EMERGING INFECTIOUS DISEASES®

CDC
Centers for Disease Control and Prevention

Poxvirus Infections

June 2023

John Williamson (c.1730–c.1803), *Recovering Smallpox Patient*, c.1770. Bust, pine, boiled linseed oil. 12.6 in x 5.7 in x 9.45 in/32 cm x 14.5 cm x 24 cm. Image courtesy of Shetland Museum and Archives (Shetland Amenity Trust), Shetland Islands, Scotland.

EMERGING INFECTIOUS DISEASES®

Emerging Infectious Diseases is published monthly by the Centers for Disease Control and Prevention, 1600 Clifton Rd NE, Mailstop H16-2, Atlanta, GA 30329-4027, USA. Telephone 404-639-1960; email, eideditor@cdc.gov

EMERGING INFECTIOUS DISEASES®

Poxvirus Infections **June 2023**

On the Cover

John Williamson (c.1730–c.1803), *Recovering Smallpox Patient*, c.1770. Bust, pine, boiled linseed oil. 12.6 in x 5.7 in x 9.45 in/32 cm x 14.5 cm x 24 cm. Image courtesy of Shetland Museum and Archives (Shetland Amenity Trust). Shetland Islands, Scotland, UK.

About the Cover p. 1292

Synopses

Research

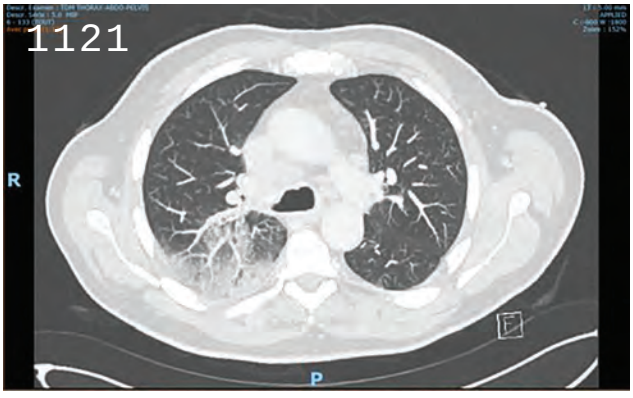

EMERGING INFECTIOUS DISEASES®
June 2023

Dispatches

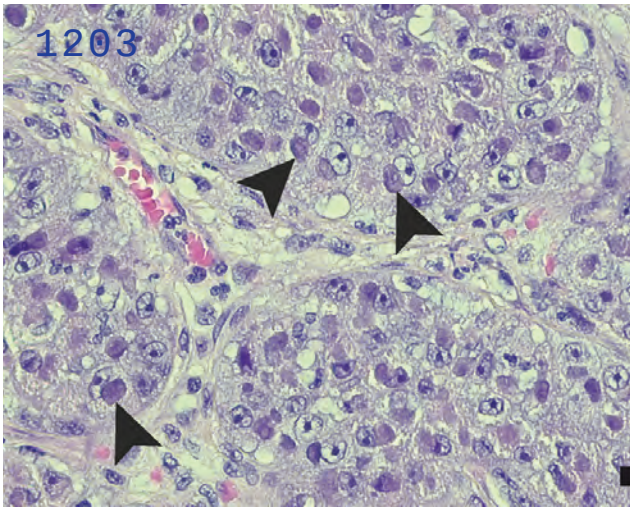

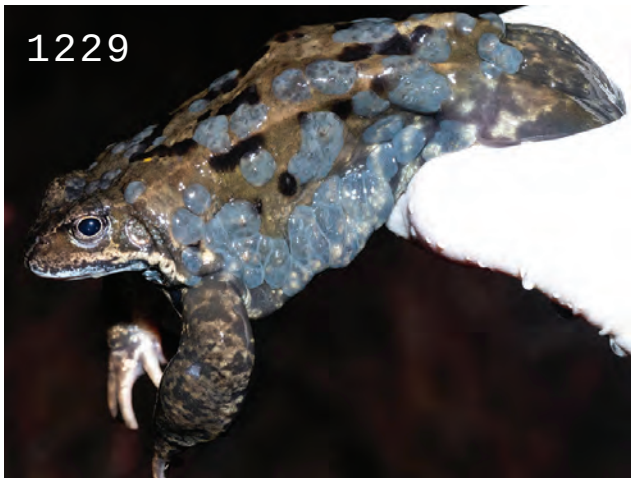

EMERGING INFECTIOUS DISEASES®
June 2023

Research Letters

About the Cover

Online Report

Emerging Infectious Diseases
Photo Quiz Articles

Volume 14, Number 9
September 2008

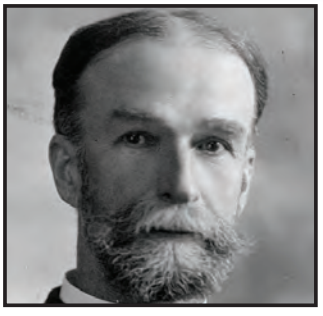

Volume 14, Number 12
December 2008

Volume 15, Number 9
September 2009 e

Volume 15, Number 10
October 2009

Volume 16, Number 6
June 2010

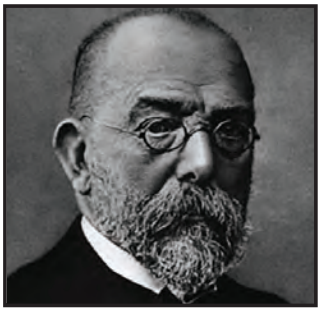

Volume 17, Number 3
March 2011

Volume 17, Number 12
December 2011

Volume 19, Number 4
April 2013

Volume 20, Number 5
May 2014

Volume 21, Number 9
September 2015

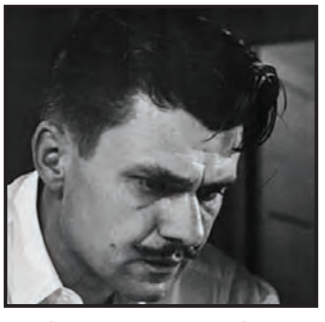

Volume 22, Number 8
August 2016

Volume 28, Number 3
March 2022

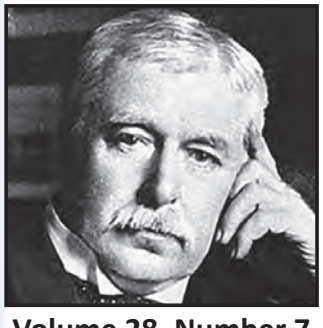

Volume 28, Number 7
July 2022

Click on the link below to read about the people behind the science.

https://bit.ly/3LN02tr

See requirements for submitting a photo quiz to EID.

https://bit.ly/3VUPqfj

EID Journal

Association of Persistent Symptoms after Lyme Neuroborreliosis and Increased Levels of Interferon-α in Blood

Sergio A. Hernández, Katarina Ogrinc, Miša Korva, Andrej Kastrin, Petra Bogovič, Tereza Rojko, Keith W. Kelley, Janis J. Weis, Franc Strle, Klemen Strle

Patients who have Lyme neuroborreliosis (LNB) might experience lingering symptoms that persist despite antibiotic drug therapy. We tested whether those symptoms are caused by maladaptive immune responses by measuring 20 immune mediators in serum and cerebrospinal fluid (CSF) in 79 LNB patients followed for 1 year. At study entry, most mediators were highly concentrated in CSF, the site of the infection. Those responses resolved with antibiotic therapy, and associations between CSF cytokines and signs and symptoms of LNB were no longer observed. In contrast, subjective symptoms that persisted after use of antibiotics were associated with increased levels of serum interferon-α (IFN-α), which were already observed at study entry, and remained increased at each subsequent timepoint. Highest IFN-α levels corresponded with severe disease. Although the infection serves as the initial trigger, sequelae after antibiotic therapy are associated with unremitting systemic IFN-α levels, consistent with the pathogenic role of this cytokine in interferonopathies in other conditions.

Lyme disease, which is caused by several species of *Borrelia burgdorferi* sensu lato complex (Lyme borreliae), is the most common vectorborne disease in the Northern Hemisphere. The US Centers for Disease Control and Prevention now estimates that nearly 500,000 new cases are diagnosed and treated for Lyme disease annually in the United States (*1*). Approximately 200,000 cases are believed to occur each year in western Europe (*2*,*3*). The first sign of the infection is usually an expanding cutaneous lesion, termed erythema migrans, which might be accompanied with nonspecific symptoms, such as headache, fever, malaise, fatigue, myalgias, and arthralgias. If untreated, spirochetes might disseminate to other organ systems, including the heart, joints, and central nervous system (CNS) (*4*,*5*). Lyme neuroborreliosis (LNB), which results from borreliae infection of the CNS, is the most common extracutaneous manifestation of Lyme disease in Europe and the second most common such manifestation in North America (*4*–*6*).

Most patients who have Lyme disease respond well to antibiotic drug therapy and their disease resolves. However, a subset of patients have sequelae, such as headache, fatigue, sleep or memory disturbance, and arthralgias or myalgias that persist for months to years after antibiotic use, termed posttreatment Lyme disease symptoms or syndrome (PTLDS) (*7*–*14*). Those sequelae might occur with each Lyme disease manifestation and are heterogenous, ranging from mild, self-resolving symptoms to debilitating syndromes that greatly impair the quality of life and require regular use of analgesics (*7*–*13*,*15*). Although PTLDS is generally more common in women and in persons who have a difficult early disease course (*12*,*15*), the underlying causes are not well understood, and biomarkers to identify patients at risk for such outcomes are lacking. Thus, treatment strategies are symptom-based and often ineffective, leaving patients and physicians in a quandary about how to restore health.

Although persistent infection is often considered as an explanation for lingering symptoms, microbiological evidence of infection in the post–antibiotic drug period is limited in humans. Two clinical trials in Europe of antibiotic drug efficacy established that only 2 (0.8%) of 244 patients had microbiologic treatment

Author affiliations: Tufts University School of Medicine, Boston, Massachusetts, USA (S.A. Hernández, K. Strle); New York State Department of Health, Albany, New York, USA (S.A. Hernández, K. Strle); University Medical Center Ljubljana, Ljubljana, Slovenia (K. Ogrinc, P. Bogovič, T. Rojko, F. Strle}; University of Ljubljana, Ljubljana (M. Korva, A. Kastrin); University of Illinois, Urbana-Champaign, Illinois, USA (K.W. Kelley); University of Utah, Salt Lake City, Utah, USA (J.J. Weis)

DOI: https://doi.org/10.3201/eid1906.221685

failure, and neither had PTLDS (*10*,*11*). Similarly, in xenodiagnostic studies, 2 of 11 patients with PTLDS were positive for borrelia DNA, but all were culture negative, implying lack of viable organisms (*16*). Findings from those microbiologic studies are substantiated by 5 clinical trials in United States and Europe that have failed to show sustained amelioration of PTLDS with additional antimicrobial drug therapy (*17*–*20*).

Emerging evidence now points to metabolic and immune system abnormalities in post-Lyme sequelae (*21*–*24*). Because Lyme borreliae do not encode toxins, the clinical manifestation of disease has been largely attributed to the host immune response. By extension, 2 longitudinal studies of erythema migrans patients demonstrated that sustained activation of this response could contribute to persistent symptoms in the post–antibiotic drug period, when few, if any, spirochetes remain (*21*,*24*). A study of US patients by Aucott et al. reported increased serum levels of CCL19 in those with PTLDS, implying that ongoing immune reactivity in peripheral tissues might contribute to PTLDS (*21*). In our study of patients in Europe, a subset who had PTLDS had increased interleukin (IL) 23 levels in serum that correlated directly with autoantibodies but not with borrelia antibodies or culture positivity, thus implicating dysregulated Th17 immunity in those symptoms (*24*). Those reports linked the immune response to PTLDS after erythema migrans. However, the potential immune etiology of persistent symptoms after neurologic manifestations of Lyme disease has not been explored.

We investigated the role of host immune responses in the clinical course and outcome of LNB, a CNS infection with a high prevalence (≈20%) of post–antibiotic drug sequelae. (*12*) We determined during infection whether immune responses in cerebrospinal fluid (CSF) correlated with signs and symptoms of LNB. In contrast, we also determined whether post-LNB sequelae were associated with increased interferon-α (IFN-α) levels in blood, supporting a role for unremitting, low-grade, systemic inflammation in those outcomes.

Methods

Patient Selection

This study included 79 adult patients who met the modified European diagnostic criteria for LNB (*4*,*14*), defined as presence of signs or symptoms indicative of neurologic involvement (i.e., radicular pain, cranial nerve paresis, meningeal signs/meningitis, tremor); CSF lymphocytic pleocytosis; and evidence of borrelial infection demonstrated by intrathecal synthesis of borrelia-specific antibodies, *Borrelia* isolation from CSF, or presence of erythema migrans. Patients were recruited on an ongoing basis in the Lyme borreliosis

Table 1. Clinical characteristics of patients at study entry stratified according to resolution or persistence of symptoms after antimicrobial drug therapy in study of persistent symptoms after Lyme neuroborreliosis and increased levels of interferon-α in blood, Slovenia*

Characteristic	Resolved, n = 52	Persistent, n = 27	p value†	Adjusted p value‡
Demographics				
Age, y	47 (15–81)	52 (15–74)	0.6	0.9
Female/male sex	15 (29)/37 (71)	16 (59)/11 (41)	0.01	**0.03**
Annual no. tick bites	2 (0–50)	1 (0–50)	0.6	0.9
Clinical characteristics at first visit				
Current or recent EM	19 (37)	9 (33)	0.8	0.9
Solitary EM	14 (27)	8 (30)	0.8	0.9
Multiple EM	5 (10)	1 (4)	0.6	0.9
No. symptoms/patient	3 (1–11)	6 (1–13)	0.02	0.1
Duration of symptoms, days	14 (3–90)	20 (3–365)	0.3	0.9
Radicular pain	14 (27)	9 (33)	0.6	0.9
Peripheral facial palsy	37 (71)	20 (74)	0.9	0.9
Laboratory findings in blood				
CRP, mg/L	1 (1–29)	1 (1–18)	0.2	0.6
ESR, mm/h	10 (2–40)	11 (1–41)	0.7	0.6
Blood leukocyte count, x 10^9 cells/L	7 (3–23)	6.5 (3–15)	0.2	0.6
Platelet count, x10^9/L	247 (134–428)	245 (165–416)	0.3	0.8
AST, μkat/L	.42 (0.18–1.1)	0.4 (0.24–1.2)	0.8	0.8
ALT, μkat/L	.43 (0.17–2.3)	0.39 (0.14–1.8)	0.5	0.8
CSF findings				
Pleocytosis	52 (100)	27 (100)	1	1
Leukocyte count, x 10^6 cells/L	73 (6–1,579)	80 (6–806)	0.4	0.9
Lymphocyte count, x 10^6/L	63 (4–1,477)	69 (4–768)	0.6	1
Borrelia culture positivity	5 (10)	3 (11)	0.9	0.9

*Values are median (range) or no. (%). Bold indicates statistically significant p values. ALT, alanine aminotransferase; AST, aspartate aminotransferase; *Borrelia, Borrelia burgdorferi* sensu lato; CRP, C-reactive protein; CSF, cerebrospinal fluid; EM, erythema migrans; ESR, erythrocyte sedimentation rate.
†Statistical analyses were performed by using Fisher exact test or Mann-Whitney nonparametric rank-sum test.
‡Values after Benjamini-Hochberg correction for multiple comparisons (false discovery rate = 0.05).

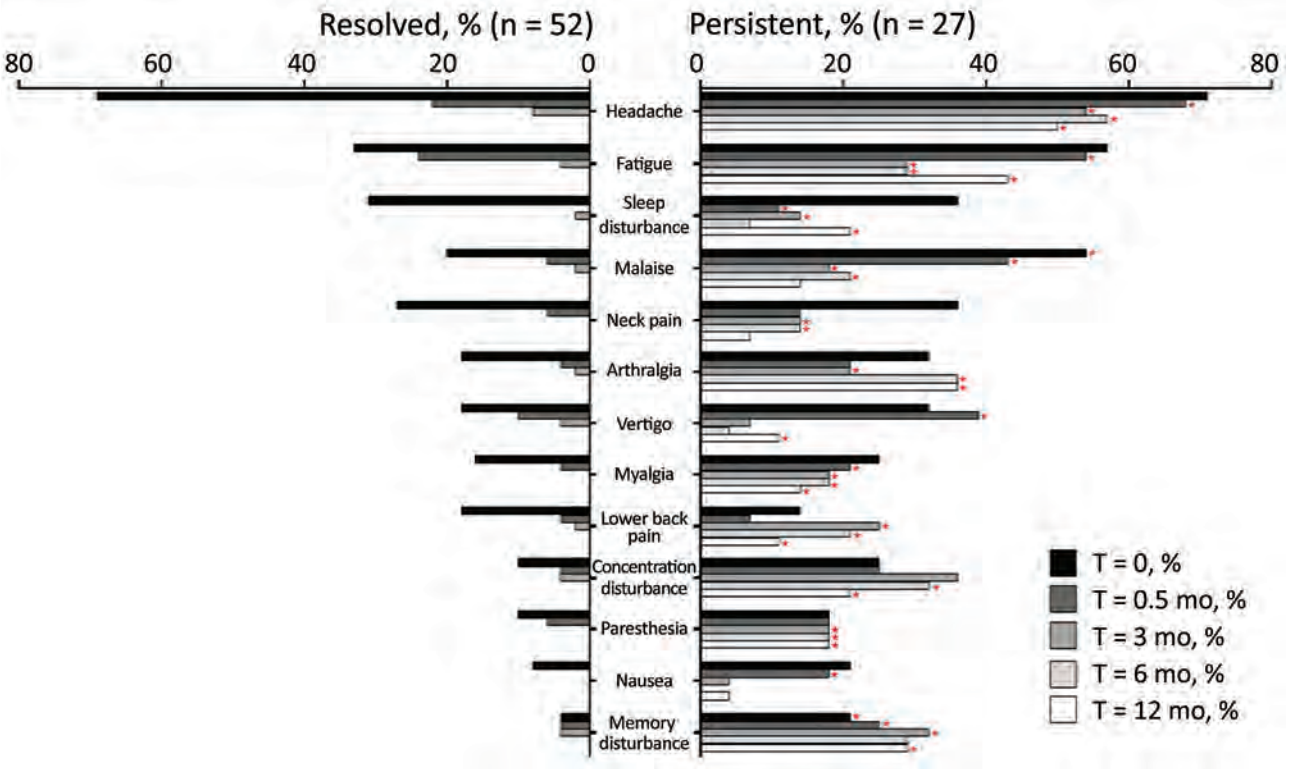

Figure 1. Individual frequency of each symptom at each follow-up timepoint in study of association of persistent symptoms after Lyme neuroborreliosis and increased levels of interferon-α in blood among patients in Slovenia.. Data in patients whose symptoms resolved are shown in the left graph and in those with persistent symptoms in the right graph. Red stars indicate symptoms that occurred at significantly higher frequency in the persistent group compared with the resolved group. p values were calculated using nonparametric Mann-Whitney rank sum tests; $p<0.05$ was considered statistically significant. T, timepoint (0 indicates baseline).

outpatient clinic at the University Medical Center Ljubljana, Ljubljana, Slovenia, during 2006–2013. The 79 patients were chosen based on availability of matched serum and CSF samples for each patient at multiple follow-up timepoints. All participants provided written informed consent, and the study was approved by the Medical Ethics Committee of the Ministry of Health of Slovenia and the Institutional Review Boards at Massachusetts General Hospital and the New York State Department of Health.

Clinical Assessment

We collected demographic and clinical information at baseline and at subsequent visits at 2 weeks and 3, 6, and 12 months after study entry by using a structured questionnaire (*12*). In addition to medical history, patients reported recurrence of tick bites, presence of EM, and severity and duration of symptoms. We also assessed signs of neurologic involvement (meningeal signs, cranial nerve damage, radiculitis, tremor) (*14*). In addition, we asked patients about any new or intensified (more severe) subjective symptoms.

We classified patients as resolved if they recovered completely with antibiotic therapy or as persistent symptoms/PTLDS if they had new or intensified subjective symptoms at 6 or 12 months after initiation of antibiotic therapy for which there was no other medical explanation. We further subgrouped patients who had PTLDS into 2 categories according to self-reported severity of symptoms based on a visual analog scale: those with mild-to-moderate symptoms that required occasional analgesics (once or twice weekly), and those who had debilitating symptoms with major impact on quality of life that required frequent use (≥3×/wk) of analgesics. In addition to clinical assessment, we obtained serum at each time point and CSF at baseline and at 3 months. We obtained serum and CSF samples during the same study visit, enabling direct comparison. Samples were stored at −80°C. The same study physician evaluated all patients over the entire study period.

Laboratory Evaluation

We assessed antibody levels (IgM and IgG) to *B. burgdorferi* sensu lato in serum and CSF by using an indirect chemiluminescence immunoassay against *OspC*

and *VlsE* recombinant antigens (LIAISON; Diasorin, https://www.diasorin.com). We determined intrathecal borrelia IgM/IgG as described; antibody index values ≥1.5 were indicative of borrelia-specific antibody production (*25*). We defined CSF pleocytosis as CSF leukocyte counts >5 × 10^6 cells/L and performed cultivation of borreliae from CSF as reported (*26*).

Cytokine and Chemokine Determinations

We assessed levels of 20 cytokines and chemokines associated with innate (CCL2, CCL3, CCL4, IL-6, IL-8, IL-10, tumor necrosis factor-α, IFN-α) and adaptive T-cell (T_H1: IFN-γ, CXCL9, CXCL10, CXCL11, CCL19, IL-12p70; T_H17: IL-17A, IL-21, IL-23; CCL21) and B-cell (CXCL12, CXCL13) immune responses in serum and CSF by using bead-based multiplex assays (EMD-Millipore, https://www.emdmillipore.com). We performed cytokine determinations in all samples in 1 complete experiment to minimize interassay variation and repeated sample freeze–thaw.

Statistical Analyses

We assessed categorical variables by using the Fisher exact test and quantitative variables by using the Mann-Whitney nonparametric rank-sum test (GraphPad.PRISM 9.2.0, https://www.graphpad.com). We adjusted p values for multiple comparisons by using the Benjamini-Hochberg procedure. We used a robust, rank-based analysis of variance to examine differences in cytokine/chemokine levels in repeated measures and using time as a within-subject factor and severity as a between-subject factor; we considered p≤0.05 statistically significant.

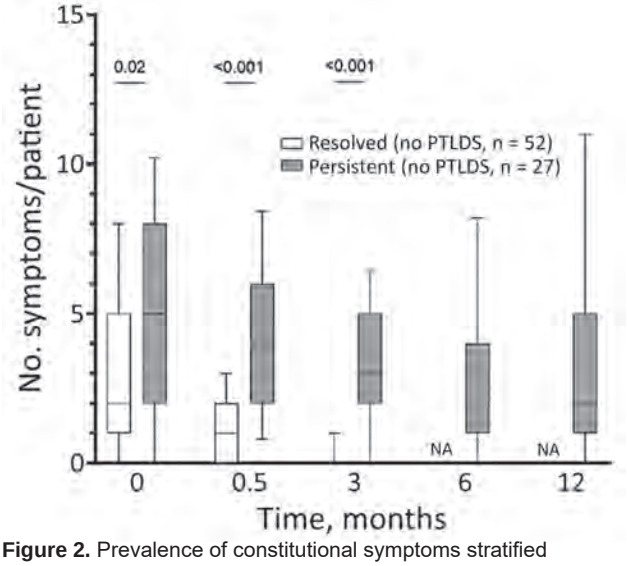

Figure 2. Prevalence of constitutional symptoms stratified according to posttreatment status in study of persistent symptoms after Lyme neuroborreliosis and increased levels of interferon-α in blood among patients in Slovenia. Total number of symptoms in Lyme neuroborreliosis patients at each time point displayed according to resolved (n = 52, white box plots) or persistent (n = 27, gray box plots) symptoms [PTLDS]). Horizontal lines within boxes indicate medians, box tops and bottoms 25th–75th percentiles, and error bars 10th–90th percentiles. Numbers above bars indicate p values. NA, not applicable; PTLDS, posttreatment Lyme disease symptoms or syndrome.

Results

Clinical Characteristics at Study Entry

A total of 79 patients were included in the study; 31 (39%) were female and 48 (61%) were male, and median age was 50 years (Table 1). Of the 79 LNB patients, 52 (66%) recovered completely after antibiotic therapy (resolved), whereas 27 (34%) had PTLDS 6–12 months after antibiotic therapy (persistent). The unusually high proportion of PTLDS patients is caused by our selection criteria, which we enriched for this patient population to enable meaningful comparisons. Compared with the resolved group, we found that patients who had PTLDS were more often female (59% vs. 41%; p = 0.03) and were more symptomatic at baseline (6 vs. 3 symptoms; p = 0.02) (Table 1). In contrast, we observed no major differences between these 2 groups for other demographic, laboratory, or clinical measurements, including the characteristic signs of LNB, Bannwarth syndrome or peripheral facial palsy.

Prevalence of Constitutional Symptoms During Follow-up

By definition, all LNB patients had signs and symptoms indicative of nervous system involvement (i.e., radiculitis, cranial nerve paresis, meningeal signs, tremor) at first visit, before antibiotic therapy. In addition to those neurologic signs and symptoms, patients often reported associated nonspecific systemic symptoms, most commonly headache, fatigue, and sleep disturbance (Figure 1). When stratified by presence of symptoms in the post–antibiotic therapy period, patients who had PTLDS had a more symptomatic early disease course, before antibiotic therapy (6 vs. 3 symptoms; p = 0.02), as well as at the conclusion of therapy (after 2 weeks, 3.5 vs. 0 symptoms; p<0.001) and at 3 months (3 vs. 0 symptoms; p<0.001) (Figure 2). Moreover, when systemic symptoms were evaluated individually, 11 of the 13 symptoms were found at higher prevalence at the initial visit for patients who later had PTLDS develop, although only malaise and memory disturbance reached statistical significance (Figure 2). Those differences became more pronounced after antibiotic therapy; at 2 weeks, patients who

Table 2. Comparison of cytokine and chemokine levels in cerebrospinal fluid and serum at study entry and 3 mo in study of association of persistent symptoms after Lyme neuroborreliosis and increased levels of interferon-α in blood, Slovenia *

Mediator	T = 0, n = 719			T = 3 mo, n = 64		
	Median CSF (range), pg/mL	Median serum (range), pg/mL	p value†	Median CSF (range), pg/mL	Median serum (range), pg/mL	p value†
Innate						
IFN-α	3 (0–64)	2 (0–187)	1	1 (0–19)	2 (0–158)	**0.0001**
IL-6	7 (0–146)	1 (0–234)	**0.0002**	1 (0–1)	1 (0–88)	0.1
IL-10	6 (0–422)	1 (0–40)	**0.0002**	1 (0–1)	1 (0–3)	1
IL-8	144 (18–1,288)	23 (0–2,159)	**0.0002**	31 (13–107)	15 (1–1,700)	**0.0002**
TNF	10 (0–150)	20 (2–385)	**0.0002**	2 (0–20)	19 (2–278)	**0.0001**
CCL2	1,096 (223–48,494)	668 (60–1,579)	**0.0002**	719 (241–1,889)	688 (287–7,311)	0.3
CCL3	49 (1–107)	25 (1–1,310)	**0.003**	38 (1–87)	21 (1–1080)	**0.0001**
CCL4	29 (1–787)	127 (29–2,567)	**0.0002**	11 (1–35)	129 (33–1,223)	**0.0001**
T_H1 adaptive						
IFN-γ	2 (0–193)	3 (0–349)	1	1 (0–11)	1 (0–32)	**0.0001**
CXCL9	2,274 (14–37,051)	1,175 (49–26,310)	**0.05**	117 (1–1,997)	853 (110–20,472)	**0.0001**
CXCL10	16,920 (137–139,804)	600 (66–4,484)	**0.0002**	905 (201–16,407)	439 (50–6,221)	**0.0001**
CXCL11	80 (1–2,640)	45 (1–534)	**0.003**	10 (1–86)	46 (1–499)	**0.0001**
CCL19	55 (10–1,598)	54 (10–939)	0.5	10 (3–362)	73 (7–1,730)	**0.0001**
IL-12p70	3 (1–17)	3 (1–1,486)	0.5	1 (1–3)	3 (1–45)	**0.0001**
T_H17 adaptive						
IL-17a	9 (4–25)	4 (0–347)	**0.0002**	7 (3–11)	5 (1–64)	**0.0001**
IL-21	3 (3–11)	3 (3–229)	0.5	20 (1–20)	20 (3–41)	0.1
IL-23	3 (3–408)	13 (0–13,296)	**0.007**	49 (0–85)	49 (0–2,123)	**0.02**
CCL21	530 (312–927)	97 (20–1,473)	**0.0002**	530 (256–1,222)	98 (20–1,323)	**0.0001**
B-cell adaptive						
CXCL12	3,760 (98–27,479)	2,875 (98–16,039)	**0.006**	1,953 (98–6,880)	2,875 (98–16,039)	**0.02**
CXCL13	187 (1–107,723)	18 (5–172)	**0.0002**	4 (1–62)	13 (1–151)	**0.0001**

*Bold indicates statistically significant p values. CCL, CC motif chemokine ligand; CSF, cerebrospinal fluid; CXCL, CXC motif chemokine ligand; IFN, interferon; IL, interleukin; T, timepoint (0 indicates baseline); TNF, tumor necrosis factor.
†Benjamini-Hochberg corrected (false discovery rate = 0.05).

had PTLDS had a higher prevalence of 9 of the 13 symptoms than did those in the resolved group (Figure 2).

Comparison of Immune Mediators in Serum and CSF

We assessed levels of 20 cytokines and chemokines associated with innate and adaptive T- and B-cell immune responses in matched serum and CSF samples at study entry and 3 months. At baseline, 12 mediators were more highly concentrated in CSF, the site of infection, than in serum (Table 2). The highest levels and the most dramatic differences were observed for CCL2 (median 1,096 pg/mL vs. 668 pg/mL; p = 0.0002), the IFN-γ–inducible chemokines CXCL9 (2,274 pg/mL vs 1,175 pg/mL; p = 0.05), and CXCL10 (16,920 pg/mL vs. 600 pg/mL; p = 0.0002), and B-cell chemoattractants CXCL12 (3,760 pg/mL vs. 2,875 pg/mL; p = 0.06) and CXCL13 (187 pg/mL vs. 18 pg/mL; p = 0.0002). Those data established that both innate and adaptive T- and B-cell immune responses are triggered during *Borrelia* infection and that those responses occur locally in CNS, the site of the disease. Conversely, TNF-α, CCL4, and IL-23 were present at greater levels in serum, suggesting that those responses occur systemically. However, by 3 months, most mediators decreased dramatically in CSF, reaching concentrations comparable to those in serum, presumably because of successful resolution of the CNS infection. Moreover, the concentrations of most mediators in serum were unremarkable and did not change between the 2 time points, further supporting the conclusion that immune responses occur locally in CSF and thereby contribute to CNS symptoms (Table 3).

Immune Responses at the Initial Visit According to PTLDS

Because the greater frequency of symptoms at first visit was associated with an unfavorable clinical outcome, we assessed whether the immune responses during early infection might predict resolution or persistence of symptoms after antibiotic drug therapy. For that purpose, we stratified cytokine and chemokine levels at initial visit, before use of antimicrobial drugs, by resolution or persistence of symptoms 6–12 months later (Table 4). In serum, 4 mediators varied greatly between patients who had persistent or resolved symptoms. Levels of 3 mediators, CXCL11, CCL19, and IL-21, were higher in patients whose symptoms resolved after antibiotic therapy, implying that they might play a protective role in the infection and contribute to symptom resolution. Those associations were lost in follow-up (data not shown), substantiating their role in the infection. In contrast, IFN-α levels were significantly higher in patients who had PTLDS

(median 18 pg/mL vs. 2 pg/mL; p = 0.01). A similar trend was observed for IL-17A and IL-23, but those differences were not significant after adjustment for multiple comparisons. In CSF, none of the mediators differentiated patients with persistent symptoms from those whose symptoms resolved, despite the association between increased CSF immune responses, symptoms, and CNS infection. This finding implies the decoupling of immune responses in CSF during infection from systemic immune responses associated with the development of PTLDS in the post–antibiotic therapy period.

Immune Responses During Follow-up According to PTLDS

IFN-α in serum was the only mediator that remained significantly increased in patients with PTLDS at each follow-up visit, compared with patients whose symptoms resolved (Figure 3, panel A). Similar results were observed when participants were further stratified according to PTLDS severity (Figure 3, panel B). Patients with severe symptoms had the highest levels of IFN-α in serum at baseline (median 35.5 pg/mL), those with moderate severity had intermediate IFN-α concentrations (9 pg/mL), and those without PTLDS had the lowest IFN-α levels (2 pg/mL) in serum. This association was observed at each subsequent time point. A similar trend was observed for IL-23, although those differences did not reach statistical significance. In contrast, other mediators did not differ by disease severity at any time point after antibiotic therapy, including CCL19, which was previously associated with PTLDS in patients after erythema migrans (*21*), and IL-10, which is a major regulatory cytokine (Figure 3, panel C). A nonparametric analysis of variance-type testing, which measured the effect of relative disease severity on cytokine levels, reinforced this association between PTLDS, IFN-α, and IL-17/IL-23 pathways (Figure 3, panel C).

We provide serum IFN-α levels for individual patients (Figure 4). Although there was overlap between disease severity groups, most patients with severe PTLDS had IFN-α levels above the third quartile of patients without PTLDS at each time point. Thus, increased serum IFN-α levels in the post–antibiotic therapy period might play a pathogenic role by contributing to ongoing symptoms after LNB.

Discussion

A subset of patients with LNB experience lingering symptoms that persist despite appropriate antimicrobial therapy. The etiology of such symptoms is unclear, and effective biomarkers and treatment strategies

Table 3. Association of inflammatory mediators in cerebrospinal fluid and serum at study entry with posttreatment Lyme disease symptoms 6 or 12 mo after acute illness in study of association of persistent symptoms after Lyme neuroborreliosis and increased levels of interferon-α in blood, Slovenia*

	Cerebrospinal fluid, n = 67			Serum, n = 78		
Mediator	Median (range) PTLDS, pg/mL, n = 24	Median (range) no PTLDS, pg/mL, n = 43	p value†	Median (range) PTLDS, pg/mL, n = 27	Median (range) no PTLDS, pg/mL, n = 51	p value†
Innate						
IFN-α	10 (0–64)	3 (0–64)	0.8	18 (0–187)	2 (0–129)	**0.05**
IL-6	3 (1–73)	8 (0–146)	0.9	1 (1–234)	1 (0–115)	1
IL-10	127 (22–1,288)	168 (18–860)	0.9	32 (1–381)	20 (0–2,159)	0.5
IL-8	4 (0–241)	6 (0–422)	0.8	1 (0–7)	1 (0–40)	0.5
TNF	9 (0–98)	10 (0–150)	0.9	17 (7–164)	20 (2–385)	0.4
CCL2	985 (223–48,494)	1,111 (311–6,099)	0.9	697 (245–1,234)	650 (60–1,579)	0.6
CCL3	45 (1–95)	50 (1–107)	0.8	24 (1–268)	26 (1–1,310)	0.8
CCL4	29 (1–787)	29 (1–105)	1	154 (65–1,405)	116 (29–2,567)	0.4
T_H1 adaptive						
IFN-γ	3 (0–193)	2 (0–30)	0.9	3 (0–349)	1 (0–24)	0.3
CXCL9	1,524 (29–21,800)	2,370 (14–37,051)	0.9	916 (433–3,819)	1,396 (49–26,310)	0.7
CXCL10	10,410 (260–118,875)	17,794 (137–139,804)	0.9	555 (231–4,484)	622 (66–3,422)	0.8
CXCL11	74 (2–2,645)	86 (1–1,194)	0.9	10 (1–151)	66 (2–534)	**0.05**
CCL19	68 (10–1,062)	53 (10–1,598)	0.9	31 (10–484)	74 (10–939)	**0.05**
IL-12p70	1 (1–17)	3 (1–12)	0.9	3 (1–1,486)	1 (1–21)	0.2
T_H17 adaptive						
IL-17a	10 (5–25)	8 (4–21)	0.8	6 (1–347)	4 (1–13)	0.1
IL-21	3 (3–10)	3 (3–11)	0.9	3 (3–10)	3 (3–229)	**0.05**
IL-23	3 (3–47)	3 (3–498)	0.9	22 (0–931)	9 (0–13,296)	0.8
CCL21	563 (376–804)	530 (312–927)	0.9	98 (20–989)	95 (20–1,473)	0.8
B-cell adaptive						
CXCL12	4,384 (98–27,479)	2,950 (98–24,080)	0.9	2,882 (98–9,061)	2,868 (98–16,039)	0.8
CXCL13	272 (5–107,723)	114 (5–50,000)	0.8	24 (5–123)	18 (5–172)	0.6

*Bold indicates statistically significant p values. CCL, CC motif chemokine ligand; CSF, cerebrospinal fluid; CXCL, CXC motif chemokine ligand; IFN, interferon; IL, interleukin; PTLDS, posttreatment Lyme disease symptoms; TNF, tumor necrosis factor.
†Benjamini-Hochberg corrected (false discovery rate = 0.05).

Table 4. Cytokine and chemokine levels at study entry vs 3 mo in cerebrospinal fluid and serum in study of association of persistent symptoms after Lyme neuroborreliosis and increased levels of interferon-α in blood, Slovenia*

	Cerebrospinal fluid			Serum		
Mediator	T = 0, median (range), pg/mL, n = 67	T = 3, median (range), pg/mL, n = 64	p value†	T = 0, median (range), pg/mL, n = 78	T = 3, median (range), pg/mL, n = 74	p value†
Innate						
IFN-α	3 (0–64)	1 (0–19)	**0.0005**	2 (0–187)	2 (0–158)	0.7
IL-6	7 (0–146)	1 (0–1)	0.6	1 (0–234)	1 (0–88)	**0.0007**
IL-8	144 (18–1,288)	1 (0–1)	**0.001**	1 (0–40)	15 (1–1,700)	**0.0007**
IL-10	6 (0–422)	31 (13–107)	0.4	23 (0–2,159)	1 (0–3)	0.2
TNF	10 (0–150)	2 (0–20)	**0.001**	20 (2–385)	19 (2–278)	0.8
CCL2	1,096 (223–48,494)	719 (241–1,889)	**0.001**	668 (60–1,579)	688 (287–7,311)	0.4
CCL3	49 (1–107)	38 (1–87)	**0.001**	25 (1–1,310)	21 (1–1,080)	0.8
CCL4	29 (1–787)	11 (1–35)	**0.001**	127 (29–2,567)	129 (33–1,223)	0.8
T_H1 adaptive						
IFN-γ	2 (0–193)	1 (0–11)	**0.003**	3 (0–349)	1 (0–32)	0.8
CXCL9	2,274 (14–37,051)	117 (1–1,997)	**0.001**	1,175 (49–26,310)	853 (110–20,472)	**0.03**
CXCL10	16,920 (137–139,804)	905 (201–16,407)	**0.001**	600 (66–4,484)	439 (50–6,221)	**0.03**
CXCL11	80 (1–2,640)	10 (1–86)	**0.001**	45 (1–534)	46 (1–499)	0.9
CCL19	55 (10–1,598)	10 (3–362)	**0.001**	54 (10–939)	73 (7–1,730)	0.7
IL-12p70	3 (1–17)	1 (1–3)	**0.001**	3 (1–1,486)	3 (1–45)	0.2
T_H17 adaptive						
IL-17a	9 (4–25)	7 (3–11)	**0.001**	4 (0–347)	5 (1–64)	0.9
IL-21	3 (3–11)	20 (1–20)	**0.009**	3 (3–229)	20 (3–41)	**0.0007**
IL-23	3 (3–408)	49 (0–85)	**0.003**	13 (0–13,296)	49 (0–2,123)	**0.005**
CCL21	530 (312–927)	530 (256–1,222)	**0.001**	97 (20–1,473)	98 (20–1,323)	0.9
B-cell adaptive						
CXCL12	3,760 (98–27,479)	1,953 (98–6,880)	0.2	2,875 (98–16,039)	2,875 (98–16,039)	0.8
CXCL13	187 (1–107,723)	4 (1–62)	**0.001**	18 (5–172)	13 (1–151)	0.2

*Bold indicates statistically significant p values. CCL, CC motif chemokine ligand; CSF, cerebrospinal fluid; CXCL, CXC motif chemokine ligand; IFN, interferon; IL, interleukin; T, timepoint (0 indicates baseline); TNF, tumor necrosis factor.
†Benjamini-Hochberg corrected (false discovery rate = 0.05).

are lacking. The usefulness of this report is that it defines IFN-α as a distinguishing marker and possibly a mediator of post-Lyme sequelae. These findings have potential implications for diagnosis of patients and treatment for this condition.

Prolonged systemic symptoms have been observed after several bacterial and viral infections, including infectious mononucleosis, influenza, Q fever, and COVID-19 (*27*,*28*). Despite the diversity of triggering agents, several common themes have emerged. As a generalization, those sequelae comprise a constellation of nonspecific symptoms that occur more frequently after severe early infection; they also are believed to represent a postinfectious process and are indistinguishable by standard clinical, demographic, or laboratory markers (*27*). Those observations are also applicable to patients who have Lyme disease, including LNB, ≈10%–20% of whom report lingering symptoms after antimicrobial drug therapy for *Borrelia* infection (*7*–*13*). Combined, those studies suggest that, despite different triggers, the underlying pathophysiology of postinfectious sequelae might be similar.

In the absence of microbiological evidence of persistent infection, other hypotheses have been proposed to explain lingering symptoms after Lyme disease. Those hypotheses include retained spirochetal antigens (*29*,*30*), metabolic irregularities (*31*), and excessive inflammation (*21*,*23*,*24*), all of which could arguably be linked to inappropriate activation of host immune responses. Insights from our study of patients with LNB, along with 2 previous reports of patients with erythema migrans who were followed longitudinally to evaluate their posttreatment status (*21*,*24*), support the role of maladaptive immune responses in PTLDS. Moreover, those studies suggest that the stage for dysregulated immunity is set early in infection. In all 3 studies, heightened levels of PTLDS-associated inflammatory mediators were observed at first visit, before antimicrobial drug therapy, implying that *Borrelia* infection serves as the initial trigger for these responses (*21*,*24*). However, the sustained immune activity in the post–antibiotic therapy period, which occurs concurrently with post-Lyme sequelae, appears to represent a postinfectious process (*10*,*11*,*24*). Similar observations have been made in patients with postinfectious Lyme arthritis who have persistent synovitis for months to years after receiving antibiotics (*23*,*32*). Thus, a range of post-Lyme complications have been linked to dysregulated host immunity.

What is driving unremitting inflammation in the absence of an ongoing infection is not yet entirely clear. One possibility is that spirochetal remnants, such as *Borrelia* peptidoglycan, which is not easily

cleared, continue to stimulate immune responses in the postinfectious period (*29*,*30*). However, given that such components presumably also persist in patients whose symptoms resolve after treatment with antibiotics, this finding alone is unlikely the entire explanation for post-Lyme sequelae. Alternatively, several studies in Lyme arthritis point to infection-induced autoimmune phenomena as a potential reason for persistent postinfectious arthritis (*23*). Finally, in mice and in humans, genetic predisposition might contribute to dysregulated immunity (*33*–*35*). Those possibilities, and probably other unidentified mechanisms, are not mutually exclusive. Depending on the condition, multiple factors might play a role. This concept is supported at least partially by distinct immune signatures associated with PTLDS across different patient populations, including CCL19 in erythema migrans patients in the United States (*21*), IL-23 in erythema migrans patients in Europe (*24*), and IFN-α in patients who have LNB. Nevertheless, the preponderance of evidence across distinct manifestations underscores the role of maladaptive immune responses as both effectors and biomarkers of post–antibiotic therapy sequelae after Lyme disease.

In this longitudinal study, both CSF and serum were available at multiple time points over 1 year. This approach enabled tracking of immunologic responses systemically and locally in CSF during the clinical course and outcome of LNB. This analysis showed that, during CNS infection, the innate and adaptive immune responses are highly concentrated in CSF, the site of the disease. Those responses resolve after antimicrobial drug therapy and presumed resolution of CNS infection. This contraction of immune responses in CSF coincides with resolution of neurologic signs and symptoms of LNB (radiculitis, cranial nerve damage, meningeal

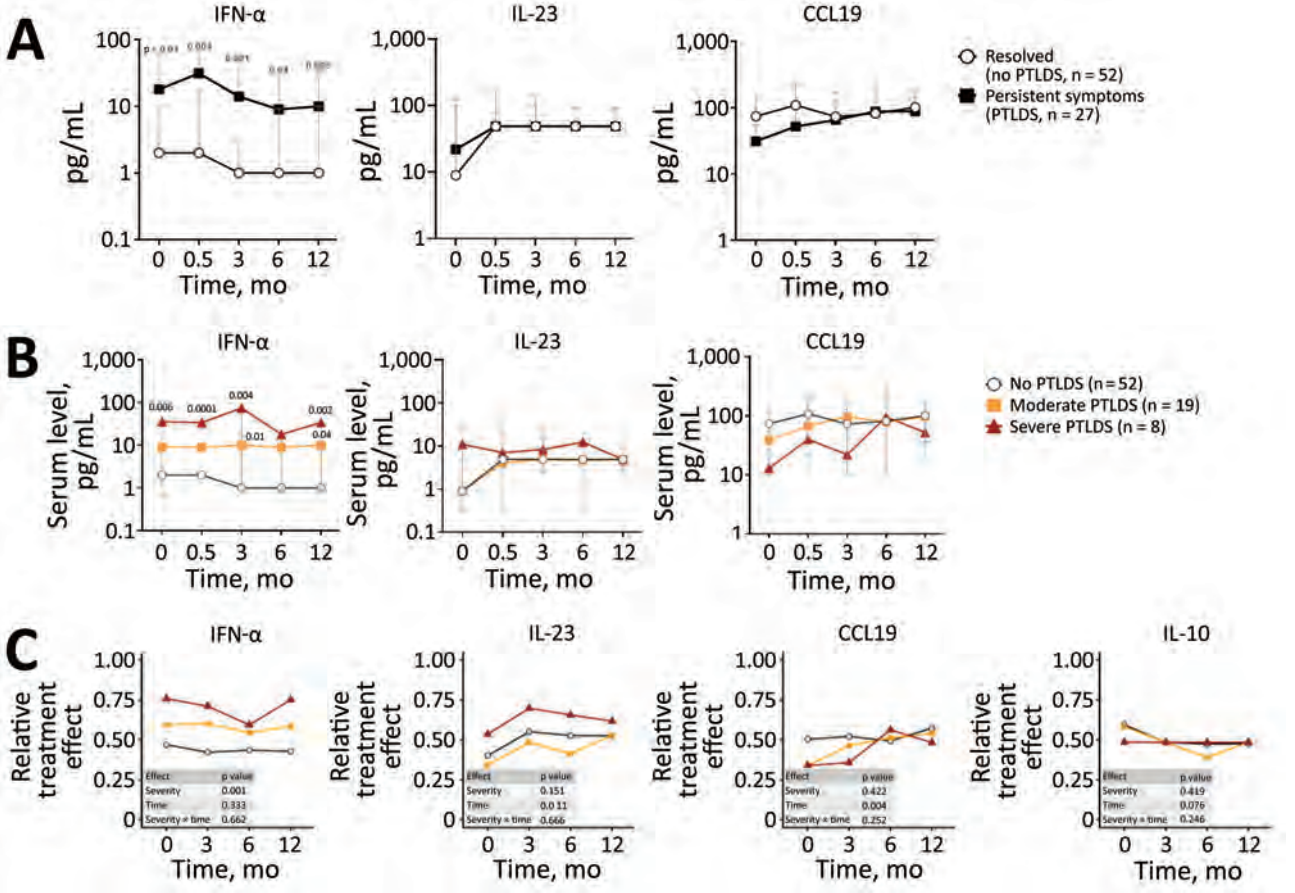

Figure 3. Cytokine and chemokine levels in serum of patients in Slovenia who had Lyme neuroborreliosis in study of association of persistent symptoms after Lyme neuroborreliosis and increased levels of interferon-α in blood. Prevalence of constitutional symptoms is stratified according to PTLDS severity during the 1-year follow-up period. A) Median serum levels of IFN-α, IL-23, and CCL19 during 1 year of follow-up stratified by presence or absence of PTLDS. B) Median serum levels of IFN-α, IL-23, and CCL19 graphed according to disease severity. p values above red line correspond to the comparison between patients with severe PTLDS vs those with no PTLDS (resolved). p values above yellow lines represent significant differences between the no PTLDS and moderate PTLDS groups. C) Analysis of variance comparison of relative effect of disease severity or time on cytokine levels in serum. Error bars indicate10th–90th percentiles. CCL, CC motif chemokine ligand; IFN, interferon; IL, interleukin; PTLDS, posttreatment Lyme disease symptoms or syndrome.

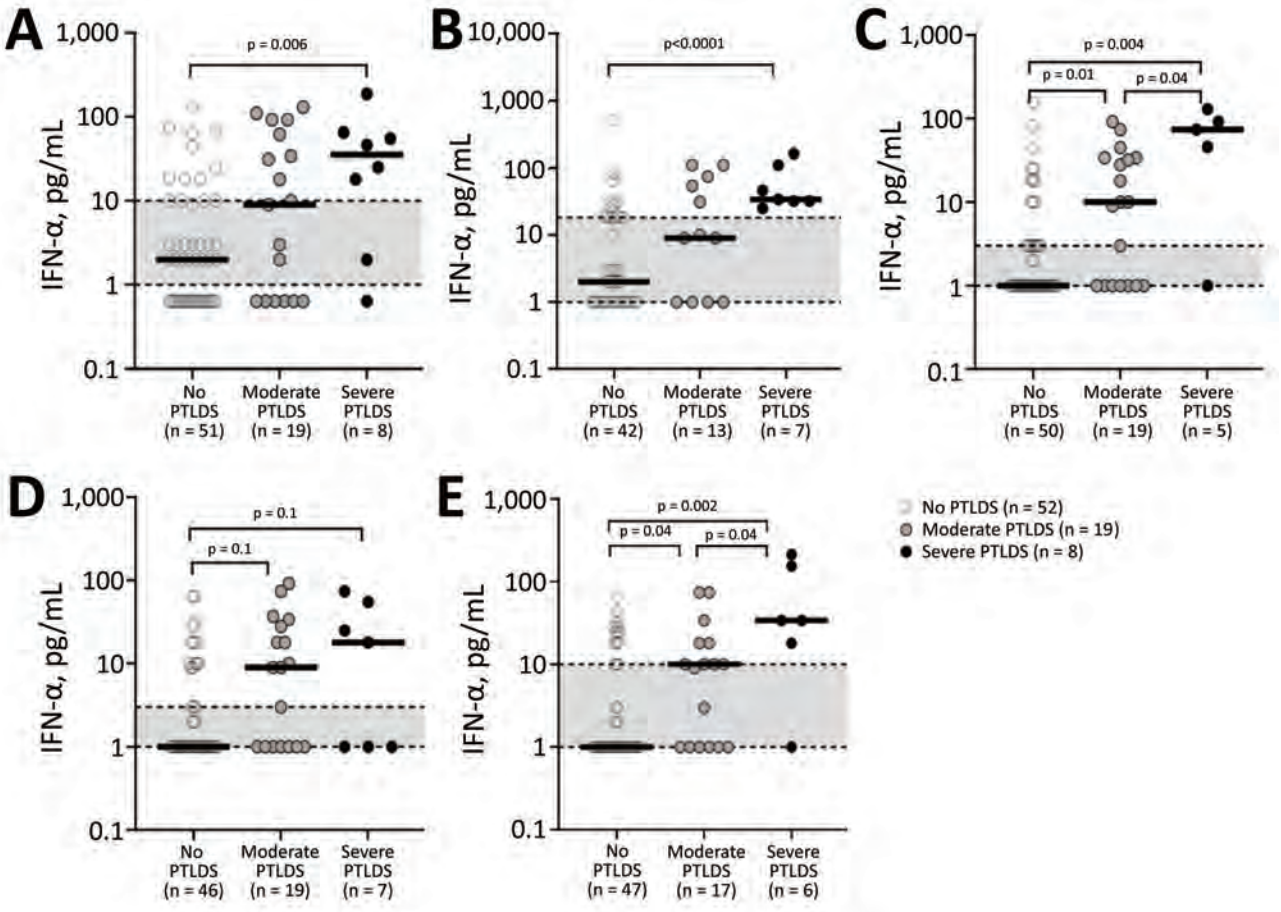

Figure 4. Serum IFN-α levels of individual patients with Lyme neuroborreliosis in Slovenia at each follow-up timepoint according to PTLDS severity in study of association of persistent symptoms after Lyme neuroborreliosis and increased levels of interferon-α in blood. A) T = 0; B) T = 2 wks; C) T = 3 mo; D) T = 6 mo; E) T = 12 mo. Levels of interferon-α in serum for individual patients throughout the 1-year follow-up are shown. Solid black lines symbolize median values, and shaded area between dotted lines indicates interquartile range. Statistical analyses were performed by using nonparametric Mann-Whitney rank-sum tests. Significant p values for each comparison are shown above the corresponding brackets. IFN, interferon; PTLDS, posttreatment Lyme disease symptoms or syndrome.

signs/meningism, tremor), thereby linking the infection and inflammation in CSF with CNS disease. In contrast, the nonspecific lingering symptoms after LNB are associated with increased IFN-α levels in serum. Those results imply that sustained systemic immune responses and associated symptomology are decoupled from infection-driven immune responses in CSF. This interpretation is consistent with the notion that type 1 IFNs represent a maladaptive immune response that contributes to disease pathology but not to control of *Borrelia* infection. In murine models, type 1 IFN responses are associated with development of arthritis in the absence of spirochetal eradication (*36*,*37*). In humans, increased IFN-α activity has been observed in patients with a history of Lyme disease and persistent cognitive deficits months to years after receiving antimicrobial drugs (*17*). Those observations provide new considerations for treatment approaches that prioritize targeting the immune response after appropriate antibiotic regimens, a treatment algorithm used successfully in post–antibiotic therapy for Lyme arthritis (*23*,*38*).

Although this study does not establish causality, the association between increased systemic IFN-α levels and PTLDS is nonetheless intriguing. This cytokine plays a central role in maladaptive hyperinflammatory immune responses in type 1 interferonopathies in other infections and autoimmune diseases, including COVID-19, influenza, and lupus (*39*). The pathologic effects of IFN-α are also apparent from treatment studies in cancer and chronic viral hepatitis in which administration of this cytokine often results in adverse events, particularly influenza-like symptoms, such as fever, chills, myalgia, headache, and nausea, as well as neurologic and psychiatric sequelae (*40*,*41*). Those symptoms, which are remarkably similar to those

in patients with PTLDS, occur in most patients undergoing IFN-α therapy and might lead to discontinuation of treatment. Lessons learned from these studies could offer major insights into novel therapeutic approaches that target IFN-α in Lyme disease. However, before such strategies can be considered, our initial observations need to be validated in larger cohorts of patients with PTLDS and appropriate control groups. Nevertheless, emerging anti–IFN-α therapies offer hope for more effective treatment strategies for patients with debilitating lingering symptoms after LNB and perhaps other manifestations of Lyme disease.

Acknowledgments

We thank the patients and physicians for participating in this study.

This study was supported by the National Institutes of Health (NIAID: R21AI144916, R01 AI150157-01 and NIAMS: K01AR062098); the Massachusetts General Hospital Executive Committee on Research Interim Support Fund, and the Wadsworth Center, New York State Department of Health startup funds to K.S. and the Slovenian Research Agency (P3-0296, J3-1744, and J3-8195) to F.S.

K.S., F.S., and K.O. designed the study. K.S., S.H., M.K., and AK conducted experiments and data analyses. K.O., F.S., P.B., and T.R. examined patients who had LNB, made diagnosis, and collected clinical samples and clinical information. S.H., M.K., A.K., and K.S. performed statistical analyses and contributed to generation of tables and figures. S.H., K.S., F.S., K.O., K.W.K., and J.J.W. helped with interpretation of data and in writing the manuscript. All authors reviewed and approved the manuscript.

K.S. served as a consultant for T2 Biosystems, Roche, BioMerieux, and the New York State Biodefense Fund for the development of a diagnostic assays in Lyme borreliosis. F.S. served on the scientific advisory board for Roche on Lyme disease serologic diagnostics and on the scientific advisory board for Pfizer on Lyme disease vaccine and is an unpaid member of the steering committee of the ESCMID Study Group on Lyme Borreliosis/ESGBOR. Other authors report no conflict of interests.

About the Author

Mr. Hernández is a research assistant at Tufts University School of Medicine. His primary research interests are understanding protective and pathogenic immune responses in Lyme borreliosis, infection-triggered autoimmunity, and its molecular underpinnings.

References

1. Kugeler KJ, Schwartz AM, Delorey MJ, Mead PS, Hinckley AF. Estimating the frequency of Lyme disease diagnoses, United States, 2010–2018. Emerg Infect Dis. 2021;27:616–9. https://doi.org/10.3201/eid2702.202731
2. Hubálek Z. Epidemiology of lyme borreliosis. Curr Probl Dermatol. 2009;37:31–50. https://doi.org/10.1159/000213069
3. Sykes RA, Makiello P. An estimate of Lyme borreliosis incidence in western Europe. J Public Health (Oxf). 2017;39:74–81.
4. Stanek G, Wormser GP, Gray J, Strle F. Lyme borreliosis. Lancet. 2012;379:461–73. https://doi.org/10.1016/S0140-6736(11)60103-7
5. Steere AC, Strle F, Wormser GP, Hu LT, Branda JA, Hovius JW, et al. Lyme borreliosis. Nat Rev Dis Primers. 2016;2:16090. https://doi.org/10.1038/nrdp.2016.90
6. Koedel U, Fingerle V, Pfister HW. Lyme neuroborreliosis-epidemiology, diagnosis and management. Nat Rev Neurol. 2015;11:446–56. https://doi.org/10.1038/nrneurol.2015.121
7. Aucott JN. Posttreatment Lyme disease syndrome. Infect Dis Clin North Am. 2015;29:309–23. https://doi.org/10.1016/j.idc.2015.02.012
8. Steere AC. Posttreatment Lyme disease syndromes: distinct pathogenesis caused by maladaptive host responses. J Clin Invest. 2020;130:2148–51. https://doi.org/10.1172/JCI138062
9. Feder HM Jr, Johnson BJ, O'Connell S, Shapiro ED, Steere AC, Wormser GP; Ad Hoc International Lyme Disease Group. A critical appraisal of "chronic Lyme disease". N Engl J Med. 2007;357:1422–30. https://doi.org/10.1056/NEJMra072023
10. Stupica D, Lusa L, Ruzić-Sabljić E, Cerar T, Strle F. Treatment of erythema migrans with doxycycline for 10 days versus 15 days. Clin Infect Dis. 2012;55:343–50. https://doi.org/10.1093/cid/cis402
11. Stupica D, Lusa L, Cerar T, Ružić-Sabljić E, Strle F. Comparison of post–Lyme borreliosis symptoms in erythema migrans patients with positive and negative *Borrelia burgdorferi* sensu lato skin culture. Vector Borne Zoonotic Dis. 2011;11:883–9. https://doi.org/10.1089/vbz.2010.0018
12. Ogrinc K, Lusa L, Lotrič-Furlan S, Bogovič P, Stupica D, Cerar T, et al. Course and outcome of early European Lyme neuroborreliosis (Bannwarth syndrome): clinical and laboratory findings. Clin Infect Dis. 2016;63:346–53. https://doi.org/10.1093/cid/ciw299
13. Wormser GP, Dattwyler RJ, Shapiro ED, Halperin JJ, Steere AC, Klempner MS, et al. The clinical assessment, treatment, and prevention of lyme disease, human granulocytic anaplasmosis, and babesiosis: clinical practice guidelines by the Infectious Diseases Society of America. Clin Infect Dis. 2006;43:1089–134. https://doi.org/10.1086/508667
14. Mygland A, Ljostad U, Fingerle V, Rupprecht T, Schmutzhard E, Steiner I, et al. EFNS guidelines on the diagnosis and management of European Lyme neuroborreliosis. Eur J Neurol. 2010;17:8–16, e1–4.
15. Boršič K, Blagus R, Cerar T, Strle F, Stupica D. Clinical course, serologic response, and long-term outcome in elderly patients with early Lyme borreliosis. J Clin Med. 2018;7:506. https://doi.org/10.3390/jcm7120506
16. Marques A, Telford SR III, Turk SP, Chung E, Williams C, Dardick K, et al. Xenodiagnosis to detect *Borrelia burgdorferi* infection: a first-in-human study. Clin Infect Dis. 2014;58:937–45. https://doi.org/10.1093/cid/cit939
17. Fallon BA, Keilp JG, Corbera KM, Petkova E, Britton CB, Dwyer E, et al. A randomized, placebo-controlled trial of repeated IV antibiotic therapy for Lyme encephalopathy.

Neurology. 2008;70:992–1003. https://doi.org/10.1212/01.WNL.0000284604.61160.2d
18. Klempner MS, Hu LT, Evans J, Schmid CH, Johnson GM, Trevino RP, et al. Two controlled trials of antibiotic treatment in patients with persistent symptoms and a history of Lyme disease. N Engl J Med. 2001;345:85–92. https://doi.org/10.1056/NEJM200107123450202
19. Krupp LB, Hyman LG, Grimson R, Coyle PK, Melville P, Ahnn S, et al. Study and treatment of post Lyme disease (STOP-LD): a randomized double masked clinical trial. Neurology. 2003;60:1923–30. https://doi.org/10.1212/01.WNL.0000071227.23769.9E
20. Berende A, ter Hofstede HJ, Vos FJ, van Middendorp H, Vogelaar ML, Tromp M, et al. Randomized trial of longer-term therapy for symptoms attributed to Lyme disease. N Engl J Med. 2016;374:1209–20. https://doi.org/10.1056/NEJMoa1505425
21. Aucott JN, Soloski MJ, Rebman AW, Crowder LA, Lahey LJ, Wagner CA, et al. CCL19 as a chemokine risk factor for posttreatment Lyme disease syndrome: a prospective clinical cohort study. Clin Vaccine Immunol. 2016;23:757–66. https://doi.org/10.1128/CVI.00071-16
22. Jacek E, Fallon BA, Chandra A, Crow MK, Wormser GP, Alaedini A. Increased IFNα activity and differential antibody response in patients with a history of Lyme disease and persistent cognitive deficits. J Neuroimmunol. 2013;255:85–91. https://doi.org/10.1016/j.jneuroim.2012.10.011
23. Lochhead RB, Strle K, Arvikar SL, Weis JJ, Steere AC. Lyme arthritis: linking infection, inflammation and autoimmunity. Nat Rev Rheumatol. 2021;17:449–61. https://doi.org/10.1038/s41584-021-00648-5
24. Strle K, Stupica D, Drouin EE, Steere AC, Strle F. Elevated levels of IL-23 in a subset of patients with post-Lyme disease symptoms following erythema migrans. Clin Infect Dis. 2014;58:372–80. https://doi.org/10.1093/cid/cit735
25. Reiber H, Peter JB. Cerebrospinal fluid analysis: disease-related data patterns and evaluation programs. J Neurol Sci. 2001;184:101–22. https://doi.org/10.1016/S0022-510X(00)00501-3
26. Ruzić-Sabljić E, Maraspin V, Lotric-Furlan S, Jurca T, Logar M, Pikelj-Pecnik A, et al. Characterization of *Borrelia burgdorferi* sensu lato strains isolated from human material in Slovenia. Wien Klin Wochenschr. 2002;114:544–50.
27. Hickie I, Davenport T, Wakefield D, Vollmer-Conna U, Cameron B, Vernon SD, et al.; Dubbo Infection Outcomes Study Group. Post-infective and chronic fatigue syndromes precipitated by viral and non-viral pathogens: prospective cohort study. BMJ. 2006;333:575. https://doi.org/10.1136/bmj.38933.585764.AE
28. Carfì A, Bernabei R, Landi F, Gemelli Against C-P-ACSG; Gemelli Against COVID-19 Post-Acute Care Study Group. Persistent symptoms in patients after acute COVID-19. JAMA. 2020;324:603–5. https://doi.org/10.1001/jama.2020.12603
29. Bockenstedt LK, Gonzalez DG, Haberman AM, Belperron AA. Spirochete antigens persist near cartilage after murine Lyme borreliosis therapy. J Clin Invest. 2012;122:2652–60. https://doi.org/10.1172/JCI58813
30. Jutras BL, Lochhead RB, Kloos ZA, Biboy J, Strle K, Booth CJ, et al. *Borrelia burgdorferi* peptidoglycan is a persistent antigen in patients with Lyme arthritis. Proc Natl Acad Sci U S A. 2019;116:13498–507. https://doi.org/10.1073/pnas.1904170116
31. Fitzgerald BL, Graham B, Delorey MJ, Pegalajar-Jurado A, Islam MN, Wormser GP, et al. Metabolic response in patients with post-treatment Lyme disease symptoms/syndrome. Clin Infect Dis. 2021;73:e2342–9. https://doi.org/10.1093/cid/ciaa1455
32. Li X, McHugh GA, Damle N, Sikand VK, Glickstein L, Steere AC. Burden and viability of *Borrelia burgdorferi* in skin and joints of patients with erythema migrans or Lyme arthritis. Arthritis Rheum. 2011;63:2238–47. https://doi.org/10.1002/art.30384
33. Li J, Ma Y, Paquette JK, Richards AC, Mulvey MA, Zachary JF, et al. The Cdkn2a gene product p19 alternative reading frame (p19ARF) is a critical regulator of IFNβ-mediated Lyme arthritis. PLoS Pathog. 2022;18:e1010365. https://doi.org/10.1371/journal.ppat.1010365
34. Strle K, Shin JJ, Glickstein LJ, Steere AC. Association of a Toll-like receptor 1 polymorphism with heightened Th1 inflammatory responses and antibiotic-refractory Lyme arthritis. Arthritis Rheum. 2012;64:1497–507. https://doi.org/10.1002/art.34383
35. Paquette JK, Ma Y, Fisher C, Li J, Lee SB, Zachary JF, et al. Genetic control of Lyme arthritis by *Borrelia burgdorferi* arthritis-associated locus 1 is dependent on localized differential production of IFN-β and requires upregulation of myostatin. J Immunol. 2017;199:3525–34. https://doi.org/10.4049/jimmunol.1701011
36. Petzke MM, Iyer R, Love AC, Spieler Z, Brooks A, Schwartz I. *Borrelia burgdorferi* induces a type I interferon response during early stages of disseminated infection in mice. BMC Microbiol. 2016;16:29. https://doi.org/10.1186/s12866-016-0644-4
37. Miller JC, Ma Y, Bian J, Sheehan KC, Zachary JF, Weis JH, et al. A critical role for type I IFN in arthritis development following *Borrelia burgdorferi* infection of mice. J Immunol. 2008;181:8492–503. https://doi.org/10.4049/jimmunol.181.12.8492
38. Arvikar SL, Steere AC. Diagnosis and treatment of Lyme arthritis. Infect Dis Clin North Am. 2015;29:269–80. https://doi.org/10.1016/j.idc.2015.02.004
39. Crow YJ, Stetson DB. The type I interferonopathies: 10 years on. Nat Rev Immunol. 2021.
40. Sleijfer S, Bannink M, Van Gool AR, Kruit WH, Stoter G. Side effects of interferon-alpha therapy. Pharm World Sci. 2005;27:423–31. https://doi.org/10.1007/s11096-005-1319-7
41. Capuron L, Miller AH. Cytokines and psychopathology: lessons from interferon-alpha. Biol Psychiatry. 2004;56:819–24. https://doi.org/10.1016/j.biopsych.2004.02.009

Address for correspondence: Klemen Strle, Tufts University School of Medicine, 145 Harrison Ave., Boston, MA 01222, USA; email: kstrle@broadinstitute.org

Probable Transmission of SARS-CoV-2 from African Lion to Zoo Employees, Indiana, USA, 2021

Audrey A. Siegrist,[1] Kira L. Richardson, Ria R. Ghai, Brian Pope, Jamie Yeadon, Betsy Culp, Casey Barton Behravesh, Lixia Liu, Jennifer A. Brown, Leslie V. Boyer

We describe animal-to-human transmission of SARS-CoV-2 in a zoo setting in Indiana, USA. A vaccinated African lion with physical limitations requiring hand feeding tested positive for SARS-CoV-2 after onset of respiratory signs. Zoo employees were screened, monitored prospectively for onset of symptoms, then rescreened as indicated; results were confirmed by using reverse transcription PCR and whole-genome virus sequencing when possible. Traceback investigation narrowed the source of infection to 1 of 6 persons. Three exposed employees subsequently had onset of symptoms, 2 with viral genomes identical to the lion's. Forward contact tracing investigation confirmed probable lion-to-human transmission. Close contact with large cats is a risk factor for bidirectional zoonotic SARS-CoV-2 transmission that should be considered when occupational health and biosecurity practices at zoos are designed and implemented. SARS-CoV-2 rapid testing and detection methods for big cats and other susceptible animals should be developed and validated to enable timely implementation of One Health investigations.

Although SARS-CoV-2 is primarily transmitted from person-to-person (*1*), it is considered zoonotic because of natural infections observed in a range of mammalian species (*2*,*3*). The broad host range of SARS-CoV-2 is evident from natural infections occurring in zoos, sanctuaries, and aquaria, most frequently in big cats (*3*), but also in mustelids (*4*), nonhuman primates (*5*), and others. Zoo outbreaks typically begin after close contact with an infected zookeeper (*6*–*10*). One Health investigations have shown transmission of SARS-CoV-2 from human to animals (*4*,*8*,*9*,*11*–*14*), but examples of animal-to-human transmission are rare (*15*–*19*).

We report a multispecies cluster of SARS-CoV-2 infections associated with an infected African lion (*Panthera leo*) at a seasonal, mid-sized, Association of Zoos and Aquariums–accredited zoo in Indiana, USA. The lion's likely source of exposure was a fully vaccinated, asymptomatic employee, and forward transmission from the lion to other fully vaccinated employees probably occurred.

Methods

Setting

The sentinel case occurred in December 2021, when the zoo was closed for the season. The lion was housed alone in a building with an indoor/outdoor enclosure located >30 feet from other animal enclosures. Feeding and veterinary procedures were conducted indoors by dedicated staff with assigned key access. Susceptible species elsewhere in the zoo included a snow leopard (*Panthera uncia*), Amur tigers (*Panthera tigris altaica*), Amur leopards (*Panthera pardus orientalis*), North American river otters (*Lontra canadensis*), and several species of nonhuman primates. All susceptible animals, including the lion, had received 2 doses of Zoetis experimental mink coronavirus vaccine (https://www.zoetis.com) during September–November 2021. Animal health was overseen by a full-time onsite veterinarian.

Zoo practice before the outbreak included SARS-CoV-2 prevention measures from the Zoo and Aquarium All Hazards Partnership (*20*,*21*), such as suspending behind-the-scenes tours and close-distance behavioral training for susceptible species. Employees were required to complete the COVID-19 vaccination series, practice social distancing, monitor for

Author affiliations: Potawatomi Zoo, South Bend, Indiana, USA (A.A. Siegrist, B. Culp); Indiana Department of Health, Indianapolis, Indiana, USA (K.L. Richardson, B. Pope, J. Yeadon, L. Liu, J.A. Brown); Centers for Disease Control and Prevention, Atlanta, Georgia, USA (R.R. Ghai, C. Barton Behravesh); University of Arizona, Tucson, Arizona, USA (L.V. Boyer)

DOI: https://doi.org/10.3201/eid2906.230150

[1]Current affiliation: Fresno Chaffee Zoo, Fresno, California, USA.

COVID-19 symptoms, and, when ill, exclude themselves from work. Disinfectant foot baths were placed at enclosure entrances, and high-pressure cleaning methods were replaced by methods less likely to aerosolize infectious material. Employees were required to wear surgical masks at all times and nitrile gloves during feedings.

Sentinel Case

The lion was a geriatric (20-year-old) male with chronic renal insufficiency and severe degenerative intervertebral disc disease prohibiting normal range of motion for self-grooming of the caudal body. He was vaccinated with the Zoetis vaccine on September 14 and October 7, 2021. Routine care included hand feeding twice daily, therapeutic laser treatments of the spine and hindquarters, corticosteroids, gabapentin, renal supplements, and mesenchymal stem cell treatments. On December 18, employees observed coughing, dyspnea, shivering, lethargy, sneezing, nasal discharge, anorexia, and exposed nictitans. Marbofloxacin treatment was initiated. Nasal swabs were collected on December 18 and 23. He was euthanized on December 23 because of declining mobility associated with intervertebral disc disease. The acute clinical signs attributed to SARS-CoV-2 had largely resolved and were not a factor in the euthanasia decision.

Investigation

We initiated an investigation on December 18 to identify the source of the lion's exposure and the potential for forward transmission (Figure 1). We defined a confirmed cluster-associated case as illness in a human or animal at the zoo with laboratory evidence for the same strain as the sentinel case, based on genomic sequencing of a clinical sample. We defined a probable cluster-associated case as illness in a human or animal at the zoo with laboratory evidence for SARS-CoV-2 based on reverse transcription PCR (RT-PCR) or rapid antigen test of a clinical sample but for which no genomic sequencing information was available.

For both traceback and forward contact tracing investigations, we assumed the exposure period to begin 10 days before illness onset, with probable acquisition within 5 days prior. We assumed the infectious period to begin 2 days before illness and extend 10 days after illness onset. We considered any person who entered the enclosure during the lion's exposure or infectious period to be a lion contact. We classified the care provided by lion contacts as cranial (e.g., feeding and nasal swabbing with ≤2 feet between

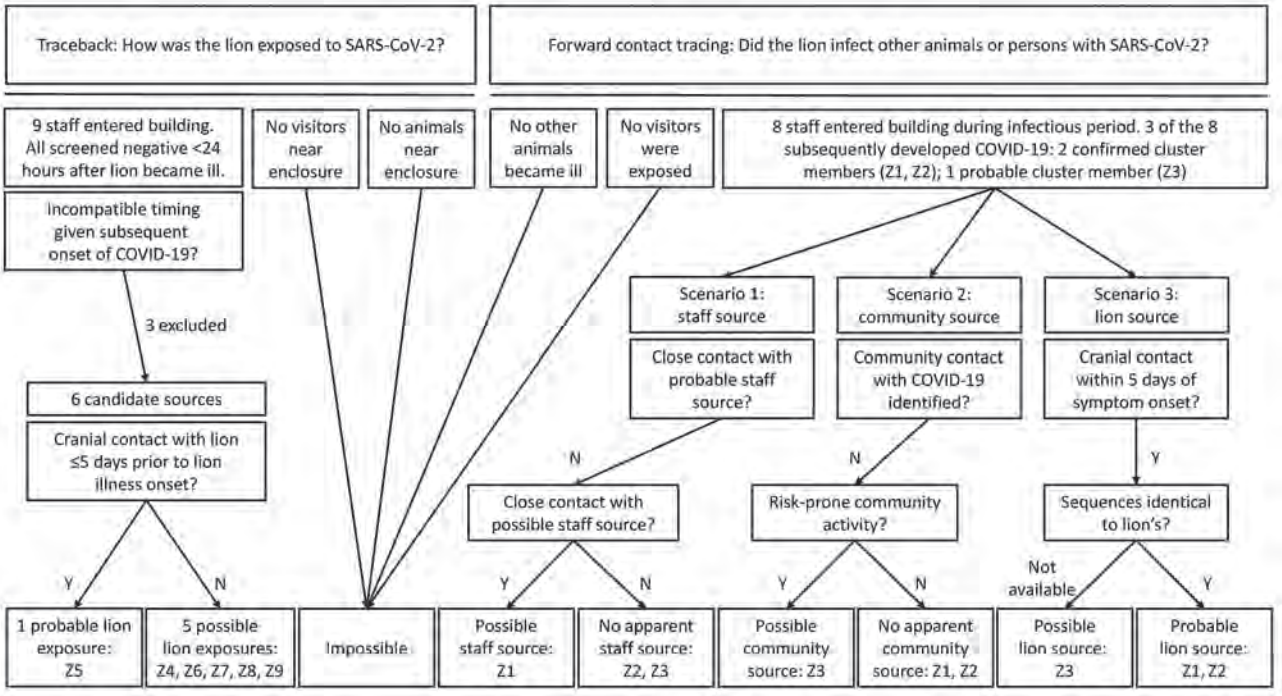

Figure 1. Traceback and forward contact tracing investigations of SARS-CoV-2 transmission between an African lion and zoo employees, Indiana, USA, 2021–2022. The traceback investigation narrowed the potential source of the lion's SARS-CoV-2 infection to 6 zoo employees who had lion contact within 10 days, 1 of whom (employee Z5) had cranial contact within 5 days of the lion's illness onset but did not have close contact with employees Z1, Z2, or Z3. Possible human sources were identified for Z1 (close occupational contact with Z7) and for Z3 (community activity), although in neither case were these potential sources shown to carry the virus. Employees Z1, Z2, and Z3 all had symptoms and had confirmed SARS-CoV-2 infection 3 days after their most recent cranial contact with the sick lion.

human and lion heads) or caudal (e.g., arthritis care and injections performed ≈9 feet from the lion's head). We defined close contact between persons as proximity of <6 feet for >15 minutes in 1 day.

Sentinel Case Investigation

We screened nasal swab samples from the lion onsite on December 18 by using a lateral flow immunoassay validated for human use (DiaTrust COVID-19 Ag Home Test; Celltrion, https://www.celltrionhealthcare.com). We sent aliquots of samples to the US Department of Agriculture's National Veterinary Services Laboratories for confirmatory testing. Necropsy was performed on December 23 at the Michigan State University Veterinary Diagnostic Laboratory.

Traceback Investigation

We screened nasopharyngeal swab samples from all employees exposed to the lion within the 10 days before his illness onset onsite by using lateral flow immunoassay on December 18 and 19. We reviewed personnel schedules, keeper and veterinary daily reports, maintenance logs, lion treatment schedules, veterinary examination notes, security logs, and social media pages for dates and nature of interactions among lion contacts.

Forward Contact Tracing Investigation

We screened lion contacts with subsequent symptoms suggestive of infection onsite for SARS-COV-2 by lateral flow immunoassay within 24 hours of symptom onset. The Indiana Department of Health confirmed the results by using a TaqPath COVID-19 Combo Kit RT-PCR (ThermoFisher, https://www.thermofisher.com).

An Indiana Department of Health epidemiologist conducted interviews of infected personnel. Those interviews covered symptoms, vaccination history, and exposures to other zoo employees and the public during the 10 days before their onset of illness. We verified location history for activity outside the zoo for these persons through credit or debit card transaction data where possible. We cross-referenced contact data with zoo records. We deidentified data summaries for analysis.

Relatedness of genomic sequences was analyzed by the authors (L.L., B.P., and J.L.) by comparing samples with 10 closely related samples collected during August 2021–February 2022 throughout the state of Indiana. We sequenced all samples in 1 run by using Clear Dx WGS SARS-CoV-2 Reagent Kit 2.0 (Clear Labs, https://www.clearlabs.com), which contained midnight primers.

We used the Pangolin COVID-19 Lineage Assigner (https://pangolin.cog-uk.io) to identify lineage from FASTA files generated by Clear Dx. We constructed the phylogenetic tree in CLC Genomics Workbench 21.0.3 (QIAGEN, https://www.qiagen.com) using classical sequencing analysis tools.

Infection Control

Upon detection of SARS-CoV-2 in the lion, employees providing care for susceptible species at the zoo were required to wear N95 respirators. Those entering the lion building also used face shields, disposable gowns, shoe covers, and gloves. Lion building access was restricted further, and laser treatments were discontinued. Work assignments were altered so that employees providing care to the lion would not come in contact with other susceptible animals (*22*).

Results

Sentinel Case Investigation

We detected evidence of SARS-CoV-2 in the lion through onsite screening on December 18. We detected further evidence of SARS-CoV-2 by RT-PCR in nasal swab samples from December 18 and December 23, and in nasal turbinate, lung tissue, and intestinal tissues obtained at necropsy on December 23. Extracted RNA from both nasal swab samples produced high-quality 29,707-nt sequences for genomic sequencing (SARS-CoV-2 Delta variant, AY.103 lineage). Necropsy confirmed intervertebral disc degeneration, chronic renal disease, chronic lower airway disease, and severe rhinitis.

Traceback Investigation

Nine people (employees Z1–Z9) entered the lion building at some time during the lion's potential exposure period during December 8–18 (Figure 1). All 9 reported being asymptomatic on December 18. Eight had screening tests on December 18, and 1 had a screening test on December 19; all were negative. Employees Z1, Z2, and Z3 had onset of COVID-19 during December 21–24, with infectious periods that began on or after December 19 (Figure 2). Employee Z5 had cranial contact during the lion's 5-day probable acquisition period. Employees Z4, Z6, Z7, Z8, and Z9 had lion contact 6–10 days before onset of the lion's illness, performed caudal activities exclusively, or both.

Forward Contact Tracing Investigation

No additional animals at the zoo had illness suggestive of SARS-CoV-2 infection (Figure 1). Eight persons

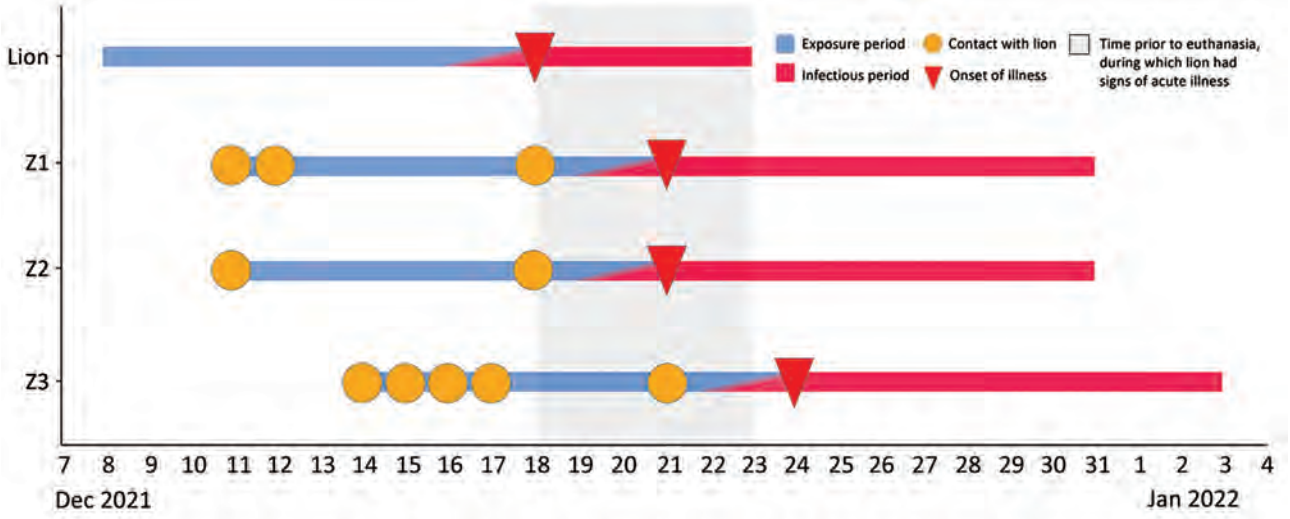

Figure 2. Timeline of probable transmission of SARS-CoV-2 from an African lion to zoo employees, Indiana, USA, 2021–2022. The lion's likely exposure period was December 8–17, and his infectious period was December 16 through euthanasia on December 23. During the lion's infectious period, employees Z1 and Z2 each had a single day of cranial contact with him, coinciding with the day of the lion's illness onset. Z3 had cranial contact with the lion on 3 occasions during his infectious period. Figure highlights the lack of overlap between Z1 and Z2's infectious period and the lion's exposure period, and between Z3's infectious period and Z1 and Z2's exposure periods.

entered the lion building during the lion's infectious period (December 16–23). Employees Z1, Z2, and Z3 were fully vaccinated and previously healthy, each of whom was involved in cranial care 3 days before having onset of upper respiratory symptoms. Each of those 3 employees was positive on rapid antigen test within 24 hours after symptom onset and had subsequent RT-PCR confirmation of SARS-CoV-2 infection. Samples from patients Z1 and Z2 were suitable for sequencing; the sample from Z3 was of insufficient quality for sequencing.

The sequences generated from lion samples on December 18 and 23 were identical to those from Z1 and Z2 samples. The 10 community comparators varied from the cluster sequences by 12–24 nt (Figure 3).

Employees Z5, Z8, and Z9 had no close contact with Z1, Z2, or Z3 during their exposure periods. Z4 had close contact with Z2 on December 18, the day that both had negative screening tests. Z6 entered the lion enclosure at the same time as Z3, but was maintaining >6 feet distance, 9 days before Z3's symptom onset. Z7 had close contact with Z1 on December 11, 12, and 18. Z7 worked in the lion enclosure with Z2, but that contact took place a full 10 days before Z2's onset of symptoms and was at >6 feet for <15 minutes. Z7 also worked in the lion enclosure with Z3 for <15 minutes and at a distance of >6 feet 8 days before Z3's onset of symptoms. Employee Z3 had no known exposures outside of the zoo but did participate in community social activities with risk for unrecognized transmission of SARS-CoV-2 on several occasions during the 10 days before onset of symptoms.

Discussion

This multispecies cluster of SARS-CoV-2 included 3 confirmed cases (2 human, 1 felid) and 1 probable case (human). The identical genomic sequences detected in samples from the confirmed cases demonstrate that the infections were acquired in a common setting. Given that the zoo was closed to visitors, the source of infection for the sentinel case was almost certainly 1 of 6 asymptomatic employees who tested negative on the day of the lion's diagnosis and who subsequently reported no signs of illness. Among those 6, employee Z5, the only person who had cranial contact within 5 days before the lion's onset of illness and who did not later have symptomatic COVID-19, was the most likely source of the lion's infection.

To determine whether lion-to-human transmission took place, we considered 3 scenarios (Figure 1). The first scenario posits that zoo employees acquired infection from the same human source as the lion. Although employee-to-employee transmission could not be ruled out on an individual basis, no pathway of transmission could be identified that explained all probable cases within the cluster.

The second scenario posits that zoo employees acquired infection from an unrelated community source. For employee Z3, whose viral genome was unknown, community acquisition is possible. Employees Z1 and Z2 had low-risk social

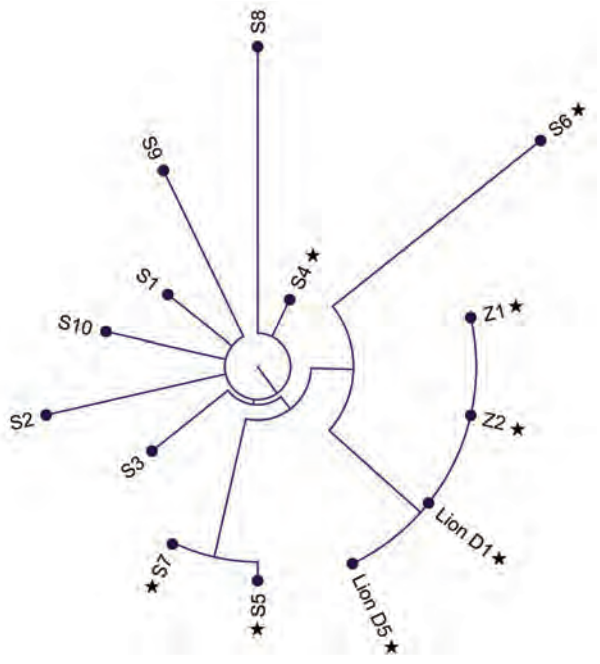

Figure 3. Phylogenetic tree of SARS-CoV-2 Delta variant, AY.103 lineage, genome sequences from an African lion (day 1 and day 5) and 2 zoo employees (Z1 and Z2) shown in comparison with reference sequences from COVID-19 patients from 7 counties in Indiana, USA, August 2021–February 2022. Reference sequences are labeled chronologically as S1 to S10. Stars indicate specimens collected in December 2021.

behavior with no other identified sources of SARS-CoV-2 transmission from the community, and samples from both yielded sequences genetically identical to the lion's viral strain. Although it is technically feasible that each of them, independently, could have acquired the cluster strain from asymptomatic community carriers, the chance of this happening are extremely low.

The third scenario posits that at least 1 zoo employee acquired infection from the lion. During cranial-end procedures, the lion breathed, roared, and coughed within arm's length of staff. Each person that had symptom onset after the lion was involved in cranial-end care while the lion was sick, and each had symptoms 3 days after that exposure. Lion-to-human transmission of SARS-CoV-2 is, therefore, the most probable explanation for their infections.

Our investigation strongly suggests that lion-to-human transmission took place in 2, and possibly 3, instances, which is important for at least 2 reasons. First, animal-to-person transmission of SARS-CoV-2 is an occupational health risk for veterinary and animal care staff that interact closely with susceptible animals. Second, transmission occurred despite an up-to-date SARS-CoV-2 vaccination history in every person involved, including the person or persons who likely transmitted the virus to the lion, the lion, and the person or persons who likely became infected from the lion. Although SARS-CoV-2 transmission from vaccinated persons to vaccinated zoo animals has been documented previously (*23*), our results show that transmission can also occur from vaccinated zoo animals to vaccinated persons. Many human vaccine efficacy studies indicate reductions in COVID-19 disease severity after vaccination (*24*,*25*); however, further research is needed to determine if the same is true of zoonotic SARS-CoV-2 transmission among vaccinated persons and animals.

The unique setting for these cases minimized the number of potential exposure pathways required to reach this conclusion. Initiation of the investigation and heightened safety measures on the day of sentinel case discovery improved analysis and contained spread. Timely screening, prospective monitoring for symptom development, cross-referencing of occupational and interview data, and genomic sequencing combined to allow inferences of causality.

Swabbing of leonine nasal passages for SARS-CoV-2 diagnosis has been reported (*26*), but neither the sampling method nor the use of tests designed for human diagnosis has been formally validated. Rapid testing methods applicable to animals should be developed and validated to enable timely implementation of biosecurity measures.

The first limitation of our study is the limited number of community samples that were available for the sequencing analysis. Second, rapid tests may not reliably establish SARS-CoV-2 negative status. Third, the distance associated with close contact and exposure and infectious periods for lions were assumed to be similar to those for humans, although these have not been established. Finally, diminished immune response of this geriatric, chronically ill lion may have precluded a robust response to vaccination, limiting the generalizability of conclusions related to viral shedding after vaccination.

Timely human-animal-environmental assessments and implementation of appropriate biosafety interventions are essential for both animal and human health during community outbreaks of SARS-CoV-2. A One Health approach, which connects the health of persons, animals, and environment (*27*), should be used to respond to susceptible zoo animals, particularly those requiring close human contact, that develop clinical signs compatible with

SARS-CoV-2 infection. Close contact with large cats should be considered a risk factor for bidirectional zoonotic SARS-CoV-2 transmission, regardless of prior immunization. This consideration may be especially warranted in the cases of geriatric animals or those with underlying health conditions.

About the Author

Dr. Siegrist is a practicing zoo animal veterinarian currently affiliated with the Fresno Chaffee Zoo, Fresno, California, USA. Her research interests include envenomation of captive animals by native reptiles and arthropods and One Health investigation of infectious disease outbreaks.

References

1. Centers for Disease Control and Prevention. How COVID-19 spreads. 2021 [cited 2022 Jul 1]. https://www.cdc.gov/coronavirus/2019-ncov/prevent-getting-sick/how-covid-spreads.html
2. Ghai RR, Carpenter A, Liew AY, Martin KB, Herring MK, Gerber SI, et al. Animal reservoirs and hosts for emerging alphacoronaviruses and betacoronaviruses. Emerg Infect Dis. 2021;27:1015–22. https://doi.org/10.3201/eid2704.203945
3. World Organisation for Animal Health. COVID-19 events in animals. 2022 [cited 2022 Jul 1]. https://www.woah.org/en/what-we-offer/emergency-and-resilience/covid-19
4. Oreshkova N, Molenaar RJ, Vreman S, Harders F, Oude Munnink BBO, Hakze-van der Honing R, et al. SARS-CoV-2 infection in farmed minks, the Netherlands, April and May. Euro Surveill. 2020;25:2001005. https://doi.org/10.2807/1560-7917.ES.2020.25.23.2001005
5. San Diego Zoo. San Diego Zoo Safari Park gorillas recovering after SARS-CoV-2 diagnosis. 2021 [cited 2022 Aug 23]. https://sandiegozoowildlifealliance.org/pressroom/news-releases/san-diego-zoo-safari-park-gorillas-recovering-after-sars-cov-2-diagnosis
6. Cushing AC, Sawatzki K, Grome HN, Puryear WB, Kelly N, Runstadler J. Duration of antigen shedding and development of antibody titers in Malayan tigers (*Panthera tigris jacksoni*) naturally infected with SARS-CoV-2. J Zoo Wildl Med. 2021;52:1224–8. https://doi.org/10.1638/2021-0042
7. Grome HN, Meyer B, Read E, Buchanan M, Cushing A, Sawatzki K, et al. SARS-CoV-2 outbreak among Malayan tigers and humans, Tennessee, USA, 2020. Emerg Infect Dis. 2022;28:833–6. https://doi.org/10.3201/eid2804.212219
8. Koeppel KN, Mendes A, Strydom A, Rotherham L, Mulumba M, Venter M. SARS-CoV-2 reverse zoonoses to pumas and lions, South Africa. Viruses. 2022;14:120. https://doi.org/10.3390/v14010120
9. McAloose D, Laverack M, Wang L, Killian ML, Caserta LC, Yuan F, et al. From people to *Panthera*: natural SARS-CoV-2 infection in tigers and lions at the Bronx Zoo. MBio. 2020;11:e02220–20. https://doi.org/10.1128/mBio.02220-20
10. Mitchell PK, Martins M, Reilly T, Caserta LC, Anderson RR, Cronk BD, et al. SARS-CoV-2 B.1.1.7 variant infection in Malayan tigers, Virginia, USA. Emerg Infect Dis. 2021;27:3171–3. https://doi.org/10.3201/eid2712.211234
11. Alberto-Orlando S, Calderon JL, Leon-Sosa A, Patiño L, Zambrano-Alvarado MN, Pasquel-Villa LD, et al. SARS-CoV-2 transmission from infected owner to household dogs and cats is associated with food sharing. Int J Infect Dis. 2022;122:295–9. https://doi.org/10.1016/j.ijid.2022.05.049
12. Sit THC, Brackman CJ, Ip SM, Tam KWS, Law PYT, To EMW, et al. Infection of dogs with SARS-CoV-2. Nature. 2020;586:776–8. https://doi.org/10.1038/s41586-020-2334-5
13. Oude Munnink BB, Sikkema RS, Nieuwenhuijse DF, Molenaar RJ, Munger E, Molenkamp R, et al. Transmission of SARS-CoV-2 on mink farms between humans and mink and back to humans. Science. 2021;371:172–7. https://doi.org/10.1126/science.abe5901
14. Wendling NM, Carpenter A, Liew A, Ghai RR, Gallardo-Romero N, Stoddard RA, et al. Transmission of SARS-CoV-2 Delta variant (B.1.617.2) from a fully vaccinated human to a canine in Georgia, July 2021. Zoonoses Public Health. 2022;69:587–92. https://doi.org/10.1111/zph.12944
15. Rabalski L, Kosinski M, Mazur-Panasiuk N, Szewczyk B, Bienkowska-Szewczyk K, Kant R, et al. Zoonotic spill-over of SARS-CoV-2: mink-adapted virus in humans. Clin Microbiol Infect. 2022;28:451.e1–4. https://doi.org/10.1016/j.cmi.2021.12.001
16. Kuchipudi SV, Surendran-Nair M, Ruden RM, Yon M, Nissly RH, Vandegrift KJ, et al. Multiple spillovers from humans and onward transmission of SARS-CoV-2 in white-tailed deer. Proc Natl Acad Sci U S A. 2022;119:e2121644119. https://doi.org/10.1073/pnas.2121644119
17. Hammer AS, Quaade ML, Rasmussen TB, Fonager J, Rasmussen M, Mundbjerg K, et al. SARS-CoV-2 transmission between mink (*Neovison vison*) and humans, Denmark. Emerg Infect Dis. 2021;27:547–51. https://doi.org/10.3201/eid2702.203794
18. Sila T, Sunghan J, Laochareonsuk W, Surasombatpattana S, Kongkamol C, Ingviya T, et al. Suspected cat-to-human transmission of SARS-CoV-2, Thailand, July–September 2021. Emerg Infect Dis. 2022;28:1485–8. https://doi.org/10.3201/eid2807.212605
19. Yen HL, Sit THC, Brackman CJ, Chuk SSY, Gu H, Tam KWS, et al.; HKU-SPH study team. Transmission of SARS-CoV-2 delta variant (AY.127) from pet hamsters to humans, leading to onward human-to-human transmission: a case study. Lancet. 2022;399:1070–8. https://doi.org/10.1016/S0140-6736(22)00326-9
20. Zoo and Aquarium All Hazards Partnership. Updated guidance for working around non-domestic felid species during the SARS CoV-2 pandemic. 2021 [cited 2022 Jul 20]. https://zahp.org/wp-content/uploads/2021/11/COVID19-guidance-Felid-TAG-29Oct21.pdf
21. Zoo and Aquarium All Hazards Partnership. COVID-19 infection prevention and control assessment tool for captive wildlife facilities: zoos, sanctuaries, aquaria, and wild animal rehabilitation centers. 2021 [cited 2022 Jul 20]. https://zahp.org/wp-content/uploads/2021/11/COVID-19-Infection-Prevention-and-Control-Assessment-Tool-for-Captive-Wildlife-Facilities-1.pdf
22. Centers for Disease Control and Prevention. Reducing the risk of SARS-CoV-2 spreading between people and wildlife. 2021 [cited 2022 Nov 26]. https://www.cdc.gov/healthypets/covid-19/wildlife.html
23. Allender MC, Adkesson MJ, Langan JN, Delk KW, Meehan T, Aitken-Palmer C, et al. Multi-species outbreak of SARS-CoV-2 Delta variant in a zoological institution, with the detection in two new families of carnivores. Transbound Emerg Dis. 2022;69:e3060–75. https://doi.org/10.1111/tbed.14662
24. Tenforde MW, Self WH, Adams K, Gaglani M, Ginde AA, McNeal T, et al.; Influenza and Other Viruses in the Acutely Ill (IVY) Network. Association between mRNA vaccination

and COVID-19 hospitalization and disease severity. JAMA. 2021;326:2043–54. https://doi.org/10.1001/jama.2021.19499
25. Lauring AS, Tenforde MW, Chappell JD, Gaglani M, Ginde AA, McNeal T, et al.; Influenza and Other Viruses in the Acutely Ill (IVY) Network. Clinical severity of, and effectiveness of mRNA vaccines against, covid-19 from omicron, delta, and alpha SARS-CoV-2 variants in the United States: prospective observational study. BMJ. 2022;376:e069761. https://doi.org/10.1136/bmj-2021-069761
26. Centers for Disease Control and Prevention Investigation of an outbreak of SARS-CoV-2 infection among African lions at Utah's Hogle Zoo. Zoonoses and One Health Updates webinar. 2022 May 4 [cited 2022 Nov 26]. https://www.cdc.gov/onehealth/zohu/2022/may.html
27. Centers for Disease Control and Prevention. One Health basics. 2022 [cited 2022 Nov 26]. https://www.cdc.gov/onehealth/basics/index.html

Address for correspondence: Leslie Boyer, University of Arizona Health Sciences Center, Department of Pathology, 1501 N Campbell Ave, PO Box 245043, Rm 5205, Tucson, AZ 85724, USA; email: leslie@email.arizona.edu

Epidemiologic Characteristics of Mpox among People Experiencing Homelessness, Los Angeles County, California, USA, 2022

Hannah K. Brosnan, Karen W. Yeh, Padma S. Jones, Sohum Gokhale, Dalia Regos-Stewart, Hang Tran, Kathleen Poortinga, Phoebe Danza, Rebecca Fisher, Lauren E. Finn, Chelsea Foo, Alicia H. Chang

In Los Angeles County, California, USA, public health surveillance identified 118 mpox cases among persons experiencing homelessness (PEH) during July–September 2022. Age and sex were similar for mpox case-patients among PEH and in the general population. Seventy-one (60%) PEH mpox case-patients were living with HIV, 35 (49%) of them virally suppressed. Hospitalization was required for 21% of case-patients because of severe disease. Sexual contact was likely the primary mode of transmission; 84% of patients reported sexual contact ≤3 weeks before symptom onset. PEH case-patients lived in shelters, encampments, cars, or on the street, or stayed briefly with friends or family (couch surfed). Some case-patients stayed at multiple locations during the 3-week incubation period. Public health follow-up and contact tracing detected no secondary mpox cases among PEH in congregate shelters or encampments. Equitable efforts should continue to identify, treat, and prevent mpox among PEH, who often experience severe disease.

Since May 2022, laboratory-confirmed cases of mpox have been reported across nonendemic countries including the United States, mostly among men who have sex with men (*1*,*2*). Persons experiencing homelessness (PEH) are disproportionately affected by infectious diseases compared with the general population because of several factors, including close living quarters in shelters and encampments; lack of consistent access to hygiene facilities when living on the streets; less access to healthcare services; and coexisting medical, mental, and substance use disorders that may increase susceptibility or pose barriers to prevention and treatment (*3*–*6*). Minimal literature exists on the characteristics and epidemiology of mpox among PEH. Los Angeles County, California, USA, has a large, heterogeneous PEH population, estimated at 69,144 persons experiencing sheltered and unsheltered homelessness; 10% identify as gay, lesbian, bisexual, or questioning (*7*,*8*). Because widespread transmission of mpox among PEH became a concern at the outset of the local outbreak, the Los Angeles County Department of Public Health (LACDPH) initiated this study to review demographics, discern patterns of transmission, and identify risk factors unique to PEH to better understand the effect of mpox among that vulnerable population and determine the need for changes to existing surveillance and mitigation strategies. This study was evaluated by an LACDPH internal review board, which determined it meets criteria for not being human subject research and review was not needed.

Author affiliation: Los Angeles County Department of Public Health, Los Angeles, California, USA

DOI: https://doi.org/10.3201/eid2906.230021

Methods

In accordance with Centers for Disease Control and Prevention (CDC) emergency mpox response guidelines, LACDPH implemented mpox case surveillance and investigation beginning in May 2022 (*9*). We handled both probable and confirmed cases reported to LACDPH equally as actual mpox cases (*10*). In addition to mandatory laboratory reporting of positive mpox and orthopox virus test results, LACDPH required healthcare providers to report all mpox or orthopoxvirus infections, hospitalizations, and deaths within 1 working day after identification using an online form (*11*,*12*). Medical provider forms were used to collect demographic, clinical, and epidemiologic information, including preinfection residential

situations (Appendix Table 1, https://wwwnc.cdc.gov/EID/article/29/6/23-0021-App1.pdf). Providers had the option to send photographs and additional medical records to LACDPH to complement the mandatory report form. We combined race and ethnicity data from all mpox case reports. Classification options were mutually exclusive and consisted of black or African American, Latinx/Hispanic, white, and other. All case-patients reporting Latinx/Hispanic ethnicity were grouped into that category regardless of any racial identification. Case-patients identifying as American Indian/Alaska Native, Asian, multirace, Native Hawaiian/Pacific Islander, or any other unspecified category, were grouped under the category other because <5 case-patients indicated each of those options.

LACDPH matched mpox cases to HIV cases in the electronic HIV registry (eHARS) to obtain co-infection, viral suppression, and CD4 counts. We categorized mpox cases as virally suppressed if the most recent HIV viral load on record was <200 copies/mL and performed ≤12 months before mpox diagnosis. We used most recent CD4 counts after mpox diagnosis to categorize HIV/mpox co-infections by level of immune suppression.

Trained investigators conducted structured interviews with all mpox case-patients reachable by phone or in person to collect additional risk factor data, assist with isolation housing and treatment, and initiate contact tracing; 3 phone calls, 3 texts, and 2 home visits were attempted for each case. Interview data included sexual orientation, symptoms and clinical history, employment, housing status and locations (Appendix Table 2), sexual history during the 3-week mpox incubation period before symptom onset, and other behavioral characteristics. The interviewer also asked mpox case-patients to name and provide phone numbers and addresses for all their intimate contacts. After the initial interview, we contacted mpox case-patients weekly until symptoms resolved and also gathered follow-up data on hospitalizations and treatments. Potential mpox contacts for whom we had information were called, texted, or visited by LACDPH staff for follow-up to review symptoms or arrange for mpox testing or vaccination.

LACDPH verified housing status for mpox case-patients for whom homelessness was noted in the mandatory healthcare provider report forms or who answered affirmatively to experiencing homelessness in the interview. The purpose of verifying housing was to confirm or amend homelessness status according to Department of Housing and Urban Development (HUD) and CDC definitions (*13*,*14*) during the 3 weeks before symptom onset. Verification methods included requesting and reviewing medical records from hospitals or clinics, and cross-checking against records from existing LACDPH communicable disease databases, other Los Angeles County department databases, and the local Homeless Management Information System, the data system required by HUD for providers receiving federal funds for the administration of homeless services (*15*). The Homeless Management Information System contains cumulative profiles and service records of persons who have entered emergency, transitional, or permanent shelter or who have received street outreach services for care and case management.

We included in this report mpox cases diagnosed among PEH during July 16–September 22, 2022. After verifying homelessness status, we categorized PEH case-patients by primary residential situation on the basis of where they spent the highest number of nights during the 3-week incubation period; we also recorded, categorized, and referred for public health follow-up additional locations where case-patients slept during the 3-week incubation period. Location categories were sheltered–congregate (emergency, transitional, and domestic violence shelters, and recuperative care centers); sheltered–other (noncongregate temporary housing such as hotels, motels, or couch surfing [staying briefly with friends or family] in private homes); unsheltered–encampment (living with others in places or structures not meant for human habitation, such as parks, streets, or vehicles); unsheltered–other (living alone in places or structures not meant for human habitation, such as parks, streets, or vehicles); and unknown.

We referred facility addresses identified during the interview and verification processes to field public health nurses who worked with facility staff to set up any necessary activities for outreach, education, symptom surveillance, clinical evaluation and testing, and vaccination of staff and residents. Each site was monitored for ≥3 weeks after an infectious PEH mpox case-patient was moved to dedicated isolation housing. If there were additional symptomatic persons reported, each site was monitored further until negative results were reported from mpox or orthopox testing. We cross-referenced locations for all mpox cases among PEH and among the general population when sufficient address information was available. We performed all analyses using SAS version 9.4 (SAS institute, https://www.sas.com).

Results

During July 16–September 22, 2022, a total of 118 mpox cases among PEH and 1,805 total mpox cases were

reported in Los Angeles County. PEH cases peaked at 26 during the week of August 6, 2022, whereas non-PEH cases peaked at 271 the week of July 30 (Figure). Most (62/118, 53%) PEH mpox case-patients were 30–39 years of age (Table 1). By gender identity, 108 (92%) identified as men, 5 (4%) as women, and 5 (4%) as other (includes transgender female, transgender male, or another gender identity). By race/ethnicity, 49 (42%) were categorized as Latinx/Hispanic, 37 (31%) black or African American, 18 (15%) white, and 7 (6%) other (American Indian/Alaska Native, Asian, multirace, or Native Hawaiian/Pacific Islander); race/ethnicity were unknown for 7 (6%). By sexual orientation, 64 (54%) identified as gay or lesbian, 21 (18%) as bisexual or by another term, and 14 (12%) as straight or heterosexual; 5 (4%) preferred not to state, and sexual orientation was unknown for 14 (12%).

HIV prevalence among PEH mpox case-patients was 60% (N = 71), among whom 36 (51%) had unsuppressed viral loads and 10 (14%) had a CD4 count <200 copies/mL. Clinical severity of mpox required hospitalization for 25 (21%) PEH, 19 of whom were HIV positive. A total of 42 (35%) PEH mpox case-patients received treatment with tecovirimat.

Among the 118 PEH mpox case-patients, public health staff were able to locate and interview 101 (86%) (Table 2). Of those interviewed, 21 (21%) reported exposure to a known or symptomatic mpox case-patient; none named exposure sources or provided additional details. When those 21 were cross-checked against records from all mpox cases, only 1 was named as a contact in a mpox case among the general population.

A total of 24 (24%) PEH mpox case-patients reported attending a large event ≤3 weeks before symptom onset. Seventy-four (73%) reported sexual contact; 23 (23%) denied sexual contact. Among those who were sexually active, 30 (41%) reported 1 sexual partner, 31 (42%) 2–5 partners, and 11 (15%) ≥6 partners. Nearly half (34/74; 46%) of sexually active PEH mpox case-patients reported meeting partners through mobile phone applications; others reported meeting through bath houses, sex clubs, or social events. Nine (12%) respondents reported engaging in group sex; 11 (15%) reported participating in transactional sex, defined as exchanging sex for money, drugs, food, housing, or other unspecified favors.

Among the 23 PEH mpox case-patients who denied sexual contact during the structured interview with public health investigators, 11 (48%) reported sexual contact to their healthcare providers as documented in notes within the mandatory reporting forms or medical records that were submitted to LACDPH. One of those 11 case-patients reported having been sexually assaulted to public health staff outside of the structured interview. Among the 12 case-patients with no report of sexual activity from interviews or records, 3 reported other possible sources of mpox transmission (1 self-reported trying on unwashed found clothing; 1 reported sharing food, utensils, dishes, bathrooms, and razor blades; and 1 reported staying at a shelter), although investigators were unable to confirm those sources. The other 9 mpox case-patients with no report of sexual activity reported no other possible sources of transmission.

Using data from healthcare provider reports and mpox case interviews, LACDPH was able to determine the primary residential situation in the 3 weeks before symptom onset for 112 (95%) PEH mpox case-patients; 55 (47%) were grouped in the sheltered–noncongregate category. Of these, 49 were couch surfing in private homes, 4 used temporary vouchers to stay in private rooms with bathrooms in hotels/motels, and 2 stayed in private rooms with bathrooms in hotels/motels used specifically for emergency housing. Of 37 (31%) PEH grouped as unsheltered–other, 18 were living outdoors

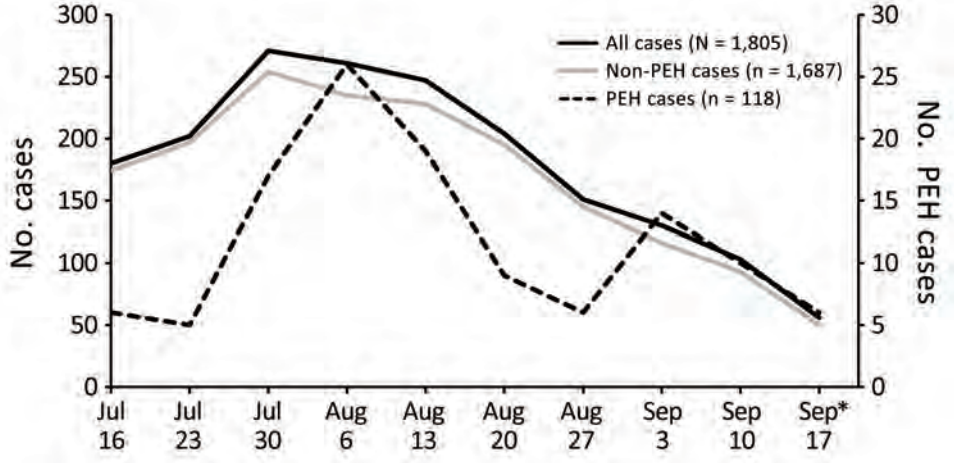

Figure. Mpox cases by week among persons experiencing homelessness, Los Angeles County, California, USA, July 16–September 22, 2022. Scales for the y-axes differ substantially to underscore patterns but do not permit direct comparisons.

Table 1. Characteristics of mpox case-patients experiencing homelessness, Los Angeles County, California, USA, July 16–September 22, 2022*

Characteristic	No. (%)
Total	118 (100)
Age, y	
0–17	0 (0)
18–29	20 (17)
30–39	62 (53)
40–49	27 (23)
≥50	9 (8)
Unknown	0 (0)
Gender identity	
M	108 (92)
F	5 (4)
Other†	5 (4)
Race/ethnicity‡	
Black/African American	37 (31)
Hispanic	49 (42)
White	18 (15)
Other: American Indian/Alaska Native, Asian, Native Hawaiian/Pacific Islander, multirace, other race	7 (6)
Unknown	7 (6)
Sexual orientation	
Gay or lesbian	64 (54)
Straight or heterosexual	14 (12)
Bisexual or another term	21 (18)
Prefer not to state	5 (4)
Unknown	14 (12)
HIV status§	
Positive	71 (60)
No match to HIV registry	47 (40)
Viral suppression among PEH with HIV,¶ n = 71	
Y	35 (49)
N	36 (51)
CD4 count, cells/mm^2, among PEH with HIV and prior CD4,# n = 70	
<200	10 (14)
≥200	60 (85)
Primary living situation**	
Sheltered–congregate	8 (7)
Sheltered–other	55 (47)
Unsheltered–encampment	12 (10)
Unsheltered–other	37 (31)
Unknown	6 (5)

*PEH, people experiencing homelessness.
†Transgender male, transgender female, gender nonbinary, gender nonconforming, other gender.
‡Race categories were based on self-reports from laboratory reports or interviews. Race categories with <5 respondents were combined as other (American Indian/Alaska Native, Asian, Native Hawaiian/Pacific Islander, multirace, other race).
§HIV status according to case match to HIV registry.
¶Most recent HIV viral load <200 copies/mL occurring within the prior 12 months.
#Most recent CD4 count.
**Primary living situation at time of exposure. Sheltered–congregate: specifically in congregate sheltered settings such as homeless or transitional shelters, domestic violence shelters, recuperative care centers; sheltered–other: noncongregate temporary housing such as hotels/motels used for emergency housing, or couch surfing in private homes; unsheltered–encampment: sharing residence with groups of other persons in places or structures not meant for human habitation; unsheltered–other: residing in places or structures not meant for human habitation such as parks, streets, or vehicles.

but not associated with an encampment, 10 were unsheltered with details unknown, and 9 were living in vehicles. We grouped 12 (10%) in the unsheltered–encampment category, 8 (7%) as sheltered–congregate, and 6 (5%) as unknown (Table 1). Twenty-nine (25%) PEH mpox case-patients reported spending nights at >1 location within the 3-week incubation timeframe before onset of symptoms, among whom 14 spent most nights couch surfing (7 moved around from private home to private home), 5 spent some nights outdoors or in a vehicle, 4 spent time in a commercial hotel, 1 in an emergency shelter, 1 incarcerated, and 1 in a non-PEH setting; 1 additional location was unknown. No mpox case-patient was identified as sharing the same encampment or address with another case-patient.

Among the 21 PEH mpox case-patients who reported exposure to a person with known mpox or mpox symptoms, 10 couch surfed, 6 lived in encampments, 2 lived in emergency shelters, and 3 lived alone on the streets. One of the 21 case-patients who reported exposure to a known mpox case-patient reported exchanging sex for services. Of the 11 PEH mpox case-patients who reported exchanging sex for services, 5 were sheltered (3 couch surfing, 1 living in

a group home, and 1 in a shelter) and 6 were unsheltered (1 in an encampment, 2 in vehicles, and 2 alone on the streets). There were no additional details for 1 of the unsheltered PEH mpox case-patients who exchanged sex for services.

Discussion

In this large descriptive series of mpox cases among PEH, mpox case-patients were proportionally similar by age and race to the underlying PEH population in Los Angeles County but disproportionally by

Table 2. Self-reported behavioral characteristics among mpox case-patients experiencing homelessness interviewed in Los Angeles County, California, USA, July 16–September 22, 2022

Characteristic	No. (%)
Total interviewed*	101 (86)
Reported exposure to monkeypox case	
Y	21 (21)
N	45 (45)
Don't know	34 (34
Did not answer	1 (1)
Attended large public or private event	
Y	24 (24)
N	75 (74)
Did not answer	2 (2)
Traveled	
Y	5 (5)
N	94 (93)
Did not answer	2 (2)
Had sexual contact with ≥1 partners	
Y	74 (73)
N	23 (23)
Did not answer	4 (4)
No. of partners, n = 74	
Unknown	2 (3)
1	30 (40)
2–5	31 (42)
≥6	11 (15)
Venues for meeting sex partners,† n = 74	
Online apps	34 (46)
Social event, bathhouse, sex club	5 (7)
Other	20 (27)
All other venues	17 (23)
Not applicable, e.g., long-term partner	11 (15)
Participated in group sex, n = 74	
Y	9 (12)
N	65 (88)
Gave or received drugs/money/favors/food/housing for sex, n = 74	
Y	11 (15)
N	63 (85)
Signs and symptoms†	
Rash, including lesions or skin bumps	96 (95)
Malaise: general feeling of illness/weakness	63 (62)
Fever	62 (61)
Enlarged lymph nodes	54 (53)
Headache	51 (51)
Myalgia	49 (49)
Chills	47 (47)
Pruritis	45 (45)
Back pain	31 (31)
Vomiting or nausea	24 (24)
Rectal pain	23 (23)
Cough	22 (22)
Abdominal pain	21 (21)
Runny nose	17 (17)
Pus or blood on stools	14 (14)
Rectal bleeding	11 (11)
Eye lesions	7 (7)
Conjunctivitis	5 (5)
Tenesmus	5 (5)

*Among 118 mpox case-patients experiencing homelessness.
†Not mutually exclusive categories.

sex (higher male proportion) (*7*,*8*). Our finding of a high proportion of male than female PEH mpox case-patients is similar among the general population (*16*). No mpox cases were identified among minors experiencing homelessness. HIV prevalence was higher among PEH mpox case-patients (60%) than among overall mpox case-patients reported from Los Angeles County and 7 other US jurisdictions (38%) (*17*). Positive referral bias might partially explain higher documented HIV prevalence; PEH with poorly controlled HIV might be more likely to seek care and receive a diagnosis because of more severe mpox illness. However, it is also possible that PEH with HIV are more susceptible because of discontinuous HIV care, disruptions in housing, and other risk factors, which might indicate higher actual prevalence.

After acquiring mpox, PEH are more vulnerable to severe disease. CDC reported 23% of persons with severe mpox who received medical consultation services through direct requests from local jurisdictions were PEH (*18*). Among our cohort of 118 PEH mpox case-patients, disease was severe enough in 21% to require hospitalization, and consistent with CDC findings, those hospitalizations comprised 27% of all mpox hospitalizations in Los Angeles County (data not shown). Los Angeles County maintains dedicated isolation housing outside of clinics for PEH mpox cases, so those hospitalizations were not for the purpose of isolation or housing. Additional details on coexisting medical conditions other than HIV that may have contributed to disease severity were not available and remain gaps in the data.

Of the 47% of mpox case-patients in sheltered–noncongregate settings, 89% were couch surfers, who are difficult to identify using traditional surveillance methods without dedicated questions delving into housing details. Couch surfers are not included in PEH population estimates from the point-in-time counts required by HUD in the Continuums of Care (*19*) and may rapidly cycle between private homes and streets to shelters (*20*). PEH who predominantly couch surf warrant further study to better understand their risk factors for communicable diseases and inform disease prevention strategies.

Similar to the situation for mpox cases among the general population, the primary mode of transmission for PEH mpox cases appeared to be through sexual contact; 84% of PEH mpox case-patients reported this risk factor, 73% to an LACDPH interviewer and 11% to another healthcare provider. California lists mpox under the California Division of Occupational Safety and Health's Aerosol Transmissible Diseases standards, which includes both aerosol-borne diseases and select diseases transmitted through droplets (*21*). This designation requires shelter employees to use more stringent protections, including wearing fit-tested N95 respirators when interacting with persons suspected of having or confirmed to have mpox infection. However, despite our initial concerns about respiratory transmission of mpox and potential spread through droplets or fomites in congregate settings, we found no evidence of any transmission within shelters to either PEH or staff. Masking requirements in response to COVID-19 in Los Angeles County during the 2022 mpox outbreak may have affected mpox transmission in congregate settings. However, the lack of transmission within shelters is consistent with anecdotal reports from other jurisdictions (San Francisco Department of Public Health, New York State Department of Health, pers. comm., email, July 26, 2022) and with a Cook County, Illinois, USA, report of an exposure in a correctional facility where investigation by symptom monitoring and serologic testing after a single mpox case in a jail resident found no secondary cases (*22*). Similarly, no transmission in encampments, considered congregate settings by Los Angeles County, was identified despite potential sharing of sleeping bags, clothes, and utensils in settings with poor access to cleaning and laundry services. One PEH mpox case-patient did report exposure without sexual contact through wearing found clothing. Additional research is needed to identify nonsexual transmission among PEH, especially among encampment residents where follow-up and contact tracing are challenging. Transmission among couch surfers appeared to follow patterns among the general population. Addresses provided by couch surfers did not match addresses for any other recorded mpox case, so it was difficult to fully assess transmission characteristics for couch surfers.

Among limitations to this report, LACDPH surveillance data were limited by reliance on provider and laboratory reporting of positive test results. In a historically marginalized population that experiences multiple barriers to healthcare, it is probable that not all PEH with mpox symptoms received the necessary medical attention for diagnosis and treatment. A serosurvey conducted by CDC among 209 persons experiencing homelessness found 3 possible missed cases of mpox (*23*), suggesting a small, but present, negative case detection bias from mpox surveillance based on case reporting. This bias may also have affected LACDPH's assessment of transmission within shelters and encampments, particularly because contact tracing is more challenging among PEH than among the general population. Symptomatic

persons may have been afraid of the stigma of mpox or losing housing and not come forward despite receiving public health outreach, education, onsite testing, and vaccination in shelters and encampments, which had 1 reported mpox case among PEH. LACDPH field staff relied on self-reports and did not conduct physical exams or serology testing as part of onsite follow-up.

In addition, case-patient information was self-reported through interviews, and LACDPH had minimal ability to confirm or verify responses. For example, among the 21 persons who reported contact with an mpox case-patient, no confirmation was possible because case-patients provided no contact names. Because sexual history can be a sensitive topic, mpox case-patients might have been hesitant to disclose information to a public health investigator who had no previous therapeutic relationship with the patient. The 11 persons who disclosed sexual encounters only to healthcare providers other than the interviewer, and the revelation outside of the interview by 1 PEH of having been sexually assaulted, suggests collection of incomplete risk factor data. In addition, this experience with collecting data from persons affected by a sexually transmitted disease reinforces the need for public health surveillance and interventions to be designed and implemented with sensitivity within a trauma-informed framework.

Our findings illustrate the medical vulnerability of PEH, the heterogeneity of their living situations, and the importance of designing disease surveillance methods that capture the complex risk factors and exposures unique to this population. Questionnaires that include sensitive topics may be more successful when implemented after a therapeutic or other trust-based relationship has been established. Developers of public health interventions to prevent and control disease among PEH should consider how differences in living situations can affect disease transmission. Equitable public health efforts should continue to identify, treat, and prevent mpox cases among PEH, who often experience severe cases in part because of barriers to accessing healthcare.

Acknowledgments

The authors acknowledge Clara Tyson, Jamila Tutor, Lylybell Fields, Suzane Kim, Emily Huang, Karin Chuang, Laura Luengas, Angela Tobias, Amber Lung, Kate Setterlund, Caroline Quintero, Roberto Gonzalez Coronado, Joanna Hernandez, Melissa Pruna, Rafa Alam, Jessy Fields, and Tahira Islam and the staff of the Acute Communicable Disease Control People Experiencing Homelessness COVID-19 Response Team.

Public health surveillance and analysis for this manuscript were completed as part of 2019–2024 ELC Cooperative Agreement activities under CDC grant no. 6 NU50CK000498-01-09 and CDC PS 18-1802.

About the Author

Ms. Brosnan is a supervising epidemiologist with the Los Angeles County Department of Public Health Acute Communicable Disease Control Program's COVID-19 Response Team for People Experiencing Homelessness. She is interested in using surveillance data to inform programmatic interventions to reach vulnerable populations.

References

1. Minhaj FS, Ogale YP, Whitehill F, Schultz J, Foote M, Davidson W, et al.; Monkeypox Response Team 2022. Monkeypox outbreak—nine states, May 2022. MMWR Morb Mortal Wkly Rep. 2022;71:764–9. https://doi.org/10.15585/mmwr.mm7123e1
2. World Health Organization. Multi-country monkeypox outbreak in non-endemic countries [cited 2022 Oct 5]. https://www.who.int/emergencies/disease-outbreak-news/item/2022-DON385
3. Liu CY, Chai SJ, Watt JP. Communicable disease among people experiencing homelessness in California. Epidemiol Infect. 2020;148:e85. https://doi.org/10.1017/S0950268820000722
4. Aldridge RW, Story A, Hwang SW, Nordentoft M, Luchenski SA, Hartwell G, et al. Morbidity and mortality in homeless individuals, prisoners, sex workers, and individuals with substance use disorders in high-income countries: a systematic review and meta-analysis. Lancet. 2018;391:241–50. https://doi.org/0.1016/S0140-6736(17)31869-X
5. Fazel S, Geddes JR, Kushel M. The health of homeless people in high-income countries: descriptive epidemiology, health consequences, and clinical and policy recommendations. Lancet. 2014;384:1529–40. https://doi.org/10.1016/S0140-6736(14)61132-6
6. Lebrun-Harris LA, Baggett TP, Jenkins DM, Sripipatana A, Sharma R, Hayashi AS, et al. Health status and health care experiences among homeless patients in federally supported health centers: findings from the 2009 patient survey. Health Serv Res. 2013;48:992–1017. https://doi.org/10.1111/1475-6773.12009
7. Los Angeles Homeless Services Authority. 2022 Greater Los Angeles homeless count—Los Angeles County [cited 2022 Oct 16]. https://www.lahsa.org/documents?id=%206515%20-%20Lacounty%20Hc22%20Data%20Summary
8. Los Angeles Homeless Services Authority. 2022 Greater Los Angeles homeless count deck [cited 2023 Mar 16]. https://www.lahsa.org/documents?id=6545-2022-greater-los-angeles-homeless-count-deck.pdf
9. Centers for Disease Control and Prevention. Case reporting recommendations for health departments [cited 2022 Oct 12]. https://www.cdc.gov/poxvirus/mpox/health-departments/case-reporting.html
10. Centers for Disease Control and Prevention. Case definitions for use in monkeypox response [cited 2022 Oct 26]. https://www.cdc.gov/poxvirus/monkeypox/clinicians/case-definition.html

11. California Department of Public Health. Title 17, California code of regulations (CCR) §2500, §2593, §2641.5–2643.20, and §2800–2812 reportable diseases and conditions [cited 2023 Mar 16]. https://www.cdph.ca.gov/Programs/CID/DCDC/CDPH%20Document%20Library/ReportableDiseases.pdf
12. County of Los Angeles Public Health. MPOX information for health professionals [cited 2023 Mar 16]. http://publichealth.lacounty.gov/acd/Monkeypox
13. US Department of Housing and Urban Development. HUD Exchange. Criteria for defining homeless [cited 2022 Oct 26]. https://files.hudexchange.info/resources/documents/HomelessDefinition_RecordkeepingRequirementsandCriteria.pdf
14. Centers for Disease Control and Prevention. Defining homelessness in public health data collection: considerations and examples [cited 2022 Oct 26]. https://www.cdc.gov/orr/science/homelessness/definition.html
15. US Department of Housing and Development. Homeless management information system (HMIS) fact sheet [cited 2023 March 15]. https://files.hudexchange.info/resources/documents/HMISFactSheet.pdf
16. Los Angeles County Department of Public Health. Los Angeles County mpox summary (weekly) [cited 2023 Mar 19]. http://publichealth.lacounty.gov/media/monkeypox/data/index.htm
17. Curran KG, Eberly K, Russell OO, Snyder RE, Phillips EK, Tang EC, et al.; Monkeypox, HIV, and STI Team. HIV and sexually transmitted infections among persons with monkeypox—eight U.S. jurisdictions, May 17–July 22, 2022. MMWR Morb Mortal Wkly Rep. 2022;71:1141–7. https://doi.org/10.15585/mmwr.mm7136a1
18. Miller MJ, Cash-Goldwasser S, Marx GE, Schrodt CA, Kimball A, Padgett K, et al.; CDC Severe Monkeypox Investigations Team. Severe monkeypox in hospitalized patients—United States, August 10–October 10, 2022. MMWR Morb Mortal Wkly Rep. 2022;71:1412–7. https://doi.org/10.15585/mmwr.mm7144e1
19. US Department of Housing and Urban Development. HUD Exchange. Point-in-time count and housing inventory count [cited 2023 Mar 17]. https://www.hudexchange.info/programs/hdx/pit-hic
20. Petry L, Hill C, Milburn N, Rice E. Who Is couch-surfing and who is on the streets? Disparities among racial and sexual minority youth in experiences of homelessness. J Adolesc Health. 2022;70:743–50. https://doi.org/10.1016/j.jadohealth.2021.10.039
21. California Department of Public Health. California Code of Regulations, Title 8, Section 5199, Appendix A [cited 2023 Mar 17]. https://www.dir.ca.gov/title8/5199.html
22. Hagan LM, Beeson A, Hughes S, Hassan R, Tietje L, Meehan AA, et al. Monkeypox Case Investigation—Cook County Jail, Chicago, Illinois, July–August 2022. MMWR Morb Mortal Wkly Rep. 2022;71:1271–7. https://doi.org/10.15585/mmwr.mm7140e2
23. Waddell CJ, Filardo TD, Prasad N, Pellegrini GJ Jr, Persad N, Carson WC, et al. Possible undetected mpox infection among persons accessing homeless services and staying in encampments—San Francisco, California, October–November 2022. MMWR Morb Mortal Wkly Rep. 2023;72:227–31. https://doi.org/10.15585/mmwr.mm7209a3

Address for correspondence: Alicia H. Chang, Los Angeles County Department of Public Health, 123 W Manchester Blvd, Inglewood, CA 90301, USA; email: alchang@ph.lacounty.gov

Case Studies and Literature Review of *Francisella tularensis*–Related Prosthetic Joint Infection

Léa Ponderand, Thomas Guimard, Estibaliz Lazaro, Henry Dupuy, Olivia Peuchant, Nathalie Roch, Philippe Deroche, Tristan Ferry, Max Maurin, Aurélie Hennebique, Sandrine Boisset, Isabelle Pelloux, Yvan Caspar

In support of improving patient care, this activity has been planned and implemented by Medscape, LLC and Emerging Infectious Diseases. Medscape, LLC is jointly accredited with commendation by the Accreditation Council for Continuing Medical Education (ACCME), the Accreditation Council for Pharmacy Education (ACPE), and the American Nurses Credentialing Center (ANCC), to provide continuing education for the healthcare team.

Medscape, LLC designates this Journal-based CME activity for a maximum of 1.00 ***AMA PRA Category 1 Credit(s)™***. Physicians should claim only the credit commensurate with the extent of their participation in the activity.

Successful completion of this CME activity, which includes participation in the evaluation component, enables the participant to earn up to 1.0 MOC points in the American Board of Internal Medicine's (ABIM) Maintenance of Certification (MOC) program. Participants will earn MOC points equivalent to the amount of CME credits claimed for the activity. It is the CME activity provider's responsibility to submit participant completion information to ACCME for the purpose of granting ABIM MOC credit.

All other clinicians completing this activity will be issued a certificate of participation. To participate in this journal CME activity: (1) review the learning objectives and author disclosures; (2) study the education content; (3) take the post-test with a 75% minimum passing score and complete the evaluation at http://www.medscape.org/journal/eid; and (4) view/print certificate. For CME questions, see page 1295.

NOTE: It is Medscape's policy to avoid the use of Brand names in accredited activities. However, in an effort to be as clear as possible, the use of brand names should not be viewed as a promotion of any brand or as an endorsement by Medscape of specific products.

Release date: May 18, 2023; Expiration date: May 18, 2024

Learning Objectives

Upon completion of this activity, participants will be able to:

- Assess clinical presentation and course of *Francisella tularensis* prosthetic joint infection, based on a case series of 3 cases of *F. tularensis* subsp. *holarctica*–related prosthetic joint infection in France between 2016 and 2019 and a review of 5 other cases reported in the literature.
- Evaluate the diagnosis and laboratory findings of *Francisella tularensis* prosthetic joint infection, based on a case series of 3 cases of *F. tularensis* subsp. *holarctica*–related prosthetic joint infection in France between 2016 and 2019 and review of 5 other cases reported in the literature.
- Examine the treatment of *Francisella tularensis* prosthetic joint infection, based on a case series of 3 cases of *F. tularensis* subsp. *holarctica*–related prosthetic joint infection in France between 2016 and 2019 and review of 5 other cases reported in the literature.

CME Editor

Jill Russell, BA, Technical Writer/Editor, Emerging Infectious Diseases. *Disclosure: Jill Russell, BA, has no relevant financial relationships.*

CME Author

Laurie Barclay, MD, freelance writer and reviewer, Medscape, LLC. *Disclosure: Laurie Barclay, MD, has no relevant financial relationships.*

Authors

Léa Ponderand, PharmD; Thomas Guimard, MD; Estibaliz Lazaro, MD, PhD; Henry Dupuy, MD; Olivia Peuchant, PharmD, PhD; Nathalie Roch, MD; Philippe Deroche, MD; Tristan Ferry, MD, PhD; Max Maurin, MD, PhD; Aurélie Hennebique, PharmD, PhD; Sandrine Boisset, PharmD, PhD; Isabelle Pelloux, MD; and ***Yvan Caspar, PharmD, PhD.***

Tularemia is a zoonotic infection caused by *Francisella tularensis*. Its most typical manifestations in humans are ulceroglandular and glandular; infections in prosthetic joints are rare. We report 3 cases of *F. tularensis* subspecies *holarctica*–related prosthetic joint infection that occurred in France during 2016–2019. We also reviewed relevant literature and found only 5 other cases of *Francisella*-related prosthetic joint infections worldwide, which we summarized. Among those 8 patients, clinical symptoms appeared 7 days to 19 years after the joint placement and were nonspecific to tularemia. Although positive cultures are typically obtained in only 10% of tularemia cases, strains grew in all 8 of the patients. *F. tularensis* was initially identified in 2 patients by matrix-assisted laser desorption/ionization time-of-flight mass spectrometry; molecular methods were used for 6 patients. Surgical treatment in conjunction with long-term antimicrobial treatment resulted in favorable outcomes; no relapses were seen after 6 months of follow-up.

Francisella tularensis is a fastidious, gram-negative coccobacillus that can cause tularemia, a zoonotic disease. Two subspecies are responsible for human cases: *F. tularensis* subspecies *tularensis* (type A strains) and *F. tularensis* subsp. *holarctica* (type B strains) (*1*). Tularemia is a reemerging disease that has occurred recently both sporadically and in outbreaks worldwide. No vaccines are available, and antibiotic classes effective in treatment are limited to aminoglycosides, fluoroquinolones, and tetracyclines (*2*,*3*).

Potential reservoirs and vectors in both the terrestrial and aquatic cycles of this bacterium are varied. Six main clinical forms of tularemia have been described (glandular, ulceroglandular, oropharyngeal, oculoglandular, pneumonic, and typhoidal), depending on the route of bacterial inoculation. Tularemia can be transmitted through direct contact with infected animals (hares, rabbits, small rodents, etc.); through the bites of blood-sucking arthropods; through consumption of contaminated food or water; through conjunctival inoculation with contaminated fingers, materials, or aerosolized particles; or through the lungs, either by inhaling infectious aerosols or by the hematogenous spread of bacteria (*4*–*7*).

Severe infections are predominantly associated with *F. tularensis* subsp. *tularensis*, which is present only in North America, whereas *F. tularensis* subsp. *holarctica*, the only subspecies found in both Europe and North America, largely causes incapacitating and chronic disease with large or multiple lymphadenopathies (*8*). According to data from the French National Reference Center for *Francisella* (FNRCF) and from mandatory notifications to the French Public Health Agency, the ulceroglandular and glandular forms account for most (72%) clinical forms of the disease (*9*). Bone and joint infections (BJIs) and prosthetic joint infections (PJIs) related to *F. tularensis* are extremely rare and have been reported sporadically in literature (*10*–*13*). BJIs are primarily related to staphylococci, streptococci, or gram-negative rods, but any bacterial species can cause an infection in the presence of prosthetic material (*14*,*15*). We report 3 cases of *F. tularensis*–related PJIs occurring during 2016–2019 in France, as well as the results of a literature review on BJIs and PJIs related to this highly pathogenic bacterium (Tables 1, 2).

Material and Methods

The following methods and laboratory precautions were used at the FNRCF to confirm the diagnosis of tularemia. For F. tularensis culturing, samples and strains were housed in a Biosafety Level 3 laboratory. Samples were seeded on chocolate agar and incubated at 37°C in a CO_2-enriched atmosphere for 10 days. Methods for identifying F. tularensis subsp. holarctica varied among the 3 patient cases described in this article. Before 2018 (case 1), specific real-time insertion sequence F. tularensis (ISFtu2) PCR and sequencing of the 16S 23S intergenic region (16) were used to confirm identification at the subspecies level. Since 2018 (cases 2 and 3), F. tularensis subsp. holarctica identification has been confirmed using in-house ISFtu2 PCR and F. tularensis subsp. holarctica–specific PCR, according to previously published protocols (17,18). Before 2018 (case 1), serologic testing was performed using in-house microagglutination test (MAT) and in-house indirect immunofluorescence assay (IFA). Since 2018, ELISA

Author affiliations: Grenoble Alpes University Hospital Center, Grenoble, France (L. Ponderand, M. Maurin, A. Hennebique, S. Boisset, I. Pelloux, Y. Caspar); Univ. Grenoble Alpes, CNRS, CEA, IBS, Grenoble, France (L. Ponderand, S. Boisset, Y. Caspar); Departmental Hospital Center of Vendée, La Roche sur Yon, France (T. Guimard); University Hospital Center of Haut-Lévêque, Pessac, France (E. Lazaro, H. Dupuy); University Hospital Center of Bordeaux, Bordeaux, France (O. Peuchant); William Morey Hospital Center, Chalon-sur-Saône, France (N. Roch); Dracy-le-Fort Orthopedic Center, Dracy-le-Fort, France (P. Deroche); Claude Bernard University Lyon 1, CNRS ENS Lyon, INSERM, Lyon, France (T. Ferry); Croix-Rousse University Hospital Center, Hospices Civils de Lyon, Lyon (T. Ferry); Univ. Grenoble Alpes, CNRS, Grenoble INP, TIMC-IMAG, Grenoble (M. Maurin, A. Hennebique)

DOI: https://doi.org/10.3201/eid2906.221395

(Serion Diagnostics) (case 2) and chemiluminescent immunoassay (Vircell) have replaced the MAT method.

For this study, we performed retrospective antibiotic susceptibility testing to determine the MIC of 7 antibiotics (gentamicin, ciprofloxacin, levofloxacin, rifampin, erythromycin, azithromycin, and doxycycline). We used an in-house broth microdilution method, as previously described (*19*).

For the retrospective case search, we performed a PubMed search for published cases of PJI caused by *F. tularensis* using the terms "*Francisella* AND joint AND infection" with no restriction of date or language. In total, 21 articles matched the searched criteria, but only 5 cases corresponded to PJI.

Results

Case 1

A 49-year-old man living in Vendée County, France, was hospitalized in March 2016 for a left femoral neck fracture after a fall. The patient underwent hip arthroplasty with prosthesis placement. His medical history

Table 1. Clinical and biologic characteristics of patients with *Francisella tularensis*–related prosthetic joint infection*

Characteristic	Case 1	2	3	4 (*10*)	5 (*11*)	6 (*11*)	7 (*12*)	8 (*13*)
Country	France	France	France	United States	Switzerland	Czech Republic	United States	Canada
Region	Vendée	Gironde	Aube	Colorado	NS	NS	Illinois	Ontario
Age, y	49	70	68	58	84	84	77	68
Sex	M	M	M	M	F	M	M	M
Exposure factors	Rural residence, dog	Hunter	Retired butcher, cooking with wild game	Farmer, possible rabbit carcass handling	Airborne transmission (rabbit barn in neighbor's house)	Walk in tularemia-endemic area	Hunter	Hunter, tick bite 6 mo before surgery
Type of surgery	Left THR	Left TKA	Left THR	Left TKA	Right knee prosthesis	Right TKA	Right THR	Right TKA
Delay between diagnosis and prosthesis implantation	35 d	12 y	19 y	9 mo	12 y	8 y	7 d	6 mo
Clinical symptoms	Infected scar, fever	Feverish confusion, bilateral mediastinal and hilar lymphadenopathy, knee swelling	Joint pain	Repeated joint effusion	Erythema, joint pain	Fever, abdominal pain, confusion, painful knee effusion	Fever, joint pain and swelling, bullous skin lesion with itching	Joint pain, warm and swollen knee
CRP, mg/L	21	100	58	NA	81	98	16	NA
Leukocytes, G/L	4.45	4	NA	NA	NA	NA	NA	NA
Sample type	Abscess	Joint aspiration	3 tissues	Joint aspiration	7 tissues	Joint aspiration	Joint aspiration	Joint aspiration
No. positive samples/total	1/1	1/1	2/3	1/1	6/7	1/1	1/1	1/1
Delay to positivity	NA	7 d	5 d	24 h–48 h	12 d	4 d	7 d	3 d
Identification	Vitek 2 GN Biochemical assay; ISFtu2 PCR +; specific *F. tularensis* subspecies *holarctica* PCR	Specific *Francisella* PCR; ISFtu2 PCR +; 16S-23S PCR + sequencing	MALDI-TOF MS (Microflex LT); ISFtu2 PCR +; specific *F. tularensis* subspecies *holarctica* PCR	Sequencing	16S rRNA gene sequencing	16 S rRNA gene sequencing	MALDI-TOF MS	Sequencing
Serologic results	MAT 640; IFA IgG 1,280; IgM 640	ELISA IgG 1.5; IgM 3.58; IFA IgG 640; IgM 640	MAT 160	ND	IgM 232.6 U/mL; IgG 126.4 U/mL	MAT 80	Positive (titers NA)	MAT 320

*CRP, C-reactive protein; IFA, immunofluorescence assay; MALDI-TOF MS, matrix-assisted laser desorption/ionization time-of-flight mass spectrometry; MAT, microagglutination test; Microflex LT, Bruker Daltonics; NA, not available; ND, not done; NS, not specified; THR, total hip replacement; TKA, total knee arthroplasty; +, positive.

Table 2. Surgery, antibiotic treatment, and follow-up of patients with *Francisella tularensis*-related prosthesis joint infection

Characteristic	Case 1	2	3	4 (*10*)	5 (*11*)	6 (*11*)	7 (*12*)	8 (*13*)
Surgery	1-stage revision joint replacement	1-stage revision joint replacement	1-stage revision with partial joint replacement	Repeated joint aspiration	2-stage revision joint replacement	Repeated joint aspiration	DAIR	2-stage revision joint replacement
Antibiotic treatment								
Before surgery	DOX 100 mg 2×/d until surgery	OFX 200 mg 2×/d for 6 wk	ND	ND	AMC	AMC	ND	IV cloxacillin 2 g/6 h for 10 d, oral cloxacillin 500 mg 4×/d
After surgery	CIP 750 mg 2×/d + DOX 100 mg x2 2×/d for 9 wk	IV CIP 500 mg 2×/d + IV AMK 1,200 mg for 5 d, CIP 500 mg 2×/d for 6 wk	CIP 750 mg 2×/d 3 mo, lifetime treatment by DOX 100 mg 2×/d	DOX, dosage NA	DOX 100 mg 2×/d for 6 wk	DOX 100 mg 2×/d for 20 d + GEN 240 mg for 10 d, CIP 500 mg 2×/d for 20 d	DOX 100 mg 2×/d for 12 mo	IV CFZ 2g/8h 6 wk + RIF 300 mg 2×/d, CIP 500 mg 2×/d + RIF 300 mg 2×/d >6 mo
Progress at follow up	No relapse, no biologic inflammatory limp, chronic joint pain	Biologic surveillance, favorable evolution	Favorable evolution with mild limp	No relapse, persistence of knee swelling	Favorable evolution	Small pain-free effusion at 24 mo	Resolution of pain and skin lesion	Resolution of symptoms under treatment
Staff monitoring or prophylaxis	Prophylactic DOX or CIP	NA	Clinical and serologic	NA	Serologic	Prophylactic DOX	NA	NA

*AMC, amoxicillin/clavulanic acid; AMK, amikacin; CFZ, cefazolin; CIP, ciprofloxacin; DOX, doxycycline; DAIR, debridement, antibiotics, implant retention; GEN, gentamicin; IV, intravenous; NA, not available; ND, not done; OFX, ofloxacin; RIF, rifampin.

included active smoking and alcoholic cirrhosis since 2008. One month later, the patient was transferred to the intensive care unit for hepatic encephalopathy. During his hospitalization, an abscess developed near the prosthesis scar; surgical site infection was suspected. A computed tomography (CT) scan of the pelvis revealed soft tissue infection of the left hip; the periosteal image was compatible with osteitis (Figure 1). The patient's blood culture results were negative, C-reactive protein (CRP) was 21 mg/L (reference <10 mg/L), and leukocyte count was 4.45 giga (G)/L (4.1–9.9 G/L). After 2 days, a specimen from the abscess demonstrated growth of a small gram-negative coccobacillus on chocolate agar under 5% CO_2 enrichment, which was not identified by Vitek-MS matrix-assisted laser desorption/ionization time-of-flight (MALDI-TOF) mass spectrometry (bioMérieux). *F. tularensis* was suspected on the basis of results of the Vitek 2 GN biochemical assay (bioMérieux) 1 day later. The strain was sent to the FNRCF, where *F. tularensis* subsp. *holarctica* infection was confirmed. Serologic results from MAT were positive (640 [reference <80]), and elevated IgM (640 [reference <80) and IgG (1,280 [reference <80]) titers were confirmed by IFA. The patient received a course of doxycycline (100 mg 2×/d for 1 mo), then underwent a 1-stage revision joint replacement; respiratory precautions (KN95 masks) were in place for all persons in the operating theater to prevent secondary transmission through contaminated droplets. Gentamicin (3 mg/kg) was administered during surgery, followed by ciprofloxacin (750 mg) and doxycycline (100 mg 2×/d), both for 9 weeks. Five samples collected during surgery remained sterile.

Although the infection was cured, the patient still had joint pain without fever or biologic inflammatory syndrome 4 years later. The patient was not a hunter but lived in a rural, *Francisella*-endemic area of France and owned a dog, which sometimes brought wild animals or game that could have been infected. The patient did not eat game meat, however, and he did not leave the hospital between the initial prosthetic hip surgery and the appearance of the abscess. We proposed 2 hypotheses to explain the infection: contamination occurred a few days before the patient's fall and bacteria were already present in his blood, leading to prosthesis contamination and abscess; or contamination occurred intraoperatively because of skin contamination after the fall. Multiple skin scratches, bruises, and wounds were described. Unfortunately, no serum samples were available to assess the date of contamination. Monitoring of laboratory staff included prophylactic treatment with doxycycline or ciprofloxacin. Because surgeons were protected with gloves, glasses, and surgical masks, and no injuries were reported involving contaminated materials, no monitoring was performed.

Case 2

A 70-year-old man was hospitalized in August 2018 with fever, confusion, headache, cervical pain, and

lower limb weakness. He lived in a forested rural area in Gironde County, France, and had been experiencing asthenia and anorexia for several months. His medical history included diabetes, high blood pressure, dyslipidemia, and regular alcohol consumption. He underwent a left knee replacement with total knee prosthesis in 2006. Laboratory examinations revealed a CRP level of 100 mg/L (reference <10 mg/L) and leukocyte count of 4 G/L (4.1–9.9 G/L). Cerebrospinal fluid (CSF) and blood culture samples were taken, and treatment with ceftriaxone and acyclovir was initiated. The culture of both samples remained sterile, and results of herpes simplex virus/varicella zoster virus PCR were also negative. The patient had not traveled abroad but had birds at home (hens, pigeons, and doves) and was a fisherman and hunter. CT and positron emission tomography demonstrated bilateral mediastinal and hilar lymphadenopathies associated with diffuse condensation of the upper right pulmonary lobe, compatible with infection (Figure 2). *Legionella pneumophila* and *Streptococcus pneumonia* urinary antigen test results were negative. Bronchoalveolar lavage did not identify any pathogen, but white blood cell count identified 60% gamma-delta T cells in the lymphocyte fraction (40% of total leukocytes), possibly indicating infection with an intracellular bacterium. At a follow-up visit 20 days later, the patient felt better but was still experiencing evening fever (38°C) without chills or night sweats. Clinical examination revealed swelling of the left knee. Joint aspiration revealed a leukocyte count of 99,000 cells/mm^3 (reference <1,700 cells/mm^3) with 70% lymphocytes. Unexpectedly, gray-white, smooth, and small colonies grew after 7 days on chocolate agar under 5% CO_2 enrichment; the bacteria were identified as *F. tularensis* by PCR targeting the gene encoding *F. tularensis* outer membrane protein A after failure to confirm identification with Biotyper MALDI-TOF mass spectrometry (Bruker Daltonics). Results of a *Francisella*-specific PCR performed directly on joint aspirate was also positive. The strains and samples were sent to FNRCF, where the strain was confirmed as *F. tularensis* subsp. *holarctica*. Results of the mediastinal lymph node biopsy, however, were PCR-negative.

Serologic samples from early September 2018 showed elevated IgM titers of 3.58 (reference <0.45) and IgG titers of 1.5 (reference <0.62) by ELISA (Serion Diagnostics) and titers of 640 (IgM) and 640 (IgG) by IFA, corroborating recent *F. tularensis* infection. Antibiotic therapy with ofloxacin (200 mg 2×/d) was administered for 6 weeks, and a 1-stage joint

Figure 1. Computed tomography scan of pelvis in case 1 showing large abscess of the left hip with a periosteal image compatible with an osteitis in case of *Francisella tularensis*–related prosthetic joint infection, France

replacement was performed in March 2019. Of 5 samples taken during surgery, 2 were found to be positive for *Francisella* by ISFtu2 PCR; however, because of a small bacterial concentration, results for the specific but less sensitive *F. tularensis* subsp. *holarctica* PCR remained negative. The fifth culture was sterile. Ciprofloxacin (500 mg 2×/d) and amikacin (1,200 mg 1×/d) were started during surgery; amikacin was stopped after 5 days. By April, the wound was sufficiently healed and CRP had decreased to 13.5 mg/L, enabling the patient to return home; ciprofloxacin was continued for 6 weeks. His progress was favorable for clinical and biologic healing.

The suspected mode of contamination was infection by animal or aerosol, and initial pulmonary symptoms indicated likely airborne contamination

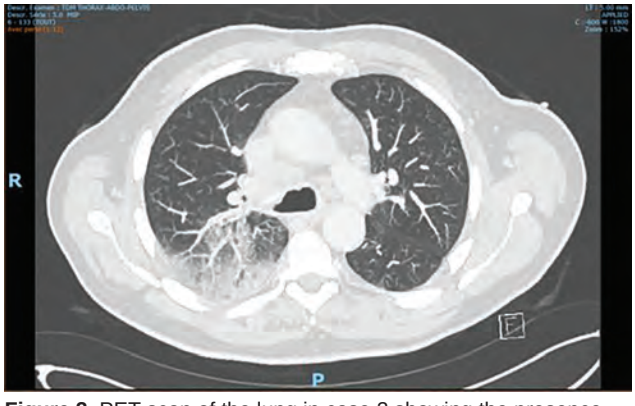

Figure 2. PET scan of the lung in case 2 showing the presence of bilateral mediastinohilar lymphadenopathies associated with a diffuse condensation of the upper right pulmonary lobe in case of *Francisella tularensis*–related prosthetic joint infection, France.

that could have occurred by inhaling contaminated aerosols or dust. The patient was fishing at the time symptoms appeared, so inhaling contaminated water droplets seems a plausible source because of the possible aquatic reservoir of this bacterium (*4*,*20*).

Case 3

A 68-year-old man living in Aube County, France, with a medical history of left hip prosthesis implantation in 2000 and right knee prosthesis implantation in 2008 was evaluated in August 2019 for lateral discomfort on his left side, functional hip difficulties, and pain adjacent to his hip prosthesis. Radiography revealed no major prosthesis degradation. Scintigraphy was positive, however, and CT performed in September revealed wear and a cavity in the metal socket of the prosthesis. A 1-stage revision of the joint was performed in October 2019 to replace the metal socket of the prosthesis. The stem was not unsealed and was therefore left in place; the surgeon noted a joint exudate and fibrosis during the operation. CRP was 58 mg/L. Unexpectedly, 2 of 3 samples obtained during surgery grew a fastidious Gram-negative coccobacillus, identified as *F. tularensis* by Biotyper MALDI-TOF mass spectrometry after 5 days on chocolate agar of aerobic cultures with 5% CO_2 enrichment. The strains and samples were sent to FNRCF, where the strain was confirmed as *F. tularensis* subsp. *holarctica*. Results of MAT (160 [reference <20]) were positive. Ciprofloxacin (750 mg 2×/d) was administered for 3 months.

After requesting a notice from Centre de Référence des Infections Ostéo-Articulaires Complexes, the reference center for the management of BJIs, and because the stem of the initial prosthesis was in place, lifetime antibiotic treatment with doxycycline (100 mg 2×/d) was recommended; long-term oral suppressive antibiotic therapy to maintain a functioning prosthesis can be recommended when removing all the components of the prosthesis is not possible. The patient's progress was favorable; he demonstrated good healing and biologic inflammatory syndrome regression and had a slight limp after 3 months. The patient was a retired butcher who often made pâté with wild game, which probably led to contamination by direct contact with infected animals or meat. No monitoring was performed for surgeons and surgical staff. However, laboratory staff follow-up care included clinical and serologic monitoring.

Laboratory Safety

For all 3 cases, before *F. tularensis* was suspected or confirmed, samples and strains were handled under Biosafety Level 2 conditions in clinical microbiology laboratories. Samples were rapidly sent to the FNRCF to confirm identification. MIC determinations were performed a posteriori on the 3 strains from France (Table 3). MICs were the lowest for ciprofloxacin (0.016–0.032 mg/L) and levofloxacin (0.032 mg/L), and no resistance to aminoglycosides, rifampin, fluoroquinolones, or tetracyclines was observed. The erythromycin MIC of 2 mg/L confirmed that the 3 strains belonged to biovar I of *F. tularensis* subsp. *holarctica* (*19*,*21*).

Discussion

Prosthetic joint replacement is a common surgery increasingly used to improve quality of life (*22*,*23*). Several recommendations to limit infection at the surgical site exist (*24*–*26*), which are either preoperative (skin disinfection by shower with antiseptic or antimicrobial soap, nasal and cutaneous decolonization of *S. aureus*), perioperative (perioperative antiseptic use, intraoperative systemic antimicrobial prophylaxis, asepsis of the operative environment), or postoperative (postoperative antimicrobial prophylaxis). Despite those preventive measures, prosthetic joint infections occur in 1%–2% of patients (*27*–*29*). The most common pathogens described are staphylococci (*S. aureus* and coagulase-negative staphylococci), isolated in 50%–60% of the cases; streptococci; and enterococci (together accounting for 10%). Aerobic

Table 3. MICs of 3 strains of *Francisella tularensis* subspecies *holarctica* obtained by broth microdilution method, France*

Antibiotics	MICs, mg/L			Breakpoints for susceptibility, mg/L
	Case 1	Case 2	Case 3	
Gentamicin	0.5	0.5	0.5	4†
Ciprofloxacin	0.016	0.032	0.016	0.25†
Levofloxacin	0.032	0.032	0.032	0.5†
Rifampin	0.5	0.5	0.5	1‡
Erythromycin	2	2	2	16‡
Azythromycin	1	1	1	4‡
Doxycycline	0.25	0.25	0.25	4†

*The assay medium was CAMHB supplemented with 2% PolyViteX (CAMHB-PVX; bioMérieux) and adjusted to pH 7.1+0.1 as recommended (17). MICs were read after 48 h of incubation and were interpreted using the Clinical and Laboratory Standards Institute susceptibility breakpoints for *Francisella tularensis* when available or the *Haemophilus influenzae* European Committee on Antimicrobial Susceptibility Testing breakpoints.
†Clinical and Laboratory Standards Institute breakpoint.
‡*H. influenzae* European Committee on Antimicrobial Susceptibility Testing breakpoint.

gram-negative rods and anaerobic bacteria are isolated from <10% of knee and hip prosthetic joint infections. However, 5%–34% of prosthetic infections remain culture-negative because of previous antimicrobial treatment or because fastidious or low-inoculum pathogens can remain undetectable by classic culture or PCR methods (*27*,*28*,*30*).

Prosthetic joint infection is an extremely rare form of tularemia; we found only 5 cases reported in the literature to date (Tables 1, 2) (*10*–*13*). Of the 8 cases of prosthetic infections summarized in this article, 7 (88%) occurred in men ≥49 years of age (range 49–84 years). The knee prosthesis was infected in 5 (62.5%) patients and hip prostheses in 3 (37.5%) patients. In all but 2 patients, clinical symptoms appeared >6 months after joint placement (7 days–19 years, median 4 years) and were unspecific to tularemia. Fever, joint pain, and joint exudate were often described, and inflammatory blood markers, where reported, usually increased (CRP range 16–100 mg/L). Inoculation of *F. tularensis* at the surface of the prosthesis seems to be possible in 3 different ways: through direct transfer from contaminated skin wounds or ulcers during surgery (case 1), after surgery through direct skin contamination close to the surgical site scar, or by hematologic spread of the bacteria from an initial infection site distant from the prosthesis (cases 2 and 3). In the reported BJI cases, the initial contamination was suspected to occur through direct transmission from an animal reservoir, either by ingestion of undercooked meat prepared from an infected animal or contact with infected carcasses (cases 2, 3, 4, 7, and 8); possibly by an arthropod bite, as in case 8, in which the patient noted a tick bite 6 months before his initial knee arthroplasty; or by inhalation of contaminated aerosols or dust (cases 1, 5, and 6). For some patients, infectious symptoms were absent or mild, suggesting that the bacteria might be able to survive in a quiescent form with low virulence levels after seeding on the prosthesis. Mechanisms similar to those involved in the long-term persistence of *F. tularensis* subsp. *holarctica* in soil and water might occur, such as switching to a viable but noncultivable state or biofilm formation (*4*; C.D. Brunet et al., unpub. data, https://www.biorxiv.org/content/10.1101/2022.02.18.480867v3). Biofilm formation has been described for the *Francisella* species in vitro and might be a key mechanism in human pathogenesis and infection, especially PJIs (*28*,*31*).

According to the World Health Organization definition of tularemia, presumptive cases are defined as cases in persons with clinical symptoms compatible with tularemia and either positive DNA detection in 1 clinical sample or a single positive serum sample. An infection is confirmed when an *F. tularensis* strain is isolated and identified in culture or by a 4-fold increase in IgM or IgG titers in paired serum specimens (*17*). Although tularemia is primarily identified by serologic assays, the proportion of diagnoses assessed by molecular methods on tissue samples is increasing because of the development of specific PCRs or the availability of 16S rDNA sequencing. Positive bacterial cultures are usually obtained in <10% of cases (*7*,*16*) because *F. tularensis* is a fastidious bacterium that requires cysteine-supplemented agar (*17*). Growth occurs in 2–4 days of incubation at 37°C in aerobic or CO_2-enriched atmosphere, and colonies are gray-white, round, and smooth with a small halo (*32*,*33*). Surprisingly, in these 8 cases, the diagnosis was made by positive culture on joint aspiration or perioperative tissues. This finding highlights the major need for rapid seeding of fresh tissues on an agar media to enable the growth of this fastidious bacterium from human samples (*34*). Serologic testing, when performed, identified mostly high titers in MAT, ELISA, or IFA, confirming *Francisella* infection, but was performed after the initial diagnosis. The identification of 1 strain was suspected on the basis of results of the Vitek 2 GN assay. MALDI-TOF mass spectrometry enabled identification of 2 strains but did not provide subspecies distinction (*35*–*37*). *F. tularensis* has been identified using the in vitro diagnosis database of the Biotyper mass spectrometer since 2017 (partial integration of 5 species of the security-relevant library as a library extension) only if the extension was added to the database by the user. In contrast, the Vitek MS database does not contain any *F. tularensis* spectra. In 7 of 8 cases, the strain was identified or confirmed by molecular methods (Table 1). Because of the high level of 16S rDNA similarity among the *Francisella* species (98.5%–99.9%), 16S rDNA amplification and sequencing enables identifying the bacterium only to the genus level (*38*). Species or subspecies determination requires PCR targeting specific genes, such as *ISFtu2*, *23kDa*, *tul4*, or *fopA* (*39*). Some of those targets, however, might cross-react with *F. novicida*, *F. philomiragia*, or *Francisella*-like endosymbionts. Additional techniques are necessary to identify *F. tularensis* subspecies, such as PCR targeting a junction between ISFtu2 and a flanking 3′ region (*18*), identification on the basis of size differences of amplified DNA products (Ft-M19, ISFtu2, RD1, and pdpD-2 assay) (*17*,*40*), and amplification and sequencing of the 16S-23S rRNA intergenic spacer region (*16*).

Strategies for PJI treatment combine surgical interventions and antimicrobial therapy. Overall, in cases of early infection (≤15 days after prosthesis placement), prosthesis retention with debridement is recommended. In chronic infection, prosthesis removal is the best option, performed as either a 1-stage or 2-stage replacement procedure, depending on the patient history, the bacterium identified, and susceptibility to antibiotics. Those surgical treatments are associated with a long duration (4–6 weeks) of antimicrobial therapy adapted to the antibiotic susceptibility of the bacteria identified (*28*,*41*,*42*). Several guidelines for tularemia treatment have been published (*2*,*17*,*43*,*44*). The antibiotic classes recommended for first-line treatment of tularemia are aminoglycosides, fluoroquinolones, and tetracycline because the bacterium is intrinsically resistant to many other antibiotic classes (all β-lactams, TMP/SXT, clindamycin, glycopeptides, and daptomycin) (*19*). For severe tularemia cases, parenteral gentamicin (5 mg/kg/d) treatment is recommended depending on the clinical response. In moderate cases, oral ciprofloxacin (800–1,000 mg/d) or doxycycline (200 mg/d) can be administered for a minimum duration of 10–14 days. However, those recommendations have not yet been established for BJIs. Of the 8 cases we reviewed, 5 patients underwent 1- or 2-stage revision joint replacement; 1 underwent debridement, antibiotic, and implant retention; and 2 underwent regular joint aspiration without prosthesis replacement. For 2 patients, aminoglycosides were administered during and after the surgery (120 mg amikacin for 5 days and 240 mg gentamicin for 10 days), followed by monotherapy with ciprofloxacin (500 mg 2×/d for 20 days). Three patients received monotherapy; 1 patient took ciprofloxacin (750 mg 2×/d) for 3 months, and 2 patients were prescribed doxycycline (100 mg 2×/d) for 6 weeks or 12 months. Combination therapy was administered in 2 other cases, consisting of ciprofloxacin with rifampin for >6 months or ciprofloxacin with doxycycline for 9 weeks. When information was available, the patients' follow-up visits revealed favorable progress without joint infection relapse.

Strains have not been reported that are resistant to the recommended first-line antibiotic classes. A comprehensive review reported low MICs for ciprofloxacin (≤0.002–0.125 mg/L), gentamicin (≤0.016–2 mg/L), and doxycycline (0.064–4 mg/L) against *F. tularensis* strains (*19*). Aminoglycosides penetrate slowly intracellularly and are effective against extracellular bacteria. On the basis of our previous comprehensive review of antimicrobial susceptibility testing data in vitro, in cellular model, and in mice model of infection (*19*), we advise using aminoglycoside for only a short period during and after surgery, when a bacteremic phase can occur, to rapidly kill extracellular bacteria and prevent hematologic spread after surgery. Combining aminoglycosides with ciprofloxacin might confer the highest efficacy because of the rapid penetration of fluoroquinolones in bones and joint tissues and their efficient activity against the intracellular niche of *Francisella*. Thus, combining aminoglycosides and fluoroquinolones might be considered in these severe cases (*44*). Ciprofloxacin and doxycycline, alone or in combination, can be used for long-term treatment. Interest in combination therapy with rifampin has not been demonstrated, but in vitro activity of rifampin against *Francisella* has been observed (MICs range 0.094–3 mg/L), and its excellent bone diffusion might enhance successful outcomes, as demonstrated by case 1 (*13*,*19*,*21*,*45*). However, rifampin is not recommended for tularemia treatment because of insufficient in vivo data (*19*).

Because of the difficulty and delay involved in identifying *Francisella* strains, laboratory staff can be exposed to bacteria without recommended precautions. During surgical interventions, surgeons can be exposed through contact with infectious materials, accidental inoculation, or exposure to aerosols and infectious droplets. World Health Organization guidelines distinguish 3 situations: proven accidental laboratory exposure, potential exposure to *F. tularensis* aerosols, and unlikely exposure. Antibiotic prophylaxis (1,000 mg ciprofloxacin or 200 mg doxycycline for 14 days) or clinical follow-up was recommended according to exposure risk (*17*).

In conclusion, PJI is an unusual clinical manifestation of tularemia that might be underestimated because of the fastidious culture conditions and difficulty in strain identification. Infection might occur in tularemia-endemic areas or in the presence of risk factors. The combination of surgical and extended antibiotic treatment generally leads to favorable outcomes.

About the Author

Dr. Ponderand is a clinical microbiologist at Grenoble Alpes University Hospital Center. Her primary research interests include applied research with clinical improvement, such as rapid bacterial identification and rapid antimicrobial susceptibility testing in septicemia, or fundamental research on *Francisella tularensis* pathogenesis in collaboration with the French National Reference Center for *Francisella*.

References

1. Oyston PCF, Sjostedt A, Titball RW. Tularaemia: bioterrorism defence renews interest in *Francisella tularensis*. Nat Rev Microbiol. 2004;2:967–78. https://doi.org/10.1038/nrmicro1045
2. Boisset S, Caspar Y, Sutera V, Maurin M. New therapeutic approaches for treatment of tularaemia: a review. Front Cell Infect Microbiol. 2014;4:40. https://doi.org/10.3389/fcimb.2014.00040
3. Maurin M, Mersali NF, Raoult D. Bactericidal activities of antibiotics against intracellular *Francisella tularensis*. Antimicrob Agents Chemother. 2000;44:3428–31. https://doi.org/10.1128/AAC.44.12.3428-3431.2000
4. Hennebique A, Boisset S, Maurin M. Tularemia as a waterborne disease: a review. Emerg Microbes Infect. 2019;8:1027–42. https://doi.org/10.1080/22221751.2019.1638734
5. Burckhardt F, Hoffmann D, Jahn K, Heuner K, Jacob D, Vogt M, et al. Oropharyngeal tularemia from freshly pressed grape must. N Engl J Med. 2018;379:197–9.
6. Eren Gok S, Kocagul Celikbas A, Baykam N, Atay Buyukdemirci A, Eroglu MN, Evren Kemer O, et al. Evaluation of tularemia cases focusing on the oculoglandular form. J Infect Dev Ctries. 2014;8:1277–84. https://doi.org/10.3855/jidc.3996
7. Maurin M, Gyuranecz M. Tularaemia: clinical aspects in Europe. Lancet Infect Dis. 2016;16:113–24. https://doi.org/10.1016/S1473-3099(15)00355-2
8. Petersen JM, Molins CR. Subpopulations of *Francisella tularensis ssp. tularensis* and *holarctica*: identification and associated epidemiology. Future Microbiol. 2010;5:649–61. https://doi.org/10.2217/fmb.10.17
9. Mailles A, Vaillant V. 10 years of surveillance of human tularaemia in France. Euro Surveill. 2014;19:20956. https://doi.org/10.2807/1560-7917.ES2014.19.45.20956
10. Azua EN, Voss LA. Tularemia in a prosthetic joint infection. Orthopedics. 2020;43:e54–6. https://doi.org/10.3928/01477447-20190627-01
11. Chrdle A, Trnka T, Musil D, Fucentese SF, Bode P, Keller PM, et al. *Francisella tularensis* periprosthetic joint infections diagnosed with growth in cultures. J Clin Microbiol. 2019;57:e00339-19. https://doi.org/10.1128/JCM.00339-19
12. Rawal H, Patel A, Moran M. Unusual case of prosthetic joint infection caused by *Francisella tularensis*. BMJ Case Rep. 2017;2017:2017.
13. Cooper CL, Van Caeseele P, Canvin J, Nicolle LE. Chronic prosthetic device infection with *Francisella tularensis*. Clin Infect Dis. 1999;29:1589–91. https://doi.org/10.1086/313550
14. French Infectious Diseases Society (SPILF). Clinical recommendations for prosthetic joint infection by the Société de pathologie infectieuse de langue française [in French] [cited 2021 Jan 12]. https://www.infectiologie.com/fr/recommandations.html
15. Beam E, Osmon D. Prosthetic joint infection update. Infect Dis Clin North Am. 2018;32:843–59. https://doi.org/10.1016/j.idc.2018.06.005
16. Maurin M, Pelloux I, Brion JP, Del Banõ JN, Picard A. Human tularemia in France, 2006–2010. Clin Infect Dis. 2011;53:e133–41. https://doi.org/10.1093/cid/cir612
17. World Health Organization. WHO guidelines on tularaemia. Geneva: The Organization: 2007 [cited 2020 Apr 7]. https://apps.who.int/iris/handle/10665/43793
18. Kugeler KJ, Pappert R, Zhou Y, Petersen JM. Real-time PCR for *Francisella tularensis* types A and B. Emerg Infect Dis. 2006;12:1799–801. https://doi.org/10.3201/eid1211.060629
19. Caspar Y, Maurin M. *Francisella tularensis* susceptibility to antibiotics: a comprehensive review of the data obtained *In vitro* and in animal models. Front Cell Infect Microbiol. 2017;7:122. https://doi.org/10.3389/fcimb.2017.00122
20. Brunet CD, Hennebique A, Peyroux J, Pelloux I, Caspar Y, Maurin M. Presence of *Francisella tularensis* subsp. *holarctica* DNA in the aquatic environment in France. Microorganisms. 2021;9:1398. https://doi.org/10.3390/microorganisms9071398
21. Caspar Y, Hennebique A, Maurin M. Antibiotic susceptibility of *Francisella tularensis subsp. holarctica* strains isolated from tularaemia patients in France between 2006 and 2016. J Antimicrob Chemother. 2018;73:687–91. https://doi.org/10.1093/jac/dkx460
22. Ferguson RJ, Palmer AJ, Taylor A, Porter ML, Malchau H, Glyn-Jones S. Hip replacement. Lancet. 2018;392:1662–71.
23. Price AJ, Alvand A, Troelsen A, Katz JN, Hooper G, Gray A, et al. Knee replacement. Lancet. 2018;392:1672–82.
24. Kapadia BH, Berg RA, Daley JA, Fritz J, Bhave A, Mont MA. Periprosthetic joint infection. Lancet. 2016;387:386–94. https://doi.org/10.1016/S0140-6736(14)61798-0
25. Allegranzi B, Zayed B, Bischoff P, Kubilay NZ, de Jonge S, de Vries F, et al.; WHO Guidelines Development Group. New WHO recommendations on intraoperative and postoperative measures for surgical site infection prevention: an evidence-based global perspective. Lancet Infect Dis. 2016;16:e288–303. https://doi.org/10.1016/S1473-3099(16)30402-9
26. Berríos-Torres SI, Umscheid CA, Bratzler DW, Leas B, Stone EC, Kelz RR, et al.; Healthcare Infection Control Practices Advisory Committee. Centers for Disease Control and Prevention guideline for the prevention of surgical site infection, 2017. JAMA Surg. 2017;152:784–91. https://doi.org/10.1001/jamasurg.2017.0904
27. Tande AJ, Patel R. Prosthetic joint infection. Clin Microbiol Rev. 2014;27:302–45. https://doi.org/10.1128/CMR.00111-13
28. Zimmerli W, Trampuz A, Ochsner PE. Prosthetic-joint infections. N Engl J Med. 2004;351:1645–54. https://doi.org/10.1056/NEJMra040181
29. Debarge R, Nicolle MC, Pinaroli A, Ait Si Selmi T, Neyret P. Surgical site infection after total knee arthroplasty: a monocenter analysis of 923 first-intention implantations [in French]. Rev Chir Orthop Repar Appar Mot. 2007;93:582–7.
30. Million M, Bellevegue L, Labussiere AS, Dekel M, Ferry T, Deroche P, et al. Culture-negative prosthetic joint arthritis related to *Coxiella burnetii*. Am J Med. 2014;127:786.e7–10. https://doi.org/10.1016/j.amjmed.2014.03.013
31. van Hoek ML. Biofilms: an advancement in our understanding of *Francisella* species. Virulence. 2013;4:833–46. https://doi.org/10.4161/viru.27023
32. Centers for Disease Control and Prevention, American Society for Microbiology, Association of Public Health Laboratories. Basic protocols for Level A laboratories for the presumptive identification of *Francisella tularensis* [cited 2021 Jan 12]. https://www.epa.gov/sites/production/files/2015-07/documents/cdc-ftularemia.pdf
33. Ellis J, Oyston PCF, Green M, Titball RW. Tularemia. Clin Microbiol Rev. 2002;15:631–46. https://doi.org/10.1128/CMR.15.4.631-646.2002
34. Petersen JM, Schriefer ME, Gage KL, Montenieri JA, Carter LG, Stanley M, et al. Methods for enhanced culture recovery of *Francisella tularensis*. Appl Environ Microbiol. 2004;70:3733–5. https://doi.org/10.1128/AEM.70.6.3733-3735.2004
35. Karatuna O, Celebi B, Can S, Akyar I, Kilic S. The use of Matrix-assisted laser desorption ionization-time of flight

mass spectrometry in the identification of *Francisella tularensis*. Bosn J Basic Med Sci. 2016;16:132–8.
36. López-Ramos I, Hernández M, Rodríguez-Lázaro D, Gutiérrez MP, Zarzosa P, Orduña A, et al. Quick identification and epidemiological characterization of *Francisella tularensis* by MALDI-TOF mass spectrometry. J Microbiol Methods. 2020;177:106055. https://doi.org/10.1016/j.mimet.2020.106055
37. Regoui S, Hennebique A, Girard T, Boisset S, Caspar Y, Maurin M. Optimized MALDI TOF mass spectrometry identification of *Francisella tularensis* Subsp. holarctica. Microorganisms. 2020;8:1143. https://doi.org/10.3390/microorganisms8081143
38. Forsman M, Sandström G, Sjöstedt A. Analysis of 16S ribosomal DNA sequences of *Francisella* strains and utilization for determination of the phylogeny of the genus and for identification of strains by PCR. Int J Syst Evol Microbiol. 1994;44:38–46.
39. Versage JL, Severin DDM, Chu MC, Petersen JM. Development of a multitarget real-time TaqMan PCR assay for enhanced detection of *Francisella tularensis* in complex specimens. J Clin Microbiol. 2003;41:5492–9. https://doi.org/10.1128/JCM.41.12.5492-5499.2003
40. Johansson A, Farlow J, Larsson P, Dukerich M, Chambers E, Byström M, et al. Worldwide genetic relationships among *Francisella tularensis* isolates determined by multiple-locus variable-number tandem repeat analysis. J Bacteriol. 2004;186:5808–18. https://doi.org/10.1128/JB.186.17.5808-5818.2004
41. Osmon DR, Berbari EF, Berendt AR, Lew D, Zimmerli W, Steckelberg JM, et al.; Infectious Diseases Society of America. Diagnosis and management of prosthetic joint infection: clinical practice guidelines by the Infectious Diseases Society of America. Clin Infect Dis. 2013;56:e1–25. https://doi.org/10.1093/cid/cis803
42. Tande AJ, Gomez-Urena EO, Berbari EF, Osmon DR. Management of prosthetic joint infection. Infect Dis Clin North Am. 2017;31:237–52. https://doi.org/10.1016/j.idc.2017.01.009
43. Hepburn MJ, Simpson AJH. Tularemia: current diagnosis and treatment options. Expert Rev Anti Infect Ther. 2008;6:231–40. https://doi.org/10.1586/14787210.6.2.231
44. Bossi P, Tegnell A, Baka A, van Loock F, Werner A, Hendriks J, et al. Bichat guidelines for the clinical management of tularaemia and bioterrorism-related tularaemia. Euro Surveill. 2004;9:27–8. https://doi.org/10.2807/esm.09.12.00503-en
45. Thabit AK, Fatani DF, Bamakhrama MS, Barnawi OA, Basudan LO, Alhejaili SF. Antibiotic penetration into bone and joints: an updated review. Int J Infect Dis. 2019;81:128–36. https://doi.org/10.1016/j.ijid.2019.02.005

Address for correspondence: Yvan Caspar, Laboratoire de Bactériologie-Hygiène hospitalière, Centre National de Référence des *Francisella,* Centre Hospitalier Universitaire Grenoble Alpes, Grenoble, CS10217 38043 CEDEX, France; email: ycaspar@chu-grenoble.fr

etymologia revisited

Originally published in March 2019

Streptomycin

strep'to-mi'sin

In the late 1930s, Selman Waksman, a soil microbiologist working at the New Jersey Agricultural Station of Rutgers University, began a large-scale program to screen soil bacteria for antimicrobial activity. By 1943, Albert Schatz, a PhD student working in Waksman's laboratory, had isolated streptomycin from *Streptomyces griseus* (from the Greek *strepto-* ["twisted"] + *mykēs* ["fungus"] and the Latin *griseus*, "gray").

In 1944, Willam H. Feldman and H. Corwin Hinshaw at the Mayo Clinic showed its efficacy against *Mycobacterium tuberculosis*. Waksman was awarded a Nobel Prize in 1952 for his discovery of streptomycin, although much of the credit for the discovery has since been ascribed to Schatz. Schatz later successfully sued to be legally recognized as a co-discoverer of streptomycin.

References:

1. Comroe JH Jr. Pay dirt: the story of streptomycin. Part I. From Waksman to Waksman. Am Rev Respir Dis. 1978;117:773–81.
2. Wainwright M. Streptomycin: discovery and resultant controversy. Hist Philos Life Sci. 1991;13:97–124.

https://wwwnc.cdc.gov/eid/article/25/3/et-2503_article

Neurologic Complications of Babesiosis, United States, 2011–2021

Sara Locke,[1] Jane O'Bryan,[1] Adeel S. Zubair, Melissa Rethana, Anne Spichler Moffarah, Peter J. Krause,[2] Shelli F. Farhadian[2]

Medscape CME Activity

In support of improving patient care, this activity has been planned and implemented by Medscape, LLC and Emerging Infectious Diseases. Medscape, LLC is jointly accredited with commendation by the Accreditation Council for Continuing Medical Education (ACCME), the Accreditation Council for Pharmacy Education (ACPE), and the American Nurses Credentialing Center (ANCC), to provide continuing education for the healthcare team.

Medscape, LLC designates this Journal-based CME activity for a maximum of 1.00 ***AMA PRA Category 1 Credit(s)™***. Physicians should claim only the credit commensurate with the extent of their participation in the activity.

Successful completion of this CME activity, which includes participation in the evaluation component, enables the participant to earn up to 1.0 MOC points in the American Board of Internal Medicine's (ABIM) Maintenance of Certification (MOC) program. Participants will earn MOC points equivalent to the amount of CME credits claimed for the activity. It is the CME activity provider's responsibility to submit participant completion information to ACCME for the purpose of granting ABIM MOC credit.

All other clinicians completing this activity will be issued a certificate of participation. To participate in this journal CME activity: (1) review the learning objectives and author disclosures; (2) study the education content; (3) take the post-test with a 75% minimum passing score and complete the evaluation at http://www.medscape.org/journal/eid; and (4) view/print certificate. For CME questions, see page 1296.

NOTE: It is Medscape's policy to avoid the use of Brand names in accredited activities. However, in an effort to be as clear as possible, the use of brand names should not be viewed as a promotion of any brand or as an endorsement by Medscape of specific products.

Release date: May 19, 2023; Expiration date: May 19, 2024

Learning Objectives

Upon completion of this activity, participants will be able to:

- Assess the type and frequency of neurologic complications of babesiosis, on the basis of a record review of all adult patients admitted to Yale-New Haven Hospital from January 2011 to October 2021 for laboratory-confirmed babesiosis
- Evaluate the risk factors predisposing patients to neurologic complications of babesiosis and outcomes, on the basis of a record review of all adult patients admitted to Yale-New Haven Hospital from January 2011 to October 2021 for laboratory-confirmed babesiosis
- Determine the clinical implications of the type and frequency of neurologic complications of babesiosis and risk factors predisposing patients to neurologic complications, on the basis of a record review of all adult patients admitted to Yale-New Haven Hospital from January 2011 to October 2021 for laboratory-confirmed babesiosis.

CME Editor

Cheryl Salerno, BA, Technical Writer/Editor, Emerging Infectious Diseases. *Disclosure: Cheryl Salerno, BA, has no relevant financial relationships.*

CME Author

Laurie Barclay, MD, freelance writer and reviewer, Medscape, LLC. *Disclosure: Laurie Barclay, MD, has no relevant financial relationships.*

Authors

Sara Locke, BA; Jane O'Bryan, MPH; Adeel S. Zubair, MD; Melissa Rethana, MD; Anne Spichler-Moffarah, MD, PhD; Peter J. Krause, MD; and ***Shelli F. Farhadian, MD, PhD.***

Author affiliations: Yale School of Medicine, New Haven, Connecticut, USA (S. Locke, J. O'Bryan, A.S. Zubair, M. Rethana, A. Spichler Moffarah, P.J. Krause, S.F. Farhadian); Frank H. Netter MD School of Medicine at Quinnipiac University, North Haven, Connecticut, USA (J. O'Bryan); Yale School of Public Health, New Haven (P.J. Krause, S.F. Farhadian).

DOI: http://doi.org/10.3201/eid2906.221890

[1]These first authors contributed equally to this article.

[2]These senior authors contributed equally to this article.

Babesiosis is a globally distributed parasitic infection caused by intraerythrocytic protozoa. The full spectrum of neurologic symptoms, the underlying neuropathophysiology, and neurologic risk factors are poorly understood. Our study sought to describe the type and frequency of neurologic complications of babesiosis in a group of hospitalized patients and assess risk factors that might predispose patients to neurologic complications. We reviewed medical records of adult patients who were admitted to Yale-New Haven Hospital, New Haven, Connecticut, USA, during January 2011–October 2021 with laboratory-confirmed babesiosis. More than half of the 163 patients experienced ≥1 neurologic symptoms during their hospital admissions. The most frequent symptoms were headache, confusion/delirium, and impaired consciousness. Neurologic symptoms were associated with high-grade parasitemia, renal failure, and history of diabetes mellitus. Clinicians working in endemic areas should recognize the range of symptoms associated with babesiosis, including neurologic.

Babesiosis is an emerging parasitic infection with global distribution. The infection is caused by intraerythrocytic protozoa of the genus *Babesia*. During the past 2 decades, the incidence of babesiosis has increased, particularly in the northeastern and northern midwestern United States. The Centers for Disease Control and Prevention reported an increased babesiosis incidence in Connecticut, USA, from 2011 (2.1 cases/100,000 persons) to 2019 (9 cases/100,000 persons), more than 10 times the incidence reported nationally during that time period (*1*). More than 100 species of *Babesia* have been described in wild and domestic animals. The predominant species causing human disease in the United States is *B. microti* (*1*–*3*). The disease is transmitted primarily through the bite of an infected ixodid tick, which is capable of transmitting several pathogens at the same time, including *Borrelia burgdorferi*, the cause of Lyme disease (*2*–*5*). Babesiosis is less commonly transmitted via blood transfusion, organ transplantation, or through the placenta (*2*,*3*,*6*).

Although most persons with babesiosis experience nonspecific influenza-like symptoms, more severe and prolonged disease can occur in persons >50 years of age; those who are immunocompromised due to asplenia, cancer, or HIV/AIDS or who are receiving immunosuppressive drugs; and those who have chronic heart, lung, renal, or liver disease (*2*,*7*,*8*). Severe infection is associated with high-grade parasitemia and organ failure (e.g., acute respiratory distress syndrome, congestive heart failure, severe hemolytic anemia, or renal failure) and death (*2*,*8*–*11*). Little has been published about babesiosis-induced central nervous system dysfunction (*12*,*13*). Neurologic complications include headache, syncope, neuropathy, retinal nerve infarcts, and altered state of consciousness (*9*,*12*,*14*–*20*). The full spectrum of neurologic complications and underlying pathophysiology are poorly understood, as are factors that predispose patients to neurologic complications.

We conducted this study to investigate the type and frequency of neurologic complications of babesiosis in a group of hospitalized patients and to assess risk factors that predispose patients to neurologic complications. We hypothesized that patients with a diagnosis of babesiosis commonly experience neurologic system manifestations and that those symptoms are most frequent in patients with severe babesiosis. Accordingly, we conducted a retrospective medical record review of all adult patients admitted to Yale-New Haven Hospital (YNHH) in New Haven, Connecticut, USA, during 2011–2021 with laboratory-confirmed babesiosis.

Methods

Design and Setting

The sample population included all adult patients (≥18 years of age) admitted to YNHH during January 2011–October 2021 with a diagnosis of babesiosis. Patients were required to have *Babesia* parasites present on thin blood smear or amplification of *B. microti* DNA by PCR to be included. Eligible patients were identified in collaboration with the Yale Center for Clinical Investigation Joint Data Analytics Team.

Data Collection

We obtained approval for study procedures from the Yale University Human Investigation Committee before data collection (HIC protocol #2000030420). We performed comprehensive medical record reviews and systematically abstracted study variables by using a standardized medical questionnaire (*21*). We recorded demographic and clinical variables, including the following underlying conditions and comorbidities: chronic cardiac, pulmonary, renal, or hepatic conditions; dementia; diabetes mellitus; hypertension; malignancy; migraine; seizure; stroke; and immunocompromised status.

We recorded all neurologic symptoms and complications documented at the time of hospital admission: acute cerebrovascular disease, acute syncope, ataxia/gait disturbance, confusion/delirium, facial droop, focal weakness, headache, impaired consciousness, nerve pain, tremor, language deficit, vision impairment, vertigo, and seizure. The neurologic

symptoms and complications we recorded were then independently confirmed by 2 neurologists. We defined confusion/delirium as a deficit in mental status characterized by disorientation, bewilderment, or difficulty following commands (*22*). We categorized impaired consciousness (i.e., diminished arousal and response to stimulation) on the basis of severity using the Glasgow Coma Scale, classifying symptoms as either lethargy, obtundation, stupor, or coma (*23*). Lethargy is a mild reduction in alertness, obtundation is a moderate reduction in alertness, stupor is a condition of deep sleep in which the patient can only be aroused by vigorous external stimulation, and coma refers to a complete lack of motor response to any stimuli from the external environment (*23*,*24*).

We abstracted key laboratory variables related to the severity of infection. We computed median laboratory values and interquartile ranges (IQRs) on the basis of either the recorded minimum or maximum laboratory value, as appropriate. Laboratory parameters included peak parasitemia, minimum hematocrit and platelet count, and maximum blood urea nitrogen, creatinine, aspartate aminotransferase and alanine aminotransferase. We calculated glomerular filtration rate by using the 2021 Chronic Kidney Disease Epidemiology Collaboration equation (*25*).

Statistical Analysis

We performed statistical analyses by using SAS Studio 3.8 (SAS Institute Inc.). We summarized demographic characteristics of the sample by using appropriate descriptive statistics. We categorized patients according to peak parasitemia (group 1, <1.0%; group 2, 1.0% −10.0%; group 3, >10.0%) (Table 1). For patients with peak thin blood smear results reported as <1%, we used a value of 0.9% in calculations. We compared those subgroups to determine if neurologic manifestations were more frequent in patients with high parasitemia. Given the nonparametric distribution of those data, we reported medians and IQRs for hematologic, hepatic, and renal function laboratory tests. We used Wilcoxon 2-sample tests to compare laboratory results among patients with and without the most common neurologic symptoms.

To represent the distribution density of neurologic symptoms by peak parasitemia, we used Prism 9 software (GraphPad Software) to generate violin plots. We analyzed the relationship between peak parasitemia and each reported neurologic symptom by using Mann-Whitney U tests for continuous variables.

We used univariate logistic regression models to test associations between comorbid conditions and the 3 most common neurologic symptoms: headache, confusion/delirium, and impaired consciousness. We noted variables that were significant in unadjusted univariate analysis and entered them into a multivariate model for each neurologic symptom. We set the significance level for univariate and multivariate analysis to $p<0.05$.

Results

Demographic and Clinical Characteristics

We identified a total of 163 hospitalized patients with laboratory-confirmed babesiosis during the study period (January 2011–October 2021**)**. The median age was 67 years (IQR 45–89; range 30–93). Most patients were male (n = 104 [63.8%]). The study population was predominately White or Caucasian (n = 118 [74.7%]). Most patients (n = 160 [98.2%]) were diagnosed with babesiosis by a blood smear positive for intra-erythrocytic organisms that were consistent with *Babesia*. Three patients were diagnosed with babesiosis on the basis of a positive PCR blood specimen in the context of an appropriate acute clinical syndrome. Most patients (n = 117 [71.8%]) had ≥1 medical comorbidity at admission. The most common comorbidities were

Table 1. Neurologic symptoms during hospital admissions for babesiosis in patients admitted to Yale-New Haven Hospital, New Haven, Connecticut, USA, January 2011–October 2021*

Neurologic symptom	No. (%) patients	Peak parasitemia, no. (%) patients			p value
		<1.0%, n = 45	1.0%–10.0%, n = 81	>10.0%, n = 37	
Headache	52 (31.9)	14 (31.1)	28 (34.6)	10 (27.0)	0.711
Confusion/delirium	27 (16.6)	2 (4.4)	13 (16.1)	12 (32.4)	**0.003**
Impaired consciousness	24 (14.7)	4 (8.9)	9 (11.1)	11 (29.7)	**0.018**
Ataxia/gait disorder	17 (10.4)	3 (6.7)	10 (12.4)	4 (10.8)	0.632
Vision impairment	10 (6.1)	5 (11.1)	4 (4.9)	1 (2.7)	0.266
Acute syncope	6 (3.7)	2 (4.4)	4 (4.9)	0 (0.0)	0.482
Language deficit	5 (3.1)	0 (0.0)	5 (6.2)	0 (0.0)	0.106
Nerve pain	4 (2.5)	1 (2.2)	2 (2.5)	1 (2.7)	1.000
Focal weakness	3 (1.8)	1 (2.2)	1 (1.2)	1 (2.7)	0.794
Tremor	3 (1.8)	1 (2.2)	2 (2.5)	0 (0.0)	1.000
Seizure	2 (1.3)	1 (2.2)	0 (0.0)	1 (2.7)	0.252

*Total sample (n = 163); Column percentages do not sum to 100% due to many patients being affected by multiple neurologic conditions throughout hospitalization. Boldface type indicates statistical significance.

hypertension (n = 82 [50.3%]), immunodeficiency (n = 40 [24.5%]), and cardiac disorder (n = 39 [23.9%]). Most of the immunodeficient patients (n = 21 [52.5%]) were asplenic. Other comorbid conditions included diabetes (n = 23 [14.1%]), stroke (n = 13 [8.0%]), chronic kidney disease (n = 8 [4.9%]), migraine (n = 4 [2.5%]), dementia (n = 3 [1.84%]), and seizure disorder (n = 2 [1.2%]). Twelve patients (7.4%) had erythema migrans rash, indicating active co-infection with Lyme disease.

Neurologic Symptoms of Babesiosis

We recorded the frequency of neurologic symptoms experienced by patients admitted to YNHH for babesiosis (Table 1). More than half (n = 97 [59.5%]) experienced ≥1 neurologic symptoms. The most frequent symptoms were headache (n = 52 [31.9%]), confusion/delirium (n = 27 [16.6%]), impaired consciousness (n = 24 [14.7%]), ataxia/gait disorder (n = 17 [10.4%]), and vision impairment (n = 10 [6.1%]). Patients noted to have impaired consciousness were 20 (12.3%) classified as lethargic, 3 (1.8%) as obtunded, and 1 (0.6%) as stuporous.

Confusion/Delirium and Parasitemia

Although we found no association between the degree of parasitemia and the presence of any neurologic symptoms, patients with confusion/delirium and impaired consciousness were significantly more likely to have a higher peak parasitemia than those without these symptoms (Figure). All 163 hospitalized patients were stratified by peak parasitemia into 3 groups: peak parasitemia of <1% (n = 45), peak parasitemia of 1.0%–10% (n = 81), and peak parasitemia of >10% (n = 37). The 27 patients with confusion/delirium were also stratified into the peak parasitemia groups. Among the 45 patients with a peak parasitemia <1%, 2 (4.4%) patients experienced confusion/delirium. Among the 81 patients with a peak parasitemia of 1.0%–10%, 13 (16.1%) experienced confusion/delirium. Among the 37 patients with a peak parasitemia of >10%, 12 (32.4%) experienced confusion/delirium (Table 1). The median peak parasitemia of the patients who experienced confusion/delirium was significantly higher than that of the patients who did not experience confusion/delirium (p = 0.001) (Figure). Those findings indicate that as parasitemia increases, so does the prevalence of confusion/delirium.

Impaired Consciousness and Parasitemia

We found a significant association between peak parasitemia and impaired consciousness (p<0.005). Of the 163 hospitalized patients, 14.7% experienced impaired consciousness at the time of hospital admission. When we stratified by peak parasitemia groups, we observed impaired consciousness in 4 (8.9%) of the group with the lowest (<1%) peak parasitemia, 9 (11.1%) of the group with mid (1.0%–10%) peak parasitemia, and 11 (29.7%) of those in the group with the highest (>10%) peak parasitemia. That distribution was similar to that of patients with confusion/delirium. Patients with impaired consciousness (of any degree) had a higher median peak parasitemia than those without impaired consciousness (p = 0.014) (Figure).

Ophthalmologic Symptoms

Ten (6.1%) patients reported transient vision impairment, one of whom was formally evaluated by the ophthalmology department after reportedly seeing different colored lights and shapes when she closed her eyes. Ophthalmologic examination revealed no evidence of ocular infection or inflammation.

Neuroimaging Findings

Thirty-three (20.2%) of the hospitalized patients underwent neuroimaging with cranial computerized tomography (n = 28), brain magnetic resonance imaging (n = 7), or electroencephalogram (n = 2) (Table 2). Only 2 patients had acute abnormalities seen on neuroimaging, 1 with ischemic stroke and 1 with subarachnoid hemorrhage. The patient who suffered a stroke had fever, malaise, and anemia; an episode of expressive aphasia during an acute babesiosis episode resulting from a small, left-middle cerebral artery stroke, confirmed on imaging to be secondary to high-grade internal carotid artery stenosis. The patient with a subarachnoid hemorrhage had confusion and jaundice and was in critical condition because of multiorgan failure, including respiratory, kidney, and liver failure, and disseminated intravascular coagulation. Computed tomography revealed subarachnoid hemorrhage, most conspicuous within the left frontal lobe. Most other patients who underwent neuroimaging had nonspecific white matter changes and some element of volume loss, which were considered to be related to chronic disease and aging. Electroencephalograms results were unremarkable for both patients who underwent this examination.

Laboratory Findings

We assessed laboratory measures of hematologic, hepatic, and renal function among patients with the most frequently reported neurologic symptoms: headache, confusion/delirium, and impaired consciousness.

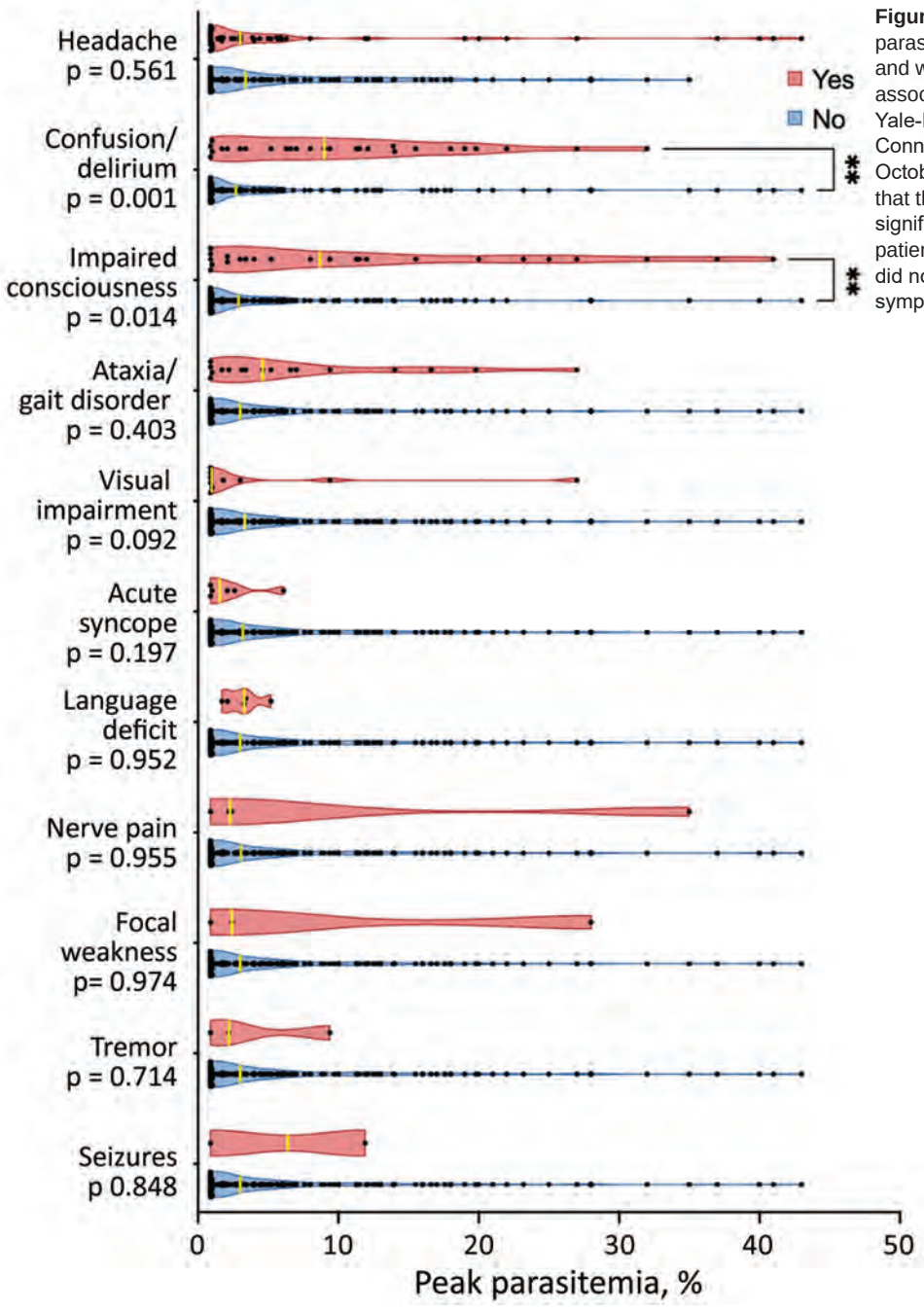

Figure. Violin plot depicting the peak parasitemia distribution in patients with and without select neurologic symptoms associated with babesiosis admitted to Yale-New Haven Hospital, New Haven, Connecticut, USA, January 2011–October 2021. Asterisks (**) indicate that the median peak parasitemia significantly differed between the patients who did and the patients who did not experience the specific symptom ($p<0.05$).

Anemia was common in the overall sample population. Median hematocrit was 26.7% for male patients (reference range 40%–52%) and 25% for female patients (reference range 37%–53%). Patients with impaired consciousness had a lower hematocrit than did those without impaired consciousness (23.6% vs. 26.4%; p = 0.024) (Table 3). Patients with confusion/delirium and those with impaired consciousness had significantly higher median blood urea nitrogen and creatinine values and significantly lower glomerular filtration rate compared with patients without these symptoms (Table 3).

Six patients underwent lumbar puncture during hospital admission. The indications for lumbar puncture were headache (n = 2), confusion (n = 2), unresponsive state (n = 1), and confusion with bilateral hearing loss (n = 1). None of those patients were found to have a pleocytosis (i.e., all had cerebrospinal fluid [CSF] leukocyte counts <5 cells/μL). One patient had slightly elevated CSF protein (82 g/dL);

Table 2. Imaging indications and findings in patients with neurologic symptoms associated with babesiosis admitted to Yale-New Haven Hospital, New Haven, Connecticut, USA, January 2011–October 2021*

Imaging	No. (%) patients
Neuroimaging modality	
Computed tomography	28 (17.2)
Magnetic resonance imaging	7 (4.3)
Electroencephalogram	2 (1.2)
Indication	
Altered mental status/confusion	15 (9.2)
Headache	8 (4.9)
Fever	5 (3.1)
Evaluate CNS abnormalities	3 (1.8)
Weakness	3 (1.8)
Dizziness	1 (0.6)
Dysphagia, slurred speech	1 (0.6)
Fall	1 (0.6)
Head injury	1 (0.6)
Visual changes	1 (0.6)
Syncope	1 (0.6)
Numbness	1 (0.6)
Fatigue	1 (0.6)
Seizure	1 (0.6)
Findings	
Nonspecific white matter changes	23 (14.1)
Volume loss	14 (8.6)
Acute changes	2 (1.2)
Evidence of previous stroke	3 (1.8)

*Total sample consisted of 163 patients. Neuroimaging modalities and indications sum to >33 because some patients received multiple imaging modalities or had multiple indications. CNS, central nervous system.

CSF parameters were otherwise within reference ranges. Five of the 6 patients who underwent lumbar puncture were tested for Lyme antibody in CSF, but results were negative in all cases.

Risk Factors for Neurologic Complications

Univariate logistic regression models tested associations between comorbid conditions and the 3 most common neurologic symptoms: headache, confusion/delirium, and impaired consciousness. In univariate modeling, we found significant associations ($p<0.05$) between hypertension, diabetes mellitus, and stroke/transient ischemic attack and the presence of confusion/delirium during hospital admission. Those same factors were also significantly associated with impaired consciousness in univariate analysis and were entered into multivariate models of the respective complications (Table 4).

Multivariate analysis revealed increased adjusted odds of confusion/delirium (OR 3.04 [95% CI 1.11–8.34]; $p = 0.031$) and impaired consciousness (OR 5.36 [95% CI 1.98–14.48]; $p<0.001$) among patients with diabetes mellitus. There was a significant association between stroke/transient ischemic attack and confusion/delirium in univariate modeling, but the association was nonsignificant in the multivariate model ($p = 0.079$). Patients affected by confusion/delirium or impaired consciousness tended to be older (median age 72.5 years [IQR 55.5–89.5]) compared with patients without these symptoms (median age 66.5 years [IQR 46.5–86.5]) ($p = 0.012$).

Outcomes

The median length of hospital stay was 6.5 (IQR 2.5–10.5) days for patients with confusion/delirium or impaired consciousness compared with 5 (IQR 2–8) days for those without those symptoms ($p = 0.019$). A greater percentage of patients with those symptoms were admitted to the intensive care unit (55.3% vs. 44.7%; $p = 0.002$). Four (2.5%) of the 163 patients in the study group died during hospitalization. Among those 4 patients, 2 had neurologic complications. One experienced ataxia/gait disturbance, confusion/delirium, impaired consciousness, tremor, and vision impairment. The other patient experienced confusion/delirium and impaired consciousness.

Discussion

More than half (59.5%) of the 163 patients admitted to YNHH with babesiosis had ≥1 neurologic complication. Confusion/delirium and impaired consciousness were the 2 most common severe neurologic complications among our study patients. Other severe neurologic symptoms, including seizure or stroke, were seldom reported. Confusion/delirium and impaired consciousness were significantly associated with high peak parasitemia ($p<0.005$) and with markers of renal injury. We also found that the prevalences of confusion/delirium and of impaired consciousness were greater in patients with diabetes mellitus. Although Lyme disease can cause several neurologic complications, including confusion/delirium and impaired consciousness, less than one tenth of patients hospitalized for babesiosis had an erythema migrans rash. We found no relationship between babesiosis–Lyme disease co-infection and prevalence of neurologic complications (*26*–*28*).

The etiology of *Babesia*-associated neurologic symptoms is unknown. Central nervous system complications observed in *B. bovis* in cattle and *B. canis* in dogs are thought to be caused by erythrocyte, platelet, and leukocyte cytoadherence to vascular endothelium with vascular obstruction, excessive proinflammatory cytokine activation associated with high parasitemia, or both (*12*,*29*–*32*). One of the patients in our study had an acute left-middle cerebral artery stroke consistent with vascular obstruction; however, a direct link between stroke and this parasitic infection cannot

Table 3. Laboratory result comparisons by neurologic symptoms in patients with babesiosis admitted to Yale-New Haven Hospital, New Haven, Connecticut, USA, January 2011–October 2021*

Laboratory result, median (IQR)	Reference range	Headache			Confusion/delirium			Impaired consciousness		
		Yes, n = 52	No, n = 111	p value†	Yes, n = 27	No, n = 136	p value†	Yes, n = 24	No, n = 139	p value†
Hematologic function										
Lowest hematocrit	M, 40%–52%; F, 37%–53%	25.9 (16.2–35.6)	26.0 (19.4–32.6)	0.581	24.0 (16.5–31.5)	26.4 (18.8–34)	0.088	23.6 (15.7–31.5)	26.4 (18.9–33.9)	0.024
Lowest platelet count	150–400 × 10^9/L	78.5 (4.0–153.0)	82.0 (23.0–141.0)	0.881	68.0 (1.0–135.0)	82.0 (–5.0 to 230.0)	0.339	59.5 (–5.0 to 124.0)	84.0 (17.0–151.0)	0.084
Hepatic function										
Highest AST	3–40 U/L	66.0 (25.5–106.5)	76.0 (38.0–114.0)	0.277	76.0 (42.0–110.0)	75.5 (32.5–118.5)	0.813	81.0 (48.0–114.0)	75.0 (33.0–117.0)	0.909
Highest ALT	3–40 U/L	61.0 (10.0–112.0)	63.0 (9.0–117.0)	0.809	54.0 (8.0–100.0)	63.5 (12.5–114.5)	0.568	49.0 (4.0–102.0)	63.0 (13.0–113.0)	0.441
Renal function										
Highest BUN	7–20 mg/dL	17.0 (4.5–29.5)	24.0 (5.0–43.0)	**0.002**	31.0 (–3.0 to 65.0)	20.0 (5.5–34.5)	0.025	33.0 (0.0–66.0)	20.0 (5.0–35.0)	**0.005**
Highest creatinine	0.5–1.2 mg/dL	1.00 (0.96–1.40)	1.1 (0.3–1.9)	0.091	1.5 (0.7–2.3)	1.0 (0.5–1.5)	**<0.001**	1.5 (0.3–2.7)	1.0 (0.5–1.5)	**0.002**
Lowest GFR	≥60 mL/min	76.0 (37.5–114.5)	67.0 (21.0–113.0)	**0.007**	46.0 (3.0–89.0)	73.0 (33.5–112.5)	**<0.001**	47.0 (1.0–93.0)	73.0 (33.0–113.0)	**0.003**

*Boldface indicates significance. ALT, alanine transaminase; AST, aspartate transaminase; BUN, blood urea nitrogen; GFR, glomerular filtration rate; IQR, interquartile range.
†By Wilcoxon 2-sample test.

be established with a single case. Retinopathy has been documented in both cerebral malaria and babesiosis and is thought to be the result of vascular obstruction in the brain and retina (*33*–*35*).

We noted an association between renal impairment (defined by elevated blood urea nitrogen and creatinine and low glomerular filtration rate) and patients who experienced confusion/delirium or impaired consciousness. Confusion/delirium and impaired consciousness may be a direct result of impaired renal function (i.e., secondary to uremia). Alternatively, those neurologic symptoms and renal impairment might be a consequence of a common pathologic mechanism, such as microvascular obstruction from cytoadhering infected erythrocytes or excessive proinflammatory cytokine release. Animal studies likewise have found an association between renal complications and cerebral complications of babesiosis (*31*,*36*–*38*).

Limitations of this study include the retrospective nature of the study design, the lack of histopathologic data, and incomplete access to prehospitalization data, including severity of comorbid conditions and medication use. Our sample size of 163 patients is modest because severe cases of babesiosis requiring hospitalization are uncommon.

Table 4. Associations between comorbid conditions and neurologic symptoms in patients with babesiosis admitted to Yale-New Haven Hospital, New Haven, Connecticut, USA, January 2011–October 2021*

Comorbid condition	Confusion/ delirium, no. (%)	Adjusted odds of confusion/delirium		Impaired consciousness, no. (%)	Adjusted odds of impaired consciousness	
		OR (95% CI)	p value		OR (95% CI)	p value
Diabetes mellitus						
No	140 (13.6)	1.00		140 (10.7)		
Yes	23 (34.8)	3.04 (1.11–8.34)	**0.031**	23 (39.1)	5.36 (1.98–14.48)	**<0.001**
Stroke/transient ischemic attack						
No	150 (14.7)					
Yes	13 (38.5)	3.06 (0.88–10.66)	0.079			

*Univariate logistic regression models tested associations between the following comorbid conditions and the 3 most frequent neurologic symptoms (headache, confusion/delirium, impaired consciousness): cardiac disorder, hypertension, diabetes mellitus, immunocompromised status, stroke/transient ischemic attack, obesity, chronic kidney disease, migraine, and malignancy. Variables that were significant in unadjusted univariate analysis were entered into a multivariate model for each neurologic symptom. The significance level for univariate and multivariate analysis was set to p<0.05.
Boldface indicates statistical significance.

This study cohort reflects the clinical manifestations of babesiosis patients who experienced severe infection that required hospitalization and, as such, the results may not be directly applicable to all patients with babesiosis. Neurologic symptom severity scores were not available, and duration of symptoms after discharge is unknown, although most patients had cleared or improved neurologic symptoms by the time of discharge. The long-term outcomes of neurologic complications of babesiosis warrant further research.

The lack of histopathologic data limits the specificity of our findings. Patients with severe infections other than babesiosis may also experience many of the neurologic complications described in this study. Regarding the patients we studied, it is challenging to delineate whether signs and symptoms were part of the typical course of systemic infection, were worsened by the presence of babesiosis, or were characteristic of the babesiosis agent itself. Despite those limitations, this study provides a baseline description of the prevalence of neurologic complications of babesiosis.

In conclusion, more than half of the patients admitted to YNHH from January 2011–October 2021 for acute babesiosis experienced ≥1 neurologic complication. Confusion/delirium and impaired consciousness were each significantly associated with peak parasitemia, renal impairment, and preexisting diabetes mellitus. Further research is needed to clarify the pathogenesis of neurologic manifestations of babesiosis and determine possible long-term neurologic sequelae. Clinicians caring for patients in endemic areas should be aware that babesiosis can manifest with a range of symptoms, including neurologic.

This work was supported by the National Institute of Mental Health and the National Institute on Aging of the National Institutes of Health (K23 MH118999 and T35 AG049685); the Llura A. Gund Laboratory for Vector-borne Diseases; and the Gordon and Llura Gund Foundation. The content is solely the responsibility of the authors and does not necessarily represent the official views of the National Institutes of Health.

P.J.K. is on the board of the American Lyme Disease Foundation, for which he receives no remuneration, and coauthored a chapter on babesiosis in UpToDate. All other authors report no potential conflicts.

About the Author

Ms. Locke is a second-year medical student at Yale School of Medicine, New Haven, Connecticut. She is interested in the epidemiology of vector-borne diseases.

References

1. Centers for Disease Control and Prevention. Surveillance for babesiosis—United States, 2019 Annual Summary. Atlanta: The Centers; 2021 [cited 2023 Mar 17]. https://www.cdc.gov/parasites/babesiosis/resources/Surveillance_Babesiosis_US_2019.pdf
2. Vannier E, Krause PJ. Human babesiosis. N Engl J Med. 2012;366:2397–407. https://doi.org/10.1056/NEJMra1202018
3. Herwaldt BL, Linden JV, Bosserman E, Young C, Olkowska D, Wilson M. Transfusion-associated babesiosis in the United States: a description of cases. Ann Intern Med. 2011; 155:509–19. https://doi.org/10.7326/0003-4819-155-8-201110180-00362
4. Knapp KL, Rice NA. Human coinfection with *Borrelia burgdorferi* and *Babesia microti* in the United States. J Parasitol Res. 2015;2015:587131. https://doi.org/10.1155/2015/587131
5. Diuk-Wasser MA, Vannier E, Krause PJ. Coinfection by *Ixodes* tick-borne pathogens: Ecological, epidemiological, and clinical consequences. Trends Parasitol. 2016;32:30–42. https://doi.org/10.1016/j.pt.2015.09.008
6. Fox LM, Wingerter S, Ahmed A, Arnold A, Chou J, Rhein L, et al. Neonatal babesiosis: case report and review of the literature. Pediatr Infect Dis J. 2006;25:169–73. https://doi.org/10.1097/01.inf.0000195438.09628.b0
7. Krause PJ, Gewurz BE, Hill D, Marty FM, Vannier E, Foppa IM, et al. Persistent and relapsing babesiosis in immunocompromised patients. Clin Infect Dis. 2008;46:370–6. https://doi.org/10.1086/525852
8. Akel T, Mobarakai N. Hematologic manifestations of babesiosis. Ann Clin Microbiol Antimicrob. 2017;16:6. https://doi.org/10.1186/s12941-017-0179-z
9. Hatcher JC, Greenberg PD, Antique J, Jimenez-Lucho VE. Severe babesiosis in Long Island: review of 34 cases and their complications. Clin Infect Dis. 2001;32:1117–25. https://doi.org/10.1086/319742
10. Krause PJ, Auwaerter PG, Bannuru RR, Branda JA, Falck-Ytter YT, Lantos PM, et al. Clinical practice guidelines by the Infectious Diseases Society of America (IDSA): 2020 guideline on diagnosis and management of babesiosis. Clin Infect Dis. 2021;72:185–9. https://doi.org/10.1093/cid/ciab050
11. Vannier EG, Diuk-Wasser MA, Ben Mamoun C, Krause PJ. Babesiosis. Infect Dis Clin North Am. 2015;29:357–70. https://doi.org/10.1016/j.idc.2015.02.008
12 Usmani-Brown S, Halperin JJ, Krause PJ. Neurological manifestations of human babesiosis. Handb Clin Neurol. 2013;114:199–203. https://doi.org/10.1016/B978-0-444-53490-3.00014-5
13. Bradshaw MJ, Bloch KC. Tick-borne infections of the central nervous system. In: Hasbun R, Bloch KC, Bhimraj MDA, editors. Neurological complications of infectious diseases. Cham: Springer International Publishing; 2021. p. 325–49.
14. Ortiz JF, Millhouse PW, Morillo Cox Á, Campoverde L, Kaur A, Wirth M, et al. Babesiosis: Appreciating the pathophysiology and diverse sequela of the infection. Cureus. 2020;12:e11085. https://doi.org/10.7759/cureus.11085
15. Sun T, Tenenbaum MJ, Greenspan J, Teichberg S, Wang RT, Degnan T, et al. Morphologic and clinical observations in human infection with *Babesia microti.* J Infect Dis. 1983;148:239–48. https://doi.org/10.1093/infdis/148.2.239
16. Venigalla T, Adekayode C, Doreswamy S, Al-Sudani H, Sekhar S. Atypical presentation of babesiosis with neurological manifestations as well as hematological

manifestations. Cureus. 2022;14:e26811. https://doi.org/10.7759/cureus.26811
17. Ruebush TK II, Cassaday PB, Marsh HJ, Lisker SA, Voorhees DB, Mahoney EB, et al. Human babesiosis on Nantucket Island. Clinical features. Ann Intern Med. 1977;86:6–9. https://doi.org/10.7326/0003-4819-86-1-6
18 Maxwell SP, Brooks C, McNeely CL, Thomas KC. Neurological pain, psychological symptoms, and diagnostic struggles among patients with tick-borne diseases. Healthcare (Basel). 2022;10:1178. https://doi.org/10.3390/healthcare10071178
19. Oleson CV, Sivalingam JJ, O'Neill BJ, Staas WE Jr. Transverse myelitis secondary to coexistent Lyme disease and babesiosis. J Spinal Cord Med. 2003;26:168–71. https://doi.org/10.1080/10790268.2003.11754578
20. Reese M, Maru D. Unexplained recurrent fevers and the importance of inquiring about occupation: a case report. The Medicine Forum. 2016. https://doi.org/10.29046/TMF.017.1.012
21. Krause PJ, McKay K, Thompson CA, Sikand VK, Lentz R, Lepore T, et al.; Deer-Associated Infection Study Group. Disease-specific diagnosis of coinfecting tickborne zoonoses: babesiosis, human granulocytic ehrlichiosis, and Lyme disease. Clin Infect Dis. 2002;34:1184–91. https://doi.org/10.1086/339813
22. Walker HK. The origins of the history and physical examination. In: Walker HK, Hall WD, Hurst JW, editors. Clinical methods: the history, physical, and laboratory examinations. Boston: Butterworths; 1990.
23. Teasdale G, Jennett B. Assessment of coma and impaired consciousness. A practical scale. Lancet. 1974;304:81–4. https://doi.org/10.1016/S0140-6736(74)91639-0
24. Edwards SL. Using the Glasgow Coma Scale: analysis and limitations. Br J Nurs. 2001;10:92–101. https://doi.org/10.12968/bjon.2001.10.2.5391
25. Inker LA, Eneanya ND, Coresh J, Tighiouart H, Wang D, Sang Y, et al.; Chronic Kidney Disease Epidemiology Collaboration. New creatinine- and cystatin C-based equations to estimate GFR without race. N Engl J Med. 2021;385:1737–49. https://doi.org/10.1056/NEJMoa2102953
26. Halperin JJ. Nervous system Lyme disease—facts and fallacies. Infect Dis Clin North Am. 2022;36:579–92. https://doi.org/10.1016/j.idc.2022.02.007
27. Schwenkenbecher P, Pul R, Wurster U, Conzen J, Pars K, Hartmann H, et al. Common and uncommon neurological manifestations of neuroborreliosis leading to hospitalization. BMC Infect Dis. 2017;17:90. https://doi.org/10.1186/s12879-016-2112-z
28. Mead P. Epidemiology of Lyme disease. Infect Dis Clin North Am. 2022;36:495–521. https://doi.org/10.1016/j.idc.2022.03.004
29. Krause PJ, Daily J, Telford SR, Vannier E, Lantos P, Spielman A. Shared features in the pathobiology of babesiosis and malaria. Trends Parasitol. 2007;23:605–10. https://doi.org/10.1016/j.pt.2007.09.005
30. Puri A, Bajpai S, Meredith S, Aravind L, Krause PJ, Kumar S. Babesia microti: Pathogen genomics, genetic variability, immunodominant antigens, and pathogenesis. Front Microbiol. 2021;12:697669. https://doi.org/10.3389/fmicb.2021.697669
31. Kumar A, Kabra A, Igarashi I, Krause PJ. Animal models of the immunology and pathogenesis of human babesiosis. Trends Parasitol. 2023;39:38–52. https://doi.org/10.1016/j.pt.2022.11.003
32. Allred DR, Al-Khedery B. Antigenic variation and cytoadhesion in *Babesia bovis* and *Plasmodium falciparum*: different logics achieve the same goal. Mol Biochem Parasitol. 2004;134:27–35. https://doi.org/10.1016/j.molbiopara.2003.09.012
33. Maude RJ, Beare NA, Sayeed AA, Chang CC, Charunwatthana P, Faiz MA, et al. The spectrum of retinopathy in adults with *Plasmodium falciparum* malaria. Trans R Soc Trop Med Hyg. 2009;103:665–71. https://doi.org/10.1016/j.trstmh.2009.03.001
34. Ortiz JM, Eagle RC Jr. Ocular findings in human babesiosis (Nantucket fever). Am J Ophthalmol. 1982;93:307–11. https://doi.org/10.1016/0002-9394(82)90530-X
35. Zweifach PH, Shovlin J. Retinal nerve fiber layer infarct in a patient with babesiosis. Am J Ophthalmol. 1991;112:597–8. https://doi.org/10.1016/S0002-9394(14)76867-9
36. de Scally MP, Lobetti RG, Reyers F, Humphris D. Are urea and creatinine values reliable indicators of azotaemia in canine babesiosis? J S Afr Vet Assoc. 2004;75:121–4. https://doi.org/10.4102/jsava.v75i3.466
37. Aikawa M, Pongponratn E, Tegoshi T, Nakamura K, Nagatake T, Cochrane A, et al. A study on the pathogenesis of human cerebral malaria and cerebral babesiosis. Mem Inst Oswaldo Cruz. 1992;87 (Suppl 3):297–301. https://doi.org/10.1590/S0074-02761992000700051
38. Tsuji M, Fujioka H, Arai S, Taniyama H, Ishihara C, Aikawa M. A mouse model for cerebral babesiosis. Parasitol Today. 1996;12:203–5. https://doi.org/10.1016/0169-4758(96)40002-3

Address for correspondence: Shelli Farhadian, Yale School of Medicine, 135 College St, New Haven, CT, USA 06520; email: shelli.farhadian@yale.edu

SARS-CoV-2 Seroprevalence Studies in Pets, Spain

Sandra Barroso-Arévalo, Lidia Sánchez-Morales,
Jose A. Barasona, Lucas Domínguez, José M. Sánchez-Vizcaíno

SARS-CoV-2 can infect domestic animals such as cats and dogs. The zoonotic origin of the disease requires surveillance on animals. Seroprevalence studies are useful tools for detecting previous exposure because the short period of virus shedding in animals makes detection of the virus difficult. We report on an extensive serosurvey on pets in Spain that covered 23 months. We included animals with exposure to SARS-CoV-2–infected persons, random animals, and stray animals in the study. We also evaluated epidemiologic variables such as human accumulated incidence and spatial location. We detected neutralizing antibodies in 3.59% of animals and showed a correlation between COVID-19 incidence in humans and positivity to antibody detection in pets. This study shows that more pets were infected with SARS-CoV-2 than in previous reports based on molecular research, and the findings highlight the need to establish preventive measures to avoid reverse zoonosis events.

Since December 2019, the entire world has experienced the pandemic produced by the novel betacoronavirus SARS-CoV-2. This virus is the causative agent of COVID-19, a severe acute respiratory disease that has resulted in >700 million cases and >6.8 million confirmed deaths (*1*). Although the origin of the virus has not been clarified yet, it is thought to have originated from an animal reservoir and subsequently been transmitted to humans by a direct spillover event (*2*–*4*). Moreover, as the pandemic has progressed, numerous cases of natural SARS-CoV-2 infection have been reported in different animal species, such as minks, cats, dogs, ferrets, nonhuman primates, tigers, and otters (*5*). Most of those cases were associated with exposure to infected humans, a phenomenon defined as reverse zoonosis. This susceptibility is probably due to high homology between the human angiotensin–converting enzyme 2 (ACE2) receptor and those in several animal species; this receptor plays a key role in the virus entry into the cell (*6*,*7*).

Considering the zoonotic origin of the virus and the ongoing pandemic, both active and passive surveillance should be conducted on animals. Surveillance is particularly important for common pets, such as cats and dogs, because human-to-pet transmission is more likely to occur through close contact between owners and pets. That fact is evidenced by the great number of studies reporting SARS-CoV-2 infection and the presence of antibodies in cats and dogs all over the world (*8*–*14*). Quantitative reverse transcription PCR (qRT-PCR) is used to confirm SARS-CoV-2 infection in animals because of its high sensitivity and specificity (*15*). However, the period of viral shedding in animals is fairly short, according to experimental (*16*) and field (*9*) data; therefore, the detection of viral RNA from pet samples is fortuitous. qRT-PCR–based results confirm the infection by direct detection of the agent; serologic diagnosis may be useful to identify previous exposure in cats and dogs because these species develop a strong antibody-based response to viral infection with SARS-CoV-2 (*17*–*19*). Seroprevalence studies may extend our knowledge about the real prevalence of COVID-19 in pets; it is crucial to use a serologic test with high specificity to avoid cross-reactivity. Thus, the virus neutralization test (VNT) is a recommended technique because it can detect specific neutralizing antibodies against the virus. This assay, in combination with a simpler test for initial serum screening, could obtain specific and reliable results.

In this study, we performed an extensive serosurvey on cats and dogs in Spain, a country that has been severely affected by the COVID-19 pandemic, with >11 million cases and 100,000 thousand deaths (*1*) so far. We performed initial antibody detection using a

Author affiliations: VISAVET Health Surveillance Center, Madrid, Spain (S. Barroso-Arévalo, L. Sánchez-Morales, J.A. Barasona, L. Domínguez, J.M. Sánchez-Vizcaíno); Complutense University of Madrid, Madrid (S. Barroso-Arévalo, J.A. Barasona, L. Domínguez, J.M. Sánchez-Vizcaíno)

DOI: https://doi.org/10.3201/eid2906.221737

previously validated screening ELISA (*20*) and posterior confirmation using VNT. The results provide insights into the occurrence of COVID-19 and its spatial distribution in pets throughout the waves of the pandemic. The ethics committee for animal experiments at Complutense University of Madrid approved all the protocols (project license 14/2020).

Materials and Methods

Animal Sample Collection

Practitioners from hospitals, clinics, or Animal Protection Centers (APCs) in Spain collected serum samples from cats (n = 861) and dogs (n = 1,039) in accordance with the guidelines of good experimental practices, following European, national, and regional regulations. Samples were subsequently sent to the Health Surveillance Centre (VISAVET) at the Complutense University of Madrid (Madrid, Spain) by a transport company under the regulations stated in the UN3373 Biological Substance, Category B (21), and ARRIVE 2.0 guidelines (22). Owners and keepers were duly informed of the purpose of the study and the data protection policy and provided written consent for each pet. Serum samples were collected in tubes without any anticoagulant and kept refrigerated until shipment. At the laboratory, samples were stored at −80°C until analysis. When possible, further samples for qRT-PCR analysis were taken following the methods previously described (20).

To avoid a potential sampling bias, the survey included animals with known exposure to persons infected with SARS-CoV-2 as confirmed by qRT-PCR or antigen test, as well as nonexposed animals. We included domestic animals, defined as pets living in houses and animals from APCs (513 cats, 967 dogs), and stray animals, defined as free-ranging dogs or cats captured for sterilization and sampling (304 cats, 54 dogs). The presence or absence of clinical signs compatible with the disease (i.e., respiratory and digestive symptoms, anorexia, and apathy) was recorded for every animal. The study period was January 2020–November 2021. Sampling included animals from 11 autonomous communities in Spain: Andalucía, Aragón, Castilla la Mancha, Castilla y León, Cataluña, Ceuta, Madrid, País Vasco, Valencia, Navarra, and Murcia.

ELISA Based on RBD

We performed an indirect ELISA test based on the receptor-binding domain (RBD) of the virus as a screening test (Raybiotech, https://www.raybiotech.com). We adapted the ELISA to each species by using a specific anti-species conjugate. In brief, we covered coated plates with 100 µL of 1:40 diluted serum in phosphate-buffered saline (PBS) containing 0.05% Tween 20 (PBS-T) and incubated at 37°C for 30 minutes. We then washed the plates 4 times, added 100 µL of the specific anti-species HRP-conjugated IgG (Jackson Immuno Research Laboratories, https://www.jacksonimmuno.com) diluted 1:18,000 in PBS-T, and incubated the solution at 37°C for 15 minutes. After 4 more washes, we added 100 µL of SureBlue Reserve TMB microwell peroxidase substrate (TMB) (KPL, https://kpl.com) and incubated the plates in the dark for 10 minutes. We stopped the reaction by adding 100 µL of H_2SO_4 (3M, https://www.3m.com) to each well. We determined absorbance at 450 nm using an Anthos 2001 plate reader (Labtec, https://anthos-labtec.nl). We determined the endpoint cutoff by the analysis of a receiver operating characteristic (ROC) curve based on positive divided by negative (P/N) values. Validation of this ELISA test was extensively described (*20*).

Virus and Cells

SARS-CoV-2 MAD6 isolated from a 69-year-old male patient in Madrid, Spain, belonging to the B.1 (Pango v.3.1.162021-11-04) lineage, was provided by Dr. Luis Enjuanes from the National Biotechnology Centre (CNB) at the Higher Council for Scientific Research (CSIC). We prepared Vero E6 cells provided by the Carlos III Healthcare Institute (Madrid, Spain) or ATCC to reproduce the SARS-CoV-2 stocks. We incubated cells at 37°C under 5% CO_2 in GIBCO Roswell Park Memorial Institute (RPMI) 1640 medium with L-glutamine (Lonza Group Ltd, https://www.lonza.com) and supplemented with 100 IU/mL penicillin, 100 µg/mL streptomycin, and 10% fetal bovine serum (FBS) (Merck KGaA, https://www.emdgroup.com). We determined SARS-CoV-2 titers via a 50% tissue culture infectious dose ($TCID_{50}$) assay.

VNT for Detection of Specific Neutralizing Antibodies against SARS-CoV-2

We used VNT to confirm the presence of neutralizing antibodies against SARS-CoV-2 in all the samples that showed a doubtful or positive result to the screening ELISA. In brief, we performed the VNT in duplicate in 96-well plates by incubating 25 µL of 2-fold serially diluted serum with 25 µL of 100 $TCID_{50}$/mL of SARS-CoV-2. We incubated the virus/serum mixture at 37°C with 5% CO_2. After 1 hour, we added 200 µL of Vero E6 cell suspension to the mixtures and incubated the plates at 37°C with 5% CO_2. We determined the neutralization titers at 5

days postinfection. We recorded the titer of a sample as the reciprocal of the highest serum dilution that provided at least 100% neutralization of the reference virus, as determined by the visualization of cytopathic effect (CPE). We additionally determined cell viability after VNT by using a violet crystal assay to confirm the results observed by microscopy. At the end of VNT (5 days postinfection), we dried the cells, added 200 μL of 0.5% crystal violet solution (Sigma-Aldrich, https://www.sigmaaldrich.com), and incubated the solution at room temperature for 20 minutes. Finally, we removed the crystal violet for the visualization of CPE or cellular tapestry. We determined cell viability by comparing each well with both the virus and the cell control wells.

Data Analysis

We organized surveillance data on sampled dogs and cats by origin source, date, and results of diagnostic tests against SARS-CoV-2 in all the samples. We structured spatial data at the province level to reduce sampling bias between rural and urban scenarios. We conducted statistical analysis using SPSS Statistics 20 (IBM, http://www.spss.com) and R version 3.5.0 (The R Project for Statistical Computing, https://www.r-project.org). We used dplyr R package (*23*) for database exploration. We performed a descriptive analysis of seroprevalence from ELISA and VNT tests to calculate average ranges per species, sampling groups, and period at 95% CI. We studied variations in these parameters between groups and among different province-periods (3 months per period) with known human incidence of SARS-CoV-2 by a generalized linear mixed model (GzLMM) using a binomial distribution and probit link function. Thus, the response variable of the model was the presence (as 1) or absence (as 0) of a positive case to ELISA and confirmed by VNT test, with the reference value in the binomial distribution. We included sampling location as a random effect factor in the model; we included incidence of SARS-CoV-2 in humans, proportion of stray sampled animals, and contact with ≥1 person infected with SARS-CoV-2 at the province-period level as independent factors. We applied a protocol for data adjustment and checked the assumptions on the residuals of the model (*24*). We considered outcomes of $p < 0.05$ statistically significant.

Results

Detection of Neutralizing Antibodies against SARS-CoV-2

A total of 68 samples tested positive to ELISA, and 3 were doubtful samples. We used VNT to determine the presence of specific and neutralizing antibodies against SARS-CoV-2 in those ELISA positive and doubtful (n = 71) samples from cats and dogs. Positive results were confirmed in 66/71 ELISA-positive samples (ELISA specificity = 92.95) (Table 1). A total of 66 animals (3.59% of the total) showed neutralizing antibodies, 28 cats (seroprevalence of 3.43%), and 38 dogs (seroprevalence of 3.73%) (Figure 1). Overall, 60 positive cases were domestic animals whereas 6 stray animals resulted positive. All the stray animals that showed neutralizing antibodies were cats. Out of the 66 positive animals, 44 had contact with ≥1 person infected with SARS-CoV-2; 16 of those also had symptoms compatible with the infection, including sneezing, cough, and diarrhea. Out of the 60 positive domestic animals, 44 were pets living in houses, and 16 were housed in APCs. Six animals that showed neutralizing antibodies were also positive by qRT-PCR. VNT titers varied among samples; the lowest recorded was 1:32 and the highest 1:256. We observed no statistical differences in the VNT titers for cats and dogs.

Table 1. Distribution of cats and dogs testing positive for SARS-CoV-2 by location and type, Spain*

	No. cats infected/total		No. dogs infected/total		
Autonomous community	Domestic	Stray	Domestic	Stray	Total no. animals
Andalucía	6/305	0/89	15/616	0/2	21/1,012
Aragon	0/19	3/36	0/2	0/13	3/70
Cataluña	2/27	0/6	2/35	0/4	4/72
Castilla La Mancha	0/2	2/117	0/16	0/14	2/149
Castilla y León	7/37	0/13	0/14	0/1	7/65
Ceuta	0/5	0/0	2/19	0/0	2/24
Madrid	6/93	0/12	16/236	0/18	22/359
Murcia	0/7	0/0	0/8	0/0	0/15
Navarra	0/0	0/0	0/3	0/0	0/3
País Vasco	1/17	0/0	3/18	0/0	4/35
Valencia	0/1	0/31	0/0	0/0	0/32
Total no. animals	27/817		38/1,019		65/1,836

*Animal origin is domestic (animal living in a house or housed in Animal Protection Centers) or stray (free-ranging animals captured for sterilization and sampling). The numbers shown correspond to the number of animals positive by virus neutralization test-with respect to the total number of animals sampled.

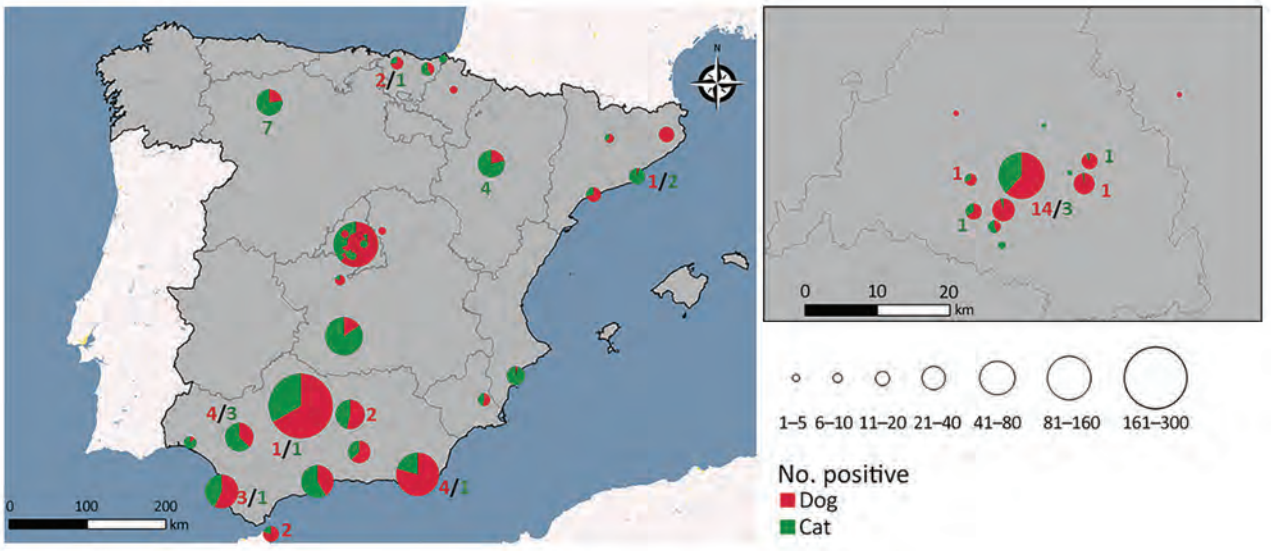

Figure 1. Spatial distribution of sampled animals and those testing positive for SARS-CoV-2 by neutralizing antibodies in study of SARS-CoV-2 seroprevalence studies in pets, Spain. Map at right shows detail of boxed area at left. Red numbers indicate number of positive dogs; green numbers indicate number of positive cats.

Factors Explaining SARS-CoV-2 Seroprevalence in Pets

When we considered the GzLMM on the seroprevalence variations obtained by VNT, we observed statistical differences once controlled by other factors, such as sampling locations and periods among groups (Table 2). The overall risk for SARS-CoV-2 seroprevalence in pets increased proportionally to the human incidence of this pathogen ($\beta = 4.85$; $p<0.001$) (Figure 2). In fact, we observed a higher risk for seroprevalence in animals with previous contact with ≥1 positive person ($\beta = 8.23$; $p<0.001$). The risk for SARS-CoV-2 seroprevalence in stray animals was significantly lower than in domestic animals ($\beta = -4.63$; $p<0.001$).

Discussion

Since the beginning of the COVID-19 pandemic, many studies have shown that pet cats and dogs are susceptible to SARS-CoV-2 infection, both experimentally (*16*) and naturally (*18*,*25*). Active infection in pets triggers the development of an effective immune response based on neutralizing antibodies, as previously demonstrated (*17*,*19*). Positivity by PCR tests lasts as long as the active infection does, 5–17 days (*19*,*26*). This short period in which positive PCR results are obtained hinders the detection of minor infections that typically occur in pets. In contrast, antibodies persist in serum for longer periods, <28 weeks (*27*), which makes those tests a helpful tool for evaluating previous exposure to the disease. Here, we evaluated a large number of samples from cats and dogs in Spain during a 23-month period, demonstrating a higher rate of antibody positivity than in previous seroprevalence studies. As we expected, the risk for SARS-CoV-2 seroprevalence in stray animals was lower than that for domestic animals. We have observed that seropositivity in animals increased proportionally to the human incidence of SARS-CoV-2. Therefore, the epidemiology of the disease in the human population has an effect on animal seroprevalence.

Taking into account the current state of the COVID-19 pandemic, we cannot rule out changes in the epidemiology of the disease. As new variants emerge, SARS-CoV-2 can adapt to other hosts such as cats and dogs. Clarifying the distribution of the disease in cats and dogs can reveal infection trends in these species.

Table 2. Variations of SARS-CoV-2 seroprevalence in pets by human contact, Spain*

Model terms	Estimate	SE	Z value	p value
Intercept	−1.274	0.240	−5.307	<0.001
Human incidence	0.001	0.001	4.852	<0.001
Contact	0.116	0.014	8.234	<0.001
Stray	−0.058	0.012	−4.628	<0.001

*Generalized linear mixed model output to explain variations of SARS-CoV-2 seroprevalence in pets in relation to the officially registered human incidence of SARS-CoV-2, the proportion of animals with previous contact with ≥1 positive person (Contact), and the proportion of stray animals. Sampling location was considered a random effect factor.

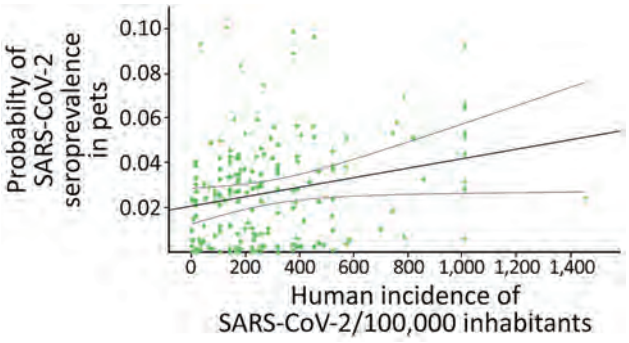

Figure 2. Predicted probability of SARS-CoV-2 seroprevalence in pets as related to registered human incidence (cases per 100,000 inhabitants) at the province-period (3 months each period) level in study of SARS-CoV-2 seroprevalence studies in pets, Spain. The black line marks the trend and slope of the correlation. Lighter gray lines show 95% CIs.

This study has several strengths in addition to the large number of samples analyzed. We have monitored both animals in contact with SARS-CoV-2–infected persons as well as animals with no previous exposure to the disease; we also analyzed a high number of samples from stray animals, which can give us information about infections caused by environmental contamination and virus circulation in the field. Moreover, the period of our study was long, which enabled us to evaluate infection trends in pets during the different waves in the human population. Because the study ended in November 2021, our results reflect the seroprevalence triggered by 3 consecutive variants of SARS-CoV-2: B.1, Alpha, and Delta. According to the sequencing reports from the government of Spain, B.1 variant was the most prevalent strain during March 2020–March 2021. More recently, the Alpha variant became dominant in the country until September 2021, the point in which the Delta variant replaced Alpha. The Omicron variant was introduced in Spain in December 2021, so no information about seroprevalence during the Omicron wave was available for this study. We note that the viral strain used for VNT in this study was the B.1 strain. The specificity of antibodies against this variant may have influenced the titers of neutralizing antibodies obtained from serum samples during subsequent waves, and, therefore, underestimated the level of antibodies in some cases.

The percentage of seropositivity in this work was slightly higher (3.56%) in comparison with other studies with similar sample size, as previously described in the United States (0.17%) (*28*), Italy (4.04%) (*10*), Germany (0.43%) (*29*), and the Netherlands (0.3%) (*30*). This finding could be related to the high COVID-19 incidence in humans in Spain during the study period. In January 2021, accumulated incidence reached ≈900 positive/100,000 inhabitants in Spain, followed by a few months in which the accumulated incidence exceeded 100 positive/100,000 inhabitants until July, when another peak was reached (700 positive/100,000 inhabitants). Subsequently, accumulated incidence had a large drop and remained <100 positive/100,000 inhabitants during September–November 2021. As demonstrated by the GzLMM, the incidence of SARS-CoV-2 infection in the human population was related to higher positivity to VNT in pets. This finding highlights the importance of taking preventive measures and minimizing contact with domestic animals when humans become infected. Because the epidemiologic scenario of the disease may change at any time due to the high rate of genomic mutation of the virus and the apparition of new variants, it is crucial to limit the contagion of susceptible species.

Previous studies on pets in Spain have demonstrated a low prevalence of positive animals by PCR (*11*,*20*). However, as we have demonstrated, more animals have been exposed to the virus. In all those cases, we can confirm that the exposure resulted in an active infection because the animals were able to develop an effective immune response based on neutralizing antibodies. We suspect that SARS-CoV-2 infection in pets is anecdotic because in none of the positive cases we described did the owners detect severe symptoms in the animals. Although some animals had antibodies and were experiencing clinical signs at the time of sampling (30.3%), such as sneezes, dyspnea, nasal discharge, coughs, vomiting, or depression, the relationship between those signs and the SARS-CoV-2 infection is not clear enough. Antibodies remain undetectable in serum until 8–10 days postinfection (*19*), leading to a delay between a positive result to antibody detection and the infection. In addition, a high percentage of the animals were sampled during their attendance at the veterinary clinic, and the symptoms reported as the reason for the visit might be unrelated to SARS-CoV-2 infection; comorbidities may cause a biased result.

We confirmed that stray animals had neutralizing antibodies, as do domestic animals in contact with SARS-CoV-2–infected persons. Those results are in line with those from other studies that confirmed the presence of neutralizing antibodies in stray animals (*31*–*33*). However, the seroprevalence in this group of animals was very low; the domestic animals represented 4.05% of the animals with neutralizing antibodies, compared with 1.69% in the case of stray animals. Those results make sense

because domestic animals are more likely to be in contact with infected persons and share potentially contaminated spaces than stray animals. In those cases, the exposure to the virus may be related to the times that humans fed the stray colonies and to the presence of infectious excretions in the areas frequented by stray cats and dogs. Another potential route of transmission is animal-to-animal transmission, which has been demonstrated in the case of stray cats (*9*). These results suggest that virus circulation in stray populations is low, although special care should be taken in practices that may pose a risk, such as the feeding of stray animals.

In conclusion, this study demonstrated higher rates of human-to-pet SARS-CoV-2 transmission than those found by direct molecular detection. As expected, the seroprevalence of the disease was higher in animals with previous exposure to infected persons, whereas the lower risk of infection in stray animals is likely caused by a low rate of exposure. In addition, the epidemiology of the disease in the human population seems to influence the seroprevalence of the infection in cats and dogs, which highlights the importance of performing active surveillance in susceptible species.

Acknowledgments

We thank Belén Rivera, Rocío Sánchez, and Deborah López for their excellent technical support, as well as all the members of the COVID-VISAVET team. We also thank all the veterinary clinics and owners who participated in this study and Luis Enjuanes for kindly providing us the virus.

This research was funded by the Institute of Health Carlos III, project "Estudio del potencial impacto del COVID19 en mascotas y linces" (reference: COV20/01385), and also financed as part of the European Union's response to the COVID-19 pandemic, being the financing entities the Community of Madrid and the European Union, through the European Regional Development Fund with the "REACT ANTICIPA-UCM" project (reference PR38/21).

Author contributions: conceptualization: S.B.-A., L.D., J.M.S.-V.; data curation: S.B.-A., L.S.-M., J.A.B.; formal analysis: S.B.-A., L.S.-M., J.A.B.; funding acquisition: J.M.S.-V., L.D.; laboratory analyses: S.B.-A., L.S.-M.; methodology: S.B.-A., L.S.-M., J.A.B., J.M.S.-V.; project administration: J.M.S.-V.; resources: L.D., J.M.S.-V.; software: S.B.-A., L.S.-M., J.A.B.; supervision: L.D., J.M.S.-V.; validation: S.B.-A., L.S.-M., J.A.B., J.M.S.-V.; visualization: S.B.-A., L.S.-M., J.A.B.; original draft preparation: S.B.-A., L.S.-M., J.A.B.; manuscript review and editing: S.B.-A., L.S.-M., J.A.B., L.D., J.M.S.-V.

About the Author

Dr. Barroso-Arévalo is a postdoctoral researcher at the SUAT-VISAVET team of the Complutense University of Madrid. Her research interests include SARS-CoV-2 and African swine fever viruses, general virus pathogenesis, immunology, and vaccine development.

References

1. World Health Organization. COVID-19 weekly epidemiological update—March 2022. 2022 [cited 2023 Apr 10]. https://www.who.int/publications/m/item/weekly-operational-update-on-covid-19---30-march-2022
2. Lau SKP, Luk HKH, Wong ACP, Li KSM, Zhu L, He Z, et al. Possible bat origin of severe acute respiratory syndrome coronavirus 2. Emerg Infect Dis. 2020;26:1542–7. https://doi.org/10.3201/eid2607.200092
3. World Health Organization. Origin of SARS-CoV-2. Reference no. WHO/2019-nCoV/FAQ/Virus_origin/2020.1. 2020 Mar 26 [cited 2023 Apr 12]. https://apps.who.int/iris/bitstream/handle/10665/332197/WHO-2019-nCoV-FAQ-Virus_origin-2020.1-eng.pdf
4. Wong G, Bi Y-H, Wang Q-H, Chen X-W, Zhang Z-G, Yao Y-G. Zoonotic origins of human coronavirus 2019 (HCoV-19 / SARS-CoV-2): why is this work important? Zool Res. 2020;41:213–9. https://doi.org/10.24272/j.issn.2095-8137.2020.031
5. World Organisation for Animal Health. SARS-CoV-2 in animals—situation report 8. 2021 Dec 31 [cited 2023 Apr 12]. https://www.woah.org/app/uploads/2022/01/sars-cov-2-situation-report-8.pdf
6. Sun K, Gu L, Ma L, Duan Y. Atlas of ACE2 gene expression reveals novel insights into transmission of SARS-CoV-2. Heliyon. 2021;7:e05850. https://doi.org/10.1016/j.heliyon.2020.e05850
7. Kim Y, Gaudreault NN, Meekins DA, Perera KD, Bold D, Trujillo JD, et al. Effects of spike mutations in SARS-CoV-2 variants of concern on human or animal ACE2-mediated virus entry and neutralization. Microbiol Spectr. 2022;10:e0178921. https://doi.org/10.1128/spectrum.01789-21
8. Hamer SA, Pauvolid-Corrêa A, Zecca IB, Davila E, Auckland LD, Roundy CM, et al. SARS-CoV-2 infections and viral isolations among serially tested cats and dogs in households with infected owners in Texas, USA. Viruses. 2021;13:938. https://doi.org/10.3390/v13050938
9. Hobbs EC, Reid TJ. Animals and SARS-CoV-2: species susceptibility and viral transmission in experimental and natural conditions, and the potential implications for community transmission. Transbound Emerg Dis. 2021;68:1850–67. https://doi.org/10.1111/tbed.13885
10. Patterson EI, Elia G, Grassi A, Giordano A, Desario C, Medardo M, et al. Evidence of exposure to SARS-CoV-2 in cats and dogs from households in Italy. Nat Commun. 2020;11:6231. https://doi.org/10.1038/s41467-020-20097-0
11. Ruiz-Arrondo I, Portillo A, Palomar AM, Santibáñez S, Santibáñez P, Cervera C, et al. Detection of SARS-CoV-2 in pets living with COVID-19 owners diagnosed during the COVID-19 lockdown in Spain: A case of an asymptomatic cat with SARS-CoV-2 in Europe. Transbound Emerg Dis. 2021;68:973–6. https://doi.org/10.1111/tbed.13803
12. Barroso-Arévalo S, Rivera B, Domínguez L, Sánchez-Vizcaíno JM. First detection of SARS-CoV-2 B.1.1.7 variant of concern in an asymptomatic dog in Spain. Viruses. 2021;13:1379. https://doi.org/10.3390/v13071379

13. Gortázar C, Barroso-Arévalo S, Ferreras-Colino E, Isla J, de la Fuente G, Rivera B, et al. Natural SARS-CoV-2 infection in kept ferrets, Spain. Emerg Infect Dis. 2021;27:1994–6. https://doi.org/10.3201/eid2707.210096
14. Zhao S, Schuurman N, Li W, Wang C, Smit LAM, Broens EM, et al. Serologic screening of severe acute respiratory syndrome coronavirus 2 infection in cats and dogs during first coronavirus disease wave, the Netherlands. Emerg Infect Dis. 2021;27:1362–70. https://doi.org/10.3201/eid2705.204055
15. Corman VM, Landt O, Kaiser M, Molenkamp R, Meijer A, Chu DK, et al. Detection of 2019 novel coronavirus (2019-nCoV) by real-time RT-PCR. Euro Surveill. 2020;25:2000045. https://doi.org/10.2807/1560-7917.ES.2020.25.3.2000045
16. Bosco-Lauth AM, Hartwig AE, Porter SM, Gordy PW, Nehring M, Byas AD, et al. Experimental infection of domestic dogs and cats with SARS-CoV-2: pathogenesis, transmission, and response to reexposure in cats. Proc Natl Acad Sci U S A. 2020;117:26382–8. https://doi.org/10.1073/pnas.2013102117
17. Shi J, Wen Z, Zhong G, Yang H, Wang C, Huang B, et al. Susceptibility of ferrets, cats, dogs, and other domesticated animals to SARS-coronavirus 2. Science. 2020;368:1016–20. https://doi.org/10.1126/science.abb7015
18. Bao L, Song Z, Xue J, Gao H, Liu J, Wang J, et al. Susceptibility and attenuated transmissibility of SARS-CoV-2 in domestic cats. J Infect Dis. 2021;223:1313–21. https://doi.org/10.1093/infdis/jiab104
19. Barroso-Arévalo S, Sánchez-Morales L, Barasona JA, Rivera B, Sánchez R, Risalde MA, et al. Evaluation of the clinical evolution and transmission of SARS-CoV-2 infection in cats by simulating natural routes of infection. Vet Res Commun. 2022;46:837–52. https://doi.org/10.1007/s11259-022-09908-5
20. Barroso-Arévalo S, Barneto A, Ramos ÁM, Rivera B, Sánchez R, Sánchez-Morales L, et al. Large-scale study on virological and serological prevalence of SARS-CoV-2 in cats and dogs in Spain. Transbound Emerg Dis. 2022;69:e759–74. https://doi.org/10.1111/tbed.14366
21. World Health Organization. Guidance on regulations for the transport of infectious substances 2021–2022. Licence: CC BY-NC-SA 3.0. Geneva: The Organization; 2021.
22. Percie du Sert N, Hurst V, Ahluwalia A, Alam S, Avey MT, Baker M, et al. The ARRIVE guidelines 2.0: Updated guidelines for reporting animal research. PLoS Biol. 2020;18:e3000410. https://doi.org/10.1371/journal.pbio. 3000410
23. Wickham H, Francois R. dplyr: a grammar of data manipulation. R package version 0.4.3. 2015 [cited 2023 Apr 3]. https://cran.r-project.org/web/packages/dplyr/index.html
24. Zuur AF, Ieno EN, Elphick CS. A protocol for data exploration to avoid common statistical problems. Methods Ecol Evol. 2010;1:3–14. https://doi.org/10.1111/j.2041-210X.2009.00001.x
25. Sit THC, Brackman CJ, Ip SM, Tam KWS, Law PYT, To EMW, et al. Infection of dogs with SARS-CoV-2. Nature. 2020;586:776–8. https://doi.org/10.1038/s41586-020-2334-5
26. Neira V, Brito B, Agüero B, Berrios F, Valdés V, Gutierrez A, et al. A household case evidences shorter shedding of SARS-CoV-2 in naturally infected cats compared to their human owners. Emerg Microbes Infect. 2021;10:376–83. https://doi.org/10.1080/22221751.2020.1863132
27. Jara LM, Ferradas C, Schiaffino F, Sánchez-Carrión C, Martínez-Vela A, Ulloa A, et al. Evidence of neutralizing antibodies against SARS-CoV-2 in domestic cats living with owners with a history of COVID-19 in Lima - Peru. One Health. 2021;13:100318. 10.1016/j.onehlt.2021.100318 https://doi.org/10.1016/j.onehlt.2021.100318
28. Barua S, Hoque M, Adekanmbi F, Kelly P, Jenkins-Moore M, Torchetti MK, et al. Antibodies to SARS-CoV-2 in dogs and cats, USA. Emerg Microbes Infect. 2021;10:1669–74. https://doi.org/10.1080/22221751.2021.1967101
29. Michelitsch A, Hoffmann D, Wernike K, Beer M. Occurrence of antibodies against SARS-CoV-2 in the domestic cat population of Germany. Vaccines (Basel). 2020;8:772. https://doi.org/10.3390/vaccines8040772
30. Zhao S, Schuurman N, Li W, Wang C, Smit LAM, Broens EM, et al. Serologic screening of severe acute respiratory syndrome coronavirus 2 infection in cats and dogs during first coronavirus disease wave, the Netherlands. Emerg Infect Dis. 2021;27:1362–70. https://doi.org/10.3201/eid2705.204055
31. Zhang Q, Zhang H, Gao J, Huang K, Yang Y, Hui X, et al. A serological survey of SARS-CoV-2 in cat in Wuhan. Emerg Microbes Infect. 2020;9:2013–9. https://doi.org/10.1080/22221751.2020.1817796
32. Dias HG, Resck MEB, Caldas GC, Resck AF, da Silva NV, Dos Santos AMV, et al. Neutralizing antibodies for SARS-CoV-2 in stray animals from Rio de Janeiro, Brazil. PLoS One. 2021;16:e0248578. https://doi.org/10.1371/journal.pone.0248578
33. van der Leij WJR, Broens EM, Hesselink JW, Schuurman N, Vernooij JCM, Egberink HF. Serological screening for antibodies against SARS-CoV-2 in Dutch shelter cats. Viruses. 2021;13:1634. https://doi.org/10.3390/v13081634

Address for correspondence: Sandra Barroso Arévalo, Complutense University of Madrid—Animal Health, AV Puerta del Hierro SN Madrid, Madrid 28040, Spain; email: sandrabarroso@ucm.es

Similar Prevalence of *Plasmodium falciparum* and Non–*P. falciparum* Malaria Infections among Schoolchildren, Tanzania[1]

Rachel Sendor,[2] Cedar L. Mitchell,[2] Frank Chacky, Ally Mohamed, Lwidiko E. Mhamilawa, Fabrizio Molteni, Ssanyu Nyinondi, Bilali Kabula, Humphrey Mkali, Erik J. Reaves, Naomi Serbantez, Chonge Kitojo, Twilumba Makene, Thwai Kyaw, Meredith Muller, Alexis Mwanza, Erin L. Eckert, Jonathan B. Parr, Jessica T. Lin,[3] Jonathan J. Juliano,[3] Billy Ngasala[3]

Achieving malaria elimination requires considering both *Plasmodium falciparum* and non–*P. falciparum* infections. We determined prevalence and geographic distribution of 4 *Plasmodium* spp. by performing PCR on dried blood spots collected within 8 regions of Tanzania during 2017. Among 3,456 schoolchildren, 22% had *P. falciparum*, 24% had *P. ovale* spp., 4% had *P. malariae*, and 0.3% had *P. vivax* infections. Most (91%) schoolchildren with *P. ovale* infections had low parasite densities; 64% of *P. ovale* infections were single-species infections, and 35% of those were detected in low malaria endemic regions. *P. malariae* infections were predominantly (73%) co-infections with *P. falciparum*. *P. vivax* was detected mostly in northern and eastern regions. Co-infections with ≥1 non–*P. falciparum* species occurred in 43% of *P. falciparum* infections. A high prevalence of *P. ovale* infections exists among schoolchildren in Tanzania, underscoring the need for detection and treatment strategies that target non–*P. falciparum* species.

Author affiliations: University of North Carolina, Chapel Hill, North Carolina, USA (R. Sendor, C.L. Mitchell, T. Kyaw, M. Muller, A. Mwanza, J.B. Parr, J.T. Lin, J.J. Juliano); National Malaria Control Programme, Dodoma, Tanzania (F. Chacky, A. Mohamed); Muhimbili University of Health and Allied Sciences, Dar es Salaam, Tanzania (L.E. Mhamilawa, T. Makene, B. Ngasala); Swiss Tropical and Public Health Institute, Basel, Switzerland (F. Molteni); RTI International, Dar es Salaam (S. Nyinondi, B. Kabula, H. Mkali); US Centers for Disease Control and Prevention, Dar es Salaam (E.J. Reaves); US Agency for International Development, Dar es Salaam (N. Serbantez, C. Kitojo); RTI International, Washington, DC, USA (E.L. Eckert); Uppsala University, Uppsala, Sweden (B. Ngasala)

DOI: https://doi.org/10.3201/eid2906.221016

Sub-Saharan Africa harbors 95% of the global malaria burden (*1*). National surveys conducted by ministries of health throughout Africa regularly assess *Plasmodium falciparum* prevalence (2); however, little is known about the prevalence and geographic distribution of non–*P. falciparum* (hereafter nonfalciparum) malaria species, such as *P. malariae*, *P. vivax*, and *P. ovale curtisi* or *P. ovale wallikeri* (hereafter *P. ovale*) (*3*–*8*). Although the clinical prevalence of nonfalciparum malaria in sub-Saharan Africa is dwarfed by *P. falciparum* (*9*), nonfalciparum species can still cause disease. *P. malariae* has been associated with increased risk for anemia (*10*) and other complications, such as chronic nephrotic syndrome (*11*,*12*). *P. vivax* can cause severe anemia, pregnancy-related complications, and death after recurrent infections, but infections in sub-Saharan Africa are infrequent (*13*–*15*). Clinical consequences of *P. ovale* infections have been mostly described in travelers and have been associated with severe infection in case reports (*16*).

Declining *P. falciparum* prevalence in East Africa might be associated with increasing nonfalciparum infections (*17*–*20*). However, comprehensive surveys of nonfalciparum malaria in sub-Saharan Africa have been infrequent because detection of those species remains challenging (*11*,*17*). Field diagnostic methods, such as microscopy and pan–*Plasmodium* spp. lactate dehydrogenase (LDH) or histidine-rich protein 2 (HRP2)–based rapid diagnostic tests (RDTs), lack

[1]Data from this study were presented as a virtual poster at the American Society of Tropical Medicine and Hygiene conference, November 17–21, 2021.

[2]These first authors contributed equally to this article.

[3]These senior authors contributed equally to this article.

sensitivity to detect nonfalciparum species (*11*,*17*). Nonfalciparum malaria parasite densities are often low, and most infected persons might not seek care. Mixed infections with *P. falciparum* can also complicate detection of nonfalciparum species (*3*,*17*). Molecular detection methods can sensitively detect nonfalciparum malaria species, but those methods remain largely confined to research use.

In Tanzania, the prevalence of malaria is high, accounting for 4.1% of global malaria deaths in 2020 (*1*). Although ≈93% of the population in mainland Tanzania is at risk for malaria, transmission throughout the country is highly heterogeneous (*21*). Transmission patterns are largely driven by geographic features of the country. Malaria transmission is low, unstable, and seasonal across the arid highlands and in urban centers; moderate and seasonally variable in southern, northern, and northwestern areas; and high and perennial along the coastal, lake, and southern lowland regions (*21*,*22*). Decades of concentrated malaria control interventions helped lower the national prevalence from 18% in 2008 to 7% in 2017 (*23*). Most reported malaria cases in Tanzania have been attributed to *P. falciparum* (*9*,*21*), but recent studies have also identified *P. malariae*, *P. vivax*, and *P. ovale* transmission (*4*,*18*,*24*,*25*). Given the widespread use of *P. falciparum*–specific HRP2-based RDTs for malaria diagnosis, the propensity for missed detection or misclassification of nonfalciparum species in Tanzania is high, and large-scale, geographically representative studies to assess spatial distributions of nonfalciparum malaria species are lacking. We used molecular methods to analyze blood samples collected during a national survey of schoolchildren in Tanzania and comprehensively characterize nonfalciparum malaria epidemiology.

Materials and Methods

Study Design

The 2017 School Malaria Parasitological Survey (SMPS) was a cross-sectional study of children who were 5–16 years of age and enrolled in public primary schools in mainland Tanzania. Methods for site selection and survey design mirrored the 2015 SMPS and have been previously described (*22*). Study regions were selected through a multistage sampling scheme to maintain geographic representation and reflect the heterogeneity of malaria transmission across Tanzania (*22*,*26*). The number of schools randomly selected per region was proportional to each region's respective population (*22*,*26*). Within each school, an average of 100 students were randomly selected for screening. After consent, each student was interviewed to obtain demographic and clinical characteristics, a malaria RDT was performed, and a dried blood spot (DBS) sample was collected (*22*,*26*). The survey largely coincided with each region's rainy season. From among students who provided a DBS, we selected a stratified random subpopulation for nonfalciparum malaria testing. To maintain representativeness, we selected students in proportions that equaled regional proportions reflected within the broader survey population.

Informed consent had been obtained from students and their legal guardians before survey data or blood sample collection, and ethical clearance was given by the Tanzania National Institute for Medical Research. Analysis of de-identified samples was approved by the Institutional Review Board of the University of North Carolina, Chapel Hill (approval no. 19-1495).

During the survey, malaria detection was conducted by using CareStart Malaria Pf/PAN (HRP2/pLDH) Ag Combo RDTs (AccessBio, https://www.accessbio.net) that were specific for *P. falciparum* HRP2 and pan-pLDH antigens. RDTs were considered positive if they were positive for either antigen. Schools and councils were grouped into epidemiologic malaria transmission risk strata on the basis of *P. falciparum* prevalences in children estimated from the 2014–15 Tanzania SMPS (*22*,*26*). *P. falciparum* prevalence was defined as very low if <5%, low if 5 to <10%, moderate if 10 to <50%, and high if ≥50% (*22*,*26*). DBS samples collected on Whatman filter paper (Cytiva, https://www.cytivalifesciences.com) were shipped to the University of North Carolina (Chapel Hill, NC, USA) for molecular testing.

Molecular Detection

We extracted DNA from three 6-mm punches from each DBS sample by using a Chelex method (*27*) and performed real-time PCR targeting the 18S rRNA subunit of malaria as previously described (*28*) (Appendix Table 1, https://wwwnc.cdc.gov/EID/article/29/6/22-1016-App1.pdf). We performed PCR for each *Plasmodium* spp. independently with appropriate controls. We prepared positive controls for *P. falciparum* detection by using whole human blood and cultured *P. falciparum* strain 3D7 parasites (BEI Resources, https://www.beiresources.org) to create mock DBS samples and for nonfalciparum species detection by using plasmid DNA (BEI Resources). We serially diluted the control samples and extracted DNA as described. We estimated semiquantitative parasitemias for nonfalciparum species by assuming 6 18S rRNA gene copies/parasite (*28*) and multiplying by 4.0 to account for the 4-fold

dilution of blood: ≈26 μL blood from 3 DBS punches (29) in 100 μL final volume of eluted DNA. We performed 40 PCR cycles for *P. malariae* and *P. falciparum* and 45 PCR cycles for *P. ovale* and *P. vivax* to enable detection of low-density infections (*28*). We previously validated this approach by using 390 negative controls comprising water (n = 22) and human DNA (n = 368) and >170 positive controls with decreasing nonfalciparum parasite densities; no false-positives were detected (*28*). We assessed PCR specificity by testing against 10 controls from each of the other *Plasmodium* spp.; no false positives were detected (Appendix Table 2). Our laboratory at the University of North Carolina participates in the World Health Organization malaria molecular quality assurance scheme, identifying and determining *Plasmodium* spp. in blinded samples every 6 months, and has consistently achieved high marks for assay performance across species. In this study, we did not detect false-positive amplification among 20 negative controls per each species-specific assay (Appendix Table 3). We performed further real-time PCR on a subset of *P. ovale*–positive samples to distinguish between *P. ovale wallikeri* and *P. ovale curtisi* (*30*,*31*). To evaluate potential bias from differences in PCR cycle numbers between species, we conducted a sensitivity analysis of randomly selected students (n = 750) stratified by malaria transmission risk. We performed semiquantitative real-time PCR of the 18S rRNA gene to 45 cycles to detect *P. falciparum* and *P. malariae* infections.

Analysis

We calculated overall malaria species-specific prevalences and prevalence of single- and mixed-species infections. We did not adjust prevalences for sampling weight because nonfalciparum samples were selected randomly and in equal proportion to the broader survey sample.

We performed descriptive statistical analyses of student characteristics according to *Plasmodium* spp. We analyzed differences between *P. falciparum* and nonfalciparum single-species infections by using Pearson χ^2 and Kruskal-Wallis rank-sum tests assuming nonnormality and applied Fisher exact test for small frequency counts. We performed similar analyses to compare malaria-positive and -negative students according to *Plasmodium* spp. Missing data were summarized, but we performed analyses on nonmissing data only.

Spatial Mapping

We assessed regional variation in prevalence of each species through geospatial mapping by council and region. We aggregated numbers of infections and students by council and estimated and mapped council-level prevalences for each species. We calculated scaled prevalences by dividing the proportion of each council's prevalence by the highest council prevalence for each *Plasmodium* species, as follows:

$$\frac{P_{d_i}}{Max\{P_{d_1}, \ldots, P_{d_{59}}\}}$$

where P is the prevalence for a given council, d_i. We calculated and mapped differences between scaled nonfalciparum and scaled *P. falciparum* prevalences for each council. This method compared prevalence estimates between each nonfalciparum species and *P. falciparum*, while accounting for differences in the absolute burden of each species.

We performed analyses by using R version 4.0.2 (The R Project for Statistical Computing, https://www.r-project.org) and used the eulerr (https://cran-r-project.org/package=eulerr) and sf version 0.9–7 (*32*) packages for prevalence visualization and mapping. We sourced shapefiles from the Global Administrative Areas database (https://gadm.org) and collected elevation measurements from the US National Aeronautics and Space Administration, Shuttle Radar Topography Mission (https://www.nasa.gov).

Results

Study Population

We selected a total of 3,456 students from 180 schools across 8 geographic regions for nonfalciparum malaria testing from among 17,131 students in the SMPS who had available DBS samples. We did not detect differences in student characteristics between those in the nonfalciparum malaria and SMPS DBS populations (Appendix Table 4). Median (interquartile range [IQR]) student age in the nonfalciparum study population was 11 (9–13) years; distribution of male (51%) and female (49%) students was similar. Malaria dual-antigen RDTs were positive in 20% of students. Most students attended schools in regions classified as high (51%) or moderate (13%) malaria transmission risk (Table 1, https://wwwnc.cdc.gov/EID/article/29/6/22-1016-T1.htm).

Species Prevalence Determined by PCR

We identified *P. falciparum* infections in 22% (95% CI 21%–23%, n = 755), *P. ovale* in 24% (95% CI 22%–25%, n = 814), *P. malariae* in 4% (95% CI 3%–5%, n = 136), and *P. vivax* in 0.3% (95% CI 0.2%–0.6%,

n = 11) of students, including single- and mixed-species infections (Appendix Table 5). Most (64%, n = 519) *P. ovale* infections were single-species infections; 28% (n = 224) were co-infections with *P. falciparum* only (Figure 1). Conversely, most (40%, n = 55) *P. malariae* infections were co-infections with both *P. ovale* and *P. falciparum*; 32% (n = 44) were co-infections with *P. falciparum* only. We determined 36% (n = 4) of *P. vivax* infections were single-species infections, and 43% (n = 326) of *P. falciparum* infections were co-infections with ≥1 non-falciparum malaria species.

We conducted a sensitivity analysis, detecting *P. falciparum* and *P. malariae* by using PCR cycle thresholds of <45 to evaluate different PCR cycles between assays. We observed 25% (95% CI 21%–29%) *P. falciparum* and 3% (95% CI 2%–5%) *P. malariae* prevalences, weighted according to student distribution within the total nonfalciparum population by transmission risk strata (Appendix Table 6). Within that subset, 2.5% (n = 4) of *P. falciparum* and 10% (n = 2) of *P. malariae* infections were detected at cycle thresholds of 40–45. Thus, >97% of *P. falciparum* and 90% of *P. malariae* infections were detectable by the primary 40-cycle assay in our study.

We evaluated differences in student characteristics according to *Plasmodium* spp. infection (Table 1; Appendix Table 7). We detected *P. ovale* single-species infections more frequently than *P. falciparum* infections in slightly younger (median 11 vs. 12 years of age; p<0.001) and female (54% vs. 45%; p = 0.009) students. Comparing RDT sensitivity to PCR, we observed 8% (n = 40) of students with *P. ovale* single-species infections were RDT-positive for any band, whereas 33% (n = 8) of those with *P. malariae* and 69% (n = 295) with *P. falciparum* single-species infections were RDT-positive. Co-infections with *P. falciparum* and nonfalciparum were RDT-positive in 78% (n = 253/325) of cases detected by PCR. Although only 3% (n = 13) of *P. falciparum* single-species infections and no *P. malariae* or *P. vivax* single-species infections were detected in low transmission risk strata, 35% (n = 181) of *P. ovale* single-species infections occurred in regions classified as low or very low malaria transmission

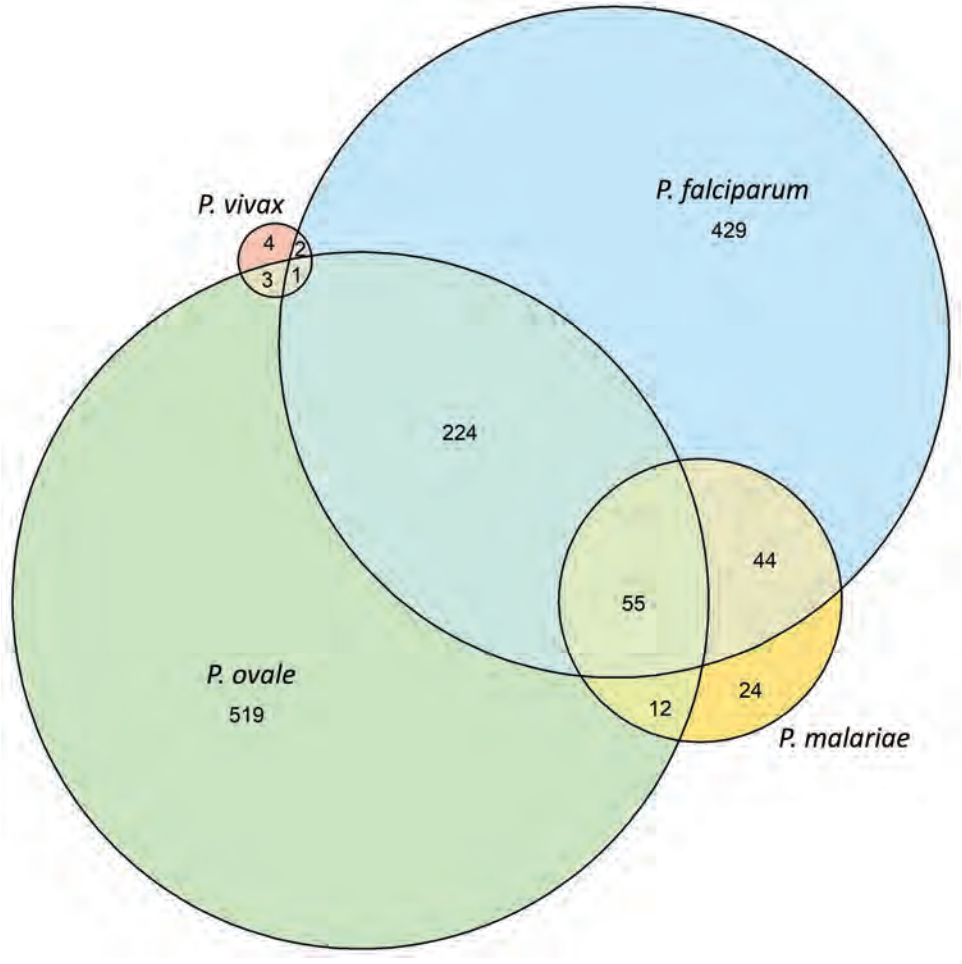

Figure 1. Distribution of *Plasmodium* spp. infections among schoolchildren, Tanzania. Prevalence estimates according to species: *P. falciparum*, 21.8% (95% CI 20.5%–23.3%, n = 755); *P. ovale*, 23.6% (95% CI 22.2%–25.0%, n = 814); *P. malariae*, 3.9% (95% CI 3.3%–4.6%, n = 136); *P. vivax*: 0.3% (95% CI 0.2%–0.6%, n = 11). *P. vivax* + *P. malariae* co-infection (n = 1) is not shown.

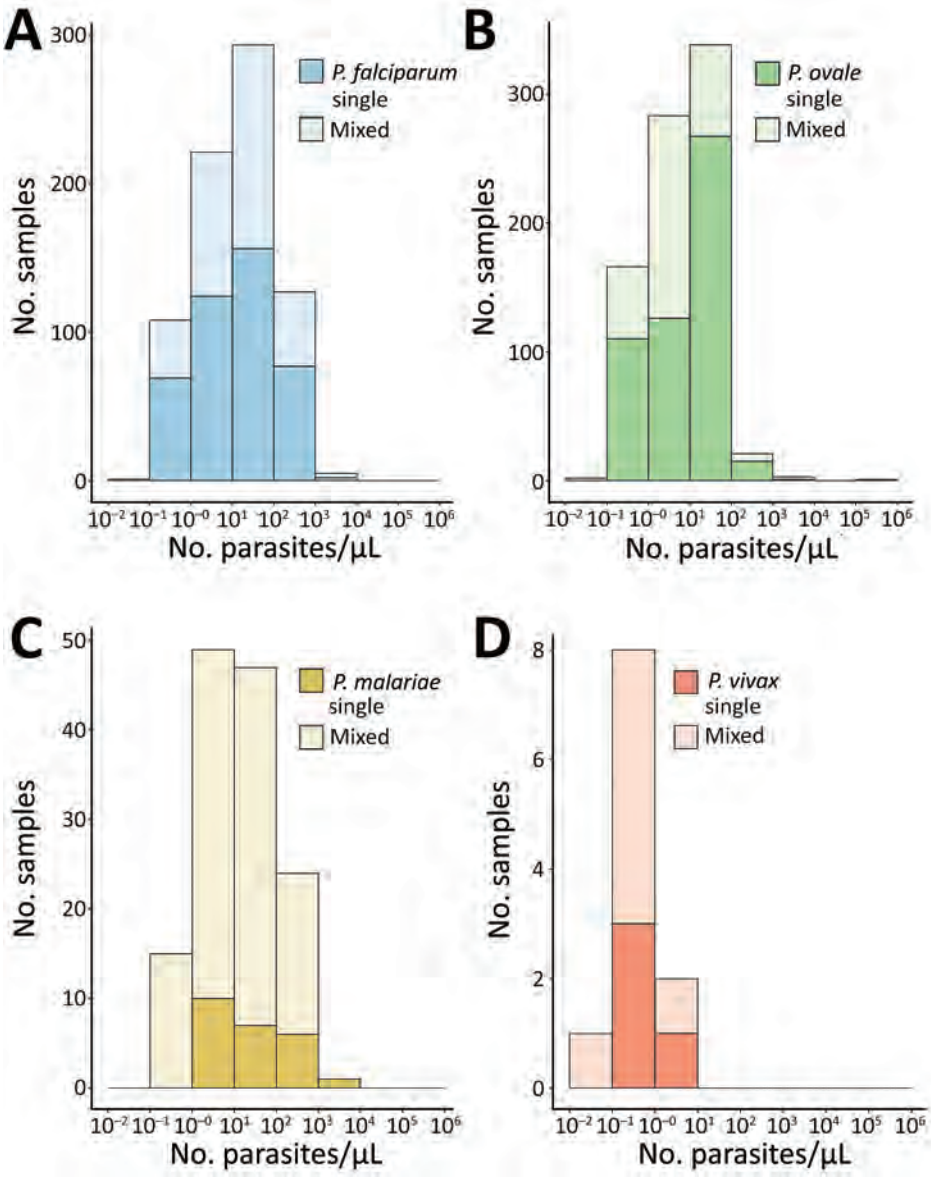

Figure 2. Estimated parasite density distributions according to malaria species in study of similar prevalence of *Plasmodium falciparum* and non–*P. falciparum* malaria infections among schoolchildren, Tanzania. We estimated *Plasmodium* spp. parasite densities for single infections and co-infections (mixed) by using semiquantitative PCR and species-specific primers (Appendix Table 1, https://wwwnc.cdc.gov/EID/article/29/6/22-1016-App1.pdf). Mixed infections included *P. falciparum* and nonfalciparum co-infections. Number of samples varied by species. *P. ovale* and *P. vivax* parasite densities were detected by using 45 PCR cycles; other species were determined by using 40 PCR cycles. A) *P. falciparum*: median (IQR) density was 11.4 (2.5–54.7) parasites/µL for single-species infections (n = 429) and 16.5 (3.5–56.9) parasites/µL for mixed-species infections (n = 326) (p = 0.117). B) *P. ovale*: median (IQR) density was 13.5 (1.3–30.1) parasites/µL for single-species infections (n = 519) and 3.1 (1.2–11.4) parasites/µL for mixed-species infections (n = 295) (p<0.001). C) *P. malariae*: median (IQR) density was 16.1 (3.8–164.0) parasites/µL for single-species infections (n = 24) and 11.2 (2.6–53.9) parasites/µL for mixed-species infections ([n = 112) (p = 0.169). D) *P. vivax*: median (IQR) density was 0.4 (0.2–0.9) parasites/µL for single-species infections (n = 4) and 0.7 (0.5–0.8) parasites/µL for mixed-species infections (n = 7) (p = 0.571). IQR, interquartile range.

risk. High epidemiologic risk strata harbored most single-species infections across all 4 *Plasmodium* spp. and also mixed infections with *P. falciparum*.

Parasite Density

Malaria parasitemia estimated by semiquantitative PCR was low across nonfalciparum species (Figure 2). Median (IQR; min–max) *P. ovale* density was 7.2 (1.3–25.0; 0.1–168,596) parasites/µL, comparable to *P. malariae* density at 11.7 (2.7–54.9; 0.3–1,214) parasites/µL. *P. vivax* density was ≈0.6 (0.3–0.8; 0.1–8.1) parasites/µL. Although 18% (n = 25) of *P. malariae* infections had a parasite density >100 parasites/µL, we rarely observed that level for *P. ovale* (3%, n = 25) and never for *P. vivax*. *P. falciparum* density was also low at 13.1 (2.6–55.9; 0.1–8,248) parasites/µL; however, 17% (n = 132) of *P. falciparum* cases had a parasite density >100 parasites/µL, and 3% (n = 24) had >500 parasites/µL. Median (IQR) density among *P. ovale* mixed infections was 3.1 (1.2–11.4) parasites/µL and 13.5 (1.3–30.1) parasites/µL for *P. ovale* single-species infections (p<0.001), whereas densities were similar between single- and mixed-species infections among the other malaria species (Figure 2).

P. ovale Species Determination

Among 814 samples positive for *P. ovale*, 60 (7%) samples with the highest parasitemia were selected for PCR to distinguish between *P. ovale wallikeri* and *P. ovale curtisi*. Species determination by PCR was

Table 2. Number of students infected with *Plasmodium* spp. and school characteristics in study of similar prevalence of *Plasmodium falciparum* and non–*P. falciparum* malaria infections among schoolchildren, Tanzania*

School characteristics‡	*Plasmodium* spp. infections†				Total, n = 3,456
	Pf, n = 755	Po, n = 814	Pm, n = 136	Pv, n = 11	
Elevation, m					
Median (IQR)	1,182 (506–1,370)	1,225 (1,124–1,427)	1,167 (320–1,370)	1,333 (1,100–1,398)	1,230 (1,058–1,467)
Minimum–maximum	54–1,901	47–2,167	54–1,677	184–1,467	34–2,167
<1,500	707 (26.5)	693 (26.0)	129 (4.8)	11 (0.4)	2,667 (100)
≥1,500	48 (6.1)	121 (15.3)	7 (0.9)	0	789 (100)
Region‡					
Arusha	3 (0.5)	23 (4.2)	0	0	552 (100)
Iringa	1 (0.3)	30 (9.4)	0	0	320 (100)
Kagera	196 (31.7)	273 (44.1)	39 (6.3)	6 (1.0)	619 (100)
Mara	157 (34.7)	102 (22.6)	19 (4.2)	2 (0.4)	452 (100)
Mtwara	146 (47.6)	62 (20.2)	38 (12.4)	1 (0.3)	307 (100)
Rukwa	49 (16.3)	118 (39.2)	6 (2.0)	0	301 (100)
Tabora	122 (29.5)	139 (33.7)	25 (6.1)	0	413 (100)
Tanga	81 (16.5)	67 (13.6)	9 (1.8)	2 (0.4)	492 (100)

*Values are no. (%) students unless otherwise indicated. IQR, interquartile range; Pf, *Plasmodium falciparum;* Pm, *P. malariae*; Po, *P. ovale* spp.; Pv, *P. vivax.*
†Totals and percentages in each species-specific column represent student-level prevalences and include single- and mixed-species infections.
‡Listed regions correspond to mapped regions in Figure 3.

successful in 35% (n = 21) of samples; *P. ovale curtisi* was detected in 17 samples and *P. ovale wallikeri* in 9 samples. We identified *P. ovale curtisi* and *P. ovale wallikeri* co-infections in 5 students. We did not perform further characterization because of limited sample sizes.

Geographic Distribution

We detected *P. ovale* across all 8 regions sampled in Tanzania, indicating widespread distribution (Table 2; Figures 3, 4). *P. ovale* prevalence was highest within the northern Kagera (34%, n = 273) and central Tabora (17%, n = 139) regions. We detected *P. ovale*

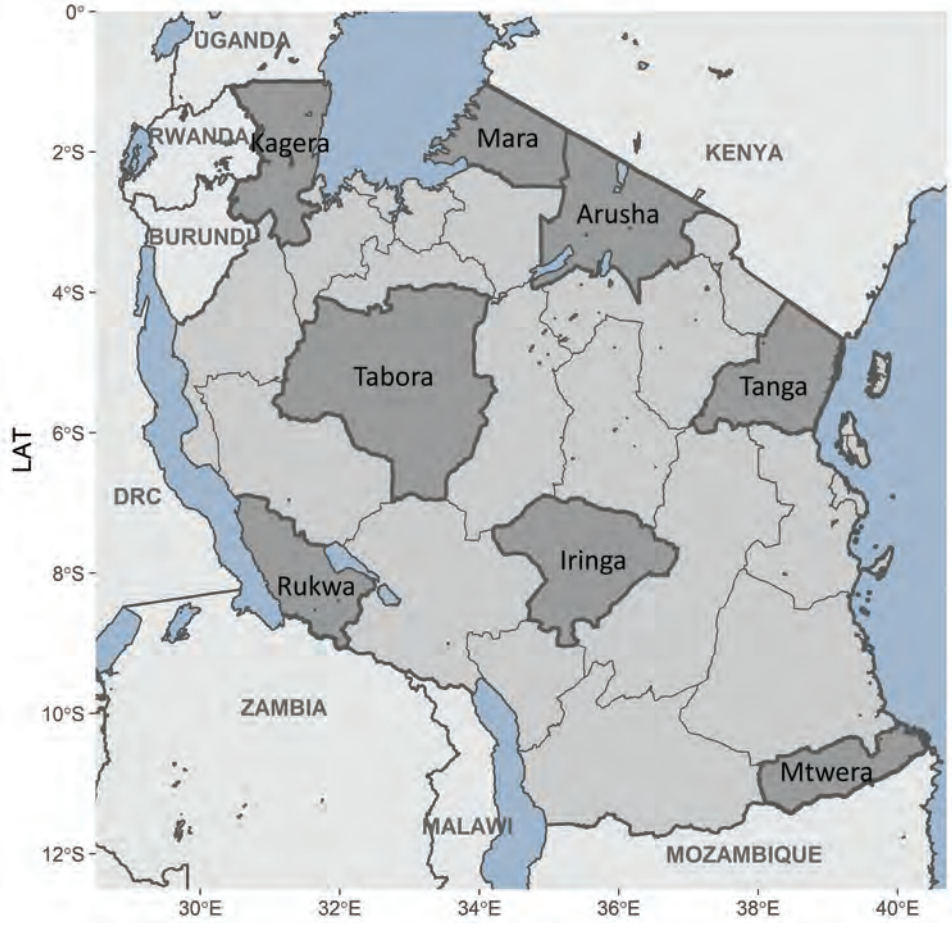

Figure 3. Locations of 8 survey regions within mainland Tanzania (dark gray shading) in study of similar prevalence of *Plasmodium falciparum* and non–*P. falciparum* malaria infections among schoolchildren, Tanzania.

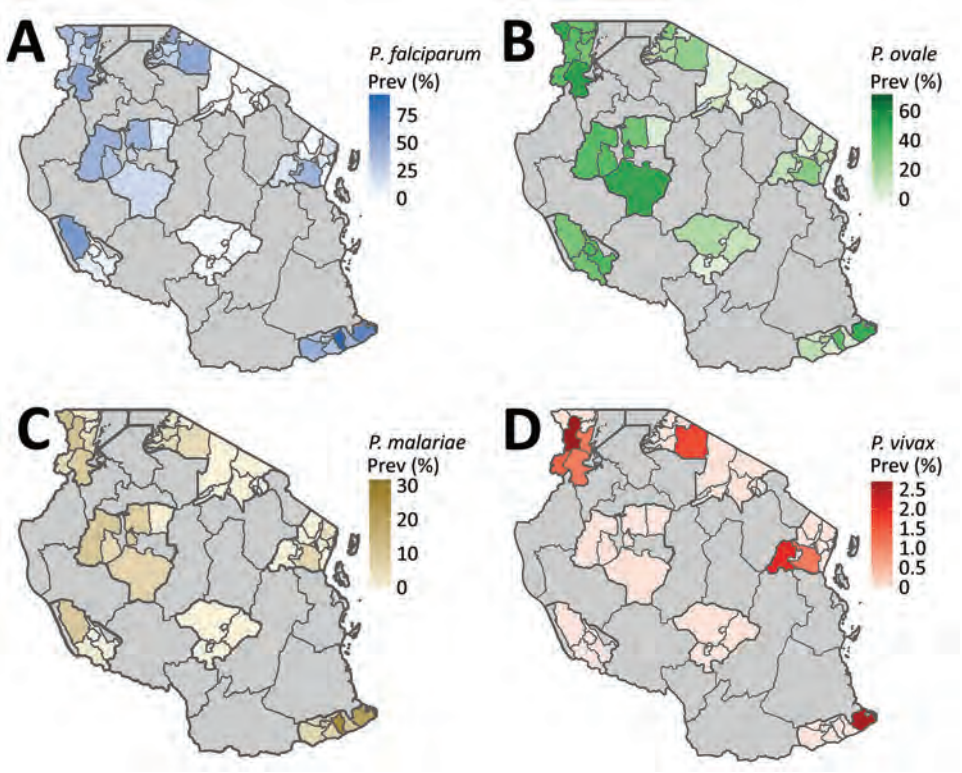

Figure 4. Spatial distribution of regional and school council–level malaria prevalence by species in study of similar prevalence of *Plasmodium falciparum* and non–*P. falciparum* malaria infections among schoolchildren, Tanzania. A) *P. falciparum*; B) *P. ovale*; C) *P. malariae*; D) *P. vivax*.

curtisi infections in 6 of 8 regions (all but Arusha and Rukwa) and *P. ovale wallikeri* in 5 of 8 (Kagera, Mara, Tabora, Tanga, and Iringa) regions. We observed high prevalence of *P. malariae* in Kagera (29%, n = 39) and in southernmost Mtwara (28%, n = 38), and *P. vivax* was predominantly distributed along the northwestern borders of Tanzania in Kagera (55%, n = 6); select, isolated cases of *P. vivax* were also detected in southern and eastern regions. Arusha and Iringa did not have any cases of *P. malariae* or *P. vivax* infections and had the lowest frequencies of *P. ovale* (3%, n = 23, in Arusha; 4%, n = 30, in Iringa) and *P. falciparum* (0.4%, n = 3, in Arusha; 0.1%, n = 1, in Iringa) infections.

We detected malaria infections in students who were predominantly located at elevations <1,500 m, including 85% (n = 693) infected by *P. ovale*, 94% (n = 707) by *P. falciparum*, 95% (n = 129) by *P. malariae*, and 100% (n = 11) by *P. vivax* (Table 2). Most (77%, n = 2,667) students enrolled in our study were from schools located at elevations <1,500 m. Among students located at elevations >1,500, *P. ovale* infections were detected most frequently in 15% (n = 121) of students compared with 6% (n = 48) infected with *P. falciparum*, 1% (n = 7) infected with *P. malariae*, and 0% infected with *P. vivax*.

We compared scaled prevalence estimates for nonfalciparum species with *P. falciparum* and identified areas where prevalences were higher than expected for *P. ovale* and *P. malariae* on the basis of *P. falciparum* frequency (Figure 5); *P. vivax* infections were too infrequent for comparison. In the southern and southwestern highlands and northwestern lake regions (Iringa, Rukwa, Tabora, and Kagera), scaled *P. ovale* prevalences were higher than *P. falciparum* prevalences. Scaled prevalence of *P. malariae* was notably higher than that of *P. falciparum* in the Karagwe council in Kagera and Mtwara municipal council in Mtwara. In most other areas, scaled prevalence of *P. malariae* was similar to or lower than *P. falciparum* prevalence.

Discussion

Our study describes a large nationally representative molecular survey of nonfalciparum malaria epidemiology across Tanzania. We used real-time PCR to estimate nonfalciparum infection prevalences in school-aged children in 8 regions of the country selected to maintain geographic diversity and malaria transmission risk heterogeneity. One quarter (24%) of schoolchildren harbored *P. ovale* parasites, comparable to the 22% *P. falciparum* prevalence in the population, and 64% of *P. ovale* infections were single-species infections. *P. malariae* was observed in 4% of students, of which most were co-infected with other malaria species. *P. vivax* infections were rare (0.3% prevalence).

High *P. ovale* prevalence could be attributed to several factors. First, we increased the number of PCR cycles for *P. ovale* detection to 45 to enable detection of low-density infections, which comprised 91% of all *P. ovale* infections identified (Appendix Table 8). This approach has precedence (*17*,*25*,*31*), as low-density parasitemia is characteristic of *P. ovale* infections, making detection challenging. Using 40-cycle PCR for *P. ovale* yielded a 0.8% prevalence estimate in our previous work in the Democratic Republic of the Congo (*5*). The prevalence of *P. ovale* infections positive at <40 cycles in this study was 9% (n = 75), confirming most infections occurred at very low parasite densities. Second, many large-scale molecular surveys of nonfalciparum malaria have focused on adults or all-age cohorts, whereas school-aged children are increasingly recognized as the main contributors to asymptomatic and infectious malaria reservoirs (*33*–*35*). Finally, the high prevalence of *P. ovale* in our study might reflect increasing *P. ovale* transmission despite malaria control efforts targeting *P. falciparum*. Increasing or persistent transmission of *P. ovale* and *P. malariae* amid a *P. falciparum* decline has been observed in molecular surveys from Tanzania and nearby Kenya and Uganda, including in symptomatic cases (*17*,*18*,*24*,*36*). The causes of increased transmission are unclear but might include hypnozoite-induced relapses of *P. ovale* infections not treated by artemisinin-based combination therapies, insect day-biting, or outdoor vectors that evade bed nets.

In contrast to findings from other studies (*11*,*36*–*39*), we found that *P. ovale* infections occurred more commonly as single-species infections than did other nonfalciparum species infections, although increased sensitivity of *P. ovale*–specific PCR might partially explain those observations. *P. ovale* single-species infections were rarely detected by RDTs, rendering them more difficult to detect and treat. In addition, *P. ovale* single-species infections were largely the only infections identified within regions categorized as low risk for malaria transmission, suggesting an unexpected transmission risk in areas where prevention measures might be less common and *P. falciparum* risk is not a particular concern. Our scaled differential prevalence map similarly highlighted several councils where *P. ovale* and *P. malariae* prevalences were proportionally higher than expected on the basis of *P. falciparum* frequency. Taken together, those characteristics indicate a hidden burden of *P. ovale* infections in Tanzania.

Detection of *P. vivax* in this study is notable given the infection control challenges posed by this species. Infections were predominately detected in the northwest/Lake regions of Tanzania and in the east, where several other studies have also observed low *P. vivax* prevalences (*4*,*24*,*40*). *P. malariae* prevalence of 4% aligns with recent research in the region that also identified low infection prevalences (2.5% in Malawi, 4.1% in Democratic Republic of the Congo, and 3.3% symptomatic and 5.3% asymptomatic cases in western Kenya) (*12*,*28*,*39*). Estimated parasite densities were low across nonfalciparum species, as expected. *P. falciparum* parasite densities were also relatively low (median 13.1 parasites/μL), likely because of the predominantly asymptomatic population. In addition, mapping confirmed low or nonexistent prevalence of nonfalciparum malaria within the northern highlands of Arusha and southern highlands and midlands of Iringa.

The first limitation of our study is that using different PCR cycling times for different species introduces ascertainment bias. Because *P. malariae* and *P. falciparum* assays were run at 40 rather than 45 cycles, their relative prevalences compared with prevalence for *P. ovale* might be underestimated. However, we

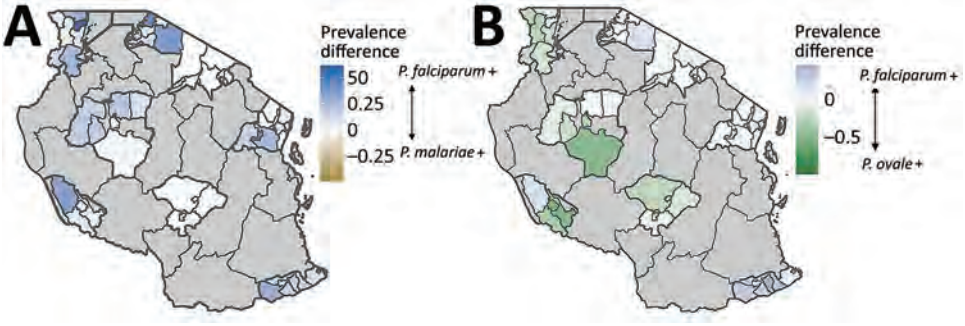

Figure 5. Differential scaled prevalences between *Plasmodium malariae* or *P. ovale* and *P. falciparum* at the school council level in study of similar prevalence of *Plasmodium falciparum* and non–*P. falciparum* malaria infections among schoolchildren, Tanzania. A) Blue shading indicates councils where *P. falciparum* scaled prevalence is greater (indicated by + in key) than *P. malariae* scaled prevalence; gold indicates regions where *P. malariae* scaled prevalence is greater. B) Light blue shading indicates councils where *P. falciparum* scaled prevalence is greater than *P. ovale* spp. scaled prevalence; green indicates regions where *P. ovale* scaled prevalence is greater. Comparison of scaled prevalences for *P. falciparum* and *P. vivax* is not depicted because the low number of *P. vivax* infections biased the scaled measurement.

performed a sensitivity analysis to quantify this bias, which indicated that only an additional 2.5% of *P. falciparum* and 10% of *P. malariae* infections would be detected by using 45 cycles, suggesting minimal underestimation of reported *P. falciparum* and *P. malariae* prevalences and no meaningful effect on overall conclusions. Weighting sensitivity analysis results to the total study population yielded a *P. falciparum* prevalence of 25% if 45 cycles were used compared with the observed prevalence of 22%. Despite this result, prevalences could still be underestimated given lower probabilities of detecting very low density infections because of PCR limits of detection in concert with small volumes of template DNA used in the assays (2 μL for *P. malariae, P. ovale*, and *P. falciparum*; 5 μL for *P. vivax*). Second, our study did not sample all geographic regions in Tanzania, and findings cannot be extrapolated to other age groups with differing malaria risk profiles. School-based sampling likely underestimated prevalence of symptomatic or severe malaria infection in school-aged children because children might have been absent because of illness. Finally, the cross-sectional survey design revealed little about clinical implications of prevalent nonfalciparum infections, especially given substantial nonrandom missingness in fever data, or the extent to which infections represented chronic infection carriage versus transient parasitemia.

In conclusion, the overall high prevalence and broad geographic distribution of *P. ovale* and, to a lesser extent, *P. malariae* and the more focal distribution of *P. vivax* in this study underscore an urgent need to elucidate clinical prevalence and transmission patterns of those species to inform malaria control programs in Tanzania. Current treatment protocols in Tanzania do not regularly address hypnozoite liver-stage *P. ovale* infection, and relapses are expected after blood-stage clearance by artemisinin-based combination therapy (*41*). Accumulating evidence exists for increases in previously unappreciated nonfalciparum malaria infections in sub-Saharan Africa (*38*). Molecular detection methods, such as PCR, and new treatment strategies will be required for continued progress toward malaria control and elimination.

Acknowledgments

We thank the 2017 SMPS study administrators and staff for their tireless work implementing the survey and students for participating in the study.

The following reagents were obtained through BEI Resources, National Institute of Allergy and Infectious Diseases, National Institutes of Health: diagnostic plasmids containing the small subunit 18S ribosomal RNA gene from *Plasmodium malariae*, MRA-179; *Plasmodium ovale*, MRA-180; and *Plasmodium vivax*, MRA-178, contributed by Peter A. Zimmerman; and *Plasmodium falciparum*, strain 3D7, MRA-102, contributed by Daniel J. Carucci.

This study was funded by the US National Institutes of Health (K24AI134990 and R01TW010870 to J.J.J.; T32AI070114 to C.L.M.; R21AI152260 to J.T.L.; R21AI148579 to J.T.L. and J.B.P.; R01AI139520 to J.B.P., R.S., and C.L.M.; and T32AI070114 to R.S.); Global Fund, which funded the survey; and US President's Malaria Initiative via the US Agency for International Development Okoa Maisha Dhibiti Malaria (cooperative agreement no. 72062118CA-00002) implemented by RTI International under the terms of an interagency agreement with the US Centers for Disease Control and Prevention for data management and facilitation of the initial processing and exporting of blood samples. Funding sources had no role in the study design, analysis, or writing of the manuscript.

The findings and conclusions in this report are those of the author(s) and do not necessarily represent the official position of the US Centers for Disease Control and Prevention, the President's Malaria Initiative via the US Agency for International Development, or other employing organizations or sources of funding.

About the Author

Ms. Sendor is a doctoral student at the University of North Carolina, Chapel Hill. Her research interests focus on malaria epidemiology.

References

1. World Health Organization. World malaria report 2021 [cited 2021 Dec 13]. https://www.who.int/teams/global-malaria-programme/reports/world-malaria-report-2021
2. Alegana VA, Macharia PM, Muchiri S, Mumo E, Oyugi E, Kamau A, et al. *Plasmodium falciparum* parasite prevalence in East Africa: updating data for malaria stratification. PLOS Glob Public Health. 2021;1:e0000014. https://doi.org/10.1371/journal.pgph.0000014
3. Oriero EC, Amenga-Etego L, Ishengoma DS, Amambua-Ngwa A. *Plasmodium malariae*, current knowledge and future research opportunities on a neglected malaria parasite species. Crit Rev Microbiol. 2021;47:44–56. https://doi.org/10.1080/1040841X.2020.1838440
4. Kim MJ, Jung BK, Chai JY, Eom KS, Yong TS, Min DY, et al. High malaria prevalence among schoolchildren on Kome Island, Tanzania. Korean J Parasitol. 2015;53:571–4. https://doi.org/10.3347/kjp.2015.53.5.571
5. Mitchell CL, Brazeau NF, Keeler C, Mwandagalirwa MK, Tshefu AK, Juliano JJ, et al. Under the radar: epidemiology of *Plasmodium ovale* in the Democratic Republic of the Congo.

J Infect Dis. 2021;223:1005–14. https://doi.org/10.1093/infdis/jiaa478
6. Björkman A, Shakely D, Ali AS, Morris U, Mkali H, Abbas AK, et al. From high to low malaria transmission in Zanzibar—challenges and opportunities to achieve elimination. BMC Med. 2019;17:14. https://doi.org/10.1186/s12916-018-1243-z
7. Bousema JT, Drakeley CJ, Mens PF, Arens T, Houben R, Omar SA, et al. Increased *Plasmodium falciparum* gametocyte production in mixed infections with *P. malariae*. Am J Trop Med Hyg. 2008;78:442–8. https://doi.org/10.4269/ajtmh.2008.78.442
8. Sutherland CJ. Persistent parasitism: the adaptive biology of *malariae* and *ovale* malaria. Trends Parasitol. 2016;32:808–19. https://doi.org/10.1016/j.pt.2016.07.001
9. World Health Organization. World malaria report 2020 [cited 2021 Aug 29]. https://www.who.int/publications-detail-redirect/9789240015791
10. Langford S, Douglas NM, Lampah DA, Simpson JA, Kenangalem E, Sugiarto P, et al. *Plasmodium malariae* infection associated with a high burden of anemia: a hospital-based surveillance study. PLoS Negl Trop Dis. 2015;9:e0004195. https://doi.org/10.1371/journal.pntd.0004195
11. Mueller I, Zimmerman PA, Reeder JC. *Plasmodium malariae* and *Plasmodium ovale*—the "bashful" malaria parasites. Trends Parasitol. 2007;23:278–83. https://doi.org/10.1016/j.pt.2007.04.009
12. Lo E, Nguyen K, Nguyen J, Hemming-Schroeder E, Xu J, Etemesi H, et al. *Plasmodium malariae* prevalence and *csp* gene diversity, Kenya, 2014 and 2015. Emerg Infect Dis. 2017;23:601–10. https://doi.org/10.3201/eid2304.161245
13. Twohig KA, Pfeffer DA, Baird JK, Price RN, Zimmerman PA, Hay SI, et al. Growing evidence of *Plasmodium vivax* across malaria-endemic Africa. PLoS Negl Trop Dis. 2019;13:e0007140. https://doi.org/10.1371/journal.pntd.0007140
14. Howes RE, Battle KE, Mendis KN, Smith DL, Cibulskis RE, Baird JK, et al. Global epidemiology of *Plasmodium vivax*. Am J Trop Med Hyg. 2016;95:15–34. https://doi.org/10.4269/ajtmh.16-0141
15. Price RN, Commons RJ, Battle KE, Thriemer K, Mendis K. *Plasmodium vivax* in the era of the shrinking *P. falciparum* map. Trends Parasitol. 2020;36:560–70. https://doi.org/10.1016/j.pt.2020.03.009
16 Groger M, Fischer HS, Veletzky L, Lalremruata A, Ramharter M. A systematic review of the clinical presentation, treatment and relapse characteristics of human *Plasmodium ovale* malaria. Malar J. 2017;16:112. https://doi.org/10.1186/s12936-017-1759-2
17. Akala HM, Watson OJ, Mitei KK, Juma DW, Verity R, Ingasia LA, et al. *Plasmodium* interspecies interactions during a period of increasing prevalence of *Plasmodium ovale* in symptomatic individuals seeking treatment: an observational study. Lancet Microbe. 2021;2:e141–50. https://doi.org/10.1016/S2666-5247(21)00009-4
18. Yman V, Wandell G, Mutemi DD, Miglar A, Asghar M, Hammar U, et al. Persistent transmission of *Plasmodium malariae* and *Plasmodium ovale* species in an area of declining *Plasmodium falciparum* transmission in eastern Tanzania. PLoS Negl Trop Dis. 2019;13:e0007414. https://doi.org/10.1371/journal.pntd.0007414
19 Doctor SM, Liu Y, Anderson OG, Whitesell AN, Mwandagalirwa MK, Muwonga J, et al. Low prevalence of *Plasmodium malariae* and *Plasmodium ovale* mono-infections among children in the Democratic Republic of the Congo: a population-based, cross-sectional study. Malar J. 2016;15:350. https://doi.org/10.1186/s12936-016-1409-0
20. Taylor SM, Messina JP, Hand CC, Juliano JJ, Muwonga J, Tshefu AK, et al. Molecular malaria epidemiology: mapping and burden estimates for the Democratic Republic of the Congo, 2007. PLoS One. 2011;6:e16420. https://doi.org/10.1371/journal.pone.0016420
21 US Agency for International Development. US President's Malaria Initiative. Tanzania malaria operational plan FY 2015 [cited 2021 Aug 30]. https://d1u4sg1s9ptc4z.cloudfront.net/uploads/2021/03/fy-2015-tanzania-malaria-operational-plan.pdf
22. Chacky F, Runge M, Rumisha SF, Machafuko P, Chaki P, Massaga JJ, et al. Nationwide school malaria parasitaemia survey in public primary schools, the United Republic of Tanzania. Malar J. 2018;17:452. https://doi.org/10.1186/s12936-018-2601-1
23. Tanzania Ministry of Health, Community Development, Gender, Elderly and Children; Ministry of Health Zanzibar; National Bureau of Statistics and Office of the Chief Government Statistician Zanzibar; ICF USA. Tanzania malaria indicator survey 2017 [cited 2021 Aug 30]. https://dhsprogram.com/pubs/pdf/MIS31/MIS31.pdf
24. Cook J, Xu W, Msellem M, Vonk M, Bergström B, Gosling R, et al. Mass screening and treatment on the basis of results of a *Plasmodium falciparum*–specific rapid diagnostic test did not reduce malaria incidence in Zanzibar. J Infect Dis. 2015;211:1476–83. https://doi.org/10.1093/infdis/jiu655
25. Tarimo BB, Nyasembe VO, Ngasala B, Basham C, Rutagi IJ, Muller M, et al. Seasonality and transmissibility of *Plasmodium ovale* in Bagamoyo District, Tanzania. Parasit Vectors. 2022;15:56. https://doi.org/10.1186/s13071-022-05181-2
26. Mitchell CL, Ngasala B, Janko MM, Chacky F, Edwards JK, Pence BW, et al. Evaluating malaria prevalence and land cover across varying transmission intensity in Tanzania using a cross-sectional survey of school-aged children. Malar J. 2022;21:80. https://doi.org/10.1186/s12936-022-04107-8
27 Teyssier NB, Chen A, Duarte EM, Sit R, Greenhouse B, Tessema SK. Optimization of whole-genome sequencing of *Plasmodium falciparum* from low-density dried blood spot samples. Malar J. 2021;20:116. https://doi.org/10.1186/s12936-021-03630-4
28. Gumbo A, Topazian HM, Mwanza A, Mitchell CL, Puerto-Meredith S, Njiko R, et al. Occurrence and distribution of nonfalciparum malaria parasite species among adolescents and adults in Malawi. J Infect Dis. 2022;225:257–68. https://doi.org/10.1093/infdis/jiab353
29. Hewawasam E, Liu G, Jeffery DW, Gibson RA, Muhlhausler BS. Estimation of the volume of blood in a small disc punched from a dried blood spot card. Eur J Lipid Sci Technol. 2018;120:1700362. https://doi.org/10.1002/ejlt.201700362
30. Perandin F, Manca N, Calderaro A, Piccolo G, Galati L, Ricci L, et al. Development of a real-time PCR assay for detection of *Plasmodium falciparum*, *Plasmodium vivax*, and *Plasmodium ovale* for routine clinical diagnosis. J Clin Microbiol. 2004;42:1214–9. https://doi.org/10.1128/JCM.42.3.1214-1219.2004
31. Calderaro A, Piccolo G, Gorrini C, Montecchini S, Rossi S, Medici MC, et al. A new real-time PCR for the detection of *Plasmodium ovale wallikeri*. PLoS One. 2012;7:e48033. https://doi.org/10.1371/journal.pone.0048033
32. Pebesma E. Simple features for R: standardized support for spatial vector data. R J. 2018;10:439–46. https://doi.org/10.32614/RJ-2018-009

33. Abdulraheem MA, Ernest M, Ugwuanyi I, Abkallo HM, Nishikawa S, Adeleke M, et al. High prevalence of *Plasmodium malariae* and *Plasmodium ovale* in co-infections with *Plasmodium falciparum* in asymptomatic malaria parasite carriers in southwestern Nigeria. Int J Parasitol. 2022;52:23–33. https://doi.org/10.1016/j.ijpara.2021.06.003
34. Andolina C, Rek JC, Briggs J, Okoth J, Musiime A, Ramjith J, et al. Sources of persistent malaria transmission in a setting with effective malaria control in eastern Uganda: a longitudinal, observational cohort study. Lancet Infect Dis. 2021 ;21:1568–78. https://doi.org/10.1016/S1473-3099(21)00072-4
35. Walldorf JA, Cohee LM, Coalson JE, Bauleni A, Nkanaunena K, Kapito-Tembo A, et al. School-age children are a reservoir of malaria infection in Malawi. PLoS One. 2015;10:e0134061. https://doi.org/10.1371/journal.pone.0134061
36. Betson M, Clifford S, Stanton M, Kabatereine NB, Stothard JR. Emergence of nonfalciparum *Plasmodium* infection despite regular artemisinin combination therapy in an 18-month longitudinal study of Ugandan children and their mothers. J Infect Dis. 2018;217:1099–109. https://doi.org/10.1093/infdis/jix686
37. Bruce MC, Macheso A, Kelly-Hope LA, Nkhoma S, McConnachie A, Molyneux ME. Effect of transmission setting and mixed species infections on clinical measures of malaria in Malawi. PLoS One. 2008;3:e2775. https://doi.org/10.1371/journal.pone.0002775
38. Hawadak J, Dongang Nana RR, Singh V. Global trend of *Plasmodium malariae* and *Plasmodium ovale* spp. malaria infections in the last two decades (2000–2020): a systematic review and meta-analysis. Parasit Vectors. 2021;14:297. https://doi.org/10.1186/s13071-021-04797-0
39. Parr JB, Kieto E, Phanzu F, Mansiangi P, Mwandagalirwa K, Mvuama N, et al. Analysis of false-negative rapid diagnostic tests for symptomatic malaria in the Democratic Republic of the Congo. Sci Rep. 2021;11:6495. https://doi.org/10.1038/s41598-021-85913-z
40. Baltzell KA, Shakely D, Hsiang M, Kemere J, Ali AS, Björkman A, et al. Prevalence of PCR detectable malaria infection among febrile patients with a negative *Plasmodium falciparum* specific rapid diagnostic test in Zanzibar. Am J Trop Med Hyg. 2013;88:289–91. https://doi.org/10.4269/ajtmh.2012.12-0095
41. Groger M, Veletzky L, Lalremruata A, Cattaneo C, Mischlinger J, Manego Zoleko R, et al. Prospective clinical and molecular evaluation of potential *Plasmodium ovale curtisi* and *wallikeri* relapses in a high-transmission setting. Clin Infect Dis. 2019;69:2119–26. https://doi.org/10.1093/cid/ciz131

Address for correspondence: Jonathan Juliano, University of North Carolina at Chapel Hill, 111 Mason Farm Rd, 2340B, MBRB, CB#7036, Chapel Hill, NC 27713, USA; email: jjuliano@med.unc.edu

etymologia revisited

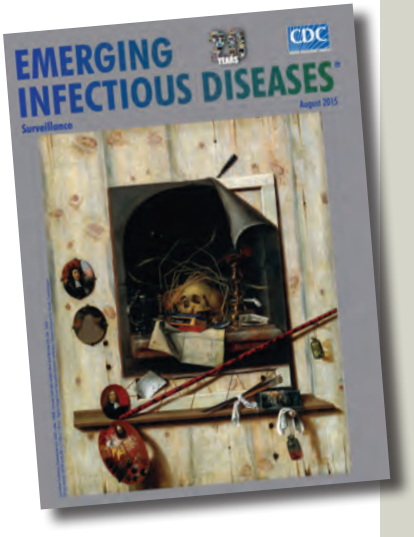

Originally published in August 2015

Escherichia coli

[esh″ə-rik′e-ə co′lī]

A gram-negative, facultatively anaerobic rod, *Escherichia coli* was named for Theodor Escherich, a German-Austrian pediatrician. Escherich isolated a variety of bacteria from infant fecal samples by using his own anaerobic culture methods and Hans Christian Gram's new staining technique. Escherich originally named the common colon bacillus *Bacterium coli commune*. Castellani and Chalmers proposed the name *E. coli* in 1919, but it was not officially recognized until 1958.

References:

1. Oberbauer BA. Theodor Escherich—Leben und Werk. Munich: Futuramed-Verlag; 1992.
2. Shulman ST, Friedmann HC, Sims RH. Theodor Escherich: the first pediatric infectious diseases physician? Clin Infect Dis. 2007;45:1025–9 .

https://wwwnc.cdc.gov/eid/article/21/8/et-2108_article

Early SARS-CoV-2 Reinfections Involving the Same or Different Genomic Lineages, Spain

Cristina Rodríguez-Grande, Agustín Estévez, Rosalía Palomino-Cabrera, Andrea Molero-Salinas, Daniel Peñas-Utrilla, Marta Herranz, Amadeo Sanz-Pérez, Luis Alcalá, Cristina Veintimilla, Pilar Catalán, Carolina Martínez-Laperche, Roberto Alonso, Patricia Muñoz, Laura Pérez-Lago,[1] Darío García de Viedma,[1] on behalf of the Gregorio Marañón Microbiology-ID COVID 19 Study Group[2]

Centers for Disease Control and Prevention guidelines consider SARS-CoV-2 reinfection when sequential COVID-19 episodes occur ≥90 days apart. However, genomic diversity acquired over recent COVID-19 waves could mean previous infection provides insufficient cross-protection. We used genomic analysis to assess the percentage of early reinfections in a sample of 26 patients with 2 COVID-19 episodes separated by 20–45 days. Among sampled patients, 11 (42%) had reinfections involving different SARS-CoV-2 variants or subvariants. Another 4 cases were probable reinfections; 3 involved different strains from the same lineage or sublineage. Host genomic analysis confirmed the 2 sequential specimens belonged to the same patient. Among all reinfections, 36.4% involved non-Omicron, then Omicron lineages. Early reinfections showed no specific clinical patterns; 45% were among unvaccinated or incompletely vaccinated persons, 27% were among persons <18 years of age, and 64% of patients had no risk factors. Time between sequential positive SARS-CoV-2 PCRs to consider reinfection should be re-evaluated.

Estimates of the burden of SARS-CoV-2 reinfections continue to be crucial for assessing new SARS-CoV-2 variants with immune escape potential (*1*). Genomic analysis of SARS-CoV-2 strains involved in sequential COVID-19 episodes has been key to assessing the proportion of reinfections, differentiating reinfection from persistent infection, and characterizing reinfection in detail.

Centers for Disease Control and Prevention (CDC) guidelines for consideration of SARS-CoV-2 reinfection require evidence of 2 sequential COVID-19 episodes separated by ≥90 days and ≥1 negative RT-PCR in between (*2*). However, inclusion criterion for most studies that have focused on COVID-19 reinfection have usually required 45–60 days between sequential episodes (*3*,*4*). This timeframe maximizes factors that increase the likelihood of reinfection, including the chance of cure of the first episode, clearance of the strain involved in the first episode, and possibility of reexposure to another positive case. Following this philosophy, we reported a systematic population-based analysis of reinfections during the first, second, and third pandemic waves in Spain (*5*). Some studies conducted during Omicron waves described an increase in the proportion of reinfections (*6*,*7*) and a shorter interval between reinfection episodes, such as early reinfections in ≤60 days. In this study, we aimed to evaluate the possibility of finding reinfections when they are even less likely, <45 days between episodes, and assess which SARS-CoV-2 variants were involved. The study was

Author affiliations: Gregorio Marañón General University Hospital, Madrid, Spain (C. Rodríguez-Grande, A. Estévez, R. Palomino-Cabrera, A. Molero-Salinas, D. Peñas-Utrilla, M. Herranz, A. Sanz-Pérez, L. Alcalá, C. Veintimilla, P. Catalán, C. Martínez-Laperche, R. Alonso, P. Muñoz, L. Pérez-Lago, D. García de Viedma); Instituto de Investigación Sanitaria Gregorio Marañón (IiSGM), Madrid (C. Rodríguez-Grande, A. Estévez, R. Palomino-Cabrera, A. Molero-Salinas, D. Peñas-Utrilla, A. Sanz-Pérez, L. Pérez-Lago, D. García de Viedma); Universidad Complutense, Madrid (R. Alonso, P. Muñoz); Centro de Investigación Biomédica en Red (CIBER) de Enfermedades Respiratorias-CIBERES, Madrid (R. Alonso, P. Muñoz, D. García de Viedma)

DOI: https://doi.org/10.3201/eid2906.221696

[1]This senior authors contributed equally to this article.

[2]Additional members of the Gregorio Marañón Microbiology-ID COVID-19 Study Group who contributed data are listed at the end of this article.

based on the 15,794 COVID-19 cases diagnosed during November 26, 2021–August 21, 2022, at Gregorio Marañón General University Hospital, a tertiary hospital that serves 650,000 inhabitants in the population of Madrid, Spain.

Material and Methods

Specimens

We selected all cases with 2 sequential COVID-19 episodes at an interval of 20–45 days by considering the time between the last positive reverse transcription PCR (RT-PCR) specimen in the first episode and the first positive specimen in the second episode. We also requested cases for which ≥1 positive specimen was available in our stored collection, among those taken in the first 10 days of each sequential episode, and for which the specimens had sufficient viral load (cycle threshold [Ct] ≤32) to maximize the chance of obtaining optimal coverage in whole-genome sequence analysis. To minimize the possibility of including potentially persistent cases, we excluded cases that had clinical conditions or admissions to hospital services that likely corresponded to immunocompromised status.

We used remnants of nasopharyngeal swab specimens previously used for diagnostic purposes via TaqPath COVID-19 CE-IVD RT-PCR kit (ThermoFisher Scientific, https://www.thermofisher.com) during November 26, 2021–August 21, 2022. We extracted viral RNA from nasopharyngeal exudates by using the KingFisher instrument (ThermoFisher Scientific). We used 16 μL of RNA as a template for reverse transcription by using LunaScript RT SuperMix Kit (New England Biolabs, https://www.neb.com).

Whole-Genome Sequencing

We performed whole-genome amplification of SARS-CoV-2 (Appendix, https://wwwnc.cdc.gov/EID/article/29/6/22-1696-App1.pdf). We deposited sequences above the GISAID quality thresholds into the GISAID database (https://www.gisaid.org); we submitted sequences below the GISAID threshold to the European Nucleotide archive (https://www.ebi.ac.uk/ena; project no. PRJEB56460) (Appendix Tables 1–3).

We considered a case to be a reinfection if different lineages or sublineages were involved in each sequential episode. We also assigned cases as probable reinfections when the sequential strains belonged to the same lineage or sublineage and the sequential strains harbored specific single-nucleotide variants (SNVs) not shared between the first and second episode, indicating that the sequence from the second episode was not derived from the first episode.

Minority Variant Analysis

We assessed whether the strain involved in the first episode persisted as a minority variant (i.e., trace of the virus) in the second episode. In each early reinfection case, we used Integrative Genomics Viewer version 2.14.1 (Broad Institute, https://www.broadinstitute.org) to visually inspected SNV alleles called in the strain involved in the first episode in the sequences obtained from the strains involved in the second episode.

Short Tandem Repeat Analysis

We conducted short tandem repeat analysis to ensure that the tested specimens from sequential episodes of all reinfection and probable reinfection cases belonged to the same patient. We used the Mentype Chimera PCR Amplification Kit (Biotype, https://www.biotype.de) to examine 12 noncoding short tandem repeat loci and the sex-specific amylogenic locus on specimens (Appendix).

Results

The first Omicron variant in our study population was identified during late November 2021. Delta and Omicron variants coexisted during November 26, 2021–January 15, 2022. The study population yielded 66 (0.42%) cases with 2 sequential COVID-19 cases that fulfilled our criteria (Figure). From this initial selection, we excluded 23 cases with clinical conditions or hospitalizations that likely corresponded to an immunocompromised status to minimize the inclusion of potentially persistent cases. Of the remaining 43 cases, 29 had positive specimens in our stored collection representative of 2 sequential episodes that could be analyzed by WGS. For 26 cases (89.7%), we obtained sequences of optimal quality and good coverage from 2 sequential episodes that enabled us to perform a one-to-one genomic comparison of both sequences (Figure).

In 11 (42%) of the 26 cases, genomic analysis indicated that reinfection occurred and involved different lineages or sublineages in each episode (Figure). Among those 11 cases, 4 involved non-Omicron followed by Omicron variants (i.e., Delta to Omicron BA.1); 4 involved 2 different Omicron lineages (BA.1.17 to B.1.1.529, BA.5 to BA.1.1, BA.5 to BA.2, and BA.2.36 to BA.5.1); and 3 involved different Omicron sublineages (BA.1.17 and BA.1.1, 10 differential SNVs; BA.1 and BA.1.1, 8 SNVs; and BA.5.2 and BA.5.1, 13 SNVs).

We considered another 4 cases to be probable reinfections (Figure): 3 involved different strains from

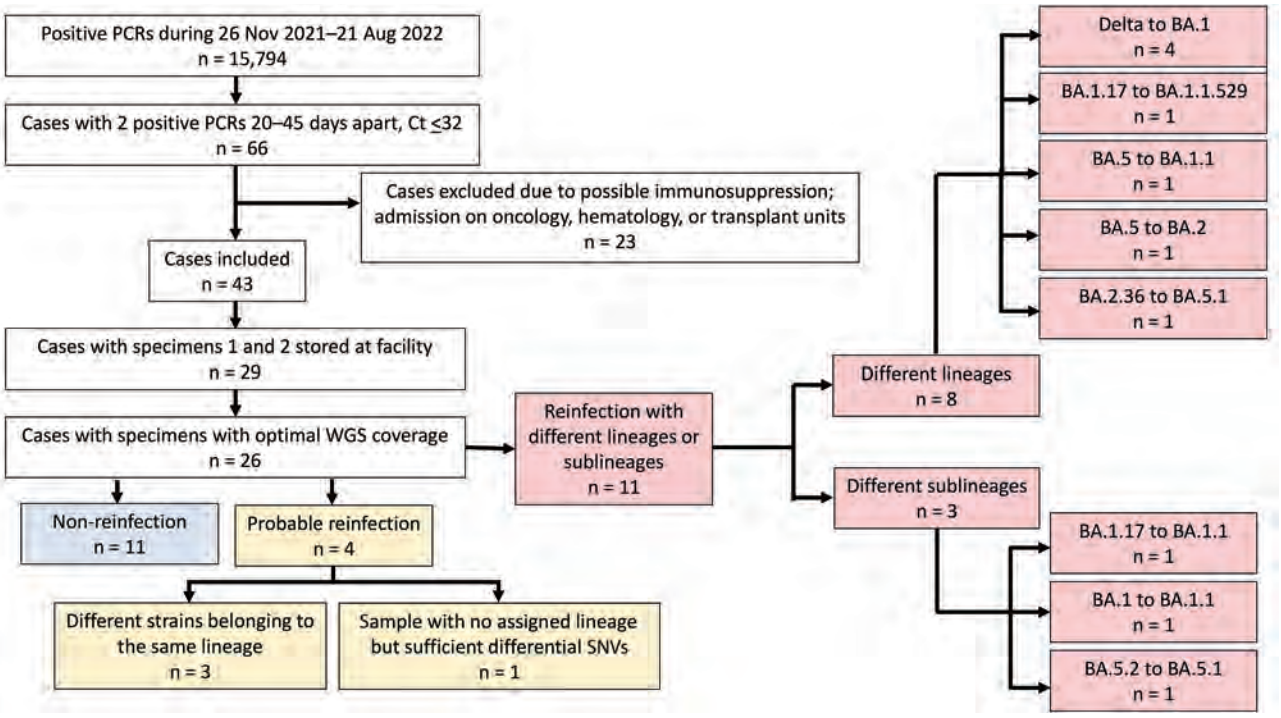

Figure. Flowchart of case selection in a study of early SARS-CoV-2 reinfection involving the same or different genomic lineages, Spain. PCR-positive cases were diagnosed by our tertiary hospital, which covers 650,000 inhabitants in the population of Madrid. Among 26 cases with optimal coverage for WGS, 11 were reinfections (red boxes), 4 of which were non-Omicron to Omicron lineage reinfections. Probable reinfection cases (yellow boxes; patients 23–26) showed enough unique SNV differences between the sequences from their sequential specimens to be suspect of reinfection (Appendix Table 3, https://wwwnc.cdc.gov/EID/article/29/6/22-1696-App1.pdf). Ct, cycle threshold; SNV, single-nucleotide variants; WGS, whole-genome sequencing.

the same sublineage (BA.2, BA.1.1, and BA.1.17); in the fourth case (case 26), we were unable to assign the variant in 1 of the specimens. In all 4 cases, we observed differential SNVs (4–8 SNVs) between the sequences from the sequential episodes. All the differential SNV calls between the sequential episodes were robust, as indicated by the good sequencing coverage (73–2,847 nt depth) observed in those positions (Appendix Table 3). The distribution of the differential SNVs between the sequential sequences in these cases pointed to independent evolutionary pathways; 1–4 SNVs in the first episode were absent in the second, and 3–5 SNVs in the second episode were absent in the first. Those observations ruled out the possibility that the sequence from the second episode evolved from the first sequence, thus indicating that 2 unrelated strains were involved in each of the sequential episodes.

Because of the short time between COVID-19 episodes in our study, we assessed whether the strain involved in the first episode of early reinfected cases could still be traced as remnant minority variants in the second episode. A thorough visual review of SNVs called in the second episode did not identify any minority calls corresponding to SNVs identified in the first episode strain, which indicated that the strain involved in the first episode had been cleared by the time the second infection was established.

We further refined the characterization of reinfections by also performing host genomic characterization to clean up any laboratory errors and ensure that the sequential specimens belonged to the same patient. We performed short tandem repeat analysis on specimens from 15 of 16 cases assigned as reinfections or probable reinfections. For all 15 cases, host genetic analysis confirmed that the 2 sequential specimens used in the study belonged to the same patient. For the remaining 1 case (case 10), no host material was available.

A review of the clinical characteristics of the 11 cases of early SARS-CoV-2 reinfections did not suggest a specific pattern: 63.6% were among female patients, patient ages were 8–88 years, 36.4% of patients had not been vaccinated, and 9.1% had incomplete vaccination schedules (Table 1). Among the unvaccinated case-patients, most were young (8–29 years of age). In most (54.5%) reinfections, symptoms were mild, and 5 patients were asymptomatic. Relevant risk factors were high blood pressure (27.3%), heart disease (18.2%), diabetes (18.2%), and previous ictus

(18.3%). In 50% of cases, a SARS-CoV-2 RT-PCR was requested before a procedure or intervention at the hospital or after exposure to a COVID-19 case (Table 2). SARS-CoV-2 antibody serology testing was not available before the first episode for all but 2 cases (cases 10 and 11), but in those cases, serologic results were negative. None of the patients died.

Among the 4 probable reinfections, patient ages were 58–81 years, 2 were male, and 3 had a full vaccination schedule before the first COVID-19 episode (Table 2). Three of the probable reinfections were asymptomatic, but we have no clinical information regarding the COVID-19 episode in the fourth patient. Relevant risk factors were high blood pressure (100%), diabetes (75%), chronic kidney disease (50%), and heart disease (50%).

Another 11 cases in the analysis were not reinfections but short-term persistence involving the same strain. The evolution of the Ct values in those cases was consistent with persistence because most (82%) had higher Ct in the second specimen; 2 had Ct values that were not markedly lower, 3 and 8 cycles difference. The strains corresponded to the Omicron variant and either had acquired no diversity, had 0 SNVs between sequential isolates, or had 1–5 SNVs in the second specimen, consistent with an acquisition of diversity by microevolution during the persistence period. We also reviewed the clinical charts for those case-patients (Table 3); their ages were 1–94 years and 63.6% were female. The most prevalent risk factors were high blood pressure (54.5%), overweight or obesity (54.5%), heart disease (45.5%), and autoimmune diseases (27.3%). Compared with patients who had short-term SARS-CoV-2 persistence, early reinfected patients were younger (43.3 vs. 58.5 years) and had lower baseline pathology (36.4% vs. 72.7%). In terms of clinical severity, 36.4% of patients with early reinfection were asymptomatic in the first episode and 45.5% were asymptomatic in the second episode, compared with only 18.2% of case-patients who had short-term persistence. For the early reinfection group, despite being statistically nonsignificant, the second episode tended to be less severe; in only 3 cases, the second episode was more severe than the first. Among early reinfections, 18.2% of case-patients required hospital admission for COVID-19 during the first episode and none required hospitalization for the second episodes, compared with 27.3% of patients with short-term persistence who required hospitalization. One (9.1%) patient in the short-term persistence group died due to COVID-19 versus none in the early reinfection group.

Table 1. Clinical characteristics of patients with early SARS-CoV-2 reinfection involving the same or different genomic lineages, Spain*

Characteristics	First episode, n = 11	Second episode, n = 11
Average age, y (range)	43.27 (8–88)	43.27 (8–88)
Sex		
M	4 (36.36)	4 (36.36)
F	7 (63.64)	7 (63.64)
Illness severity		
Asymptomatic	4 (36.36)	5 (45.45)
Mild	5 (45.45)	6 (54.55)
Intermediate	2 (18.18)	0
Severe	0	0
Care required		
Emergency	0	0
Hospital admission	3 (27.27)	2 (18.18)
Hospital admission for COVID-19	2 (18.18)	0
Nosocomial transmission	1 (9.09)	0
ICU	0	0
ICU for COVID-19	0	0
Underlying conditions		
None of interest	7 (63.64)	7 (63.64)
High blood pressure	3 (27.27)	3 (27.27)
COPD	1 (9.09)	1 (9.09)
Asthma	0	0
Diabetes	2 (18.18)	2 (18.18)
Ictus	2 (18.18)	2 (18.18)
Overweight/obesity	1 (9.09)	1 (9.09)
Heart disease	2 (18.18)	2 (18.18)
Autoimmune	1 (9.09)	1 (9.09)
Oncological	0	0
Chronic kidney disease	1 (9.09)	1 (9.09)
HIV infection	0	0
AIDS	0	0
Pregnant	0	0
Paxlovid use‡	0	0
Use of dexamethasone	0	0
Death	0	0
Vaccines and serology		
Complete vaccination schedule	6 (54.55)	6 (54.55)
Incomplete vaccination schedule	1 (9.09)	1 (9.09)
Unvaccinated	4 (36.36)	4 (36.36)
Previous positive serology for SARS-CoV-2	0	0
Previous negative serology for SARS-CoV-2	2 (18.18)	2 (18.18)
Serology not available	9 (81.82)	9 (81.82)

*Values are no. (%) except as indicated. COPD, chronic obstructive pulmonary disease; ICU, intensive care unit.
†Illness severity was defined according to the following criteria: mild, general unrest, cough, diarrhea, cephalgia, fever, anosmia, myalgias, rhinorrhea; moderate, previous symptoms plus dyspnea, mild respiratory failure, or unilateral pneumonia; severe, previously listed symptoms plus bilateral pneumonia or severe respiratory failure.
‡Nirmatrelvir/ritonavir.

Discussion

Most studies focusing on COVID-19 reinfections followed the CDC guidelines during the first waves of the pandemic (*8*). Nevertheless, the guidelines need to be reviewed in the current epidemiologic context, which is substantially different from when most reinfection studies were conducted. One crucial

difference is the emergence of the Omicron variant at the end of 2021. Omicron is markedly different from previous variants, harboring a constellation of >55 mutations, 32 of which are in the spike, and 15 mutations map to the receptor-binding domain. Those mutations triggered alarm about the possibility of immune escape from the protection conferred by pre-Omicron variant infections. Those suspicions were confirmed, and Omicron was shown to be barely neutralized by serum from convalescent patients (*9*).

The lack of Omicron neutralization during in vitro exposure to serum from vaccinated or convalescent case-patients infected with earlier variants led to consideration that reinfections were likely to increase. A large study in South Africa demonstrated that risk assessments for reinfection with Omicron were higher than for pre-Omicron variants (*7*). Similarly, the 6.8% reinfection rate with Omicron in Marseille, France, was markedly higher than infection rates (0.2%–1.5%) in pre-Omicron pandemic waves (*6*).

If Omicron escapes the protection associated with infection from earlier variants, then higher rates of Omicron reinfection could be expected to occur within a shorter time after the first episode (i.e., early reinfections) than was seen with previous variants. This shorter reinfection time was noted in Italy (*10*), where Omicron reinfections occurred 25–60 days after the first COVID-19 episode involving the Delta variant,

Table 2. Clinical characteristics of patients with early SARS-CoV-2 reinfection or probable reinfection involving the same or different genomic lineages, Spain*

Pt. no.	Age, y/sex	Underlying conditions	Illness severity, 1st/2nd episode†	COVID-19 care required, 1st/2nd episode	COVID-19 treatment	Vaccine schedule	Inter-infection period, d	PCR Ct, 1st/2nd episode	Reason for PCR, 1st/2nd episode	SARS-CoV-2 variant, 1st/2nd episode
Reinfections										
1	29/M	None	Mild/mild	N/N	N	N	37	24/22	Symp/symp	AY.127/BA.1.1.1
2	12/M	None	Mild/mild	N/N	N	N	34	30/19	Symp/symp	AY.124/BA.1.1
3	8/F	None	Asymp/mild	N/N	N	N	37	30/22	PE/symp	B.1.617.2 Delta plus/BA.1.1
4	85/F	HBP, DM, obesity	Asymp/mild	N/N	N	Complete, Pfizer	41	32/25	PP/PE	BA.1.17/BA.1.1
5	27/F	None	Mild/asymp	N/N	N	Complete, AstraZeneca/ Pfizer	42	22/32	PP/PP	BA.1.17/B.1.1.529
6	28/F	None	Asymp/mild	N/N	N	Complete, Pfizer/ Moderna	27	32/16	PE/symp	BA.1/BA.1.1
7	42/F	None	Mild/mild	N/N	N	Incomplete, Pfizer	41	32/20	Symp/symp	AY.122/BA.1.17
8	11/F	None	Asymp/ asymp	N/N	N	N	22	30/27	PP/PP	BA.2.36/BA.5.1
9	88/M	COPD, ictus, heart disease, CKD	Mod/asymp	Hospital admission/N	Steroids	Complete, Pfizer	25	13/26	Symp/PP	BA.5/BA.2
10	63/F	HBP, systemic sclerosis	Mild/asymp	N/N	N	Incomplete, AstraZeneca	20	19/32	Symp/PP	BA.5/BA.1.1
11	83/M	HBP, DM, ictus, heart disease	Mod/asymp	Hospital admission/N	Steroids	Complete, Pfizer	27	16/32	Symp/PP	BA.5.2/BA.5.1
Probable reinfections										
23	74/F	HBP, DM, heart disease	NA/NA	NA/NA	NA	Complete, Pfizer	21	31/16	NA/NA	BA.2/BA.2
24	81/M	HBP, DM, heart disease, CKD	Mod/asymp	Hospital admission/ hospital admission	Steroids	Complete, Pfizer	45	22/30	Symp/PP	BA.1.1/BA.1.1
25	64/F	HBP, CKD	Mild/asymp	Emergency/ N	N	Incomplete, Pfizer	26	32/30	Symp/symp	BA.1.17/BA.1.17
26	58/M	HBP, DM	Asymp/ asymp	N/N	N	Complete, Pfizer	24	29/30	PP/PP	BA.2/unassigned

*Asymp, asymptomatic; CKD, chronic kidney disease; COPD, chronic obstructive pulmonary disease; DM, diabetes mellitus; HBP, high blood pressure; ICU, intensive care unit; NA, not available; PP, pre-procedure; PE, postexposure; symp, symptoms.
†Severity of illness was defined according to the following criteria: mild, general unrest, cough, diarrhea, headache, fever, anosmia, dysgeusia, myalgia, rhinorrhea; Moderate, the above symptoms plus dyspnea, mild respiratory failure, or unilateral pneumonia; Severe, the above symptoms plus bilateral pneumonia or unilateral pneumonia with respiratory failure.

whereas reinfections involving Omicron in both sequential episodes (BA.1 to BA.2) were identified within the standard time range for reinfection, ≥90 days. Likewise, in Belgium, most early reinfections (<60 days) identified involved Omicron after a Delta infection (*11*). Other studies have also reported shorter times (24 days and 39 days) between episodes involving non-Omicron to Omicron reinfections (*11*,*12*).

To identify early non-Omicron followed by Omicron infections and classify variants as Omicron or non-Omicron, many previous studies relied on indirect inference methods, not WGS. In one study, spike gene target failure, which could be detected in Delta but not Omicron in the TaqPath RT-PCR, was used as a proxy marker to assign the variant (*11*). In another study, variants of concern (VOCs) were inferred by determining changes in the melting patterns of probes used in RT-PCR to target regions where marker SNVs are located (*4*). Although such inferences are useful and practicable, they can only assign reinfections involving certain VOCs, thereby missing possible early reinfections involving the same lineages or even sublineages, which can only be addressed by WGS characterization.

In our study, we tried to optimize the characterization of early reinfections in the Omicron era by performing WGS to cover all possible variants involved, narrowing the time range between episodes to <45 days to capture the earliest reinfections, and fine-tuning the analysis as much as possible by host genetic analysis to ensure that the 2 sequential specimens used for genomic viral comparison belonged to the same patient. During the study period, we detected a total of 66 (0.42%) cases with sequential RT-PCR–positive specimens in an interval of 20–45 days. That percentage was higher than the cases with sequential positives 45–90 days (8 cases, 0.05%) or >90 days (38 cases, 0.24%) apart.

One relevant finding was that among suspected cases of early reinfection, we confirmed early reinfection in 38% (11/29) of cases with specimens available for sequencing. In addition, the time interval between episodes was very short, 20–42 days. A recent systematic review on SARS-CoV-2 reinfections also determined a period of 23–57 days for reinfections (*8*), below the standard 90-day threshold, despite including data from studies published before May 22, 2022; data from the latest waves were also probably underrepresented. More recent criteria for considering reinfections enable reduction to ≥45 days between episodes for persons with symptoms, evidence of close contact with a confirmed case, and no evidence of other causes of infection (*2*). Our data indicate that even those updated guidelines would miss the early reinfections that we highlight, and these combined findings should lead to reconsideration of the more stringent and longer period of ≥90 days between episodes used in the CDC guidelines.

About one third (36.4%) of the early reinfections in our study involved sequential infection with non-Omicron followed by Omicron variants, which is consistent with previous descriptions of Omicron

Table 3. Clinical characteristics of case-patients with short-term SARS-CoV-2 persistence in study of early SARS-CoV-2 reinfection involving the same or different genomic lineages, Spain*

Characteristic	Value, n = 11
Average age, y (range)	58.5 (1–94)
Sex	
M	4 (36.4)
F	7 (63.6)
Illness severity	
Asymptomatic	2 (18.2)
Mild	4 (36.4)
Intermediate	2 (18.2)
Severe	2 (18.2)
Care required	
Emergency	1 (9.1)
Hospital admission	6 (54.5)
Hospital admission for COVID-19	3 (27.3)
Nosocomial transmission	1 (9.1)
ICU	0
ICU for COVID-19	0
Underlying conditions	
None of interest	3 (27.3)
High blood pressure	6 (54.5)
COPD	2 (18.2)
Asthma	1 (9.1)
Diabetes	0
Ictus	1 (9.1)
Overweight/obesity	6 (54.5)
Heart disease	5 (45.5)
Autoimmune	3 (27.3)
Oncological	2 (18.2)
Chronic kidney disease	2 (18.2)
HIV infection	1 (9.1)
AIDS	0
Pregnant	0
Paxlovid use‡	1 (9.1)
Remdesivir use	3 (27.3)
Tocilizumab use	1 (9.1)
Dexamethasone use	4 (36.4)
Death	1 (9.1)
Vaccines and serology	
Complete vaccination schedule	8 (72.7)
Incomplete vaccination schedule	1 (9.1)
Unvaccinated	2 (18.2)
Previous positive serology for SARS-CoV-2	3 (27.3)
Previous negative serology for SARS-CoV-2	2 (18.2)
Serology not available	6 (54.5)

*Values are no. (%) except as indicated. COPD, chronic obstructive pulmonary disease; ICU, intensive care unit.
†Illness severity was defined according to the following criteria: mild, general unrest, cough, diarrhea, cephalgia, fever, anosmia, myalgias, rhinorrhea; moderate, previous symptoms plus dyspnea, mild respiratory failure, or unilateral pneumonia; severe, previously listed symptoms plus bilateral pneumonia or severe respiratory failure.
‡Nirmatrelvir/ritonavir.

variants capable of causing immediate reinfection of patients newly recovered from COVID-19 (*9*). However, because of our nontargeted WGS-based design, we were able to identify not only early reinfections involving non-Omicron followed by Omicron variants but also reinfections with different Omicron lineages, different sublineages belonging to the same Omicron lineage, and even different strains from the same sublineage that were missed in other studies that used indirect inference methods. Our findings support reformulating the assumption that early infections are mainly restricted to a non-Omicron–Omicron alternation, because of the lack of cross-protection caused by major Omicron genetic differences.

Among the 4 probable early reinfections in our study, 3 cases involved 2 strains from the same sublineage. One case (case 23) constituted one of the shortest time intervals between episodes, 21 days apart, which contrasts with other studies that only found reinfections with the same variant for episodes ≥90 days apart. This probable early reinfection showed 8 SNVs between strains from the same lineage in the 2 separate episodes. In addition, several observations led us to reinforce its assignment as an early reinfection. First, the patient had 3 RT-PCR–negative specimens between the 2 RT-PCR–positive specimens 21 days apart, which sustains the hypothesis of early reinfection versus the alternative explanation of persistence. Second, the Ct value of the second specimen was 16, whereas the Ct of the first specimen was 31. We generally expect an increased Ct value, or reduced viral load, for a second specimen in cases of persistence, but a new reinfection should correspond to a lower Ct value, as noted in that case. Third, for persistence we expect a sequential acquisition of SNVs from the first strain during the persistence period. To the contrary, in that case, when we analyzed the distribution of the 8 SNVs identified between the 2 sequential specimens, 4 SNVs were only identified in the first specimen and another 4 were identified only in the second specimen, which is more consistent with the involvement of 2 independent strains, each with 4 proper SNVs.

The robustness of our assignation of early reinfections is supported by the precautionary consideration of the possibility of specimens belonging to different persons could be mishandled or misclassified, thereby leading to erroneous assignment as reinfections (*13*). However, we confirmed the hosts in all our reinfections by performing host analysis. Most of the literature focused on COVID-19 reinfections, with just a few exceptions (*5*,*13*,*14*), lacks host control.

We identified no common clinical pattern among early reinfection cases by sex, age, risk factors, or clinical conditions. Although we did not achieve strong statistical support because of our small sample size, we observed a tendency for the second episode in early reinfections to be equally or less severe than the previous episode. Of note, more than half (63.6%) of the reinfections were cases with no clinical history, which means that we need to broaden the circumstances for suspecting early reinfections.

In our analysis, despite the efforts to minimize the interference of persistence in case selection by ruling out cases with positive PCRs between episodes and patients with immunosuppression, we still identified 11 cases in which the same strain was found in the 2 sequential episodes, even though 27.3% of those cases had no clinical history to justify persistence. Although those were cases of short-term persistence, our findings could help expand clinical patterns to consider unexpected persistence, which is different from long-term persistence that occurs mainly in immunosuppressed persons (*15*,*16*). Despite the short-term nature of such persistence, the findings could still be relevant, depending on clinical interpretations and isolation measures.

Our data fill a gap in observations of the time range between sequential COVID-19 episodes that has generally been missing from the literature. In addition, our study period covered the 6th, most recent, COVID-19 wave, to provide new information on reinfections in a scenario in which SARS-CoV-2 VOCs are emerging and the population has extensive vaccine coverage. To reinforce the robustness of our findings, we also provided additional analytical rigor and refinement by including host genetic analysis in the assignment of reinfection.

In conclusion, our study provides new data on early reinfections involving Omicron and other variants. These findings shorten the time between episodes in which reinfection can occur and broaden the clinical profile for reinfection beyond unvaccinated young persons. We showed that early reinfections are not exclusively associated with the impaired protection expected of a non-Omicron to Omicron sequence but also can involve very similar strains. Because early reinfection can occur in various clinical and epidemiologic circumstances, guidelines for assigning reinfection to only ≥90 days between sequential SARS-CoV-2–positive PCRs should be reevaluated.

Additional members of Gregorio Marañón Microbiology-ID COVID 19 Study Group: Teresa Aldámiz, Ana Álvarez-Uría, Elena Bermúdez, Emilio Bouza, Sergio Buenestado-Serrano, Almudena Burillo, Raquel Carrillo, Emilia

Cercenado, Alejandro Cobos, Cristina Díez, Pilar Escribano, Chiara Fanciulli, Alicia Galar, Mª Dolores García, Paloma Gijón, Helmuth Guillén, Jesús Guinea, Álvaro Irigoyen, Martha Kestler, Juan Carlos López, Marina Machado, Mercedes Marín, Pablo Martín-Rabadán, Pedro Montilla, Belén Padilla, María Palomo, María Jesús Pérez-Granda, Leire Pérez, Elena Reigadas, Cristina Rincón, Belén Rodríguez, Sara Rodríguez, Adriana Rojas, María Jesús Ruiz-Serrano, Carlos Sánchez, Mar Sánchez, Julia Serrano, Francisco Tejerina, Maricela Valerio, Mª, Lara Vesperinas, Teresa Vicente, and Sofía de la Villa.

Acknowledgments

We thank the Genomics Unit of Gregorio Marañón University Hospital for support in the sequencing runs. We thank Janet Dawson for her help in editing and proofreading.

This work was supported by Instituto de Salud Carlos III (project no. PI21/01823) together with the FEDER fund "A way of making Europe," and by the European Centre for Disease Prevention and Control (project no. 2021/PHF/23776), and Instituto de Investigación Sanitaria Gregorio Marañón (project no. 2021-II-PI-01). Additional funding from the Miguel Servet contract (no. CPII20/0000175) to L.P.L. and Predoctoral de Formación en Investigación en Salud contract (no. FI20/00129) to C.R.G.

About the Author

Ms. Rodríguez-Grande is a PhD candidate at Instituto de Investigación Sanitaria Gregorio Marañón, Madrid, Spain. Her research interests include molecular and genomic epidemiology of tuberculosis and SARS-CoV-2.

References

1. Planas D, Saunders N, Maes P, Guivel-Benhassine F, Planchais C, Buchrieser J, et al. Considerable escape of SARS-CoV-2 Omicron to antibody neutralization. Nature. 2022;602:671–5. https://doi.org/10.1038/s41586-021-04389-z
2. Centers for Disease Control and Prevention. Investigative criteria for suspected cases of SARS-CoV-2 reinfection (ICR) [cited 2022 Nov 4]. https://www.cdc.gov/coronavirus/2019-ncov/php/invest-criteria.html#print%0Ahttps://www.cdc.gov/coronavirus/2019-ncov/php/invest-criteria.html
3. Flacco ME, Acuti Martellucci C, Baccolini V, De Vito C, Renzi E, Villari P, et al. Risk of reinfection and disease after SARS-CoV-2 primary infection: meta-analysis. Eur J Clin Invest. 2022;52:e13845. https://doi.org/10.1111/eci.13845
4. Vera-Lise I, Dominik E, Elisabeth R, Kerstin H, Raffael F, Angelika X, et al. "Rapid reinfections with different or same Omicron SARS-CoV-2 sub-variants." J Infect. 2022;85:e96–8. https://doi.org/10.1016/j.jinf.2022.07.003
5. Rodríguez-Grande C, Alcalá L, Estévez A, Sola-Campoy PJ, Buenestado-Serrano S, Martínez-Laperche C, et al.; Gregorio Marañón Microbiology-ID COVID 19 Study Group. Systematic genomic and clinical analysis of severe acute respiratory syndrome coronavirus 2 reinfections and recurrences involving the same strain. Emerg Infect Dis. 2022;28:85–94. https://doi.org/10.3201/eid2801.211952
6. Nguyen NN, Houhamdi L, Hoang VT, Stoupan D, Fournier PE, Raoult D, et al. High rate of reinfection with the SARS-CoV-2 Omicron variant. J Infect. 2022;85:174–211. https://doi.org/10.1016/j.jinf.2022.04.034
7. Pulliam JRC, van Schalkwyk C, Govender N, von Gottberg A, Cohen C, Groome MJ, et al. Increased risk of SARS-CoV-2 reinfection associated with emergence of Omicron in South Africa. Science. 2022;376(6593):eabn4947. https://doi.org/10.1126/science.abn4947
8. Toro-Huamanchumo CJ, Hilario-Gomez MM, Pinedo-Castillo L, Zumarán-Nuñez CJ, Espinoza-Gonzales F, Caballero-Alvarado J, et al. Clinical and epidemiological features of patients with COVID-19 reinfection: a systematic review. New Microbes New Infect. 2022;48:101021. https://doi.org/10.1016/j.nmni.2022.101021
9. Carreño JM, Alshammary H, Tcheou J, Singh G, Raskin AJ, Kawabata H, et al.; PSP-PARIS Study Group. Activity of convalescent and vaccine serum against SARS-CoV-2 Omicron. Nature. 2022;602:682–8. https://doi.org/10.1038/s41586-022-04399-5
10. Mencacci A, Gili A, Camilloni B, Bicchieraro G, Spaccapelo R, Bietta C, et al. Immediate reinfection with Omicron variant after clearance of a previous SARS-CoV-2 infection. J Infect Public Health. 2022;15:983–5. https://doi.org/10.1016/j.jiph.2022.07.013
11. Nevejan L, Cuypers L, Laenen L, Van Loo L, Vermeulen F, Wollants E, et al. Early SARS-CoV-2 reinfections within 60 days and implications for retesting policies. Emerg Infect Dis. 2022;28:1729–31. https://doi.org/10.3201/eid2808.220617
12. Seid AG, Yirko T, Sayeed S, Plipat N. Infection with SARS-CoV-2 Omicron variant 24 days after non-Omicron infection, Pennsylvania, USA. Emerg Infect Dis. 2022;28:1911–3. https://doi.org/10.3201/eid2809.220539
13. Pérez-Lago L, Machado M, Herranz M, Sola-Campoy PJ, Suárez-González J, Martínez-Laperche C, et al.; Gregorio Marañón Microbiology-ID COVID-19 Study Group. Host genetic analysis should be mandatory for proper classification of COVID-19 reinfections. Open Forum Infect Dis. 2021;8:ofab402. https://doi.org/10.1093/ofid/ofab402
14. Tillet RL, Sevinsky JR, Hartley PD, Kerwin H, Crawford N, Gorzalski A, et al. Genomic evidence for reinfection with SARS-CoV-2: a case study. Lancet Infect Dis. 2021;21:52–8. PubMed https://doi.org/10.1016/S1473-3099(20)30764-7
15. Pérez-Lago L, Aldámiz-Echevarría T, García-Martínez R, Pérez-Latorre L, Herranz M, Sola-Campoy PJ, et al.; on behalf of Gregorio Marañón Microbiology-ID Covid Study Group. Different within-host viral evolution dynamics in severely immunosuppressed cases with persistent SARS-CoV-2. Biomedicines. 2021;9:808. https://doi.org/10.3390/biomedicines9070808
16. Baang JH, Smith C, Mirabelli C, Valesano AL, Manthei DM, Bachman MA, et al. Prolonged severe acute respiratory syndrome coronavirus 2 replication in an immunocompromised patient. J Infect Dis. 2021;223:23–7. https://doi.org/10.1093/infdis/jiaa666

Address for correspondence: Laura Pérez-Lago or Darío García de Viedma; Hospital General Universitario Gregorio Marañón, Dr. Esquerdo 46, Madrid 28007, Spain; email: lperezg00@gmail.com or dgviedma2@gmail.com

SARS-CoV-2 Vaccine Effectiveness against Omicron Variant in Infection-Naive Population, Australia, 2022

Lauren E. Bloomfield, Sera Ngeh, Gemma Cadby, Kate Hutcheon, Paul V. Effler

SARS-CoV-2 transmission in Western Australia, Australia, was negligible until a wave of Omicron variant infections emerged in February 2022, when >90% of adults had been vaccinated. This unique pandemic enabled assessment of SARS-CoV-2 vaccine effectiveness (VE) without potential interference from background immunity from prior infection. We matched 188,950 persons who had a positive PCR test result during February–May 2022 to negative controls by age, week of test, and other possible confounders. Overall, 3-dose VE was 42.0% against infection and 81.7% against hospitalization or death. A primary series of 2 viral-vectored vaccines followed by an mRNA booster provided significantly longer protection against infection >60 days after vaccination than a 3-dose series of mRNA vaccine. In a population free from non–vaccine-derived background immunity, vaccines against the ancestral spike protein were ≈80% effective for preventing serious outcomes from infection with the SARS-CoV-2 Omicron variant.

Until February 2022, Western Australia (WA), Australia, successfully delayed sustained transmission of SARS-CoV-2 by using rigorous international quarantine and state border entry restrictions, supported by comprehensive local outbreak control measures when breaches occurred. Data corroborating no substantive community transmission of SARS-CoV-2 in WA until February 2022 include the incidence of reported laboratory-confirmed SARS-CoV-2 infections (Figure 1) and serologic testing of blood donors. By the time WA lifted restrictions and experienced the first wave of SARS-CoV-2 infection, >90% of the state's residents ≥16 years of age had received ≥2 doses of a SARS-CoV-2 vaccine (*1*). The WA public health laboratory, PathWest Laboratory, determined which SARS-CoV-2 variants were circulating in the state during the first pandemic wave. During the study period (February 1–May 31, 2022), all 2,695 specimens for which lineage could be assigned were the Omicron variant, of which 2,668 (99%) were designated as BA.1 or BA.2 sublineage (Figure 2).

This unique pandemic experience enabled real-world assessment of vaccine effectiveness (VE) without potential bias caused by population-level background immunity resulting from prior infection. With this study, we assessed VE for mRNA vaccines and viral-vectored SARS-CoV-2 vaccines against laboratory-confirmed infection and severe illness caused exclusively by the Omicron variant in a SARS-CoV-2–naive population. This work was approved by the WA Department of Health Human Research Ethics Committee (RGS0000005522).

Methods

Study Design

We used a test-negative case–control design to compare persons ≥16 years of age who had positive PCR SARS-CoV-2 test results with matched controls who were SARS-CoV-2 negative. We compared the odds of vaccination among those with PCR-confirmed SARS-CoV-2 infection or severe COVID-19 with the odds of vaccination among matched PCR-confirmed negative controls.

Data Linkage

In early 2020, WA created a statewide linked data repository to collect information essential for public health

Author affiliations: The University of Notre Dame Australia, Fremantle, Western Australia, Australia (L.E. Bloomfield); Western Australia Department of Health, East Perth, Western Australia, Australia (L.E. Bloomfield, S. Ngeh, G. Cadby, K. Hutcheon, P.V. Effler)

DOI: https://doi.org/10.3201/eid2906.230130

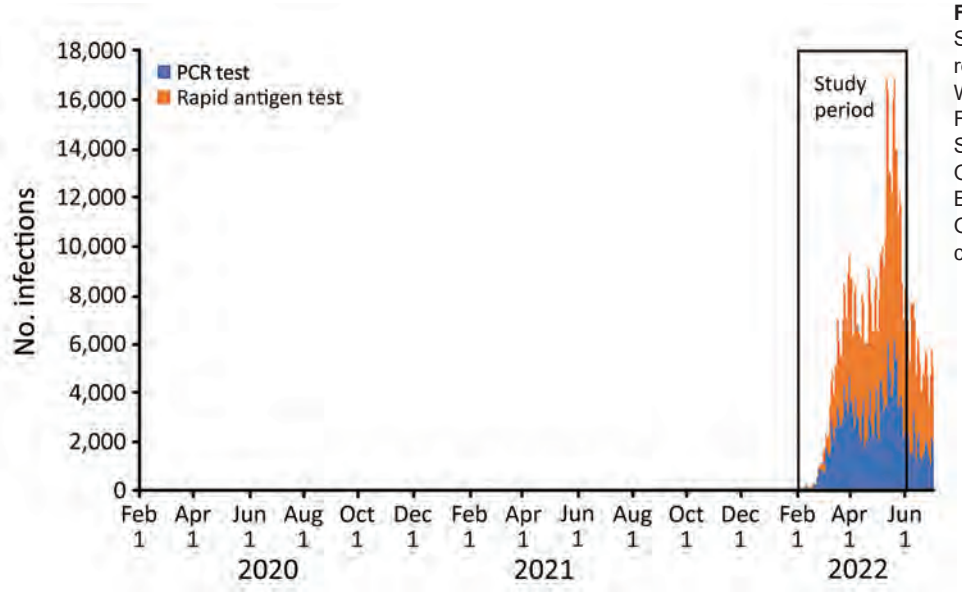

Figure 1. Number of SARS-CoV-2–positive test results reported by day, by test type, Western Australia, Australia, February 1–June 30, 2022. Source: COVID-19 Public Health Operations, WA Health (D. Barth, COVID-19 Public Health Operations, WA, Australia, pers. comm., email, 2022 Dec 1).

management of the pandemic, including SARS-CoV-2 vaccinations that began in February 2021 (*2*). In brief, COVID-19 vaccination data from the Australian Immunisation Register (AIR; Appendix, https://wwwnc.cdc.gov/EID/article/29/6/23-0131-App1.pdf) were linked to existing WA Department of Health data collections, including statewide hospital admission data, mortality data, and SARS-CoV-2 pathology test results.

Ascertainment of Infection

All persons with ≥1 SARS-CoV-2 PCR tests performed within the study period were eligible for inclusion. We included in the analysis only a person's first positive or negative PCR test result during the study period. Persons who initially tested negative but subsequently tested positive during the study period were removed from the negative test pool and reclassified as a case-patient (i.e., each person appeared once in the dataset, as either a case-patient or a control). Because the reason for SARS-CoV-2 testing was not recorded in the data repository, we excluded persons with >20 test results reported during January 2020–May 2022 because those persons were probably subjected to regular asymptomatic screening for employment purposes. We also excluded persons with only SARS-CoV-2 rapid antigen test (RAT) results because negative RAT results were not required to be reported and compliance with mandatory reporting of positive RAT results is unknown.

Vaccination Data

For this analysis, we established vaccination status at the time of the person's eligible SARS-CoV-2 PCR test result by linking the person to their respective SARS-CoV-2 immunization history in AIR. We included in our analysis persons who received any dose of vaccine ≥14 days before the eligible PCR result and excluded persons who had received a vaccine dose <14 days before the eligible PCR result. We defined unvaccinated persons as those who had no record of receiving a SARS-CoV-2 vaccine dose before their linked PCR test result.

The vaccines analyzed were the adenovirus-vectored vaccine produced by AstraZeneca (ChAdOx1, https://www.astrazeneca.com) and the mRNA vaccines produced by Pfizer-BioNTech (BNT162b2, https://www.pfizer.com) and Moderna (mRNA-1273, https://www.modernatx.com). We defined a homologous 3-dose vaccination schedule as 2 doses of an mRNA vaccine and an mRNA booster dose, regardless of brand/manufacturer, and a heterologous 3-dose vaccination schedule as 2 doses of ChAdOx1 followed by an mRNA booster dose, regardless of brand/manufacturer. Matched pairs in which the case-patient or control had received a protein-based SARS-CoV-2 vaccine, a ChAdOx1 booster dose, or a mixed 2-dose primary schedule (ChAdOx1 and an mRNA vaccine) were few; we excluded those pairs from subanalysis examining heterologous and homologous vaccine combinations.

Hospitalization and Mortality Data

During the study period, we extracted data from the WA Hospital Morbidity Data Collection (*3*) and linked them to all SARS-CoV-2 test results for specimens collected. We defined a SARS-CoV-2 hospitalization as ≥1 inpatient admissions 0–7 days after the date of a positive PCR result. To reduce potential bias

that might be introduced through routine preadmission SARS-CoV-2 screening, we excluded admissions for patients indicated by the specialty of the admitting clinician to be unlikely to have been hospitalized for treatment of COVID-19 and for patients admitted for boarding purposes (Table 1). We also performed supplementary sensitivity analyses, which included all hospital admissions regardless of admitting clinician specialty or those defined as a COVID-19 hospitalization on the basis of select codes from the International Statistical Classification of Diseases and Related Health Problems, Tenth Revision, Australian Modification (ICD-10-AM).

The WA Registry of Births, Deaths and Marriages (https://www.wa.gov.au), the mandatory repository for death reports in WA, provided mortality data. We defined SARS-CoV-2–associated deaths as death from any cause 0–30 days after an eligible PCR test and included those cases in the analysis. We defined severe disease as SARS-CoV-2 hospitalization, an associated death, or both.

To identify pre-existing medical conditions that could potentially increase a person's risk for SARS-CoV-2 infection or severe disease, we reviewed any hospital admissions in the 24 months before their eligible PCR test. We selected 14 diagnostic categories and the ICD-10-AM codes used to define them, based on previous literature (Table 2) (*4*). If a person had any of the ICD-10-AM codes listed as either a principal or secondary diagnosis for an admission in the 24 months before their eligible PCR test, they were assigned a score of 1 for the corresponding diagnostic category. We then summed the total number of unique diagnostic categories assigned a score of 1 for each person, yielding a score of 0–14 (0 if there had been no admissions or only admissions that did not include any of the selected ICD-10-AM codes). We used this aggregate comorbidity score as a proxy index of underlying conditions and controlled for it in the analyses.

Statistical Analyses

We assessed VE by using conditional logistic regression of matched case–control pairs. We calculated adjusted odds ratios (aORs) by using the clogistic function in the Epi package in R version 4.1.0 (The R Foundation for Statistical Computing, https://www.r-project.org). Vaccine effectiveness was defined as (1 – aOR) × 100 and is presented with 95% CIs. We assessed differences between odds ratios by calculating the absolute difference between the log odds and the SEs of the difference. We calculated p values by using z-scores; to account for multiple testing, we considered $p<0.01$ significant.

Case-patients and controls were matched on week of eligible PCR test, age group (16–19 years, then 10-year intervals thereafter), sex, Aboriginality (defined as Aboriginal and/or Torres Strait Islander ancestry), Index of Relative Socioeconomic Advantage and Disadvantage decile (*5*) (a score of 1 demonstrating relatively greater disadvantage and a score of 10 indicating a relative lack of disadvantage), and comorbidity score using by the MatchIt package (*6*) on a 1:1 basis. We randomly sorted all eligible case-patients and controls by using the sample function before matching.

We calculated effectiveness by comparing unvaccinated persons with those who had received either 2 or 3 doses of vaccine. We also performed subanalyses to examine VE for breakthrough infection by time since last vaccine dose and between the homologous and heterologous 3-dose vaccination schedule. Analysis of VE against severe disease included positive case-patients (by PCR) with severe disease

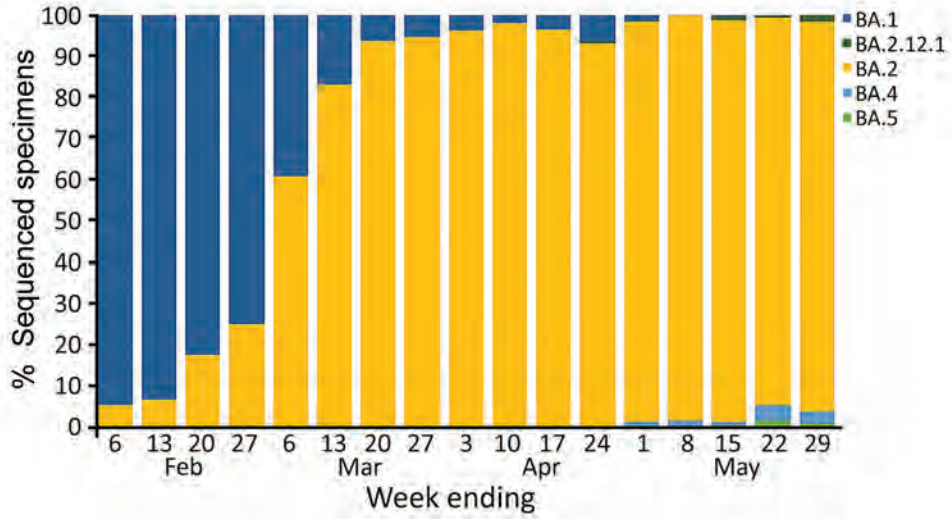

Figure 2. Weekly proportion of assigned lineages for sequenced SARS-CoV-2 specimens, by week of sample collection, Western Australia, Australia, February 1–May 31, 2022. Source: PathWest Laboratory Medicine (C. Sikazwe, Pathwest Laboratory, WA, Australia, pers. comm., email, 2022 July 15).

who, along with their matched controls, received 2 or 3 vaccine doses.

Results

A total of 1,306,453 PCR tests were reported for specimens collected during February 1, 2022–May 31, 2022, from which 188,950 positive case-patients and 188,950 negative matched controls were eligible for inclusion in the analysis (Table 3; Figure 3). Of the 377,900 study participants, 30,420 (8%) were unvaccinated at the time of testing, 84,237 (22%) had received 2 doses, and 263,243 (70%) had received 3 doses.

VE against Breakthrough Infection of Any Severity

Overall, in adjusted analyses comparing those who were unvaccinated with those who had received 2 vaccine doses, VE for preventing PCR-confirmed infection of any severity was 24.9% (95% CI 21.2%–28.4%), increasing to 42.0% (95% CI 40.2%–43.6%) for persons who had received 3 doses (Table 4). Breakthrough infection of any severity waned notably after a booster dose. For those who had received a booster dose 15–29 days before testing, VE was 70.7% (95% CI 67.4%–73.7%) but fell to 13.5% (95% CI 5.6%–20.8%) for those whose booster was administered ≥120 days before testing (Figure 4). The median time between the most recent vaccine dose and PCR test date was 21 days longer for persons who received 2 doses (101 days) than for those who received 3 doses (80 days); given the waning immunity after 3 doses, it is possible that increased time since vaccination contributed to lower VE estimates for 2 versus 3 doses.

VE against Severe Disease

Hospitalizations and deaths in the study cohort were rare. Among the 188,950 matched case-patients, there were 264 deaths within 30 days of testing and 1,456 hospital admissions within 7 days, excluding persons admitted under clinician specialties (Table 1).

Table 1. Clinician specialties for which hospital admissions were excluded from the analysis of SARS-CoV-2 vaccine effectiveness, Western Australia, Australia, February 1, 2022–May 31, 2022

Specialty
Child psychiatry/psychology
In vitro fertilization
Gynecology oncologist
Oncology
Psychogeriatrics
Psychiatry
Radiology
Nephrology/dialysis
Obstetrics
Burns
Dental surgery
Gynecology
Ophthalmology
Oral surgery
Orthopedics
Plastic and reconstructive surgery
Renal transplant surgery
Spinal surgery
Radiation oncology
General practitioner obstetrics

Overall, VE against severe disease for 2 doses of vaccine was 41.9% (95% CI 4.8%–64.5%) and increased to 81.7% (95% CI 73.9%–87.2%) for 3 doses (Table 5). The number of case-patients with severe disease in individual time strata was insufficient to permit meaningful VE estimates to be generated by time since last vaccination.

VE for Homologous versus Heterologous 3-Dose Series

Our analysis of VE by different vaccine series was restricted to 100,142 case-patients who received either a homologous or heterologous series of 3-dose vaccination (Table 6), as defined previously, and their

Table 2. ICD-10-AM hospital admission codes used to identify and categorize underlying conditions and construct a comorbidity score for each person included in a study of SARS-CoV-2 vaccine effectiveness, Western Australia, Australia, 2022*

Underlying condition category	ICD-10-AM codes
Respiratory disease	J40–J47; J81; J84; E84
Diabetes	E10–E14
Anemia/splenic issues	D50–D59; D60–D63; D73
Down syndrome	Q90
Cancer	C00–C97 excl C44
Kidney disease	N18–N19; N00–N16; N25–N29
Immunocompromise	D80–D89; B24
Dementia	F00–F03; G30
Cardiac disease incl hypertension and arrhythmia	I20–I28; I05–I10; I47–I50
Stroke/TIA	G45; H34; I60–I69
Liver disease	K71–K77
Obesity	E66
Rheumatoid arthritis	M05–M06
Ulcerative colitis/Crohn's disease	K50–K51

*ICD-10-AM, International Statistical Classification of Diseases and Related Health Problems, Tenth Revision, Australian Modification; TIA, transient ischemic attack.

matched controls. Persons who were vaccinated according to the heterologous versus homologous schedule were older (median age at test 65 vs. 38 years), more likely to be male, and more likely to have ≥1 comorbidity (Table 7).

VE was higher, although not significantly, up to 60 days after administration of the booster dose among persons who received the homologous or heterologous 3-dose vaccination series. However, VE was significantly higher among those who received a heterologous 3-dose vaccination series 60 days through <120 days of follow-up (Figure 5).

Restricting the samples to those <60 years of age to account for differences in behavior that may contribute to differential breakthrough infection rates yielded similar results. We observed the same pattern of waning immunity in the homologous and the heterologous groups, and protection was significantly higher from 60 to <120 days of follow-up (data not shown) for those on the heterologous schedule

Consistent with the results for breakthrough infection, VE against severe disease was ≈10% higher for those on the heterologous schedule (85.7%, 95% CI 73.1%–92.4%) than on the homologous mRNA schedule (75.8%, 95% CI 61.5%–84.8%), although that difference was not statistically significant in the context of a relatively small number of severe outcomes (p = 0.19). Low numbers of severe outcomes also precluded further analysis of effectiveness by time since vaccination.

Sensitivity Analyses

We performed sensitivity analyses to explore the potential effects of measurement bias, including the effect of using different options for defining disease severity and selecting covariates for matching case-patients to controls. We found no statistically significant effect on VE for severe disease when we restricted hospitalizations to those likely to be for COVID-19 by selecting specific ICD-10-AM codes used for the primary diagnosis instead of the specialty of the admitting clinician (point estimates for VE after 3 doses changed from 79.2% when restricted by primary diagnosis codes to 81.7% when restricted by admitting clinician specialty). In addition, we explored using

Table 3. Demographic characteristics of matched samples for analysis of SARS-CoV-2 vaccine effectiveness, Western Australia, Australia, February 1–May 31, 2022*

Characteristic	Unvaccinated, no. (%), n = 30,420	Two doses, no. (%), n = 84,237	Three doses, no. (%), n = 263,243	Total, no. (%), n = 377,900
Age group, y				
16–19	1,470 (4.8)	13,645 (16.2)	14,451 (5.5)	29,566 (7.8)
20–29	9,851 (32.4)	28,569 (33.9)	50,886 (19.3)	89,306 (23.6)
30–39	9,083 (29.9)	20,395 (24.2)	58,914 (22.4)	88,392 (23.4)
40–49	4,294 (14.1)	11,672 (13.9)	58,712 (22.3)	74,678 (19.8)
50–59	2,519 (8.3)	5,709 (6.8)	42,446 (16.1)	50,674 (13.4)
60–69	1,646 (5.4)	2,517 (3.0)	21,903 (8.3)	26,066 (6.9)
70–79	849 (2.8)	932 (1.1)	9,577 (3.6)	11,358 (3.0)
≥80	708 (2.3)	798 (0.9)	6,354 (2.4)	7,860 (2.1)
Sex				
F	14,180 (46.6)	40,940 (48.6)	144,180 (54.8)	199,300 (52.7)
M	15,972 (52.5)	43,143 (51.2)	118,699 (45.1)	177,814 (47.1)
Unspecified	268 (0.9)	154 (0.2)	364 (0.1)	786 (0.2)
Aboriginal Status				
Non-Aboriginal	29,367 (96.5)	80,418 (95.5)	259,701 (98.7)	369,486 (97.8)
Aboriginal	1,053 (3.5)	3,819 (4.5)	3,542 (1.3)	8,414 (2.2)
No. comorbidities				
0	29,269 (96.2)	80,583 (95.7)	246,896 (93.8)	356,748 (94.4)
1	221 (0.7)	852 (1.0)	3,929 (1.5)	5,002 (1.3)
2	596 (2.0)	2,046 (2.4)	9,008 (3.4)	11,650 (3.1)
3	46 (0.2)	120 (0.1)	778 (0.3)	944 (0.2)
4	195 (0.6)	404 (0.5)	1,815 (0.7)	2,414 (0.6)
≥5	93 (0.3)	229 (0.3)	817 (0.3)	1,142 (0.3)
IRSAD				
1	345 (1.1)	390 (0.5)	515 (0.2)	1,250 (0.3)
2	2,090 (6.9)	5,893 (7.0)	12,425 (4.7)	20,408 (5.4)
3	658 (2.2)	2,242 (2.7)	5,636 (2.1)	8,536 (2.3)
4	2,893 (9.5)	9,375 (11.1)	24,962 (9.5)	37,230 (9.9)
5	2,649 (8.7)	9,784 (11.6)	26,867 (10.2)	39,300 (10.4)
6	3,446 (11.3)	9,734 (11.6)	25,666 (9.8)	38,846 (10.3)
7	3,296 (10.8)	10,479 (12.4)	28,123 (10.7)	41,898 (11.1)
8	3,967 (13.0)	13,371 (15.9)	39,974 (15.2)	57,312 (15.2)
9	6,186 (20.3)	13,719 (16.3)	51,589 (19.6)	71,494 (18.9)
10	4,890 (16.1)	9,250 (11.0)	47,486 (18.0)	61,626 (16.3)

*IRSAD, Index of Relative Socioeconomic Advantage and Disadvantage.

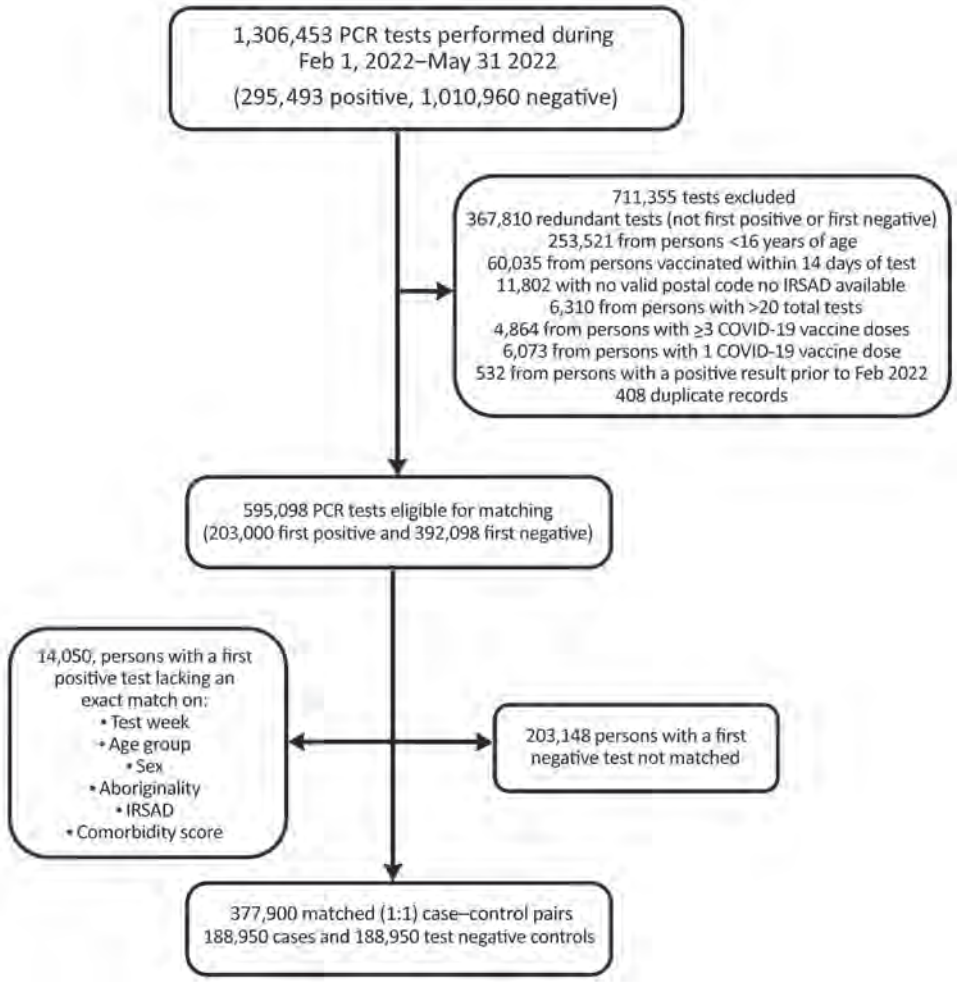

Figure 3. Selection of SARS-CoV-2 cases positive by PCR and of negative controls for analysis of vaccine effectiveness, Western Australia, Australia, February 1–May 31, 2022. IRSAD, Index of Relative Socioeconomic Advantage and Disadvantage.

different time frames to capture hospitalizations after a positive PCR, specifically 0–14, 2–14, and 2–9 days. VE estimates for severe disease did not differ significantly when we varied the window for hospitalization from 0–7 days to these alternate time frames.

Last, we re-ran the analyses while individually and sequentially adding covariates of interest to the matching algorithm to explore potential effects of confounding. Matching by age group and week of PCR test was sufficient to produce stable VE estimates that were statistically similar to those observed when matching on the full set of covariates for infection of any severity and severe disease.

Discussion

The ability of WA to limit the introduction of SARS-CoV-2 and prevent sustained local transmission 2 years into the pandemic provides a rare opportunity to assess VE in a population without potential confounding from prior asymptomatic or undiagnosed infection, factors that could affect VE assessments performed in almost all other settings. An assessment of VE in Sydney, New South Wales, Australia, also cited low rates of SARS-CoV-2 background infections in its study population, but WA and metropolitan Sydney have had different pandemic experiences (*4*). Cohort follow-up for the New South Wales study

Table 4. Vaccine effectiveness against breakthrough SARS-CoV-2 infection of any severity, 2 or 3 doses versus unvaccinated, Western Australia, Australia, February 1, 2022–May 31, 2022*

Case-patients		Controls		
Vaccinated	Unvaccinated	Vaccinated	Unvaccinated	Vaccine effectiveness, %, (95% CI)†
16,306	6,060	17,292	5,074	24.9 (21.2–28.4)
103,741	14,299	108,863	9,177	42.0 (40.2–43.6)

*Case-patient (SARS-CoV-2 positive) and control (SARS-CoV-2 negative) pairs (infection status determined by PCR) matched by age group, sex, Aboriginality, testing week, Index of Relative Socioeconomic Advantage and Disadvantage decile and comorbidities.
†Vaccine effectiveness = 1 – adjusted odds ratio (ascertained by using conditional logistic regression of matched pairs).

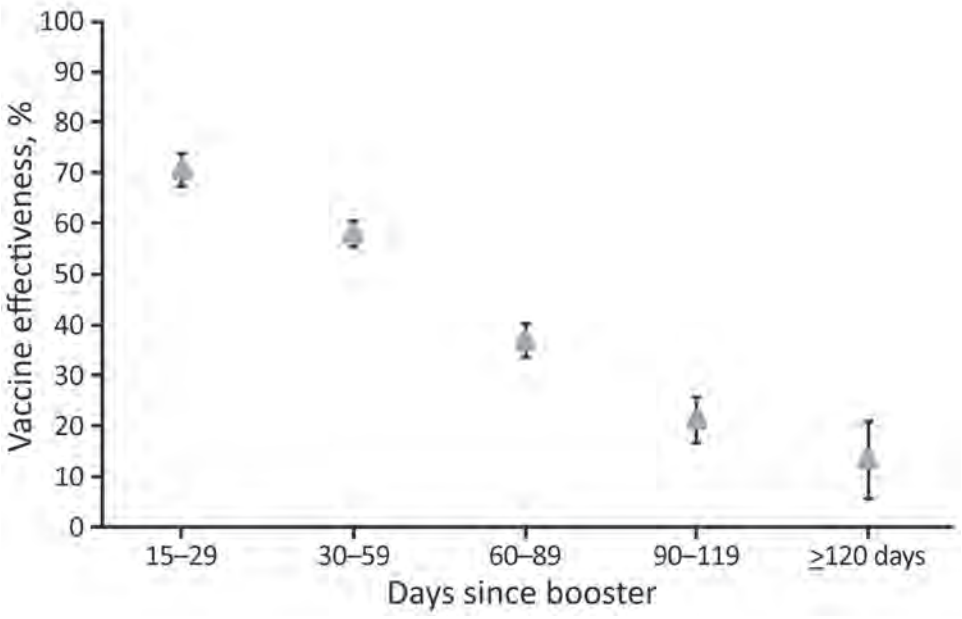

Figure 4. Vaccine effectiveness against breakthrough infection of any severity, by time since first booster dose versus unvaccinated controls, Western Australia, Australia, February 1–May 31, 2022. Error bars indicate 95% CIs.

began in January 2022, by which time 157,880 SARS-CoV-2 infections had been reported in the Sydney metropolitan area, largely the result of a protracted outbreak of the Delta variant in 2021 (*7*). Given that an estimated 40% of all SARS-CoV-2 infections are thought to be asymptomatic (*8*) and that the degree of underascertainment of those with mild illness who do not seek testing is unknown, it is difficult to quantify with certainty the extent of prior SARS-CoV-2 infection in the Sydney cohort. In contrast, the very low number of locally acquired infections identified before mid-February 2022 in WA (in the context of high rates of testing and robust contact tracing) and the extremely low rate of nucleocapsid antibody positivity among WA blood donor specimens collected during late February–early March 2022 (*9*) provide convincing evidence that prior SARS-CoV-2 infection was close to negligible among the population used for our analysis.

Most of our key findings are consistent with those from previous studies (*10*–*12*). First, overall VE against breakthrough infection of any severity across the full study period for persons who received 2 doses of vaccine was low (24.9% vs. 42.0% for those who received 3 doses). Subanalyses demonstrated that for those who received a booster dose, VE against any infection was near 71% at 15–29 days after vaccination but declined to <14% by 120 days.

Second, protection against severe disease after 3 vaccine doses was much higher than that after 2 doses; overall VE was estimated to be >80%. This finding is relevant because there has been concern that the level of protection afforded by vaccines based on the spike protein of the ancestral strain would be inadequate against Omicron variants, necessitating development of new bivalent vaccines designed to enhance the immune response to Omicron-specific epitopes (*10*).

This study showed considerable protection from monovalent vaccines against clinically severe illness during an exclusively Omicron wave among a population with negligible background immunity from exposure to the ancestral lineage or previous variants of concern. Our study definitively demonstrates that ancestral strain vaccines still provide substantial protection against severe disease caused by newer variants among a population free from potential confounding of previous immunity conferred by natural infection with an earlier variant.

Table 5. Vaccine effectiveness against severe COVID-19, 2 or 3 doses versus unvaccinated, Western Australia, Australia, February 1, 2022–May 31, 2022*

	Case-patients, hospital admission or death		Controls		
Vaccination status	Vaccinated	Unvaccinated	Vaccinated	Unvaccinated	Vaccine effectiveness, % (95% CI)†
Two doses	131	69	148	52	41.9 (4.8–64.5)
Three doses	795	259	982	72	81.7 (73.9–87.2)

*Severe disease was defined as hospitalization for SARS-CoV-2 infection with 7 d of positive SARS-CoV-2 PCR results and/or death from any cause.
†Vaccine effectiveness calculated with conditional logistic regression by using case–control pairs matched by week of testing, age group, sex, Aboriginality, Index of Relative Socioeconomic Advantage and Disadvantage, and comorbidity score.

Table 6. Dosing schedule for case-patients and controls included in the heterologous versus homologous 3-dose vaccination schedule analysis of SARS-CoV-2 vaccine effectiveness, Western Australia, Australia, February 1, 2022–May 31, 2022*

Dose 1	Dose 2	Dose 3	No. (%)
Homologous 3-dose vaccination schedules			
BNT162b2 mRNA	BNT162b2 mRNA	BNT162b2 mRNA	112,939 (75.7)
BNT162b2 mRNA	BNT162b2 mRNA	mRNA-1273	30,676 (20.6)
mRNA-1273	mRNA-1273	mRNA-1273	3,721 (2.5)
mRNA-1273	mRNA-1273	BNT162b2 mRNA	1,775 (1.2)
mRNA-1273	BNT162b2 mRNA	BNT162b2 mRNA	22 (0)
mRNA-1273	BNT162b2 mRNA	mRNA-1273	9 (0)
BNT162b2 mRNA	mRNA-1273	mRNA-1273	7 (0)
BNT162b2 mRNA	mRNA-1273	BNT162b2 mRNA	2 (0)
Heterologous 3-dose vaccination schedules			
ChAdOx1	ChAdOx1	BNT162b2 mRNA	18,925 (78.2)
ChAdOx1	ChAdOx1	mRNA-1273	5,261 (21.8)

*BNT162b2, Pfizer-BioNTech (https://www.pfizer.com); ChAdOx1, AstraZeneca (https://www.astrazeneca.com); mRNA-1273, Moderna (https://www.modernatx.com).

Vaccine-derived cross-protection observed in our setting may have implications for SARS-CoV-2 vaccine science going forward, specifically for assessing the need to continually design new variant-specific vaccines as the virus evolves. Although greater follow-up time is needed, these data support the hypothesis that vaccine effectiveness against severe disease caused by Omicron is likely to be substantially higher than the estimates against symptomatic disease, as has been observed for previous variants of concern (*13*–*15*).

We observed that a heterologous schedule consisting of 2 primary doses of ChAdOx1 followed by a booster dose of an mRNA vaccine provided significantly greater protection against infection >60 days after the last dose, compared with a homologous 3-dose

Table 7. Demographic characteristics of matched pairs for analysis for homologous versus heterologous 3-dose schedule SARS-CoV-2 vaccine effectiveness subanalysis, Western Australia, Australia, February 1, 2022–May 31, 2022*

Characteristic	Homologous schedule, no. (%)	Heterologous schedule, no. (%)
Age group, y		
16–19	8,409 (5.4)	0 (0.2)
20–29	33,199 (23.5)	249 (6.8)
30–39	42,223 (29.0)	268 (6.0)
40–49	44,699 (28.4)	291 (2.7)
50–59	17,565 (11.3)	4,449 (16.8)
60–69	1,442 (1.2)	10,897 (38.4)
70–79	370 (0.3)	5,923 (21.0)
≥80	1,244 (0.9)	2,109 (8.0)
Sex		
F	84,961 (55.8)	11,458 (46.2)
M	63,950 (43.9)	12,706 (53.4)
Unspecified	240 (0.3)	25 (0.5)
Aboriginal Status		
Non-Aboriginal	147,475 (98.7)	24,069 (99.2)
Aboriginal	1,676 (1.3)	117 (0.8)
No. comorbidities		
0	143,910 (96.6)	19,940 (85.0)
1	1,656 (1.0)	780 (2.7)
2	2,997 (1.9)	2,284 (8.0)
3	153 (0.1)	258 (0.9)
4	337 (0.2)	624 (2.3)
≥5	98 (0.1)	300 (1.1)
IRSAD		
1	306 (0.3)	31 (0.5)
2	6,641 (4.7)	1,024 (4.7)
3	3,074 (2.1)	561 (2.3)
4	12,710 (8.6)	2,649 (10.7)
5	14,401 (9.4)	2,756 (10.5)
6	14,992 (10.2)	1,846 (8.4)
7	15,669 (10.5)	2,268 (9.5)
8	23,381 (15.4)	2,825 (11.7)
9	30,236 (20.4)	4,827 (20.4)
10	27,741 (18.5)	5,399 (21.4)

*IRSAD, Index of Relative Socioeconomic Advantage and Disadvantage.

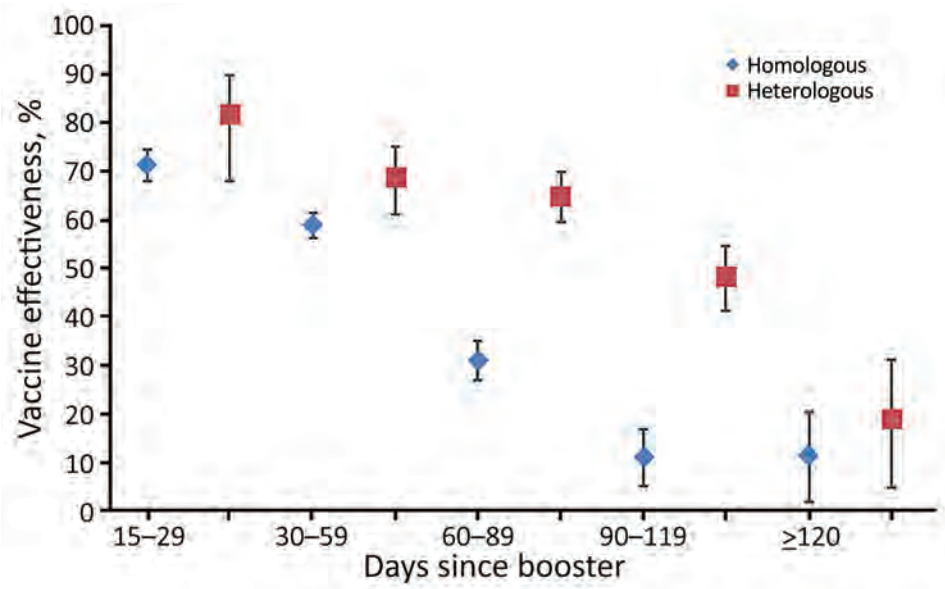

Figure 5. Vaccine effectiveness against breakthrough infection of any severity, by time since booster vaccination, for homologous (all mRNA vaccines) versus heterologous (ChAdOx1 primary, mRNA booster) vaccination series, Western Australia, Australia, February 1–May 31, 2022. Error bars indicate 95% CIs.

series of mRNA-based vaccines (mostly 3 doses of BNT162b2). This finding is unlikely to be explained by recipients of the heterologous vaccine schedule being inherently less prone to COVID-19 because after the association between ChAdOx1 and thrombotic events was identified, ChAdOx1 was almost entirely administered to persons >60 years of age across Australia. However, in accordance with guidance in Australia about brand-based differences for recommended first- and second-dose intervals, the median time between 2 doses of an mRNA primary series in our cohort was 27 days; for a ChAdOx1 primary series, it was 84 days. It is therefore possible that the longer interval between doses contributed to the more durable protection we observed with the heterologous schedule.

A study of Omicron infections in England found that VE against symptomatic illness was similar between those who received 2 doses of either ChAdOx1 or BNT162b2 followed by a booster dose of BNT162b2, specifically 62.4% and 67.2% given 2–4 weeks after the booster, falling to 39.6% and 45.7%, respectively, after ≥10 weeks (*10*). One key difference between our setting and that of the study in England is that in late 2020, the United Kingdom began recommending up to 12 weeks between the first and second doses of BNT162b2, a practice uncommon in the WA cohort, and a longer interval between BNT162b2 doses has been shown to enhance immunogenicity (*13*).

Alternatively, the superior performance of the heterologous schedule in protecting against Omicron infection in WA may be a real phenomenon, unmasked without interference from substantial levels of background immunity caused by prior infections with earlier variants. The enhanced immune response, and in some instances clinical protection against non-Omicron variants, produced by heterologous vaccination schedules has been documented in a variety of settings (*14*,*15*).

Among the limitations of our study, our analysis was restricted to using PCR test results from licensed laboratories to determine a person's status as a case-patient or control and excluded self-administered RATs reported by the general public. This approach was necessary because RAT results were not systematically linked to other datasets used in this analysis. However, even if possible, including RAT results in our setting would have been methodically undesirable because reporting of negative RAT results is not mandatory and the degree of underreporting of positive RAT results by the public is not quantifiable. Furthermore, because there may be relevant differences between those who seek PCR testing and those who choose to self-administer a RAT, including only positive RAT results would have the potential to introduce significant bias when using a VE study design that explicitly relies on matching test-positive case-patients to similar test-negative controls.

Another limitation is that although we attempted to control for relevant confounders, we were limited by the information available in the data repository, and the potential for residual confounding remains. For example, without knowing the reasons for obtaining a PCR test, we could not exclude tests performed for asymptomatic screening, perhaps before an elective hospital admission or for work requirements. Instead, to account for this limitation, we created a surrogate by excluding all tests for persons with >20 tests over the study period and admissions to hospital

services not likely to be treating COVID-19. Likewise, because we were not able to directly access information about a person's comorbidities, we created a comorbidity score based on hospital ICD-10-AM codes accumulated in the previous 2 years. Although we believe those strategies reduced confounding, they are probably imperfect proxies.

Among the strengths of this study, first, the entire cohort of persons ≥16 years of age who were tested for SARS-CoV-2 by PCR was eligible for inclusion, which resulted in a large sample, probably representative of the population at risk during the study period. Second, we accessed all SARS-CoV-2 PCR results from every private and public clinical laboratory in the state notified to the WA Department of Health as required by law. Third, we used a comprehensive linked data collection, which included hospitalization data from public and private hospitals and mortality data for the entire state. Fourth, vaccination status was obtained from a population-based, whole-of-life, mandatory national immunization register. AIR data are generally considered to be of good quality (*16*), and there was a strong incentive for persons to be sure that their COVID-19 vaccination record was accurate and up to date because activities such as employment and attending public venues were dependent on vaccination status (*17*). Last, the pandemic experience in WA enabled assessment of VE in a SARS-CoV-2 infection–naive cohort, which eliminated potential interference from non–vaccine-derived prior immunity.

In summary, as a result of a sustained, concerted effort to prevent introduction and spread of SARS-CoV-2 during the first 2 years of the pandemic, WA was in a unique position to evaluate, on the basis of the ancestral spike protein, the effectiveness of vaccines to prevent infection and severe disease caused by the Omicron variant in a population that had not experienced prior local SARS-CoV-2 transmission. We demonstrated that VE against infection of any severity was ≈70% up to 1 month after vaccination but waned to very low levels by 4 months. Compared with a homologous 3-dose mRNA vaccine series, a heterologous series consisting of 2 doses of ChAdOx1 followed by an mRNA booster provided significantly longer protection after 60 days, up to 4 months. Protection against hospitalization and death after 3 doses was high (i.e., ≈80%), reinforcing the value of SARS-CoV-2 vaccines for preventing serious outcomes from SARS-CoV-2 infection.

Acknowledgments

We thank Paul Knight and Dylan Barth for providing SARS-CoV-2 testing and case data (Figure 1). We also thank Chisha Sikazwe, Avram Levy, and staff within the Microbial Surveillance unit at PathWest Laboratory Medicine, Perth, Western Australia, for providing lineage data (Figure 2). Last, we thank the staff at the Western Australian Data Linkage Branch, Death Registrations, COVID-19 Pathology Data Collection, Hospital Morbidity Data Collection, and AIR for providing linked health data.

About the Author

Dr. Bloomfield is a communicable disease epidemiologist with the Immunisation Program in the WA Department of Health, and a senior lecturer for Population and Preventive Health, School of Medicine (Fremantle), University of Notre Dame Australia.

References

1. Australian Government. COVID-19 vaccine roll-out: 01 February 2022 [cited 2023 Jan 30]. https://www.health.gov.au/sites/default/files/documents/2022/02/covid-19-vaccine-rollout-update-1-february-2022.pdf
2. Eitelhuber T, Ngeh S, Bloomfield L, Chandaria B, Effler P. Using data linkage to monitor COVID-19 vaccination: development of a vaccination linked data repository. Int J Popul Data Sci. 2022;5. https://doi.org/10.23889/ijpds.v5i4.1730
3. Government of Western Australia Department of Health. Hospital morbidity data collection: data specifications [cited 2023 Jan 30]. https://www.health.wa.gov.au/-/media/Corp/Policy-Frameworks/Information-Management/Patient%20Activity%20Data/Supporting/Hospital-Morbidity-Data-Collection-Data-Specifications-2022.pdf
4. Liu B, Gidding H, Stepien S, Cretikos M, Macartney K. Relative effectiveness of COVID-19 vaccination with 3 compared to 2 doses against SARS-CoV-2 B.1.1.529 (Omicron) among an Australian population with low prior rates of SARS-CoV-2 infection. Vaccine. 2022;40:6288–94. https://doi.org/10.1016/j.vaccine.2022.09.029
5. Australian Bureau of Statistics. 2033.0.55.001—Census of Population and Housing: Socio-Economic Indexes for Areas (SEIFA), Australia, 2016 [cited 2023 Jan 30]. https://www.abs.gov.au/AUSSTATS/abs@.nsf/DetailsPage/2033.0.55.0012016?OpenDocument
6. Ho D, Imai K, King G, Stuart EA. MatchIt: nonparametric preprocessing for parametric causal inference. J Stat Softw. 2011;42:1–28. https://doi.org/10.18637/jss.v042.i08
7. Government NSW. COVID-19 cases data [cited 2023 Jan 30]. https://data.nsw.gov.au/nsw-covid-19-data/cases
8. Ma Q, Liu J, Liu Q, Kang L, Liu R, Jing W, et al. Global percentage of asymptomatic SARS-CoV-2 infections among the tested population and individuals with confirmed COVID-19 diagnosis: a systematic review and meta-analysis. JAMA Netw Open. 2021;4:e2137257. https://doi.org/10.1001/jamanetworkopen.2021.37257
9. Australian Government. COVID-19 vaccine roll-out: 01 February 2022 [cited 2023 Jan 30]. https://www.health.gov.au/sites/default/files/documents/2022/02/covid-19-vaccine-rollout-update-1-february-2022.pdf
10. Andrews N, Stowe J, Kirsebom F, Toffa S, Rickeard T, Gallagher E, et al. Covid-19 vaccine effectiveness against the Omicron (B.1.1.529) variant. N Engl J Med. 2022;386:1532–46. https://doi.org/10.1056/NEJMoa2119451

11. Chemaitelly H, Tang P, Hasan MR, AlMukdad S, Yassine HM, Benslimane FM, et al. Waning of BNT162b2 vaccine protection against SARS-CoV-2 infection in Qatar. N Engl J Med. 2021;385:e83. https://doi.org/10.1056/NEJMoa2114114
12. Kirsebom FCM, Andrews N, Stowe J, Toffa S, Sachdeva R, Gallagher E, et al. COVID-19 vaccine effectiveness against the omicron (BA.2) variant in England. Lancet Infect. Dis. 2022;22:931–3. https://doi.org/10.1016/S1473-3099(22)00309-7
13. Payne RP, Longet S, Austin JA, Skelly DT, Dejnirattisai W, Adele S, et al.; PITCH Consortium. Immunogenicity of standard and extended dosing intervals of BNT162b2 mRNA vaccine. Cell. 2021;184:5699–5714.e11. https://doi.org/10.1016/j.cell.2021.10.011
14. Schmidt T, Klemis V, Schub D, Mihm J, Hielscher F, Marx S, et al. Immunogenicity and reactogenicity of heterologous ChAdOx1 nCoV-19/mRNA vaccination. Nat Med. 2021;27:1530–5. https://doi.org/10.1038/s41591-021-01464-w
15. Liu X, Shaw RH, Stuart ASV, Greenland M, Aley PK, Andrews NJ, et al.; Com-COV Study Group. Safety and immunogenicity of heterologous versus homologous prime-boost schedules with an adenoviral vectored and mRNA COVID-19 vaccine (Com-COV): a single-blind, randomised, non-inferiority trial. Lancet. 2021;398:856–69. https://doi.org/10.1016/S0140-6736(21)01694-9
16. Dalton LG, Meder KN, Beard FH, Dey A, Hull BP, Macartney KK, et al. How accurately does the Australian Immunisation Register identify children overdue for vaccine doses? A national cross-sectional study. Commun Dis Intell. 2018;2022:46. https://doi.org/10.33321/cdi.2022.46.10
17. Government of Western Australia. Proof of COVID-19 vaccination to expand state-wide from Monday 31 January [cited 2023 Jan 30]. https://www.wa.gov.au/government/announcements/proof-of-covid-19-vaccination-expand-state-wide-monday-31-january

Address for correspondence: Paul V. Effler, Immunisation Program, Communicable Disease Control Directorate, WA Department of Health, 189 Royal St, East Perth, WA 6004, Australia; email: paul.effler@health.wa.gov.au

etymologia revisited

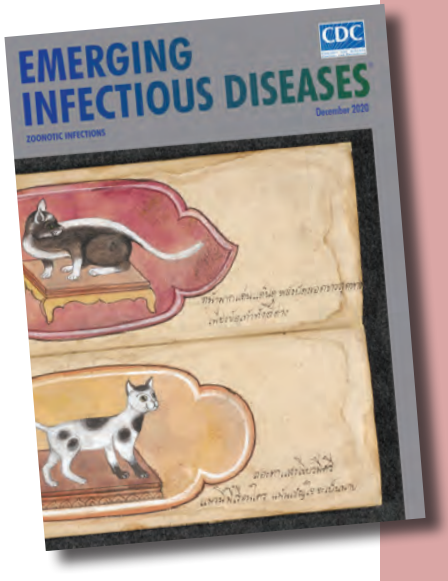

Originally published in December 2020

Salmonella

[sal′′mo-nel′ə]

Named in honor of Daniel Elmer Salmon, an American veterinary pathologist, *Salmonella* is a genus of motile, gram-negative bacillus, nonspore-forming, aerobic to facultatively anaerobic bacteria of the family Enterobacteriaceae. In 1880, Karl Joseph Eberth was the first to observe *Salmonella* from specimens of patients with typhoid fever (from the Greek *typhōdes* [like smoke; delirious]), which was formerly called *Eberthella typhosa* in his tribute. In 1884, Georg Gaffky successfully isolated this bacillus (later described as *Salmonella* Typhi) from patients with typhoid fever, confirming Eberth's findings. Shortly afterward, Salmon and his assistant Theobald Smith, an American bacteriologist, isolated *Salmonella* Choleraesuis from swine, incorrectly assuming that this germ was the causative agent of hog cholera. Later, Joseph Lignières, a French bacteriologist, proposed the genus name *Salmonella* in recognition of Salmon's efforts.

References:

1. Dorland's Illustrated Medical Dictionary. 32nd ed. Philadelphia: Elsevier Saunders; 2012.
2. Gossner CM, Le Hello S, de Jong B, Rolfhamre P, Faensen D, Weill FX, et al. Around the world in 1,475 Salmonella geo-serotypes [Another Dimension]. Emerg Infect Dis. 2016;22:1298–302.
3. Issenhuth-Jeanjean S, Roggentin P, Mikoleit M, Guibourdenche M, de Pinna E, Nair S, et al. Supplement 2008-2010 (no. 48) to the White-Kauffmann-Le Minor scheme. Res Microbiol. 2014;165:526–30.
4. Salmon DE. The discovery of the germ of swine-plague. Science. 1884;3:155–8.
5. Su LH, Chiu CH. Salmonella: clinical importance and evolution of nomenclature. Chang Gung Med J. 2007;30:210–9.

Increased Incidence of Legionellosis after Improved Diagnostic Methods, New Zealand, 2000–2020

Frances F. Graham, David Harte, Jane Zhang, Caroline Fyfe, Michael.G. Baker

Legionellosis, notably Legionnaires' disease, is recognized globally and in New Zealand (Aotearoa) as a major cause of community-acquired pneumonia. We analyzed the temporal, geographic, and demographic epidemiology and microbiology of Legionnaires' disease in New Zealand by using notification and laboratory-based surveillance data for 2000–2020. We used Poisson regression models to estimate incidence rate ratios and 95% CIs to compare demographic and organism trends over 2 time periods (2000–2009 and 2010–2020). The mean annual incidence rate increased from 1.6 cases/100,000 population for 2000–2009 to 3.9 cases/100,000 population for 2010–2020. This increase corresponded with a change in diagnostic testing from predominantly serology with some culture to almost entirely molecular methods using PCR. There was also a marked shift in the identified dominant causative organism, from *Legionella pneumophila* to *L. longbeachae*. Surveillance for legionellosis could be further enhanced by greater use of molecular typing of isolates.

Legionellosis is caused by the gram-negative bacterium *Legionella*. This infection is predominantly the consequence of an environmental exposure to legionellae, which are ubiquitous in water and moist soil ecosystems. Incidence and seroprevalence studies show that the infection has a global distribution (*1*,*2*). The severity of disease varies from mild febrile illness (Pontiac fever, incubation period commonly 24–48 hours) (*3*) to serious and sometimes fatal pneumonia (Legionnaires' disease, incubation period commonly 2–10 days) (*4*). Recognized infection risk factors for legionellosis include smoking, chronic obstructive pulmonary disease, diabetes, various conditions associated with immunodeficiency, male sex, and increasing age (*4*).

Author affiliations: University of Otago, Wellington, New Zealand (F.F. Graham, J. Zhang, C. Fyle, M.G. Baker); Environmental Science and Research, Wellington (D. Harte)

DOI: https://doi.org/10.3201/eid2906.221598

Disease surveillance for legionellosis began in New Zealand (Aotearoa) in 1979 with the collection of laboratory-based data (cases positive for *Legionella* species); additional data were available starting in June 1980, when the disease became notifiable (*5*). A review of national surveillance data for 1979–2009 showed that the annual incidence rate for laboratory-identified cases was 2.5 cases/100,000 persons and 1.4 cases/100,000 persons for notified cases (*6*); the disparity was caused by not all laboratory-identified cases being notified.

Inhalation of aerosolized bacteria from an environmental source is the usual means of *Legionella* transmission. Environmental surveillance shows that *Legionella* species are widely distributed in New Zealand (*7*). Commonly identified sources are engineered environments, such as wet cooling towers and water distribution systems, which can be reservoirs and amplifiers of the bacteria, particularly *L. pneumophila* (*1*). Aerosolized dust inhalation from handling compost and potting mix materials is most probably a major transmission route contributing to the cases of legionellosis caused by *L. longbeachae* (*8*), which is the predominant species that causes disease in New Zealand (*9*).

During 1980–2000, all cases of legionellosis were diagnosed in New Zealand by using traditional laboratory methods, notably culture isolation and direct fluorescent-antibody staining of respiratory tract specimens, and serology by immunofluorescent antibody testing. During that period, the *Legionella* urinary antigen test (UAT), followed by nucleic acid amplification test (NAAT), became established diagnostic tools. Since 2000, there has been an increasing shift toward NAATs, primarily PCR testing, and this method has dominated from 2015 onward.

The aims of this study were to provide an updated analysis of the epidemiology of legionellosis

in New Zealand, focusing on differences between 2 periods (2000–2009 and 2010–2020); examine the influence of changing diagnostic methods on the temporal and geographic distribution of notified and laboratory-identified legionellosis cases; and review changes in the causative species. Our findings are intended to be used to improve surveillance, prevention, and management of legionellosis.

Methods

Surveillance Data and Case Definitions

We used 2 data sources to describe the epidemiology of legionellosis (including Legionnaires' disease and Pontiac fever) in New Zealand: notifiable disease data and laboratory-based surveillance data (Appendix, https://wwwnc.cdc.gov/EID/article/29/6/22-1598-App1.pdf). We analyzed all reported cases of Legionnaires' disease and Pontiac fever. Pontiac fever cases are a small proportion of legionellosis notifications (3 cases, 0.1% during 2000–2020), possibly because Pontiac fever is a milder and self-resolving illness, which consequently is mostly untested and therefore unreported (*6*).

A confirmed case of legionellosis requires a clinically compatible disease with ≥1 form of laboratory evidence: *Legionella* culture isolated from a clinical specimen; a ≥4-fold increase in immunofluorescent antibody titer against *Legionella* spp. to ≥256 between acute-phase and convalescent-phase paired serum samples tested in parallel by using pooled antigen at the same reference laboratory; and detection of *L. pneumophila* serogroup 1 by antigen in urine or positive NAAT result (*10*). A probable case is defined as a clinically compatible disease with laboratory evidence of *Legionella* infection showing ≥1 antibody titers ≥512 but without a demonstrated 4-fold titer increase.

Statistical Analysis

We used Poisson regression to estimate the incidence rates, age-standardized to 2013 New Zealand census population age-structure, for legionellosis over 2 periods: 2000–2009 (preceding a major shift to NAAT) and 2010–2020 (after the effect of a shift to NAAT and change in diagnostic criteria/case definition). The null hypothesis was that there was no change in the rates of legionellosis cases in these time periods. We calculated the annual incidence rate (legionellosis cases/100,000 population) by dividing reported cases by each mid-year census estimate and multiplying by 100,000. We did not calculate rates when a category had <5 notified cases. We performed statistical analysis by using SAS version 9.4 (SAS Institute, https://www.sas.com).

Results

Case Incidence and Temporal Trends

A total of 2,628 legionellosis cases were notified during 2000–2020, an overall mean annual incidence rate of 2.7 cases/100,000 population. The mean annual incidence rate increased from 1.6 cases/100,000 population in 2000–2009 to 3.9 cases/100,000 population in 2010–2020 (Figure 1). We observed marked increases in legionellosis cases in 2003, 2010, and 2015 and decreases in the periods between those years (Appendix Table 1).

A total of 2,675 laboratory-identified cases that fit the case definition were reported during the study period. Of the laboratory-identified cases that met the case definition, 1,942 (72.6%) were confirmed and 733 (27.4%) were probable. The incidence rate for laboratory-identified cases (confirmed and probable cases combined) averaged 2.8 cases/100,000 population/year (range 1.3 cases/100,000 population in 2002 and 2006 to 5.4 cases/100,000 population in 2015) (Figure 1).

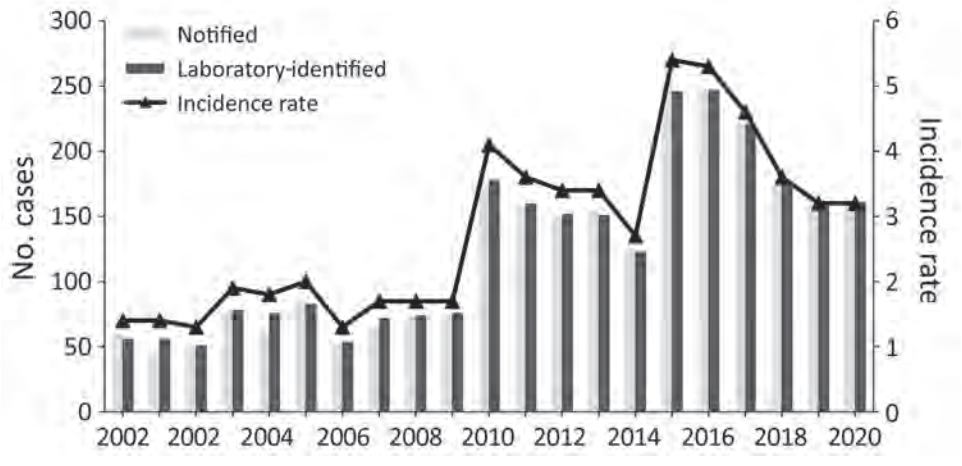

Figure 1. Notification and laboratory-identified case numbers and incidence rates (cases/100,000 population), by year, in study of increased incidence of legionellosis after improved diagnostic methods, New Zealand, 2000–2020.

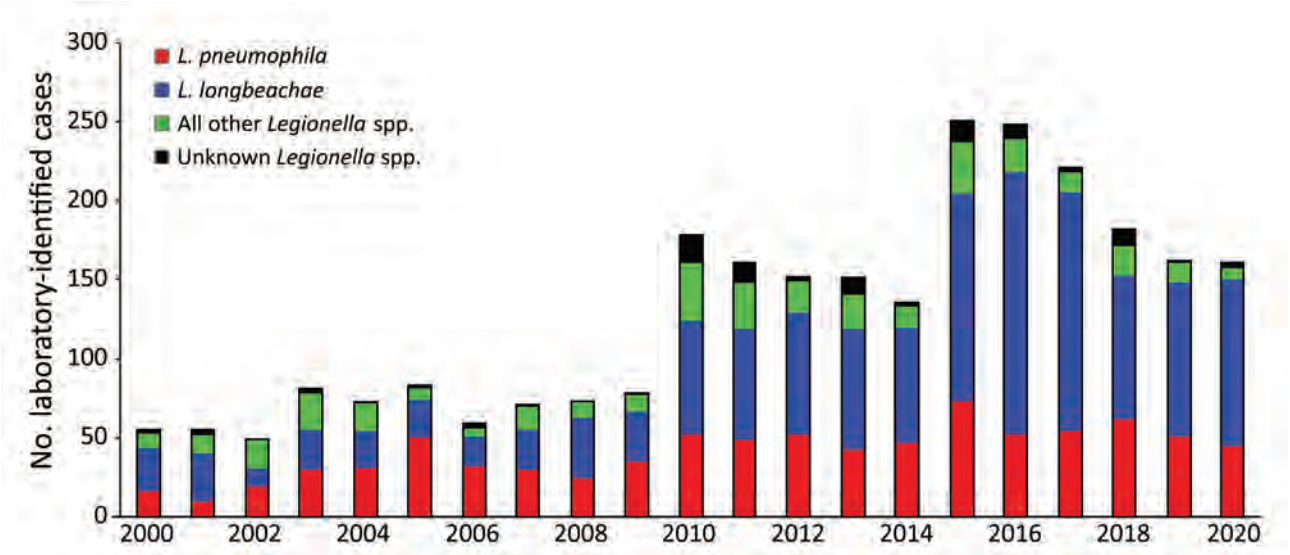

Figure 2. Laboratory-identified legionellosis cases, by species and year, in study of increased incidence of legionellosis after improved diagnostic methods, New Zealand, 2000–2020.

Causative *Legionella* Species

We grouped the number of *Legionella* species identified through laboratory-based surveillance during 2000–2020 as *L. longbeachae*, *L. pneumophila*, or other (Figure 2; Appendix Table 2). *L. longbeachae* was identified as the causative agent for 51.0% of all legionellosis cases over the 21-year period (Appendix Table 2). *L. pneumophila* accounted for 31.2% of all cases, followed by other *Legionella* spp. (13.5%) and unidentified *Legionella* spp. (4.3%) (Appendix Table 2).

During 2000–2009, the annual laboratory-identified clinical case numbers caused by *L. pneumophila* infection were similar to those caused by *L. longbeachae* (*L. pneumophila*, 26.4 cases/year; *L. longbeachae*, 25.2 cases/year). During 2010–2020, *L. longbeachae* case numbers increased 4-fold to average 101.3 cases/year (55.6%, 1,114/2,002 cases), compared with a doubling in *L. pneumophila* case numbers to an average of 51.8 cases/year (28.5%, 571/20,02 cases). We found a marked increase in the number of *L. longbeachae* cases in which the serogroup was unidentified (32 cases in 2010 increasing to 61 cases in 2020); those cases were identified by using a molecular method that did not differentiate between *L. longbeachae* serogroups 1 and 2. (Appendix Table 2).

Method of Case Identification

The method of initial diagnosis that gave a positive *Legionella* result changed over time (Figure 3; Appendix Table 3). The number of cases diagnosed by using PCR increased progressively from 2010 onward, whereas the number of cases diagnosed by traditional methods of serology and culture

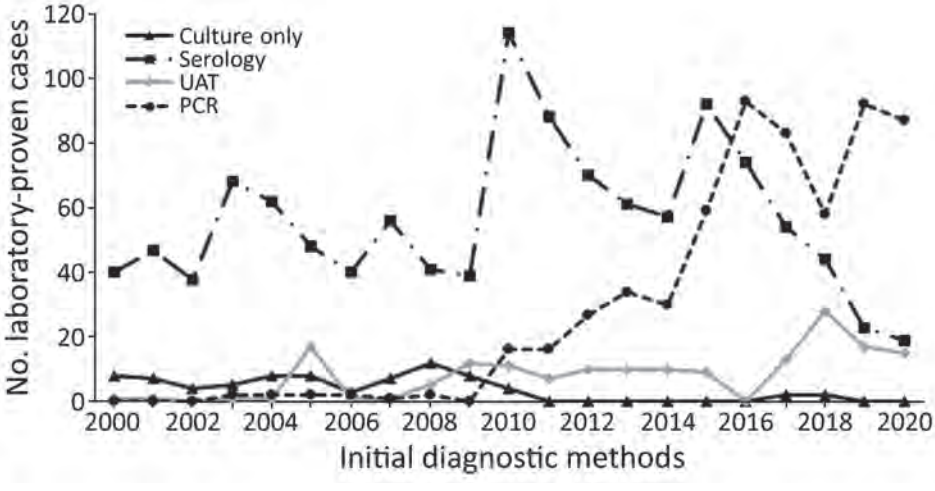

Figure 3. Laboratory-identified legionellosis, by initial diagnostic method and year, in study of increased incidence of legionellosis after improved diagnostic methods, New Zealand, 2000–2020. UAT, urine antigen test.

isolation alone decreased. This observation is reinforced (Appendix Table 3) and shows a major increase in cases diagnosed by using molecular methods between the 2 10-year periods compared with more traditional methods (culture, serology, and UAT).

Demographic Characteristics

Except for 2003, legionellosis incidence and age-standardized rates were highest in adults ≥60 years of age, followed by adults 40–59 years of age and children and younger adults (0–39 years of age) (Table 1; Figure 4). Compared with 2000–2009, legionellosis incidence and age-standardized rates were much higher in 2010–2020. Rates increased across all age, sex, and ethnic groups (Table 1; Appendix Tables 4, 5). The association of age with the incidence of legionellosis demonstrates increasing incidence with age for all *Legionella* species, especially in the population ≥60 years of age (Table 1). During 2000–2020, the number of notified cases (n = 2,628) was also higher for male (62.7%) than female (37.1%) patients, an overall ratio of 1.7:1.

We recorded ethnicity for 2,508 (95.4%) notified cases during 2000–2020 and compiled age-stratified and age-standardized rates of legionellosis for European, Māori, Pacific Peoples, and other ethnicities (Appendix Tables 4, 5). Focusing on age-standardized rates for the 2010–2020 period, the European ethnic group had the highest notification rate (3.9 cases/100,000 population), followed by Pacific Peoples (3.1 cases/100,000 population), Māori (2.8 cases/100,000 population), and other ethnic group persons (1.7 cases/100,000 population). The age-standardized rates increased for all ethnicities over the 2 time periods. A notable change in the second time period (2010–2020) was that the ethnic gradient toward higher rates in Europeans was reduced because rates had increased more markedly for Māori, Pacific Peoples, and other ethnic groups over that observation period (Table 1).

Regional Distribution

We compiled the rates of legionellosis incidence calculated for each district health board (DHB) area that had ≥5 diagnosed cases (divided into quintiles based on mean rate/100,000 population) for 2000–2009 and 2010–2020 (Figure 5; Appendix, Appendix Table 6). The two highest quintiles were well above the mean national notifiable incidence rate of 2.7 cases/100,000 population. In the South Island, large changes in the legionellosis rate were observed on the West Coast (2.0 cases/100,000 population in 2000–2009 and 10.6 cases/100,000 population in 2010–2020), partly influenced by the small population size. The Canterbury DHBs of the South Island showed consistently high rates (9.1 cases/100,000 population in 2000–2009 and 9.8 cases/100,000 population in 2010–2020). In the North Island, large changes in the incidence rate were observed in Northland, with an observed increase in mean annual incidence from 2.0 cases/100,000 population in 2000–2009 to 6.0 cases/100,000 population in 2010–2020. Conversely, a decrease in incidence rates was observed across the 3 Auckland DHBs; the Central Auckland DHB had the largest decrease in mean annual incidence, from 5.5 cases/100,000 population in 2000–2009 to 3.3 cases/100,000 population in 2010–2020. Conversely, a decrease in incidence rates was observed across the 3 Auckland DHBs; the Central Auckland DHB had the largest decrease in mean annual incidence, from 5.5 cases/100,000 population in 2000–2009 to 3.3 cases/100,000 population in 2010–2020.

Case Outcome

The hospitalization status was recorded on EpiSurv (https://surv.esr.cri.nz) for 95.8% (2,518/2,628) notified cases during 2000–2020. Of those case-patients, most (82.0%, 2,066/2,518) were hospitalized; 90 (3.6%) recorded unknown hospitalization status. The risk for hospitalization decreased over time: 91.4% (588/643 case-patients) were hospitalized during 2000–2009 but only 74.5% (14,78/1,985 case-patients) during 2010–2020. The highest percentage of hospitalized case-patients was ≥60 years of age for both periods, 82.3% (375 cases) in 2000–2009 and 81.1% (1,308 cases) in 2010–2020. The rate of hospitalization for legionellosis increased from 14.2 cases/100,000 population in 2000–2009 to 31.4 cases/100,000 population in 2010–2020.

A total of 61 deaths attributed to legionellosis were reported during 2000–2020, giving an overall case-fatality risk (CFR) of 2.7% (range 0.4%–8.9%). The CFR decreased from 4.0% (26 deaths/643 notified cases) during 2000–2009 to 1.8% (35 deaths/1985 notified cases) in 2010–2020. Throughout the study period, an increased CFR was consistently associated with advanced age and male sex. The increase in cases was associated with a marked decrease in CFR for *L. longbeachae* but little change for *L. pneumophila* (Appendix Table 7). The increase in case detection during 2010–2020 identified a larger number of less severe cases, which effectively increased the denominator of nonfatal cases and decreased the observed CFR by ≈60%. This effect was particularly marked

for *L. longbeachae*, for which the CFR has decreased by 80% and is now markedly less than that observed for *L. pneumophila* (Appendix Table 7). The legionellosis mortality rate increased slightly between study periods, from 0.6 deaths/100,000 population in 2000–2009 to 0.7 deaths/100,000 population in 2010–2020.

Risk Factors

The surveillance system routinely collects data on a range of environmental exposures reported by cases along with key host factors that are known to predispose to legionellosis (Table 2). An environmental exposure risk was reported for 1,744 (68.4%) of laboratory-identified cases recorded in the EpiSurv

Table 1. Characteristics of notified cases by patient age group, sex, ethnicity, and *Legionella* species, New Zealand, 2000–2020*

	2000–2009				2010–2020				Comparison of 2 periods, IRR (95% CI)
Category	No. cases	Crude rate	ASR† (95% CI)	IRR (95% CI)	No. cases	Crude rate	ASR† (95% CI)	IRR (95% CI)	
Age group, y									
Total	643	1.6	1.5 (1.4–1.6)	NA	1,985	3.9	3.8 (3.6–3.9)	NA	2.5 (2.3–2.7)
<1–39	46	0.2	NA	Referent	99	0.4	NA	Referent	1.7 (1.2–2.9)
40–59	219	1.9	NA	9.1 (6.6–12.5)	619	5.0	NA	12.8 (10.3–15.8)	2.5 (2.1–2.9)
≥60	378	4.5	NA	21.9 (16.1–29.7)	1,267	11.8	NA	32.8 (26.7–40.2)	2.6 (2.3–2.9)
Sex									
M	383	1.9	1.9 (1.7–2.11)	1.7 (1.4–2.0)	1,265	5.0	5.0 (4.7–5.2)	1.9 (1.8–2.1)	2.6 (2.3–2. 9)
F	254	1.2	1.1 (1.0–1.3)	Referent	720	2.7	3.0 (2.4–2.8)	Referent	2.3 (2.0–2.6)
Unknown	6	NA			0	NA			
Ethnicity									
European	517	2.3	2.1 (1.9–2.3)	Referent	1,620	4.5	3.9 (3.7–4.1)	Referent	1.85 (1.67–2.04)
Māori	27	0.5	0.7 (0.4–1.1)	0.35 (0.22–0.55)	149	1.7	2.8 (1.4–3.3)	0.73 (0.61–0.88)	3.89 (2.42–6.25)
Pacific Peoples	13	0.6	0.7 (0.3–1.1)	0.32 (0.17–0.58)	72	1.7	3.1 (2.3–3.9)	0.80 (0.62–1.03)	4.63 (2.42–8.88)
Other	17	0.2	0.2 (0.1–0.4)	0.11 (0.07–0.19)	93	1.1	1.7 (1.4–2.1)	0.45 (0.36–0.56)	7.46 (4.31–12.9)
Unknown	69	NA			51	NA			
Laboratory status									
Confirmed	537	1.3	0.9 (0.8–0.9)	Referent	1,700	3.3	2.4 (2.2–2.5)	Referent	2.7 (2.5–3.0)
Probable	106	0.2	0.2 (0.1–0.2)	0.2 (0.2–0.23)	285	0.6	0.4 (0.3–0.4)	0.2 (0.1–0.2)	2.2 (1.7–2.7)
L. pneumophila									
Total	256	6.2	NA	NA	527	11.2	NA	NA	1.80 (1.57–1.94)
<1–39	9	0.3		Referent	58	0.8		Referent	2.67 (2.31–2.86)
40–59	58	1.0		1.41 (0.97–1.73)	196	2.9		2.85 (2.19–3.12)	2.90 (2.50–3.04)
≥60	189	3.2		13.6 (9.42–16.5)	273	4.9		5.15 (3.99–5.63)	1.53 (1.33–1.88)
L. longbeachae									
Total	161	3.9	NA	NA	1,062	22.6	NA	NA	5.79 (5.49–6.12)
1–39	5	0.1		Referent	39	0.6		Referent	2.00 (1.96–2.29)
40–59	56	1.0		2.60 (1.70–3.26)	284	3.8		1.76 (1.41–1.85)	3.80 (3.68–3.96)
≥60	98	2.4		7.50 (5.00–9.42)	739	14.6		11.02 (8.86–11.51)	6.10 (6.26–6.67)
Other species									
Total	87	2.1	NA	NA	251	5.3	NA	NA	2.52 (2.16–2.89)
<1–39	11	0.1		Referent	50	0.7		Referent	7.00 (6.43–7.69)
40–59	35	0.5		3.24 (1.94–4.56)	79	1.2		2.21 (1.55–2.64)	2.40 (1.90–2.50)
≥60	41	0.9		4.30 (2.58–5.99)	122	2.3		4.56 (3.26–5.34)	2.56 (2.35–2.83)
Unknown	139	NA			145	NA			

*Crude rate is cases per 100,000 population. ASR, age-standardized rate; IRR, incidence rate ratio; NA, not applicable.
†Age standardized to the New Zealand population age structure at the 2013 census.

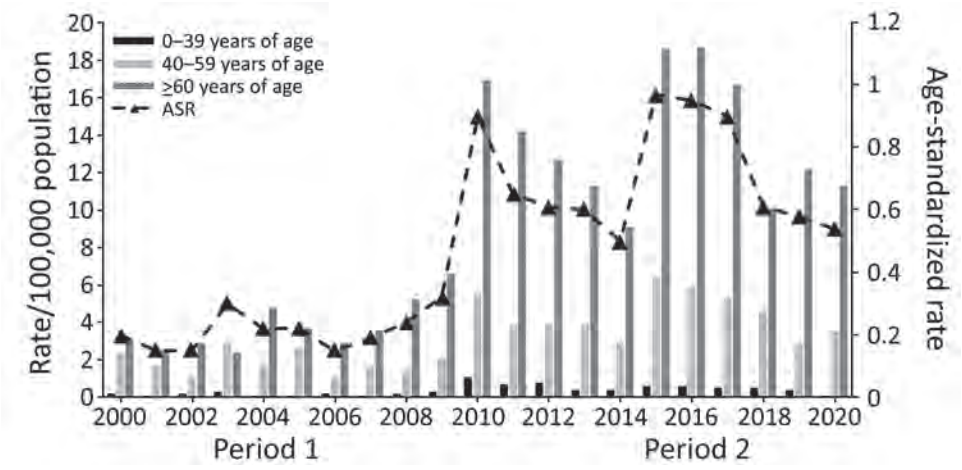

Figure 4. Incidence rate and ASR of legionellosis notifications, by age group and year (time-period), in study of increased incidence of legionellosis after improved diagnostic methods, New Zealand, 2000–2020. Period 1, 2000–2009; period 2, 2010–2020.ASR, age-standardized rate.

database during 2000–2020. More detailed exposure data were available for the second decade and showed that 1,054 (41.4%) case-patients reported contact with compost/potting mix or soil during their incubation period (Table 2). A total of 155 (6.2%) of the number of reported notified case-patients had a history of overseas travel during the incubation period. Smoking and an immunosuppressive or debilitating condition were commonly reported by notified case-patients (Table 2).

Discussion

This study provides a comprehensive analysis of the epidemiology of legionellosis over the 21-year period of 2000–2020 in New Zealand by using notifications and national laboratory-based surveillance of *Legionella* cases. The study period saw a large increase in disease incidence driven by several factors that we investigated.

A major finding is the marked increase in the reported incidence of legionellosis from 2010 onward (Figure 1; Appendix Table 1). This increase is associated with improved case ascertainment, likely driven by increased clinical awareness of legionellosis and increased availability of specific laboratory testing for legionellosis. The marked increase in legionellosis notifications during 2015 and 2016 was caused by the LegiNZ prospective study, which provided a 12-month period (May 2015–May 2016) of intensified surveillance (*11*). During that study, all lower respiratory samples from hospitalized notified-case patients who had suspected pneumonia were tested for *Legionella* spp. by PCR. An increase in case detection in 17 regions (Figure 5) was expected, with the national 86% increase more likely caused by historical underdiagnosis of the disease, rather than an increase in disease burden (*12*). For that reason, the legionellosis rate of 3.9 cases/100,000 during 2010–2020 probably provides a more valid estimate of the true population rate than seen previously; the higher rate of 5.4 cases/100,000 population detected by the LegiNZ study is likely to be particularly robust. Those rates put New Zealand above an estimated global mean rate of 2.8 cases/100,000 population (95% CI 2.7–2.9 cases/100,000 population) derived from the reported contribution of *Legionella* species to community-acquired pneumonia in multiple countries (*1*). The relatively small increase in the mortality rate of legionellosis during this period (from 0.6 deaths/100,000 population in 2000–2009 to 0.7 deaths/100,000 population in 2010–2020) is also consistent with the conclusion of greater case ascertainment of less severe cases being the main driver of the apparent increase in disease incidence during this period.

Unlike jurisdictions outside New Zealand that observed a temporary decrease in legionellosis at the beginning of the COVID-19 pandemic (*13*), rates for New Zealand did not appear to have been affected in 2020 (Figure 1). This finding suggests that environmental exposures to *Legionella* species may not have changed in New Zealand during this period, which could reflect the COVID-19 elimination strategy that enabled ordinary life to continue for most of that year, with only a few weeks under lockdown (*14*). The pandemic and its response had complex effects on the epidemiology of many infectious diseases and their surveillance. For example, studies undertaken in other jurisdictions outside New Zealand have identified greatly increased *Legionella* microbial contamination in building water systems (cooling towers) linked to extreme water stagnation caused by prolonged closures of

commercial buildings, reinforcing the need for monitoring water and air conditioning systems (*15*).

The findings of this study have shown the dramatic shift in legionellosis diagnosis during a period when traditional techniques were largely replaced by molecular methods and UAT. However, a key limitation of UAT is that it cannot detect organisms other than *L. pneumophila* serogroup 1 (*16*); some authors have suggested that a total dependence on this diagnostic assay may miss up to 40% of legionellosis cases (*17*). Another limitation of UAT is that it does not generate material that can be used for typing methods. In New Zealand, the *Legionella* UAT has been used by several laboratories since 1998 but has decreased utility because of the high proportion of legionellosis caused by non–*L. pneumophila* species, such as *L. longbeachae* (Figure 3; Appendix Table 3). In this setting, a negative UAT result does not exclude legionellosis and necessitates further testing to elucidate either exclusion or inclusion. Because only 20.3% of the 2,675 cases diagnosed during the study period were caused by *L. pneumophila* serogroup 1 infection (Appendix Table 2), potentially 80% of cases could be missed if only UAT were used. A recent evaluation of the UAT for the diagnosis of *L. longbeachae* infection indicated a sensitivity of 59.1% and specificity of 82.2% (*18*). Further development of the assay should improve sensitivity to strengthen its application as a useful diagnosis tool, particularly in laboratories in which there is limited molecular testing capacity and because of the ease of specimen collection and rapidity of diagnosis (*18*).

During the 1990s, the drive for better diagnostic methods led to development of several PCRs. However, a combination of factors, including test cost, reagent quality issues, contamination problems, and the lack of trained and skilled staff, resulted in the initial slow adoption of molecular diagnostics for legionellosis (*19*). The technology has now matured, and since 2010, when some laboratories in New Zealand began routine molecular diagnostic testing for legionellosis, it has now become the method of first choice. This change was caused by the availability of more robust and sensitive assays for the detection of many difficult to diagnose diseases, in addition to legionellosis, and the overall reduction in test costs.

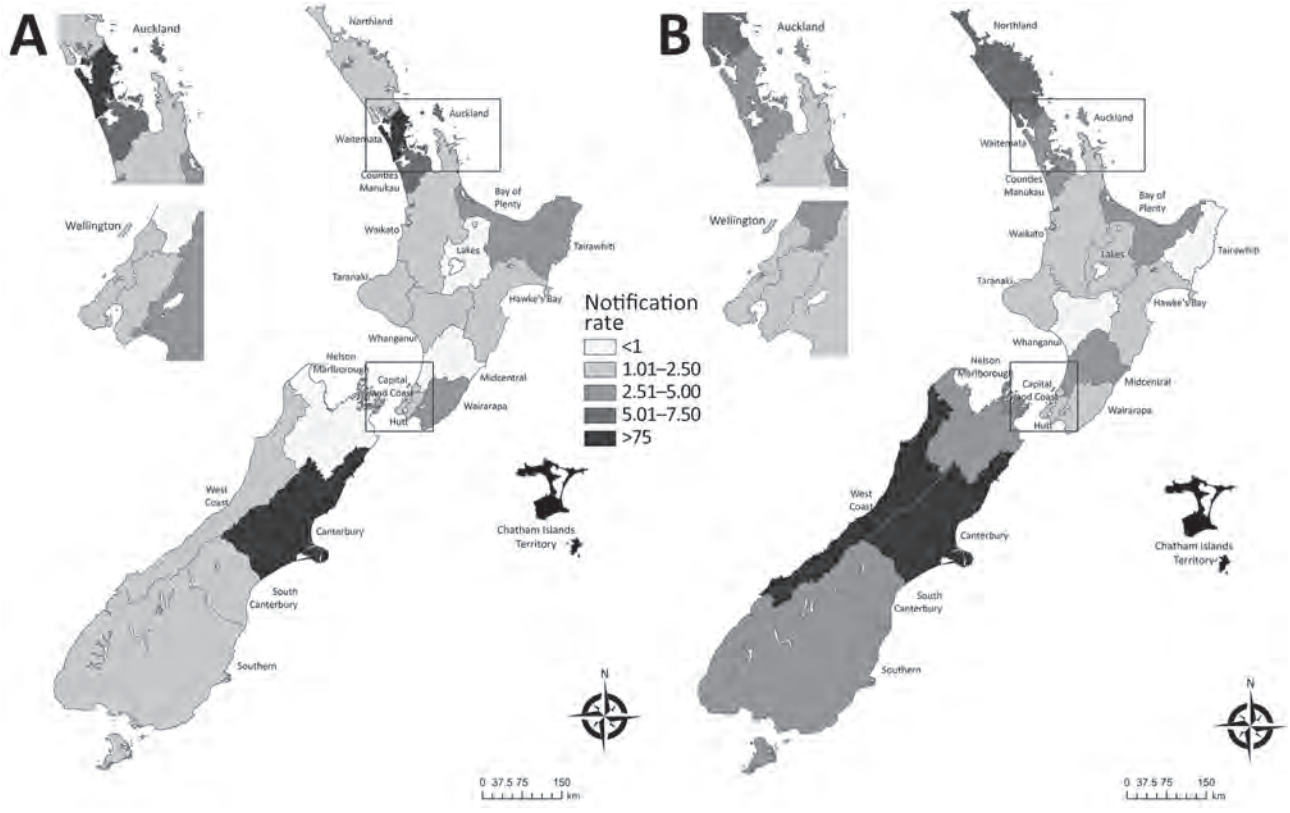

Figure 5. Geographic pattern of mean legionellosis notification rates (cases/100,000 population) by New Zealand District Health Board in study of increased incidence of legionellosis after improved diagnostic methods, New Zealand, 2000–2020. A) 2000–2009; B) 2010–2020. Insets show enlarged areas around the cities of Auckland and Wellington. Maps generated in ArcGIS version 10.8 (https://www.arcgis.com/index.html) by using District Health Board data (Appendix, https://wwwnc.cdc.gov/EID/article/29/6/22-1598-App1.pdf).

Table 2. Increased incidence of legionellosis after improved diagnostic methods, showing risk factors associated with notified case-patients who had legionellosis and percentages reporting exposure, New Zealand, 2000–2020*

Risk factor	No. (%) cases		Odds ratio (95% CI), 2010–2020 compared with 2000–2009
	2000–2009	2010–2020	
Hospital-acquired	2 (0.3)	6 (0.2)	0.8 (0.2–3.8)
Overseas travel during incubation period	43 (6.7)	112 (4.4)	0.65 (0.45–0.93)
Contact with definite or suspected environmental source	307 (47.5)	1,437 (56.4)	1.43 (1.09–1.3)
Compost source contact	ID	1,054 (41.4)	ID
Water source contact	ID	91 (3.6)	ID
Smoker or ex-smoker	120 (18.6)	326 (12.8)	0.64 (0.51–0.81)
Preexisting immunocompromised or debilitating condition	174 (26.9)	666 (26.1)	0.97 (0.79–1.27)
Total	646 (100.0)	2,547 (100.0)	NA

*Percentages refer to notified case-patients who answered yes for the total number of notified cases for which a response was recorded. Some notified case-patients had ≥1 risk factor recorded. ID, incomplete data (no comparison could be made); NA, not applicable.

Molecular testing for legionellosis has also been driven by its superior diagnostic utility compared with traditional methods because it enables detection of all *Legionella* species and can obtain a result within hours of sample collection (*20*).

The shift in laboratory methods during 2000–2020 has influenced the ability of routine surveillance to detect the contribution of species and serogroups. We observed a marked increase in *L. longbeachae* cases compared with other species, such as *L. pneumophila*, since 2010 (Figure 2; Appendix Table 2). We also observed a decrease in the identification of the serogroup for *Legionella* species caused by reductions in the use of the traditional methods, namely culture and serology, which risks gaps in surveillance information and can hinder cluster analysis and source tracing (Appendix Table 2) (21). This trend was caused by increased use of PCR testing alone that identifies the species, but not the serogroup of the *Legionella* species. No single laboratory test combines both optimal diagnostic accuracy with the ability to epidemiologically type the causative agent. To achieve this feature, a combination of molecular testing supported by culture, serologic testing, or both is required (19). In recent years, whole-genome sequencing has emerged as a major tool to support epidemiologic investigation (suspected clusters and outbreaks) of Legionnaires' disease and for characterization of new strains, but this method still requires the culture isolation of the bacterium.

The results of this study show that the rates of legionellosis were highest in adults >60 years of age and in male notified case-patients, consistent with previously reported research (6). As the population ages in New Zealand, the burden of legionellosis is likely to continue to increase in the absence of effective measures to prevent or adequately control the risk for infection. Legionellosis rates were higher in persons from Europe compared with Māori, Pacific Peoples, and persons of other ethnicities during 2000–2009, even after age standardization. Those differences largely disappeared during 2010–2020, corresponding with increased case ascertainment. This pattern is different from that seen for other serious infectious diseases, for which rates are markedly higher for Māori and Pacific Peoples (22). Those unexpected differences need further investigation to see if there is systematic underdiagnosis of legionellosis across ethnic groups or if differences in exposure might explain the pattern seen.

This analysis found that infections caused by *L. longbeachae* increasingly dominated over those caused by *L. pneumophila* (Figure 2; Appendix Table 2). The largest contribution to this increase in *L. longbeachae* cases came from persons ≥60 years of age (Table 1). Early spring–summer clusters of *L. longbeachae* infections are seen each year and might be linked to increased gardening activity in warmer months, which has been shown to provide several psychological, physical, and social benefits for older persons (*23*). In contrast, *L. pneumophila* infections appear to be spread evenly throughout the year, and transmission by aerosols containing contaminated water from cooling towers was the most identified source from outbreak investigations in New Zealand. Decreased incidence rates observed across the 3 Auckland DHBs between decades might reflect introduction of a bylaw in 2015 requiring owners to register their industrial wet cooling tower systems annually and monitor *Legionella* bacteria levels (*24*). In contrast, higher incidence rates in the Northland region might reflect the readiness of clinicians to consider testing for *Legionella* species in response to the national surveillance study (*11*).

Our study also provides data on major risk factors, exposures, and potential transmission settings. Few cases were classified as hospital acquired. A small percentage (6.2%) were classified as travel-associated, based on having a history of overseas travel during the incubation period. That percentage is lower than that for Europe, where 14.7% of detected Legionnaires' disease cases in 2019 were linked to travel

abroad, of which 79% were linked to overnight stays in hotels (*25*). This difference is observed despite New Zealand having among the highest per capita international travel rates in the world, with >3 million residents departing New Zealand in 2019 (*26*).

Our study has several limitations associated with the use of routinely collected surveillance data. The most critical limitation is the long-term underascertainment of legionellosis. This limitation has been partially corrected by using more sensitive molecular testing, resulting in a marked increase in measured rates of legionellosis during the 2010–2020 period. A further limitation is the incomplete reporting of some variables.

More research on the epidemiology of legionellosis in New Zealand is warranted. The high percentage of hospitalizations (82.0%) reported during the study period means that those data can be analyzed to provide a useful basis to identify emerging issues and determine priorities for prevention. For example, the discharge data could be used to estimate the economic cost of hospitalized cases of legionellosis in New Zealand. It would also be useful to investigate the contribution of *Legionella* infection to the burden of community-acquired pneumonia of mild-to-moderate severity, which will often be treated empirically outside the hospital setting without any etiologic diagnosis. Proposed interventions to reduce the effect of legionellosis in New Zealand should also be evaluated after they are implemented to determine their efficacy.

Acknowledgments

We thank Yvonne Galloway for providing assistance with legionellosis surveillance data and the technical staff of the Legionella Reference Laboratory, Environmental Science and Research for providing scientific analyses. The surveillance data underlying the results presented in this study are available from the Institute of Environmental Science and Research, which contributes to the New Zealand public health surveillance effort under contract with the New Zealand Ministry of Health.

About the Author

Dr. Graham recently received a doctoral degree in public health focusing on the environmental epidemiology of legionellosis in New Zealand at the University of Otago, Wellington, New Zealand. Her primary research interests are infectious disease epidemiology and surveillance and infection prevention and control with a focus on legionellosis.

References

1. Graham FF, Finn N, White P, Hales S, Baker MG. Global Perspective of *Legionella* infection in community-acquired pneumonia: a systematic review and meta-analysis of observational studies. Int J Environ Res Public Health. 2022;19:1907. https://doi.org/10.3390/ijerph19031907
2. Graham FF, Hales S, White PS, Baker MG. Review Global seroprevalence of legionellosis—a systematic review and meta-analysis. Sci Rep. 2020;10:7337. https://doi.org/10.1038/s41598-020-63740-y
3. Bartram J, Chartier Y, Lee JV, Pond K, Surman-Lee S. *Legionella* and the prevention of legionellosis. Geneva: World Health Organization; 2007.
4. Marston BJ, Lipman HB, Breiman RF. Surveillance for Legionnaires' disease. Risk factors for morbidity and mortality. Arch Intern Med. 1994;154:2417–22. https://doi.org/10.1001/archinte.1994.00420210049006
5. Graham FF. The mysterious illness that drove them to their knees—Ah, that Legionnaires' disease—a historical reflection of the work in Legionnaires' disease in New Zealand (1978 to mid-1990s) and the 'One Health' paradigm. One Health. 2020;10:100149. https://doi.org/10.1016/j.onehlt.2020.100149
6. Graham FF, White PS, Harte DJ, Kingham SP. Changing epidemiological trends of legionellosis in New Zealand, 1979–2009. Epidemiol Infect. 2012;140:1481–96. https://doi.org/10.1017/S0950268811000975
7. Graham FF, Harte DJ, Baker MG. Environmental investigation and surveillance for *Legionella* in Aotearoa New Zealand, 2000–2020. Curr Microbiol. 2023;80:156. https://doi.org/10.1007/s00284-023-03261-9
8. Whiley H, Bentham R. *Legionella longbeachae* and legionellosis. Emerg Infect Dis. 2011;17:579–83. https://doi.org/10.3201/eid1704.100446
9. Kenagy E, Priest PC, Cameron CM, Smith D, Scott P, Cho V, et al. Risk factors for *Legionella longbeachae* Legionnaires' disease, New Zealand. Emerg Infect Dis. 2017;23:1148–54. https://doi.org/10.3201/eid2307.161429
10. Wellington Ministry of Health. 2012. Communicable disease control manual: legionellosis [cited 2023 Apr 12]. https://www.health.govt.nz/our-work/diseases-and-conditions/communicable-disease-control-manual/legionellosis
11. Priest PC, Slow S, Chambers ST, Cameron CM, Balm MN, Beale MW, et al. The burden of Legionnaires' disease in New Zealand (LegiNZ): a national surveillance study. Lancet Infect Dis. 2019;19:770–7. https://doi.org/10.1016/S1473-3099(19)30113-6
12. Harte D. Laboratory-based legionellosis surveillance, 2015. New Zealand Public Health Surveill Rep. 2016;14:A1–3.
13. Riccò M. Impact of lockdown and non-pharmaceutical interventions on the epidemiology of Legionnaires' disease. Acta Biomed. 2022;93:e2022090.
14. Baker MG, Wilson N, Blakely T. Elimination could be the optimal response strategy for covid-19 and other emerging pandemic diseases. BMJ. 2020;371:m4907. https://doi.org/10.1136/bmj.m4907
15. Palazzolo C, Maffongelli G, D'Abramo A, Lepore L, Mariano A, Vulcano A, et al. *Legionella* pneumonia: increased risk after COVID-19 lockdown? Italy, May to June 2020. Euro Surveill. 2020;25:2001372. https://doi.org/10.2807/1560-7917.ES.2020.25.30.2001372
16. Shimada T, Noguchi Y, Jackson JL, Miyashita J, Hayashino Y, Kamiya T, et al. Systematic review and metaanalysis: urinary antigen tests for Legionellosis. Chest. 2009;136:1576–85. https://doi.org/10.1378/chest.08-2602

17. Fields BS, Benson RF, Besser RE. *Legionella* and Legionnaires' disease: 25 years of investigation. Clin Microbiol Rev. 2002; 15:506–26. https://doi.org/10.1128/CMR.15.3.506-526.2002
18. Podmore R, Schousboe M. Evaluation of a new *Legionella longbeachae* urine antigen test in patients diagnosed with pneumonia. New Zealand J Medical Lab Sci. 2020;74:20–1.
19. Pierre DM, Baron J, Yu VL, Stout JE. Diagnostic testing for Legionnaires' disease. Ann Clin Microbiol Antimicrob. 2017;16:59. https://doi.org/10.1186/s12941-017-0229-6
20. Mercante JW, Winchell JM. Current and emerging *Legionella* diagnostics for laboratory and outbreak investigations. Clin Microbiol Rev. 2015;28:95–133. https://doi.org/10.1128/CMR.00029-14
21. Orkis LT, Harrison LH, Mertz KJ, Brooks MM, Bibby KJ, Stout JE. Environmental sources of community-acquired Legionnaires' disease: a review. Int J Hyg Environ Health. 2018;221:764–74. https://doi.org/10.1016/j.ijheh.2018.04.013
22. Baker MG, Barnard LT, Kvalsvig A, Verrall A, Zhang J, Keall M, et al. Increasing incidence of serious infectious diseases and inequalities in New Zealand: a national epidemiological study. Lancet. 2012;379:1112–9. https://doi.org/10.1016/S0140-6736(11)61780-7
23. Scott TL, Masser BM, Pachana NA. Positive aging benefits of home and community gardening activities: older adults report enhanced self-esteem, productive endeavours, social engagement and exercise. SAGE Open Med. 2020; 8:2050312120901732. https://doi.org/10.1177/2050312120901732
24. Stephens C. Property maintenance and nuisance bylaw. 2020 review findings report. Auckland (New Zealand): Auckland Council; 2020.
25. European Centre for Disease Prevention and Control. Legionnaires' disease. Annual epidemiological report for 2019. 2021 [cited 2023 Apr 12]. https://www.ecdc.europa.eu/sites/default/files/documents/AER-legionnaires-2019.pdf
26. Statistics New Zealand. Table: NZ-resident traveller departure totals, 2021 [2023 Apr 12]. http://infoshare.stats.govt.nz/ViewTable.aspx?pxID=2056e0fd-3522-4f24-9632-7a947bd3e1bf

Address for correspondence: Frances F. Graham, Department of Public Health, University of Otago, PO Box 7343, Wellington South 6242, New Zealand; email: grafr148@student.otago.ac.nz

Risk Factors for Non-O157 Shiga Toxin–Producing *Escherichia coli* Infections, United States

Ellyn P. Marder,[1] Zhaohui Cui, Beau B. Bruce, LaTonia Clay Richardson, Michelle M. Boyle, Paul R. Cieslak, Nicole Comstock, Sarah Lathrop, Katie Garman, Suzanne McGuire, Danyel Olson, Duc J. Vugia, Siri Wilson, Patricia M. Griffin, Carlota Medus

Shiga toxin–producing *Escherichia coli* (STEC) causes acute diarrheal illness. To determine risk factors for non-O157 STEC infection, we enrolled 939 patients and 2,464 healthy controls in a case–control study conducted in 10 US sites. The highest population-attributable fractions for domestically acquired infections were for eating lettuce (39%), tomatoes (21%), or at a fast-food restaurant (23%). Exposures with 10%–19% population attributable fractions included eating at a table service restaurant, eating watermelon, eating chicken, pork, beef, or iceberg lettuce prepared in a restaurant, eating exotic fruit, taking acid-reducing medication, and living or working on or visiting a farm. Significant exposures with high individual-level risk (odds ratio >10) among those >1 year of age who did not travel internationally were all from farm animal environments. To markedly decrease the number of STEC-related illnesses, prevention measures should focus on decreasing contamination of produce and improving the safety of foods prepared in restaurants.

Non-O157 Shiga toxin–producing *Escherichia coli* (STEC), which encompasses all STEC serogroups other than O157, causes an estimated 219,000 US infections annually (*1*). Typical symptoms are diarrhea, abdominal cramps, and vomiting, and hemolytic uremic syndrome occurs in 1% (*2*); deaths from STEC are rare. Incidence is highest among children (*2*). Most strains isolated from US residents belong to 1 of 6 serogroups, defined by O antigens (*3*–*5*) (S. Browning, Centers for Disease Control and Prevention, December 18, 2020 email).

Non-O157 STEC infections were underdiagnosed for decades because laboratories lacked practical detection methods (*4*,*6*–*9*). Culture-independent diagnostic tests for Shiga toxin became available in 1995. The number of laboratories using enzyme immunoassays and PCR tests to identify non-O157 STEC has been increasing since then. Reported infections increased further after non-O157 STEC infection was designated a nationally notifiable infection in 2000 (*2*,*10*).

Investigations of non-O157 STEC outbreaks have identified transmission routes, including foodborne, waterborne, from contact with animals and their environments, and person-to-person contact (*11*,*12*). Because little is known about risk factors for sporadic infections, the Foodborne Diseases Active Surveillance Network (FoodNet) conducted a large, multisite, case–control study to identify risks for sporadic non-O157 STEC infections in the United States. Centers for Disease Control and Prevention (CDC) and FoodNet site institutional review boards approved the study protocol. We obtained verbal consent from all

Author affiliations: Centers for Disease Control and Prevention, Atlanta, Georgia, USA (E.P. Marder, Z. Cui, B.B. Bruce, L. Clay Richardson, P.M. Griffin); Maryland Department of Health, Baltimore, Maryland, USA (M.M. Boyle); Oregon Health Authority, Portland, Oregon, USA (P.R. Cieslak); Colorado Department of Public Health and Environment, Denver, Colorado, USA (N. Comstock); University of New Mexico, Albuquerque, New Mexico, USA (S. Lathrop); Tennessee Department of Health, Nashville, Tennessee, USA (K. Garman); New York State Department of Health, Albany, New York, USA (S. McGuire); Connecticut Emerging Infections Program, New Haven, Connecticut, USA (D. Olson); California Department of Public Health, Richmond, California, USA (D.J. Vugia); Georgia Department of Public Health, Atlanta (S. Wilson); Minnesota Department of Health, Saint Paul, Minnesota, USA (C. Medus)

DOI: https://doi.org/10.3201/eid2906.221521

[1]Current affiliation: Washington State Department of Health, Shoreline, Washington, USA.

persons ≥18 years of age and parents or legal guardians of children <18 years of age and verbal assent (in addition to parent or guardian consent) from children 12–17 years of age.

Methods

During 2012–2015, FoodNet conducted active, population-based surveillance for laboratory-diagnosed STEC infections in 10 sites, covering an estimated 49 million persons (15% of the US population in 2014). The catchment area included Connecticut, Georgia, Maryland, Minnesota, New Mexico, Oregon, and Tennessee and selected counties in California, Colorado, and New York. We recruited patients from each site for a consecutive 36-month period during July 1, 2012–September 1, 2015. We defined a case as isolation of non-O157 STEC from a clinical specimen of an ill person residing in a FoodNet site. We excluded cases in which a pathogen other than non-O157 STEC was detected in a non-O157 STEC–positive specimen, or the patient was lost to follow-up, did not speak English or Spanish, was part of an outbreak (except for the index patient in each site), or was not the first case in their household. We attempted to enroll 3 controls per case, matched on county and stratified by age groups: 0–1, 2–5, 6–17, 18–39, 40–59, or ≥60 years. We selected controls in all except the youngest age group from commercially available lists of residential telephone numbers, by county, that included age ranges. We selected controls <2 years of age from birth registries. We enrolled controls within 60 days after the matched case-patient's specimen collection date. We excluded controls who did not speak English or Spanish.

We interviewed patients and controls or their guardians by telephone using a standard questionnaire that covered 385 variables and had sections on health, travel, water, animals, foods, and demographics. Most exposures, including international travel, were for the 7 days before illness began; controls were asked about exposures during the same period as case-patients. The questionnaire defined fast-food restaurants as places where food is ordered and paid for at a counter or drive-through and table-service restaurants as all sit-down or table-service restaurants.

Clinical laboratories submitted specimens that had Shiga toxin (determined by immunoassay) or Shiga toxin genes (determined by PCR) to state public health laboratories. State public health laboratory staff identified non-O157 specimens and submitted them to CDC for serologic testing to determine O and H antigens. CDC used whole-genome sequencing to confirm the absence of O157 genes on rough isolates.

We included all enrolled participants in descriptive analyses. International travel was examined in univariable analysis. Those reporting international travel were excluded from other risk factor analyses, which were conducted separately for infants <1 and persons ≥1 years of age. To control for confounding in the main risk factor analysis, we rematched controls with cases using the nearest-neighbors approach (*13*). For a given exposure, we calculated Gower distance on the basis of age, sex, state, and all exposures except the one under consideration (*14*). Using logistic regression, we established an overall threshold for Gower distance at which it was more likely that a matched control was a patient's nearest neighbor than a randomly selected control. We matched up to 20 controls within the Gower distance with the nearest case-patient and ensured that each control was matched to only 1 case-patient. Of note, distance between 85% of patient–control pairs matched during recruitment exceeded that threshold. We excluded case-patients without matches within the threshold from the analysis for the exposure under consideration. After rematching patients with controls, information was available for patients for all but 5 exposures in at least 92% of cases: municipal water away from home (89%), private well water away from home (85%), spring water away from home (85%), prepackaged iceberg lettuce (84%), and prepackaged romaine lettuce (87%). Information was available for all except 4 exposures for at least 92% of controls: municipal water away from home (91%), contact with someone with diarrheal illness (90%), private well water away from home (82%), and spring water away from home (81%). We did not conduct imputation because results were unlikely to be affected by the low rates of missing data.

For our analyses, we calculated odds ratios (ORs) and population attributable fractions (PAFs) to identify both individual risk and percentages at which illnesses in the population could be decreased. Because prevalence of some exposures was low among case-patients, controls, or both, we applied Firth bias-reduced penalized-likelihood logistic regression to estimate ORs and 95% CIs for each exposure, after adjusting for the matched strata generated by the nearest-neighbors approach. We calculated and adjusted p values for multiple testing using the Benjamini-Yekutieli method (*15*). We considered associations statistically significant if adjusted p was <0.05 and 95% CIs did not include 1.0. We calculated PAF using a method described elsewhere (*16*) and calculated 95% CIs for PAFs using the 95% confidence limits of ORs. We did not assess the overall statistical significance of our logistic regression models because each included only the ex-

posure under consideration and the strata of matched case-control pairs (Appendix Table 2, https://wwwnc.cdc.gov/EID/article/29/6/22-1521-App1.pdf).

Results

We identified 1,988 non-O157 STEC case-patients and We identified 1,988 non-O157 STEC case-patients and 2,464 controls meeting inclusion criteria; we excluded 324 of the case-patients according to exclusion criteria (Figure). Of the 1,644 eligible patients remaining, 407 could not be reached and 318 refused to participate, leaving 939 (56.4%) total cases in the study. Nine serogroups accounted for 83% of isolates from enrolled case-patients: O26 (263, 28%), O103 (216, 23%), O111 (135, 14%), O121 (46, 5%), O118 (37, 4%), O186 (23, 2%), O5 (22, 2%), O145 (21, 2%), and O45 (21, 2%) (Table 1, https://wwwnc.cdc.gov/EID/article/29/6/22-1521-T1.htm). The remainder of the results is limited to enrolled case-patients.

Nearly all patients (99%) reported diarrhea (median duration 7 days, interquartile range 5–10 days) (Table 1). Other common signs and symptoms were abdominal pain (89%), fatigue (71%), bloody feces (58%), and nausea (53%). Seventeen percent of patients were hospitalized, and 8 (1%) had hemolytic uremic syndrome develop.

International travel was significantly associated with infection in univariable analysis; 138/939 (15%) patients reported international travel, compared with 31/2,464 (1%) controls (matched OR 14.2, 95% CI 9.0–23.3) (Table 1). The most common destination among patients traveling internationally was Mexico (68, 49%). The rank order of non-O157 STEC serotypes among international travelers was similar to that for domestic cases except for the absence of O121. O186 (11/23, 48%) and O118 (11/37, 30%) were the serogroups with the highest percentages of patients who had recently traveled internationally.

Most patients (801/939) and controls (2,433/2,464), including 27 infant case-patients and 68 infant controls, had not recently traveled internationally. Patient median age was 18 years (interquartile range 4–35 years); 57% were female, 90% White, and 17% of Hispanic ethnicity (Table 2). Median age was significantly lower for patients (18 years) than for controls (22 years). Patients were also more likely than controls to be White (90% vs. 87%) and of Hispanic ethnicity (17% vs. 10%) and less likely to be Black (5% vs. 7%). Among FoodNet sites, the most cases were in Minnesota (226, 28%), followed by Tennessee (107, 13%), Oregon (91, 11%), Georgia (88, 11%), California (61, 8%), New York (58, 7%), Colorado (54, 7%), Connecticut (46, 6%), New

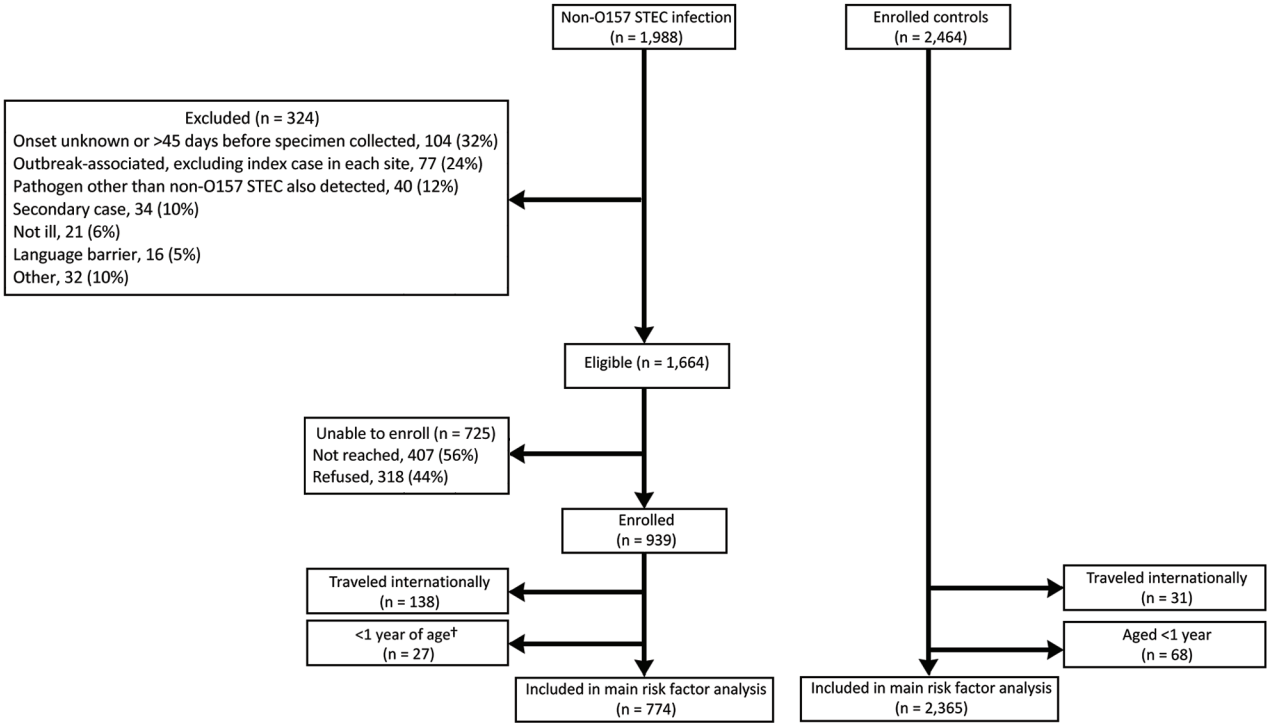

Figure. Flowchart for inclusion/exclusion in study of risk factors for non-O157 STEC infections, United States. **Campylobacter*, n = 11; *Salmonella*, n = 8; *Cryptosporidium*, n = 7; STEC O157, n = 7; *C. difficile*, n = 2; *Giardia*, n = 2; *Cryptosporidium* and *Giardia*, n = 1; norovirus, n = 1; *Shigella*, n = 1. †An additional 3 infants who traveled internationally were included in the Traveled internationally box above. STEC, Shiga toxin–producing *Escherichia coli*.

Mexico (40, 5%), and Maryland (30, 4%). International travel was the only factor significantly associated with infection among 3/30 (10%) infants, compared with none among 68 controls (OR 32.8, 95% CI 1.5–4,607.2). No food, environmental, water, or other exposure we examined among infants who had not traveled internationally was significantly associated with illness (Appendix Table 1).

Among persons ≥1 year of age who had not traveled internationally, significant PAFs (>20%) were largest for eating lettuce (PAF 39.3%; OR 2.6), tomatoes (PAF 21.3%; OR 1.7), or at a fast-food restaurant (PAF 22.5%; OR 1.7) (Table 3, https://wwwnc.cdc.gov/EID/article/29/6/22-1521-T3.htm). Other produce exposures with high PAFs (10%–19%) were eating watermelon (PAF 19.0%; OR 2.4), including prepared inside the home (PAF 10.9%; OR 1.7); eating tomatoes prepared in a restaurant (PAF 13.7%; OR 2.5); eating exotic fruit, such as kiwi, avocado, or mango (PAF 13.2%; OR 1.7); and eating iceberg lettuce prepared in a restaurant (PAF 12.9%; OR 2.7). The highest ORs among fruit and vegetable exposures were for raspberries (PAF 2.2%; OR 7.7), cantaloupe (PAF 3.2%; OR 4.3), exotic fruit (PAF 5.8%; OR 3.9), and pineapple (PAF 3.8%; OR 3.6) prepared in a restaurant. However, <8% of patients had exposure to any 1 of those.

Eating at a table service restaurant also had a high PAF (19.4%; OR 1.7). Of the 24 food-related risk factors identified, 17 were related to preparation in a restaurant and 1 to preparation inside the home; the other 6 did not specify a place of preparation. Meats with significant high PAFs (10%–19%) were chicken prepared in a restaurant (PAF 16.3%; OR 1.6), pork prepared in a restaurant (PAF 10.2%; OR 2.9), and beef prepared at a table-service restaurant (PAF 10.1%; OR 2.1). The highest OR among meat and seafood products was for eating pink hamburger from a table-service restaurant (PAF 3.4%; OR 9.0). Eating ground beef hamburger (PAF 5.8%; OR 2.4) at a table-service restaurant was also a significant risk factor. However, 9 of 21 factors significantly associated with lower risk of illness were related to beef (Appendix Table 2).

Although living or working on or visiting a farm, petting zoo, or fair (PAF 14.7%; OR 8.0) was the only significant environmental exposure with a PAF ≥10%, many significant animal environment-associated exposures had ORs >10. Those included exposures to calves, chickens, cows, goats, horses, pigs, and sheep. Taking stomach acid-reducing medications in the 4 weeks before illness (PAF 11.3%; OR 2.1) was the only other significant risk factor with PAF ≥10% or OR >10.

Among the 5 risk factors for STEC O26 infection, only 1, contact with someone with diarrheal illness (PAF 10.8%, OR 5.7), had a PAF ≥10%; the other 4, all with ORs ≥10, were animal environment exposures. Among the 7 risk factors associated with STEC O103 infection, 3 had PAFs ≥10% and the other 4 had ORs >14. The highest PAFs were for living or working on, or visiting a farm, petting zoo, or fair (PAF 22.0%, OR 7.2) and for eating iceberg lettuce in a restaurant (PAF 20.1; OR 4.5). One risk factor was identified for STEC O111: living or working on, or visiting a farm, petting zoo, or fair (PAF 20.3%; OR 15.4) (Table 4).

Table 2. Demographic characteristics of case-patients with non-O157 Shiga toxin–producing *Escherichia coli* infection and controls without international travel, FoodNet case–control study, United States, 2012–2015*

Characteristic	Case-patients, n = 801	Controls, n = 2,433
Age, y median (IQR)	18 (4–35)	22 (6–39)
Sex		
F	457/801 (57)	1,425/2,410 (59)
M	344/801 (43)	982/2,410 (41)
Race		
White	667/739 (90)	2,016/2,310 (87)
Black	35/739 (5)	167/2,310 (7)
Asian	15/739 (2)	46/2,310 (2)
Ethnicity		
Hispanic	133/789 (17)	236/2,399 (10)†

*Values are no. positive/no. for whom data were available (%) except as indicated.
†p<0.05 compared with case-patients.

Discussion

We found non-O157 STEC infections were associated with international travel and domestic exposure to a wide variety of foods and animal environments. Among 18 food consumption risks with site of consumption indicated, 94% were in restaurants. The wide variety of foods implicated suggests that sources of infection, and thus control measures, for non-157 STEC are more similar to those for *Salmonella* than to those for STEC O157 (*17*). Control measures focused on improving the food safety system, in particular for produce and restaurants, are likely to decrease illness the most.

Our finding of large population-level risks attributable to eating at restaurants is notable because most food is consumed at home (*18*). FoodNet studies also identified restaurants as risks for STEC O157 (*19*) and *Campylobacter* (*20*) infections. A study from Australia linked non-O157 STEC illnesses to catered meals (*21*). In a review of US restaurant outbreaks, food handling and preparation practices were implicated in about half and food contaminated before entering the restaurant in about one quarter of *Salmonella* outbreaks (data for STEC not provided) (*22*,*23*). Policies that help promote a culture of food safety for restaurants include

Table 4. Risk factors associated with domestically acquired non-O157 Shiga toxin–producing *Escherichia coli* infections by serogroup, FoodNet case–control study, United States, 2012–2015*

Serogroup and exposure†	Case-patients	Controls	Multivariable analysis		
			OR (95% CI)	PAF (95% CI)	p value§
O26, n = 231					
Contact with someone with diarrheal illness	16/122 (13)	11/370 (3)	5.7 (2.4–14.4)	10.8 (7.6–12.2)	0.04
Environmental					
Live or work on, or visit a farm, petting zoo, or fair					
With chickens present	11/143 (8)	1/410 (0)	35.5 (6.9–319.6)	7.5 (6.6–7.7)	0.003
With cows present	11/140 (8)	4/399 (1)	13.6 (3.6–62.0)	7.3 (5.7–7.7)	0.04
With cows or calves present	11/141 (8)	5/394 (1)	13.7 (3.5–65.5)	7.2 (5.6–7.7)	0.04
Visit a farm with chickens present	7/139 (5)	1/421 (0)	24.3 (4.7–172.0)	4.8 (4.0–5.0)	0.04
O103, n = 179					
Environmental					
Live or work on, or visit a farm, petting zoo, or fair	24/94 (26)	22/315 (7)	7.2(2.9–19.4)	22.0 (16.6–24.2)	0.008
With cows or calves present	12/95 (13)	6/334 (2)	24.9 (5.3–169.3)	12.1 (10.2–12.6)	0.008
With calves present	7/97 (7)	2/330 (1)	60.8 (6.7–2,615.0)	7.1 (6.1–7.2)	0.02
Live on a farm	11/101 (11)	5/328 (2)	15.8 (3.8–77.8)	10.2 (8.1–10.8)	0.02
Contact with wild deer or elk or their droppings	9/98 (9)	2/327 (1)	14.6 (3.7–69.1)	8.6 (6.7–9.1)	0.02
Visit a farm with horses present	5/93 (5)	1/316 (0)	60.1 (6.4–5,983.0)	5.3 (4.5–5.4)	0.02
Fruits and vegetables					
Iceberg lettuce prepared outside the home	24/93 (26)	37/290 (13)	4.5 (2.1–9.9)	20.1 (13.7–23.2)	0.02
O111, n = 104					
Environmental					
Live on, visit, or work on a farm, petting zoo, or fair	13/60 (22)	11/190 (6)	15.4 (4.1–73.9)	20.3 (16.3–21.4)	0.03

*Values are no. exposures/no. for whom data were available (%) except as indicated. OR, odds ratio; PAF, population attributable fractions.
†In the 7 d before illness unless otherwise specified. Interviewers told respondents to consider foods prepared at any home to be prepared at home and foods prepared at a restaurant or commercial food service establishment to be prepared outside the home.
‡All cases included were in nontravelers >1 y old; each serogroup-specific analysis had 2,365 noninfant, nontraveler controls. The overall number of cases for each serogroup-specific analysis is listed in the respective section header. During nearest-neighbors matching, cases and controls without a match were excluded for the exposure under consideration. Thus, the numbers of cases and controls that were matched and included in the analysis of each exposure is smaller than the total.
§p adjusted for multiple testing using Benjamini-Hochberg-Yekutieli method.

staff training in and oversight of food preparation and purchase agreement requirements that foods meet or exceed standards promoted by the Food Safety Modernization Act and the US Department of Agriculture's Food Safety and Inspection Service. Health officials can also drive improved adherence to the Food and Drug Administration Food Code or stricter local regulations.

Our analysis indicated that eating lettuce, tomatoes, and other produce commonly consumed raw accounts for a large proportion of illnesses. One review of STEC found that row crop vegetables were associated with more outbreaks than any other food and significantly more non-O157 outbreaks than beef (*12*). Produce also transmits a high proportion of foodborne illnesses caused by other pathogens (*17*,*23*–*25*). Identifying particular growing areas and farms as sources of produce associated with outbreaks would provide a more efficient targeted process for preventing contamination before produce arrives at restaurants or stores (*26*). Produce growers, suppliers, sellers, and commercial establishments should adhere to guidelines to assure that produce is safe when purchased. The Food and Drug Administration is charged with implementing the Produce Safety Rule, part of the Food Safety Modernization Act, which includes requiring routine inspections of large produce farms. Best practice standards for biosecurity and water management should recognize the risk from environmental contamination caused by wildlife and from the use of untreated water contaminated with fecal matter from food-producing animals on crops (*26*,*27*). Preventing cross-contamination of produce from meat in restaurants and homes is also essential.

Further regulatory measures could decrease transmission of non-O157 STEC. In 2012, similar to the practice for STEC O157 since 1994, the Food Safety and Inspection Service named the 6 non-O157 STEC serogroups (O26, O103, O111, O121, O145, and O45) most frequently linked to human illness as adulterants in raw, nonintact beef products (*28*). Although we observed inverse associations for some beef exposures, the consumption of any beef at a table service restaurant had a PAF of 10.1% and pink ground beef hamburger had an OR of 9, indicating those are high-risk exposures. We found eating ground beef hamburgers from fast-food restaurants was not associated with illness, similar to the finding of a FoodNet study of STEC O157 infections conducted during 1996–1997 (*19*). Those findings suggest that standard hamburger cooking procedures in fast-food restaurants are effective. PAFs of 16% for chicken and 10% for pork prepared in a restaurant suggest that those meats might transmit non-O157 STEC. US outbreaks caused by O157 but not non-O157 STEC have been linked to those foods (*29*).

We identified a wide variety of risky exposures related to infection from animals; visiting, living on, or working on a farm, petting zoo, or fair had the highest PAF (14.7%). Visiting (PAF 8.2%) and living on (PAF 5.2%) a farm each conferred risk. The study implicated specific animal types, including calves, chickens, cows, goats, horses, pigs, or sheep, as well as contact with horse feed and with wild deer or elk or their droppings. Contact with farm animals, particularly but not exclusively ruminants, or their environments is a known risk factor for both non-O157 (*20*,*21*,*27*,*30*) and O157 STEC infections (19,32,33). Handwashing is essential for preventing infections in these settings. Guidelines have been published for behaviors in public settings with animals (*34*); development of guidelines for nonpublic settings could help avert infections.

Although risk factors that have high PAFs provide the largest opportunities for reducing illnesses, many exposures had significantly high ORs, particularly animal contact and environmental exposures, which also signal potential targets for reducing infections. Very high ORs (6.8–66.9) indicating high individual-level risk were identified for exposure to environments with calves, cows, chickens, goats, horses, pigs, and sheep. Other exposures with high ORs (4.3–7.7) were, in descending order, eating raspberries in a restaurant, drinking untreated water, and eating cantaloupe in a restaurant. Drinking untreated water was also identified as a risk factor for O157 STEC infection in another FoodNet case–control study (*22*).

The similarity of serotypes in our study to those more recently causing illness indicates that the most notable risk factors we found likely remain current. The top 4 serogroups in our study, which accounted for 70% of isolates, were the same as the top 4 named adulterants in 2012. They were also the top 4 non-O157 STEC isolates reported to national surveillance during the study period (74% of isolates) and in the years with the most recently validated data, 2016–2018 (78% of isolates) (S. Browning, Centers for Disease Control and Prevention, December 18, 2020 email). The next 5 most common serogroups in our study were all among the top 11 serogroups nationally during the study period and 2016–2018. Regional variations in sources may influence serotype frequency but variations in laboratory practices may also affect frequency data (*35*,*36*). For example, some public health laboratories attempt to identify only the 3 most common serogroups, others test for the top 6, and others routinely send all isolates to CDC for serogrouping. It is possible that our study protocol requiring that all non-O157 STEC isolates be sent to CDC for serotyping resulted in recognition of illnesses caused by less common serogroups.

Nearest-neighbor matching approaches have a solid theoretical basis in epidemiologic research (*37*–*39*), but applying this method to matching in case–control studies of enteric diseases is recent (*13*). Although it is impossible to account for every possible confounder when selecting controls, this approach allows the most closely matched controls to be selected for each case. The nearest-neighbor approach permitted better control of confounding and would be expected to produce less-biased estimates than our original scheme that matched only on age, sex, and geography. One apparent benefit of our study approach was that we did not observe the large number of spurious inverse effects for vegetable and fruit items that have been seen in other studies (*20*,*31*,*41*).

Our study was limited to cases reported to public health departments and thus dependent on infected persons seeking health care and providers obtaining fecal specimens, so data may not be representative of all non-O157 STEC illnesses (*40*). We only enrolled patients residing in the FoodNet catchment area, which is not completely representative of the US population (*41*). In addition, patients were significantly more likely than controls to be Hispanic, possibly because controls were selected from purchased commercial lists of telephone numbers that included only landlines; persons of Hispanic ethnicity were more likely than others to live in households with only cellular telephones during the study (*42*). As in any case–control study, there were probably nondifferential information biases (e.g., differences in the way patients remember and report exposures compared with controls). Finally, unlike in outbreak investigations, in which a particular exposure can be confirmed as the source, associations in studies of sporadic infections do not confirm a particular source because of the possibility of residual confounding. Although we used an advanced method to control for confounding, residual confounding for some associations and for common coexposures was still likely. For example, many salads include both lettuce (PAF = 39.3%) and tomato (PAF = 21.3%); eating a tomato might be associated with illness only because it is consumed with contaminated lettuce. However, a major strength of studies of sporadic cases is that, unlike outbreak investigations, they can identify the exposures associated with the most illnesses in a population; conclusions about associations can be bolstered by information from outbreaks and microbiologic studies of sources. Studies such as ours can be used to target interventions that reduce the most illnesses in a population and evaluate the effectiveness of the intervention.

In conclusion, sporadic non-O157 STEC infections were associated with a wide variety of food and farm animal environment-associated exposures, reflecting widespread carriage by animals. As for *Salmonella*, non-O157 STEC are a diverse group of organisms, widely distributed in food-producing and wild animals; many foods contaminated with animal feces transmit these pathogens. Therefore, non-O157 STEC infections might best be prevented by widespread improvements in food safety systems. To have the greatest effect in reducing the incidence of these infections, control measures should focus on decreasing contamination of produce consumed raw, especially lettuce, as well as improving the safety of food consumed in restaurants and decreasing transmission from animal environments. Such measures would also decrease illnesses caused by other enteric pathogens (*30*,*32*). Control measures that could be effective include decreasing carriage of pathogens by food animals, decreasing contamination of farm environments with food animal fecal matter, and decreasing contamination of foods of animal origin at slaughter. Transmission directly from farm animal environments could be decreased by improving hand hygiene; for example, by designing systems in which handwashing is the default behavior after exposure to those environments.

Acknowledgments

We thank Ruth Luna-Gierke, Raj Mody, Mary Patrick, Rebecca Lindsey, Haley Martin, Devon Stoneburg, Nancy Strockbine, Aimee Geissler, Danielle Tack, Beth Karp, and Kristin Holt for helpful contributions. We recognize epidemiologists and laboratory partners in FoodNet sites for providing data.

Funding was provided by the Emerging Infections Program, CDC; Food Safety and Inspection Service, US Department of Agriculture; and the Center for Food Safety and Applied Nutrition, US Food and Drug Administration.

About the Author

Dr. Marder is a senior epidemiologist at the Washington State Department of Health, where she works on COVID-19 surveillance. Previously, Dr. Marder was a surveillance epidemiologist with the Foodborne Diseases Active Surveillance Network, where she conducted epidemiologic studies and analyses of enteric illnesses.

References

1. Collier SA, Deng L, Adam EA, Benedict KA, Beshearse EM, Blackstock AJ, et al. Estimate of burden and direct healthcare cost of infectious waterborne disease in the United States. Emerg Infect Dis. 2021;27:140–9. https://doi.org/10.3201/eid2701.190676
2. Gould LH, Mody RK, Ong KL, Clogher P, Cronquist A, Garman KN, et al. Increased recognition of non-O157 Shiga toxin-producing *Escherichia coli* infections in the United States during 2000–2010: epidemiologic features and comparison with *E. coli* O157 infections. Foodborne Pathog Dis. 2013;10:453–60. https://doi.org/10.1089/fpd.2012.1401
3. Brooks HT, Sowers EG, Wells JG, Greene KD, Griffin PM, Hoekstra RM, et al. Non-O157 Shiga toxin–producing *Escherichia coli* infections in the United States, 1983–2002. J Infect Dis. 2005;192:1422–9. https://doi.org/10.1086/466536
4. Strockbine NA, Bopp CA, Barrett TJ. Overview of detection and subtyping methods. In: Kaper JB, O'Brien AD, editors. *Escherichia coli* O157:H7 and other Shiga toxin–producing *E. coli* strains. Washington: American Society for Microbiology; 1998. p. 331–56.
5. Hoefer D, Hurd S, Medus C, Cronquist A, Hanna S, Hatch J, et al. Laboratory practices for the identification of Shiga toxin–producing *Escherichia coli* infections in the United States, 2007. Foodborne Pathog Dis. 2011;8:555–60. https://doi.org/10.1089/fpd.2010.0764
6. Stigi KA, MacDonald JK, Tellez-Marfin AA, Lofy KH. Laboratory practices and incidence of non-O157 Shiga toxin–producing *Escherichia coli* infections. Emerg Infect Dis. 2012;18:477–9. https://doi.org/10.3201/eid1803.111358
7. Hughes JM, Wilson, Johnson KE, Thorpe CM, Sears CL. The emerging clinical importance of non-O157 Shiga toxin–producing *Escherichia coli*. Clin Infect Dis. 2006;43:1587–95. https://doi.org/10.1086/509573
8. Bettelheim KA. The non-O157 Shiga-toxigenic (verocytotoxigenic) *Escherichia coli*; under-rated pathogens. Crit Rev Microbiol. 2007;33:67–87. https://doi.org/10.1080/10408410601172172
9. Centers for Disease Control and Prevention. Recommendations for diagnosis of Shiga toxin–producing *Escherichia coli* infections by clinical laboratories. Morb Mortal Wkly Rep. 2009;58(RR-12):1–14.
10. Centers for Disease Control and Prevention. National Enteric Disease Surveillance: Shiga toxin–producing *Escherichia coli* (STEC) annual report, 2015. 2017 [cited 2023 Apr 10]. https://www.cdc.gov/nationalsurveillance/pdfs/STEC_Annual_Summary_2015-508c.pdf
11. Luna-Gierke RE, Griffin PM, Gould LH, Herman K, Bopp CA, Strockbine N, et al. Outbreaks of non-O157 Shiga toxin–producing *Escherichia coli* infection: USA. Epidemiol Infect. 2014;142:2270–80. https://doi.org/10.1017/S0950268813003233
12. Tack DM, Kisselburgh HM, Richardson LC, Geissler A, Griffin PM, Payne DC, et al. Shiga toxin–producing *Escherichia coli* outbreaks in the United States, 2010–2017. Microorganisms. 2021;9:1521. https://doi.org/10.3390/microorganisms9071529
13. Cui Z, Marder EP, Click ES, Hoekstra RM, Bruce BB. Nearest-neighbors matching for case-control study analyses: better risk factor identification from a study of sporadic campylobacteriosis in the United States. Epidemiol. 2022;33:633–41; https://doi.org/10.1097/EDE.0000000000001504
14. Gower JC. A general coefficient of similarity and some of its properties. Biometrics. 1971;27:857–71. https://doi.org/10.2307/2528823
15. Benjamini Y, Yekutieli D. The control of the false discovery rate in multiple testing under dependency. Ann Stat. 2001;29:1165–88. https://doi.org/10.1214/aos/1013699998
16. Bruzzi P, Green SB, Byar DP, Brinton LA, Schairer C. Estimating the population attributable risk for multiple risk factors using case-control data. Am J Epidemiol. 1985;122:904–14. https://doi.org/10.1093/oxfordjournals.aje.a114174

17. Centers for Disease Control and Prevention. The Interagency Food Safety Analytics Collaboration. Foodborne illness source attribution estimates for 2020 for *Salmonella*, *Escherichia coli* O157, and *Listeria monocytogenes* using multi-year outbreak surveillance data, United States. 2022 [cited 2023 Apr 10]. https://www.cdc.gov/foodsafety/ifsac/pdf/p19-2020-report-triagency-508.pdf
18. Economic Research Service, United States Department of Agriculture. COVID-19 working paper: shares of commodity consumption at home, restaurants, fast food places, schools, and other away-from-home places: 2013–16 [cited 2023 Apr 10]. https://www.ers.usda.gov/webdocs/publications/100138/ap-085.pdf
19. Kassenborg HD, Hedberg CW, Hoekstra M, Evans MC, Chin AE, Marcus R, et al. Farm visits and undercooked hamburgers as major risk factors for sporadic *Escherichia coli* O157:H7 infection: data from a case-control study in 5 FoodNet sites. Clin Infect Dis 2004;38(Suppl 3):S271–8.
20. McPherson M, Lalor K, Combs B, Raupach J, Stafford R, Kirk MD. Serogroup-specific risk factors for Shiga toxin–producing *Escherichia coli* infection in Australia. Clin Infect Dis. 2009;49:249–56. https://doi.org/10.1086/599370
21. Hsuan C, Ryan-Ibarra S, DeBurgh K, Jacobson DM. Association of paid sick leave laws on foodborne illness rates. Am J Prev Med. 2017;53:609–15. https://doi.org/10.1016/j.amepre.2017.06.029
22. Voetsch AC, Kennedy MH, Keene WE, Smith KE, Rabatsky-ehr T, Zansky S, et al. Risk factors for sporadic Shiga toxin–producing *Escherichia coli* O157 infections in FoodNet sites, 1999–2000. Epidemiol Infect. 2007;135:993–1000. https://doi.org/10.1017/S0950268806007564
23. Angelo KM, Nisler AL, Hall AJ, Brown LG, Gould LH. Epidemiology of restaurant-associated foodborne disease outbreaks, United Sates, 1998–2013. Epidemiol Infect. 2017;145:523–34. https://doi.org/10.1017/S0950268816002314
24. Bennett SD, Sodha SV, Ayers TL, Lynch MF, Gould LH, Tauxe RV. Produce-associated foodborne disease outbreaks, USA, 1998–2013. Epidemiol Infect. 2018;146:1397–406. https://doi.org/10.1017/S0950268818001620
25. Painter JA, Hoekstra RM, Ayers T, Tauxe RV, Braden CR, Angulo FJ, et al. Attribution of foodborne illnesses, hospitalizations, and deaths to food commodities by using outbreak data, United States, 1998–2008. Emerg Infect Dis. 2013;19:407–15. https://doi.org/10.3201/eid1903.111866
26. Marshall KE, Hezemer A, Seelman SL, Fatica MK, Blessington T, Hajmeer M, et al. Lessons learned from a decade of investigations of Shiga toxin–producing *Escherichia coli* outbreaks linked to leafy greens, United States and Canada. Emerg Infect Dis. 2020;26:2319–28. https://doi.org/10.3201/eid2610.191418
27. Bottichio L, Keaton A, Thomas D, Fulton T, Tiffany A, Frick A, et al. Shiga toxin–producing *Escherichia coli* infections associated with romaine lettuce—United States, 2018. Clin Infect Dis. 2020;71:e323–30. https://doi.org/10.1093/cid/ciz1182
28. US Department of Agriculture. USDA targeting six additional strains of E. coli in raw beef trim starting Monday, May 31, 2012 [cited 2023 Apr 10]. https://www.usda.gov/media/press-releases/2012/05/31/usda-targeting-six-additional-strains-ecoli-raw-beef-trim-starting
29. Centers for Disease Control and Prevention. National Outbreak Reporting System Dashboard. [cited 2023 Apr 7]. https://wwwn.cdc.gov/norsdashboard
30. Friedman CR, Hoekstra RM, Samuel M, Marcus R, Bender J, Shiferaw B, et al; Emerging Infections Program FoodNet Working Group. Risk factors for sporadic *Campylobacter* infection in the United States: a case-control study in FoodNet sites. Clin Infect Dis. 2004;38(Suppl 3):S285–96. https://doi.org/10.1086/381598
31. Friesema I, Schotsborg M, Heck M, Van Pelt W. Risk factors for sporadic Shiga toxin–producing *Escherichia coli* O157 and non-O157 illness in the Netherlands, 2008–2012, using periodically surveyed controls. Epidemiol Infect. 2015;143:1360–7. https://doi.org/10.1017/S0950268814002349
32. Hale CR, Scallan E, Cronquist AB, Dunn J, Smith K, Robinson T, et al. Estimates of enteric illness attributable to contact with animals and their environments in the United States. Clin Infect Dis. 2012;54(Suppl_5):S472–9. https://doi.org/10.1093/cid/cis051
33. Heiman KE, Mody RK, Johnson SD, Griffin PM, Gould LH. *Escherichia coli* O157 outbreaks in the United States, 2003–2012. Emerg Infect Dis. 2015;21:1293–301. https://doi.org/10.3201/eid2108.141364
34. Daly RF, House J, Stanek D, Stobierski MG; National Association of State Public Health Veterinarians Animal Contact Compendium Committee. Compendium of measures to prevent disease associated with animals in public settings, 2017. J Am Vet Med Assoc. 2017;215:1268–92.
35. Centers for Disease Control and Prevention. Laboratory-confirmed non-O157 Shiga toxin–producing *Escherichia coli*—Connecticut, 2000–2005. Morb Mortal Wkly Rep. 2007;56:29–31.
36. Hedican EB, Medus C, Besser JM, Juni BA, Koziol B, Taylor C, et al. Characteristics of O157 versus non-O157 Shiga toxin–producing *Escherichia coli* infections in Minnesota, 2000–2006. Clin Infect Dis. 2009;49:358–64. https://doi.org/10.1086/600302
37. Rosenbaum P, Rubin DB. The bias due to incomplete matching. Biometrics. 1985;41:103–16. https://doi.org/10.2307/2530647
38. Stuart EA. Matching methods for causal inference: a review and a look forward. Statist Sci. 2010;25:1–21. https://doi.org/10.1214/09-STS313
39. Shirts BH, Bennett ST, Jackson BR. Using patients like my patient for clinical decision support: institution-specific probability of celiac disease diagnosis using simplified near-neighbor classification. J Gen Intern Med. 2013;28:1565–72. https://doi.org/10.1007/s11606-013-2443-z
40. Scallan E, Jones TF, Cronquist A, Thomas S, Frenzen P, Hoefer D, et al. Factors associated with seeking medical care and submitting a stool sample in estimating the burden of foodborne illness. Foodborne Pathog Dis. 2007;3:432–8. https://doi.org/10.1089/fpd.2006.3.432
41. Hardnett FP, Hoekstra RM, Kennedy M, Charles L, Angulo FJ. Epidemiologic issues in study design and data analysis related to FoodNet activities. Clin Infect Dis. 2004;38(S3):S121–6. https://doi.org/10.1086/381602
42. Blumberg SJ, Luke JV; National Center for Health Statistics. Wireless substitution: early release of estimates from the National Health Interview Survey, January–June 2017 [cited 2023 Apr 10]. https://www.cdc.gov/nchs/data/nhis/earlyrelease/wireless201712.pdf

Address for correspondence: Ellyn P. Marder, Washington State Department of Health, 1610 NE 150th St, Shoreline, WA 98155, USA; email: Ellyn.Marder@doh.wa.gov

Evolution of Avian Influenza Virus (H3) with Spillover into Humans, China

Jiaying Yang,[1] Ye Zhang,[1] Lei Yang,[1] Xiyan Li, Hong Bo, Jia Liu, Min Tan, Wenfei Zhu, Yuelong Shu, Dayan Wang

The continuous evolution of avian influenza viruses (AIVs) of subtype H3 in China and the emergence of human infection with AIV subtype H3N8 highlight their threat to public health. Through surveillance in poultry-associated environments during 2009–2022, we isolated and sequenced 188 H3 AIVs across China. Performing large-scale sequence analysis with publicly available data, we identified 4 sublineages of H3 AIVs established in domestic ducks in China via multiple introductions from wild birds from Eurasia. Using full-genome analysis, we identified 126 distinct genotypes, of which the H3N2 G23 genotype predominated recently. H3N8 G25 viruses, which spilled over from birds to humans, might have been generated by reassortment between H3N2 G23, wild bird H3N8, and poultry H9N2 before February 2021. Mammal-adapted and drug-resistance substitutions occasionally occurred in H3 AIVs. Ongoing surveillance for H3 AIVs and risk assessment are imperative for potential pandemic preparedness.

Avian influenza viruses (AIVs) of subtype H3 are highly prevalent among waterfowl globally, causing mild or no apparent signs of illness in birds (*1*–*5*). H3 AIV has shown the potential for cross-species transmission and was the origin of other animal influenza viruses, which caused epidemics in horses, dogs, seals, and pigs (*6*–*9*). In 1968, H3 AIV contributed its hemagglutinin (HA) gene to the human influenza (H3N2) pandemic viruses, and it is still unknown whether an intermediate host was involved (*10*).

Author affiliations: National Institute for Viral Disease Control and Prevention, Chinese Center for Disease Control and Prevention, Key Laboratory for Medical Virology, Beijing, China (J. Yang, Y. Zhang, L. Yang, X. Li, H. Bo, J. Liu, M. Tan, W. Zhu, D. Wang); School of Public Health (Shenzhen), Shenzhen campus of Sun Yat-sen University, Shenzhen, China (J. Yang, Y. Shu); Institute of Pathogen Biology of Chinese Academy of Medical Science/Peking Union Medical College, Beijing (Y. Shu)

DOI: https://doi.org/10.3201/eid2906.221786

In April 2022, the first human infection with AIV (H3N8) was reported; the case was in a 4-year-old boy whose family reared chickens and silky fowls in Henan Province, China (*11*). After infection, the patient exhibited recurrent fever and severe pneumonia. In May 2022, a second case was identified in 5-year-old boy with mild influenza symptoms, who had visited the live poultry market (LPM) in Hunan Province, China (*12*). Those cases raised concern over whether H3N8 AIVs will cause a major public health threat (*13*).

In China, H3 AIVs have been dynamically circulating in poultry and wild birds across multiple regions (*14*). H3 combinations with multiple neuraminidase (NA) subtypes (N1–N8) were reported, among which H3N2 and H3N8 predominated (*14*–*16*). Phylogenetically, those viruses belonged to the Eurasian lineage, which is widespread in wild birds across Eurasia (*3*,*14*,*17*,*18*). Reassortment events often occurred at LPMs (*16*,*19*–*22*). During 2009–2022, we conducted country-level AIV surveillance in poultry-associated environments and performed a large-scale genetic analysis to provide a comprehensive picture of the evolution of H3 AIVs in China.

Methods

During January 2009–June 2022, we collected environmental samples monthly from avian-linked environments across 31 provinces in the China mainland according to AIV surveillance guideline of Chinese Center for Disease Control and Prevention. We isolated and sequenced 188 H3 viruses (32 have been previously published [*15*]). The sequences were deposited in the GISAID EpiFlu database (https://www.gisaid.org; accession nos. EPI2210281–1516) (Appendix Table 1, https://wwwnc.cdc.gov/EID/article/29/6/22-1786-App1.pdf).

[1]These authors contributed equally to this article.

We performed sequence alignments with available sequences from the GISAID EpiFlu database as of June 25, 2022, by using MAFFT version 7.222 (*23*). We reconstructed maximum-likelihood phylogenies of all segments by using FastTree version 2.1.11 (*24*). The resulting trees were classified into divergent lineages or sublineages. Genotypes were assigned by the combination of lineages for each segment of full-genome viruses.

To estimate the time to the most recent common ancestor (tMRCA) of H3N8 viruses of humans, we used Bayesian Markov chain Monte Carlo analyses for each gene in BEAST version 1.10.4 (*25*). We then generated maximum clade credibility trees (Appendix).

Results

Isolation and Sequencing of H3 AIVs

During January 2009–June 2022, we isolated 188 H3 AIVs from the poultry-associated environmental samples: 167 H3N2, 7 H3N3, 3 H3N6, 10 H3N8, and 1 H3 with NA unknown (Appendix Table 1). The H3N2 AIVs were widely distributed across 15 provinces, mainly in southern China (Figure 1, panel A). We isolated H3 AIVs with other NA subtypes (N3, N6, and N8) in 2–8 provinces. More than three quarters of the H3 viruses (149/188, 79.3%) were isolated from the samples collected from LPMs (Appendix Table 2). Before 2014, we isolated and sequenced <6 strains of H3 AIVs per year (Figure 1, panel B). Since 2014, we obtained more isolates, most (48) in 2018. All H3 isolates were sequenced, and we recovered the full genomes from 185 of the isolates (Appendix Table 1).

Evolution of H3 Genes in China

To elucidate the evolution of H3 AIVs in China, we performed a phylogenetic analysis of HA genes of the H3 AIVs sequenced in this study, along with sequences available from the GISAID EpiFlu Database (Figure 2). The HA genes of all viruses in this study were grouped into the Eurasian lineage, sharing a nucleotide homology of 79.2%–100.0%. In brief, the major branch of Eurasian avian H3 lineage containing viruses in recent decades could be further classified into 10 sublineages (named by the geographic distributions: China-1, China-2, China-3, China-4, Asia, Europe-Asia, worldwide-1, worldwide-2, North America-1, and Korea); other minor branches at the bottom of the phylogenetic tree included the North America-2 sublineage and early strains sampled during 1972–1992 (Figure 2; Appendix Figure 1). H3 AIVs collected from wild birds, poultry, or poultry-associated environments in China in recent decades were distributed in 8 sublineages, except sublineages North America-1, North America-2, and Korea, which were only identified in North America and South Korea.

Sublineages China-1, China-2, China-3, and China-4 consisted of AIVs almost all collected from poultry or poultry-associated environments in China in addition to a few viruses from Vietnam (18) and Cambodia (1) (Appendix Figure 1). Domestic ducks acted as the main host for China-1 (48/166), China-2 (63/111), China-3 (80/110), and China-4 (15/23)

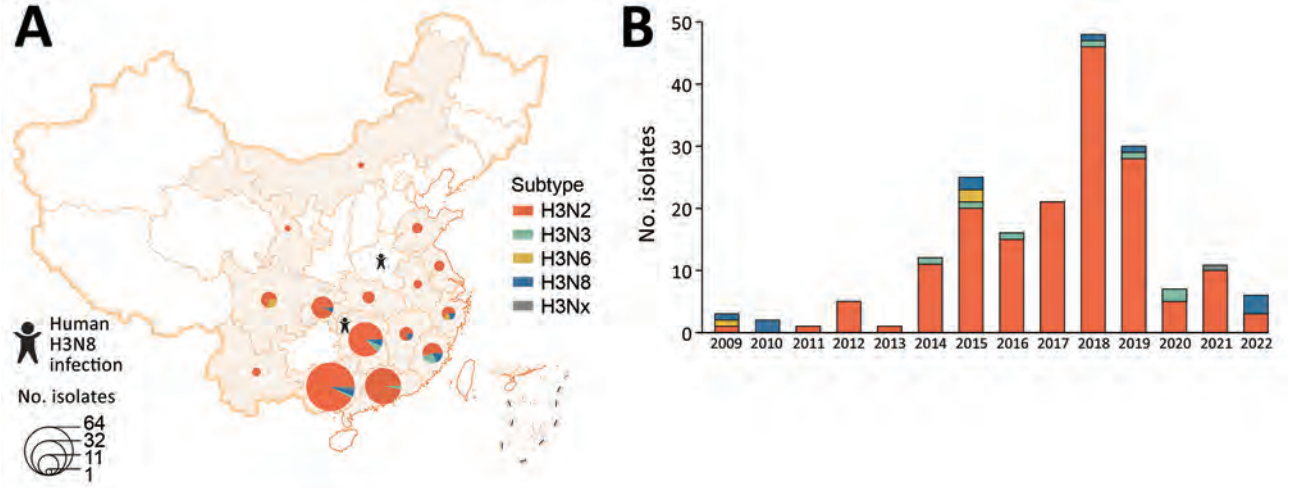

Figure 1. Spatial and temporal distribution of avian influenza virus subtype H3 isolated from poultry-associated environments, China, 2009–2022. A) Spatial distribution of environmental H3 subtype viruses. One H3 isolate without neuraminidase (NA) subtype was designated as H3Nx. Provinces where human infections with H3N8 were reported are noted. B) Number of environmental H3 subtype isolates per year. This figure includes all H3 isolates sequenced by the Chinese National Influenza Center. Additional metadata are available in Appendix Table 1 (https://wwwnc.cdc.gov/EID/article/29/6/22-1786-App1.pdf).

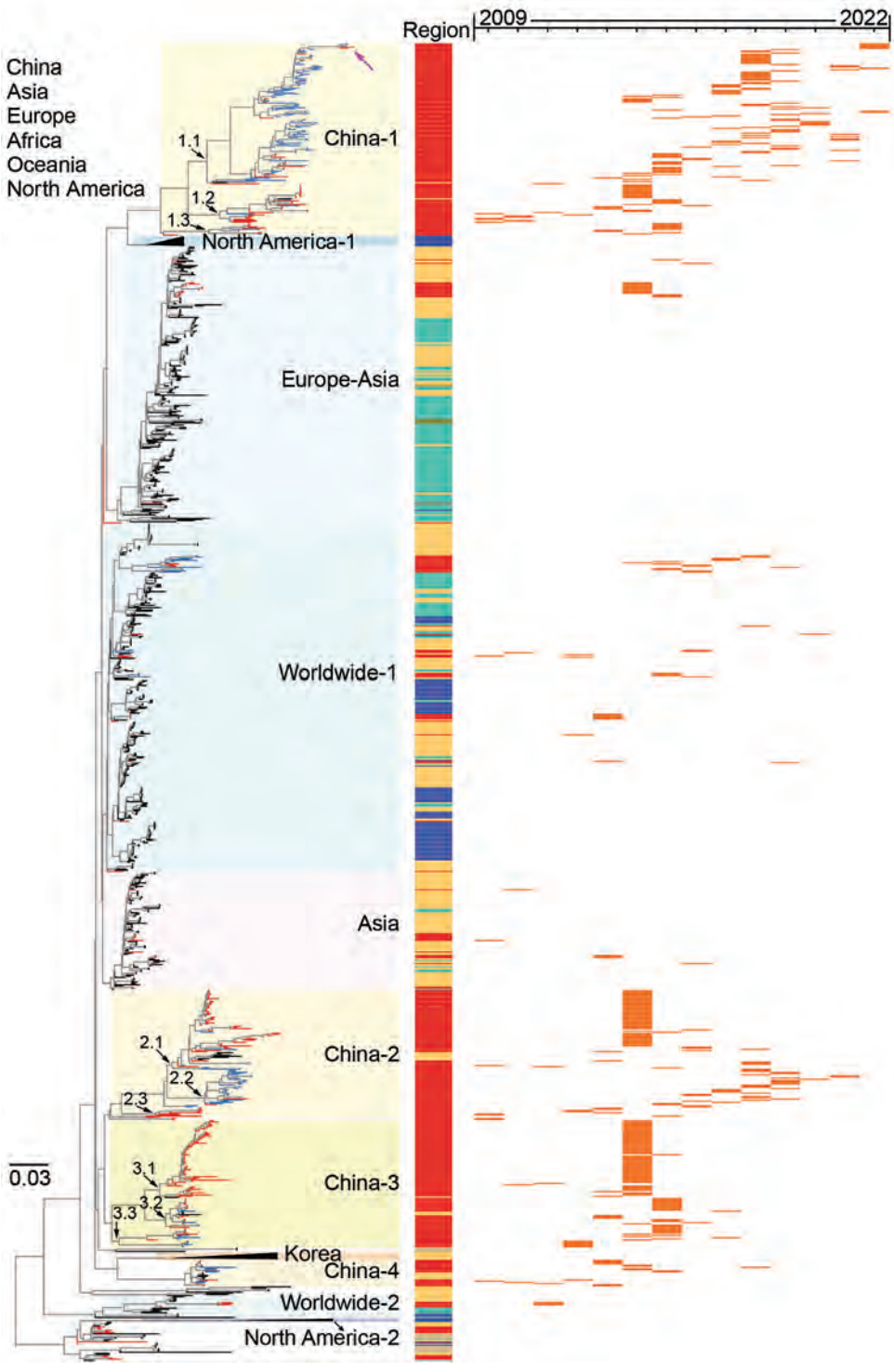

Figure 2. Maximum-likelihood phylogenetic tree of hemagglutinin genes of avian influenza viruses subtype H3 from China (n = 1,291) and reference sequences from GISAID (https://www.gisaid.org). Blue tree sections indicate sequences reported in this study; red tree sections indicate other H3 sequences from China; violet arrow at top of tree indicates human H3N8 virus. For clarity, some clades are collapsed. Sublineages are shown with different background colors on the phylogenetic tree. Subgroups in sublineages China-1, China-2, and China-3 are marked with black arrows at the nodes. The sampling locations are annotated with colored bars adjacent to the tree. For the H3 viruses sampled in China during 2009–2022, the sampling year of each of these viruses is shown on the right panel with orange horizontal bars. The phylogenetic tree of the H3 genes with more detailed information is shown in Appendix Figure 1 (https://wwwnc.cdc.gov/EID/article/29/6/22-1786-App1.pdf). Scale bar indicates nucleotide substitutions per site.

(Appendix Table 3). Each sublineage comprised various NA subtypes (Appendix Figure 1). The most common subtype was H3N2 (270), followed by H3N8 (41), H3N6 (19), H3N3 (12), and H3N9 (1), except for 67 H3 AIVs with NA unknown. A high proportion (397/410, 96.8%) of these viruses have been sampled since 2009, whereas recent isolates were primarily consolidated in the China-1 and China-2 sublineages (Figure 2).

The China-1 sublineage had evolved into 3 distinct subgroups, with prevalence spanning different times. Most of our isolates (101/185, 54.6%) fell into the China-1.1 subgroup, which circulated during

2008–2022. Of note, 3 H3N8 strains sampled in Fujian (2) and Guangxi (1) Provinces in 2022 had a close relationship with 2 human H3N8 strains and together formed a miniature phylogenetic group (Appendix Figure 1). The China-1.2 subgroup was detected during 2009–2016 and the China-1.3 subgroup during 2013–2015 (Figure 2; Appendix Figure 1).

The China-2 and China-3 sublineages have evolved into 3 subgroups, and the China-2.2 subgroup mainly comprised environmental H3 viruses (29/31, 93.5%) sequenced in this study during 2015–2021 (Figure 2; Appendix, Appendix Figure 1). H3 viruses of sublineages Asia, Europe-Asia, worldwide-1, and worldwide-2 were occasionally detected in poultry and wild birds in China, but no stable cluster was established (Appendix, Appendix Figure 1).

Reassortment with NA Genes

We detected multiple NA subtypes in each H3 sublineage. We performed phylogenetic analyses for 4 major NA subtypes: N2, N3, N6, and N8. Almost all NA genes of H3 AIVs in our study were clustered within the Eurasian lineage, and 8 H3N8 AIVs had NA genes derived from the North American lineage (Appendix Figure 2, panels A–D).

The N2 genes of AIVs in the Eurasian lineage could be further classified into sublineages, and most H3N2 viruses in this study were clustered in the Eurasian-2 sublineage (Appendix). We also found H3N3 strains closely related to the human-origin influenza (H10N3) virus and H3N6 closely related to highly pathogenic AIV (HPAIV) subtype H5N6 (Appendix).

Most NA genes of H3N8 viruses (43/59) from China belonged to the North American lineage, closely related to AIVs from different regions (e.g., Russia, Vietnam, South Korea, and North America). Of note, the NA genes of human H3N8 and H10N8 viruses belonged to distinct groups (Figure 3), and 3 environmental strains sequenced in this study were highly homologous to the human H3N8 viruses. Few H3N8 strains from China fell into the Eurasian lineage (Figure 3).

Reassortment with Internal Genes

In the phylogenetic tree of each internal gene, a large proportion of H3 AIVs in China belonged to the Eurasian wild bird reservoir (Appendix Figure 3). Some H3 AIVs had internal genes derived from ZJ-5 sublineage (of the wild bird viruses), poultry H5N1/H5N6 sublineage, poultry H9N2 ZJ-HJ/07 sublineage, or waterfowl H6 sublineage (Appendix). Each internal gene has only 1 or 2 virus sequences that belong to the H9N2 ZJ-HJ/07 sublineage. In 2022, a total of 3 environmental and 2 human H3N8 viruses contained all internal genes belonging to the H9N2 ZJ-HJ/07 sublineage.

Emergence of Multiple Genotypes

Assessment of the diversity of genome constellations indicated that prolific reassortments of the H3 AIVs had occurred in China in past decades. On the basis of the sublineage classification of all 8 gene segments, we identified 126 genotypes among 284 full-genome H3 viruses sampled in China during 2009–2022 (Appendix Figure 4). We found evidence of dynamic emergence for 73 genotypes (G1–G73) from 212 H3N2 genomes, 11 genotypes (G1–G11) from 14 H3N3, 17 (G1–G17) from 25 H3N6, and 25 (G1–G25) from 33 H3N8 (Appendix). H3N2 G23 had been detected in multiple years and provinces during 2014–2022 (Appendix Figure 4, panel A, Figure 5, panel A). H3N8 G25, which had been detected in both environmental and human viruses in 2022, acquired HA genes from the China-1 H3 sublineage, NA genes from the North American N8 lineage, and all 6 internal gene from poultry H9N2 ZJ-HJ/07 sublineage viruses (Appendix Table 4).

Emergence of H3N8 G25 Viruses

We further traced the origin of the H3N8 G25 viruses. When we compared the genetic diversity of G25 genotype viruses, the results showed that these viruses shared a higher similarity in HA (98.4%–99.1%) and NA genes (98.8%–99.3%) and a lower similarity in other internal genes (polymerase basic [PB] 2, 93.9%–100.0%; PB1, 91.6%–99.9%; polymerase acidic [PA], 93.4%–99.6%; nucleocapsid, 94.5%–99.9%; matrix (M), 95.3%–100.0%; and nonstructural, 97.0%–98.7%). This finding indicated that after the emergence of prior H3N8 G25 virus, dynamic reassortment might occur between H3N8 and poultry H9N2 viruses.

To elucidate the timing of H3N8 G25 virus emergence, we performed coalescent analyses and calculated the estimated tMRCA of all 8 segments (Appendix Figures 6–13). The median tMRCA among the HA genes was estimated to be February 2021 (95% highest posterior density [HPD] October 2020–May 2021). The HA genes closely related to those of H3N8 G25 viruses were from H3N2 G23 AIVs isolated from Guangxi and Guangdong Provinces, particularly A/environment/Guangxi/44461/2019 (H3N2), sampled in December 2019 (Figure 4, panels A, C). The median tMRCA among the NA genes of the H3N8 G25 viruses was estimated to be August 2020 (95% HPD November 2019–March 2021). H6N8

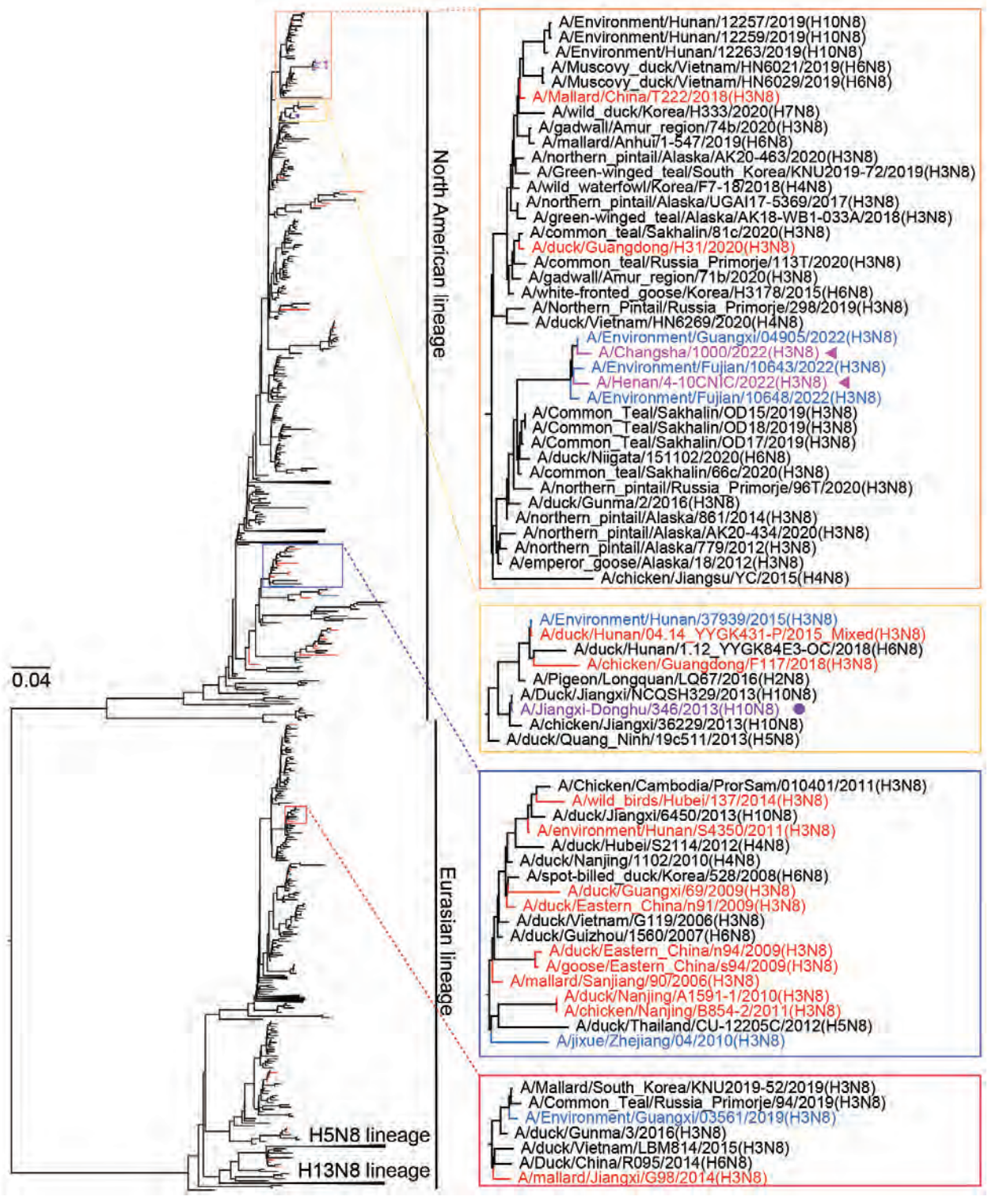

Figure 3. Maximum-likelihood phylogenetic tree of avian influenza virus subtype N8 genes from China (n = 1,106) and reference sequences from GISAID (https://www.gisaid.org). Blue tree sections indicate sequences of H3 subtype viruses reported in this study; red tree sections indicate other H3 subtype viruses from China. For of clarity, some clades are collapsed. Representative clusters are indicated in shaded boxes and magnified on the right. Violet arrows indicate human H3N8 viruses; purple solid circle indicates human H10N8 virus. The phylogenetic tree of N8 genes with more complete information is shown in Appendix Figure 2, panel D (https://wwwnc.cdc.gov/EID/article/29/6/22-1786-App1.pdf). Scale bar indicates nucleotide substitutions per site.

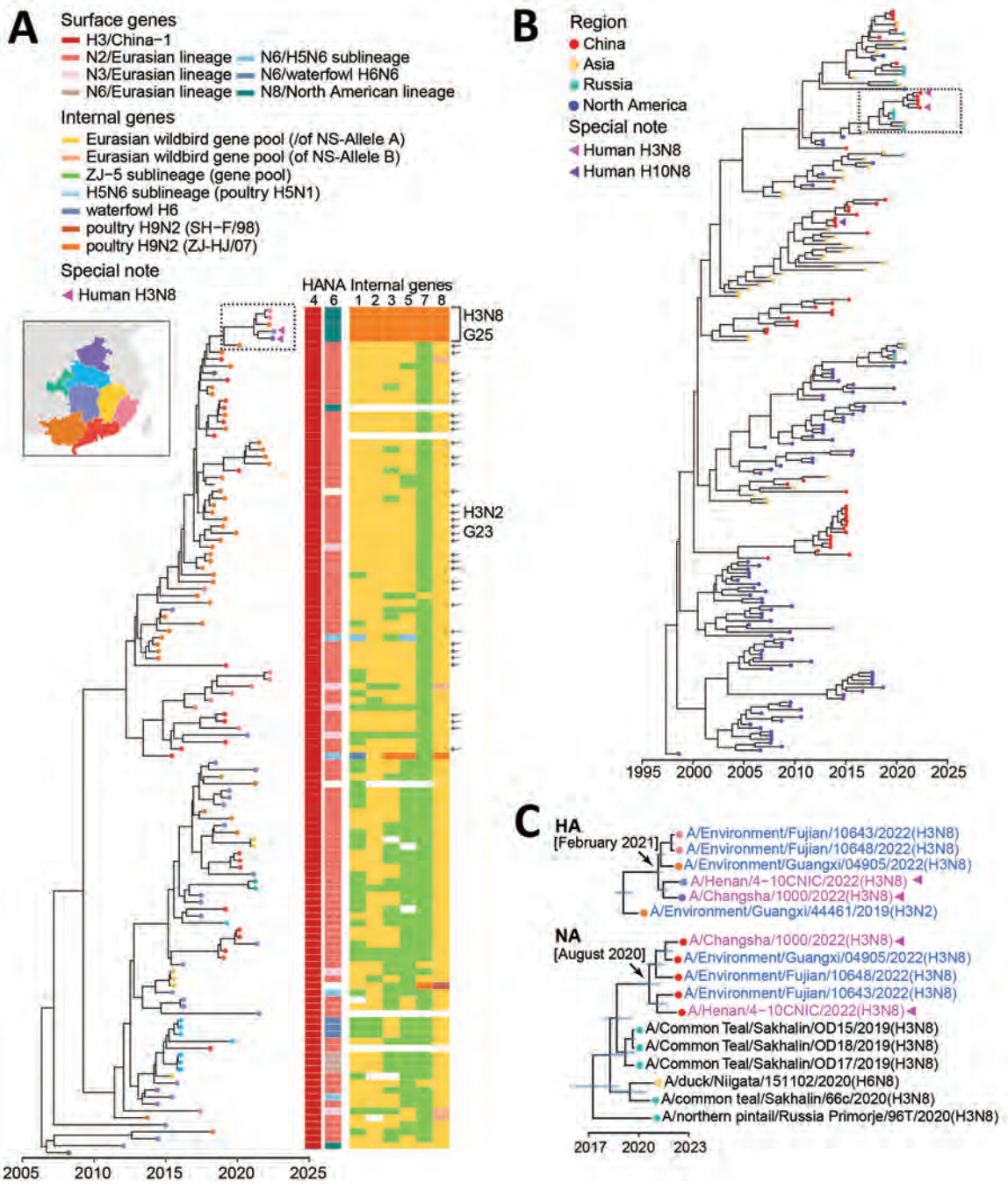

Figure 4. Bayesian time-resolved phylogenetic tree of hemagglutinin (HA) genes from avian influenza subtype H3 viruses and neuraminidase (NA) genes from subtype N8 viruses from China and reference sequences from GISAID (https://www.gisaid.org). A) Maximum clade credibility tree of HA genes of the China-1.1 H3 subgroup (n = 122). Tip points are colored by provinces (corresponding to the fill color in the map). Violet triangles indicate human H3N8 viruses. The lineage origins of each gene segment of H3 AIVs are represented by different colored tiles adjacent to the tree; the tile is blank if the sequence is unavailable. H3N2 G23 viruses are indicated with arrows. H3N8 G25 viruses are indicated within the bracket. The fully resolved tree with detailed information is depicted in Appendix Figure 6 (https://wwwnc.cdc.gov/EID/article/29/6/22-1786-App1.pdf). B) Maximum clade credibility tree of N8 genes (n = 202). Tip points are colored by region. Violet triangles indicate human H3N8 viruses; purple triangle indicates human H10N8 virus. Virus names of the representative cluster (in the dashed box) are shown in panel C. The fully resolved tree with detailed information is depicted in Appendix Figure 7. C) Clades in the dashed box in panels A and B. Trees are drawn to the same scale. Blue indicates H3 avian influenza viruses sequenced in this study; violet indicates human H3N8 viruses. For HA (top) and NA (bottom) genes, branch tips are colored as in panels A and B. Blue node bars correspond to the 95% credible intervals of node heights. Arrows indicate the most recent common ancestors of HA and NA genes of H3N8 G25 viruses.

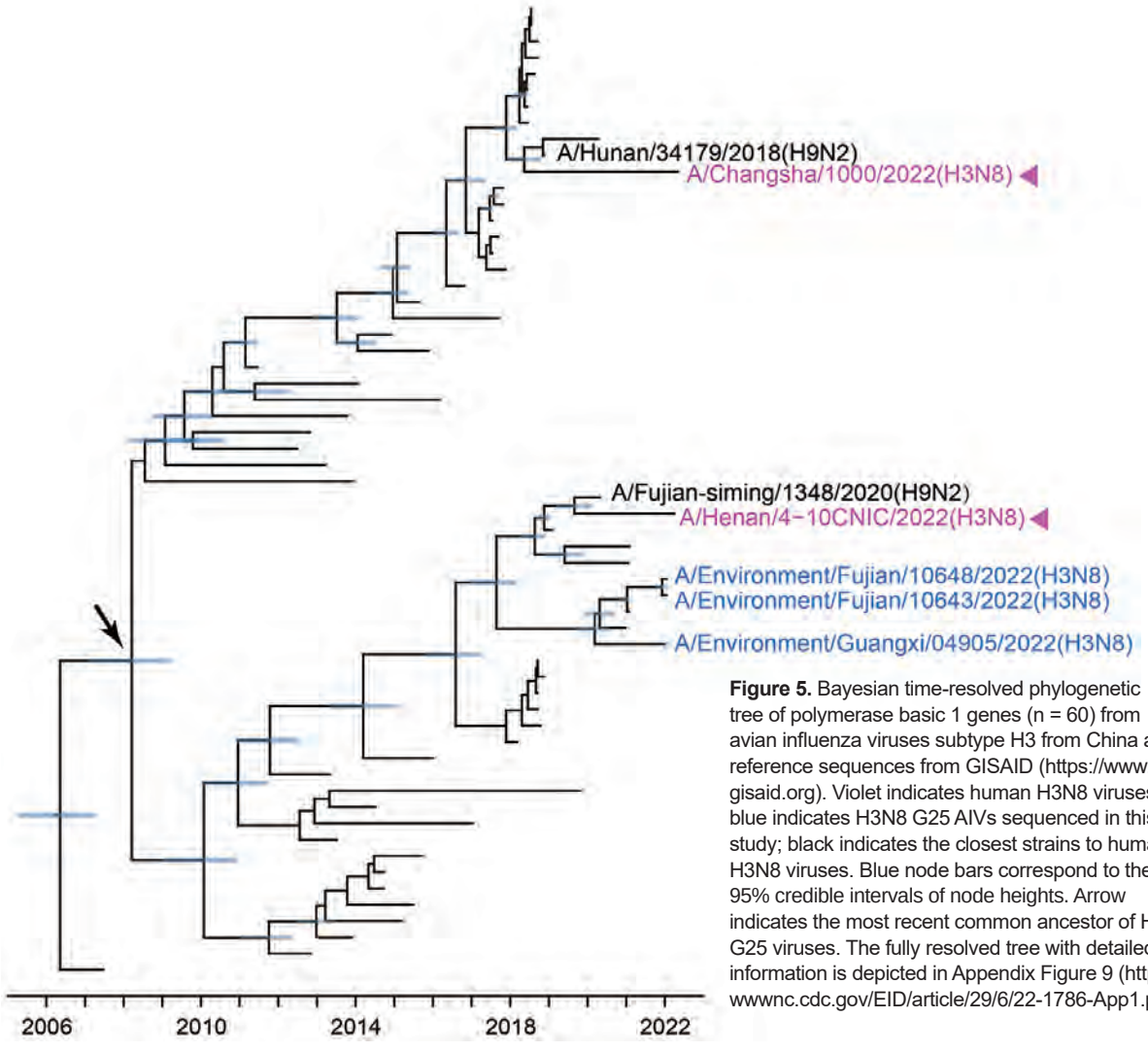

Figure 5. Bayesian time-resolved phylogenetic tree of polymerase basic 1 genes (n = 60) from avian influenza viruses subtype H3 from China and reference sequences from GISAID (https://www.gisaid.org). Violet indicates human H3N8 viruses; blue indicates H3N8 G25 AIVs sequenced in this study; black indicates the closest strains to human H3N8 viruses. Blue node bars correspond to the 95% credible intervals of node heights. Arrow indicates the most recent common ancestor of H3N8 G25 viruses. The fully resolved tree with detailed information is depicted in Appendix Figure 9 (https://wwwnc.cdc.gov/EID/article/29/6/22-1786-App1.pdf).

AIV isolated in Japan and H3N8 AIV isolated in the Russian Far East during 2019–2020 were closely related to H3N8 G25 viruses, specifically A/common teal/Sakhalin/OD17/2019 (H3N8) virus (Figure 4, panels B, C).

The internal genes of the H3N8 G25 viruses showed earlier tMRCAs than that estimated for HA and NA genes (Appendix Figure 8–13). The internal genes of H3N8 G25 viruses scattered within different subclades without forming a cluster alone. The closest H9N2 viruses to the human H3N8 viruses also differed. For example, the common ancestry of PB1 genes of the H3N8 G25 viruses could be dated back to March 2008 (95% HPD March 2007–May 2009). A/Fujian-siming/1348/2020 (H9N2) was closely related to human H3N8 virus A/Henan/4–10CNIC/2022, and A/Hunan/34179/2018 (H9N2) was close to human H3N8 virus A/Changsha/1000/2022 (Figure 5). Other internal genes of the H3N8 G25 viruses had been estimated to have tMRCAs tracing back to 2010–2018 (Appendix Figure 8–13). Those results further indicate that H3N8 G25 viruses dynamically reassorted with H9N2 viruses.

Molecular Characterization of the H3 AIVs

We investigated the molecular markers of H3 AIVs in China (Appendix Table 5). One human H3N8 isolate, A/Henan/4-10CNIC/2022, had 228G/S in the receptor binding site, which might alter the binding preference to human-type receptors (*26*). Three H3 AIVs previously sampled from poultry in 2014 had an aspartic acid at position 190, which might alter receptor specificity (*26*).

Key molecular markers associated with increased capacity for receptor binding, viral replication, and pathogenicity in mammals were found in the internal gene segments of avian H3 viruses in China (Appendix Table 5). E627K and E627V in PB2 genes were exclusively detected in human H3N8 viruses, suggesting adaptation of these viruses to mammals. Other mutations such as R389K, I292V, and A588V in PB2, which might be associated with increased polymerase activity and replication in mammalian and avian cells (*27*,*28*) and virulence in mice (*29*), were also found in 2 human isolates and several avian H3 viruses. All H3 AIVs contained N30D, T215A, and P41A in the M1 genes, which might alter the virulence in mice (*30*) and affect growth and transmission in the guinea pig model (*31*).

We identified host signature amino acids in PB2 and PA genes (PB2-702R, PA-356R, PA-409N) (*32*) in human H3N8 isolates and few H3 AIVs, except for A/Changsha/1000/2022, which had PB2-702K (Appendix Table 5, Figure 14). We also analyzed the substitutions related to antiviral drug resistance (Appendix Table 5). Two human H3N8 viruses contained an S31N mutation in the M2 gene, suggesting resistance to amantadine and rimantadine (*33*). In the M2 protein, 26 of 337 H3 AIVs contained drug-resistance mutation V27I/A and 15 contained S31N. Mutations, such as E119V/A/D and H274Y (N2 numbering) were not identified in NA gene, suggesting that all H3 viruses might be sensitive to NA inhibitors (e.g., oseltamivir) (*34*); however, 3 H3 AIVs possessed Q136L, E119G, or H274R, which might affect their drug sensitivity.

Discussion

The natural reservoir for AIVs is waterfowl; the viruses are spread worldwide by wild bird migration and introduced to domestic poultry across the wild bird–poultry interface (*35*). H3 AIVs have continuously circulated in poultry and wild birds across China (*14*). In China, 4 sublineages (China-1, China-2, China-3, and China-4) of HA genes evolved from the Eurasian lineage and became established in poultry, especially in domestic ducks, after introduction in recent decades. Currently, H3 viruses in China-1 and China-2 sublineages are cocirculating in poultry, with the China-1 sublineage predominating. Although frequent introductions from wild birds to poultry have been observed in other sublineages (e.g., worldwide-1), it is inevitable that continuous introductions will result in new sublineages in poultry (*36*). Our surveillance results also showed that H3N2 predominated among H3 AIVs in poultry-associated environments during 2009–2022. Consistent results for birds were revealed by the available avian strains in GISAID (Appendix Figure 15), although most were collected during 2013–2015 because of strengthened surveillance during the influenza (H7N9) outbreak (*37*–*39*).

Phylogenetic analyses revealed intense reassortment of the H3 AIVs, generating multiple genotypes. On the basis of the sublineage classification, we identified 126 genotypes from 284 H3 AIVs during 2009–2022. Most were transient, and the H3N2 G23 genotype seems to have stabilized in recent years, predominating in southern China. The H3N8 G25 viruses, which had caused human infection, contained complete internal gene cassettes originating from poultry H9N2 ZJ-HJ/07 sublineage, which has persistently circulated in chickens in China and named G57 genotype H9N2 AIVs (*40*). Similar to the pattern of H7N9 AIVs (*41*), H3N8 G25 AIVs might be adapted in chickens rather than ducks.

The H3N8 G25 viruses exhibited distinct tMRCAs among 8 segments. Molecular dating of HA and NA genes of the H3N8 G25 viruses implied that the ancestral virus might have been generated through reassortment between the H3N2 G23 virus and wild bird H3N8 virus before February 2021 (95% HPD October 2020–May 2021). However, the internal genes of the H3N8 G25 viruses showed much earlier tMRCAs than those of HA and NA, indicating that sequential reassortments underlie the emerging of H3N8 G25 viruses.

H3 AIVs have existed for a long time, but to our knowledge, no human infection had been reported until 2022. After reassortment with 6 internal genes of H9N2, current H3N8 AIVs seem to have the advantage of infecting humans (*42*). Ongoing adaptation in mammals after continuous human infections may underlie emergence of pandemic strains. The H3N8 G25 viruses had acquired human-adapted mutations after infecting humans (Appendix Figure 14), such as 228G/S in the HA gene and E627K/V in the PB2 gene, which were also present in 1968 H3N2 pandemic strains (*43*). This finding indicates the pandemic potential of the newly emerged H3N8 AIVs.

For risk assessment of the pandemic potential, human population immunity to a newly emerged animal virus is a critical parameter. HA inhibition assays among poultry workers (*12*) and the general population (*44*) showed seropositivity for the human seasonal H3N2 virus but very low seroprevalence against the newly emerged H3N8 virus. Those results suggest little antigenic cross-reactivity between human seasonal H3N2 virus and the current H3N8

virus and that the human population has little or no preexisting immunity to emerging H3N8 viruses. No drug-resistance mutation to NA inhibitors was observed in H3N8 G25 viruses; therefore, vaccine and drug stockpiles are needed for the potential pandemic preparation.

H3 AIVs have been isolated from asymptomatic ducks (*45*). Recent studies indicate that the newly emerged H3N8 AIVs are pathogenic to chickens (*12*,*46*). Our samples were collected exclusively from avian-linked environments (including LPMs, poultry farms, backyards, and slaughterhouses), according to surveillance guidelines. Thus, we were unable to link the isolated H3 AIVs to specific host information. Poultry sampling might provide helpful information about H3 AIV activity in China. The species of poultry in the LPMs might be confounding factors for the spatiotemporal differences. In this study, the sampling sites were geographically dispersed, and the data were collected from a small number of LPMs. Considering the large number of LPMs in China, especially in rural areas, representativeness of the data might be biased.

AIV surveillance has greatly improved since HPAIV H5N1 infected humans in Hong Kong in 1997 (*47*). However, gaps still exist, and new virus is unpredictable. The AIVs circulating and evolving in poultry might have a preferential ability to transmit to humans directly across the poultry–human interface (*48*). The H3N8 G25 viruses, with increased human receptor binding and low population immunity (*12*), had raised concern for pandemic potential. Dual receptor-binding profiles (*49*,*50*) and mutations associated with enhanced virus replication and pathogenicity in mammals were also found in many H3 AIVs. Surveillance and research of H3 AIVs, as well as the drugs and vaccine capacity, should be strengthened for pandemic preparedness.

Acknowledgments

We thank the authors and laboratories for sharing the AIVs sequences in the GISAID database.

This study was supported by the National Key Research and Development Program of China (2022YFC2303800, 2021YFC2300100) and the National Nature Science Foundation of China (81961128002, 31970643).

The opinions expressed by authors contributing to this journal do not necessarily reflect the opinions of the Chinese Center for Disease Control and Prevention or the institutions with which the authors are affiliated.

About the Author

Dr. J. Yang studies in the Chinese National Influenza Center, National Institute for Viral Disease Control and Prevention, Chinese Center for Disease Control and Prevention, and the School of Public Health (Shenzhen), Shenzhen campus of Sun Yat-sen University. Her research interests include epidemiology and evolutionary analysis of influenza viruses.

References

1. Pu J, Zhang GZ, Ma JH, Xia YJ, Liu QF, Jiang ZL, et al. Serologic evidence of prevalent avian H3 subtype influenza virus infection in chickens. Avian Dis. 2009;53:198–204. https://doi.org/10.1637/8410-071708-Reg.1
2. Hollander LP, Fojtik A, Kienzle-Dean C, Davis-Fields N, Poulson RL, Davis B, et al. Prevalence of influenza A viruses in ducks sampled in northwestern Minnesota and evidence for predominance of H3N8 and H4N6 subtypes in mallards, 2007–2016. Avian Dis. 2019;63(sp1):126–30. https://doi.org/10.1637/11851-041918-Reg.1
3. Kang HM, Kim MC, Choi JG, Batchuluun D, Erdene-Ochir TO, Paek MR, et al. Genetic analyses of avian influenza viruses in Mongolia, 2007 to 2009, and their relationships with Korean isolates from domestic poultry and wild birds. Poult Sci. 2011;90:2229–42. https://doi.org/10.3382/ps.2011-01524
4. Soda K, Kashiwabara M, Miura K, Ung TTH, Nguyen HLK, Ito H, et al. Characterization of H3 subtype avian influenza viruses isolated from poultry in Vietnam. Virus Genes. 2020;56:712–23. https://doi.org/10.1007/s11262-020-01797-7
5. Choi JG, Kang HM, Kim MC, Paek MR, Kim HR, Kim BS, et al. Genetic relationship of H3 subtype avian influenza viruses isolated from domestic ducks and wild birds in Korea and their pathogenic potential in chickens and ducks. Vet Microbiol. 2012;155:147–57. https://doi.org/10.1016/j.vetmic.2011.08.028
6. Anthony SJ, St Leger JA, Pugliares K, Ip HS, Chan JM, Carpenter ZW, et al. Emergence of fatal avian influenza in New England harbor seals. MBio. 2012;3:e00166–12. https://doi.org/10.1128/mBio.00166-12
7. Guo Y, Wang M, Kawaoka Y, Gorman O, Ito T, Saito T, et al. Characterization of a new avian-like influenza A virus from horses in China. Virology. 1992;188:245–55. https://doi.org/10.1016/0042-6822(92)90754-D
8. Tu J, Zhou H, Jiang T, Li C, Zhang A, Guo X, et al. Isolation and molecular characterization of equine H3N8 influenza viruses from pigs in China. Arch Virol. 2009;154:887–90. https://doi.org/10.1007/s00705-009-0381-1
9. Crawford PC, Dubovi EJ, Castleman WL, Stephenson I, Gibbs EP, Chen L, et al. Transmission of equine influenza virus to dogs. Science. 2005;310:482–5. https://doi.org/10.1126/science.1117950
10. Guan Y, Vijaykrishna D, Bahl J, Zhu H, Wang J, Smith GJ. The emergence of pandemic influenza viruses. Protein Cell. 2010;1:9–13. https://doi.org/10.1007/s13238-010-0008-z
11. Bao P, Liu Y, Zhang X, Fan H, Zhao J, Mu M, et al. Human infection with a reassortment avian influenza A H3N8 virus: an epidemiological investigation study. Nat Commun. 2022;13:6817. https://doi.org/10.1038/s41467-022-34601-1
12. Yang R, Sun H, Gao F, Luo K, Huang Z, Tong Q, et al. Human infection of avian influenza A H3N8 virus and the viral origins: a descriptive study. Lancet Microbe. 2022;3:e824–34. https://doi.org/10.1016/S2666-5247(22)00192-6

13. Yassine HM, Smatti MK. Will influenza A(H3N8) cause a major public health threat? Int J Infect Dis. 2022;124:35–7. https://doi.org/10.1016/j.ijid.2022.08.028
14. Yang J, Yang L, Zhu W, Wang D, Shu Y. Epidemiological and genetic characteristics of the H3 subtype avian influenza viruses in China. China CDC Wkly. 2021;3:929–36. https://doi.org/10.46234/ccdcw2021.225
15. Zou S, Tang J, Zhang Y, Liu L, Li X, Meng Y, et al. Molecular characterization of H3 subtype avian influenza viruses based on poultry-related environmental surveillance in China between 2014 and 2017. Virology. 2020;542:8–19. https://doi.org/10.1016/j.virol.2020.01.003
16. Cui H, Shi Y, Ruan T, Li X, Teng Q, Chen H, et al. Phylogenetic analysis and pathogenicity of H3 subtype avian influenza viruses isolated from live poultry markets in China. Sci Rep. 2016;6:27360. https://doi.org/10.1038/srep27360
17. Suttie A, Karlsson EA, Deng YM, Hurt AC, Greenhill AR, Barr IG, et al. Avian influenza in the Greater Mekong Subregion, 2003–2018. Infect Genet Evol. 2019;74:103920. https://doi.org/10.1016/j.meegid.2019.103920
18. Olszewska M, Smietanka K, Minta Z. Phylogenetic studies of H3 low pathogenic avian influenza viruses isolated from wild mallards in Poland. Acta Vet Hung. 2013;61:416–24. https://doi.org/10.1556/avet.2013.017
19. Li X, Yang J, Liu B, Jia Y, Guo J, Gao X, et al. Co-circulation of H5N6, H3N2, H3N8, and emergence of novel reassortant H3N6 in a local community in Hunan Province in China. Sci Rep. 2016;6:25549. https://doi.org/10.1038/srep25549
20. Yang D, Liu J, Ju H, Ge F, Wang J, Li X, et al. Genetic analysis of H3N2 avian influenza viruses isolated from live poultry markets and poultry slaughterhouses in Shanghai, China in 2013. Virus Genes. 2015;51:25–32. https://doi.org/10.1007/s11262-015-1198-5
21. Li C, Yu M, Liu L, Sun H. Characterization of a novel H3N2 influenza virus isolated from domestic ducks in China. Virus Genes. 2016;52:568–72. https://doi.org/10.1007/s11262-016-1323-0
22. Liu M, He S, Walker D, Zhou N, Perez DR, Mo B, et al. The influenza virus gene pool in a poultry market in south central China. Virology. 2003;305:267–75. https://doi.org/10.1006/viro.2002.1762
23. Katoh K, Standley DM. MAFFT multiple sequence alignment software version 7: improvements in performance and usability. Mol Biol Evol. 2013;30:772–80. https://doi.org/10.1093/molbev/mst010
24. Price MN, Dehal PS, Arkin AP. FastTree 2—approximately maximum-likelihood trees for large alignments. PLoS One. 2010;5:e9490. https://doi.org/10.1371/journal.pone.0009490
25. Suchard MA, Lemey P, Baele G, Ayres DL, Drummond AJ, Rambaut A. Bayesian phylogenetic and phylodynamic data integration using BEAST 1.10. Virus Evol. 2018;4:vey016. https://doi.org/10.1093/ve/vey016
26. Thompson AJ, Paulson JC. Adaptation of influenza viruses to human airway receptors. J Biol Chem. 2021;296:100017. https://doi.org/10.1074/jbc.REV120.013309
27. Hu M, Yuan S, Zhang K, Singh K, Ma Q, Zhou J, et al. PB2 substitutions V598T/I increase the virulence of H7N9 influenza A virus in mammals. Virology. 2017;501:92–101. https://doi.org/10.1016/j.virol.2016.11.008
28. Gao W, Zu Z, Liu J, Song J, Wang X, Wang C, et al. Prevailing I292V PB2 mutation in avian influenza H9N2 virus increases viral polymerase function and attenuates IFN-β induction in human cells. J Gen Virol. 2019;100:1273–81. https://doi.org/10.1099/jgv.0.001294
29. Xiao C, Ma W, Sun N, Huang L, Li Y, Zeng Z, et al. PB2-588 V promotes the mammalian adaptation of H10N8, H7N9 and H9N2 avian influenza viruses. Sci Rep. 2016;6:19474. https://doi.org/10.1038/srep19474
30. Fan S, Deng G, Song J, Tian G, Suo Y, Jiang Y, et al. Two amino acid residues in the matrix protein M1 contribute to the virulence difference of H5N1 avian influenza viruses in mice. Virology. 2009;384:28–32. https://doi.org/10.1016/j.virol.2008.11.044
31. Campbell PJ, Kyriakis CS, Marshall N, Suppiah S, Seladi-Schulman J, Danzy S, et al. Residue 41 of the Eurasian avian-like swine influenza A virus matrix protein modulates virion filament length and efficiency of contact transmission. J Virol. 2014;88:7569–77. https://doi.org/10.1128/JVI.00119-14
32. Liu Q, Lu L, Sun Z, Chen G-W, Wen Y, Jiang S. Genomic signature and protein sequence analysis of a novel influenza A (H7N9) virus that causes an outbreak in humans in China. Microbes Infect. 2013;15:432–9. https://doi.org/10.1016/j.micinf.2013.04.004
33. Lee J, Song YJ, Park JH, Lee JH, Baek YH, Song MS, et al. Emergence of amantadine-resistant H3N2 avian influenza A virus in South Korea. J Clin Microbiol. 2008;46:3788–90. https://doi.org/10.1128/JCM.01427-08
34. Nguyen HT, Fry AM, Gubareva LV. Neuraminidase inhibitor resistance in influenza viruses and laboratory testing methods. Antivir Ther. 2012;17:159–73. https://doi.org/10.3851/IMP2067
35. Hill NJ, Smith LM, Muzaffar SB, Nagel JL, Prosser DJ, Sullivan JD, et al. Crossroads of highly pathogenic H5N1: overlap between wild and domestic birds in the Black Sea-Mediterranean impacts global transmission. Virus Evol. 2021;7:veaa093. https://doi.org/10.1093/ve/veaa093
36. Hassan KE, Saad N, Abozeid HH, Shany S, El-Kady MF, Arafa A, et al. Genotyping and reassortment analysis of highly pathogenic avian influenza viruses H5N8 and H5N2 from Egypt reveals successive annual replacement of genotypes. Infect Genet Evol. 2020;84:104375. https://doi.org/10.1016/j.meegid.2020.104375
37. Liu W, Fan H, Raghwani J, Lam TT, Li J, Pybus OG, et al. Occurrence and reassortment of avian influenza A (H7N9) viruses derived from coinfected birds in China. J Virol. 2014;88:13344–51. https://doi.org/10.1128/JVI.01777-14
38. Yu X, Jin T, Cui Y, Pu X, Li J, Xu J, et al. Influenza H7N9 and H9N2 viruses: coexistence in poultry linked to human H7N9 infection and genome characteristics. J Virol. 2014;88:3423–31. https://doi.org/10.1128/JVI.02059-13
39. Lu J, Wu J, Zeng X, Guan D, Zou L, Yi L, et al. Continuing reassortment leads to the genetic diversity of influenza virus H7N9 in Guangdong, China. J Virol. 2014;88:8297–306. https://doi.org/10.1128/JVI.00630-14
40. Wang J, Jin X, Hu J, Wu Y, Zhang M, Li X, et al. Genetic evolution characteristics of genotype G57 virus, a dominant genotype of H9N2 avian influenza virus. Front Microbiol. 2021;12:633835. https://doi.org/10.3389/fmicb.2021.633835
41. Pu J, Wang S, Yin Y, Zhang G, Carter RA, Wang J, et al. Evolution of the H9N2 influenza genotype that facilitated the genesis of the novel H7N9 virus. Proc Natl Acad Sci U S A. 2015;112:548–53. https://doi.org/10.1073/pnas.1422456112
42. Pu J, Yin Y, Liu J, Wang X, Zhou Y, Wang Z, et al. Reassortment with dominant chicken H9N2 influenza virus contributed to the fifth H7N9 virus human epidemic. J Virol. 2021;95:e01578-20. https://doi.org/10.1128/JVI.01578-20
43. \Medina RA, García-Sastre A. Influenza A viruses: new research developments. Nat Rev Microbiol. 2011;9:590–603. https://doi.org/10.1038/nrmicro2613
44. Sit THC, Sun W, Tse ACN, Brackman CJ, Cheng SMS, Tang AWY, et al. Novel zoonotic avian influenza A(H3N8)

virus in chicken, Hong Kong, China. Emerg Infect Dis. 2022;28:2009–15. https://doi.org/10.3201/eid2810.221067
45. Deng G, Tan D, Shi J, Cui P, Jiang Y, Liu L, et al. Complex reassortment of multiple subtypes of avian influenza viruses in domestic ducks at the Dongting Lake Region of China. J Virol. 2013;87:9452–62. https://doi.org/10.1128/JVI.00776-13
46. Wan Z, Jiang W, Gong J, Zhao Z, Tang T, Li Y, et al. Emergence of chicken infection with novel reassortant H3N8 avian influenza viruses genetically close to human H3N8 isolate, China. Emerg Microbes Infect. 2022;11:2553–5. https://doi.org/10.1080/22221751.2022.2128437
47. Yuen KY, Chan PK, Peiris M, Tsang DN, Que TL, Shortridge KF, et al. Clinical features and rapid viral diagnosis of human disease associated with avian influenza A H5N1 virus. Lancet. 1998;351:467–71. https://doi.org/10.1016/S0140-6736(98)01182-9
48. Freidl GS, Meijer A, de Bruin E, de Nardi M, Munoz O, Capua I, et al.; FLURISK Consortium. Influenza at the animal-human interface: a review of the literature for virological evidence of human infection with swine or avian influenza viruses other than A(H5N1). Euro Surveill. 2014; 19:8–26. https://doi.org/10.2807/1560-7917.ES2014.19.18.20793
49. Tian J, Li M, Li Y, Bai X, Song X, Zhao Z, et al. H3N8 subtype avian influenza virus originated from wild birds exhibited dual receptor-binding profiles. J Infect. 2023;86:e36–39. https://doi.org/10.1016/j.jinf.2022.10.023
50. Guan L, Shi J, Kong X, Ma S, Zhang Y, Yin X, et al. H3N2 avian influenza viruses detected in live poultry markets in China bind to human-type receptors and transmit in guinea pigs and ferrets. Emerg Microbes Infect. 2019;8:1280–90. https://doi.org/10.1080/22221751.2019.1660590

Address for correspondence: Dayan Wang, Chinese Center for Disease Control and Prevention, 155 Changbai Rd, Changping District, Beijing 102206, China; email: wangdayan@ivdc.chinacdc.cn; Yuelong Shu, School of Public Health (Shenzhen), Shenzhen campus of Sun Yat-sen University, Shenzhen 518107, Guangdong, China; email: shuylong@mail.sysu.edu.cn

Detection of Novel Poxvirus from Gray Seal (*Halichoerus grypus*), Germany

Florian Pfaff, Katharina Kramer, Jacqueline King, Kati Franzke, Tanja Rosenberger, Dirk Höper, Patricia König, Donata Hoffmann, Martin Beer

We detected a novel poxvirus from a gray seal (*Halichoerus grypus*) from the North Sea, Germany. The juvenile animal showed pox-like lesions and deteriorating overall health condition and was finally euthanized. Histology, electron microscopy, sequencing, and PCR confirmed a previously undescribed poxvirus of the *Chordopoxvirinae* subfamily, tentatively named Wadden Sea poxvirus.

Members of the poxvirus subfamily *Chordopoxvirinae* (family *Poxviridae*) infect vertebrates, such as birds, reptiles, and a broad spectrum of mammals. Although some chordopoxviruses have a narrow host range, several can easily jump species barriers and cause severe disease (*1*). Considering the potential zoonotic and epizootic potential of chordopoxviruses, constant monitoring and adaptation of diagnostic procedures are essential. With the advent of metagenomic sequencing, novel chordopoxviruses have been identified that are genetically diverse and were not readily detectable by using established PCR-based diagnostics (*2*–*4*).

We report a case of a poxvirus infection in a gray seal (*Halichoerus grypus*) from the North Sea near Germany. We identified a novel chordopoxvirus that was phylogenetically divergent from other known poxviruses of gray seals.

Case Study

In June 2020, a juvenile gray seal was nursed at a rehabilitation center in Friedrichskoog, Germany (Appendix Figure 1, https://wwwnc.cdc.gov/EID/article/29/6/22-1817-App1.pdf) and was about to be released back into the wild when staff noticed pox-like lesions on its hind flipper (Appendix Figure 2). The seal's overall health condition deteriorated over the next 3 weeks, and it had dyspnea, vomiting after feeding, and apathy; it was humanely euthanized. At necropsy, the seal was in good body condition (abdominal blubber ≈35 mm, reference >30 mm). We noted 2 prominent verrucous nodules on the right hind flipper (Appendix Figure 2). We also found severe emphysema of the mediastinum and a focal, adhesive pleuritis. No other organs had lesions. Histologic examination of both nodules (Appendix) revealed severe papillary epithelial hyperplasia, acanthosis, ballooning degeneration, large eosinophilic cytoplasmatic inclusion bodies in the stratum spinosum, moderate hyperkeratosis, and severe ulceration with hemorrhages (Figure 1, panels A, B). In addition, we observed multifocal severe infiltrations of neutrophils. In the liver, we detected a focally necrotizing hepatitis with ballooning degeneration of nuclei and a focal granulomatous subcapsular hepatitis with intralesional parasites and calcification. We found further inflammatory changes in the lungs (Figure 1, panel C), which had multifocal moderate pneumonia with infiltration of mononuclear cells and neutrophils; the heart had focal severe mononuclear myocarditis; and the duodenum had moderate diffuse lymphoplasmacellular enteritis. We also observed depletion of lymphocytic organs, including a severe atrophy of the thymus.

Results of quantitative PCRs (qPCRs) specific for orthopoxvirus (*5*) and parapoxvirus (*6*), canine alphaherpesvirus 1, influenza A virus, canine morbillivirus, and *Brucella* sp. were negative for lung and skin lesion tissue. We isolated an *Escherichia coli* strain from lung, mediastinum, liver, kidney, and intestines.

We used electron microscopy to analyze lung tissue and detected typical poxvirus-like virions, which were ovoid in shape and ≈250 nm long and ≈200 nm wide (Figure 1, panel D). The surface structures resembled typical orthopox-like randomly arranged tubular

Author affiliations: Friedrich-Loeffler-Institute, Greifswald, Germany (F. Pfaff, J. King, K. Franzke, D. Höper, P. König, D. Hoffmann, M. Beer); Landeslabor Schleswig-Holstein, Neumünster, Germany (K. Kramer); Seehundstation Friedrichskoog e.V., Friedrichskoog, Germany (T. Rosenberger)

DOI: https://doi.org/10.3201/eid2906.221817

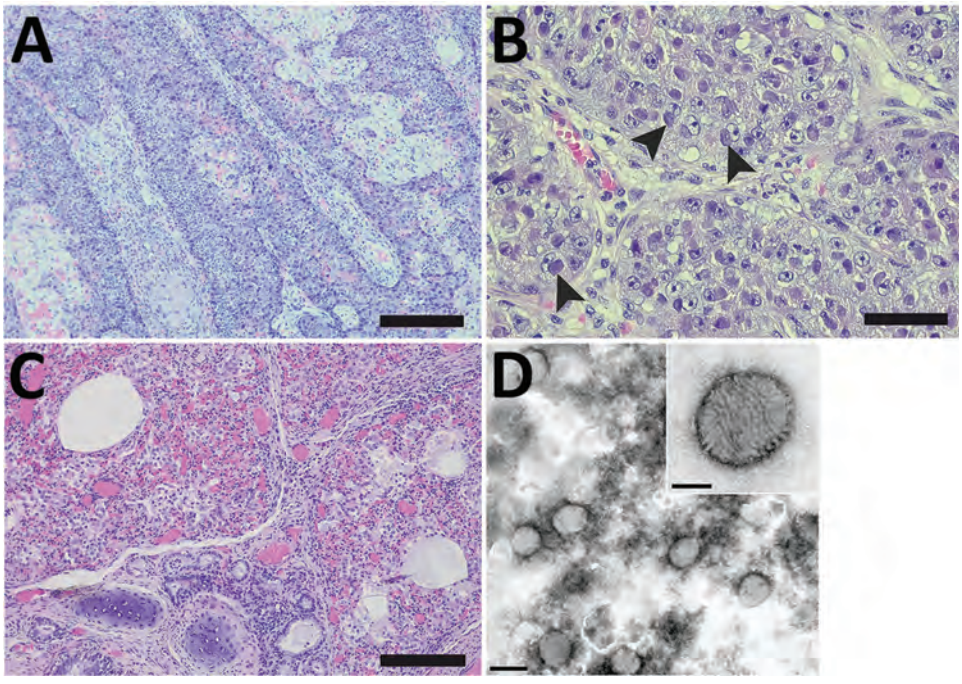

Figure 1. Histopathology and electron microscopy of nodules and lung tissue from a gray seal (*Halichoerus grypus*) with novel poxvirus, North Sea, Germany. A) Histopathology of nodules shows severe papillary epithelial hyperplasia with infiltration of neutrophils. Scale bar indicates 200 µm. B) Histopathology of ballooning degeneration of epithelial cells. Arrows indicate large eosinophilic intracytoplasmic inclusion bodies. Scale bar indicates 50 µm. C) Histopathology of the lung shows multifocal moderate pneumonia with infiltration of mononuclear cells and neutrophils with proliferation of pneumocytes type II and intra-alveolar histiocytosis, severe atelectasis, and hyperemia. Scale bar indicates 100 µm. D) Negative-contrast electron microscopy of lung tissue. Microscopy revealed poxvirus-like viral particles. Scale bar indicates 300 nm. Inset: closeup of poxvirus-like particles, which had an oval shape ≈250 nm × ≈200 nm and an irregular surface with randomly arranged tubular structures; scale bar indicates 100 nm.

units. However, the virion morphology did not enable assignment to a poxvirus genus.

We isolated DNA from a pool of lung and skin lesion tissue and sequenced DNA using Ion Torrent S5XL (Thermo Fisher Scientific, https://www.thermofisher.com) (*7*), NovaSeq (Illumina, https://www.illumina.com), and MinION Mk1C (Oxford Nanopore Technologies, https://nanoporetech.com) sequencing technologies (Appendix). We combined the reads in a hybrid assembly, which resulted in a complete poxviral genome (mean coverage ≈650). We were able to confirm completeness of the genome because the terminal repeats contained the terminal hairpin region.

We screened several organs by using 2 different virus-specific qPCRs (Appendix). Results from both qPCR panels were consistent and we detected the highest viral loads in the skin lesion and parts of the lung (Table).

We tentatively named the poxvirus Wadden Sea poxvirus (WSPV) to reflect the geographic origin of the infected gray seal, which was found in the Wadden Sea, an intertidal zone in the southeastern part of the North Sea, Germany (Appendix Figure 1). We submitted the annotated WSPV genome sequence to the International Nucleotide Sequence Database Collaboration (https://www.insdc.org; accession no. OP810554).

WSPV had one of the smallest genomes (124,614 bp) and lowest guanine-cytosine content (≈22.5%) described so far among chordopoxviruses. The unique core genome of 117,842 bp was flanked by 2 inverted terminal repeats of 3,386 bp each. We identified 124 unique potential open reading frames (ORFs), of which 3 were duplicated in the inverted terminal repeats. BLASTp (https://blast.ncbi.nlm.nih.gov/Blast.cgi) identified 111 ORFs representing orthologs of poxvirus proteins. Nine ORFs encoded proteins that were not related to known poxvirus proteins but showed sequence similarity to eukaryote proteins, and 4 ORFs remained unclassified.

Table. Quantitative PCR detection of novel poxvirus from different tissues of a gray seal (*Halichoerus grypus*), Germany*

Sample	Cycle quantification value	
	Panel 1, viral DNA polymerase	Panel 2, viral RNA polymerase
Skin lesion	9.1	8.9
Lung 1	18.2	18.2
Lung 2	32.3	31.3
Lymph nodes	25.0	24.6
Uterus	26.5	26.2
Spleen	27.2	27.2
Kidney	28.8	28.8
Blood, EDTA	32.2	31.5
Brain	32.9	33.7
Liver	33.7	32.7

*Novel virus is tentatively named Wadden Sea virus.

For phylogenetic classification, we compared the amino acid sequences encoded by 15 poxvirus core genes from WSPV with the respective homologs from 47 representative poxviruses (Appendix). WSPV formed a separate phylogenetic branch that did not fall within any of the established genera (Figure 2) and likely is a new species within a novel genus of the subfamily *Chordopoxvirinae*. Of note, a sequence comparison of the predicted WSPV DNA polymerase protein to the nonredundant BLAST database revealed a 96.3% sequence identity with a partial sequence from a Steller sea lion poxvirus (GenBank accession no. AAR06586.1), but other poxviruses had a sequence identity <77%.

Conclusions

Infections with poxviruses have been reported from gray seals and harbor seals (*Phoca vitulina*), both of which live in the North Sea, Germany. Poxviruses have also been reported in other pinniped species and infections are usually associated to subclades of parapoxviruses, called sealpox or sea lion pox virus (*8*–*10*). Ulcerative to proliferative, nodular, cutaneous, and mucosal lesions have been found in seals infected with parapoxviruses (*10*–*12*). The nodules usually heal spontaneously, but healing lasts from several weeks up to a few months. The illness rate is high, but death rates are low (*13*). Rarely, nodules in

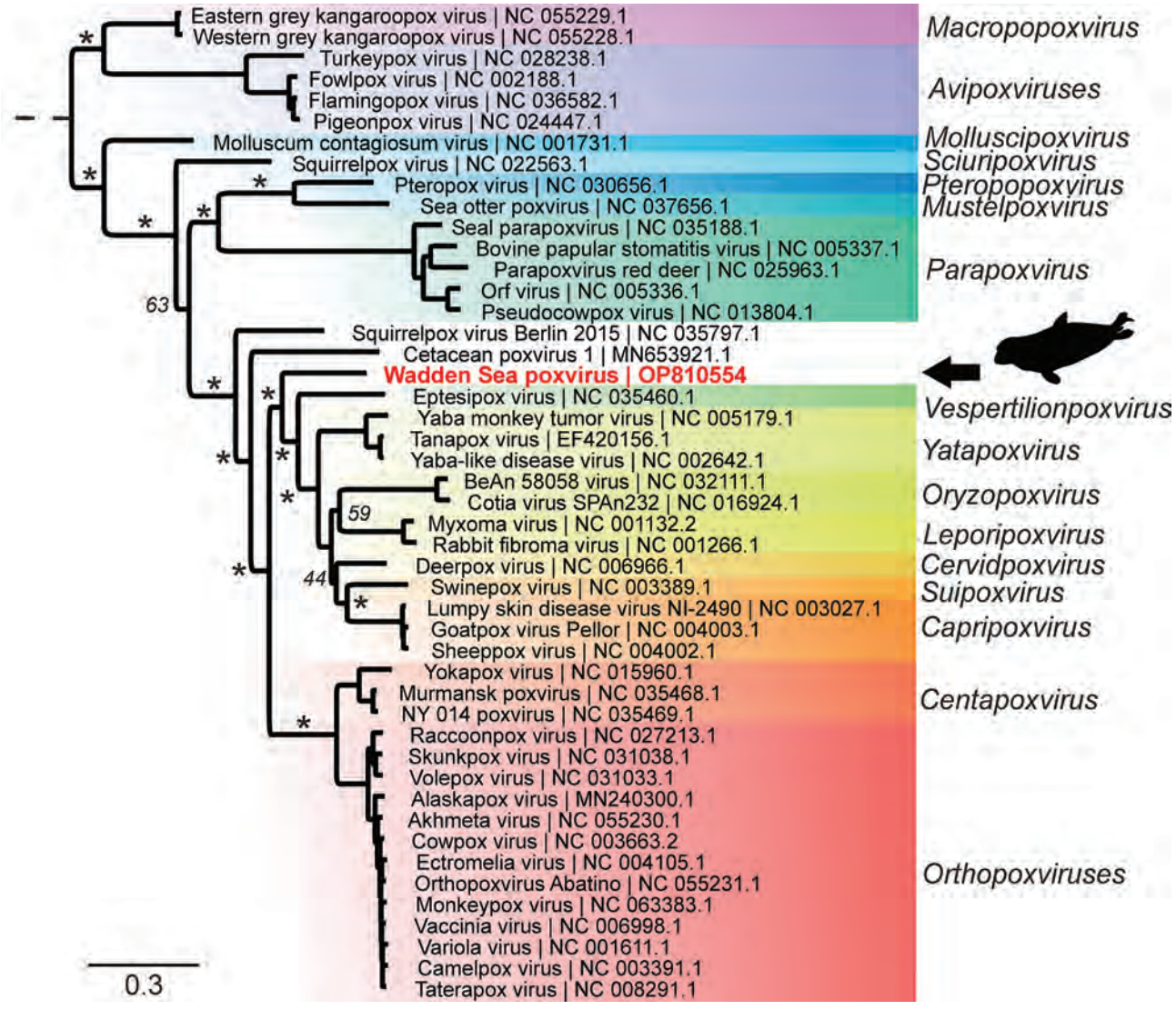

Figure 2. Phylogenetic tree of novel poxvirus detected from gray seal (*Halichoerus grypus*), Germany. Sequencing resulted in a complete poxvirus genome and the virus was tentatively named Wadden Sea poxvirus (red text). Phylogenetic analysis of 15 concatenated viral proteins (alignment of 9,130 aa) showed that Wadden Sea poxvirus (black arrow) is a member of the subfamily *Chordopoxvirinae* but might resemble a novel species distant from the established genera. Asterisks indicate major branches of the bootstrap support at >90%. Scale bar indicates amino acid substitutions per site.

the oral cavity can lead to problems during feeding, and secondary bacterial infection can fatally impair respiratory functions (*14*). However, in the case we report, we could not link the animal's overall deteriorating health condition and severe pneumonia to oral lesions. We considered the cultured *E. coli* strain a facultative pathogen that might have been involved in disease; however, postmortem contamination might be more likely.

We did not detect any parapoxvirus DNA, but sequencing revealed WSPV, a novel poxvirus that is phylogenetically distinct from any other members of the subfamily *Chordopoxvirinae*. The high loads of viral DNA in several organs (Table), and the observed histopathologic changes suggested a generalized infection with systemic pathology. Lesion associated detection of high viral loads (cycle quantification [cq] values for skin cq ≈9, for lung cq ≈18) indicated that the WSPV infection was likely responsible for the gray seal's disease and severe pneumonia. However, other factors might have been involved, and the source of infection, the potential natural reservoir, and the zoonotic potential of WSPV are unknown. None of the contact animals within the rehabilitation center had similar lesions develop and so far, no further cases have been reported.

Sequence comparison of WSPV showed that a close relative of this novel poxvirus has been detected in a cutaneous lesion of a young Steller sea lion (*Eumetopias jubatus*) from Prince William Sound, Alaska, USA (*15*). This finding suggests a geographically wide distribution of WSPV or WSPV-related viruses and the potential to infect other pinnipeds. As noted in the case we describe, WSPV can cause severe disease. Therefore, future diagnostic considerations for pox-like lesions of pinniped species should include WSPV.

Acknowledgments

We gratefully acknowledge Patrick Zitzow for excellent technical assistance with metagenomic sequencing and Mandy Jörn for the graphic design of electron microscope pictures.

About the Author

Dr. Pfaff is a biotechnologist and the head of the Laboratory for Applied Bioinformatics and Sequencing of Viral Genomes and Transcriptomes at the Friedrich-Loeffler-Institut, Greifswald, Germany. His main research interests are discovery, characterization, and classification of viruses using high-throughput sequencing and bioinformatics.

References

1. McFadden G. Poxvirus tropism. Nat Rev Microbiol. 2005;3:201–13. https://doi.org/10.1038/nrmicro1099
2. Hodo CL, Mauldin MR, Light JE, Wilkins K, Tang S, Nakazawa Y, et al. Novel poxvirus in proliferative lesions of wild rodents in east central Texas, USA. Emerg Infect Dis. 2018;24:1069–72. https://doi.org/10.3201/eid2406.172057
3. David D, Davidson I, Berkowitz A, Karniely S, Edery N, Bumbarov V, et al. A novel poxvirus isolated from an Egyptian fruit bat in Israel. Vet Med Sci. 2020;6:587–90. https://doi.org/10.1002/vms3.233
4. Wibbelt G, Tausch SH, Dabrowski PW, Kershaw O, Nitsche A, Schrick L. Berlin squirrelpox virus, a new poxvirus in red squirrels, Berlin, Germany. Emerg Infect Dis. 2017;23:1726–9. https://doi.org/10.3201/eid2310.171008
5. Olson VA, Laue T, Laker MT, Babkin IV, Drosten C, Shchelkunov SN, et al. Real-time PCR system for detection of orthopoxviruses and simultaneous identification of smallpox virus. J Clin Microbiol. 2004;42:1940–6. https://doi.org/10.1128/JCM.42.5.1940-1946.2004
6. Nitsche A, Büttner M, Wilhelm S, Pauli G, Meyer H. Real-time PCR detection of parapoxvirus DNA. Clin Chem. 2006;52:316–9. https://doi.org/10.1373/clinchem.2005.060335
7. Wylezich C, Papa A, Beer M, Höper D. A versatile sample processing workflow for metagenomic pathogen detection. Sci Rep. 2018;8:13108. https://doi.org/10.1038/s41598-018-31496-1
8. Tryland M, Klein J, Nordøy ES, Blix AS. Isolation and partial characterization of a parapoxvirus isolated from a skin lesion of a Weddell seal. Virus Res. 2005;108:83–7. https://doi.org/10.1016/j.virusres.2004.08.005
9. Costa H, Klein J, Breines EM, Nollens HH, Matassa K, Garron M, et al. A comparison of parapoxviruses in North American pinnipeds. Front Vet Sci. 2021;8:653094. https://doi.org/10.3389/fvets.2021.653094
10. Günther T, Haas L, Alawi M, Wohlsein P, Marks J, Grundhoff A, et al. Recovery of the first full-length genome sequence of a parapoxvirus directly from a clinical sample. Sci Rep. 2017;7:3734. https://doi.org/10.1038/s41598-017-03997-y
11. Roess AA, Levine RS, Barth L, Monroe BP, Carroll DS, Damon IK, et al. Sealpox virus in marine mammal rehabilitation facilities, North America, 2007–2009. Emerg Infect Dis. 2011;17:2203–8. https://doi.org/10.3201/eid1712.101945
12. Müller G, Gröters S, Siebert U, Rosenberger T, Driver J, König M, et al. Parapoxvirus infection in harbor seals (*Phoca vitulina*) from the German North Sea. Vet Pathol. 2003;40:445–54. https://doi.org/10.1354/vp.40-4-445
13. Hicks BD, Worthy GA. Sealpox in captive grey seals (*Halichoerus grypus*) and their handlers. J Wildl Dis. 1987;23:1–6. https://doi.org/10.7589/0090-3558-23.1.1
14. Tryland M. Seal parapoxvirus. In: Liu D, editor. Molecular detection of human viral pathogens, 1st edition. New York: CRC Press; 2010. p. 1029–38.
15. Bracht AJ, Brudek RL, Ewing RY, Manire CA, Burek KA, Rosa C, et al. Genetic identification of novel poxviruses of cetaceans and pinnipeds. Arch Virol. 2006;151:423–38. https://doi.org/10.1007/s00705-005-0679-6

Address for correspondence: Martin Beer, Friedrich-Loeffler-Institut, Bundesforschungsinstitut für Tiergesundheit, Südufer 10, Greifswald 17493, Germany; email: Martin.Beer@fli.de

Tanapox, South Africa, 2022

Monica Birkhead,[1] Wayne Grayson,[1] Antoinette Grobbelaar, Veerle Msimang, Naazneen Moolla, Angela Mathee, Lucille Blumberg, Terry Marshall, Daniel Morobadi, Mirjana Popara, Jacqueline Weyer

Tanapox is a rarely diagnosed zoonosis known to be endemic to equatorial Africa. All previously reported human cases were acquired within 10° north or south of the Equator, most recently 19 years ago. We describe a human case of tanapox in South Africa (24° south of the Equator). Expanded surveillance for this pathogen is warranted.

Tanapox is a rarely diagnosed zoonosis endemic to equatorial Africa. Only 4 exported cases from Africa involving either human or nonhuman primates have been reported (Table). Initial human outbreaks, in 1957 and 1962, were recorded from the Tana River Valley of Kenya, and the etiologic agent was subsequently isolated and described as Tanapox virus (TANV) (genus *Yatapoxvirus*, family *Poxviridae*) in 1965 (*1*). Subsequently, the occurrence of tanapox in research laboratory primates imported into the United States (*2*,*3*) led to a serologic survey of 12 nonhuman primate species from Kenya, Ethiopia, Cameroon, Côte d'Ivoire, Liberia, and Senegal; seropositivity was detected in all species surveyed in those countries (*8*). Therefore, nonhuman primates across equatorial Africa were surmised to be the natural reservoirs of TANV and humans incidental hosts (*3*,*8*). On the basis of the overlap between human tanapox cases and the geographic ranges of selected nonhuman primates, an ecologic niche model predicted that tanapox could be found from Somalia to Senegal, with the most southerly range above the Tropic of Capricorn (*9*).

The epidemiology and natural ecology of tanapox is largely unknown, but previous reports indicate that all infected humans are equally affected, regardless of age group and sex. Serologic surveys conducted in Tana River communities indicated 16.3% prevalence in 1971 and 9.2% in 1976 (*10*). Human-to-human transmission is rare, and although transmission from nonhuman primates to humans by contact or inoculation has been noted under laboratory conditions, natural human infections are more likely to be acquired by mechanical transmission from contaminated mouthparts of hematophagous arthropods (*2*–*4*). This vector theory arose because of the synchronicity between tanapox outbreaks and the increased arthropod activity associated with seasonal high temperatures, high rainfall, and flooding in the riparian areas in which surveillance was done (*1*,*3*,*9*). The similarities in the distribution and incidence of TANV and West Nile virus antibodies in serum samples collected in the Tana River Valley in 1971 led to the suggestion that both viruses are transmitted in the same way (i.e., by a culicine mosquito, probably a species of *Mansonia*) (*1*,*3*).

In humans, tanapox typically manifests with 1 or 2 characteristic, nodular skin lesions that are large, raised, umbilicated, and painful and generally ulcerate without becoming pustular (in contrast to lesions observed in most other poxvirus infections) (*1*,*3*,*7*). The lesions may be associated with localized lymphadenopathy, and their gradual development is preceded by a mild, short-lived febrile illness, with possible pruritus and myalgia leading to prostration and headaches (*1*–*3*,*5*,*6*). Histologically, lesions are restricted to the epithelial layers, with cells containing eosinophilic cytoplasmic inclusions and vacuolated nuclei (*1*,*2*,*7*). TANV virions are poxlike but cannot be distinguished microscopically from the other species in the genus (e.g., Yaba monkey tumor virus) or

Author affiliations: National Institute for Communicable Diseases, Johannesburg, South Africa (M. Birkhead, A. Grobbelaar, V. Msimang, N. Moolla, L. Blumberg, J. Weyer); Ampath Laboratories, Centurion, South Africa (W. Grayson, T. Marshall, D. Morobadi); University of the Witwatersrand, Johannesburg (W. Grayson, J. Weyer); South African Medical Research Council, Cape Town, South Africa (A. Mathee); University of Johannesburg, Johannesburg (A. Mathee); University of Pretoria, Pretoria, South Africa (N. Moolla, L. Blumberg, J. Weyer); Right to Care, Johannesburg (L. Blumberg); University of the Free State, Bloemfontein, South Africa (D. Morobadi); Mediclinic, Sandton, South Africa (M. Popara)

DOI: https://doi.org/10.3201/eid2906.230326

[1]These first authors contributed equally to this article.

Table. History of recorded tanapox cases in humans and nonhuman primates, 1957–2004

Year	Location of exposure	Epidemiologic description	Reference
1957	Ngau, Kenya (Tana River Valley)	Several Wapakomo school children diagnosed with tanapox	(*1*)
1962	Between Garissa and Garsen, Kenya (Tana River Valley)	About 50 case-patients from the Wapakomo tribe	(*1*)
1965–1966*	Holding facilities of primate supplier, USA	Infected macaques from the same supplier, distributed to 3 primate research centers in Oregon, California, and Texas, USA	(*2*–*4*)
1966–1968†	Laboratory-acquired	Several laboratory workers in Oregon and California became infected after handling of laboratory macaques	(*2*–*4*)
1971†	Laboratory-acquired	Human volunteer was inoculated with tanapox virus, and clinical progression of the disease was monitored and recorded	(*1*)
1979–1983	Mongala, Democratic Republic of Congo (then Zaire)	A total of 357 cases reported, of which 264 were confirmed by laboratory testing	(*3*)
1999	Bagamoyo, Tanzania	Traveler from Germany diagnosed with tanapox upon return from Tanzania	(*5*)
2002†	Sierra Leone	Person from Sierra Leone admitted to hospital in New York, USA, 2 weeks after arrival from Sierra Leone	(*6*)
2004	Republic of Congo	Volunteer working with chimpanzees has onset of tanapox; only diagnosed after return to USA	(*7*)

*Initially identified as Yaba-like disease virus; subsequent research indicated homology with *Tanapoxvirus*.
†Date of report (date of actual case not published).

from *Orthopoxvirus* virions (*3*,*7*). Clinical differential diagnoses have included cutaneous anthrax, other poxvirus infections, sporotrichosis, *Mycobacterium marinum* infection, spotted fever group rickettsial infections, tropical ulcers, insect bites, and scabies (*3*,*7*,*9*). The disease is self-limiting, with no recorded fatalities (*3*). We describe a case of tanapox in South Africa, 19 years after the last published report of human tanapox (*7*).

The Study

We obtained written consent from the patient in this study and received ethics clearance from the Faculty of Health Sciences of University of the Witwatersrand, Johannesburg (approval no. M210752). During February 2–6, 2022, a 61-year old woman served as a volunteer in Kruger National Park (KNP), South Africa. She stayed in a tented bush camp along the banks of the Sand River, ≈20 km from the town of Skukuza (24°59′43″ S, 31°35′34″E) (Figure 1; Appendix Figure 1, https://wwwnc.cdc.gov/EID/article/29/6/23-0326-App1.pdf). The woman noted large numbers of arthropods (e.g., spiders, insects, and ticks) around the camp site and reported being bitten on several occasions on various body parts (especially on her hands, shoulders, arms, and back). Because of heavy

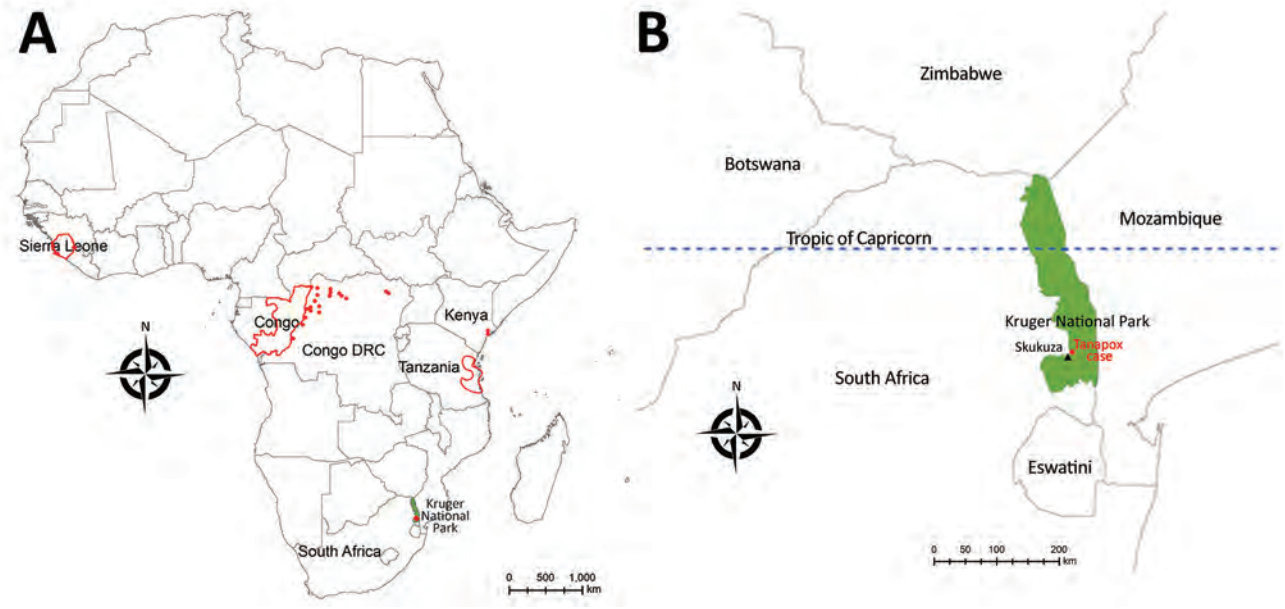

Figure 1. Geographic distribution of recorded human cases of tanapox. A) Locations of previous tanapox cases reported in the literature. Red dots indicate cases acquired locally; red outlines indicate regions of countries visited by travelers to Africa. B) Location of the case acquired in Kruger National Park, South Africa, 2022. Green shading shows the park's location; black triangle indicates town of Skukuza.

rains, trails were overgrown, so bushwalks resulted in scratches on her arms, and many ticks were found on her clothing. During February 7–9, she continued her visit to KNP as a guest in air-conditioned accommodation and had no further direct contact with vegetation. She reported no direct contact with primates, although vervet monkeys (*Chlorocebus pygerythrus*) are seen near the camps.

Two days after her return to urban Johannesburg, she experienced pruritus at the base of her thumb on the dorsal side of her right hand and noticed a pale blister forming there, followed 2 days later by another blister on the side of her left hand. Initially, both papules were round and white with erythematous edges (Appendix Figure 2, panel A), but they became dome-shaped, firm, smooth, umbilicated nodules 12–15 mm in size (Appendix Figure 2, panels B, C). A third lesion formed on the woman's mid-upper back but was perforated through chafing from clothing. About 3 days after the appearance of the first lesion, the woman reported feeling unwell, fatigued, and feverish and had severe headaches. No lymphadenopathy was recorded. The lesions were persistently painful and hypersensitive, but none were cystic or became pustular. Instead, they became ulcerated, open, and dry (Appendix Figure 2, panel D), and all 3 resolved over a period of 6 weeks, leaving slight discoloration. After discovering the third lesion, the woman sought medical attention. Differential diagnoses included allergies, cellulitis, erysipelas, pyoderma gangrenosum, or granulomas caused by foreign bodies or insect bites (e.g., mango fly bites).

Histopathologic examination of a lesion biopsy indicated a possible pox infection, given the presence of acidophilic intracytoplasmic inclusion bodies and cellular vacuolation (Figure 2, panel A). The lesion was confined to the epithelial layers with many cells that had vacuolated nuclei, and we observed ballooning cells in the deeper epithelial layer (Figure 2, panel B). Subsequently, we took an additional biopsy for electron microscopy and 2 lesion swab specimens for molecular characterization. After routine processing (Appendix), we observed numerous brick-shaped virions 287 nm x 221 nm with distinct surface tubules and generally an outer membrane layer (capsular form) (Figure 2, panel C). We used 1 dry swab sample for PCR analysis (Appendix), and partial sequence analysis indicated clustering with available TANV sequences (Appendix Figure 3). Attempts at full genomic sequencing and virus isolation (from the second swab specimen) were unsuccessful, possibly because of the limited clinical material available.

Recent surveys of the mosquito distribution in southern Africa have found that 2 culicine genera (*Culex* and *Mansonia*) comprise 91% of the mosquito population in the town of Skukuza (*11*). Weather conditions at the time of the case exposure were conducive to vector replication; recent rainfall was up to 147% higher than the average annual cumulative total (*12*), and ambient temperatures were 100°F–104°F (38°C–40°C) (*13*). In terms of virus reservoirs, a limitation of Monroe et al.'s model (*9*) was that the restricted range of recorded human cases determined the exclusion of many other primates with extensive geographic ranges. Our report extends this range beyond the most southerly predictions of the model, which increases the pool of potential reservoir hosts.

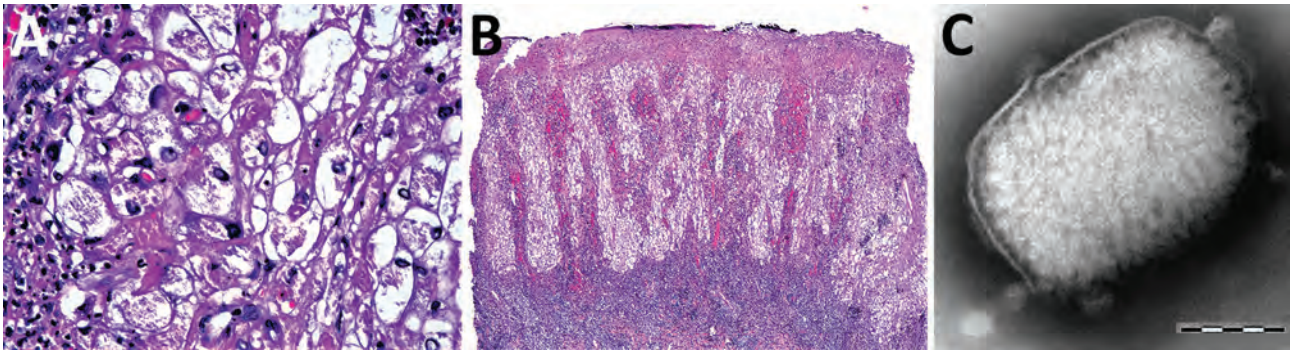

Figure 2. Diagnostic light and electron microscopy of tanapox lesion biopsies from a case-patient, South Africa, 2022. A) High-power photomicrograph of initial skin biopsy, showing prominent vacuolation of epidermal keratinocytes, granular intracytoplasmic inclusions, and intranuclear pseudoinclusions. Hematoxylin and eosin stain; original magnification ×400. B) Low-power photomicrograph of initial skin biopsy, showing a superficially eroded hyperplastic epidermis, with cytoplasmic pallor and a dense underlying superficial dermal lymphoid infiltrate. Hematoxylin and eosin stain; original magnification ×40. C) Negatively stained tanapox virus virion with surface tubules evident beneath the remains of the surrounding membrane. Virion dimensions were 159–327 nm × 186–289 nm. Scale bar indicates 100 nm.

Conclusions

The clinical findings for this reported case were in keeping with previous clinical reports of tanapox, and the diagnosis was supported by histopathology, electron microscopy, and molecular analyses. The importance and continuing relevance of histopathology and microscopy to the diagnosis and investigation of zoonotic disease were clearly illustrated. Given that tanapox is a vectorborne disease, many drivers, including anthropogenic destruction of wildlife habitats, environmental instability, and global climate change, may influence its emergence (*14*). Improved surveillance, including studies relating to the ecology and epidemiology of TANV in vectors, hosts, and humans, is warranted.

Acknowledgments

We thank Nosihle Msomi for her support in sequencing and sequencing analysis performed in this study.

About the Author

Dr. Birkhead is a medical scientist in the electron microscopy laboratory of the National Institute for Communicable Diseases, a division of the National Health Laboratory Service, in Johannesburg, South Africa. Her primary research interests include the use of ultrastructural information for diagnoses of and research on human infectious diseases.

References

1. Downie AW, Taylor-Robinson CH, Caunt AE, Nelson GS, Manson-Bahr PEC, Matthews TCH. Tanapox: a new disease caused by a pox virus. BMJ. 1971;1:363–8. https://doi.org/10.1136/bmj.1.5745.363
2. Downie AW, España C. A comparative study of Tanapox and Yaba viruses. J Gen Virol. 1973;19:37–49. https://doi.org/10.1099/0022-1317-19-1-37
3. Jezek Z, Arita I, Szczeniowski M, Paluku KM, Kalisa R, Nakano JH. Human tanapox in Zaire: clinical and epidemiological observations on cases confirmed by laboratory studies. Bull. World Health Organ. 1985;63:1027–35.
4. Downie AW, España C. Comparison of Tanapox virus and Yaba-like viruses causing epidemic disease in monkeys. J Hyg (Lond). 1972;70:23–32. https://doi.org/10.1017/S0022172400022051
5. Croitoru AG, Birge MB, Rudikoff D, Tan MH, Phelps RG. Tanapox virus infection. Skinmed. 2002;1:156–7. https://doi.org/10.1111/j.1540-9740.2002.01778.x
6. Stich A, Meyer H, Köhler B, Fleischer K. Tanapox: first report in a European traveller and identification by PCR. Trans R Soc Trop Med Hyg. 2002;96:178–9. https://doi.org/10.1016/S0035-9203(02)90295-6
7. Dhar AD, Werchniak AE, Li Y, Brennick JB, Goldsmith CS, Kline R, et al. Tanapox infection in a college student. N Engl J Med. 2004;350:361–6. https://doi.org/10.1056/NEJMoa031467
8. Downie AW. Serological evidence of infection with Tana and Yaba pox viruses among several species of monkey. J Hyg (Lond). 1974;72:245–50. https://doi.org/10.1017/S0022172400023445
9. Monroe BP, Nakazawa YJ, Reynolds MG, Carroll DS. Estimating the geographic distribution of human Tanapox and potential reservoirs using ecological niche modeling. Int J Health Geogr. 2014;13:34. https://doi.org/10.1186/1476-072X-13-34
10. Axford JS, Downie AW. Tanapox. A serological survey of the lower Tana River Valley. J Hyg (Lond). 1979;83:273–6. https://doi.org/10.1017/S0022172400026061
11. Cornel AJ, Lee Y, Almeida APG, Johnson T, Mouatcho J, Venter M, et al. Mosquito community composition in South Africa and some neighboring countries. Parasit Vectors. 2018;11:331. https://doi.org/10.1186/s13071-018-2824-6
12. SANparks Scientific Services. Data and information resources: Kruger climate and rainfall [cited 2023 Mar 27]. https://www.sanparks.org/scientific-services/wp-content/uploads/2022/01/December.pdf
13. Meteoblue. Weather history and climate archive [cited 2023 Mar 27]. https://www.meteoblue.com/en/weather/history-climate/weatherarchive/skukuza_south-africa_954955
14. Carlson CJ, Albery GF, Merow C, Trisos CH, Zipfel CM, Eskew EA, et al. Climate change increases cross-species viral transmission risk. Nature. 2022;607:555–62. https://doi.org/10.1038/s41586-022-04788-w

Address for correspondence: Monica Birkhead, National Institute for Communicable Diseases, Private Bag X4, Sandringham, 2192, South Africa; email: monicab@nicd.ac.za

Replication of Novel Zoonotic-Like Influenza A(H3N8) Virus in Ex Vivo Human Bronchus and Lung

Kenrie P.Y. Hui, John C.W. Ho, Ka-Chun Ng, Samuel M.S. Cheng, Ko-Yung Sit, Timmy W.K. Au, Leo L.M. Poon, John M. Nicholls, Malik Peiris, Michael C.W. Chan

Human infection with avian influenza A(H3N8) virus is uncommon but can lead to acute respiratory distress syndrome. In explant cultures of the human bronchus and lung, novel H3N8 virus showed limited replication efficiency in bronchial and lung tissue but had a higher replication than avian H3N8 virus in lung tissue.

Avian influenza viruses (AIVs) with reassortments between AIVs from domestic poultry and wild birds sporadically cross species barriers, leading to human infections. Viruses with internal genes of H9N2, hemagglutinin, and neuraminidase acquired from wild birds constitute the zoonotic H5N1, H7N9, and H10N8 viruses (*1*–*3*) and can lead to severe influenza.

In 2022, two human infections with novel influenza A(H3N8) viruses were reported in Henan and Hunan Province, China (*4*,*5*). The first case was identified in a 4-year-old boy with acute respiratory distress syndrome, and the second case occurred in a 5-year-old boy with mild disease. Phylogenetic analysis revealed that the novel H3N8 viruses were triple reassortments containing the Eurasian avian H3 gene of wild-bird origin, the North American avian N8 gene derived from the wild bird AIV, and G57 genotype H9N2 internal genes from AIVs found in poultry in China (*6*,*7*). H3N8 viruses that are genetically similar to the zoonotic H3N8 viruses reported in China (*4*,*5*) have been isolated in poultry markets in Hong Kong, China (*8*). Those novel avian H3N8 viruses are antigenically distant from contemporary human influenza A(H3N2) viruses, and little cross-reactive immunity to these chicken H3N8 viruses exists in the human population (*8*). We assessed the replication of the novel influenza A(H3N8) virus in human ex vivo bronchus and lung tissues (Appendix, https://wwwnc.cdc.gov/EID/article/29/6/22-1680-App1.pdf).

Author affiliations: The University of Hong Kong School of Public Health, Hong Kong, China (K.P.Y. Hui, J.C.W. Ho, K.-C. Ng, S.M.S. Cheng, L.L.M. Poon, M. Peiris, M.C.W. Chan); Centre for Immunology and Infection, Hong Kong (K.P.Y. Hui, J.C.W. Ho, L.L.M. Poon, M. Peiris, M.C.W. Chan); The University of Hong Kong Division of Cardiothoracic Surgery, Hong Kong (K.-Y. Sit, T.W.K. Au); The University of Hong Kong School of Clinical Medicine, Hong Kong (J.M. Nicholls)

DOI: https://doi.org/10.3201/eid2906.221680

The Study

The viruses used in this study were H9N2/Y280, pH1N1, avH3N8/MP16, novel H3N8, and H5N1/483 (Appendix Table 1). The novel H3N8 virus was isolated from chickens and is genetically closely related to the virus causing zoonotic human disease in China (A/Henan/4-10CNIC/2022/H3N8) (*8*). Their hemagglutinin genes share a 99.1% similarity, and the neuraminidase genes share a 98.7% similarity. The avH3N8 virus was isolated from wild bird droppings in Mai Po, Hong Kong, and is genetically unrelated to the virus causing zoonotic disease in China. The novel H3N8 virus failed to propagate in Madin-Darby canine kidney (MDCK) cells but could be propagated in eggs and titrated in chicken embryo fibroblasts (DF-1), whereas the other strains could be propagated and titrated in MDCK cells. We performed titration in cells that support the replication of the influenza A viruses rather than in all DF-1 cells, because pH1N1 virus did not replicate in DF-1 cells. We investigated the virus replication kinetics by measuring viral matrix protein segment RNA in culture supernatants using real-time quantitative reverse transcription PCR and 50% tissue culture infectious dose ($TCID_{50}$) assay for infectious virus titers (Figure 1).

In bronchial tissues, pH1N1 virus had a higher level of viral RNA than did avH3N8, novel H3N8, and H5N1, whereas levels of viral RNA of H9N2 virus were higher than those of avH3N8 and H5N1 virus (Figure 1, panels A, C). The viral RNA levels of avH3N8, novel H3N8, and H5N1 virus were similar.

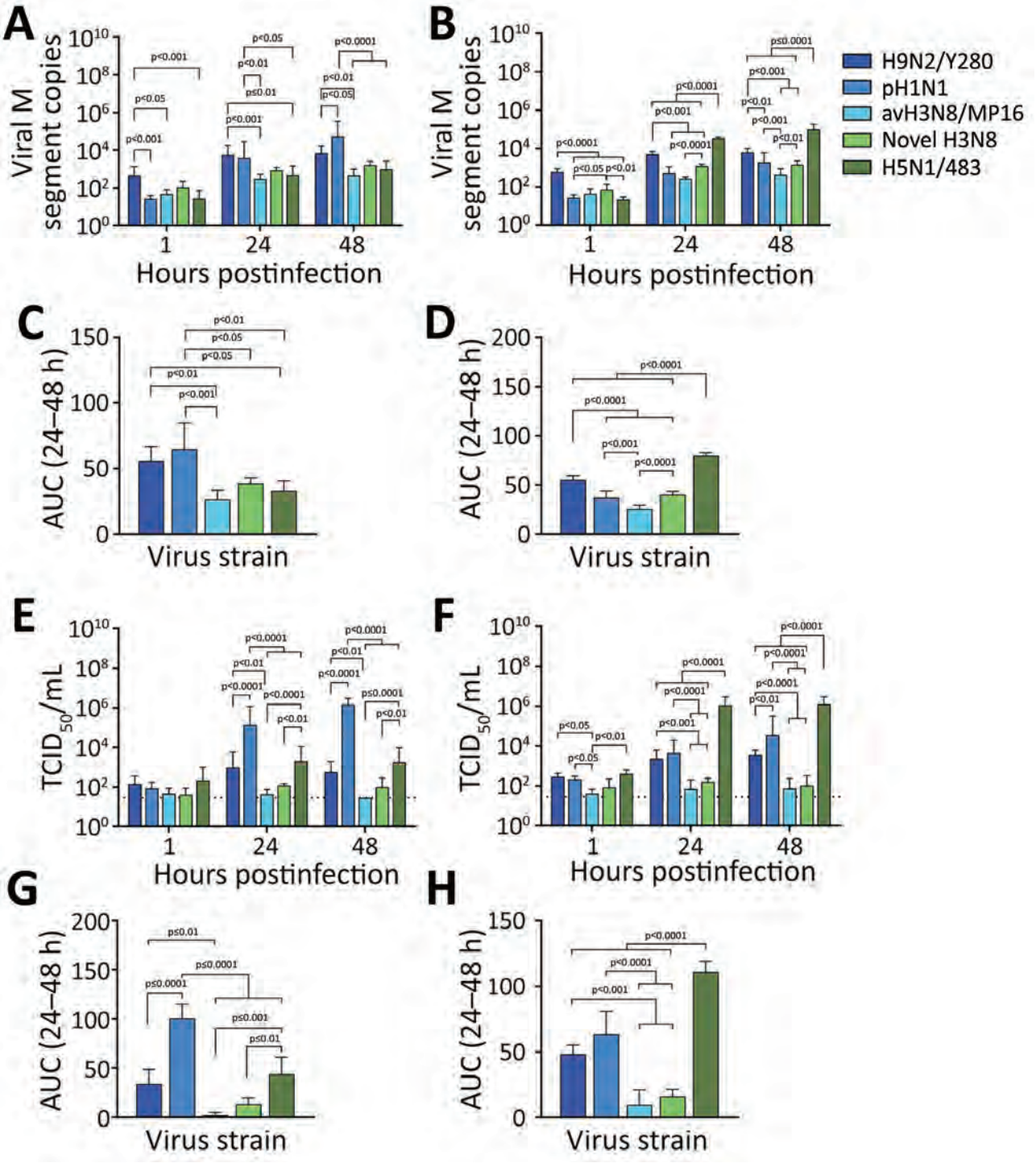

Figure 1. Comparative replication competence of zoonotic-like influenza A(H3N8) viruses isolated from chicken and other human and avian viruses in ex vivo cultures of human bronchus and lung tissue. Viral M segment RNA copies (A, B) and viral titers (E, F) in culture supernatants were collected at 1, 24, and 48 hours postinfection with H9N2/Y280, pH1N1, avH3N8/MP16, novel H3N8, or H5N1/483 viruses and measured by quantitative reverse transcription PCR (A, B) and $TCID_{50}$ (E, F). C, D) Viral load from panels A and B by virus strain. G, H) Viral titers from panels E and F by virus strain. Data are geometric mean ±SD. Statistical analysis was performed using 2-way (A, B, E, F)or 1-way (C, D, G, H) analysis of variance followed by Tukey posttest; $p<0.05$ was considered to be statistically significant. Detailed information on viruses used in study is provided in the Appendix (https://wwwnc.cdc.gov/EID/article/29/6/22-1680-App1.pdf). AUC, area under the curve; M, matrix; $TCID_{50}$, 50% tissue culture infectious dose.

The viral RNA level of H5N1 virus was the highest among all the tested strains in human lung tissues, followed by H9N2 (Figure 1, panels B, D). Viral RNA levels of novel H3N8 and pH1N1 viruses were higher than those of avH3N8 virus. Measurement of viral RNA using quantitative reverse transcription PCR is sensitive, but it cannot distinguish defective viral particles from infectious ones. Therefore, we performed the $TCID_{50}$ assay to monitor the infectious viral titers.

As expected, replication of pH1N1 virus was the highest among all tested strains in human bronchial tissues, in both viral titers and area under the curve values (Figure 1, panels E, G). The titers of H5N1 virus were similar to those of H9N2 virus, whereas H5N1 virus had higher replication competence than did avH3N8 and novel H3N8 viruses. We observed a discrepant trend between viral RNA copies and infectious titers for H9N2. Viral RNA levels of H9N2 were similar to those of pH1N1 (Figure 1, panels A, C), but the infectious titers of H9N2 virus were significantly lower than that of pH1N1 in bronchus (Figure 1, panels E, G).

In lung tissue, H5N1 virus had the highest replication of all strains tested (Figure 1, panels F, H). Similar to pH1N1 virus, H9N2 had higher titers than the 2 H3N8 viruses in lung tissues. avH3N8 had the lowest titer measured by $TCID_{50}$. The novel H3N8 virus replicated poorly in mammalian MDCK cells but replicated efficiently in DF-1 avian cells (Appendix Figure). Those findings imply that the novel H3N8 virus has not yet adapted to mammal hosts, which was confirmed by limited replication in human bronchial and lung tissues (Figure 1, panels E, F).

We fixed infected tissues at 48 hours postinfection and stained them for influenza A nucleoprotein immunohistochemistry (Appendix). Consistent with $TCID_{50}$ findings, bronchial tissues infected with pH1N1 had the most extensive distribution of viral

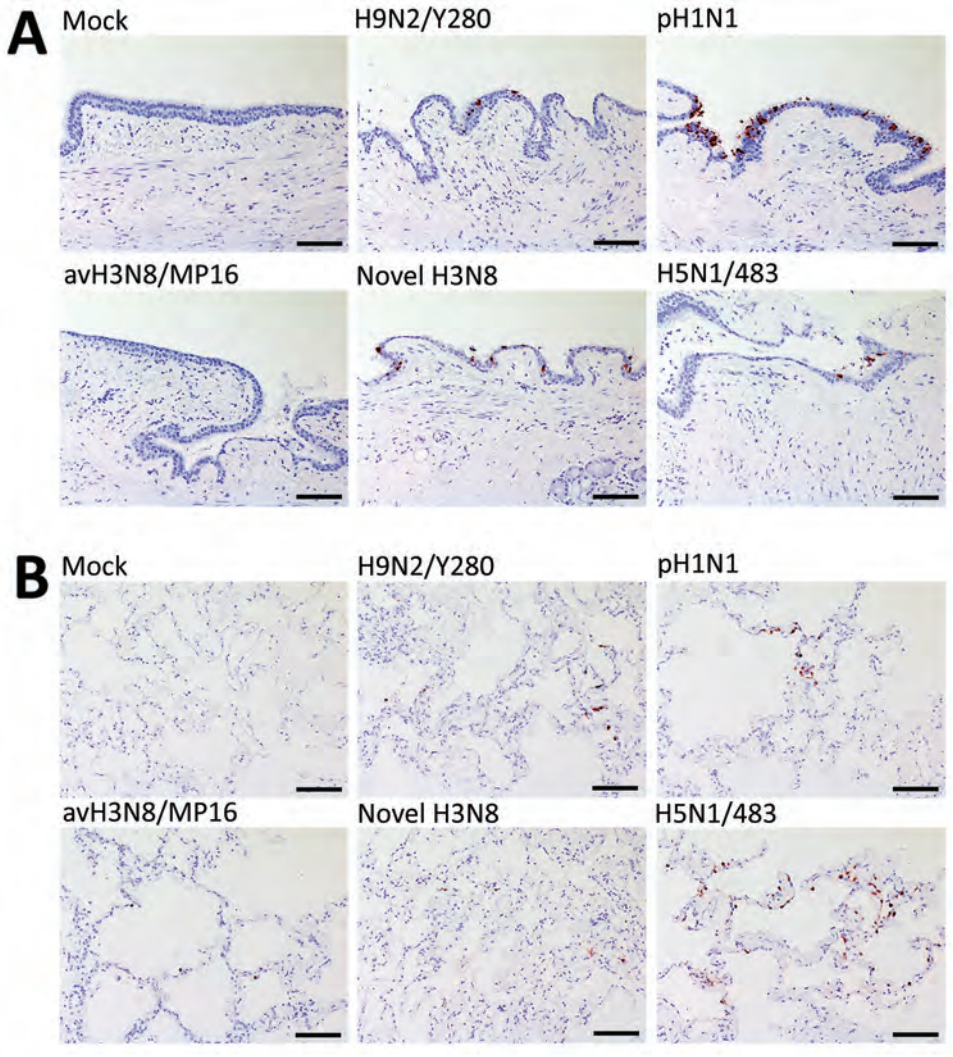

Figure 2. Tissue tropism of influenza A viruses in ex vivo cultures of human bronchus and lung tissue. Immunohistochemical staining of influenza A nucleoprotein in ex vivo cultures of human bronchial tissues (A) and lung tissues (B) at 48 hours postinfection with H9N2/Y280, pH1N1, H3N8/MP16, novel H3N8, and H5N1/483 viruses. Positive cells are indicated by red-brown color. Images are representative of 3 individual donors. Scale bar indicates 100 μm. Detailed information on viruses used in study is provided in the Appendix (https://wwwnc.cdc.gov/EID/article/29/6/22-1680-App1.pdf).

Table. Source of gene segments of novel and avian influenza A(H3N8) viruses*

Gene segment	Novel H3N8	avH3N8/MP16
Polymerase basic 2	H9N2	H3N8
Polymerase basic 1	H9N2	H6N1
Polymerase acidic	H9N2	H6N2
Hemagglutinin	H3N8	H3N8
Nucleoprotein	H9N2	H3N8
Neuraminidase	H3N8	H3N8
Matrix	H9N2	H1N1
Nonstructural	H9N2	H7N1

*Detailed information on viruses used in study is provided in the Appendix (https://wwwnc.cdc.gov/EID/article/29/6/22-1680-App1.pdf).

antigen, whereas we observed moderate levels of viral antigen staining in tissues infected with novel H3N8, H9N2, and H5N1 virus. No viral antigen staining was observed in tissues infected with avH3N8 (Figure 2, panel A). In the lung, H5N1 virus infection demonstrated the most extensive viral antigen staining, followed by infection with pH1N1, novel H3N8, and avH3N8 virus, which demonstrated the least extensive staining (Figure 2, panel B).

The discrepancy between the viral load in RNA copies and $TCID_{50}$ titers of H9N2 and avH3N8 infection suggests that infection with those viruses might produce high levels of defective particles that cannot be detected by $TCID_{50}$ assay. Immunohistochemistry staining of viral antigen serves as alternative evidence of virus replication in human tissues. The staining correlates more with $TCID_{50}$ results than with viral RNA analysis for all the viruses.

Amino acid comparisons of the novel H3N8 and avH3N8 viruses demonstrated that they shared the same stalk length in the NA gene but did not have the G228S mutation that enhances binding to mammalian receptors (Appendix Table 2). The internal genes of the novel H3N8 virus were reassorted from H9N2 virus, whereas the internal genes of the avH3N8 came from H3N8, H6N1, H6N2, H3N8, H1N1, and H7N1 (Table). Neither virus had the E627K mutation in polymerase basic 2 that confers mammal adaptation, virulence, and transmissibility. The novel H3N8 virus had the A588V mutation in polymerase basic 2 that promotes mammal adaptation, but avian H3N8 virus did not have this mutation. This difference might contribute to higher replication of the novel H3N8 virus in human lung tissue. The S31N mutation found in the matrix protein 2 of the novel H3N8 virus provided adamantane resistance.

Conclusions

Although zoonotic H3N8 viruses have a dual receptor-binding affinity of α-2,3 and α-2,6 receptors (*7*), our findings show that this factor does not confer an advantage for replication in human bronchial tissue. Our findings demonstrated inefficient replication of the novel H3N8 virus in human bronchial tissues, which implies limited efficiency to transmit among humans. This finding is in line with a recent serologic surveillance study in which no poultry workers were positive for antibodies for the novel H3N8 virus (*7*), and only 2 human cases have been documented since April 2022 (*4*,*5*). The moderate replication ability of the novel H3N8 virus in human lung tissue suggests that the virus causes less severe disease than H5N1 virus.

In summary, our findings suggest that the zoonotic-like avian H3N8 virus has limited efficiency for human-to-human transmission and, at present, is unlikely to cause severe disease in humans. However, the limited cross-reactive immunity against this novel H3N8 virus in the human population (*8*) and the emergence of novel H3N8 viruses by continuous reassortment between AIVs in wild birds and poultry demonstrate that the zoonotic and pandemic potential of avian H3N8 viruses should be closely monitored.

Acknowledgments

We thank Jenny Chan, Rachel Ching, and Kevin Fung for technical support.

This work was supported by grants from the National Institute of Allergy and Infectious Diseases, National Institutes of Health, Department of Health and Human Services (contract no. 75N93021C00016) and the Theme-Based Research Scheme (Ref: T11-712/19-N) under University Grants Committee of Hong Kong Special Administrative Region.

About the Author

Dr. Hui is an assistant professor in the School of Public Health at the University of Hong Kong. Her research interests include risk assessment, understanding the pathogenesis of emerging respiratory viruses, and the development of therapeutic options for severe influenza diseases and coronavirus infections.

References

1. Guan Y, Shortridge KF, Krauss S, Webster RG. Molecular characterization of H9N2 influenza viruses: were they the donors of the "internal" genes of H5N1 viruses in Hong Kong? Proc Natl Acad Sci U S A. 1999;96:9363–7. https://doi.org/10.1073/pnas.96.16.9363
2. Lam TT, Zhou B, Wang J, Chai Y, Shen Y, Chen X, et al. Dissemination, divergence and establishment of H7N9 influenza viruses in China. Nature. 2015;522:102–5. https://doi.org/10.1038/nature14348
3. Ma C, Lam TT, Chai Y, Wang J, Fan X, Hong W, et al. Emergence and evolution of H10 subtype influenza viruses in

poultry in China. J Virol. 2015;89:3534–41. https://doi.org/10.1128/JVI.03167-14
4. Cheng D, Dong Y, Wen S, Shi C. A child with acute respiratory distress syndrome caused by avian influenza H3N8 virus. J Infect. 2022;85:174–211. https://doi.org/10.1016/j.jinf.2022.05.007
5. Tan X, Yan X, Liu Y, Wu Y, Liu JY, Mu M, et al. A case of human infection by H3N8 influenza virus. Emerg Microbes Infect. 2022;11:2214–7. https://doi.org/10.1080/22221751.2022.2117097
6. Li Y, Li P, Xi J, Yang J, Wu H, Zhang Y, et al. Wild bird-origin H3N8 avian influenza virus exhibit well adaptation in mammalian host. J Infect. 2022;84:579–613. https://doi.org/10.1016/j.jinf.2021.12.014
7. Yang R, Sun H, Gao F, Luo K, Huang Z, Tong Q, et al. Human infection of avian influenza A H3N8 virus and the viral origins: a descriptive study. Lancet Microbe. 2022;3:e824–34. https://doi.org/10.1016/S2666-5247(22)00192-6
8. Sit THC, Sun W, Tse ACN, Brackman CJ, Cheng SMS, Tang AWY, et al. Novel zoonotic avian influenza A(H3N8) virus in chicken, Hong Kong, China. Emerg Infect Dis. 2022;28:2009–15. https://doi.org/10.3201/eid2810.221067

Address for correspondence: Michael C.W. Chan, School of Public Health, Li Ka Shing Faculty of Medicine, The University of Hong Kong, Pok Fu Lam, Hong Kong, China; email: mchan@hku.hk

Risk for Infection in Humans after Exposure to Birds Infected with Highly Pathogenic Avian Influenza A(H5N1) Virus, United States, 2022

Krista Kniss,[1] Kelsey M. Sumner,[1] Katie J. Tastad, Nathaniel M. Lewis, Lauren Jansen, Derek Julian, Mike Reh, Emily Carlson, Robin Williams, Samir Koirala, Bryan Buss, Matthew Donahue, Jennifer Palm, Leslie Kollmann, Stacy Holzbauer, Min Z. Levine, Todd Davis, John R. Barnes, Brendan Flannery, Lynnette Brammer, Alicia Fry

During February 7–September 3, 2022, a total of 39 US states experienced outbreaks of highly pathogenic avian influenza A(H5N1) virus in birds from commercial poultry farms and backyard flocks. Among persons exposed to infected birds, highly pathogenic avian influenza A(H5) viral RNA was detected in 1 respiratory specimen from 1 person.

Infection with highly pathogenic avian influenza (HPAI) virus results in high mortality rates in chickens, gallinaceous birds, and some wild bird species (*1*). Potential for HPAI virus transmission and adaptation to human hosts poses a pandemic risk (*2*). In 2021, HPAI viruses belonging to influenza A(H5N1) clade 2.3.4.4b were detected worldwide in migrating birds and commercial poultry flocks (*3*). HPAI H5N1 viruses were first detected in the United States in January 2022 in hunter-harvested wild birds in North and South Carolina (*4*); reports of infected wild and domesticated birds in other states followed. Infection risk among persons exposed to birds with H5N1 clade 2.3.4.4b infection is unknown, although 2 human cases were reported in China, 1 in Chile, 1 in Ecuador, 2 in Spain, and 1 in the United Kingdom (*5*,*6*). Using active symptom monitoring of exposed persons in the United States during February 7–September 3, 2022, we estimated the risk for symptomatic H5N1 virus infection in humans and developed a surveillance protocol for monitoring asymptomatic infection by using serologic testing among persons exposed to H5N1-infected birds.

The Study

In the United States, the US Department of Agriculture is responsible for conducting surveillance for avian influenza in wild or domesticated birds (*7*). An outbreak of HPAI in domesticated or commercial flocks was defined as ≥1 case of laboratory-confirmed avian influenza in a bird. For persons exposed (e.g., flock owners, farm workers, and cullers) to commercial poultry, backyard flocks, wild birds, and the environments of birds infected with HPAI, the Centers for Disease Control and Prevention (CDC) recommended active symptom monitoring (conducted through a mixture of phone, email, and text contact based on the jurisdiction's preference) by health departments for 10 days after their most recent exposure among persons who did not wear recommended personal protective equipment (PPE) or had a breach in PPE (*8*). State and local health departments used different criteria to determine whether a person met the criteria for active monitoring, and PPE use data may have been collected by state and local health departments

Author affiliations: Centers for Disease Control and Prevention, Atlanta, Georgia, USA (K. Kniss, K.M. Sumner, K.J. Tastad, N.M. Lewis, L. Jansen, M. Reh, B. Buss, S. Holzbauer, M.Z. Levine, T. Davis, J.R. Barnes, B. Flannery, L. Brammer, A. Fry); Nebraska Department of Health and Human Services, Lincoln, Nebraska, USA (L. Jansen, D. Julian, M. Reh, E. Carlson, R. Williams, S. Koirala, B. Buss, M. Donahue); Minnesota Department of Health, Saint Paul, Minnesota, USA (J. Palm, L. Kollmann, S. Holzbauer)

DOI: https://doi.org/10.3201/eid2906.230103

[1]These first authors contributed equally to this article.

but was not collected by CDC. Respiratory specimens (typically nasal or nasopharyngeal swabs) were collected from persons with symptoms compatible with influenza A(H5) virus infection within 10 days of their most recent exposure and tested for influenza A(H5) by real-time reverse transcription PCR (rRT-PCR) at state public health labs using the CDC Human Influenza Virus Real-Time RT-PCR Diagnostic Panel, Influenza A(H5) Subtyping Kit (*9*). Jurisdictions could also test persons without compatible symptoms at their discretion. Any influenza A(H5)–positive results from states were confirmed by testing at CDC. Confirmed diagnostic positive samples were characterized at CDC by using genomic sequencing and viral culture to determine if samples contained infectious influenza A(H5) virus. CDC collected aggregate data from state health departments, including the number of persons monitored and tested for influenza A(H5).

To assess the risk for asymptomatic human infection, alongside state and local health departments in Nebraska and Minnesota, CDC collected serum and respiratory specimens to detect influenza A(H5) virus infection among asymptomatic and symptomatic persons exposed to H5N1-infected poultry in commercial farms, backyard flocks, and wildlife rehabilitation centers experiencing animal outbreaks. All exposed persons were invited to participate in collection of acute respiratory specimens for rRT-PCR diagnostic testing of influenza A(H5) and paired acute and convalescent serum specimens collected 3–4 weeks apart for hemagglutination inhibition and microneutralization assays against A/American Wigeon/South Carolina/22-000345-001/2021 2.3.4.4.b A(H5N1) virus (*10*). Activities were conducted as part of a public health response and not considered human subjects research under federal human subject protection regulations.

During February 7–September 3, 2022, HPAI H5N1 virus infections were detected in 2,199 wild birds in 45 US states. The US Department of Agriculture's National Veterinary Services Laboratory also confirmed H5N1 outbreaks in 200 commercial poultry farms and 229 backyard flocks in 39 states (Figure). Nationally, 4,351 persons were actively monitored after exposure to these birds, and 3,658 (84%) completed the 10-day monitoring period (Table). Among persons monitored for postexposure symptoms, 134 (3%) experienced onset of ≥1 symptoms compatible with influenza virus infection and had respiratory specimens collected for diagnostic testing. All 134 symptomatic persons reported mild illness.

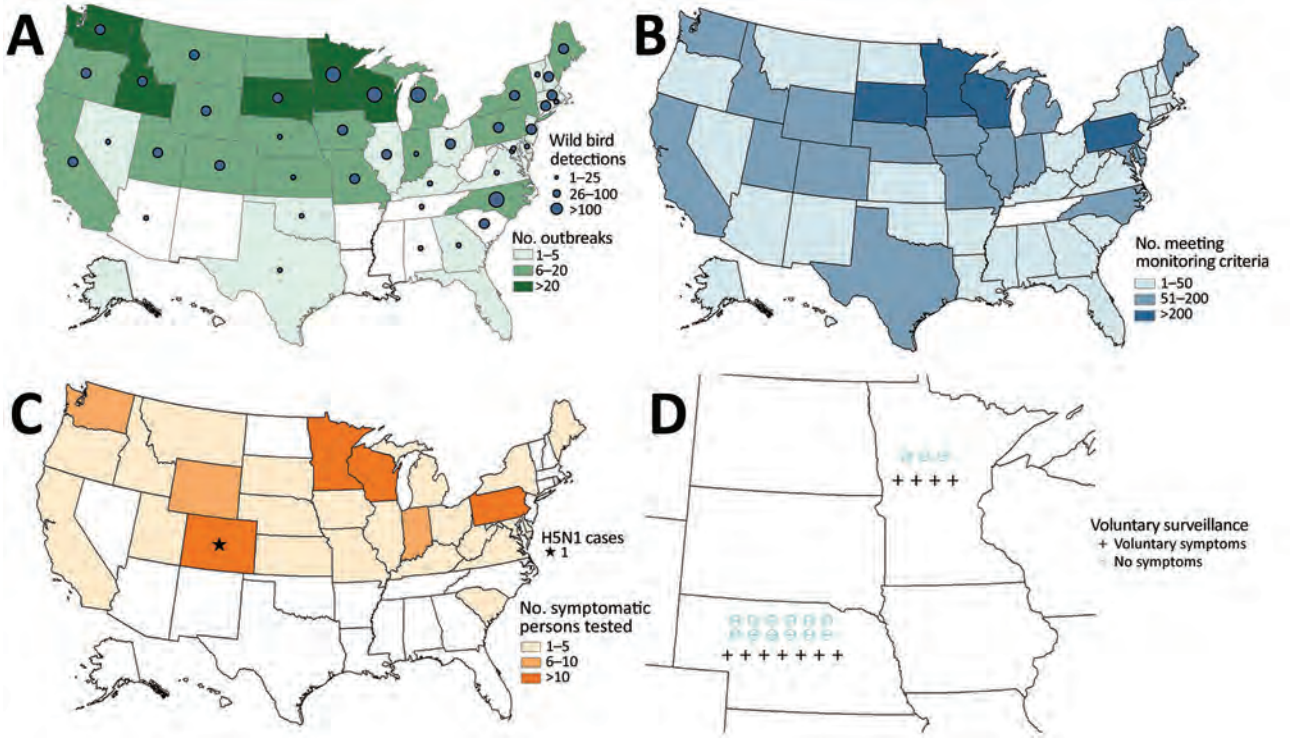

Figure. Highly pathogenic avian influenza A(H5N1) virus infection outbreaks and human exposures, United States, February 7–September 3, 2022. A) Number of outbreaks in commercial poultry and backyard flocks and number of detections of H5N1 among wild birds. B) Number of persons exposed and meeting active monitoring criteria. C) Number of persons who were symptomatic during 10-day monitoring period and number of influenza A(H5N1) virus infection cases reported. D) Number of persons in Nebraska and Minnesota who expressed interest in asymptomatic and symptomatic serologic surveillance.

Table. Characteristics of exposed persons monitored and tested for influenza A(H5) virus after exposure to highly pathogenic avian influenza A(H5N1) virus–infected birds, United States, February 7–September 3, 2022*

Characteristic	Met jurisdiction-level active monitoring criteria	Completed 10-day monitoring period	Tested through surveillance	Expressed interest in asymptomatic and symptomatic serologic surveillance
Total	4,351 (100)	3,658 (100)	154 (100)	26 (100)
Demographic characteristics				
Median age (range), y			40 (0.5–79)	40.5 (9–73)
Sex				
M				13 (50)
F				13 (50)
Symptomatic†			134 (93)	11 (42)
Hospitalized			0	0
Exposure category				
Farm worker or owner and other nonresponders	1,219 (28)	1,114 (30)	36 (27)‡	
Responders§	2,072 (48)	1,839 (50)	76 (57)‡	
Other, e.g., wildlife, veterinarian, laboratorian	87 (2)	86 (2)	22 (16)‡	
Unknown	973 (22)	619 (17)	0‡	

*Values are no. (%) except as indicated.
†Having ≥1 symptoms compatible with A(H5) infection: fever or feeling feverish or chills; cough; sore throat; runny or stuffy nose; eye tearing, redness, irritation (pink eye); sneezing; difficulty breathing; shortness of breath; fatigue (feeling very tired); muscle or body aches; headaches; nausea; vomiting; diarrhea; seizures; or rash. Ten exposed but asymptomatic persons and 10 persons without symptom history available had respiratory specimens collected under their jurisdiction's discretion or in conjunction with follow-up to the single human case detected.
‡Exposure category information only collected through surveillance for persons who reported being symptomatic.
§Defined as persons responsible for performing response activities such as culling, cleaning, and decontaminating infected premises.

One person in Colorado with reported fatigue tested positive for A(H5) by rRT-PCR (*11*).

Twenty-six persons with exposure to H5N1-infected birds in 5 investigations in Nebraska and 1 investigation in Minnesota expressed interest in the additional serum and respiratory swab sample collection, including 11 (42%) persons who reported symptoms after contact with sick birds. Nasal swab samples and paired serum specimens were obtained from 17 persons, and nasal swab samples only were obtained from 5 persons; 4 persons had no specimens tested. All 22 persons with collected nasal swab samples tested negative for influenza viruses by rRT-PCR. The 17 persons with paired serum specimens demonstrated no increase in antibody titers to influenza A(H5) 2.3.4.4b virus. Nineteen participants were present for culling of sick birds, and all reported PPE use of variable type and duration.

Conclusions

More than 4,000 persons exposed to HPAI H5N1–infected birds were monitored for symptomatic illness across the United States, and only 1 rRT-PCR–confirmed influenza A(H5) case was detected in a person. In addition, A(H5) serologic tests conducted in 2 states did not identify evidence of asymptomatic infection with influenza A(H5) 2.3.4.4b virus. Although some persons may have worn full PPE without breach, many probably had a PPE breach. Although the full extent of exposure among those monitored is unknown, our results are consistent with a low risk for avian-to-human transmission among persons exposed to wild and domesticated birds infected with influenza A(H5N1) clade 2.3.4.4b viruses detected in the United States.

Our findings are consistent with other reports. In previous years, US avian outbreaks with HPAI A(H5) viruses detected 0 human cases of infection with those viruses (*12*,*13*). In addition, no cases of human infection with H5N1 viruses were detected in Europe during 2016–2021, despite many avian H5N1 outbreaks (*14*,*15*).

At the time of this investigation, 7 persons exposed to the current H5N1 virus clade had H5N1 virus detected by rRT-PCR. Some of those cases were asymptomatic or mild and could represent contamination of the nasal mucosa instead of infection. Serologic testing of exposed persons in 2 states failed to find A(H5) in nasal mucosa or evidence of asymptomatic infection by antibody detection; however, the number of participants with serologic specimens was small, and a larger sample size is needed to confirm these findings.

One limitation of our study is that the number of persons exposed to H5N1-infected birds was underestimated because of underreporting and noncompliance with monitoring; however, jurisdictions requested employee lists and inquired about additional contacts to expand capture of those exposed. Detailed exposure information was not collected from all exposed persons, so we could not report on the influence of exposure duration or PPE use on infection risk.

Although we found that the risk for A(H5) virus transmission to the public appears to be low, close monitoring of these viruses and persons exposed to them is imperative. The virus is continuing to reassort with other North American avian influenza viruses,

increased A(H5) cases are occurring in mammals, and the risk profile could change at any moment. Influenza A(H5N1) viruses remain a potential pandemic threat, and limiting the incidence of human zoonotic infections and human-to-human transmission is critical.

Acknowledgments

We thank the state and local public health officials, particularly the members of the H5N1 Monitoring Team for their work monitoring persons exposed to birds that were infected with HPAI H5N1. We also thank the persons who participated in the active monitoring and voluntary expanded surveillance activities. We thank Crystal Holiday and Feng for their laboratory contributions.

Members of the H5N1 Monitoring Team: Carrie Edmonson and Martin Jones (Alaska Department of Health); DeJuana Grant (Alabama Department of Public Health); Haytham Safi and Laura K. Rothfeldt (Arkansas Department of Health); Erin L. Murray and Jennifer McNary (California Department of Public Health); Kristine Donschikowski and Amanda Brunner(Tuolumne County Public Health Department); June Nash and Jessica Guevara (Sacramento County Public Health); Catherine Blaser (County of San Diego Health and Human Services Agency); Laura Esbenshade and Paula Ptomey (Tulare County Health and Human Services Agency); Lissett Padgett and Samer Al Saghbini (Fresno County Department of Public Health); Evonne Koo (Monterey County Health Department); Isaac Armistead, Nisha Alden, and Elizabeth Austin (Colorado Department of Public Health and Environment); Alan Siniscalchi (Connecticut State Department of Public Health); Leslie Ayuk-Takor, Shreya Khuntia, and Saumya Rajamohan (District of Columbia Department of Health); Camille Moreno-Gorrin and Lisandra Clarke (Delaware Division of Public Health); Katherine Toothaker, Ashley Gent, Danielle Stanek, and Anna Pettit (Florida Department of Health); Amanda Feldpausch, Sayna Patel, and Katelin Reishus (Georgia Department of Public Health); Michelle Vien (Hawaii State Department of Health); Leslie Tengelsen (Idaho Department of Health and Welfare); Mallory Sinner, Connie Austin, and Melissa Cox (Illinois Department of Public Health); Layne Mounsey, Kira Richardson, Jennifer A. Brown, and Shawn M. Pence (Indiana Department of Health); Snehal Baxa and Erin Petro (Kansas Department of Health and Environment); Kelly Giesbrecht (Kentucky Department for Public Health); Alyssa McKenzie (Louisiana Department of Health); Joyce Cohen (Massachusetts Department of Public Health); David Crum and Evelyn Mahugu (Maryland Department of Health); Anna Krueger (Maine Center for Disease Control and Prevention); Sally Bidol, Anna Falkowski, James Barber, Meghan Burr-Martin, Ebonē Colbert, Smeralda Bushi, Mat Myers, Sarah Pruett, and Rosalyn Schaefer (Michigan Department of Health and Human Services); Jeffrey Sanders, Joni Scheftel, Melissa McMahon, Carrie Klumb, Malia Ireland, Leah Bauck, and Maria Bye (Minnesota Department of Health); Kate Cleavinger and Molly Baker (Missouri Department of Health and Senior Services); Jannifer Anderson (Mississippi State Department of Health); Devon Cozart (Montana Department of Public Health and Human Services); Khalil Harbi (North Carolina Department of Health and Human Services); Levi Schlosser (North Dakota Department of Health and Human Services); John Dreisig (New Hampshire Department of Health and Human Services); Deepam Thomas and Darby McDermott (New Jersey Department of Health); Samuel Scherber (New Mexico Department of Health); B. Denise Stokich (Nevada Division of Public and Behavioral Health); Andie Newman (New York State Department of Health); Nic Fisher (Ohio Department of Health); Mike Mannell and Awa Keinde (Oklahoma State Department of Health); M. Andraya Hendrick (Oregon Health Authority, Public Health Division); Sameh Boktor (Pennsylvania Department of Health); Lindsey McAda (South Carolina Department of Health and Environmental Control); Vickie Horan (South Dakota Department of Health); Emilio Gonzales (Texas Department of State Health Services); Janelle Delgadillo (Utah Department of Health and Human Services); Lisa Sollot (Virginia Department of Health), Hilary Fannin, Natalie Kwit, and Laura Ann Nicolai (Vermont Department of Health); Anna Unutzer (Washington State Department of Health); Thomas Haupt, Ian Pray, and Agela Maxted (Wisconsin Department of Health Services); Jillian Jeffrey (West Virginia Department of Health and Human Resources, Bureau for Public Health); Allison Siu (Wyoming Department of Health).

About the Author

Ms. Kniss is a surveillance epidemiologist in the Influenza Division of CDC's National Center for Immunization and Respiratory Diseases. Her primary interests include epidemiologic investigations, surveillance, and influenza.

References

1. Centers for Disease Control and Prevention. Avian influenza in birds. 2022 [cited 2022 Aug 15]. https://www.cdc.gov/flu/avianflu/avian-in-birds.htm
2. Yamaji R, Saad MD, Davis CT, Swayne DE, Wang D, Wong FYK, et al. Pandemic potential of highly pathogenic avian influenza clade 2.3.4.4 A(H5) viruses. Rev Med Virol. 2020;30:e2099. https://doi.org/10.1002/rmv.2099
3. Bevins SN, Shriner SA, Cumbee JC Jr, Dilione KE, Douglass KE, Ellis JW, et al. Intercontinental movement of highly pathogenic avian influenza A(H5N1) clade 2.3.4.4 virus to the United States, 2021. Emerg Infect Dis.

2022;28:1006–11. https://doi.org/10.3201/eid2805.220318
4. US Department of Agriculture Animal and Plant Health Inspection Service. USDA confirms highly pathogenic avian influenza in wild bird in South Carolina. 2022 [cited 2022 Mar 22]. https://www.aphis.usda.gov/aphis/newsroom/stakeholder-info/sa_by_date/sa-2022/hpai-sc
5. Pan American Health Organization. Informative note: human infection caused by avian influenza A(H5) virus in Chile—31 March 2023 [cited 2023 Apr 7]. https://www.paho.org/en/documents/informative-note-human-infection-caused-avian-influenza-ah5-virus-chile-31-march-2023
6. Centers for Disease Control and Prevention. Technical report: highly pathogenic avian influenza A(H5N1) viruses. 2023 [cited 2023 Apr 4]. https://www.cdc.gov/flu/avianflu/spotlights/2022-2023/h5n1-technical-report.htm
7. US Department of Agriculture Animal and Plant Health Inspection Service. 2022–2023 detections of highly pathogenic avian influenza. 2023 [cited 2023 Apr 7]. https://www.aphis.usda.gov/aphis/ourfocus/animalhealth/animal-disease-information/avian/avian-influenza/2022-hpai
8. Centers for Disease Control and Prevention. Information on bird flu. 2022 [cited 2022 Aug 15]. https://www.cdc.gov/flu/avianflu
9. Centers for Disease Control and Prevention. Interim guidance on testing and specimen collection for patients with suspected infection with novel influenza A viruses with the potential to cause severe disease in humans. 2022 [cited 2023 Apr 17]. https://www.cdc.gov/flu/avianflu/severe-potential.htm
10. Levine MZ, Holiday C, Liu F, Jefferson S, Gillis E, Bellamy AR, et al. Cross-reactive antibody responses to novel H5Nx influenza viruses following homologous and heterologous prime-boost vaccination with a prepandemic stockpiled A(H5N1) vaccine in humans. J Infect Dis. 2017;216(Suppl_4):S555–9. https://doi.org/10.1093/infdis/jix001
11. Centers for Disease Control and Prevention. Current U.S. bird flu situation in humans. 2022 [cited 2022 Oct 12]. https://www.cdc.gov/flu/avianflu/inhumans.htm
12. Olsen SJ, Rooney JA, Blanton L, Rolfes MA, Nelson DI, Gomez TM, et al. Estimating risk to responders exposed to avian influenza A H5 and H7 viruses in poultry, United States, 2014–2017. Emerg Infect Dis. 2019;25:1011–4. https://doi.org/10.3201/eid2505.181253
13. Arriola CS, Nelson DI, Deliberto TJ, Blanton L, Kniss K, Levine MZ, et al.; H5 Investigation Group. Infection risk for persons exposed to highly pathogenic avian influenza A H5 virus-infected birds, United States, December 2014–March 2015. Emerg Infect Dis. 2015;21:2135–40. https://doi.org/10.3201/eid2112.150904
14. Adlhoch C, Baldinelli F, Fusaro A, Terregino C. Avian influenza, a new threat to public health in Europe? Clin Microbiol Infect. 2022;28:149–51. https://doi.org/10.1016/j.cmi.2021.11.005
15. Adlhoch C, Miteva A, Zdravkova A, Miškić T, Kneževic D, Perdikaris S, et al. Estimation of the number of exposed people during highly pathogenic avian influenza virus outbreaks in EU/EEA countries, October 2016–September 2018. Zoonoses Public Health. 2019;66:874–8. https://doi.org/10.1111/zph.12629

Address for correspondence: Krista Kniss, Centers for Disease Control and Prevention, 1600 Clifton Rd NE, Mailstop H24-7, Atlanta, GA 30329-4027, USA; email: krk9@cdc.gov

Results of PCR Analysis of Mpox Clinical Samples, Sweden, 2022

Jon Edman-Wallér,[1] Ola Jonsson,[1] Gustav Backlund,[1] Shaman Muradrasoli, Klara Sondén

We compared cycle thresholds from mpox skin lesions with other specimen sites and over time from onset of clinical signs among 104 patients in Sweden. Cycle thresholds differed by anatomic site. We identified 2 early mpox cases from anorectal swab specimens after skin samples were negative, indicating necessity of sampling multiple sites.

A global outbreak of mpox was detected in May 2022 and declared a Public Health Emergency of International Concern on July 23 (*1*). We investigated how monkeypox virus (MPXV) cycle threshold (Ct) values, a proxy for viral loads, differed on the basis of specimen type and duration of illness among patients in Sweden. Ethics approval was deemed unnecessary because all analyses were based on anonymized laboratory data available from the Public Health Agency of Sweden.

The Study

As of February 19, 2023, Sweden had 260 confirmed mpox cases; peak incidence was in August 2022. During the May 24–September 2 study period, most cases were diagnosed at the Public Health Agency of Sweden. As in other countries, most cases were found among men who have sex with men. In most cases, the disease has been self-limiting, and skin lesions are the most common clinical sign (*2*).

Samples were collected from all parts of the country from patients with suspected mpox disease based on clinical observation; for this study, we included 289 samples from 104 patients with ≥1 positive test. We used in-house real-time PCR targeting the B21 gene of MPXV for diagnostic testing of all specimen types. Before setup, we tested analytic specificity in vitro against cowpox and vaccinia viruses and in silico against other orthopoxviruses.

For the analyses, we included specimen type, Ct value, and days since onset of clinical signs as variables for each sample. When multiple samples from the same patient, day, and sample site existed, we analyzed the sample with the lowest Ct. We tested Ct values from skin lesions compared with paired samples from other specimen sites from the same patient and date for statistical significance using Wilcoxon signed-rank test. We used R Core Team version 4.2.2 software (The R Project for Statistical Computing, https://cran.r-project.org) for statistical analyses and to generate graphs.

The World Health Organization recommends MPXV PCR testing primarily from skin lesions (*3*), which have higher sensitivity than other specimen types (*4*); skin lesions were the most common specimen type in our study. (Table 1). Previous studies comparing Ct from paired skin lesion and oropharyngeal samples have usually shown lower mean values in skin samples but lower values from the oropharynx in some individual cases (*5*). In our study, all but 1 skin lesion sample had lower Ct values than oropharyngeal samples taken on the same day (Figure 1). Semen was positive in 4/6 samples. Within the cohort of patients with same-day rectal and skin samples of which ≥1 was positive (n = 15), we found no significant difference in Ct values between samples from the 2 sites. This finding agreed with previous research (*3*), but only a minority of patients (n = 22) were tested, and those might have had prominent clinical signs from the rectal area (e.g., perianal lesions or proctitis).

Ct values were lowest from skin samples taken ≈1 week after onset of signs (Figure 2). Post hoc

Author affiliations: Sahlgrenska University Hospital, Gothenburg, Sweden (J. Edman-Wallér); University of Gothenburg Institute of Biomedicine, Gothenburg (J. Edman-Wallér); Linköping University Hospital, Linköping, Sweden (O. Jonsson); Falu Hospital, Falun, Sweden (G. Backlund); Public Health Agency of Sweden, Solna, Sweden (S. Muradrasoli, K. Sondén); Karolinska Institute Department of Medicine, Solna (K. Sondén)

DOI: https://doi.org/10.3201/eid2906.230253

[1]These authors contributed equally to this article.

Table. Mpox PCR tests, specimen types, and cycle threshold levels for 104 patient samples analyzed at the Public Health Agency of Sweden, May 24–September 2, 2022*

	Samples			Ct values of positive samples			Patients	
Specimen type	Total no.	No. positive	Positive, %	Median	25th percentile	75th percentile	Total no.	≥1 positive samples
Skin lesion	178	148	83.1	23.6	20.6	28.6	96	92
Rectum	22	21	95.5	23.0	21.0	31.2	22	21
Throat	16	10	62.5	30.9	27.5	32.3	15	10
Blood†	17	8	47.1	37.6	36.0	38.0	8	7
Semen	6	4	66.7	32.9	31.1	35.2	5	3
Nasopharynx	13	4	30.8	34.9	32.8	36.6	5	3
Saliva	10	8	80.0	35.1	32.0	37.0	3	3
Sputum	8	5	62.5	31.2	30.2	35.0	4	2
Urine	7	2	28.6	30.3	28.6	32.0	5	2
Other	3	1	50.0	20.6	20.6	20.6	2	1
Unknown	9	4	50.0	22.1	21.2	23.1	4	2

*Ct, cycle threshold.
†Blood includes whole blood, plasma, and serum samples.

analysis showed significantly higher Ct values from samples taken on days 1–5 after onset of signs (n = 36, median Ct = 28.2, interquartile range [IQR] 23.8–37.3) than on days 6–10 (n = 58, median = 23,2, IQR 20.7–28.3; p = 0.004), possibly because vesicular or pustular lesions that develop after a few days might have been easier to sample or have a higher actual viral load. After the initial decrease, Ct values from skin lesions increased over time (Figure 2). At 16 days after onset of signs, >50% of skin lesion samples were PCR negative. This period is in line with the clinical course documented elsewhere, in which infection usually resolves 2–4 weeks after the onset of rash (Z.M. Afshar et al., unpub data, https://doi.org/10.22541/au.165446104.43472483/v1), although cases of prolonged disease and PCR positivity have been described elsewhere (*6*). Previous research has also shown generally decreased viral loads 14 days after the first positive test (*7*).

Among 83 patients with skin lesion samples for whom data on onset of signs were available, 3 were negative based on first skin lesion samples. However, 2 of those patients were found positive from rectal samples taken the same days as the corresponding skin sample (days 3 and 4 after onset of signs) and 1 was positive in a serum sample (day of onset of signs). Those results suggest that rectal and serum testing may be more useful early in the disease course, when skin lesions are at an early stage. In addition, in 2 patients for whom dates of onset of signs were unavailable and who were found negative from first skin lesion samples, we found 1 was positive from a rectal sample and the other from a throat swab sample from the same days.

Conclusions

Our data on MPXV PCR tests during the mpox 2022 outbreak in Sweden indicate that viral levels peak in skin lesions 6–10 days after onset of signs and samples may test negative in early disease. Mpox detection rates might increase with complementary anorectal sampling in early disease or repeated skin lesion testing when patients with suspected lesions test negative soon after onset of signs. A strength of the study

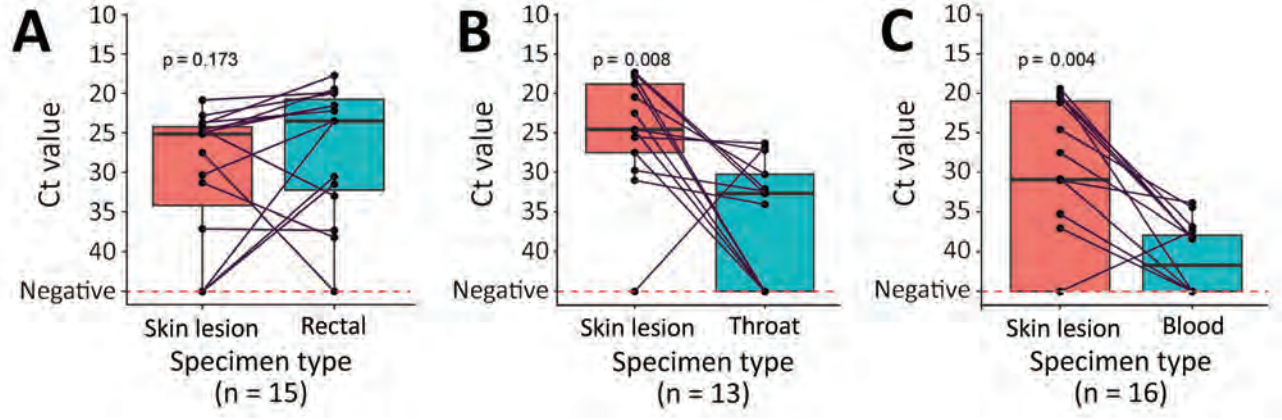

Figure 1. Mpox Ct levels of paired tests from different specimen types collected on the same day from the same patient and analyzed at the Public Health Agency of Sweden, May 24–Sep 2, 2022. Black dots indicate Ct levels of individual samples and gray lines link results from different specimen sites on the same day from the same patient. Ct, cycle threshold.

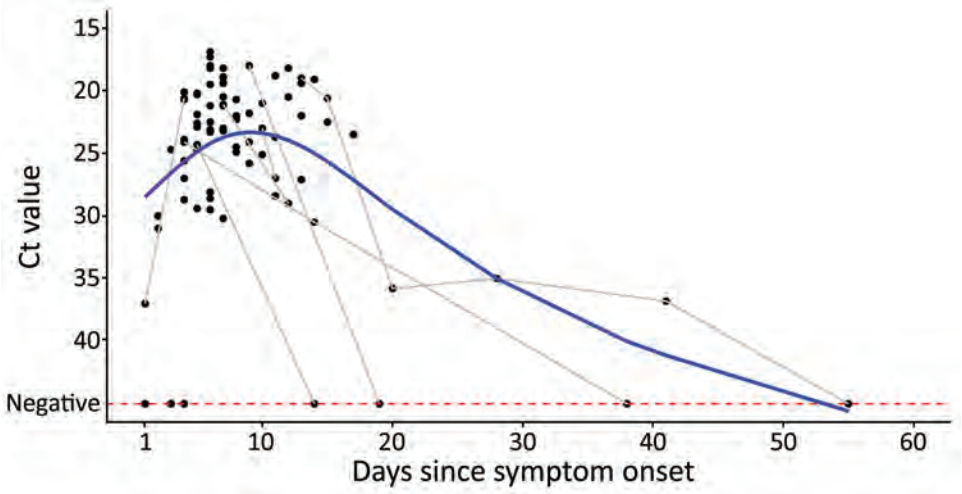

Figure 2. Mpox PCR Ct values in skin lesion samples and days since onset of signs (day 1) analyzed at the Public Health Agency of Sweden, May 24–Sep 2, 2022 (n = 83). Gray lines connect samples from the same patient. Blue line (smoothing spline) is for visualization.

was the national coverage, but because final Ct levels varied with sampling methods, extraction methods, and PCR targets, and detailed clinical data were missing in this study, our results need to be confirmed in other settings.

Acknowledgments

We thank the laboratory staff at the Public Health Agency for performing the PCR analyses.

About the Author

Dr. Edman-Wallér is a resident physician in clinical microbiology and infection protection and control in western Sweden. He is pursuing a PhD in preventive strategies for *Clostridiodes difficile* infections.

References

1. Nuzzo JB, Borio LL, Gostin LO. The WHO declaration of monkeypox as a global public health emergency. JAMA. 2022;328:615–7. https://doi.org/10.1001/jama.2022.12513
2. Vaughan AM, Cenciarelli O, Colombe S, de Sousa LA, Fischer N, Gossner CM, et al. A large multi-country outbreak of monkeypox across 41 countries in the WHO European Region, 7 March to 23 August 2022. Euro Surveill. 2022;27:2200620
3. World Health Organization. Laboratory testing for the monkeypox virus: interim guidance [cited 2022 Oct 24]. https://apps.who.int/iris/bitstream/handle/10665/354488/WHO-MPX-Laboratory-2022.1-eng.pdf
4. Martins-Filho PR, Tanajura DM, Alves Dos Santos C. Polymerase chain reaction positivity and cycle threshold values in biological samples from patients with monkeypox: a meta-analysis. Travel Med Infect Dis. 2022;50:102448. https://doi.org/10.1016/j.tmaid.2022.102448
5. Paran N, Yahalom-Ronen Y, Shifman O, Lazar S, Ben-Ami R, Yakubovsky M, et al. Monkeypox DNA levels correlate with virus infectivity in clinical samples, Israel, 2022. Euro Surveill. 2022;27:2200636. https://doi.org/10.2807/1560-7917.ES.2022.27.35.2200636
6. Pettke A, Filén F, Widgren K, Jacks A, Glans H, Andreasson S, et al. Ten-week follow-up of monkeypox case-patient, Sweden, 2022. Emerg Infect Dis. 2022;28:2074–7. https://doi.org/10.3201/eid2810.221107
7. Palich R, Burrel S, Monsel G, Nouchi A, Bleibtreu A, Seang S, et al. Viral loads in clinical samples of men with monkeypox virus infection: a French case series. Lancet Infect Dis. 2023;23:74–80. https://doi.org/10.1016/S1473-3099(22)00586-2

Address for correspondence: Jon Edman-Wallér, University of Gothenburg Sahlgrenska Academy – Biomedicine, Infectious Diseases, Postmästaregatan 10 C Mölndal 431 66, Sweden; email: jon.edman@vgregion.se

SARS-CoV-2 Seroprevalence and Cross-Variant Antibody Neutralization in Cats, United Kingdom

Grace B. Tyson, Sarah Jones, Nicola Logan, Michael McDonald, Leigh Marshall, Pablo R. Murcia, Brian J. Willett, William Weir, Margaret J. Hosie

Anthropogenic transmission of SARS-CoV-2 to pet cats highlights the importance of monitoring felids for exposure to circulating variants. We tested cats in the United Kingdom for SARS-CoV-2 antibodies; seroprevalence peaked during September 2021–February 2022. The variant-specific response in cats trailed circulating variants in humans, indicating multiple human-to-cat transmissions over a prolonged period.

The World Organisation for Animal Health reported that 26 different animal species had been infected with SARS-CoV-2 by December 31, 2022; ≈30% (8/26) of the susceptible species are felids (*1*). Animal SARS-CoV-2 infections originating from anthropogenic transmission can lead to onward animal-to-animal transmission, as described previously in mink (*2*), hamsters (*3*), and white-tailed deer (*4*). There have also been reports of animal-to-human transmission of SARS-CoV-2 from farmed mink (*2*), pet hamsters (*5*), free-ranging white-tailed deer (*6*), and a pet cat (*7*).

It is unknown whether individual SARS-CoV-2 variants are more or less likely to be transmitted from humans to cats or whether infected cats are more or less likely to develop clinical signs. The aim of this study was to assess the seroprevalence of SARS-CoV-2 infection in cats during April 2020–February 2022 in the United Kingdom. We used a pseudotype-based neutralization assay (PVNA) to measure virus neutralizing antibody titers and a confirmatory ELISA that measured antibodies recognizing the receptor binding domain of the SARS-CoV-2 spike (S) protein. We measured neutralizing titers against a panel of viral pseudotypes based on a lentiviral (HIV) backbone and bearing the S proteins of the predominant circulating variants in the United Kingdom to investigate the specificity of the neutralizing response. The University of Glasgow Veterinary Ethics Committee granted approval for the study (EA27/20).

Author affiliations: Medical Research Council—University of Glasgow Centre for Virus Research, Glasgow, Scotland, UK (G.B. Tyson, S. Jones, N. Logan, P.R. Murcia, B.J. Willett, M.J. Hosie); University of Glasgow, Glasgow (G.B. Tyson, S. Jones, M. McDonald, L. Marshall, W. Weir)

DOI: https://doi.org/10.3201/eid2906.221755

The Study

We screened residual blood samples from 2,309 cats by using PVNA at a final dilution of 1:100; the samples were submitted to the University of Glasgow Veterinary Diagnostic Services laboratory (VDS) during April 2020–February 2022 (Figure 1, panel A). The samples represented a cohort that was broadly representative of the domestic cat population in the United Kingdom, including samples from 112 of the 126 UK postcode areas (Appendix 1 Figure 1, https://wwwnc.cdc.gov/EID/article/29/6/22-1755-App1.pdf), although the samples had an uneven distribution unrelated to the local human population density. Overrepresented areas included Blackpool, Glasgow, Edinburgh, and Cambridge. The PVNA used HIV (SARS-CoV-2) pseudotypes bearing S proteins of SARS-CoV-2 ancestral D614G (B.1), Alpha (B.1.1.7), Delta (B.1.617.2) or Omicron (BA.1). Samples submitted early in the pandemic were tested against ancestral D614G (B.1) only, whereas new variants were included as they emerged (Appendix 2, https://wwwnc.cdc.gov/EID/article/29/6/22-1755-App2.xlsx). We estimated neutralization titers for positive samples by performing the PVNA with serially diluted samples.

Our results showed that SARS-CoV-2 seroprevalence in UK cats increased over time (Figure 1, panel B).

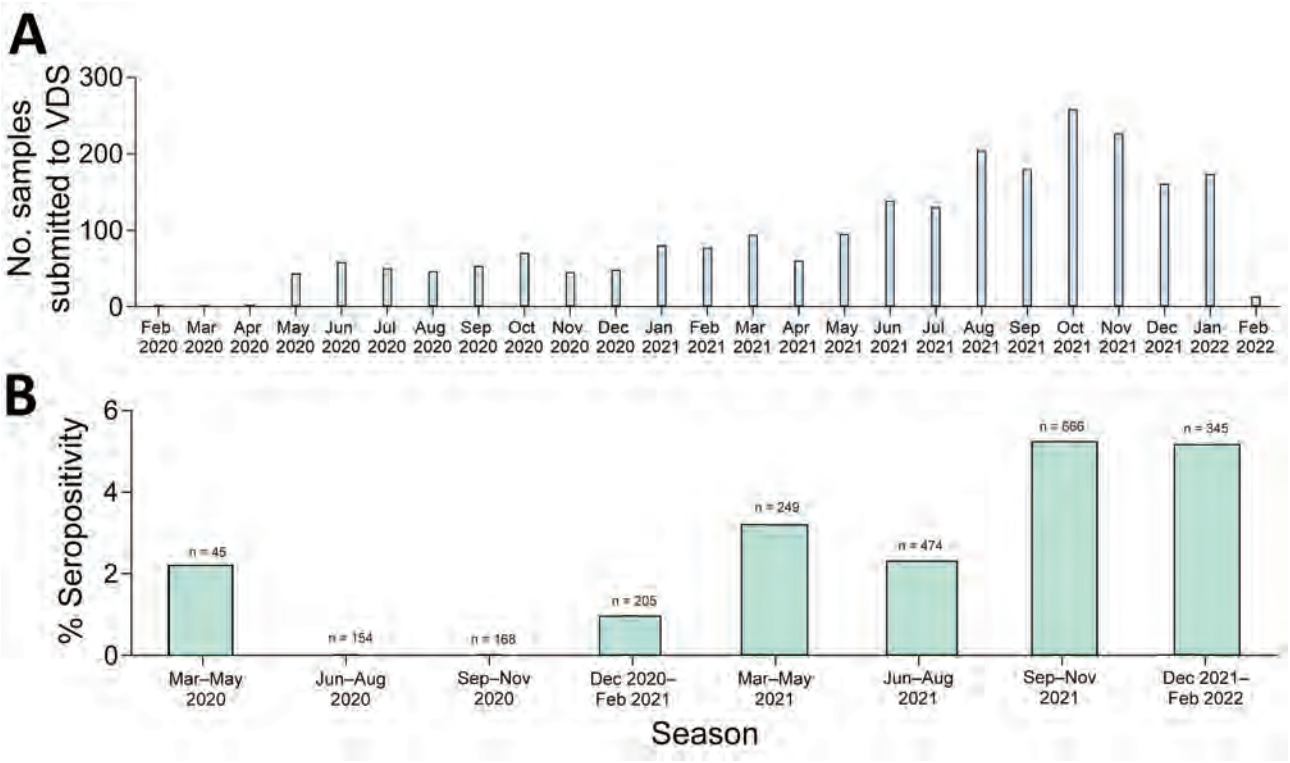

Figure 1. Seropositivity of samples included in analysis in study of SARS-CoV-2 seroprevalence and immunity in cats, United Kingdom, April 2020–February 2022. A) Number of samples tested per month. Overall seropositivity across all samples was 3.2% (75/2,309). B) Percentage seropositivity of samples per 3-month period and sample size for each period. VDS, University of Glasgow Veterinary Diagnostic Services laboratory.

Overall, the seroprevalence during the study period was 3.2% (95% CI 2.56%–4.05%; 75/2,309). Seroprevalence was highest during September–November 2021 (5.3%, 95% CI 3.69%–7.23%; 35/666) and during December 2021–February 2022 (5.2%, 95% CI 3.09%–8.05%; 18/348).

When we analyzed individual samples, we observed differences in variant-specific potencies among titers against the different SARS-CoV-2 variants: 17/75 (22.7%) samples were B.1 dominant (i.e., they possessed higher titers against B.1 than against other variants); 31/75 (41.3%) were Alpha dominant, and 27/75 (36%) were Delta dominant. On average, Delta-dominant samples displayed higher neutralization titers (mean 760) against their dominant pseudotype compared with Alpha-dominant (488; $p = 0.06$) or B.1-dominant (329; $p = 0.02$) samples (Appendix 1 Figure 2). Throughout the study period (April 2020–February 2022), no Omicron-dominant seropositive samples were identified; we anticipated this finding because only a small proportion of samples were collected after the Omicron variant emerged.

We observed an association between the dominant variant in cats and the timeline of variant emergence in the human population. Detection of new dominant variants in cats trailed detection of the variant in the humans; however, we detected dominant titers against extinct variants even after human cases had declined, possibly indicating long-lasting humoral immunity (Figure 2). We observed 3 distinct patterns of neutralization. B.1-dominant samples generally had slightly lower titers against the Alpha pseudotype than against B.1. Those samples also had significantly lower titers against both the Delta ($p<0.0001$) and Omicron ($p<0.001$) pseudotypes. Alpha-dominant samples showed slightly lower B.1 titers and markedly lower Delta and Omicron titers. Delta-dominant samples showed similar titers against the B.1, Alpha, and Omicron pseudotypes, all of which were significantly lower than their Delta titers ($p<0.0001$) (Appendix 1 Figure 3).

The trends we observed for cats thought to have been infected with the B.1 variant are similar to the patterns of neutralization in humans reported previously (*8*); Wilhelm et al. showed that humans vaccinated with an ancestral strain–based vaccine develop lower neutralization titers against the Delta and Omicron variants than against B.1 or Alpha. Another study showed that cats experimentally inoculated with either the ancestral or the Delta variant became lethargic and pyrexic, whereas Omicron-inoculated

cats did not develop any clinical signs and displayed lower levels of virus shedding, suggesting that the Omicron variant might be less pathogenic in cats as well as in humans (*9*).

Despite those distinct patterns of neutralization, the variant to which the animal was exposed can only be speculatively inferred through serologic testing in the absence of viral sequence data, even in cases in which the titer against the dominant variant is many times greater than the next highest titer. The 3 specific patterns of immunity we observed were similar to previous findings in humans (*10*). It is likely that both the antigenicity of the different variants' S proteins and the viral load during the infection period influence the breadth and potency of variant-specific neutralization.

A greater proportion of purebred cats (31/720 [4.3%, 95% CI 2.94%–6.06%]) than nonpedigree cats (39/1,300 [3%, 95% CI = 2.14%–4.08%]) were seropositive; however, this finding was not significant (p = 0.1). Purebred cats are more likely to be kept indoors only and may therefore experience more close contact with their owners, meaning they are more prone to exposure to SARS-CoV-2 if their owners become infected.

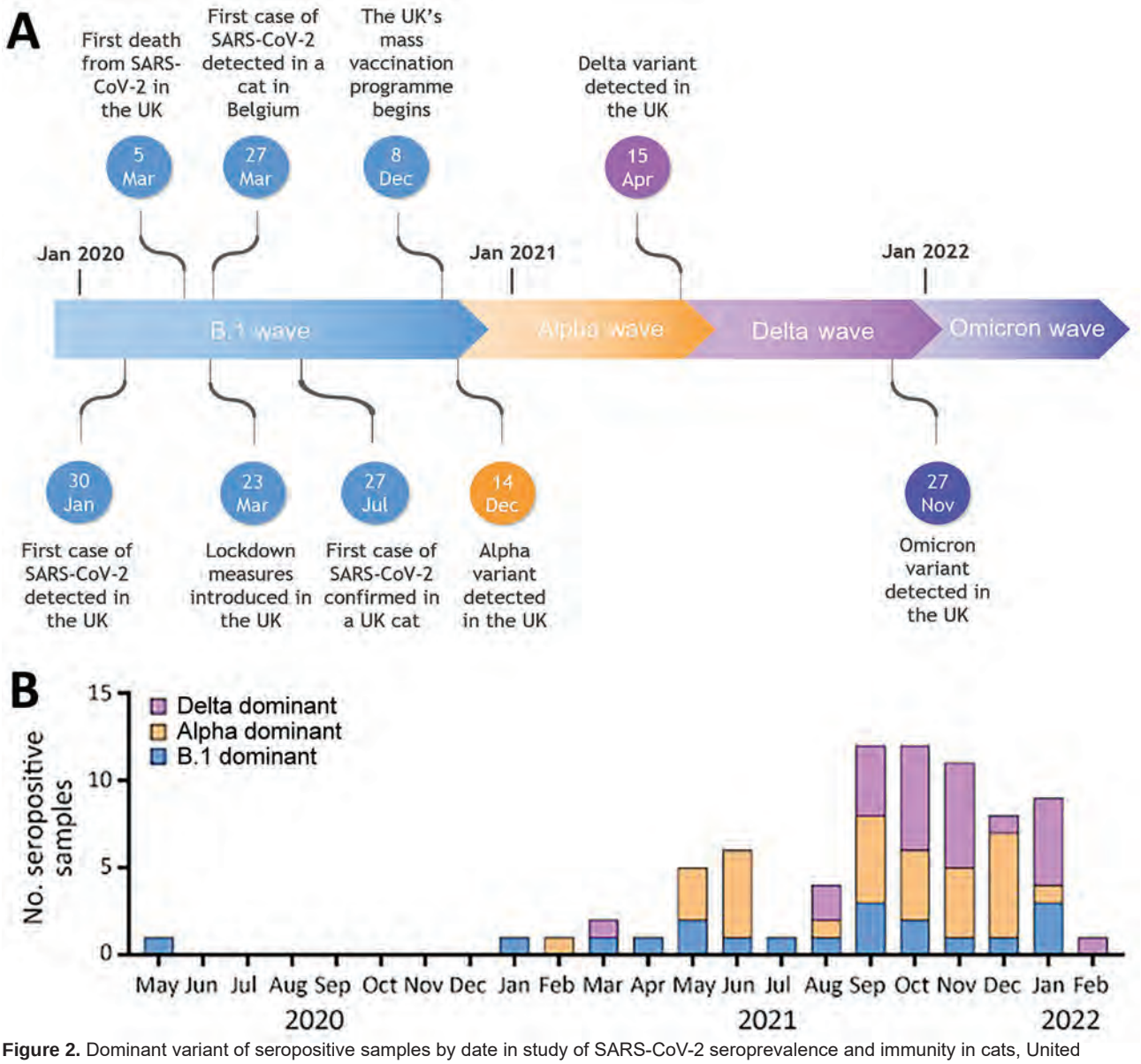

Figure 2. Dominant variant of seropositive samples by date in study of SARS-CoV-2 seroprevalence and immunity in cats, United Kingdom, April 2020–February 2022. A) Timeline of key events during the COVID-19 pandemic in the United Kingdom, including the emergence of major variants into the human population. B) Seropositive samples from cats, categorized by dominant variant and plotted by month. B.1 indicates ancestral/wild-type virus.

Table. Overview of longitudinal samples used in study of SARS-CoV-2 seroprevalence and immunity in cats, United Kingdom, April 2020–February 2022*

Sample	Days between sampling	Titer			% Decrease per day		
		B.1	Alpha	Delta	B.1	Alpha	Delta
Cat F	12	490	257	601	5.90	0.90	4.10
		146	229	303			
Cat G	175	586	677	243	0.40	0.40	0.40
		134	170	58			
Cat H	94	687	825	2,165	0.30	0.20	0.70
		474	678	685			
Cat J	175	627	719	247	0.30	0.40	0.40
		318	241	79			
Cat L	23	109	102	468	−7.20	1.40	1.60
		289	70	301			

*We used 2 samples from each of 5 animals, taken ≥12 d apart. The earlier sample was used in the overall analysis; however, newer samples were also tested. Values related to each variant are shown for each sample, with the earlier sample above and later below. Titers are color-coded by size (stronger titers and greater decreases are shown with darker shading). B.1 indicates ancestral/wild-type virus.

Although a definitive protective threshold antibody level for SARS-CoV-2 has not yet been established, waning neutralizing antibody levels in humans after vaccination have been associated with reinfection and reduced protection against novel variants (*11*). Sequential samples ≥12 days apart were collected from 5 seropositive cats. In all 5 cases, the neutralizing titers against SARS-CoV-2 waned over time. The average percentage decrease in titer per day was highly variable across samples, although for 3 of 5 cats it was consistent across all variants (Table).

Conclusions

This study demonstrated increasing seroprevalence of SARS-CoV-2 antibodies in the UK domestic cat population, consistent with results reported in a survey of cats and dogs recently conducted in Canada (*12*) and the low seroprevalence observed during the first and second waves of the pandemic (*13*,*14*). This increase could be explained by the persistence of the humoral response over time, with a consequent accumulation in the number of seropositive results in the population. In addition, increased seroprevalence during the later months of the pandemic may mean the likelihood of human-to-cat transmission is greater for newer variants that have previously been shown to be more readily transmitted between humans (*15*), although this hypothesis has not been confirmed experimentally.

This study demonstrates the importance of adopting a One Health approach to monitor SARS-CoV-2 infections in pet cats that are in close contact with their SARS-CoV-2–positive owners. Changes in transmissibility of emerging variants should be monitored in cats as well as humans.

This article was preprinted at https://www.biorxiv.org/content/10.1101/2022.11.18.517046v1.

Acknowledgments

We thank Dawn Dunbar and Andrea Bowie for assisting with sample provision.

UK Research and Innovation—Biotechnology and Biological Sciences Research Council (UKRI-BBSRC) contributed to the funding of this research.

About the Author

Miss Tyson is a PhD candidate at the MRC-University of Glasgow Centre for Virus Research, Glasgow, Scotland. Her primary research interests include viral immunology, humoral immunity, and viruses at the human–animal interface.

References

1. World Organisation for Animal Health. COVID-19—events in animals. 2022 [cited 2022 May 1]. https://www.oie.int/en/what-we-offer/emergency-and-resilience/covid-19/#ui-id-3
2. Oreshkova N, Molenaar RJ, Vreman S, Harders F, Oude Munnink BB, Hakze-van der Honing RW, et al. SARS-CoV-2 infection in farmed minks, the Netherlands, April and May 2020. Euro Surveill. 2020;25:2001005. https://doi.org/10.2807/1560-7917.ES.2020.25.23.2001005
3. Sia SF, Yan LM, Chin AWH, Fung K, Choy KT, Wong AYL, et al. Pathogenesis and transmission of SARS-CoV-2 in golden hamsters. Nature. 2020;583:834–8. https://doi.org/10.1038/s41586-020-2342-5
4. Kuchipudi SV, Surendran-Nair M, Ruden RM, Yon M, Nissly RH, Vandegrift KJ, et al. Multiple spillovers from humans and onward transmission of SARS-CoV-2 in white-tailed deer. Proc Natl Acad Sci U S A. 2022;119:e2121644119. https://doi.org/10.1073/pnas.2121644119
5. Yen HL, Sit THC, Brackman CJ, Chuk SSY, Gu H, Tam KWS, et al.; HKU-SPH Study Team. Transmission of SARS-CoV-2 delta variant (AY.127) from pet hamsters to humans, leading to onward human-to-human transmission: a case study. Lancet. 2022;399:1070–8. https://doi.org/10.1016/S0140-6736(22)00326-9
6. Pickering B, Lung O, Maguire F, Kruczkiewicz P, Kotwa JD, Buchanan T, et al. Divergent SARS-CoV-2 variant emerges in white-tailed deer with deer-to-human transmission. Nat

Microbiol. 2022;7:2011–24. https://doi.org/10.1038/s41564-022-01268-9
7. Sila T, Sunghan J, Laochareonsuk W, Surasombatpattana S, Kongkamol C, Ingviya T, et al. Suspected cat-to-human transmission of SARS-CoV-2, Thailand, July–September 2021. Emerg Infect Dis. 2022;28:1485–8. https://doi.org/10.3201/eid2807.212605
8. Wilhelm A, Widera M, Grikscheit K, Toptan T, Schenk B, Pallas C, et al. Limited neutralisation of the SARS-CoV-2 Omicron subvariants BA.1 and BA.2 by convalescent and vaccine serum and monoclonal antibodies. EBioMedicine. 2022;82:104158. https://doi.org/10.1016/j.ebiom.2022.104158
9. Martins M, do Nascimento GM, Nooruzzaman M, Yuan F, Chen C, Caserta LC, et al. The Omicron variant BA.1.1 presents a lower pathogenicity than B.1 D614G and Delta variants in a feline model of SARS-CoV-2 infection. J Virol. 2022;96:e0096122. https://doi.org/10.1128/jvi.00961-22
10. Manali M, Bissett LA, Amat JAR, Logan N, Scott S, Hughes EC, et al. SARS-CoV-2 evolution and patient immunological history shape the breadth and potency of antibody-mediated immunity. J Infect Dis. 2022;227:40–9. https://doi.org/10.1093/infdis/jiac332
11. Ahmed S, Mehta P, Paul A, Anu S, Cherian S, Shenoy V, et al. Postvaccination antibody titres predict protection against COVID-19 in patients with autoimmune diseases: survival analysis in a prospective cohort. Ann Rheum Dis. 2022;81:868–74. https://doi.org/10.1136/annrheum-dis-2021-221922
12. Bienzle D, Rousseau J, Marom D, MacNicol J, Jacobson L, Sparling S, et al. Risk factors for SARS-CoV-2 infection and illness in cats and dogs. Emerg Infect Dis. 2022;28:1154–62. https://doi.org/10.3201/eid2806.220423
13. Smith SL, Anderson ER, Cansado-Utrilla C, Prince T, Farrell S, Brant B, et al. SARS-CoV-2 neutralising antibodies in dogs and cats in the United Kingdom. Curr Res Virol Sci. 2021;2:100011. https://doi.org/10.1016/j.crviro.2021.100011
14. Mahase E. Delta variant: what is happening with transmission, hospital admissions, and restrictions? BMI. 2021;373:n1513.
15. Torjesen I. Covid-19: Omicron may be more transmissible than other variants and partly resistant to existing vaccines, scientists fear. BMJ. 2021;375:n2943. https://doi.org/10.1136/bmj.n2943

Address for correspondence: Grace Tyson, Henry Wellcome Building, Rm 434, Garscube, Glasgow, G61 1QH Scotland, UK; email: g.tyson.1@research.gla.ac.uk

Ranid Herpesvirus 3 Infection in Common Frog *Rana temporaria* Tadpoles

Francesco C. Origgi, Annette Taugbøl

Ranid herpesvirus 3 (RaHV3) is a recently discovered virus associated with skin disease in frogs. We detected RaHV3 DNA in free-ranging common frog (*Rana temporaria*) tadpoles, consistent with premetamorphic infection. Our finding reveals a critical aspect of RaHV3 pathogenesis, relevant for amphibian ecology and conservation and, potentially, for human health.

Infectious diseases have been identified as relevant stressors contributing to the ongoing global amphibian decline (*1*). The collapse of amphibian communities translates into a dramatic loss of biodiversity and critical biomass, which eventually could affect human health (*2*). Ranaviruses and chytrid fungi are primary amphibian pathogens that are causing extinction or extirpation of local amphibian populations worldwide (*3*,*4*). It is likely that other infectious organisms, yet to be characterized, might play a similar role.

Recently, 2 novel alloherpesviruses have been discovered: ranid herpesvirus 3 (RaHV3, *Batravirus ranidallo3*) in the common frog (*Rana temporaria*) and bufonid herpesvirus 1 in the common toad (*Bufo bufo*). Both viruses are associated with proliferative skin disease (*5*–*7*). RaHV3 is invariably associated with gray patchy skin proliferations corresponding to areas of epidermal hyperplasia (Figure 1) (*7*). Lesions vary in severity and size, but their clinical significance in adult frogs is unknown. Equally unclear is the potential effect of the lesions on overall host fitness, reproductive success, and susceptibility to other infectious agents.

Pathogenesis of RaHV3 is only partially understood (*7*); the actual route and timing of infection is unknown. In a transmission study performed on postmetamorphic common frogs, no specific lesions could be observed after RaHV3 inoculation (F.C. Origgi, unpub. data). Furthermore, experimental transmission studies of ranid herpesvirus 1 (RaHV1, *Batravirus ranidallo1*), the first characterized amphibian herpesvirus (*8*), indicated that the virus-associated renal adenocarcinoma most likely occurred when amphibians were infected during the early embryonic stage (premetamorphosis), but not in adult or juvenile stages (postmetamorphosis) (as reviewed in *9*). We investigated the potential occurrence of RaHV3 infection in premetamorphic free-ranging common frogs.

The Study

We collected 14 sample batches of free-ranging tadpoles (3–13 tadpoles per batch), either directly from or in close (<10 m) proximity to 5 ponds in Norway in 2022, where adult frogs with lesions consistent with RaHV3 infection were observed earlier in the year (Figure 2) (F.C. Origgi, unpub. data). We sampled the ponds 2–3 times during early June through mid-July 2022 (Appendix Table, https://wwwnc.cdc.gov/EID/article/29/6/23-0255-App1.pdf). The Gosner developmental stages for tadpoles ranged from stages 26–36.

We collected and humanely euthanized tadpoles by using tricaine methanesulfonate in strict accordance with the Animal Welfare Act (§4 in FOR-2003-03-14-349) of Norway and then preserved them in 96% ethanol. In the laboratory, we bisected each tadpole with a scalpel; we extracted DNA from 1 half as previously described (*5*) and fixed the other half in 10% buffered formalin. We amplified the partial RaHV3 genome sequence as previously described (*5*) and by using a new quantitative PCR protocol (Appendix). Initially, we extracted DNA from 3–5 tadpoles from each sampling date and pond location; if we obtained a positive signal for RaHV3 by

Authors affiliations: University of Messina, Messina, Italy (F.C. Origgi); University of Bern, Bern, Switzerland (F.C. Origgi); Norwegian Institute for Nature Research, Lillehammer, Norway (A. Taugbøl)

DOI: https://doi.org/10.3201/eid2906.230255

PCR, we tested all tadpoles collected from the same location. We processed the fixed-tissues, embedded them in paraffin, prepared 5 µm–thick sections, and stained the sections with hematoxylin and eosin in accordance with the standard protocol used at the Vetsuisse Faculty, University of Bern.

After qualitative and quantitative PCR on tadpole DNA (n = 77 samples), we found 2 of 14 sampled batches were positive for RaHV3, corresponding to 2 of the 5 tested pond locations (Lillehammer and Skytta) (Figure 2). After testing each tadpole in the positive batches, we identified 6 of 13 tadpoles from the Lillehammer pond and 1 of 4 from the Skytta pond that were positive for RaHV3 DNA; genome equivalents ranged from 2×10^1 to 2×10^7. After sequencing amplicons obtained by using qualitative PCR (*5*), we found a 100% match with the reference strain RaHV3_FO1_2015 (Genbank accession no. NC_034618.1).

We did not observe differences in histological sections of RaHV3 PCR-positive and PCR-negative tadpoles. However, RaHV3-associated changes might have been masked by the advanced autolysis observed in the examined tissue sections.

Figure 1. Ranid herpesvirus 3 infection in common frog *Rana temporaria* tadpoles, Norway. Image shows a large number of multifocal to coalescent, mildly elevated, gray patches (epidermal hyperplasia) extending over most of the integument, particularly clustering along the left flank. Between gray areas is normally pigmented skin. Image copyright © Jeroen van der Kooij.

Conclusions

Finding genomic RaHV3 DNA in free-ranging tadpoles is a major step toward understanding the pathogenesis of RaHV3-associated disease. In particular, this result supports the hypothesis that infection occurs during the frog's premetamorphic embryonic or larval stages. Experimental RaHV1 infection of leopard frogs (*Lithobates pipiens*) was successful only

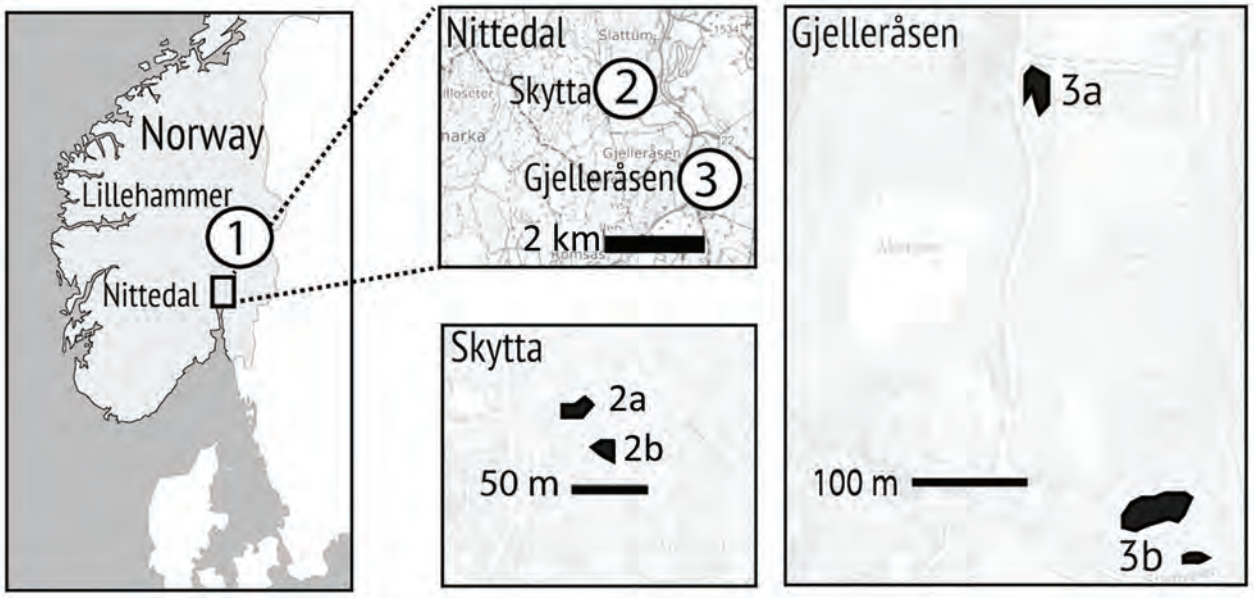

Figure 2. Location of sampling areas in study of ranid herpesvirus 3 infection in common frog *Rana temporaria* tadpoles, Norway. We collected 14 sample batches of free-ranging tadpoles (3–13 tadpoles per batch) either directly from or in close (<10 m) proximity to 5 ponds in Norway in 2022, where adult frogs with lesions consistent with ranid herpesvirus 3 (RaHV3) infection were observed earlier in the year. Maps show locations of ponds in Lillehammer, Skytta, and Gjelleråsen and the distances (in meters) between them. The 2 ponds marked collectively as 3b are linked by marshland in which adult frogs breed independently and are, therefore, treated as 1 complex. We found 2 of 14 sampled tadpole batches were positive for RaHV3 by using PCR, corresponding to pond areas in Lillehammer and Skytta. After testing each tadpole in the positive batches, we identified 6 of 13 tadpoles from the Lillehammer pond and 1 of 4 from the Skytta pond that were RaHV3-positive.

during the early embryonic stages (*9*). Why premetamorphic frogs are presumptively more susceptible to herpesvirus infections is unclear. The lack of keratinized skin in tadpoles (*10*) and the substantial immune system differences between premetamorphic and postmetamorphic life stages might partially explain the susceptibility of premetamorphic frogs to natural infection (*11*). Studies performed with RaHV1 did not clarify the natural route of infection because the embryos were experimentally inoculated with the virus in the pronephros, which is unlikely to mimic what occurs in nature (*9*). RaHV3-infected adult frogs are known to release a large number of virions embedded in sloughed keratinocytes (*5*,*7*), which could eventually be ingested by tadpoles. However, the possibility that oral ingestion of RaHV3 would cause tadpole infection, similarly to what has been shown for Ranavirus, a major amphibian pathogen (*12*), will need to be ruled out by a transmission study.

All 5 tadpole populations were collected in or near ponds where infected adults had been confirmed earlier in the Spring, but only 2 tadpole populations were RaHV3-positive and only at 1 timepoint for each pond (2 of 14 samples in total). Among the positive samples, the Lillehammer population had ≈50% and the Skytta population had ≈25% positivity rates. Reasons for discrepancies in incidence of RaHV3 infection between the different sampled populations remain unclear. Our finding suggests either sporadic RaHV3 infection within different tadpole populations, high virus lethality in infected tadpoles, or both. According to the second hypothesis, RaHV3-positive tadpoles would be difficult to detect in field conditions, because they would rapidly die and be scavenged. Herpesviruses, including alloherpesviruses, infecting a variety of animal species generally cause more severe disease and death in young, immature individuals than in adult hosts, (*13*). Accordingly, RaHV3 might be fatal to a large proportion of infected tadpoles resulting in low detection rates in the remaining viable tadpole population. No obvious tadpole die-offs had been recently reported at the sampling sites; however, those sites are not presently monitored.

In conclusion, our study opens a new venue for understanding RaHV3 pathogenesis and potential effects of RaHV3 infections on premetamorphic and postmetamorphic life stages of amphibian hosts. Understanding the short- and long-term consequences of RaHV3 and other herpesvirus infections on frog populations will be critical for amphibian conservation programs, maintaining biodiversity, and, in turn, supporting human and planetary health (*2*).

Acknowledgments

We thank the technical personnel at Vetsuisse Bern, Institute of Animal Pathology, for histological analysis and Ian Hawkins for critical review of this manuscript.

Fieldwork was funded by the Norwegian Financial Mechanism 2014–2021, project no. 2019/34/H/NZ8/00683 (ECOPOND project). Development of molecular tests was partially supported by the Vontobel Foundation (Zurich, Switzerland) and Swiss Federal Office of the Environment (FOEN; grant no. R212-1468).

About the Author

Dr. Origgi is a veterinary microbiologist and pathologist at the University of Messina and University of Bern. His research interests focus on infectious diseases and pathology of wildlife, especially reptiles and amphibians. Dr. Taugbøl is an evolutionary geneticist at the Norwegian Institute for Nature Research. Her research interests include biodiversity conservation.

References

1. Catenazzi A. State of the world's amphibians. Annu Rev Environ Resour. 2015;40:91–119. https://doi.org/10.1146/annurev-environ-102014-021358
2. Springborn MR, Weill JA, Lips KR, Ibáñez R, Ghosh A. Amphibian collapses increased malaria incidence in Central America. Environ Res Lett. 2022;17:104012. https://doi.org/10.1088/1748-9326/ac8e1d
3. Price SJ, Garner TWJ, Nichols RA, Balloux F, Ayres C, Mora-Cabello de Alba A, et al. Collapse of amphibian communities due to an introduced *Ranavirus*. Curr Biol. 2014;24:2586–91. https://doi.org/10.1016/j.cub.2014.09.028
4. Skerratt LF, Berger L, Speare R, Cashins S, McDonald KR, Phillott AD, et al. Spread of chytridiomycosis has caused the rapid global decline and extinction of frogs. EcoHealth. 2007;4:125–34. https://doi.org/10.1007/s10393-007-0093-5
5. Origgi FC, Schmidt BR, Lohmann P, Otten P, Akdesir E, Gaschen V, et al. Ranid herpesvirus 3 and proliferative dermatitis in free-ranging wild common frogs (*Rana temporaria*). Vet Pathol. 2017;54:686–94. https://doi.org/10.1177/0300985817705176
6. Origgi FC, Schmidt BR, Lohmann P, Otten P, Meier RK, Pisano SRR, et al. Bufonid herpesvirus 1 (BfHV1) associated dermatitis and mortality in free ranging common toads (*Bufo bufo*) in Switzerland. Sci Rep. 2018;8:14737. https://doi.org/10.1038/s41598-018-32841-0
7. Origgi FC, Otten P, Lohmann P, Sattler U, Wahli T, Lavazza A, et al. Herpesvirus-associated proliferative skin disease in frogs and toads: proposed pathogenesis. Vet Pathol. 2021;58:713–29. https://doi.org/10.1177/03009858211006385
8 Lucké B. A neoplastic disease of the kidney of the frog, *.Rana pipiens.* Am J Cancer. 1934;20:352–79. https://doi.org/10.1158/ajc.1934.352
9. McKinnell RG. The Lucké frog kidney tumor and its herpesvirus. Am Zool. 1973;13:97–114. https://doi.org/10.1093/icb/13.1.97
10 Marantelli G, Berger L, Speare R, Keegan L. Distribution of the amphibian chytrid *Batrachochytrium dendrobatidis* and

keratin during tadpole development. Pac Conserv Biol. 2004;10:173–9. https://doi.org/10.1071/PC040173
11. Rollins-Smith LA, Blair PJ, Davis AT. Thymus ontogeny in frogs: T-cell renewal at metamorphosis. Dev Immunol. 1992;2:207–13. https://doi.org/10.1155/1992/26251
12. Hoverman JT, Gray MJ, Miller DL. Anuran susceptibilities to ranaviruses: role of species identity, exposure route, and a novel virus isolate. Dis Aquat Organ. 2010;89:97–107. https://doi.org/10.3354/dao02200
13. Michel B, Fournier G, Lieffrig F, Costes B, Vanderplasschen A. Cyprinid herpesvirus 3. Emerg Infect Dis. 2010;16:1835–43. https://doi.org/10.3201/eid1612.100593

Address for correspondence: Francesco Origgi, Institute of Infectious Animal Diseases, Department of Veterinary Sciences, University of Messina, Viale Giovanni Palatucci sn, 98168 Messina, Italy; email: foriggi@unime.it; or Institute of Animal Pathology, Vetsuisse Faculty, University of Bern, Länggassstrasse 122, CH-3012, Bern, Switzerland; email: francesco.origgi@vetsuisse.unibe.ch

Baylisascaris procyonis Roundworm Infection in Child with Autism Spectrum Disorder, Washington, USA, 2022

Beth A. Lipton,[1] Hanna N. Oltean,[1] Roger B. Capron, Arran Hamlet, Susan P. Montgomery, Rebecca J. Chancey, Victoria J.L. Konold, Katherine E. Steffl

We describe a case of *Baylisascaris procyonis* roundworm infection in a child in Washington, USA, with autism spectrum disorder. Environmental assessment confirmed nearby raccoon habitation and *B. procyonis* eggs. *B. procyonis* infections should be considered a potential cause of human eosinophilic meningitis, particularly among young children and persons with developmental delays.

Baylisascaris spp. are ascarid worms that parasitize the small intestines of multiple species. The primary definitive host for *B. procyonis* roundworms is the raccoon (*Procyon lotor*), although other carnivores, including dogs, can serve as definitive hosts (*1*). Infected raccoons shed >1 million *B. procyonis* eggs daily; excreted eggs take 2–4 weeks to embryonate and become infective. In the western United States, the estimated prevalence of *B. procyonis* infection in raccoons is 68%–82% (*2*). Raccoons often defecate in communal locations (raccoon latrines) that are close to areas of human activity or living spaces, such as yards, decks, roofs, or attics. Humans become intermediate hosts after ingesting infective eggs that hatch into larvae, penetrate the gut wall, and migrate through tissues, potentially resulting in visceral, ocular, or neural larva migrans syndromes; neural larva migrans often manifests as acute eosinophilic meningitis. Tissue damage and clinical outcomes of baylisascariasis might be severe; permanent neurologic sequalae and death might occur because of the large size of *B. procyonis* larvae and invasive tissue migration (*3*). Severity of disease is related to host size, number of eggs ingested, larval migration pathway, and extent of host inflammatory responses (*4*,*5*). As with other parasite larva migrans, *B. procyonis* larvae are found mostly in muscle tissue; <5% of migrating larvae reach the brain (*5*). Asymptomatic and subclinical infections are known to occur. Fewer ingested eggs might result in positive serologic tests in the absence of neurologic disease (*5*,*6*).

We describe a case of *B. procyonis* infection in a child in Washington, USA, with autism spectrum disorder and history of pica who had eosinophilic meningitis. We conducted an environmental assessment of the patient's residence to assess raccoon activity and potential exposure sources.

The Study

In July 2022, a 7-year-old boy with a history of autism spectrum disorder and global developmental delay accompanied by lack of verbal ability began having episodes of mild motor impairment, lethargy, decreased responsiveness, and difficulty understanding and executing commands that lasted 45 minutes to 2 hours (first episode = day 0). He was seen at an emergency department on day 11, then hospitalized by a second emergency department the next day after a prolonged period of stumbling and lethargy. The patient had not traveled outside of Washington in the past 2 years and had no household pets. In recent weeks, the patient had played in a sandbox where nonhuman feces were observed and visited a location with farm animals.

Author affiliations: Washington State Department of Health, Shoreline, Washington, USA (B.A. Lipton, H.N. Oltean, A. Hamlet); Skagit County Health Department, Mount Vernon, Washington, USA (R.B. Capron); Centers for Disease Control and Prevention, Atlanta, Georgia, USA (A. Hamlet, S.P. Montgomery, R.J. Chancey); Seattle Children's Hospital, Seattle, Washington, USA (V.J.L. Konold, K.E. Steffl)

DOI: https://doi.org/10.3201/eid2906.230290

[1]These authors contributed equally to this article.

While hospitalized, the patient underwent several tests. A complete blood count showed peripheral eosinophilia (1,693 eosinophils/μL), and results of an upper respiratory virus and bacteria PCR panel were negative. An electroencephalogram indicated focal cerebral pathology, and brain magnetic resonance imaging showed patchy white matter disease with limited gray matter involvement (Figure 1). Cerebrospinal fluid (CSF) was collected and had negative PCR results for cytomegalovirus, enterovirus, herpes simplex virus 1, herpes simplex virus 2, herpes simplex virus 6, human parechovirus, and varicella zoster virus. CSF was Gram stain and culture negative but had a nucleated cell count of 6 cells/μL (reference range 0–5 cells/μL) with 50% eosinophils. Acute disseminated encephalomyelitis was suspected, and corticosteroid treatment was initiated. Consultation with the Centers for Disease Control and Prevention (CDC) was pursued, given the eosinophilic meningitis and possible parasitic cause of illness, after which a 10-day course of albendazole (25 mg/kg body weight/d) was initiated on day 17.

The patient's serum and CSF specimens were sent to CDC for *B. procyonis* testing. The patient's serum was positive for *B. procyonis*–specific antibodies; CSF was antibody negative. A *Toxocara* spp. IgG test was positive, although false-positive results might occur in patients with other parasitic infections, including *Baylisascaris* spp. Conversely, *B. procyonis* test cross-reactivity with toxocariasis was not expected (*7*). On day 23, the patient was discharged from the hospital. The family reported ongoing but improving symptoms 1 month after discharge.

In mid-September 2022, we performed an environmental investigation at the patient's residence. The family had never seen raccoons in the yard but noted possible animal feces at the base of a fir tree. After additional questioning, the family recalled that the patient had put material from the ground around this tree in his mouth in July; we observed a raccoon latrine at this location (Figure 2). We collected 4 fecal samples for fecal flotation analysis from the following locations: raccoon latrine (location 1, 2 samples), a grassy area away from the latrine (location 2, 1 sample), and the sandbox (location 3, 1 sample). Two samples were positive for *B. procyonis* eggs, and 2 samples were positive for non–*B. procyonis* roundworm eggs (Table).

We noted various raccoon attractants around the property, including bushes and trees, a brush pile, and a large open shed. We provided oral feedback and written materials regarding safe latrine clean-up, regular observation and prompt clean-up of feces, and methods to discourage raccoons from inhabiting nearby areas. Raccoons are not a reservoir species for rabies in Washington; therefore, we did not provide education on rabies prevention.

Reported cases of human *B. procyonis* infection are rare, despite the proximity and prevalence of infected raccoons across much of the United States (*8*). We found 37 published cases of *B. procyonis* infection in North America (33 in the United States, 4 in Canada) (*2*,*4*,*8*–*13*). Of published case reports, including this study, the median age of infected persons was 1.6 years (range 9 months–73 years); 32 (82%) persons were male, and 7 (18%) infections resulted in death. Geophagia or pica was mentioned in 21 (55%) cases, and 14 (37%) cases described developmental disabilities in the patients. Case-patients with geophagia or pica were associated with an increased risk for death, possibly because of ingestion of higher numbers of *B. procyonis* eggs. All but 2 cases described neurologic symptoms. Undetected subclinical infections and lack of commercially available testing likely leads to overestimation of the overall death rate (*5*–*7*). Baylisascariasis is not nationally notifiable in the United States but was recently added to the notifiable conditions list in Washington (*14*).

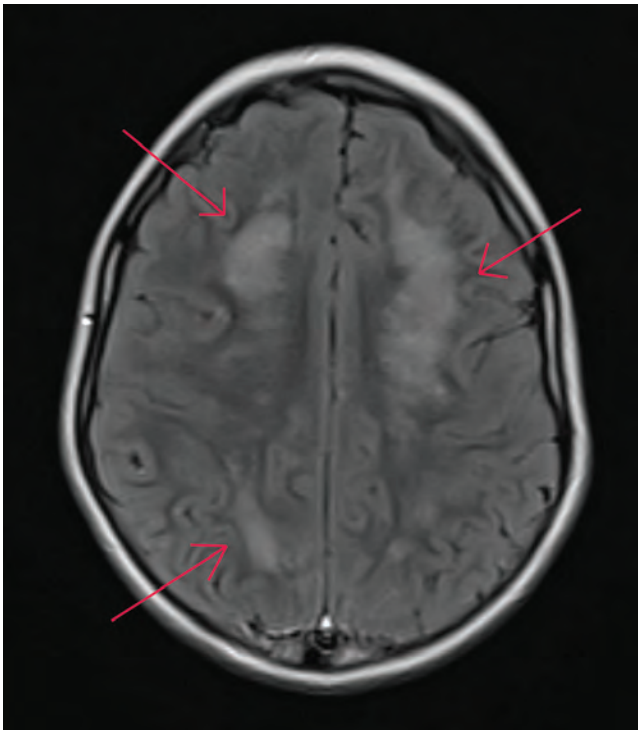

Figure 1. Magnetic resonance imaging of brain of child with autism spectrum disorder infected with *Baylisascaris procyonis* roundworms, Washington, USA, 2022. Axial section of the brain shows patchy white matter disease with limited gray matter involvement. Red arrows indicate diseased regions.

Figure 2. Raccoon latrine found at residence of child with autism spectrum disorder infected with *Baylisascaris procyonis* roundworms, Washington, USA, 2022.

Conclusions

Young children and persons with developmental delays are at high risk for *B. procyonis* infection because of hand–mouth behaviors, as are persons exposed to raccoons or environments where raccoons are frequently found (*3*). Healthcare providers should consider *B. procyonis* roundworm infections a possible cause of eosinophilic meningitis even without known patient exposure to raccoon feces. The ubiquitous nature of raccoons and the 1–4-week incubation period for infection might cause difficulty in characterizing potential exposure locations. Treatment with albendazole and corticosteroids during the early stage of infection might reduce serious tissue damage, although no treatments are totally effective (*3*,*9*). Known or suspected oral exposure to raccoon feces indicates immediate prophylactic treatment with albendazole should be considered, which might prevent disease (*10*).

Raccoon latrines have diverse locations, sizes, and appearances. Raccoons might share multiple latrines over a short period of time, increasing the accumulation of *B. procyonis* eggs (*15*). Feces are often dark and tubular; latrines might remain active for >1 year (*3*,*15*). Eggs can remain viable in the environment for years and are difficult to kill or remove. CDC provides resources on how to identify and safely clean up a latrine (*3*).

In summary, discouraging raccoons from residential areas and increased recognition of raccoon latrines can help prevent *B. procyonis* infections. Public and healthcare provider awareness of *B. procyonis* infection risks, especially for persons at higher risk such as young children and those with developmental delays, is critical for prevention and early treatment and improving disease outcome.

Acknowledgments

We thank Laura Williams and Rachel Soltys for fecal flotation analysis and study consultation and the CDC Parasitic Diseases Laboratory (Center for Global Health, Division of Parasitic Diseases and Malaria) for *B. procyonis* testing.

This report was reviewed by CDC, and the study was conducted according to applicable federal law [45 Code of Federal Regulations, part 46.102(l)(2), 21 Code of Federal Regulations, part 56; 42 United States Code (U.S.C.) §241(d); 5 U.S.C. §552a; 44 U.S.C. §3501 et seq] and CDC policy.

About the Author

Dr. Lipton is the public health veterinarian for the Washington State Department of Health, Office of Health and Science, Center for Public Health, Medical and Veterinary Sciences. Her primary research interests

Table. Fecal flotation results from environmental sampling in September 2022 at residence of child with autism spectrum disorder infected with *Baylisascaris procyonis* roundworms, Washington, USA*

Fecal sample characteristics	Organism	Result	No. eggs/g†
Location 1, pooled sample 1, raccoon latrine at base of fir tree	*B. procyonis*	Positive	14
	Non-*B. procyonis* roundworms	Negative	NA
Location 1, pooled sample 2, raccoon latrine at base of fir tree	*B. procyonis*	Negative	NA
	Non-*B. procyonis* roundworms	Negative	NA
Location 2, unidentified feces in grassy area away from raccoon latrine	*B. procyonis*	Positive	25
	Non-*B. procyonis* roundworms	Positive	1
Location 3, pooled sample, suspected cat feces in sandbox	*B. procyonis*	Negative	NA
	Non-*B. procyonis* roundworms	Positive	1

*NA, not applicable.
†No. eggs per gram of collected feces detected by fecal flotation.

focus on using epidemiological and environmental data to elucidate disease transmission at the human–animal interface.

References

1. Centers for Disease Control and Prevention. Raccoon roundworms in pet kinkajous—three states, 1999 and 2010. MMWR Morb Mortal Wkly Rep. 2011;60:302–5.
2. Hung T, Neafie RC, Mackenzie IRA. *Baylisascaris procyonis* infection in elderly person, British Columbia, Canada. Emerg Infect Dis. 2012;18:341–2. https://doi.org/10.3201/eid1802.111046
3. Centers for Disease Control and Prevention. Parasites—baylisascaris infection [cited 2022 Nov 30]. https://www.cdc.gov/parasites/baylisascaris
4. Kawakami V, Casto A, Natarajan N, Snyder A, Mosser J, Bonwitt J, et al. Notes from the field: *Baylisascaris procyonis* encephalomyelitis in a toddler—King County, Washington, 2017. MMWR Morb Mortal Wkly Rep. 2018;67:79–80. https://doi.org/10.15585/mmwr.mm6702a6
5. Weinstein SB, Lake CM, Chastain HM, Fisk D, Handali S, Kahn PL, et al. Seroprevalence of *Baylisascaris procyonis* infection among humans, Santa Barbara County, California, USA, 2014–2016. Emerg Infect Dis. 2017;23:1397–9. https://doi.org/10.3201/eid2308.170222
6. Sapp SGH, Rascoe LN, Wilkins PP, Handali S, Gray EB, Eberhard M, et al. *Baylisascaris procyonis* roundworm seroprevalence among wildlife rehabilitators, United States and Canada, 2012–2015. Emerg Infect Dis. 2016;22:2128–31. https://doi.org/10.3201/eid2212.160467
7. Rascoe LN, Santamaria C, Handali S, Dangoudoubiyam S, Kazacos KR, Wilkins PP, et al. Interlaboratory optimization and evaluation of a serological assay for diagnosis of human baylisascariasis. Clin Vaccine Immunol. 2013;20:1758–63. https://doi.org/10.1128/CVI.00387-13
8. Sircar AD, Abanyie F, Blumberg D, Chin-Hong P, Coulter KS, Cunningham D, et al. Raccoon roundworm infection associated with central nervous system disease and ocular disease—six states, 2013–2015. MMWR Morb Mortal Wkly Rep. 2016;65:930–3. https://doi.org/10.15585/mmwr.mm6535a2
9. Graeff-Teixeira C, Morassutti AL, Kazacos KR. Update on baylisascariasis, a highly pathogenic zoonotic infection. Clin Microbiol Rev. 2016;29:375–99. https://doi.org/10.1128/CMR.00044-15
10. Lauffer A, Lutz P, Flesher SL. *Baylisascaris procyonis* exposure case study. W V Med J. 2016;112:32–3.
11. Goldman-Yassen AE, Derman A, Madan RP, Radmanesh A. A worm's tale or why to avoid the raccoon latrine: a case of *Baylisascaris procyonis* meningoencephalitis. Case Rep Radiol. 2022;2022:5199863. https://doi.org/10.1155/2022/5199863
12. Dunbar M, Lu S, Chin B, Huh L, Dobson S, Al-Rawahi GN, et al. Baylisascariasis: a young boy with neural larva migrans due to the emerging raccoon round worm. Ann Clin Transl Neurol. 2018;6:397–400. https://doi.org/10.1002/acn3.694
13. Muganda GN, Akagi NE, Fagbemi OD, Chusid MJ, Nelson AM. Rapid therapeutic response of eosinophilic meningoencephalitis in a toddler with *Baylisascaris procyonis* infection. WMJ. 2018;117:130–2.
14. Washington State Legislature. Washington administrative code, title 246, chapter 246-101: notifiable conditions [cited 2022 Nov 30]. https://apps.leg.wa.gov/WAC/default.aspx?cite=246-101
15. Hirsch BT, Prange S, Hauver SA, Gehrt SD. Patterns of latrine use by raccoons (*Procyon lotor*) and implication for *Baylisascaris procyonis* transmission. J Wildl Dis. 2014;50:243–9. https://doi.org/10.7589/2013-09-251

Address for correspondence: Beth A. Lipton, Washington State Department of Health, 1610 NE 150th St, Shoreline, WA 98155, USA; email: beth.lipton@doh.wa.gov

MERS-CoV–Specific T-Cell Responses in Camels after Single MVA-MERS-S Vaccination

Christian Meyer zu Natrup, Lisa-Marie Schünemann, Giulietta Saletti, Sabrina Clever, Vanessa Herder, Sunitha Joseph, Marina Rodriguez, Ulrich Wernery, Gerd Sutter, Asisa Volz

We developed an ELISPOT assay for evaluating Middle East respiratory syndrome coronavirus (MERS-CoV)–specific T-cell responses in dromedary camels. After single modified vaccinia virus Ankara-MERS-S vaccination, seropositive camels showed increased levels of MERS-CoV–specific T cells and antibodies, indicating suitability of camel vaccinations in disease-endemic areas as a promising approach to control infection.

The Middle East respiratory syndrome coronavirus (MERS-CoV) is a betacoronavirus that is of special interest for public health. Dromedary camels have been identified as natural animal reservoirs, with >90% MERS-CoV seroprevalence reported in Middle East countries (*1*–*4*). Such permanent viral circulation within camel herds poses a constant threat of zoonotic transmission into human populations (*5*). Thus, a potentially useful approach to prevent MERS-CoV zoonoses focuses on vaccination-based reduction of spill over events from camels as a classical One Health approach (*6*,*7*).

Besides antibody responses, MERS-CoV–specific T cells probably play a major role in rapid viral clearance and long-lasting immunity against MERS-CoV infections (*8*). Although serologic assays were rapidly developed, established T-cell assays for camels are still lacking, yet urgently needed for contact tracing, epidemiology, and vaccine evaluation studies. Several MERS-CoV–specific vaccine candidates are under investigation and use different platforms, such as DNA vaccines or adenoviral vectors (*9*–*12*). A promising experimental vaccine for use in camels is recombinant modified vaccinia virus Ankara (MVA) expressing full-length MERS-CoV spike protein as antigen (MVA-MERS-S) (*13*). Experimental vaccination with MVA-MERS-S in dromedaries can induce protective immunity to MERS-CoV (*14*). Moreover, MVA-MERS-S proved safe and immunogenic in a phase Ia/b clinical study in humans (*15*). The aim of this exploratory study in Dubai, United Arab Emirates, where enzootic MERS-CoV is prevalent, was to establish an assay for detecting MERS-CoV–specific T cells in dromedary camels under field conditions.

The Study

To investigate the effect of MVA-MERS-S vaccination in naive or previously infected animals, we divided 12 adult dromedary camels into 2 cohorts: naive and MERS-CoV seropositive solely based on presence of MERS-S IgG (by ELISA) before vaccination. Eight camels had antibody titers relevant for seroconversion (optical density [OD] ratio >1.1), indicating previous MERS-CoV infection, whereas the remaining 4 camels had no MERS-specific antibodies (Table 1).

Table 1. MERS-CoV seroprevalence in 12 dromedary camels before vaccination, Dubai, United Arab Emirates*

Camel ID	Optical density ratio (ELISA)	MERS-CoV infection status/cohort
1	0.07	Naive
2	2.09	Seropositive
3	2.97	Seropositive
4	4.00	Seropositive
5	0.06	Naive
6	0.07	Naive
7	0.05	Naive
8	4.11	Seropositive
9	3.42	Seropositive
10	4.59	Seropositive
11	2.48	Seropositive
12	3.22	Seropositive

*ID, identification; MERS-CoV, Middle East respiratory syndrome coronavirus.

Author affiliations: University of Veterinary Medicine Hannover, Hanover, Germany (C. Meyer zu Natrup, L.-M. Schünemann, G. Saletti, S. Clever, A. Volz); University of Glasgow, Glasgow, Scotland, UK (V. Herder); Central Veterinary Research Laboratory, Dubai, United Arab Emirates (S. Joseph, M. Rodriguez, U. Wernery); Ludwig Maximilian University Munich, Munich, Germany (G. Sutter)

DOI: https://doi.org/10.3201/eid2906.220128

Table 2. Cohorts of dromedary camels by MERS-CoV seroprevalence and vaccine candidate used Dubai, United Arab Emirates*

Category	Type	Vaccine candidate		Total
		MVA	MVA-MERS-S	
MERS-CoV infection	Naive	1	3	4
	Seropositive	3	5	8
	Total	4	8	12

*MERS-CoV, Middle East respiratory syndrome coronavirus; MVA, modified vaccinia virus Ankara; MVA-MERS-S, modified vaccinia virus Ankara expressing full-length MERS-CoV spike protein as antigen.

Camels were either vaccinated with MVA-MERS-S or MVA as a control by using intramuscular inoculation (dose 2.5 × 10^8 PFU/2 mL) (Table 2). Animals and application sites were monitored and scored daily for an observation period of 22 days. No clinical signs or potential side effects were observed (data not shown). Analysis of the IgG response at the day of vaccination and 15 days later (Figure 1) showed no differences in MERS-CoV–specific antibodies in naive camels (MVA– and MVA-MERS-S–vaccinated camels).

One seropositive animal vaccinated with MVA showed an increased optical density (OD) ratio of 0.54, whereas the other 2 animals showed no difference or a decreased ratio of 0.19. Seropositive camels vaccinated with MVA-MERS-S (n = 5) mounted increased levels of MERS binding antibodies, with a mean titer (OD ratio) of 4.44 on day 15 compared with 3.22 at day 0 postvaccination. Two MVA-MERS-S vaccinated camels from seropositive animals showed an increased OD ratio >2.4.

To assess T-cell responses, we prepared peripheral blood mononuclear cells (PBMCs) from blood plus EDTA on different days postvaccination during the observation period. PBMCs were restimulated with 2 pools of overlapping peptides comprising either the S1 or S2 subunit of MERS-CoV spike glycoprotein (Appendix Figure, https://wwwnc.cdc.gov/EID/article/29/6/23-0128-App1.pdf) analyzed by using interferon (IFN) γ ELISpot assays.

After S1 peptide pool stimulation, we detected no IFN-γ–producing cells in the MVA-vaccinated naive animals (Figure 2, panel A). MVA-MERS-S vaccinated naive animals (n = 3) showed detectable levels of S1-specific T cells on day 6 postvaccination (mean 11.1 spot-forming T cells [SFC]/10^6 PBMCs), which further increased until day 8 postvaccination (mean 63.3 IFN-γ SFC/10^6 PBMCs).

MVA-vaccinated seropositive animals showed negligible levels of IFN-γ–producing cells, except for 1 animal that had S1-specific T cells on days 6 and 8 postvaccination (mean 217.8 IFN-γ SFC/10^6 PBMCs). Seropositive MVA-MERS-S–vaccinated animals had substantially higher activated S1-specific T-cell levels starting on day 6 postvaccination (mean 230.6 IFN-γ SFC/10^6 PBMCs), further increasing on day 8 postvaccination (mean 497.8 IFN-γ SFC/10^6 PBMCs). Subsequently, S1-specific T-cell levels decreased on day 10 (mean 110 IFN-γ SFC/10^6 PBMCs), until reaching relatively low levels at day 22 postvaccination (mean 42.8 IFN-γ SFC/10^6 PBMCs).

Upon S2 peptide stimulation, we detected lower levels of IFN-γ–producing cells compared with S1 peptide stimulation (Figure 2, panel B). The MVA-vaccinated naive camels had low levels of IFN-γ–producing cells on day 6 and 8 postvaccination (mean 38.3 IFN-γ SFC/10^6 PBMCs). MVA-MERS-S-vaccinated naive animals showed low responses in all animals; mean levels of 11.9 IFN-γ SFC/10^6 PBMCs on day 6 postvaccination increased to 36.3 IFN-γ SFC/10^6 PBMCs on day 8 postvaccination, then decreased again by day 22 postvaccination.

Two MVA-vaccinated seropositive animals mounted no detectable levels of S2-specific T cells. The same seropositive animal mounting S1-specific T cells revealed increased levels of S2-specific T cell activation on day 6 and 8 postvaccination (mean

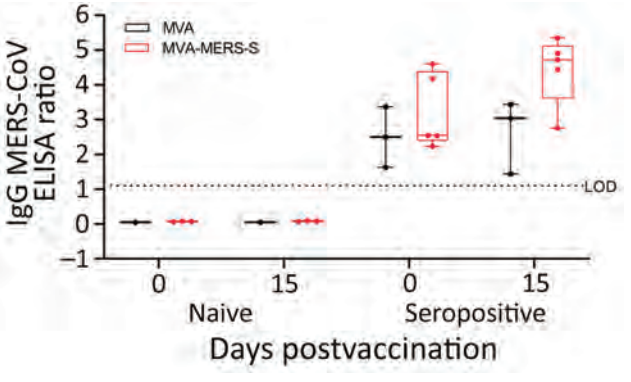

Figure 1. Antigen-specific humoral immunity after MVA-MERS-S vaccination in dromedary camels, Dubai, United Arab Emirates. MERS-CoV seropositive and naive dromedary camels were immunized once with 2.5 x 10^8 plaque-forming units of MVA-MERS-S or MVA as a vector control. Serum samples were collected on day 0 and on day 15 after single-shot vaccination. Black indicates serum samples analyzed for MERS-CoV S1 IgG by ELISA of MVA vaccinated animals and red indicates for MVA-MERS-S–vaccinated animals. Box plots show individual values (dots), median values (horizontal lines within boxes), first and third quartiles (box tops and bottoms), and minimums and maximums of value distribution (error bars). LOD, limit of detection; MERS-CoV, Middle East respiratory syndrome coronavirus; MVA, modified vaccinia virus Ankara; MVA-MERS-S, modified vaccinia virus Ankara expressing full-length MERS-CoV spike protein as antigen.

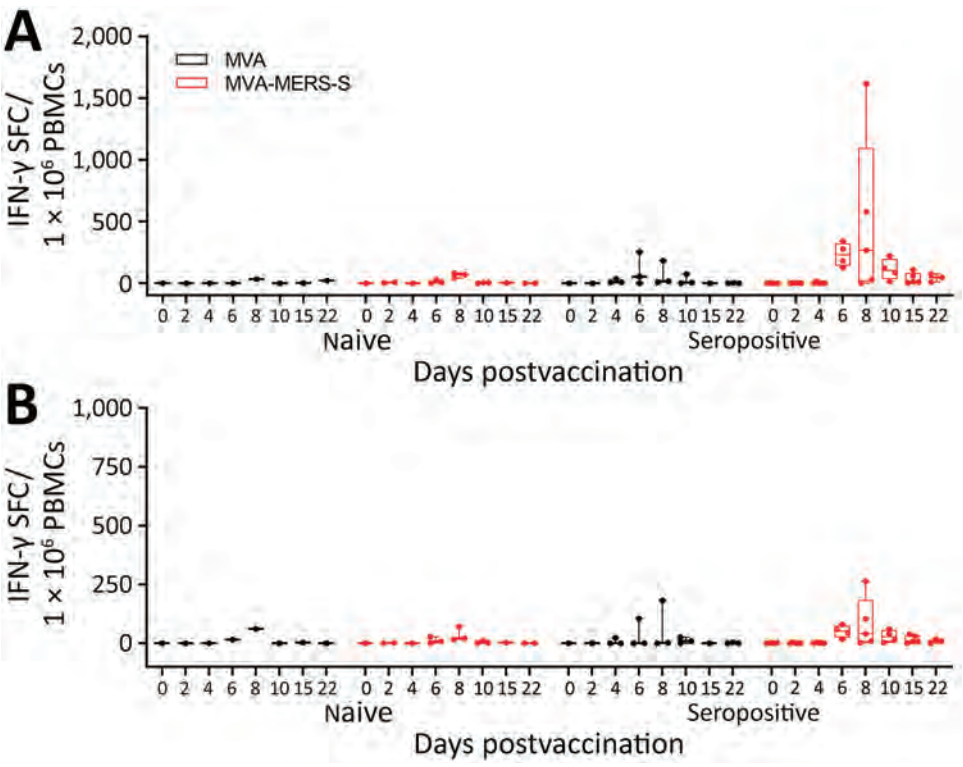

Figure 2. Antigen-specific cellular immunity after MVA-MERS-S vaccination in dromedary camels, Dubai, United Arab Emirates. PBMCs were isolated from blood samples on different days post–single-shot vaccination and IFN-γ SFCs were measured by ELISpot assay after restimulation of PBMCs from different time points with overlapping peptides comprising the MERS-CoV S1 (A) and MERS-CoV-S2 (B) protein subunit. Box plots show individual values (dots), median values (horizontal lines within boxes), first and third quartiles (box tops and bottoms), and minimums and maximums of value distribution (error bars). IFN-γ, interferon-γ; MERS-CoV, Middle East respiratory syndrome coronavirus; MVA, modified vaccinia virus Ankara; MVA-MERS-S, modified vaccinia virus Ankara expressing full-length MERS-CoV spike protein as antigen; PBMCs, peripheral blood mononuclear cells; SFCs, spot-forming T cells.

143.6 IFN-γ SFC/10^6 PBMCs). All seropositive MVA-MERS-S–vaccinated animals had levels of S2-specific T cells that increased on day 6 postvaccination (mean 50.6 IFN-γ SFC/10^6 PBMCs), further increasing on day 8 postvaccination (mean 84 IFN-γ SFC/10^6 PBMCs). Again, the S2-specific T cells subsequently decreased by day 22 postvaccination (mean 8.9 IFN-γ SFC/10^6 PBMCs).

Conclusions

This exploratory study confirms the presence of MERS-S–specific T cells in dromedary camels after a single MVA-MERS-S vaccination under field conditions as analyzed by IFN-γ ELISPOT assay. Previous infection seems not to hamper the practicability or value of vaccination trials because specific T cells were immunologically boosted in seropositive camels. These data are consistent with a recent study of humoral boost effects in seropositive camels after vaccination with a chimpanzee adenoviral vector-based MERS-CoV vaccine (*12*). This finding is relevant because serum antibodies are considered to reduce viral replication (*6*). MVA-MERS-S vaccination also reactivated humoral immune responses in seropositive camels. Our previous study confirmed that MERS-CoV-S–specific antibodies correlate with reduced viral excretion in camels (*14*). These preliminary results could have major implications for implementing future MVA-MERS-S camel vaccination studies in disease-endemic areas.

Naive MVA-MERS-S–vaccinated animals mounted fewer MERS-CoV-S–specific T cells than seropositive animals and failed to show S-specific antibodies after single MVA-MERS-S vaccination. Thus, further optimizing MVA-MERS-S–induced immunogenicity would require modifying vaccination strategies under field conditions, such as prime-boost vaccination regimens or alternative applications including intranasal immunization.

Although it is unlikely for the specific T cells detected in 1 seropositive and 1 naive camel after MVA vaccination, we cannot rule out a field infection between vaccination and sample preparation. Rather, we hypothesize that the seropositive animal could have remounted a cellular immune response caused by MVA-induced immune activation and potential coactivation of S-peptide specific T cells from previous MERS-CoV infection. In the naive camel, which did not seroconvert or mount S1-specific responses, nonspecific reactions could explain the detection of IFN-γ SFC.

The first limitation for this proof-of-concept study is that it was conducted as an exploratory study to

evaluate MERS-CoV–specific T cells in a few camels and provide a basis for further evaluation of camel vaccination in disease-endemic areas. To verify the potential protective capacity of vaccine-induced immune responses under field conditions, it will be essential to also characterize the infection status and demonstrate reduced virus excretion in vaccinated, subsequently infected animals. Future field studies could be based on MVA-MERS-S vaccination, not only in prime-only immunization cohorts but also in prime-boost applications, especially in juvenile animals, the probable main drivers of MERS-CoV transmission in camel populations (*6*). Our findings should contribute to establishing an advanced method for evaluating MERS-CoV–specific cellular immunity in dromedary camels.

This study was supported by the Federal Ministry of Education and Research (grant BMBF RAPID 01KI1723G to A.V.).

About the Author

Mr. Meyer zu Natrup is a veterinarian at the Institute of Virology at the University of Veterinary Medicine Hannover, Hannover, Germany. His primary research interest is development of innovative vaccination strategies against emerging coronaviruses.

References

1. Reusken CB, Haagmans BL, Müller MA, Gutierrez C, Godeke GJ, Meyer B, et al. Middle East respiratory syndrome coronavirus neutralising serum antibodies in dromedary camels: a comparative serological study. Lancet Infect Dis. 2013;13:859–66. https://doi.org/10.1016/S1473-3099(13)70164-6
2. Meyer B, Müller MA, Corman VM, Reusken CB, Ritz D, Godeke GJ, et al. Antibodies against MERS coronavirus in dromedary camels, United Arab Emirates, 2003 and 2013. Emerg Infect Dis. 2014;20:552–9. https://doi.org/10.3201/eid2004.131746
3. Haagmans BL, Al Dhahiry SH, Reusken CB, Raj VS, Galiano M, Myers R, et al. Middle East respiratory syndrome coronavirus in dromedary camels: an outbreak investigation. Lancet Infect Dis. 2014;14:140–5. https://doi.org/10.1016/S1473-3099(13)70690-X
4. Müller MA, Meyer B, Corman VM, Al-Masri M, Turkestani A, Ritz D, et al. Presence of Middle East respiratory syndrome coronavirus antibodies in Saudi Arabia: a nationwide, cross-sectional, serological study. Lancet Infect Dis. 2015;15:559–64. https://doi.org/10.1016/S1473-3099(15)70090-3
5. Mohd HA, Al-Tawfiq JA, Memish ZA. Middle East respiratory syndrome coronavirus (MERS-CoV) origin and animal reservoir. Virol J. 2016;13:87. https://doi.org/10.1186/s12985-016-0544-0
6. Meyer B, Juhasz J, Barua R, Das Gupta A, Hakimuddin F, Corman VM, et al. Time course of MERS-CoV infection and immunity in dromedary camels. Emerg Infect Dis. 2016;22:2171–3. https://doi.org/10.3201/eid2212.160382
7. Hemida MG, Chu DK, Poon LL, Perera RA, Alhammadi MA, Ng HY, et al. MERS coronavirus in dromedary camel herd, Saudi Arabia. Emerg Infect Dis. 2014;20:1231–4. https://doi.org/10.3201/eid2007.140571
8. Zhao J, Alshukairi AN, Baharoon SA, Ahmed WA, Bokhari AA, Nehdi AM, et al. Recovery from the Middle East respiratory syndrome is associated with antibody and T-cell responses. Sci Immunol. 2017;2:eaan5393. https://doi.org/10.1126/sciimmunol.aan5393
9. Muthumani K, Falzarano D, Reuschel EL, Tingey C, Flingai S, Villarreal DO, et al. A synthetic consensus anti-spike protein DNA vaccine induces protective immunity against Middle East respiratory syndrome coronavirus in nonhuman primates. Sci Transl Med. 2015;7:301ra132. https://doi.org/10.1126/scitranslmed.aac7462
10. Modjarrad K, Roberts CC, Mills KT, Castellano AR, Paolino K, Muthumani K, et al. Safety and immunogenicity of an anti-Middle East respiratory syndrome coronavirus DNA vaccine: a phase 1, open-label, single-arm, dose-escalation trial. Lancet Infect Dis. 2019;19:1013–22. https://doi.org/10.1016/S1473-3099(19)30266-X
11. Munster VJ, Wells D, Lambe T, Wright D, Fischer RJ, Bushmaker T, et al. Protective efficacy of a novel simian adenovirus vaccine against lethal MERS-CoV challenge in a transgenic human DPP4 mouse model. NPJ Vaccines. 2017;2:28. https://doi.org/10.1038/s41541-017-0029-1
12. Alharbi NK, Qasim I, Almasoud A, Aljami HA, Alenazi MW, Alhafufi A, et al. Humoral immunogenicity and efficacy of a single dose of ChAdOx1 MERS vaccine candidate in dromedary camels. Sci Rep. 2019;9:16292. https://doi.org/10.1038/s41598-019-52730-4
13. Volz A, Kupke A, Song F, Jany S, Fux R, Shams-Eldin H, et al. Protective efficacy of recombinant modified vaccinia virus Ankara delivering Middle East respiratory syndrome coronavirus spike glycoprotein. J Virol. 2015;89:8651–6. https://doi.org/10.1128/JVI.00614-15
14. Haagmans BL, van den Brand JM, Raj VS, Volz A, Wohlsein P, Smits SL, et al. An orthopoxvirus-based vaccine reduces virus excretion after MERS-CoV infection in dromedary camels. Science. 2016;351:77–81. https://doi.org/10.1126/science.aad1283
15. Koch T, Dahlke C, Fathi A, Kupke A, Krähling V, Okba NM, et al. Safety and immunogenicity of a modified vaccinia virus Ankara vector vaccine candidate for Middle East respiratory syndrome: an open-label, phase 1 trial. Lancet Infect Dis. 2020;20:827–38. https://doi.org/10.1016/S1473-3099(20)30248-6

Address for correspondence: Asisa Volz, Institute of Virology, University of Veterinary Medicine Hannover, Buenteweg 17, 30559 Hanover, Germany; email: asisa.volz@tiho-hannover.de

High Prevalence of SARS-CoV-2 Omicron Infection Despite High Seroprevalence, Sweden, 2022

Ramona Groenheit, Philip Bacchus,[1] Ilias Galanis,[1] Klara Sondén, Ioana Bujila, Tatiana Efimova, Fredrik Garli, Oskar Karlsson Lindsjö, Mikael Mansjö, Elin Movert, Aleksandra Pettke, Marie Rapp, Maike Sperk, Sandra Söderholm, Karin Valentin Asin, Sarah Zanetti, Maria Lind Karlberg, Andreas Bråve, Kim Blom,[2] Jonas Klingström[2]

We performed 2 surveys during 2022 to estimate point prevalences of SARS-CoV-2 infection compared with overall seroprevalence in Sweden. Point prevalence was 1.4% in March and 1.5% in September. Estimated seroprevalence was >80%, including among unvaccinated children. Continued SARS-CoV-2 surveillance is necessary for detecting emerging, possibly more pathogenic variants.

The SARS-CoV-2 Omicron variant has had strong effects on the COVID-19 pandemic. New Omicron subvariants have emerged over time and those subvariants have increased capacity to evade neutralizing antibody responses induced by both vaccines and prior infections, causing breakthrough infections and reinfections (*1*–*4*). After general PCR testing was halted in Sweden in early 2022, the possibility to track the COVID-19 situation and maintain surveillance in the general population largely depended on point prevalence surveys to detect acute SARS-CoV-2 infection by using PCR and estimates of previous infections by using serology. We performed 2 cross-sectional surveys during 2022 to estimate SARS-CoV-2 point prevalences and overall seroprevalence in Sweden.

Author affiliations: Public Health Agency of Sweden, Solna, Sweden (R. Groenheit, I. Galanis, K. Sondén, I. Bujila, T. Efimova, F. Garli, O. Karlsson Lindsjö, M. Mansjö, E. Movert, A. Pettke, M. Rapp, M. Sperk, S. Söderholm, K. Valentin Asin, S. Zanetti, M. Lind Karlberg, A. Bråve, K. Blom, J. Klingström); Swedish Armed Forces, Umeå, Sweden and Lund University, Lund, Sweden (P. Bacchus); Karolinska Institutet, Stockholm, Sweden (K. Sondén, M. Sperk, K. Blom, J. Klingström); Linköping University, Linköping, Sweden (J. Klingström)

DOI: https://doi.org/10.3201/eid2906.221862

The Study

Participants were invited from a nationwide probability-based web panel (*5*,*6*). Participants received material for sampling and instructions on how to perform self-sampling at home (Appendix, https://wwwnc.cdc.gov/EID/article/29/6/22-1862-App1.pdf). The first survey, March 21–25, covered all 21 regions in Sweden; the second survey, September 26–29, covered 11 regions in the country, representing 64% of the population. We performed surveys as part of the Public Health Agency of Sweden's assignment to monitor communicable diseases and evaluate infection control measures (in accordance with §§18 of Ordinance 2021:248 from the Swedish Parliament). All participants provided informed consent, and the legal guardian provided consent for persons <16 years of age.

In March, 11,334 persons were invited and 2,906 persons 2–96 years of age participated (Appendix Table 1). In total, we analyzed 2,659 samples for ongoing infection and 2,587 samples for serologic responses (Figure, panel A). We detected 48 PCR-positive samples showing SARS-CoV-2 infection, an estimated point prevalence of 1.4% (95% CI 0.9%–2.1%) in the population of Sweden at the end of March. One infection was caused by the Delta variant and 47 by Omicron subvariants (Appendix Table 2). Data from the national registry for communicable diseases revealed that 633 (24%) of the 2,659 participants with a valid PCR result had ≥1 previous confirmed SARS-CoV-2 infection; 79.4% had received ≥3 vaccine doses (Table 1). Among 48 participants with PCR-positive results, 4 (8.3%) had previously

[1]These authors contributed equally to this article.

[2]These senior authors contributed equally to this article.

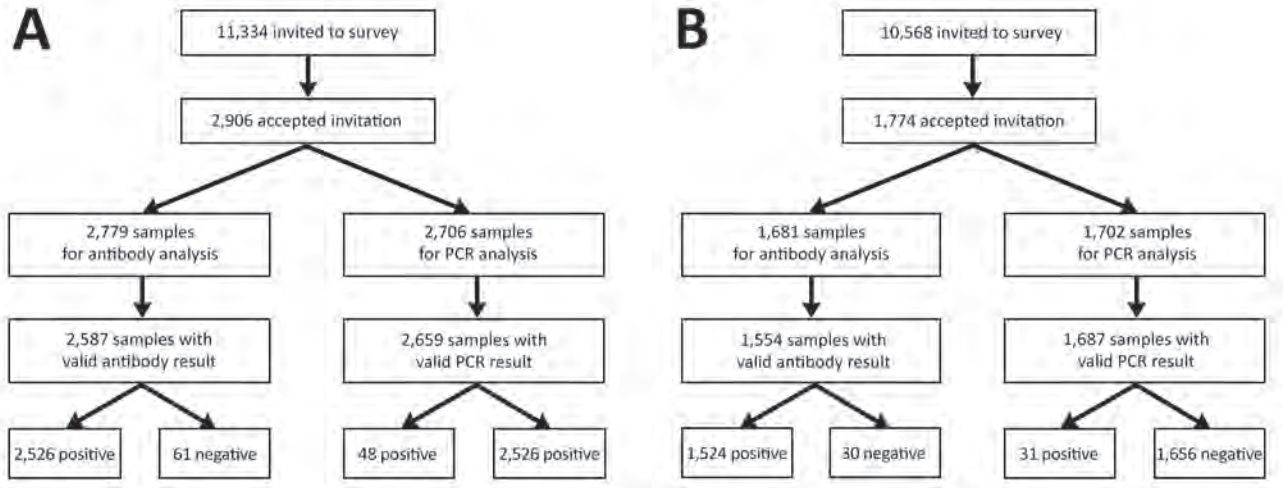

Figure. Flowchart of study participant enrollment and collected and analyzed samples in a study of prevalence of SARS-CoV-2 Omicron infection despite high seroprevalence, Sweden, 2022. A) Surveys performed during March 21–25. B) Surveys performed September 26–29. Point prevalence and Omicron subvariant data from the September study was published previously (*6*).

reported SARS-CoV-2 infections. On the basis of spike IgG data from the 2,587 participants with a valid sample for serology, we estimated a 93.3% (95% CI 91.5%–94.8%) SARS-CoV-2 seroprevalence in the population of Sweden at the end of March 2022. The estimated seroprevalence was 80.1% (95% CI 71.1%–87.4%) in children ≤11 years of age and 94.2%–98.8% in persons >11 years of age (Table 2).

In the September survey, 10,568 persons were invited and 1,774 persons 2–94 years of age participated. We were able to analyze 1,687 samples for ongoing infection (Appendix Table 1), and 1,554 samples for serologic responses (Figure, panel B). We previously reported that 31 of 1,687 participants were PCR-positive in September, that the estimated point prevalence was 1.5% (95% CI 0.9%–2.5%), and all infections were caused by Omicron subvariants (*6*). Among participants in the September survey, 485 (29%) had ≥1 previously confirmed SARS-CoV-2 infection; 85.5% had received ≥3 vaccine doses (Table 1). Among PCR-positive participants, 22 (71%) had previously reported SARS-CoV-2 infections. On the basis of spike IgG data (n = 1,554), we estimated that SARS-CoV-2 seroprevalence in Sweden was 93.1% (95% CI 89.2%–96.0%) at end of September. Estimated seroprevalence was 84.0% (95% CI 70.3%–93.3%) in persons 2–11 years of age and 84.9%–100% in persons >11 years of age (Table 2).

Using answers in the participant symptom survey, we next analyzed for symptoms in general and for symptoms among SARS-CoV-2–infected participants. Overall, 65.2% of participants in March and 67.7% of participants in September, experienced ≥1 symptom within 2 weeks before sampling. Of participants with negative PCR results, 64.6% in March and 67.3% in September had ≥1 symptom (Appendix Table 3). Among 79 PCR-positive participants, 4 had no symptoms within 2 weeks before sampling (Appendix Table 3), and 3 of those 4 experienced symptoms within 1 week after sampling.

Conclusions

Beginning February 9, 2022, mainly hospitalized persons, healthcare workers, long-term care facility staff, and at-risk persons with symptoms indicating COVID-19, were tested for SARS-CoV-2 infection in Sweden. Because the general population was no longer tested, trends in prevalence and transmission patterns were difficult to assess in real-time. To estimate point prevalence of infection in the population, Sweden needed random sampling of the population on a nationwide level.

We estimated point prevalences in Sweden of 1.4% during March 21–25 and, as previously reported (*6*), 1.5% during September 26–29. Those estimated point prevalences were higher than those in our previous national surveys (*5*). In another survey of

Table 1. Number of COVID-19 vaccine doses received by participants in surveys conducted for study of high prevalence of SARS-CoV-2 Omicron infection despite high seroprevalence, Sweden, 2022

No. doses	No. participants (%)	
	March 21–25, n = 2,659	September 26–29, n = 1,687
0	178 (6.9)	96 (6.2)
1	12 (0.5)	5 (0.3)
2	343 (13.3)	126 (8.1)
3	2,006 (77.5)	809 (52.1)
4	48 (1.9)	408 (26.3)
5	0	110 (7.1)

Table 2. Estimated SARS-CoV-2 seroprevalence by age group in study of high prevalence of SARS-CoV-2 Omicron infection despite high seroprevalence, Sweden, 2022

Age group	% Participants (95% CI)	
	March 21–25, n = 2,587	September 26–29, n = 1,554
1–11	80.1 (71.1–87.4)	84.0 (70.3–93.3)
12–19	97.2 (81.9–100.0)	84.9 (53.2–99.0)
20–29	95.9 (89.6–99.2)	92.7 (70.8–100.0)
30–49	94.2 (89.4–97.5)	95.9 (89.7–99.2)
50–64	95.3 (91.6–97.9)	95.0 (88.3–98.7)
65–79	95.0 (94.2–95.7)	96.7 (89.2–100.0)
≥80	98.8 (89.8–100.0)	100 (94.3–100.0)

healthcare workers in Stockholm during June 28–29, 2022, we observed asymptomatic SARS-CoV-2 infections in 2.3% of participants (*7*). Although healthcare workers are likely at higher risk for infection than the general population, those 3 surveys collectively indicated a continued high level of Omicron transmission in Sweden during March, June, and September 2022. Similar, or even higher, point prevalences were reported from other countries during 2022. For example, surveys performed on the general population in the United Kingdom estimated point prevalences of 6.7%–8.7% in March and 2.1%–2.5% in September for England, Scotland, Wales, and Northern Ireland (*8*). Moreover, a survey of blood donors in Denmark estimated that, by March 2022, ≈66% of the age-matched healthy population had been infected by SARS-CoV-2 in <5 months (*9*). Taken together, those and many other reports show the high capacity of Omicron to spread, including among highly vaccinated populations.

A large percentage of the population were positive for spike IgG in March and in September 2022, which can partly be explained by the high vaccine coverage in Sweden. COVID-19 vaccination was not recommended for children <12 years of age in Sweden. Hence, in the youngest, unvaccinated, age group, seroconversion was likely induced solely by infection, indicating that a large percentage (80%) of that age group had already been infected with SARS-CoV-2 by March 2022. Similar levels of infections in children have been reported from Bavaria, Germany, including seroprevalences of 67% for preschool children 1–4 years of age and 84% for school-age children 5–10 years of age in June 2022, largely caused by the Omicron variant (*10*).

Current vaccines seem to provide only limited, short-term, inhibitory effect on Omicron transmissibility (*11*). Of note, our surveys showed that among PCR-positive participants in March, 8.3% had a previously recorded SARS-CoV-2 infection, but in September, those participants increased to 71%, indicating a high level of reinfection caused by then circulating Omicron subvariants, which have shown highly increased capacity to avoid neutralizing antibodies (*12*–*14*).

In summary, we estimate that ≈1 of every 66 persons in Sweden was infected with SARS-CoV-2 by March and September 2022. Although Omicron has a high transmission capacity, current vaccines protect against severe disease, as noted by the low fatality rate observed in Omicron-infected persons in Denmark (*9*). However, because Omicron has the capacity to efficiently transmit despite high vaccine coverage, continued surveillance of the general population for early signs of new, more possibly pathogenic, emerging SARS-COV-2 variants remains crucial.

Acknowledgments

We thank all the participants in the survey for volunteering to perform self-sampling and completing symptom questionnaires. We thank the Swedish Armed Forces, whose personnel from regular units and Home Guard units collected and transported the samples.

This work was funded by grants provided to the Public Health Agency of Sweden (grant nos. S2020/0281/FS and S2020/08532 FS).

About the Author

Dr. Groenheit is a microbiologist at the Public Health Agency of Sweden, Solna, Sweden. Her primary interests include tuberculosis, especially focusing on drug resistance and molecular epidemiology, and SARS-CoV-2 prevalence and seroprevalence.

References

1. Tegally H, Moir M, Everatt J, Giovanetti M, Scheepers C, Wilkinson E, et al.; NGS-SA consortium. Emergence of SARS-CoV-2 Omicron lineages BA.4 and BA.5 in South Africa. Nat Med. 2022;28:1785–90. https://doi.org/10.1038/s41591-022-01911-2
2. Dejnirattisai W, Shaw RH, Supasa P, Liu C, Stuart AS, Pollard AJ, et al.; Com-COV2 study group. Reduced neutralisation of SARS-CoV-2 omicron B.1.1.529 variant by post-immunisation serum. Lancet. 2022;399:234–6. https://doi.org/10.1016/S0140-6736(21)02844-0
3. Tuekprakhon A, Nutalai R, Dijokaite-Guraliuc A, Zhou D, Ginn HM, Selvaraj M, et al.; OPTIC Consortium; ISARIC4C Consortium. Antibody escape of SARS-CoV-2 Omicron BA.4 and BA.5 from vaccine and BA.1 serum. Cell. 2022;185:2422–2433.e13. https://doi.org/10.1016/j.cell.2022.06.005
4. Blom K, Marking U, Havervall S, Norin NG, Gordon M, García M, et al. Immune responses after Omicron infection in triple-vaccinated health-care workers with and without previous SARS-CoV-2 infection. Lancet Infect Dis. 2022;22:943–5. https://doi.org/10.1016/S1473-3099(22)00362-0
5. Groenheit R, Beser J, Kühlmann Berenzon S, Galanis I, van Straten E, Duracz J, et al. Point prevalence of SARS-CoV-2 infection in Sweden at six time points during

2020. BMC Infect Dis. 2022;22:861. https://doi.org/10.1186/s12879-022-07858-6
6. Groenheit R, Galanis I, Sondén K, Sperk M, Movert E, Bacchus P, et al. Rapid emergence of Omicron sublineages expressing spike protein R346T. Lancet Reg Health Eur. 2023;24:100564. https://doi.org/10.1016/j.lanepe.2022.100564
7. Blom K, Havervall S, Marking U, Norin NG, Bacchus P, Groenheit R, et al. Infection rate of SARS-CoV-2 in asymptomatic healthcare workers, Sweden, June 2022. Emerg Infect Dis. 2022;28:2119–21. https://doi.org/10.3201/eid2810.221093
8. Office for National Statistics, United Kingdom. Coronavirus (COVID-19) [cited 2022 December 1]. https://www.ons.gov.uk/peoplepopulationandcommunity/healthandsocialcare/conditionsanddiseases
9. Erikstrup C, Laksafoss AD, Gladov J, Kaspersen KA, Mikkelsen S, Hindhede L, et al. Seroprevalence and infection fatality rate of the SARS-CoV-2 Omicron variant in Denmark: a nationwide serosurveillance study. Lancet Reg Health Eur. 2022;21:100479. https://doi.org/10.1016/j.lanepe.2022.100479
10. Ott R, Achenbach P, Ewald DA, Friedl N, Gemulla G, Hubmann M, et al. SARS-CoV-2 seroprevalence in preschool and school-age children. Dtsch Arztebl Int. 2022;119:765–70. https://doi.org/10.3238/arztebl.m2022.0355
11. Woodbridge Y, Amit S, Huppert A, Kopelman NM. Viral load dynamics of SARS-CoV-2 Delta and Omicron variants following multiple vaccine doses and previous infection. Nat Commun. 2022;13:6706. https://doi.org/10.1038/s41467-022-33096-0
12. Hachmann NP, Miller J, Collier AY, Ventura JD, Yu J, Rowe M, et al. Neutralization escape by SARS-CoV-2 Omicron subvariants BA.2.12.1, BA.4, and BA.5. N Engl J Med. 2022;387:86–8. https://doi.org/10.1056/NEJMc2206576
13. Qu P, Evans JP, Faraone JN, Zheng Y-M, Carlin C, Anghelina M, et al. Enhanced neutralization resistance of SARS-CoV-2 Omicron subvariants BQ.1, BQ.1.1, BA.4.6, BF.7, and BA.2.75.2. Cell Host Microbe. 2023;31:9-17.e3. https://doi.org/10.1016/j.chom.2022.11.012
14. Sheward DJ, Kim C, Fischbach J, Sato K, Muschiol S, Ehling RA, et al. Omicron sublineage BA.2.75.2 exhibits extensive escape from neutralising antibodies. Lancet Infect Dis. 2022;22:1538–40. https://doi.org/10.1016/S1473-3099(22)00663-6

Address for correspondence: Kim Blom, Public Health Agency of Sweden, Nobels väg 18, 171 65 Solna, Sweden; email: Kim.Blom@Folkhalsomyndigheten.se

Novel Avian Influenza Virus (H5N1) Clade 2.3.4.4b Reassortants in Migratory Birds, China

Jing Yang,[1] Chunge Zhang,[1] Yue Yuan,[1] Ju Sun,[1] Lu Lu,[1] Honglei Sun, Heting Sun, Dong Chu, Siyuan Qin, Jianjun Chen, Chengbo Zhang, Xiyan Hao, Weifeng Shi, Wenjun Liu, George F. Gao, Paul Digard, Samantha Lycett, Yuhai Bi

Two novel reassortant highly pathogenic avian influenza viruses (H5N1) clade 2.3.4.4b.2 were identified in dead migratory birds in China in November 2021. The viruses probably evolved among wild birds through different flyways connecting Europe and Asia. Their low antigenic reaction to vaccine antiserum indicates high risks to poultry and to public health.

Since the Gs/GD/96-lineage highly pathogenic avian influenza virus (HPAIV) (H5N1) was identified in 1996, H5 HPAIVs have evolved into divergent clades and caused continuous outbreaks in birds (*1*–*11*). Moreover, long-distance transmissions of H5 HPAIVs within a relatively short period indicate a crucial role of migratory birds in global spread of HPAIVs (*7*,*8*). Thus far, H5 viruses have undergone at least 4 waves of intercontinental transmission: H5N1 clade 2.2 during 2005–2006, H5N1 clade 2.3.2.1c during 2009–2010, H5N8 clade 2.3.4.4a and H5N1 clade 2.3.2.1c during 2014–2015, and H5Ny clade 2.3.4.4b during 2016–2017 (*2*–*8*).

Starting during 2020–2021, a new wave of HPAIV H5N1/H5N8 clade 2.3.4.4b outbreaks was reported in wild and domestic birds in Eurasia (*9*–*11*) and Africa (https://wahis.woah.org/#/event-management). Human cases of H5N1/H5N6/H5N8 infection were sporadically documented (https://www.who.int/teams/global-influenza-programme/avian-influenza/monthly-risk-assessment-summary), highlighting the zoonotic risk of H5 HPAIVs. Since 2021, H5 HPAIVs have caused at least 9 outbreaks in wild birds rather than poultry in mainland China (http://www.moa.gov.cn/gk/yjgl_1/yqfb; http://www.xmsyj.moa.gov.cn/yqfb). However, large outbreaks of H5N1 HPAIVs in domestic poultry were reported during 2021–2022 in Europe and the United States (https://www.cdc.gov/flu/avianflu/data-map-commercial.html) (A. Kandeil et al., unpub. data, https://doi.org/10.21203/rs.3.rs-2136604/v1). In this study, we explored the genetic origin, spread patterns, and antigenicity of H5N1 viruses identified from 2 dead migratory birds in China.

The Study

We collected oral swab specimens and lung tissues from a dead whooper swan in northern China (Inner Mongolia) on November 3, 2021, and a deceased black swan in eastern China (Zhejiang) on November 15, 2021. We performed virus isolation in 10-day-old specific pathogen-free chicken embryos (*12*), then confirmed results by quantitative reverse transcription PCR (Mabsky Biotech, http://www.mabsky.com).

We isolated and Sanger sequenced 3 viruses, A/whooper swan/Northern China/11.03 IMEEDSAK1-O/2021 (Ws/NC/AK1-O/2021), A/whooper swan/Northern China/11.03 IMEEDSAK2-O/2021

Author affiliations: Institute of Microbiology, Center for Influenza Research and Early-warning (CASCIRE), Chinese Academy of Sciences–The World Academy of Sciences Center of Excellence for Emerging Infectious Diseases, Chinese Academy of Sciences, Beijing, China (J. Yang, Chunge Zhang, J. Sun, W. Liu, G.F. Gao, Y. Bi); University of Chinese Academy of Sciences, Beijing (J. Yang, Chunge Zhang, W. Liu, G.F. Gao, Y. Bi); Shandong First Medical University, Taian, China (Y. Yuan, W. Shi, Y. Bi); Shanxi Agricultural University, Taigu, China (J. Sun, Y. Bi); University of Edinburgh, Edinburgh, UK (L. Lu, P. Digard, S. Lycett); China Agricultural University, Beijing (Honglei Sun); State Forestry and Grassland Administration, Shenyang, China (Heting Sun, D. Chu, S. Qin); Wuhan Institute of Virology, Chinese Academy of Sciences, Wuhan, China (J. Chen); Ordos Forestry and Grassland Development Center, Ordos, China (Chengbo Zhang); Hohhot Center for Disease Control and Prevention, Hohhot, China (X. Hao)

DOI: https://doi.org/10.3201/eid2906.221723

[1]These authors contributed equally to this article.

(Ws/NC/AK2-O/2021), and A/black swan/Eastern China/11.15 ZJHZ74-Lg/2021 (Bs/EC/74-Lg/2021). We deposited whole genomes in NMDC (https://nmdc.cn; accession nos. NMDCN0000RD8–NMDCN0000RDV) and GISAID (https://www.gisaid.org; accession nos. EPI195500–EPI195523). We reconstructed phylogenetic trees for each gene of the 3 H5N1 isolates together with reference viruses from GISAID and the National Center for Biotechnology Information (https://www.ncbi.nlm.nih.gov/genomes/FLU/Database/nph-select.cgi), using the maximum-likelihood method with a general time-reversible model plus gamma distribution in RAxML 8.2.12 (https://cme.h-its.org/exelixis/web/software/raxml) (Appendix 1 Table, https://wwwnc.cdc.gov/EID/article/29/6/22-1723-App1.xlsx). We reconstructed Bayesian time-resolved phylogenetic trees in BEAST 1.10.4 (https://beast.community/index.html) using the SRD06 model, the log-normal relaxed clock model, and the Skygrid coalescent model. We mapped spatial coordinates to the post burn-in time-scaled posterior trees using a Brownian motion continuous phylogeographic model. We mapped host type and hemagglutinin (HA) or neuraminidase (NA) subtype on each posterior tree by using a discrete trait phylogeographic model with BSSVS extension to infer the most likely ancestor with statistical support (Appendix 2, https://wwwnc.cdc.gov/EID/article/29/6/22-1723-App2.pdf).

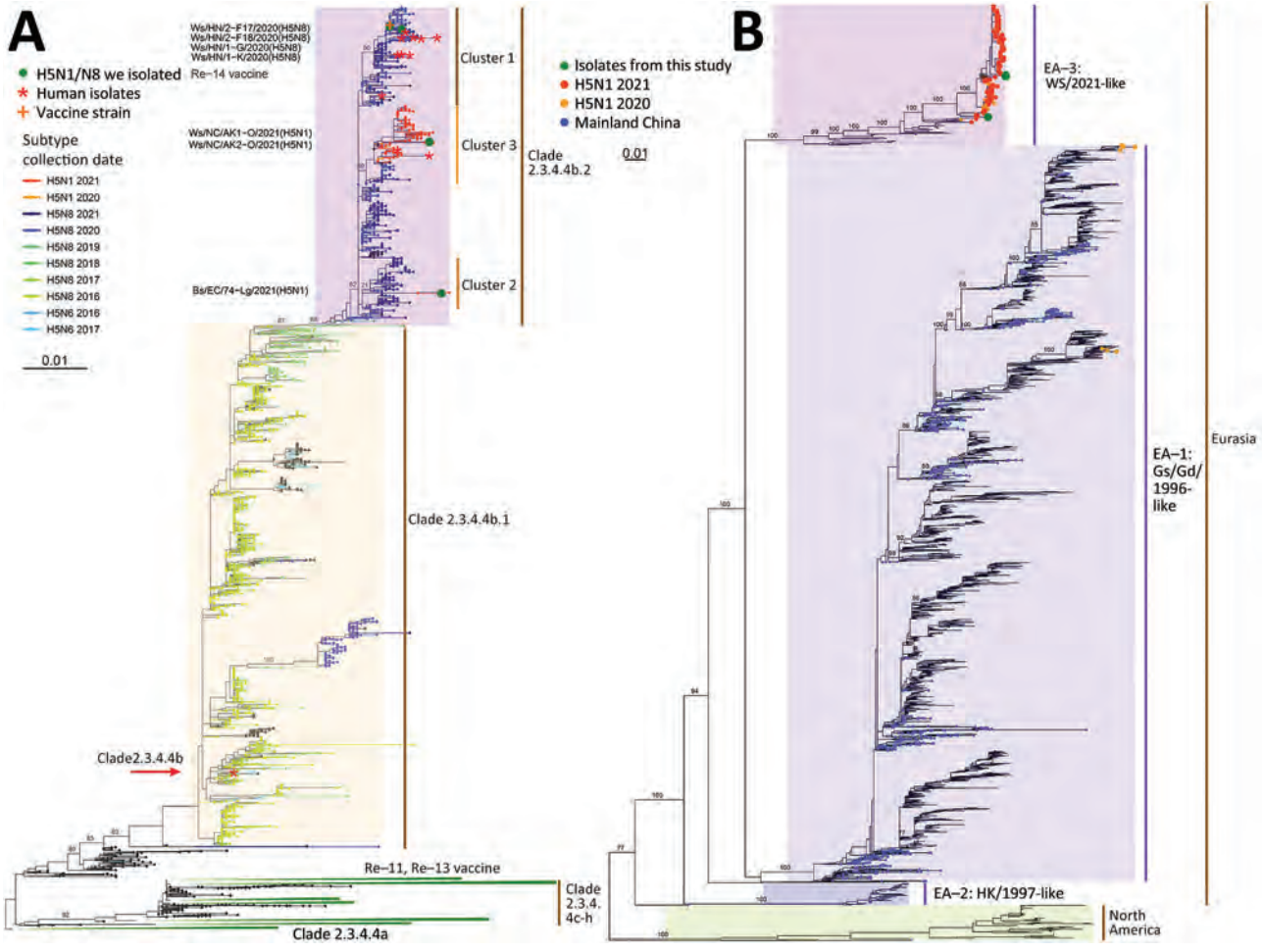

Figure 1. Phylogenetic trees for hemagglutinin genes of clade 2.3.4.4 H5Ny and neuraminidase genes of global H5N1 avian influenza viruses. A) Phylogeny of hemagglutinin genes of global clade 2.3.4.4 H5Ny avian influenza viruses. Solid green circles indicate H5N1 and H5N8 viruses from wild birds isolated in China; sequence names are listed next to corresponding circles. Red asterisks indicate human isolates. H5 vaccine seed strains used in mainland China are listed near the corresponding clades; orange cross indicates Re-14 vaccine. The major H5Ny subtypes within clade 2.3.4.4b are colored by their subtypes and collection dates. Clade 2.3.4.4b was divided into clade 2.3.4.4b.1 and clade 2.3.4.4b.2 because of >2.7% average pairwise nucleotide distance and >60% support for the 2 subclades. B) Phylogeny of global H5N1 neuraminidase genes. Colored circles indicate the novel H5N1 viruses from this study, H5N1 viruses from mainland China, and H5N1 viruses isolated in 2020 and 2021. Numbers on branches represent bootstrap support values for some major clades. Scale bar indicates number of nucleotide substitutions per site. Full phylogenetic trees of hemagglutinin genes of global H5Ny and neuraminidase genes of global H5N1 are provided at https://github.com/judyssister/globalH5N1_2021.

Table 1. HI titers of H5N1 and H5N8 highly pathogenic avian influenza viruses from wild birds in China against antiserum of H5 Re-11, Re-13, and Re-14 vaccines*

Virus	HI titers of chicken antiserum against vaccine strains and H5N1/H5N8 isolates		
	Re-11, clade2.3.4.4h	Re-13, clade2.3.4.4h	Re-14, clade2.3.4.4b
Re-11, Dk/GZ/S4184/2017(H5N6)	256	256–512	128
Re-13, Dk/FJ/S1424/2020(H5N6)	32	256	2–4
Re-14, Ws/SX/4–1/2020(H5N8)	8	16	256
Bs/EC/74-Lg/2021(H5N1)	16	8	128
Ws/NC/AK2-O/2021(H5N1)	2–4	2–4	32
Ws/HN/1-K/2020(H5N8)	8	8	64
Ws/HN/1-G/2020(H5N8)	8	8	64

*H5 Re-11 vaccine was used in poultry in mainland China during December 2018–December 2021. H5 Re-13 and Re-14 vaccines have been deployed since January 2022. HI, hemagglutination inhibition.

We performed hemagglutination inhibitor (HI) assays (https://www.who.int/publications/i/item/manual-for-the-laboratory-diagnosis-and-virological-surveillance-of-influenza) to test the reactivities of antiserum of H5 Re-11/Re-13/Re-14 vaccines against these new H5N1 isolates and H5N8 HPAIVs identified in 2020 (*10*). Re-11 (A/duck/Guizhou/S4184/2017[H5N6], clade 2.3.4.4h) was used in poultry in China during December 2018–December 2021, whereas Re-13 (A/duck/Fujian/S1424/2020[H5N6], clade 2.3.4.4h) and Re-14 (A/whooper swan/Shanxi/4–1/2020[H5N8], clade 2.3.4.4b) have been deployed since January 2022 (http://www.moa.gov.cn/govpublic).

Conclusions

We obtained 3 H5N1 HPAIVs, Ws/NC/AK1-O/2021 and Ws/NC/AK2-O/2021 from a dead whooper swan in northern China and Bs/EC/74-Lg/2021 from a dead black swan in eastern China in November 2021. Consistent with the HPAIV signature of multiple basic amino acids on HA cleavage site, these H5N1 strains caused severe histopathologic changes in the wild birds (Appendix 2 Figure 1).

Phylogenetic analyses showed that all 3 H5N1 HA genes cluster in clade 2.3.4.4b.2 (Figure 1, panel A). Most H5 avian influenza viruses (AIVs) identified during 2020–2021 were in that clade, whereas H5N8 was the dominant subtype during 2019–2021, and H5N1 strains emerged in October 2020 and increased subsequently. In NA phylogeny, most H5N1 viruses identified during 2020–2021 including those 3 H5N1 viruses, were classified into the Eurasian lineage clade EA-3 (Figure 1, panel B). However, almost all H5N1 NA genes from mainland China were identified during 1996–2018 and are clade EA-1.

Given the HA phylogenetic relationships, we defined cluster 1, 2, and 3 in clade 2.3.4.4b.2 (Figure 1, panel A). Cluster 1 includes 4 H5N8 HPAIVs identified from wild birds in 2020 (*10*) and Re-14 vaccine strain. In cluster 2, Bs/EC/74-Lg/2021 was grouped with H5N1 viruses from Japan and South Korea, showing 99.3%–99.6% sequence identity. In cluster 3, Ws/NC/AK1-O/2021 and Ws/NC/AK2-O/2021 are identical (Appendix 2 Table 1) and clustered with H5N1 viruses from Europe, possessing 99.3% nucleotide identity. Most H5N1 viruses identified during 2020–2021 belong to cluster 3. Notably, 8 H5N6 and 1 H5N8 viruses that caused human infections (*13*) are found in cluster 1. Moreover, 2 human infections with cluster 3 H5N1 viruses were reported in the United Kingdom and United States during 2021–2022 (*14*). Therefore, this virus lineage poses a nonnegligible threat to public health, despite these viruses carrying non–mammalian-adapted molecular markers (Appendix 2 Table 2) and avian-type receptor-binding propensity (Appendix 2 Figure 2).

Table 2. Amino acid substitutions on the hemagglutinin antigenic sites between H5N1 2021 and H5N8 2020 highly pathogenic avian influenza viruses and H5 vaccine seed viruses Re-11, Re-13, and Re-14 used in China*

Virus	Position of antigenic sites in hemagglutinin genes (H3 numbering)*															
	63	81	125	131	132	144	145	155	158	159	160	166	188	189	193	202
Re-11, clade2344h	D	R	R	T	S	V	A	T	N	D	A	M	A	E	N	V
Re-13, clade2344h	N	S	E	T	T	V	A	T	N	E	T	K	V	E	D	V
Re-14, clade2344b	D	R	S	E	T	A	P	I	N	D	A	I	A	E	N	I
Bs/EC/74-Lg/2021(H5N1)	D	R	N	E	T	A	P	I	N	D	A	I	A	K	D	I
Ws/NC/AK1-O/2021(H5N1)	D	R	S	E	T	A	P	I	D	D	A	I	A	K	N	I
Ws/NC/AK2-O/2021(H5N1)	D	R	S	E	T	A	P	I	D	D	A	I	A	K	N	I
Ws/HN/1-K/2020(H5N8)	D	R	S	E	T	A	P	I	N	D	A	I	A	E	N	I
Ws/HN/1-G/2020(H5N8)	D	R	S	E	T	A	P	I	N	D	A	I	A	E	N	I
Ws/HN/2-F17/2020(H5N8)	D	R	S	E	T	A	P	I	N	D	A	I	A	E	N	I
Ws/HN/2-F18/2020(H5N8)	D	R	S	E	T	A	P	I	N	D	A	I	A	E	N	I

*Positions of antigenic sites based on the H5 and H3 (sites A–E) antigenic sites.

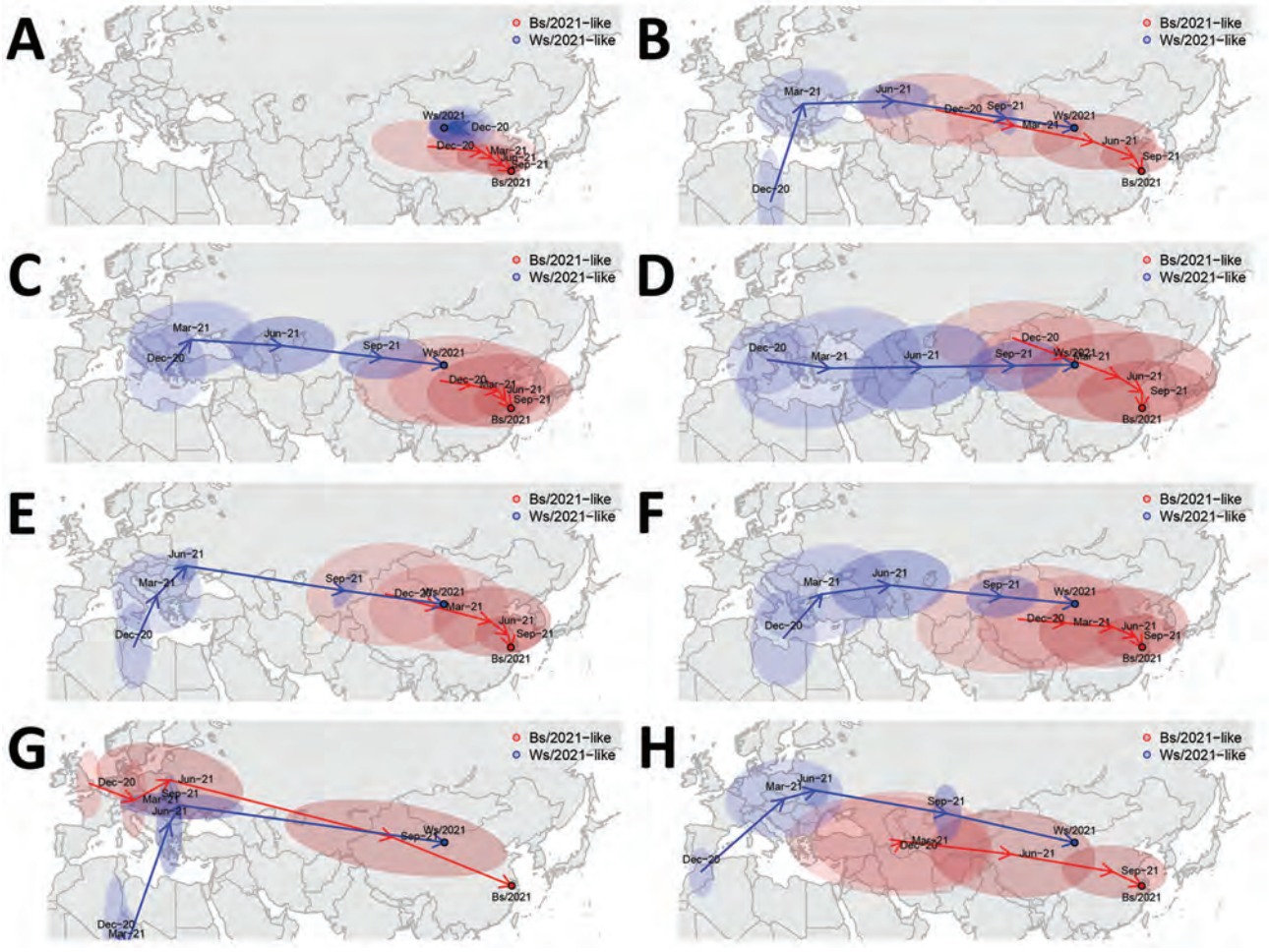

Figure 2. Spread patterns of all 8 gene segments of highly pathogenic avian influenza virus (H5N1), Bs/2021-like and Ws/2021-like reassortants, identified in migratory wild birds in China. Virus spread patterns reconstructed for 8 genes. A) polymerase basic 2 gene. B) polymerase basic 1 gene. C) polymerase acidic gene. D) hemagglutinin gene. E) nucleoprotein gene. F) neuraminidase gene. G) matrix gene. H) nonstructural protein gene. Blue indicates spread patterns of Ws/2021-like and red indicates spread patterns of Bs/2021-like H5N1. The spread patterns were adjusted by interpolating the ancestral space-time points by every 3 months from December 2020 through November 2021. Arrows represent the inferred ancestral locations at corresponding interpolated time (at 3-month intervals going back along their inferred transmission routes), and filled ellipses represent the 95% uncertainty of the inferred ancestral locations.

Current H5N1 viruses have resulted in substantial mortality in domestic and wild birds in Eurasia, Africa, and Americas (https://wahis.woah.org/#/event-management); however, they have only been identified in wild birds in mainland China. Compared with high HI antibody titers (256) between homologous antiserum and antigens of H5 vaccines, the recent H5N1/H5N8 viruses presented low HI titers (2–16) against Re-11/Re-13 antiserum (Table 1). In addition, cluster 1 H5N8 viruses had HI titers of 64 against Re-14 (cluster 1) antiserum, whereas HI titers for the H5N1 viruses were 128 for Bs/EC/74-Lg/2021 (cluster 2) and 32 for Ws/NC/AK1-O/2021 (cluster 3). This finding indicates lower antigenic identities between H5N1/H5N8 viruses circulating in wild birds and vaccines used in domestic poultry, even within the same clade. This antigenic variation may correlate to substitutions at antigenic sites (Table 2; Appendix 2 Tables 3,4, Figure 3).

Phylogenetic analyses uncovered that 3 novel H5N1 viruses could be classified into Ws/2021-like (Ws/NC/AK1-O/2021 and Ws/NC/AK2-O/2021) and Bs/2021-like (Bs/EC/74-Lg/2021) reassortants (Appendix 2 Figure 4). The viruses originated through separate reassortment events between H5N8 HPAIVs (obtaining HA and matrix [M] genes) and low pathogenic avian influenza virus pools (NA, polymerase basic 1, polymerase basic 2, polymerase acidic, nucleoprotein, and nonstructural protein genes) (Appendix 2 Figure 5–12). Phylogeographic

analyses suggested that the H5N1 viruses spread to China by long-distance bird migration through various routes (Figure 2).

We reconstructed the genetic reassortment history for these H5N1 viruses (Appendix 2 Table 5, Figures 13, 14). For the Bs/2021-like reassortant, most gene segments group with viruses from wild Anseriformes in China or its adjacent areas, whereas the M gene likely originated from an HPAIV H5N8 ancestor from Eastern Europe in approximately May 2021 before import into China through bird migration. For the Ws/2021-like reassortant, 7 gene segments originated from Europe and were potentially transmitted by wild birds in February–August 2021, whereas a unique polymerase basic 2 gene originated from an early ancestry in 2017 with unknown origin but most closely related to a Russian H3N6 low pathogenic AIV. The ancestral states of most genes of the 2 reassortants indicate origins in wild Anseriformes and likely transmission through wild Anseriformes over the summer of 2021, whereas a few genes (e.g., Bs/2021-like M gene) potentially originated from domestic poultry. However, sampling bias in sequences might affect ancestral reconstruction by discrete trait phylogeographic models.

In conclusion, we identified 3 H5N1 HPAIVs in wild birds in autumn 2021, China. The antigenic divergence highlights the high-risk introduction of H5N1 circulating in wild birds to incompletely protected vaccinated flocks in China. The H5N1 viruses have experienced complicated reassortment during long-distance spread through various bird migration routes. Therefore, we call for international cooperation on AIV monitoring in migratory birds to help early identification and intervention of the emerging and reemerging AIVs with public health risks.

Acknowledgments

We thank the submitters and originating laboratories for influenza virus genomes in the GISAID and National Center for Biotechnology Information databases.

This work was supported by the National Key R&D Program of China (grant nos. 2021YFC2300900 and 2022YFC2601602), National Natural Science Foundation of China (grant nos. 32261133524 and 32200416), Strategic Priority Research Program of Chinese Academy of Sciences (grant no. XDB29010102), Chinese Academy of Sciences' Southeast Asia Biodiversity Research Institute (grant no. 151C53KYSB20210023), Self-supporting Program of Guangzhou Laboratory (grant no. SRPG22-001), and the National Science and Technology Infrastructure of China (grant no. NPRC-32).

Y.B. is supported by the Youth Innovation Promotion Association of the Chinese Academy of Sciences (grant no. Y2021034) and Innovation Team and Talents Cultivation Program of National Administration of Traditional Chinese Medicine (grant no. ZYYCXTD-D-202208). L.L., S.L., P.D., and W.L. are supported by an Ecology and Evolution of Infectious Diseases collaborative grant with the UK Biotechnology and Biological Sciences Research Council (grant no. BB/V011286/1) and the National Natural Science Foundation of China (grant no. 32061123001). P.D. and S.L. are additionally supported by the Strategic Program grant to Roslin Institute (grant no. BB/P013740/1) and a UK research consortium on avian influenza research gaps (Flu-MAP) (grant no. BB/X006123/1) from the UK Biotechnology and Biological Sciences Research Council and Department for Environment Food and Rural Affairs. P.D. was also supported by an EU Horizon 2020 award (no. 727922 [DELTA-FLU]), and L.L and S.L are supported by an EU Horizon 2020 award (no: 874735 [VEO]).

About the Author

Dr. Yang is an assistant professor at the Institute of Microbiology, Chinese Academy of Sciences. Her research interests are focused on the evolution and spread patterns of emerging and reemerging infectious diseases.

References

1. World Health Organization, World Organization for Animal Health, Food and Agriculture Organization H5N1 Evolution Working Group. Revised and updated nomenclature for highly pathogenic avian influenza A (H5N1) viruses. Influenza Other Respir Viruses. 2014;8:384–8. https://doi.org/10.1111/irv.12230
2. Bi Y, Chen J, Zhang Z, Li M, Cai T, Sharshov K, et al. Highly pathogenic avian influenza H5N1 clade 2.3.2.1c virus in migratory birds, 2014-2015. Virol Sin. 2016;31:300–5. https://doi.org/10.1007/s12250-016-3750-4
3. Shi W, Gao GF. Emerging H5N8 avian influenza viruses. Science. 2021;372:784–6. https://doi.org/10.1126/science.abg6302
4. Liu J, Xiao H, Lei F, Zhu Q, Qin K, Zhang XW, et al. Highly pathogenic H5N1 influenza virus infection in migratory birds. Science. 2005;309:1206. https://doi.org/10.1126/science.1115273
5. Li Y, Liu L, Zhang Y, Duan Z, Tian G, Zeng X, et al. New avian influenza virus (H5N1) in wild birds, Qinghai, China. Emerg Infect Dis. 2011;17:265–7. https://doi.org/10.3201/eid1702.100732
6. Global Consortium for H5N8 and Related Influenza Viruses. Role for migratory wild birds in the global spread of avian influenza H5N8. Science. 2016;354:213–7. https://doi.org/10.1126/science.aaf8852
7. Lee DH, Torchetti MK, Hicks J, Killian ML, Bahl J, Pantin-Jackwood M, et al. Transmission dynamics of highly pathogenic avian influenza virus A(H5Nx) clade 2.3.4.4, North America, 2014–2015. Emerg Infect Dis. 2018;24:1840–8. https://doi.org/10.3201/eid2410.171891

8. Lycett SJ, Pohlmann A, Staubach C, Caliendo V, Woolhouse M, Beer M, et al.; Global Consortium for H5N8 and Related Influenza Viruses. Genesis and spread of multiple reassortants during the 2016/2017 H5 avian influenza epidemic in Eurasia. Proc Natl Acad Sci U S A. 2020;117:20814–25. https://doi.org/10.1073/pnas.2001813117
9. Sobolev I, Sharshov K, Dubovitskiy N, Kurskaya O, Alekseev A, Leonov S, et al. Highly pathogenic avian influenza A(H5N8) virus clade 2.3.4.4b, western Siberia, Russia, 2020. Emerg Infect Dis. 2021;27:2224–7. https://doi.org/10.3201/eid2708.204969
10. Li J, Zhang C, Cao J, Yang Y, Dong H, Cui Y, et al. Re-emergence of H5N8 highly pathogenic avian influenza virus in wild birds, China. Emerg Microbes Infect. 2021; 10:1819–23. https://doi.org/10.1080/22221751.2021.1968317
11. Okuya K, Mine J, Tokorozaki K, Kojima I, Esaki M, Miyazawa K, et al. Genetically diverse highly pathogenic avian influenza A(H5N1/H5N8) viruses among wild waterfowl and domestic poultry, Japan, 2021. Emerg Infect Dis. 2022;28:1451–5. https://doi.org/10.3201/eid2807.212586
12. Bi Y, Li J, Li S, Fu G, Jin T, Zhang C, et al. Dominant subtype switch in avian influenza viruses during 2016-2019 in China. Nat Commun. 2020;11:5909. https://doi.org/10.1038/s41467-020-19671-3
13. Pyankova OG, Susloparov IM, Moiseeva AA, Kolosova NP, Onkhonova GS, Danilenko AV, et al. Isolation of clade 2.3.4.4b A(H5N8), a highly pathogenic avian influenza virus, from a worker during an outbreak on a poultry farm, Russia, December 2020. Euro Surveill. 2021;26:2100439. https://doi.org/10.2807/1560-7917.ES.2021.26.24.2100439
14. Oliver I, Roberts J, Brown CS, Byrne AM, Mellon D, Hansen R, et al. A case of avian influenza A(H5N1) in England, January 2022. Euro Surveill. 2022;27:2200061. https://doi.org/10.2807/1560-7917.ES.2022.27.5.2200061

Address for correspondence: Yuhai Bi, Institute of Microbiology, Chinese Academy of Sciences, No. 1 Beichen West Rd, Chaoyang District, Beijing 100101, China; email: beeyh@im.ac.cn

Detection of *Leishmania* RNA Virus 1 in *Leishmania* (*Viannia*) *panamensis* Isolates, Panama

Kadir Gonzalez, Santiago S. De León, Vanessa Pineda, Franklyn Samudio, Zeuz Capitan-Barrios, José Antonio Suarez, Adriana Weeden, Betsi Ortiz, Margarita Rios, Brechla Moreno, Nathan D. Gundacker, Juan M. Pascale, Sandra López-Vergès, Néstor Sosa, Azael Saldaña, Leyda E. Ábrego

We detected *Leishmania* RNA virus 1 (LRV1) in 11 isolates of *Leishmania (Viannia) panamensis* collected during 2014–2019 from patients from different geographic areas in Panama. The distribution suggested a spread of LRV1 in *L. (V.) panamensis* parasites. We found no association between LRV1 and an increase in clinical pathology.

Leishmania RNA virus 1 (LRV1) belongs to the *Totiviridae* family, *Leishmaniavirus* genus, and infects different *Leishmania* lineages. This virus is not enveloped and is composed of a viral capsid ≈40 nm in diameter and a double-stranded RNA (dsRNA) of 5,280 nt (*1*,*2*). The genome has 3 open reading frames (ORF), 2 of which are coding. The *orf2* codes for the capsid protein and the *orf3* codes for an RNA-dependent RNA polymerase (RdRp). *orf1* has been described in other members of the family, but its function is unknown (*1*,*3*). This virus has been categorized in LRV1 and LRV2, according to the subgenuses of *Leishmania* in which they have been identified (*4*,*5*). The presence of LRV1 has been reported more frequently in specific regions of South America associated with cases of cutaneous leishmaniasis (CL) and mucocutaneous leishmaniasis (MCL) (*6*,*7*). *L. (Viannia) panamensis* is the predominant species and is responsible for most cases of CL in Panama (*8*,*9*) and the presence of LRV1 has been reported in 2 isolates of *L. (V.) panamensis* from Ecuador and Costa Rica (*7*,*10*).

Author affiliations: Gorgas Memorial Institute for Health Studies, Panama City, Panama (K. González, S.S. De León, V. Pineda, F. Samudio, Z. Capitan-Barrios, J.A. Suárez, A. Weeden, B. Ortíz, M. Ríos, B. Moreno, J.M. Pascale, S. López-Vergès, N. Sosa, A. Saldaña, L.E. Ábrego); University of Panama, Panama City (K. Gonzalez, S.S. De León, Z. Capitan-Barrios, A. Saldaña, L.E. Ábrego); Medical College of Wisconsin—Zablocki VA Medical Center, Milwaukee, Wisconsin, USA (N.D. Gundacker); University of New Mexico, Albuquerque, New Mexico, USA (N. Sosa)

DOI: https://doi.org/10.3201/eid2906.220012

The Study

We analyzed *Leishmania* spp. parasite isolates from clinical samples from 2014–2018 that were cryopreserved at Gorgas Memorial Institute's parasitology research department (Panama City, Panama). The Bioethics Committee of the Gorgas Memorial Institute for Health Studies approved this study (protocol no. 056/CBI/ICGES/19). We extracted clinical and epidemiologic data such as sex, age, clinical classification (location, severity, and number of lesions), and province of origin from the database. The disease was classified as nonsevere or severe according to Infectious Disease Society of America guidelines (*11*). We activated the isolates at 26°C by using Schneider's medium enriched with 25% fetal bovine serum until reaching exponential growth (2–3 $\times 10^7$ parasites/mL) (*9*). We centrifuged this concentration of parasites for 10 minutes at 3,500 rpm and divided it into 2 pellets; we used 1 pellet to extract DNA from *Leishmania* spp. for characterization and confirmation and the other to extract RNA and detect LRV1. We characterized the isolates as *L. (V.) panamensis* by the RFLP/PCR-Hsp70 methodology (*12*). For the detection of LRV1, we amplified 245 nucleotides corresponding to the *orf1* gene region using the primers described by Ito et al. (*6*,*13*) and sequenced the product by the Sanger method.

We recovered parasite isolates from 56 patients. Of those isolates, 11 (20%) were positive for LRV1, 63.3% from female patients and 36.4% from male

patients. Patient age range was 8–59 years; mean (±SD) age was 34 (±5.4) years (Appendix Table 1, https://wwwnc.cdc.gov/EID/article/29/6/22-0012-App1.pdf). All the patients came from leishmaniasis-endemic areas in Panama: 36.4% from Panama Oeste, 18.2% from Panama, 18.2% from Colón, 18.2% from Darién, and 9.0% from Coclé (Figure 1). Most of the patients had single lesions (7/11 [63.6%]); mean (±SD) was 1 (±0.2) and range 1–3 lesions per patient. Mean (±SD) time of evolution of the lesion was 50 (±9.6) days and range was 21–120 days. Most (6/11 [54.5%]) patients had an evolution time of 30 days. All the lesions were CL and were classified as nonsevere; lesions consisted of a crusty, moist ulcer with raised margins and a clean base (Table) (*11*). The lesions were distributed mainly on the arms (9/11: 81.8%); only 2 were visible elsewhere, on the leg (1/11: 9.1%) and face (1/11: 9.1%).

We performed data analysis using GraphPad Prism 5.0 software (GraphPad, https://www.graphpad.com). We performed the Kolmogorov-Smirnov test to assess the normality of the samples. To analyze the differences between groups, we performed a *t* test for Gaussian distribution data. We considered differences statistically significant when p was <0.05. We found no significant difference to suggest that those with LRV1-positive parasites developed more severe diseases (data not shown). From 10 sequences obtained in this study (GenBank accession nos. OL389058–67), we selected 6 sequences based on phylogenetic analysis quality (Appendix Table 2); those sequences clustered within the phylogenetic group of LRV1 sequences detected in the species of the subgenus *Viannia*, close to those found in isolates of *L. (V.) guyanensis* (Figure 2).

Conclusions

We detected LRV1 in 11/56 (20%) of *L. (V.) panamensis*–evaluated isolates, all of them in patients with CL, consistent with the preliminary description of the presence of LRV1 in 2 isolates of *L. (V.) panamensis* from clinical samples from Ecuador and Costa Rica, countries geographically close to Panama (*7*). The prevalence of LRV1 has been reported as higher in *Leishmania* spp. isolates from the New World (39.1%) than in those from the Old World (8.4%); prevalence also is higher in isolates from patients with severe skin forms of leishmaniasis, such as disseminated leishmaniasis and MCL, than from patients with CL (*14*).

The use of *Leishmania* spp. isolates could be a limitation for the analysis because we were able to analyze only the parasites that grew in medium. To avoid this bias, future studies analyzing the presence of the virus directly from clinical samples are needed. In South American countries, prevalence of ≈25% of LRV1 has been described in isolates of *L. (V.) braziliensis* and *L. (V.) guyanensis* from Peru (*7*), Bolivia (*14*), and Brazil (*15*). The presence of LRV1 in *L. (V.) panamensis* in this study (20%) indicates circulation of this virus in Panama, suggesting LRV1 is likely widespread across the Americas and in different *Leishmania (V.)* species. Future analysis using a higher

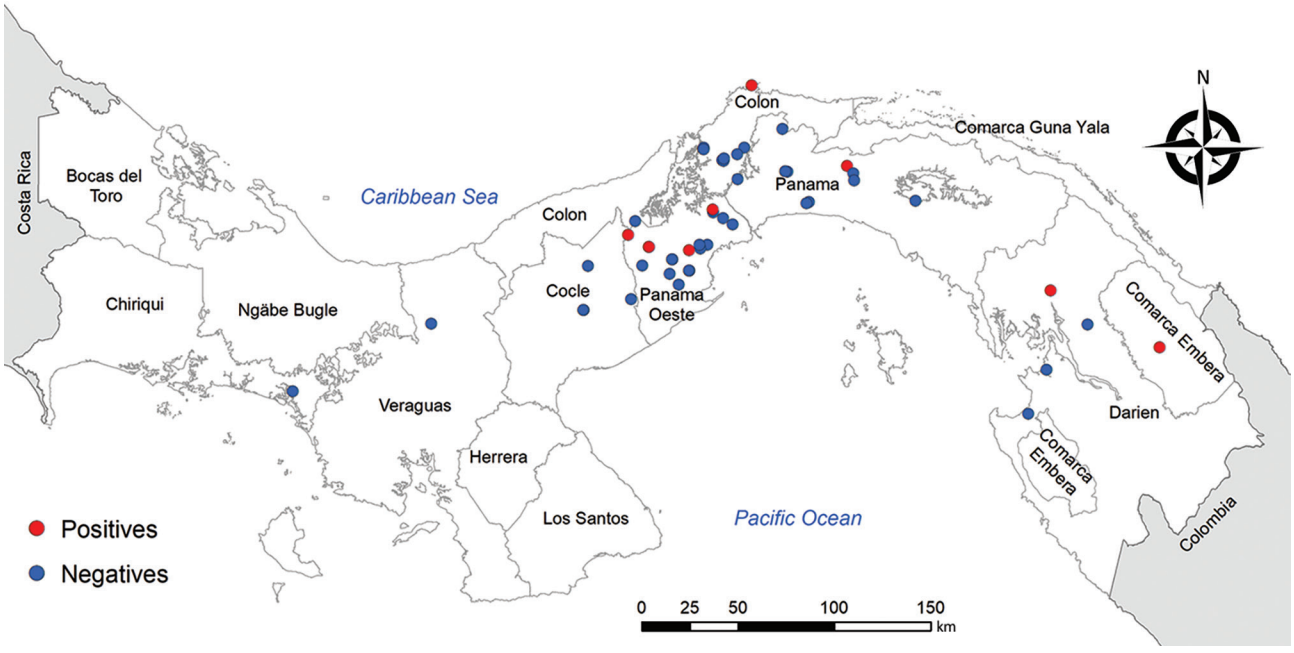

Figure 1. Distribution map of Leishmania RNA virus 1 positive and negative isolates analyzed in Panama, 2014–2018.

Table. Epidemiologic description of *Leishmania* (*Viannia*) *panamensis* isolates analyzed for LRV1, Panama, 2014–2018*

LRV1 status	No. isolates, N = 56	Mean age, y (SD)	Age range, y	Sex, no.	Duration of disease, d		No. lesions	
					Mean (SD)	Range	Mean (SD)	Range
Positive	11	34 (5.4)	8–59	4 M, 7 F	50 (9.6)	21–120	1 (0.2)	1–3
Negative	45	30 (3.1)	3–72	26 M, 19 F	67 (11)	15–365	1 (0.2)	1–6

*LRV1, *Leishmania* RNA virus 1.

number of samples is necessary to estimate LRV1 prevalence in Panama.

In this study, we found no evidence that correlates the presence of LRV1 with severe clinical forms of leishmaniasis caused by *L. (V.) panamensis*, which was consistent with previous findings of no predisposition of the Th2 response induced by LRV1 for the favorable survival of the parasite for *L. (V.) panamensis* (*7*). In addition, previous studies described a general decrease in the expression of virulence factor transcription in *L. (V.) panamensis* (*7*) compared with an earlier study of *L. (V.) braziliensis* (*10*). It is possible that *L. (V.) panamensis* strains infected with LRV1 have low expression of virulence factor, which would be reflected in the presence of uncomplicated symptoms of CL cases in the analyzed samples.

The role of LRV1 and its subtypes modulating the immune response in infection caused by *L. (V.) panamensis* is unclear. It is important to carry out studies of the virus subtypes that are circulating in the country and analyze whether the differences in the modulation of the immune response reflected in the clinical manifestations are because of intrinsic factors of the virus, the *Leishmania* species that it infects, or both.

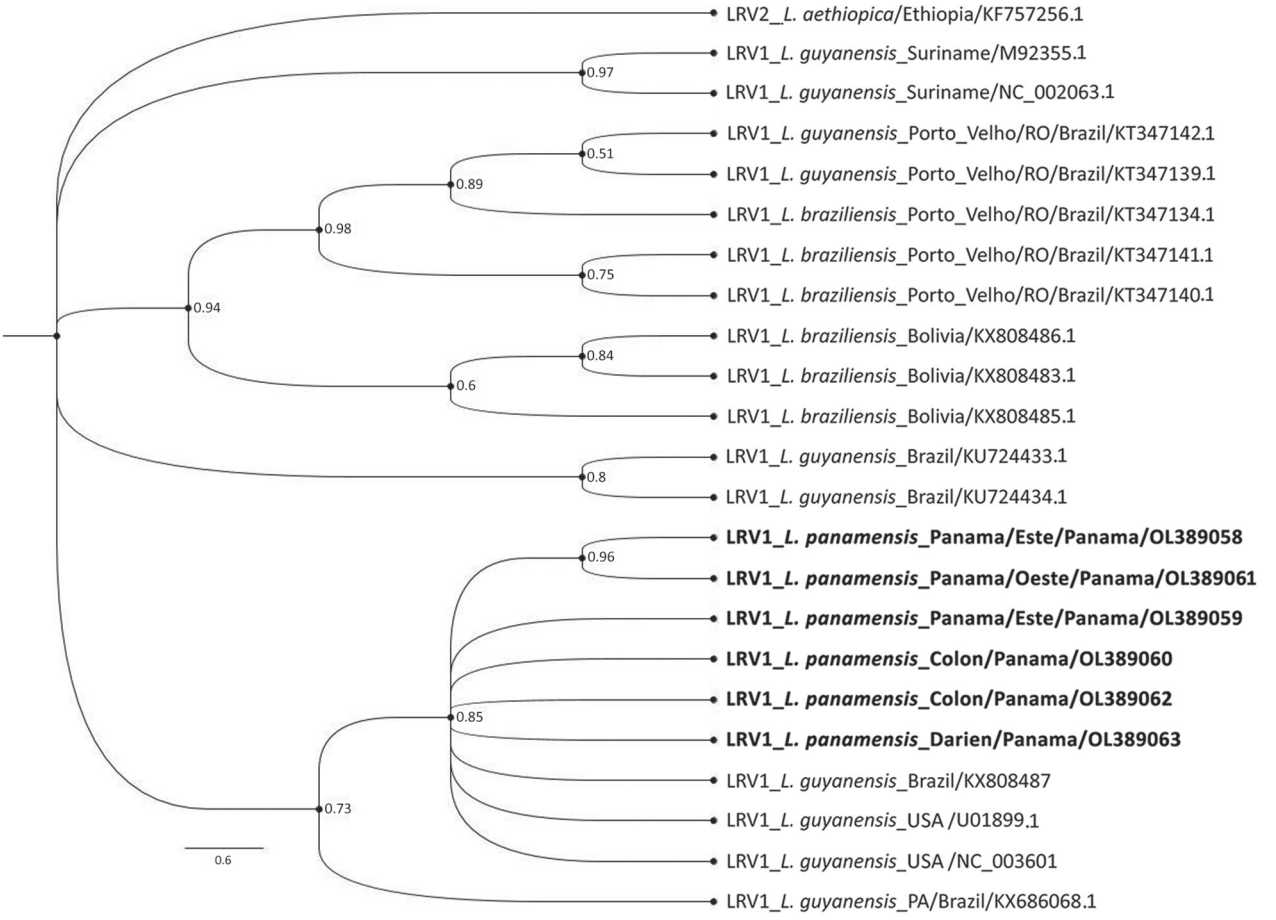

Figure 2. Phylogenetic analysis of *Leishmania* RNA virus 1 isolates analyzed in Panama, 2014–2018, and reference isolates. A phylogenetic tree reconstruction was implemented, applying Bayesian inference with the general time reversible plus gamma 4 plus invariate sites model using MrBayes version 3.2.6 phylogenetic software (https://nbisweden.github.io/MrBayes). Boldface indicates sequences obtained in this study, which are in the same clade with reference sequences from *Leishmania (Viannia) panamensis* isolates, mostly from Brazil. Numbers at each node represent clade credibility values. GenBank accession numbers are provided. Scale bar indicates substitutions per site.

In conclusion, the data we obtained show the presence of LRV1 in isolates of *L. (V.) panamensis* from Panama from different years and locations, suggesting wide spread of the virus in this species. In addition, the recent documented circulation of *L. (V.) guyanensis* and *L. (V.) braziliensis* in Panama (*9*) and the proposed association of LRV1 presence in these species with severity of disease highlight the necessity of future studies on the presence of LRV1 in non–*L. (V.) panamensis* species in Panama. The role of *Leishmania* in disease severity may depend on the species infected and the role of viral, parasite, and human host factors in pathogenesis.

Acknowledgments

We thank all the members of the Department of Research in Virology and Biotechnology, the Department of Research in Parasitology, and the clinical research unit of Gorgas Memorial Institute for Health Studies. We thank Alberto Cumbrera for map creation.

K.G., F.S., J.A.S., J.M.P., S.L.V., A.S., L.E.A. are members of the Sistema Nacional de Investigación of SENACYT, Panama.

This study was possible thanks to the support of the Sistema Nacional de Investigación (SNI-SENACYT), Panama, awarded to J.A.S., J.M.P., S.L.V., N.S., A.S., K.G., and L.E.A. This work also received administrative and financial support from Gorgas Memorial Institute for Health Studies.

About the Author

Dr. González is a medical technologist and senior health researcher at Gorgas Memorial Institute, Panama City, Panama. Primary research interests are immunopathology of cutaneous leishmaniasis and molecular characterization of *Leishmania* spp., and in vitro studies of *Leishmania (V.) panamensis* infection.

References

1. Scheffter SM, Ro YT, Chung IK, Patterson JL. The complete sequence of *Leishmania* RNA virus LRV2-1, a virus of an Old World parasite strain. Virology. 1995;212:84–90. https://doi.org/10.1006/viro.1995.1456
2. Stuart KD, Weeks R, Guilbride L, Myler PJ. Molecular organization of *Leishmania* RNA virus 1. Proc Natl Acad Sci U S A. 1992;89:8596–600. https://doi.org/10.1073/pnas.89.18.8596
3. MacBeth KJ, Patterson JL. The short transcript of *Leishmania* RNA virus is generated by RNA cleavage. J Virol. 1995; 69:3458–64. https://doi.org/10.1128/jvi.69.6.3458-3464.1995
4. Widmer G, Comeau AM, Furlong DB, Wirth DF, Patterson JL. Characterization of a RNA virus from the parasite *Leishmania*. Proc Natl Acad Sci U S A. 1989;86:5979–82. https://doi.org/10.1073/pnas.86.15.5979
5. Guilbride L, Myler PJ, Stuart K. Distribution and sequence divergence of LRV1 viruses among different *Leishmania* species. Mol Biochem Parasitol. 1992;54:101–4. https://doi.org/10.1016/0166-6851(92)90099-6
6. Cantanhêde LM, da Silva Júnior CF, Ito MM, Felipin KP, Nicolete R, Salcedo JMV, et al. Further evidence of an association between the presence of *Leishmania* RNA virus 1 and the mucosal manifestations in tegumentary leishmaniasis patients. PLoS Negl Trop Dis. 2015;9:e0004079. https://doi.org/10.1371/journal.pntd.0004079
7. Kariyawasam R, Grewal J, Lau R, Purssell A, Valencia BM, Llanos-Cuentas A, et al. Influence of leishmania RNA virus 1 on proinflammatory biomarker expression in a human macrophage model of American tegumentary leishmaniasis. J Infect Dis. 2017;216:877–86. https://doi.org/10.1093/infdis/jix416
8. Christensen HA, de Vasquez AM, Petersen JL. Short report epidemiologic studies on cutaneous leishmaniasis in eastern Panama. Am J Trop Med Hyg. 1999;60:54–7. https://doi.org/10.4269/ajtmh.1999.60.54
9. Miranda ADC, González KA, Samudio F, Pineda VJ, Calzada JE, Capitan-Barrios Z, et al. Molecular identification of parasites causing cutaneous leishmaniasis in Panama. Am J Trop Med Hyg. 2021;104:1326–34. https://doi.org/10.4269/ajtmh.20-1336
10. Kariyawasam R, Mukkala AN, Lau R, Valencia BM, Llanos-Cuentas A, Boggild AK. Virulence factor RNA transcript expression in the *Leishmania Viannia* subgenus: influence of species, isolate source, and *Leishmania* RNA virus-1. Trop Med Health. 2019;47:25. https://doi.org/10.1186/s41182-019-0153-x
11. Aronson N, Herwaldt BL, Libman M, Pearson R, Lopez-Velez R, Weina P, et al. Diagnosis and treatment of leishmaniasis: clinical practice guidelines by the Infectious Diseases Society of America (IDSA) and the American Society of Tropical Medicine and Hygiene (ASTMH). Am J Trop Med Hyg. 2017;96:24–45. https://doi.org/10.4269/ajtmh.16-84256
12. Montalvo AM, Fraga J, Maes I, Dujardin JC, Van der Auwera G. Three new sensitive and specific heat-shock protein 70 PCRs for global *Leishmania* species identification. Eur J Clin Microbiol Infect Dis. 2012;31:1453–61. https://doi.org/10.1007/s10096-011-1463-z
13. Ito MM, Catanhêde LM, Katsuragawa TH, da Silva Júnior CF, Camargo LMA, Mattos RG, et al. Correlation between presence of *Leishmania* RNA virus 1 and clinical characteristics of nasal mucosal leishmaniosis. Rev Bras Otorrinolaringol (Engl Ed). 2015;81:533–40. 10.1016/j.bjorl.2015.07.014 https://doi.org/10.1016/j.bjorl.2015.07.014
14. Saberi R, Fakhar M, Mohebali M, Anvari D, Gholami S. Global status of synchronizing *Leishmania* RNA virus in *Leishmania* parasites: a systematic review with meta-analysis. Transbound Emerg Dis. 2019;66:2244–51. https://doi.org/10.1111/tbed.13316
15. Adaui V, Lye LF, Akopyants NS, Zimic M, Llanos-Cuentas A, Garcia L, et al. Association of the endobiont double-stranded RNA virus LRV1 with treatment failure for human leishmaniasis caused by *Leishmania braziliensis* in Peru and Bolivia. J Infect Dis. 2016;213:112–21. https://doi.org/10.1093/infdis/jiv354

Address for correspondence: Leyda Abrego, Department of Research in Virology and Biotechnology, Gorgas Memorial Institute for Health Studies, Avenida Justo Arosemena, Panama City, Panama; email: labrego@gorgas.gob.pa; Azael Saldaña, Department of Research in Parasitology, Gorgas Memorial Institute for Health Studies, Avenida Justo Arosemena, Panama City, Panama; email: azael.saldana@up.ac.pa

Novel Orthonairovirus Isolated from Ticks near China–North Korea Border

Fan Li,[1] Jixu Li,[1] Jingdong Song, Qikai Yin, Kai Nie, Songtao Xu, Ying He, Shihong Fu, Guodong Liang, Qiang Wei, Huanyu Wang

We isolated a new orthonairovirus from *Dermacentor silvarum* ticks near the China–North Korea border. Phylogenetic analysis showed 71.9%–73.0% nucleic acid identity to the recently discovered Songling orthonairovirus, which causes febrile illness in humans. We recommend enhanced surveillance for infection by this new virus among humans and livestock.

Viruses of the genus *Orthonairovirus*, family *Nairoviridae*, include the consequential tick-transmitted pathogens Crimean–Congo hemorrhagic fever virus and Nairobi sheep disease virus, as well as other poorly characterized viruses that have been found in ticks and mammals. *Orthonairovirus* virions are spherical in shape (80–120-nm diameter) with 3 single-stranded RNA segments 17.1–22.8 kilobases in length and a membrane envelope (*1*–*5*). We performed surveillance in areas endemic for tick-borne encephalitis (*6*) and identified a novel orthonairovirus from *Dermacentor silvarum* ticks collected in 2021 in Jilin Province, China, near the China–North Korea border.

The Study

On April 17, 2021, we dragged corduroy to collect ticks from a forest region in Antu (118°46′E, 43°15′N), a district of the city of Yanbian in eastern Jilin Province, China, near the border with North Korea. We identified captured ticks according to morphologic keys and stored them at 4°C with wet cotton. We collected 264 ticks of 3 species—29 *Ixodes persulcatus*, 193 *Dermacentor silvarum*, and 12 *Haemaphysalis concinna*—and 30 larvae of unidentified species.

We homogenized ticks using a QIAGEN TissueLyser (QIAGEN, https://www.qiagen.com) and inoculated supernatants onto a monolayer of African green monkey kidney (Vero) E6 cells. After 3 successive passages, we observed cells for cytopathic effects. The inoculate from *Dermacentor silvarum* ticks, designated as YB_tick_2021_24, caused cytopathic effects in Vero E6 cells 96 h after inoculation (Figure 1, panels A, B). We collected cells showing cytopathic effects, then fixed and embedded them in epoxy resin. We cut ultrathin (80 nm) sections from the resin block, stained them with citrate lead and uranyl acetate, and observed them under a transmission electron microscope. We observed enveloped virus particles ≈100 nm in diameter that shared morphologic features with *Bunyavirales* viruses (Figure 1, panel C).

We extracted viral RNA from infected culture supernatants using a QIAGEN QIAamp Viral RNA Mini Kit, synthesized cDNA, prepared DNA libraries using an Illumina Nextera XT Kit (Illumina, https://www.illumina.com), and performed 150 bp paired-end sequencing using the Illumina MiniSeq System. We filtered reads on the basis of their length and mean quality values. We prepared contigs by de novo assembly and subjected them to BLASTx alignment (https://blast.ncbi.nlm.nih.gov/Blast.cgi) at E value $<10^{-4}$ against the nonredundant protein and viral proteome databases of the National Center for Biotechnology Information. We used Bowtie 2 (https://bowtie-bio.sourceforge.net/bowtie2/index.shtml) to remap the clean reads to the generated virus-related contigs (*7*). We used rapid

Author affiliations: Chinese Center for Disease Control and Prevention, Beijing, China (F. Li, J. Song, Q. Yin, K. Nie, S. Xu, Y. He, S. Fu, G. Liang, Q. Wei, H. Wang); Yanbian Korean Autonomous Prefecture Center for Disease Control and Prevention, Jilin, China (J. Li)

DOI: https://doi.org/10.3201/eid2906.230056

[1]These authors contributed equally to this article.

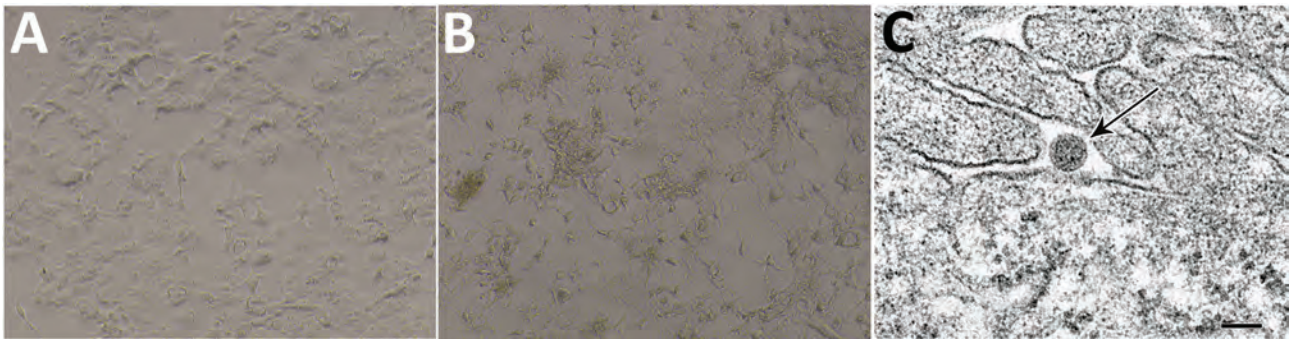

Figure 1. Discovery and characterization of novel orthonairovirus Antu virus isolate YB_tick_2021_24 from *Dermacentor silvarum* ticks in China. A) Vero E6 cells without YB_tick_2021_24 infection. Original magnification ×10. B) YB_tick_2021_24-infected Vero E6 cells showing cytopathic effects visible by light microscopy. Original magnification ×10. C) Ultrathin section electron micrograph of an isolated particle (black arrow) on a cell surface. Scale bar = 100 nM

amplification of cDNA ends (RACE) PCR and Sanger sequencing to confirm the terminal sequences of virus genomes, and deposited the new genome in GenBank (accession nos. OQ207701–3). We identified open read frames (ORFs) using ORF finder (https://www.ncbi.nlm.nih.gov/orffinder) and calculated sequence similarities using BLAST.

Our procedure generated 40,826,350 reads (6.1 Gbp), which produced 266 virus-related contigs. Three contigs, the 1,516 bp small (S), 3,936 bp medium (M), and 12,133 bp large (L) segments, were annotated to Songling virus (SLV), a previously reported

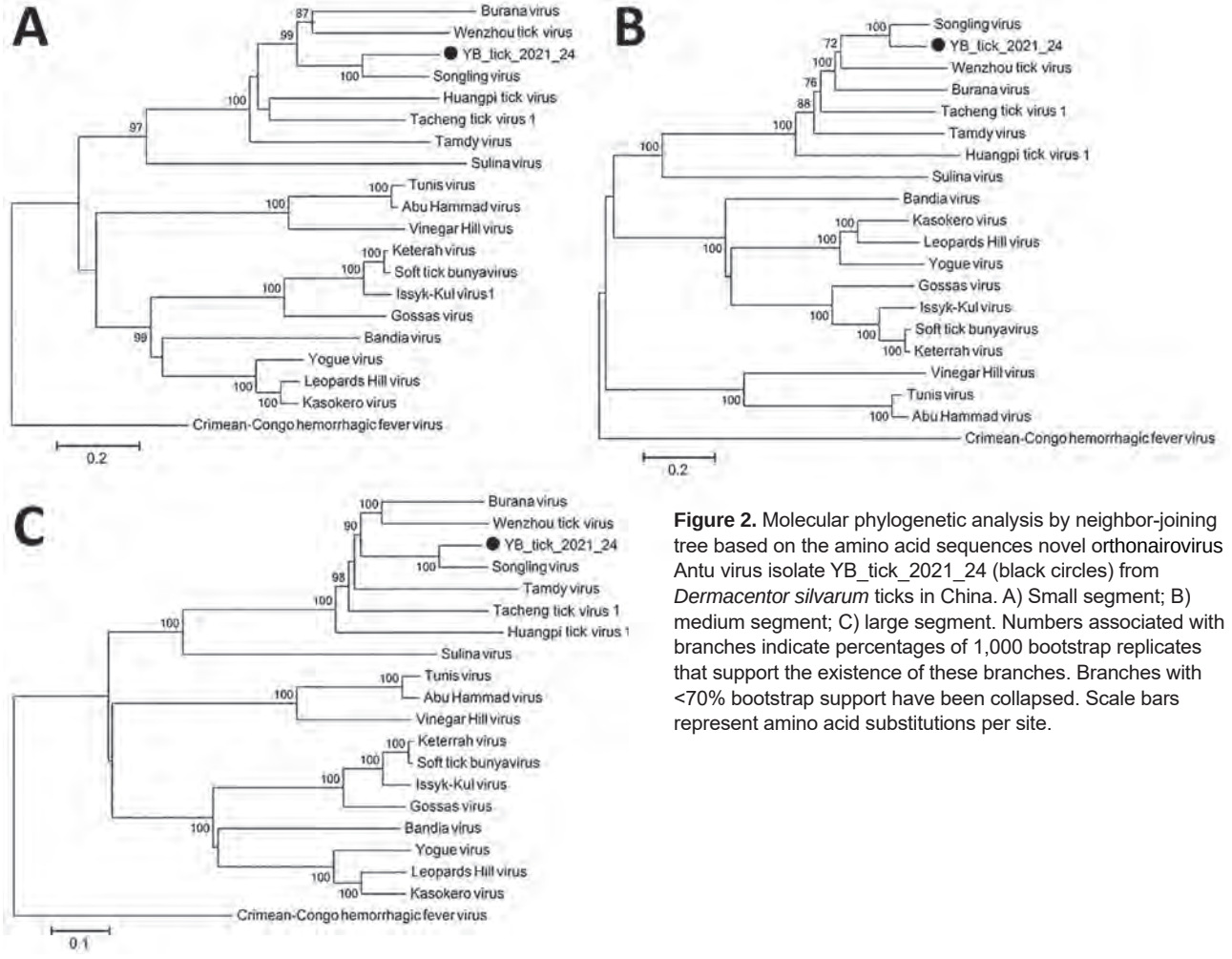

Figure 2. Molecular phylogenetic analysis by neighbor-joining tree based on the amino acid sequences novel orthonairovirus Antu virus isolate YB_tick_2021_24 (black circles) from *Dermacentor silvarum* ticks in China. A) Small segment; B) medium segment; C) large segment. Numbers associated with branches indicate percentages of 1,000 bootstrap replicates that support the existence of these branches. Branches with <70% bootstrap support have been collapsed. Scale bars represent amino acid substitutions per site.

Table. Homology comparisons of the sequence of novel orthonairovirus Antu viruses from China and other related viruses*

Protein/virus	Antu virus	SLGV	WTV	TTV	BURV	TDYV	HTV	CCHFV
Small								
Antu virus		71.5	52.6	53.7	52.1	48.9	47.4	37.3
SLGV	71.9		55.3	51.2	51.8	49.6	45.9	34.9
WTV	60.3	60.6		50.0	54.1	43.8	46.0	34.0
TTV	59.5	57.9	56.6		46.6	49.1	51.0	33.4
BURV	58.6	59.9	60.5	55.2		44.3	42.4	35.0
TDYV	56.5	58.2	54.0	57.9	53.1		45.0	34.3
HTV	55.5	55.8	55.9	58.7	52.9	55.8		35.2
CCHFV	47.6	46.8	46.8	46.5	47.9	47.7	46.3	
Medium								
Antu virus		79.5	59.9	56.3	58.7	53.8	46.9	25.4
SLGV	72.4		58.2	53.9	57.0	51.2	46.5	24.5
WTV	61.9	61.8		51.8	54.0	50.0	46.5	24.5
TTV	57.2	58	56.4		51.6	51.1	48.1	24.5
BURV	61	61.2	58.9	58		49.4	47.2	24.0
TDYV	56.6	57.5	55.9	55.1	55.4		45.7	24.4
HTV	53.7	53.9	53.4	52.9	54.2	52.1		24.6
CCHFV	41.8	40.7	40.5	40.6	41.3	42.2	40.3	
Large								
Antu virus		84.6	66.5	64.1	66.0	62.2	60.1	39.2
SLGV	73.0		65.7	64.0	65.1	61.4	60.1	38.5
WTV	63.4	63.7		63.5	69.7	61.7	60.0	38.5
TTV	61.9	62.0	62.2		63.2	59.3	60.0	38.7
BURV	63.4	63.3	66.1	61.8		61.5	60.3	38.7
TDYV	60.4	60.5	60.5	59.4	60.8		58.0	39.2
HTV	59.8	60.1	59.5	61.5	60.3	58.2		38.2
CCHFV	48.1	48.3	48.2	48.0	48.8	48.1	48.5	

*Percentage nucleotide sequence identity presented below and amino acid identity above blank cells. BURV, Burana virus; CCHFV, Crimean-Congo hemorrhagic fever virus; HTV, Huangpi tick virus; SGLV, Songling virus; TDYV, Tamdy virus; TTV, Tacheng tick virus; WTV, Wenzhou tick virus.

orthonairovirus (*8*). Average sequencing coverages remapped to the 3 contigs were 48× (S), 63× (M), and 234× (L). The final genome lengths confirmed by RACE sequencing were 1,848 bp encoding 488 aa for the S segment, 4,099 bp encoding 1,263 aa for the M segment, and 12,001 bp encoding 3,950 aa for the L segment. We performed multiple alignments using MAFFT version 7 (https://mafft.cbrc.jp/alignment/server) (*9*) and constructed a phylogenetic tree in MEGA7 (https://www.megasoftware.net) by using the neighbor-joining method with a bootstrap test for 1,000 replicates (*10*).

Phylogenetic analysis showed the strain belongs to the genus *Orthonairovirus*, family *Nairoviridae*, and is genetically related to SLV (Figure 2) (*4*,*5*,*8*,*11*). The terminal nucleotides of the S segment were identical to those of orthonairoviruses (3′ segment terminus AGAGUUUCU and 5′ segment terminus AGAAACUCU) (*5*). The termini of the M and L segments were different (Appendix Figure, https://wwwnc.cdc.gov/EID/article/29/6/23-0056-App1.pdf). Homology analysis comparing YB_tick_2021_24 with SLV sample YC585 showed 71.9% nucleic acid (na) and 71.5% aa identities for the S segment, 72.4% na and 79.5% aa identities for the M segment, and 73.0% na and 84.6% aa identities for the L segment (Table 1) (*8*). Those results indicate that the isolate represents a unique *Orthonairovirus* species. For purposes of archiving, we designated novel YB_tick_2021_24 as Antu virus and deposited the strain in the National Pathogen Resource Center (accession no. NPRC 2.3.9401).

Conclusion

We identified a novel orthonairovirus, Antu virus, in *Dermacentor silvarum* ticks collected in China near the China–North Korea border. Nucleotide and amino acid sequence homologies, combined with phylogenetic analysis of other orthonairovirus genomes, suggested that Antu virus is a new member of the genus *Orthonairovirus*, genetically related to SLV. Tamdy virus and SLV are orthonairoviruses reportedly able to infect human and livestock (*8*,*12*,*13*). Lacking direct evidence of the ability of Antu virus to infect and cause illness among humans and livestock animals, we recommend enhanced monitoring and surveillance for Antu virus infection among humans and livestock in potentially endemic areas.

This study was supported by the Science and Technology Fundamental Resources Investigation Program (grant no. 2022FY100904), the National Key Research and Development Program (grant no. 2022YFC2302700, 2022YFC2602200), and the United States National Institutes of Health Foundation (grant no. U01 AI151810).

About the Author

Dr. Fan Li is an associate professor at National Institute for Viral Disease Control and Prevention, Chinese Center for Disease Control and Prevention. Her research interests include virus discovery in disease vectors and arbovirus infections.

References

1. Garrison AR, Alkhovsky SV, Avšič-Županc T, Bente DA, Bergeron É, Burt F, et al. ICTV virus taxonomy profile: *Nairoviridae*. J Gen Virol. 2020;101:798–9. https://doi.org/10.1099/jgv.0.001485
2. Lasecka L, Baron MD. The molecular biology of nairoviruses, an emerging group of tick-borne arboviruses. Arch Virol. 2014;159:1249–65. https://doi.org/10.1007/s00705-013-1940-z
3. Bergeron É, Zivcec M, Chakrabarti AK, Nichol ST, Albariño CG, Spiropoulou CF. Recovery of recombinant Crimean Congo hemorrhagic fever virus reveals a function for non-structural glycoproteins cleavage by furin. PLoS Pathog. 2015;11:e1004879. https://doi.org/10.1371/journal.ppat.1004879
4. Walker PJ, Widen SG, Wood TG, Guzman H, Tesh RB, Vasilakis N. A global genomic characterization of nairoviruses identifies nine discrete genogroups with distinctive structural characteristics and host-vector associations. Am J Trop Med Hyg. 2016;94:1107–22. https://doi.org/10.4269/ajtmh.15-0917
5. Kuhn JH, Wiley MR, Rodriguez SE, Bào Y, Prieto K, Travassos da Rosa AP, et al. Genomic characterization of the genus *Nairovirus* (family *Bunyaviridae*). Viruses. 2016;8:164. https://doi.org/10.3390/v8060164
6. Chen X, Li F, Yin Q, Liu W, Fu S, He Y, et al. Epidemiology of tick-borne encephalitis in China, 2007–2018. PLoS One. 2019;14:e0226712. https://doi.org/10.1371/journal.pone.0226712
7. Langmead B, Salzberg SL. Fast gapped-read alignment with Bowtie 2. Nat Methods. 2012;9:357–9.
8. Ma J, Lv XL, Zhang X, Han SZ, Wang ZD, Li L, et al. Identification of a new orthonairovirus associated with human febrile illness in China. Nat Med. 2021;27:434–9. [Erratum in Nat Med. 2021;27:926.] https://doi.org/10.1038/s41591-020-01228-y
9. Katoh K, Standley DM. MAFFT multiple sequence alignment software version 7: improvements in performance and usability. Mol Biol Evol. 2013;30:772–80. https://doi.org/10.1093/molbev/mst010
10. Kumar S, Stecher G, Tamura K. MEGA7: Molecular Evolutionary Genetics Analysis version 7.0 for bigger datasets. Mol Biol Evol. 2016;33:1870–4. https://doi.org/10.1093/molbev/msw054
11. Zhou H, Ma Z, Hu T, Bi Y, Mamuti A, Yu R, et al. Tamdy virus in *Ixodid* ticks infesting bactrian camels, Xinjiang, China, 2018. Emerg Infect Dis. 2019;25:2136–8.
12. Liu X, Zhang X, Wang Z, Dong Z, Xie S, Jiang M, et al. A tentative Tamdy orthonairovirus related to febrile illness in northwestern China. Clin Infect Dis. 2020;70:2155–60. https://doi.org/10.1093/cid/ciz602
13. Moming A, Shen S, Fang Y, Zhang J, Zhang Y, Tang S, et al. Evidence of human exposure to Tamdy virus, northwest China. Emerg Infect Dis. 2021;27:3166–70. https://doi.org/10.3201/eid2712.203532

Address for correspondence: Huanyu Wang, National Institute for Viral Disease Control and Prevention, State Key Laboratory for Infectious Disease Prevention and Control, Chinese Center for Disease Control and Prevention, No.155 Changbai Rd, Changping District, Beijing 102206, China; email: wanghy@ivdc.chinacdc.cn; Qiang Wei, National Pathogen Resource Center, Chinese Center for Disease Control and Prevention, No.155 Changbai Rd, Changping District, Beijing 102206, China; email: weiqiang@chinacdc.cn

Enterovirus D68 Outbreak in Children, Finland, August–September 2022

Ville Peltola, Riikka Österback, Matti Waris, Lauri Ivaska, Paula A. Tähtinen, Miia Laine, Tytti Vuorinen

We observed an intense enterovirus D68 outbreak in children in southwest Finland in August–September 2022. We confirmed enterovirus D68 infection in 56 children hospitalized for respiratory illnesses and in 1 child with encephalitis but were not able to test all suspected patients. Continuing surveillance for enterovirus D68 is needed.

Widespread enterovirus D68 (EV-D68) epidemics occurred in the United States and in other parts of the world in 2014, 2016, and 2018 (*1*,*2*). Low-level EV-D68 detection was reported in the United States during the COVID-19 pandemic in 2020 (*3*). EV-D68 re-emerged in autumn 2021, prominently in Europe but also to some extent in the United States, and again in 2022, when reports emerged from the United States and Europe about a substantially increased circulation of EV-D68 associated with acute respiratory illnesses in children (*4*–*6*). Previous EV-D68 epidemics in Europe and the United States were associated with severe lower respiratory tract infections, wheezing illnesses, and, more rarely, acute flaccid myelitis or other neurologic presentations in children (*7*,*8*). The clinical manifestations during the outbreaks in 2022 have not been described in detail in the literature.

In Finland, EV-D68 cases were detected in 2014 and sporadically before and after that, but circulation of the virus has not been seen during recent years. All laboratory findings of enterovirus in Finland are reported in the Finnish National Infectious Diseases Register ,and some enteroviruses are typed. Hospitalizations of children because of respiratory illnesses increased rapidly in southwest Finland in August 2022. We screened children (≤16 years of age) admitted to Turku University Hospital, Turku, Finland, for respiratory or central nervous system illness associated with enterovirus (confirmed by reverse transcription PCR [RT-PCR]) and identified EV-D68 by type-specific RT-PCR and sequencing. We describe the outbreak and report the clinical features of 57 children hospitalized with EV-D68 in August–September 2022.

The Study

Turku University Hospital is the only hospital providing inpatient care for children in the Southwest Finland Hospital District, covering a population of 470,000 people, including 77,000 children and adolescents ≤16 years of age. The hospital also serves as a tertiary facility for a larger area, but our study did not include patients referred from other hospitals. Hospital policy requires that all children and adolescents with symptoms of infection at admittance be screened by a rapid RT-PCR test for SARS-CoV-2, influenza A and B, and respiratory syncytial virus (RSV). A laboratory-developed triplex RT-PCR test for enterovirus, rhinovirus, and RSV (*9*) or a 16-plex RT-PCR test for respiratory viruses including enterovirus (Allplex Respiratory Panels 1–3; Seegene, https://www.seegene.com) is performed by using nasopharyngeal swab or cerebrospinal fluid specimens for patients with a respiratory tract or central nervous system illness and negative screening test (Appendix, https://wwwnc.cdc.gov/EID/article/29/6/22-1795-App1.pdf).

When we noticed an enterovirus outbreak, we aimed to genotype viruses in all detected cases. First, we subjected specimens positive for enterovirus to typing based on partial enterovirus viral protein (VP) 1 gene sequencing after seminested PCR amplification (*10*). We observed a high prevalence of EV-D68, but the amplification succeeded only in specimens with high virus load (low cycle threshold value). Therefore, we applied an RT-PCR assay with EV-D68 VP1 gene-specific primers (*11*). Because a portion of the specimens remained untyped, we subjected them to

Author affiliations: Turku University Hospital and University of Turku, Turku, Finland

DOI: http://doi.org/10.3201/eid2906.221795

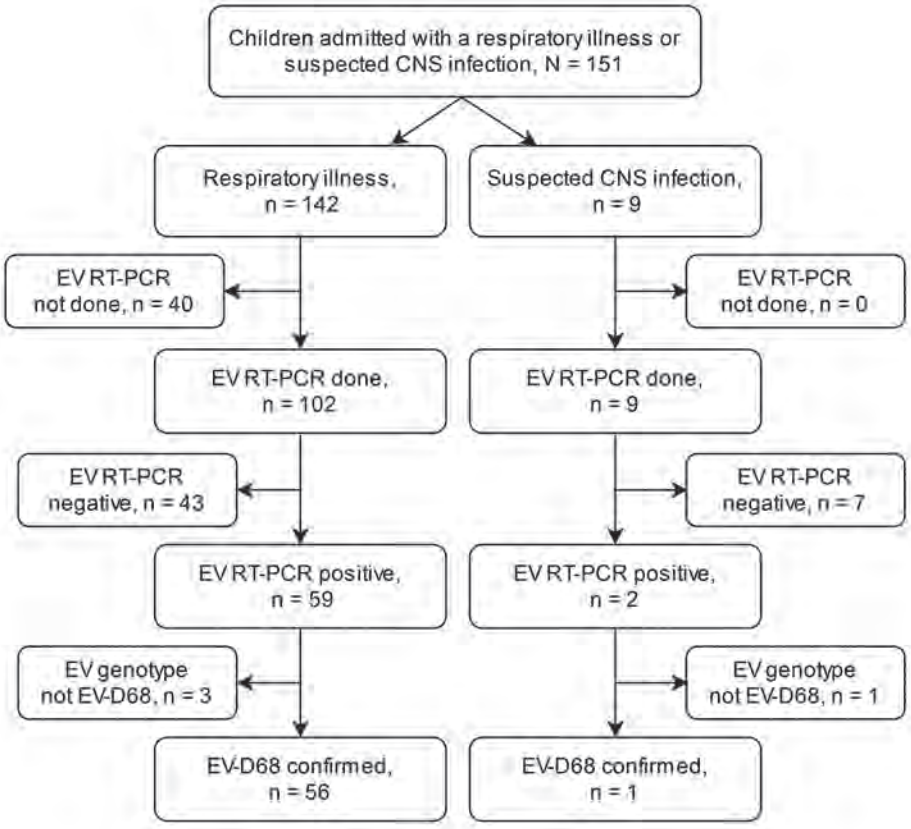

Figure 1. Flowchart of the enterovirus D68 (EV-D68) testing process of children hospitalized with respiratory illness or suspected central nervous system (CNS) infection at Turku University Hospital, Turku, Finland, during August 1–September 30, 2022. EV, enterovirus; RT-PCR, reverse transcription PCR.

a nested amplification and sequencing for the VP4/2 gene region (*9*,*12*) (Figure 1; Appendix)

In August 2022, hospitalization and intensive care unit admittances of children for wheezing illnesses and pneumonia increased rapidly at our hospital. EV-D68 was documented in most children who tested positive for enterovirus (Figure 2). During the study period of August 1–September 30, 2022, a total of 57 children were hospitalized with a confirmed EV-D68 infection. The weekly number of new EV-D68 cases ranged from 7 to 20 during the 4-week period of August 22–September 18, 2022, and decreased thereafter.

The median age of the 56 children hospitalized with EV-D68 respiratory illness was 4.23 years

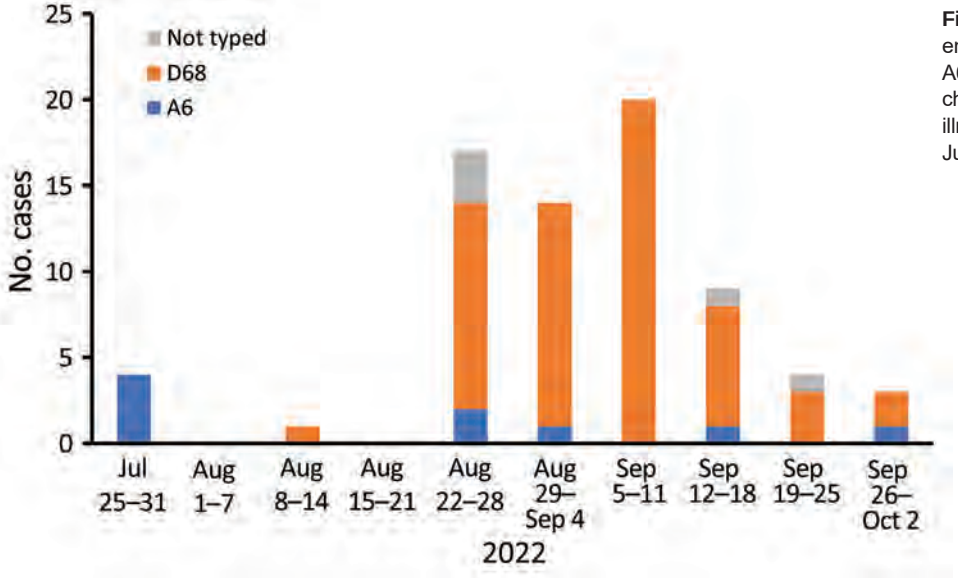

Figure 2. Weekly number of enterovirus D68, coxsackievirus A6, and nontyped enteroviruses in children hospitalized with enteroviral illness in southwest Finland during July 25–October 2, 2022.

(interquartile range 2.42–6.15 years), and most (66.1%) were male (Table). Before their most recent illness, 26.8% of the children had confirmed asthma or had been prescribed inhaled corticosteroids for suspected asthma. The primary reason for hospitalization was wheezing illness for 78.6% and pneumonia for 16.1%. The mean length of hospital stay among the children was 2.75 days (SD 2.05 days). More than half needed supplemental oxygen or other respiratory support, and 7 (12.5%) were admitted to the intensive care unit. The study population included 1 case of encephalitis and no cases of acute flaccid myelitis. The child with encephalitis manifested ataxia as the predominant symptom and did not need intensive care; EV-D68 was detected in the nasopharyngeal specimen but not in cerebrospinal fluid. All children recovered fully, and only 1 child was re-admitted to hospital within 14 days after discharge.

We detected another respiratory virus, in addition to EV-D68, in 8 (14.3%) children. Because other respiratory viruses can affect the clinical picture, we performed a sensitivity analysis of the clinical characteristics, excluding children with a co-detected virus (Appendix Table). We determined the clinical characteristics of 48 children with EV-D68 as the only detected virus to be similar to all study children.

Conclusions

The EV-D68 outbreak we studied started rapidly and was exceptionally intense but was of short duration in our area. Other parts of Finland also reported an increased number of children hospitalized with wheezing illnesses during the same timeframe. As in earlier reports, we found that the clinical picture of EV-D68 infection in hospitalized children was most often a respiratory illness characterized by wheezing and respiratory distress. In that respect, EV-D68 resembles rhinoviruses more than it does other enteroviruses (*13*).

Compared with wheezing illnesses caused by other viruses, the median age of children with EV-D68–associated illness was somewhat high (4.2 years), and a large proportion of children had a severe illness treated at the intensive care unit. Some children were simultaneously positive for another respiratory virus, but clinical manifestations were similar among those with EV-D68 only and those with co-detected viruses. Co-detection of ≥2 respiratory viruses is common in children. Although cases in this outbreak included 1 child diagnosed with encephalitis and no cases of acute flaccid myelitis, EV-D68 can cause acute flaccid myelitis and other neurologic illnesses. A study of a larger population would be needed to determine the occurrence of rare manifestations.

Table. Baseline characteristics, diagnoses, and treatment of children hospitalized with EV-D68 respiratory illness in southwest Finland. August–September 2022*

Variable	Children with EV-D68, N = 56
Median age, years (IQR)	4.23 (2.42–6.15)
Sex	
F	19 (33.9)
M	37 (66.1)
Underlying condition, any	21 (37.5)
Asthma†	15 (26.8)
Neurologic condition	5 (8.9)
Premature birth, <37+0 gestational weeks	4 (7.1)
Other condition‡	3 (5.4)
Other virus§	8 (14.3)
Diagnosis	
Wheezing illness¶	44 (78.6)
Pneumonia	9 (16.1)
Upper respiratory tract infection	3 (5.4)
Treatment	
Intensive care unit admission	7 (12.5)
Respiratory support, any	32 (57.1)
Supplemental oxygen	22 (39.3)
High flow nasal oxygen	10 (17.9)
Invasive ventilation	0 (0)
Inhaled salbutamol	53 (94.6)
Systemic corticosteroids	42 (75.0)
Antibiotics	20 (35.7)
Mean length of stay in the hospital, days (SD)	2.75 (2.05)
Readmission#	1 (1.8)

*Values are no. (%) unless otherwise indicated. IQR, interquartile range; SD, standard deviation.
†Confirmed or suspected asthma.
‡Cardiovascular condition, cystic fibrosis, or hypothyroidism.
§Rhinovirus, n = 7; SARS-CoV-2, n = 3; and human bocavirus, n = 3. Including 3 patients who had 3 or 4 viruses.
¶Bronchiolitis, wheezing bronchitis, or exacerbation of asthma.
#Within 14 days after discharge.

Active surveillance for EV-D68 is important because of its epidemic occurrence, continuous antigenic evolution (*14*), and potential to cause severe respiratory illnesses and serious neurologic conditions. Rapid multiplex RT-PCR methods are increasingly used for microbiologic diagnostics of respiratory tract infections, but these methods do not provide virus type, and some methods do not discriminate between rhinoviruses and enteroviruses. Our findings support virologic laboratory testing, especially in severe clinical cases, to determine the enterovirus type.

Our study included only 1 large pediatric hospital in Finland, and the number of EV-D68 cases is probably underestimated because of the short study period; enterovirus testing of only children negative in the screening test for SARS-CoV-2, influenza A and B, and RSV; and use of either triplex or 16-plex RT-PCR as the primary test for enterovirus. If we had used both tests or the highly sensitive triplex test for all cases, sensitivity might have been higher. We were not able to determine the lineage of genotyped EV-D68 viruses based on partial sequencing of VP1 only.

In summary, we observed a rapid onset of an EV-D68 epidemic in southwest Finland in August 2022. Most children who needed hospital treatment had a respiratory illness characterized by acute wheezing and respiratory distress. Given the virus' ability to cause acute flaccid myelitis and other neurologic illnesses, continuing surveillance for EV-D68 is needed.

Acknowledgments

We acknowledge Ulla Torkko for help in collecting the clinical data.

This study received institutional approval and was not subject to the Ethics Committee approval.

About the Author

Dr. Peltola is a professor of pediatric infectious diseases at the University of Turku, Turku, Finland. His primary research interests include epidemiology, diagnostics, treatment, and prevention of respiratory tract infections in children.

References

1. Holm-Hansen CC, Midgley SE, Fischer TK. Global emergence of enterovirus D68: a systematic review. Lancet Infect Dis. 2016;16:e64–75. https://doi.org/10.1016/S1473-3099(15)00543-5
2. Andrés C, Vila J, Creus-Costa A, Piñana M, González-Sánchez A, Esperalba J, et al. Enterovirus D68 in hospitalized children, Barcelona, Spain, 2014–2021. Emerg Infect Dis. 2022;28:1327–31. https://doi.org/10.3201/eid2807.220264
3. Shah MM, Perez A, Lively JY, Avadhanula V, Boom JA, Chappell J, et al. Enterovirus D68–associated acute respiratory illness—New Vaccine Surveillance Network, United States, July–November 2018–2020. MMWR Morb Mortal Wkly Rep. 2021;70:1623–8. https://doi.org/10.15585/mmwr.mm7047a1
4. Fall A, Gallagher N, Morris CP, Norton JM, Pekosz A, Klein E, et al. Circulation of enterovirus D68 during period of increased influenza-like illness, Maryland, USA, 2021. Emerg Infect Dis. 2022;28:1525–7. https://doi.org/10.3201/eid2807.212603
5. Ma KC, Winn A, Moline HL, Scobie HM, Midgley CM, Kirking HL, et al.; New Vaccine Surveillance Network Collaborators. Increase in acute respiratory illnesses among children and adolescents associated with rhinoviruses and enteroviruses, including enterovirus D68—United States, July–September 2022. MMWR Morb Mortal Wkly Rep. 2022;71:1265–70. https://doi.org/10.15585/mmwr.mm7140e1
6. Benschop KSM, Albert J, Anton A, Andrés C, Aranzamendi M, Armannsdóttir B, et al. Re-emergence of enterovirus D68 in Europe after easing the COVID-19 lockdown, September 2021. Euro Surveill. 2021;26:2100998. https://doi.org/10.2807/1560-7917.ES.2021.26.45.2100998
7. Midgley CM, Watson JT, Nix WA, Curns AT, Rogers SL, Brown BA, et al.; EV-D68 Working Group. Severe respiratory illness associated with a nationwide outbreak of enterovirus D68 in the USA (2014): a descriptive epidemiological investigation. Lancet Respir Med. 2015;3:879–87. https://doi.org/10.1016/S2213-2600(15)00335-5
8. Kidd S, Lopez AS, Konopka-Anstadt JL, Nix WA, Routh JA, Oberste MS. Enterovirus D68–associated acute flaccid myelitis, United States, 2020. Emerg Infect Dis. 2020;26:26. https://doi.org/10.3201/eid2610.201630
9. Österback R, Tevaluoto T, Ylinen T, Peltola V, Susi P, Hyypiä T, et al. Simultaneous detection and differentiation of human rhino- and enteroviruses in clinical specimens by real-time PCR with locked nucleic Acid probes. J Clin Microbiol. 2013;51:3960–7. https://doi.org/10.1128/JCM.01646-13
10. Nix WA, Oberste MS, Pallansch MA. Sensitive, seminested PCR amplification of VP1 sequences for direct identification of all enterovirus serotypes from original clinical specimens. J Clin Microbiol. 2006;44:2698–704. https://doi.org/10.1128/JCM.00542-06
11. Poelman R, Schuffenecker I, Van Leer-Buter C, Josset L, Niesters HG, Lina B; ESCV-ECDC EV-D68 study group. European surveillance for enterovirus D68 during the emerging North-American outbreak in 2014. J Clin Virol. 2015;71:1–9. https://doi.org/10.1016/j.jcv.2015.07.296
12. Savolainen C, Mulders MN, Hovi T. Phylogenetic analysis of rhinovirus isolates collected during successive epidemic seasons. Virus Res. 2002;85:41–6. https://doi.org/10.1016/S0168-1702(02)00016-3
13. Blomqvist S, Savolainen C, Råman L, Roivainen M, Hovi T. Human rhinovirus 87 and enterovirus 68 represent a unique serotype with rhinovirus and enterovirus features. J Clin Microbiol. 2002;40:4218–23. https://doi.org/10.1128/JCM.40.11.4218-4223.2002
14. Hodcroft EB, Dyrdak R, Andrés C, Egli A, Reist J, García Martínez de Artola D, et al. Evolution, geographic spreading, and demographic distribution of Enterovirus D68. PLoS Pathog. 2022;18:e https://doi.org/10.1371/journal.ppat.1010515

Address for correspondence: Ville Peltola, Department of Paediatrics and Adolescent Medicine, Turku University Hospital, 20521 Turku, Finland; email: ville.peltola@utu.fi

Treatment Failure in Patient with Severe Mpox and Untreated HIV, Maryland, USA

Evgenii Filippov,[1] Sanchit Duhan,[1] Laura Lehman, Bijeta Keisham, Vishal Sethi

A 33-year-old man in Baltimore, Maryland, USA, with untreated HIV infection had a 74-day course of mpox with multiorgan system involvement and unique clinical findings. In this clinical experience combining 3 novel therapeutic regimens, this patient died from severe mpox in the context of untreated HIV and advanced immunodeficiency.

In July 2022, the World Health Organization declared human mpox an international public health emergency (*1*). Mpox usually has a self-limiting illness course of 2–4 weeks; characteristic rash is the most common symptom and is associated with fever, lymphadenopathy, and fatigue in ≈50% of cases (*2*). Although ≈5.8% of confirmed cases require hospitalization, patients with advanced AIDS might be especially prone to severe mpox and death (*3*).

No medications have a proven benefit for mpox, and experience with available regimens is limited. Four medications are available under clinical trials or the US Food and Drug Administration expanded access protocol (*4*). Two of them, brincidofovir and tecovirimat (TPOXX or ST-246), have shown effectiveness against orthopoxvirus in animal models (*5*,*6*). Both medications have a safe side effect profile in humans (*7*,*8*). According to the Centers for Disease Control and Prevention (CDC), tecovirimat is the first choice and should be taken with fatty meals. For patients who experience clinically significant disease progression while receiving tecovirimat or who experience recrudescence, brincidofovir can be used as an adjunctive therapy. Another medication, cidofovir, can be used in cases of severe monkeypox virus infection, although it has a less favorable safety profile. Vaccinia immune globulin intravenous (VIG-IV) can also be used in severe illness and prophylactically in patients with T-cell deficiency who cannot receive live mpox vaccines (*4*).

We report a case of disseminated mpox treated with those novel drugs in a patient with untreated HIV who was admitted multiple times to different hospitals. Information regarding outside admissions was obtained from electronic medical records.

The Study

A 33-year-old man with untreated HIV infection sought care at an outside hospital for generalized rash, diarrhea, and odynophagia. His first skin lesion (day 0) appeared 4 days before the hospitalization, and his last sexual contact occurred with a male partner 10 days before hospitalization. He had 25–30 circular, raised lesions (vesicles, pustules, and scabs) measuring 1 × 1 cm distributed over his entire body. Some of the lesions had purulence around the circumference with a dark center. His CD4 count was 25 cells/mm^3 (reference range 500–1,500 cells/mm^3) and viral load 678,000 copies/mL (ideal range in HIV infection <20 copies/mL).

Results of blood cultures at admission were negative. Given the high clinical suspicion of mpox, superficial swab specimens were collected from skin lesions. The viral PCR result was positive for nonvariola orthopoxvirus DNA of mpox on day 6. He was treated with oral tecovirimat (600 mg 2×/d). On day 10, he was discharged with the remainder of the 14-day course and close outpatient follow-up.

Two days later, the patient was readmitted to a different outside hospital for worsening fever and painful skin lesions. He had widespread annular and pustular lesions on the face, scalp, trunk, and extremities. He could not tolerate oral tecovirimat and received further doses intravenously (days 18–23 after onset of lesions). Most of his lesions crusted during this treatment, and the fever subsided. The patient

Author affiliation: Sinai Hospital of Baltimore, Baltimore, Maryland, USA

DOI: https://doi.org/10.3201/eid2906.230059

[1]These first authors contributed equally to this article.

received a 17-day course of tecovirimat before leaving against medical advice on day 23. He was noted to be unaccepting of his HIV status and declined antiretroviral therapy (ART) during each hospital admission.

On day 44, he was readmitted to Sinai Hospital of Baltimore (Baltimore, Maryland, USA) for severe swelling in his right hand, lethargy, and fever, as well as widespread coalescing, painful, and necrotic lesions (>3 cm diameter). Several lesions were ulcerated and open, and he also had a few moist, small vesicular lesions (0.5 × 0.5 cm). CD4 count was 22 cells/mm^3, HIV viral load was 229,000 copies/mL, and leukocyte count was 11,700 cells/mm^3 (reference range 4,500–11,000 cells/μL). Ultrasonography of the right arm showed subcutaneous edema but no abscess. He declined ART throughout this hospitalization and initially deferred mpox medications. We empirically treated suspected bacterial superinfection with vancomycin and cefepime, which were later transitioned to linezolid and meropenem secondary to worsening leukocytosis and fevers.

By day 60, the patient's rash involved his left eye and arm. Orbital computed tomography showed soft tissue swelling in anterior globes but no intraorbital abnormalities. On day 65, the patient agreed to begin oral tecovirimat and adjunctive brincidofovir (2 doses given 1 week apart). Still, rash and left arm swelling worsened (Figure 1). On day 72, leukocyte count increased to ≈35,000 cells/μL with a neutrophilic predominance (89%; reference range 43%–70%); liver function tests remained unremarkable, and blood cultures remained negative. He received 1 dose of VIG-IV. The next day, severe respiratory distress developed, and we noted several lung nodules and a large left-sided pleural effusion on imaging (Figure 2). A chest tube was placed. On day 74, the patient died of cardiac arrest. The cause of death was determined to be severe monkeypox virus infection per discussion with CDC and the Maryland health department (Figure 3, https://wwwnc.cdc.gov/EID/article/29/6/23-0059-F3.htm).

Conclusions

This case demonstrated severe manifestations of mpox in the setting of untreated HIV with advanced immunodeficiency. The patient had worsening dissemination of skin lesions, presumed superinfection, periorbital swelling, and possible lung involvement. Historically, intratracheal monkeypox virus administration in Macaque monkeys caused rapidly progressive fatal pneumonia (*9*). The pulmonary nodules in this patient closely resemble those seen by Manta et al. (*10*) in a patient with pulmonary mpox. We lack pathologic evidence, but this patient's lung

Figure 1. Changes in skin lesions despite aggressive treatment with antiviral medications in patient with severe mpox and untreated HIV, Baltimore, Maryland, USA: A) left hand, B) face, C) trunk, and D) left arm and elbow. Images at left (top in panel B) taken on day 65, after 18 days of tecovirimat and 1 dose of brincidofovir. Images at right (bottom in panel B) taken on day 73, after 26 days of tecovirimat, 2 doses of brincidofovir, and 1 dose of vaccinia immune globulin intravenous.

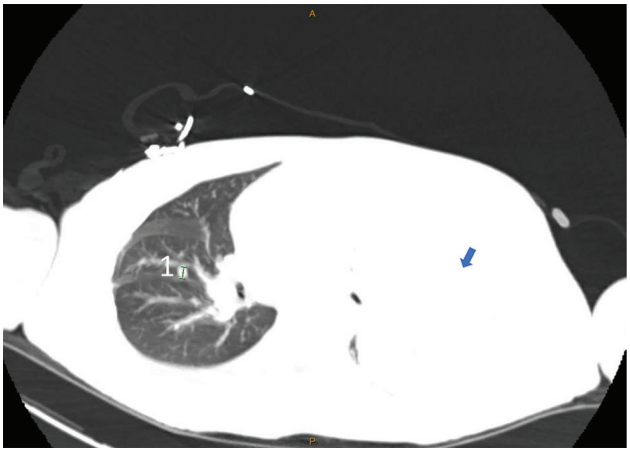

Figure 2. Computed tomography scan of lung showing right-sided pulmonary nodule (marked as 1) and large left pleural effusion (blue arrow) in patient with severe mpox and untreated HIV, Baltimore, Maryland, USA.

complications could be secondary to mpox. The role of early imaging and biopsy in identifying those lesions warrants further study.

The body of data regarding the interaction between untreated HIV and mpox is growing. Evidence suggests higher hospitalization rates, severe infections, and increased mortality rates in this subgroup. The current recommendation is to initiate ART at the time mpox is diagnosed (*11*). As seen in this case, treating mpox might not be effective without concurrent ART.

Treatment guidelines for mpox are still developing. An ongoing randomized clinical trial, Study of Tecovirimat for Human Monkeypox Virus, is intended to help determine the efficacy of oral tecovirimat (*12*). Although this patient completed more than the suggested 14-day course of tecovirimat, he intermittently declined several doses, hindering optimal treatment response. Whether the patient was taking tecovirimat with fatty meals at home, as was recommended, was unclear. Brincidofovir was well tolerated without evidence of liver toxicity. The role of initiating intravenous forms of these medications early warrants discussion. Prospective trials with the available agents in various combinations and treatment durations for managing mpox are needed.

Barriers to HIV treatment are still prevalent and include poverty, behavioral health disorders, and substance use disorders. Fear of living with HIV and lack of awareness regarding the benefits of ART also play a role; Dasgupta et al. (*13*) found that 91.5% of patients about whom clinicians sought CDC guidance were persons with HIV not taking ART. Of those, 68% were Black, as was the patient in this study. Only a few states publicly report racial disparities, which could lead to a disproportionate effects of mpox outbreaks, as was seen in the COVID-19 pandemic (*14*,*15*). The specific barriers in our case could not be elucidated.

This case adds to the limited clinical experience with these novel medications in treating mpox. We second CDC recommendations regarding the necessity of ART in patients with HIV and mpox. Barriers to HIV treatment can be detrimental to prognosis and must be preemptively identified and addressed. This case also raises the suspicion of possible pulmonary involvement, which could pave the way for further research into the spread of mpox and systemic involvement. In this case, mpox treatments deployed months into the course of illness, in the setting of untreated HIV, did not appear to alter disease progression to death.

About the Author

Dr. Filippov is a first-year resident at Sinai Hospital of Baltimore who graduated from First Moscow State University, Russia, with the honor of distinction. His primary research interest is infectious diseases, specifically HIV.

References

1. World Health Organization. WHO Director-General declares the ongoing monkeypox outbreak a Public Health Emergency of International Concern [cited 2022 Nov 24]. https://www.who.int/europe/news/item/23-07-2022-who-director-general-declares-the-ongoing-monkeypox-outbreak-a-public-health-event-of-international-concern
2. Mitjà O, Ogoina D, Titanji BK, Galvan C, Muyembe JJ, Marks M, et al. Monkeypox. Lancet. 2023;401:60–74.
3. Center=s for Disease Control and Prevention. Mpox: 2022 outbreak cases and data [cited 2022 Nov 24]. https://www.cdc.gov/poxvirus/monkeypox/response/2022/index.html
4. Centers for Disease Control and Prevention. Mpox: treatment information for healthcare professionals [cited 2022 Nov 24]. https://www.cdc.gov/poxvirus/monkeypox/clinicians/treatment.html
5. Sherwat A, Brooks JT, Birnkrant D, Kim P. Tecovirimat and the treatment of monkeypox—past, present, and future considerations. N Engl J Med. 2022;387:579–81. https://doi.org/10.1056/NEJMp2210125
6. Food and Drug Administration. FDA approves drug to treat smallpox [cited 2022 Nov 24]. https://www.fda.gov/drugs/news-events-human-drugs/fda-approves-drug-treat-smallpox
7. Alvarez-Cardona JJ, Whited LK, Chemaly RF. Brincidofovir: understanding its unique profile and potential role against adenovirus and other viral infections. Future Microbiol. 2020;15:389–400. https://doi.org/10.2217/fmb-2019-0288
8. Grosenbach DW, Honeychurch K, Rose EA, Chinsangaram J, Frimm A, Maiti B, et al. Oral tecovirimat for the treatment of smallpox. N Engl J Med. 2018;379:44–53. https://doi.org/10.1056/NEJMoa1705688
9. Goff AJ, Chapman J, Foster C, Wlazlowski C, Shamblin J, Lin K, et al. A novel respiratory model of infection with

monkeypox virus in cynomolgus macaques. J Virol. 2011;85:4898–909. https://doi.org/10.1128/JVI.02525-10
10. Manta R, Muteganya R, Gohimont N, Heymans B, Ene D. First [18F]-FDG-PET/CT images of a patient infected with monkeypox. Eur J Nucl Med Mol Imaging. 2023;50:966–7. https://doi.org/10.1007/s00259-022-06023-0
11. Centers for Disease Control and Prevention. Clinical considerations for treatment and prophylaxis of mpox infection in people who are immunocompromised [cited 2023 Feb 15]. https://www.cdc.gov/poxvirus/monkeypox/clinicians/people-with-HIV.html
12. ClinicalTrials.gov. Study of tecovirimat for human monkeypox virus (STOMP) [cited 2022 Nov 24]. https://clinicaltrials.gov/ct2/show/record/NCT05534984
13. Dasgupta S, Tie Y, Beer L, Fagan J, Weiser J. Barriers to HIV care by viral suppression status among US adults with HIV: findings from the Centers for Disease Control and Prevention Medical Monitoring Project. J Assoc Nurses AIDS Care. 2021;32:561–8. https://doi.org/10.1097/JNC.0000000000000249
14. Kuehn BM. Interim guidance for monkeypox among patients with HIV. JAMA. 2022;328:1173–4. https://doi.org/10.1001/jama.2022.14727
15. Miller MJ, Cash-Goldwasser S, Marx GE, Schrodt CA, Kimball A, Padgett K, et al.; CDC Severe Monkeypox Investigations Team. Severe monkeypox in hospitalized patients—United States, August 10–October 10, 2022. MMWR Morb Mortal Wkly Rep. 2022;71:1412–7. https://doi.org/10.15585/mmwr.mm7144e1

Address for correspondence: Sanchit Duhan, Internal Medicine, Sinai Hospital of Baltimore, 2401 W Belvedere Ave, Baltimore, MD, 21215, USA; email: s123anchit@gmail.com

Manifestations and Management of Trimethoprim/Sulfamethoxazole–Resistant *Nocardia otitidiscaviarum* Infection

Katherine Fu, Kyle White, Aliaksandr Ramaniuk, Vidya Kollu, Daniel Urbine

Author affiliations: University of Florida College of Medicine, Gainesville, Florida, USA

DOI: https://doi.org/10.3201/eid2906.221854

Nocardia can cause systemic infections with varying manifestations. Resistance patterns vary by species. We describe *N. otitidiscavarium* infection with pulmonary and cutaneous manifestations in a man in the United States. He received multidrug treatment that included trimethoprim/sulfamethoxazole but died. Our case highlights the need to treat with combination therapy until drug susceptibilities are known.

Nocardia otitidiscaviarium was first described in 1924 after being isolated from a guinea pig with ear disease (*1*). *N. otitidiscaviarium* infections account for ≈5.9% of all *Nocardia* infections (*2*,*3*). *Nocardia* can cause systemic infections with varying clinical signs. Predisposing factors are chronic lung disease, corticosteroid use, HIV infection, solid organ transplant, and solid organ malignancy (*4*). Patterns of resistance to antimicrobial therapies vary widely among *Nocardia* species. We present a case of a man with pulmonary and cutaneous manifestations of a trimethoprim/sulfamethoxazole (TMP/SMX)–resistant *N. otitidiscaviarum* infection.

The patent was a 73-year-old man in Gainesville, Florida, USA, who had severe chronic obstructive pulmonary disease, coronary artery disease, and congestive heart failure. In June 2020, he sought care for fever, productive cough, dyspnea on exertion, and a 30-pound weight loss over 4 months. Six months earlier, he had undergone computed tomography (CT) of the chest because of his smoking history and concern for unintentional weight loss. Scans revealed a 3.4-cm spiculated, cavitary, right upper lobe mass with associated precarinal and right hilar adenopathy. Subsequent positron emission tomography/CT showed a hypermetabolic wedge-shaped subpleural area of consolidation (5.0 × 4.1 cm) in the right upper lobe, consistent with pneumonia. Antimicrobial drugs were administered. Follow-up CT chest 3 months later showed progressive disease bilaterally in the upper lobes (Figure, panel A). The patient was then hospitalized and underwent bronchoscopy with bronchoalveolar lavage (BAL). We sent cultures for bacterial, including mycobacterial, and fungal testing. Pending results of the BAL gram stain and cultures, we empirically prescribed broad-spectrum antimicrobial drugs (i.e., vancomycin, cefepime, and metronidazole) for pneumonia, and the patient was discharged after clinical improvement. The BAL sample showed gram-positive branching rods (Figure, panel B), and *N. otitidiscaviarum* grew on culture. The patient was readmitted to the hospital.

At readmission, examination was remarkable for distant heart and lung sounds and a prolonged expiratory phase. The patient had no noticeable skin lesions at that time. CT of the head with contrast (implantable cardioverter device was not compatible

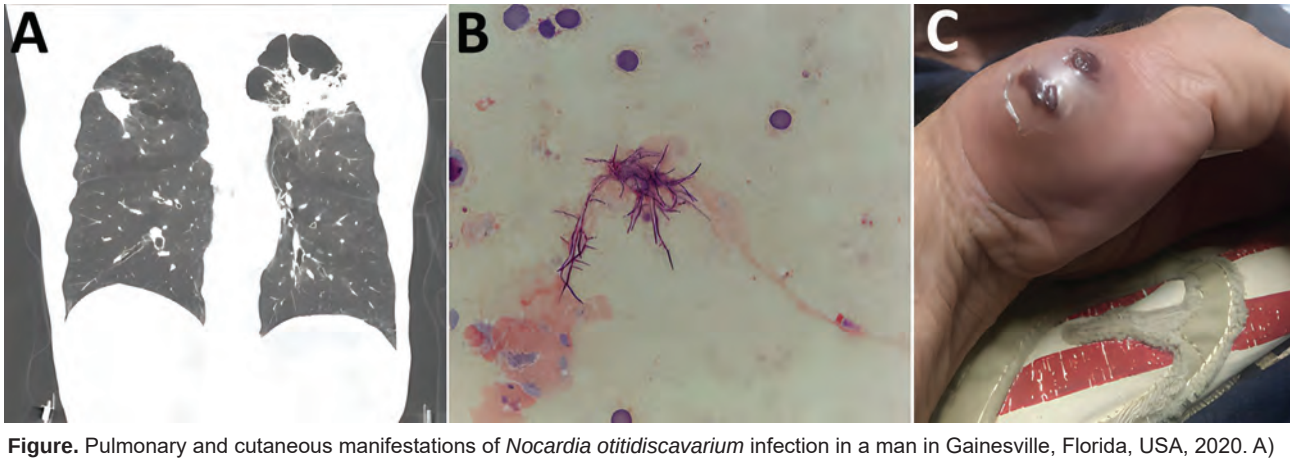

Figure. Pulmonary and cutaneous manifestations of *Nocardia otitidiscavarium* infection in a man in Gainesville, Florida, USA, 2020. A) Computed tomography of the chest showing progressive disease in the upper lobes. B) Bronchoalveolar lavage sample (Gram stain) showing gram-positive branching rods. C) Cutaneous abscess on the ulnar aspect of the right hand.

Table. Sensitivity results for *Nocardia otitidiscaviarum* isolated from a man in Gainesville, Florida, USA, 2020

Drug	Sensitivity
Amikacin	Sensitive
Amoxicillin/clavulanate	Resistant
Cefepime	Resistant
Ceftriaxone	Resistant
Ciprofloxacin	Intermediate
Clarithromycin	Sensitive
Doxycycline	Resistant
Imipenem	Intermediate
Linezolid	Sensitive
Minocycline	Intermediate
Moxifloxacin	Sensitive
Tobramycin	Intermediate
Trimethoprim/sulfamethoxazole	Resistant

with magnetic resonance imaging) revealed no focal enhancing lesions. We empirically started intravenous TMP/SMX, intravenous amikacin, and oral levofloxacin. At the same time, the patient discovered a rapidly enlarging skin lesion along the ulnar aspect of the right hand (Figure, panel C). We incised and drained the 2.5-cm abscess, and *N. otitidiscaviarum* grew in cultures with broth microdilution. On the basis of sensitivity results (Table), we discontinued TMP/SMX and levofloxacin and added linezolid and clarithromycin; amikacin remained unchanged. Unfortunately, acute renal injury developed, and a new, prolonged QTc interval was seen on electrocardiogram. Those findings were attributed to either amikacin or clarithromycin, which prompted discontinuation of the aminoglycoside and macrolide. Repeat CT of the chest at week 6 of treatment showed disease progression. The patient subsequently decided to pursue palliative care and subsequently died.

Clinical manifestations of *N. otitidiscaviarum* infection may include pneumonia, brain abscess, lung abscess, skin abscess, muscle abscess, ocular infections, bacteremia, osteomyelitis, and septic joints (*4*). The risk factor for this patient was chronic obstructive pulmonary disease. The patient had pulmonary involvement and a rapidly developing skin abscess.

Antimicrobial drug resistance of *N. otitidiscaviarum* is variable. The organism is usually sensitive to linezolid, amikacin, TMP/SMX, doxycycline, gentamicin, and minocycline. Susceptibility to carbapenems is limited; most activity is from imipenem compared with meropenem or ertapenem. *N. otitidiscaviarum* is generally resistant to amoxicillin/clavulanic acid, cefotaxime, ceftriaxone, ciprofloxacin, moxifloxacin, tobramycin, and clarithromycin (*3*–*5*).

This case demonstrates the value of considering *Nocardia* infection for patients with cavitary lung disease and concomitant soft tissue abscesses. It also highlights the need to choose appropriate initial antimicrobial therapy. In the absence of a drug susceptibility profile, clinicians should approach the selection of antibiotics with a framework that considers disease severity, the epidemiologic probability of particular species, and the most likely resistance profiles of the species. Treatment can be narrowed after the species and susceptibilities are known.

About the Author

Dr. Fu is an internal medicine resident at the University of Florida, pursuing a fellowship in pulmonology and critical care. Her research interests include global health, clinical education, pulmonary diseases, critical care, and pulmonary hypertension.

References

1. Brown-Elliott BA, Brown JM, Conville PS, Wallace RJ Jr. Clinical and laboratory features of the *Nocardia* spp. based on current molecular taxonomy. Clin Microbiol Rev. 2006;19:259–82. https://doi.org/10.1128/CMR.19.2.259-282.2006
2. Tan C-K, Lai C-C, Lin S-H, Liao CH, Chou CH, Hsu HL, et al. Clinical and microbiological characteristics of nocardiosis including those caused by emerging *Nocardia* species in Taiwan, 1998–2008. Clin Microbiol Infect. 2010;16:966–72. https://doi.org/10.1111/j.1469-0691.2009.02950.x
3. Wang H, Zhu Y, Cui Q, Wu W, Li G, Chen D, et al. Epidemiology and antimicrobial resistance profiles of the *Nocardia* species in China, 2009–2021. Microbiol Spectr. 2022;10:e01560-21. https://doi.org/10.1128/spectrum.01560-21
4. Brown-Elliot BA, Ward SC, Crist CJ, Mann LB, Wilson RW, Wallace RJ Jr. In vitro activities of linezolid against multiple *Nocardia* species. Antimicrob Agents Chemother. 2001;45:1295–7.
5. Brown-Elliott BA, Killingley J, Vasireddy S, Bridge L, Wallace RJ Jr. In vitro comparison of ertapenem, meropenem, and imipenem against isolates of rapidly growing mycobacteria and *Nocardia* by use of broth microdilution and Etest. J Clin Microbiol. 2016;54:1586–92. https://doi.org/10.1128/JCM.00298-16

Address for correspondence: Katherine Fu, Department of Medicine, University of Florida College of Medicine, 1600 SW Archer Rd, Gainesville, FL 32610, USA; email: Katherine.Fu@medicine.ufl.edu

Limited Cutaneous Leishmaniasis as Ulcerated Verrucous Plaque on Leg, Tucson, Arizona, USA[1]

Caitlyn B. Dagenet, Mitchell S. Davis, Sean Murphy, Rebecca Thiede, Keliegh S. Culpepper, Mohammad Fazel

Author affiliations: University of Arizona College of Medicine, Tucson, Arizona, USA (C.B. Dagenet, R. Thiede, M. Fazel); University of California, San Francisco, California, USA (M.S. Davis); Tucson ER and Hospital, Tucson (S. Murphy); DermPath Diagnostics, Tucson (K.S. Culpepper)

DOI: https://doi.org/10.3201/eid2906.230125

We report a 34-year-old man who had a nonhealing, verrucous plaque with central ulceration on the lower leg. This case-patient is a rare example of endemic limited cutaneous leishmaniasis in Tucson, Arizona, USA. Clinicians should be aware of this disease because its manifestations can vary for individual patients.

Cutaneous leishmaniasis (CL) is the most common form of leishmaniasis and typically manifests as solitary painless lesions at the site of sand fly bites. This disease is generally acquired in specific habitat environments conducive to its sand fly vector and reservoir hosts (*1*). Most cases of CL diagnosed in the United States are attributed to persons who travel (e.g., military, international workers) to disease-endemic countries (e.g., India, Nepal, Brazil, Sudan, and Bangladesh) (*1*,*2*)

Although the United States was classified as endemic for leishmaniasis by the World Health Organization in 2020, the state of Arizona has had few documented cases (*1*–*4*). A Medline search of authors showed only 3 cases of CL have been reported in Arizona (*1*,*2*,*4*). Of those case-patients, only 1 truly autochthonous case-patient did not report recent travel to a disease-endemic location (*1*,*2*,*4*). Despite the rarity of human CL cases, sand fly vectors (e.g., *Lutzomyia anthophora*) and hosts (e.g., *Neotoma albigula* [white-throated woodrat]) can transmit New World *Leishmania* spp. and have been documented in Arizona (*5*,*6*). We report a 34-year-old man who had a nonhealing, verrucous plaque with central ulceration on the lower leg.

Consent for publication of all patient photographs and medical information was provided by the authors at the time of article submission. The patient gave consent for their photographs and medical information to be published in print and online and with the understanding that this information mighty be publicly available.

The patient had no major medical history and no history of skin cancer or immunosuppression. He came to the dermatology clinic in Tucson, Arizona, because of a new onset of a painless lesion on the right lateral lower leg. The lesion was present for 6 weeks before the visit. Physical examination demonstrated a 2.1 × 1.1 cm solitary, nonhealing, verrucous plaque with central ulceration on the right proximal lateral pretibial region (Figure). The patient reported considerable time outdoors and recreational activities, such as mountain biking and hiking. Those activities occurred in Arizona; he specifically denied a history of recent travel outside of the United States. He also denied any trauma to the site of infection.

Shave biopsy and subsequent staining with hematoxylin and eosin showed focal ulceration with mixed acute, chronic, and granulomatous inflammatory infiltrate and minute organisms in the cytoplasm of histocytes favoring parasitized histiocytic infection. The organisms were negative by staining with periodic acid–Schiff. Microscopic examination was then completed by the Centers for Disease Control and Prevention, and small intracellular organisms compatible with protozoal amastigotes were observed within macrophages. Immunohistochemical analysis subsequently confirmed a diagnosis of leishmaniasis. The patient was referred to an infectious disease department, where observation was recommended because he had a solitary cutaneous lesion that was removed in entirety by biopsy. He also had no mucosal involvement.

In this case, the new-onset ulcerated plaque was initially most concerning for infectious versus neoplastic etiology. Although an infectious process was considered, CL was not on the original differential diagnosis given the rarity of this diagnosis in Arizona. This case helps demonstrate that leishmaniasis must be a consideration when patients in Arizona have verrucous papules or plaques.

Most autochthonous cases of CL in the Unites States have been in Texas (*6*). In 2018, a study in Texas identified 69 novel cases of leishmaniasis and 22 having documented speciation (all *L. mexicanca*) (*4*). CL is probably underreported because reporting is not required in most states, and a high rate of misdiagnosis can be presumed (*4*,*6*). Sand flies capable of transmitting *L. mexicana* have been reported in several states (*7*).

CL treatment decreases the risk for mucosal dissemination, accelerates healing of the lesion, decreases the risk for relapse, and decreases illness. Relapse

[1]This study was presented at the Pacific Dermatology Conference, Scottsdale, Arizona, USA, May 7, 2022.

Figure. Limited cutaneous leishmaniasis as ulcerated verrucous plaque on leg of patient in Tucson, Arizona, USA. A solitary, nonhealing plaque with central ulceration is shown on the right proximal lateral pretibial region.

of cutaneous disease (leishmaniasis recidivans) can occur several years after resolution of the primary lesion in treated and untreated patients (*9*). Treatment options for CL include systemic miltefosine (for *Leishmania* [*Viannia*] spp.), ketoconazole (for *L. mexicana*), and fluconazole or local therapy (antimonial drugs, topical paromomycin, or liquid nitrogen therapy) (*9*).

Treatment of leishmaniasis is determined by species, risk for mucosal dissemination, size, number, and location of lesion(s). Limited CL does not require further treatment if the findings self-resolve. CL can spontaneously resolve within 2 months to a year. CL that has ≥5 lesions; an area >5 cm; is on the face, toes, fingers, or genitalia; or has a duration >6 months might require treatment to prevent relapse or progression to mucosal disease (*2*). Other complications of CL include secondary infections and scarring (*8*).

CL treatment decreases the risk for mucosal dissemination, accelerates healing of the lesion, decreases the risk for relapse, and decreases illness. Relapse of cutaneous disease (leishmaniasis recidivans) can occur several years after resolution of the primary lesion in treated and untreated patients (*9*). Treatment options for CL include systemic miltefosine (for *Leishmania* [*Viannia*] spp.), ketoconazole (for *L. mexicana*), and fluconazole or local therapy (antimonial drugs, topical paromomycin, or liquid nitrogen therapy) (*9*).

In conclusion, CL is an increasing concern in the United States where endemic cases have been identified, most prominently the southern and southwestern regions. Our case adds to the short but increasing list of documented CL cases in Arizona. Placing CL in the differential diagnosis for new-onset verrucous plaques of unknown etiology in local disease-endemic areas of the United States is prudent. Limited CL can be managed conservatively with monitoring for recurrence once the solitary lesion has been removed, but further treatment might be necessary depending on the manifestations in an individual patient.

This study was supported by the Department of Medicine, Division of Dermatology, University of Arizona.

About the Author

Ms. Dagenet is a medical student at the University of Arizona College of Medicine in Tucson, AZ. Her primary research interests are cutaneous manifestations of disease and inflammatory dermatoses.

References

1. Asbury K, Seville MT, Pritt B, Scotch A, Rosenthal A, Grys TE, et al. The brief case: the unexpected souvenir. J Clin Microbiol. 2018;56:e01387–17. https://doi.org/10.1128/JCM.01387-17
2. Levine N. Cutaneous leishmaniasis treated with controlled localized heating. Arch Dermatol. 1992;128:759–61. https://doi.org/10.1001/archderm.1992.01680160041003
3. McIlwee BE, Weis SE, Hosler GA. Incidence of endemic human cutaneous leishmaniasis in the United States. JAMA Dermatol. 2018;154:1032–9. https://doi.org/10.1001/jamadermatol.2018.2133
4. de Almeida M, Zheng Y, Nascimento FS, Bishop H, Cama VA, Batra D, et al. Cutaneous leishmaniasis caused by an unknown *Leishmania* strain, Arizona, USA. Emerg Infect Dis. 2021;27:1714–7. https://doi.org/10.3201/eid2706.204198
5. Kerr SF, McHugh CP, Merkelz R. Short report: a focus of *Leishmania mexicana* near Tucson, Arizona. Am J Trop Med Hyg. 1999;61:378–9. https://doi.org/10.4269/ajtmh.1999.61.378
6. Clarke CF, Bradley KK, Wright JH, Glowicz J. Case report: emergence of autochthonous cutaneous leishmaniasis in northeastern Texas and southeastern Oklahoma. Am J Trop Med Hyg. 2013;88:157–61. https://doi.org/10.4269/ajtmh.2012.11-0717
7. Curtin JM, Aronson NE. Leishmaniasis in the United States: emerging issues in a region of low endemicity. Microorganisms. 2021;9:578. https://doi.org/10.3390/microorganisms9030578
8. Aronson N, Herwaldt BL, Libman M, Pearson R, Lopez-Velez R, Weina P, et al. Diagnosis and treatment of leishmaniasis: clinical practice guidelines by the Infectious Diseases Society of America (IDSA) and the American Society of Tropical Medicine and Hygiene (ASTMH). Clin Infect Dis. 2016;63:1539–57. https://doi.org/10.1093/cid/ciw742
9. McGwire BS, Satoskar AR. Leishmaniasis: clinical syndromes and treatment. QJM. 2014;107:7–14. https://doi.org/10.1093/qjmed/hct116

Address for correspondence: Mohammad Fazel, Division of Dermatology, University of Arizona College of Medicine, 7165 N Pima Canyon Dr, Tucson, AZ 85718, USA; email: morox5@arizona.edu

Genomic Surveillance of Monkeypox Virus, Minas Gerais, Brazil, 2022

Natália R. Guimarães,[1] Luiz Marcelo R. Tomé,[1] Ludmila O. Lamounier,[1] Marcos Vinícius F. Silva,[1] Maurício T. Lima, Alana Vitor B. da Costa, Kelly Cristina M. Luiz, Ronaldo de Jesus, Giliane de S. Trindade, Danilo B. Oliveira, Flávio G. da Fonseca, Ana Paula S.M. Fernandes, Jaqueline S. de Oliveira, Josiane B.P. Moura, Erna G. Kroon, Marta Giovanetti, Vagner Fonseca, Luiz Alcantara, Talita Emile R. Adelino, Felipe C. de Melo Iani

Author affiliations: Ezequiel Dias Foundation, Belo Horizonte, Brazil (N.R. Guimarães, L.M.R. Tomé, L.O. Lamounier, M.V.F. Silva, M.T. Lima, A.V.B. da Costa, K.C.M. Luiz, J.B.P. Moura, T.E.R. Adelino, F.C. de Melo Iani); Federal University of Minas Gerais, Belo Horizonte (L.M.R. Tomé, G.d.S. Trindade, F.G. da Fonseca, A.P.S.M. Fernandes, E.G. Kroon); Brazilian Ministry of Health, Distrito Federal, Brazil (R. de Jesus); Federal University of Vales do Jequitinhonha e Mucuri, Diamantina, Brazil (D.B. Oliveira); State Secretary of Health of Minas Gerais, Belo Horizonte (J.S. de Oliveira); University of Campus Bio-Medico, Rome, Italy (M. Giovanetti); Instituto Rene Rachou, Fundação Oswaldo Cruz, Belo Horizonte (M. Giovanetti, L. Alcantara); Pan American Health Organization, Distrito Federal, Brazil (V. Fonseca)

DOI: https://doi.org/10.3201/eid2906.230113

Phylogenetic analysis of 34 monkeypox virus genome sequences isolated from patients in Minas Gerais, Brazil, revealed initial importation events in early June 2022, then community transmission within the state. All generated genomes belonged to the B.1 lineage responsible for a global mpox outbreak. These findings can inform public health measures.

Human mpox (formerly monkeypox) is an emerging zoonotic disease caused by monkeypox virus (MPXV) (*1*,*2*). Since the 1970s, mpox outbreaks in humans have occurred sporadically, mainly in Africa (*3*). In early May 2022, mpox emerged worldwide, and case numbers increased substantially (*4*). On July 23, 2022, the World Health Organization (WHO) declared the mpox outbreak a Public Health Emergency of International Concern (*5*).

Genomic surveillance might be considered a fundamental approach to tracking circulating strains and investigating viral spread (*6*–*8*). By October 2022, Brazil had reported 12,378 mpox cases, and the state of Minas Gerais, located in southeast Brazil, reported a total of 838 cases through epidemiologic week 41 (*9*).

We selected 34 human MPXV-positive samples collected in Minas Gerais during June–September 2022 for whole-genome sequencing at the Central Laboratory of Public Health of Minas Gerais. The selected samples had cycle threshold values ≤30 and available epidemiologic patient data. The study was approved by the research ethics committee of the Ezequiel Dias Foundation (approval no. 62702222.6.0000.9507).

We extracted viral DNA from lesion exudate and sequenced with the Ion Torrent PGM platform (Thermo Fisher Scientific, https://www.thermofisher.com) using a set of MPXV-specific primers designed for this study by using the primalscheme platform version 1.3.2 (https://pypi.org/project/primalscheme) (Appendix Table 1, htts://wwwnc.cdc.gov/EID/article/29/6/22-0113-App1.pdf). We used the MPXV reference genome (GenBank accession no. NC_063383.1) to perform genome assembly by using Burrows-Wheeler Aligner version 0.7.17 (https://github.com/lh3/bwa), SAMtools version 1.11 (https://github.com/samtools), and iVar version 1.0 (https://github.com/andersen-lab/ivar). We used Nextclade version 2.8.1 (Nextstrain, https://clades.nextstrain.org) to assess genome quality and classification.

We used MAFFT version 7.310 (https://mafft.cbrc.jp) to align the 34 genomes obtained from this study with an additional 218 MPXV genomes collected from GISAID (https://www.gisaid.org) until October 3, 2022 (Appendix Table 2). We used BEAST version 1.10.4 (https://beast.community) to infer the Bayesian phylogeny. The Brazilian Ministry of Health Notifiable Diseases Information System provided weekly notified cases of MPXV infection in Minas Gerais.

Epidemiologic data revealed that the highest number (n = 112) of MPXV cases in Minas Gerais were reported during epidemiologic week 31 (Appendix Figure 1). The data also highlight that the metropolitan region of Belo Horizonte had the highest concentration (n = 608) of confirmed cases during June–September (Appendix Figure 2).

Using patients' clinical records, we found that 55.9% (19/34) were HIV-positive and 23.5% (8/34) reported active sexually transmitted infection. Among the screened samples, 33 were from male patients and 1 was from a female patient; patients were 22–46 (mean 32.5)

[1]These authors contributed equally to this article.

years of age. The most frequent signs and symptoms were rash (34/34, 100%), lymphadenopathy (22/34, 64.7%), and fever (21/34, 61.8%) (Appendix Figure 3). Among mpox patients, 17 reported no travel history, 15 reported travel history to the state of São Paulo, Brazil, and 1 each reported travel to London and to Portugal.

Using the Ion Torrent PGM platform, we obtained a total number of 34 MPXV genome sequences. Genome coverage was 76.2%–97.5% (mean 87%) and had an average depth of 391 × (Table). All the genomes generated in this study belonged to lineages B.1 (n = 13), B.1.1 (n = 19), B.1.2 (n = 1), and B.1.9 (n = 1), which are lineages responsible for the 2022 outbreak (*7*,*8*).

Our phylogenetic reconstruction revealed that all genomes from the 2022 mpox outbreak grouped together (Figure). Most of the genomes we obtained from Minas Gerais grouped with MPXV genomes isolated from other regions of Brazil (Figure). Our phylogenetic reconstruction revealed that the first mpox case reported in Minas Gerais, isolated from a patient with a travel history to London, UK (GISAID accession no. EPI_ISL_13780332), grouped with a genome sequence from the United Kingdom (GISAID accession no. EPI_ISL_14439774).

We also sequenced a sample from the first confirmed mpox death in Brazil, which was reported in late July 2022. That sample was collected from

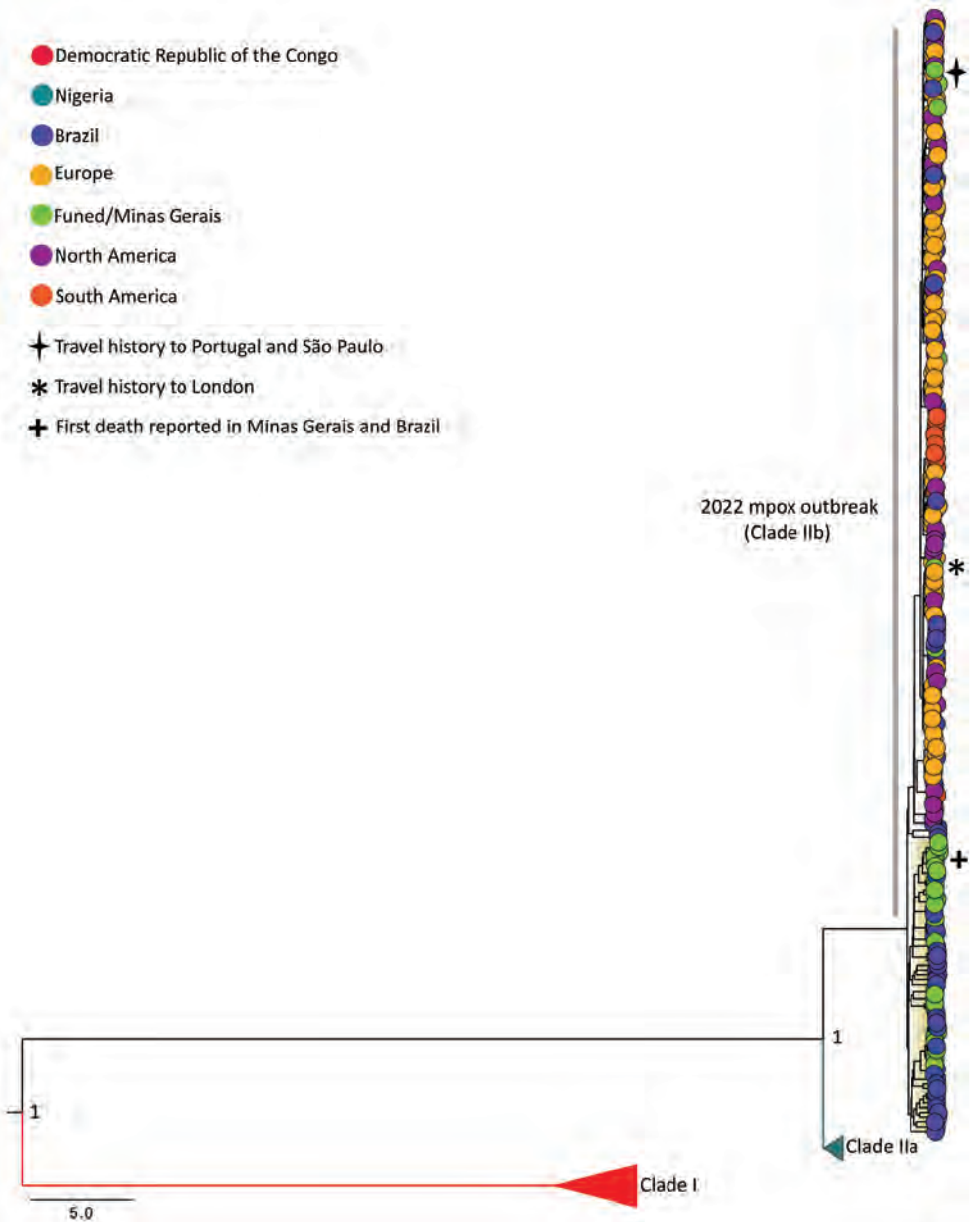

Figure. Bayesian phylogenetic tree of 34 genome sequences generated during genomic surveillance of monkeypox virus, Minas Gerais, Brazil, 2022. The tree also includes 218 reference strains available at GISAID (https://www.gisaid.org), accessed October 3, 2022. Colors represent different sampling locations. Posterior probability support is shown at key nodes for clade I, IIa, and IIb. Scale bar indicates nucleotide substitutions per site.

Table. Summary statistics of assembled genomes from genomic surveillance of monkeypox virus, Minas Gerais, Brazil, 2022*

Sample ID	Collection date	Mapped reads	Mean read depth	Coverage, %	Lineage	GISAID ID
311257928†	2022 Jun 28	241,791	208.5	90.3	B.1	EPI_ISL_13780332
311261010	2022 Jul 1	520,016	473.6	86.5	B.1.1	EPI_ISL_16650224
311261273	2022 Jul 1	478,258	447.8	90.7	B.1	EPI_ISL_16650225
311261816	2022 Jul 4	318,530	244.3	84.9	B.1	EPI_ISL_16650230
311261841	2022 Jul 4	388,417	347.0	93.5	B.1	EPI_ISL_16650229
311262116‡	2022 Jul 4	334,589	234.4	83.3	B.1	EPI_ISL_16650231
311262133	2022 Jul 4	362,965	331.9	85.3	B.1.1	EPI_ISL_16650228
311262224	2022 Jul 4	449,397	420.0	91.4	B.1	EPI_ISL_16650226
311262265	2022 Jul 4	427,206	399.6	93.6	B.1.1	EPI_ISL_16650227
311262687	2022 Jul 5	353,768	282.2	76.2	B.1.1	EPI_ISL_16650233
311262723	2022 Jul 5	342,256	266.3	81.8	B.1	EPI_ISL_16650234
311263370	2022 Jul 5	388,951	308.5	80.5	B.1.1	EPI_ISL_16650232
311265338	2022 Jul 5	344,341	299.7	82.5	B.1.1	EPI_ISL_16650238
311263885	2022 Jul 6	296,827	256.8	78.4	B.1	EPI_ISL_16650236
311263902	2022 Jul 6	394,450	332.8	79.2	B.1.1	EPI_ISL_16650235
311264859	2022 Jul 7	393,675	342.8	81.0	B.1.1	EPI_ISL_16650237
311266133	2022 Jul 8	345,305	290.7	79.1	B.1.1	EPI_ISL_16650239
311266186	2022 Jul 8	354,920	274.4	87.8	B.1	EPI_ISL_16650240
311266233	2022 Jul 8	284,916	239.2	82.9	B.1.1	EPI_ISL_16650241
311266796	2022 Jul 11	384,836	358.5	82.2	B.1.9	EPI_ISL_16650243
311267285	2022 Jul 11	351,311	325.0	79.4	B.1.1	EPI_ISL_16650242
311267311	2022 Jul 11	341,773	320.4	81.0	B.1.1	EPI_ISL_16650244
311267938	2022 Jul 12	330,526	300.1	77.1	B.1.1	EPI_ISL_16650245
311271087§	2022 Jul 15	581,432	594.2	97.5	B.1.1	EPI_ISL_16650246
311283035	2022 Aug 5	590,550	584.0	96.3	B.1	EPI_ISL_16650248
311287351	2022 Aug 12	565,565	557.1	96.5	B.1.1	EPI_ISL_16650247
311288391	2022 Aug 15	533,148	528.6	97.1	B.1.1	EPI_ISL_16650249
311291580	2022 Aug 22	520,820	554.3	91.7	B.1	EPI_ISL_16650262
311294876	2022 Aug 26	567,700	528.8	97.0	B.1	EPI_ISL_16650251
311297067	2022 Aug 31	539,498	454.0	94.7	B.1.2	EPI_ISL_16650253
311300630	2022 Sep 8	532,582	549.0	88.9	B.1.1	EPI_ISL_16650258
311300699	2022 Sep 8	476,181	514.3	82.5	B.1	EPI_ISL_16650255
311303564	2022 Sep 13	533,191	563.8	95.9	B.1.1	EPI_ISL_16650260
311309205	2022 Sep 26	546,501	564.2	92.9	B.1.1	EPI_ISL_16650265

*Genome assembly performed by using Burrows-Wheeler Aligner version 0.7.17 (https://github.com/lh3/bwa) and iVar version 1.0 (https://github.com/andersen-lab/ivar) pipeline and lineage ID was assigned to each genome by using Nextclade version 2.8.1 (Nextstrain, https://clades.nextstrain.org). GISAID, https://www.gisaid.org. ID, identification.
†First confirmed mpox case in Minas Gerais; patient had travel history to London, UK.
‡Patient had travel history to Portugal and São Paulo, Brazil.
§First mpox death reported in Minas Gerais.

a patient who resided in Minas Gerais and was in treatment for diffuse large B-cell lymphoma and HIV (*10*). The genome from that patient's sample belonged to the B.1.1 lineage, and in our phylogenetic reconstruction, it clustered with genome sequences isolated from Minas Gerais and from other states in Brazil.

Overall, our data revealed that an mpox case detected in Minas Gerais in early 2022 was related to a likely importation event, probably associated with a traveler returning from the United Kingdom, and then sustained MPXV community transmission. The first confirmed death reported in Minas Gerais was associated with a local MPXV infection described in a patient who reported several underlying conditions. These results contribute to genomic MPXV surveillance in Minas Gerais and increase the number of genome sequences from this virus available in GISAID. These findings and the available data can help future studies aiming to improve diagnostic protocols and vaccine development.

Acknowledgments

We thank all authors who have kindly deposited and shared genome data on GISAID (Appendix Table 2).

This study was financed by the Central Public Health Laboratory of Minas Gerais (Ezequiel Dias Foundation), the Brazilian Ministry of Health (grant no. SCON2021-00180), Pan American Health Organization PAHO/WHO and the National Institutes of Health (grant no. U01 AI151698) for the United World Arbovirus Research Network (UWARN). M.G. is funded by PON Ricerca e Innovazione (Research and Innovation) 2014-2020. Laboratório de Vírus and CT-Vacinas received funding from the Ministry of Science, Technology and Innovation, Brazil. G.d.S.T. is a researcher with the National Council for Scientific and Technological Development (CNPq), Brazil.

About the Author

Dr. Guimarães is a research scientist and analyst at the Ezequiel Dias Foundation. Her research interests and work include the molecular diagnosis and sequencing of SARS-CoV-2, monkeypox virus, and arboviruses, including dengue, Zika, chikungunya, and yellow fever viruses, and other pathogens of importance to public health.

References

1. McCollum AM, Damon IK. Human monkeypox. Clin Infect Dis. 2014;58:260–7. https://doi.org/10.1093/cid/cit703
2. Essbauer S, Pfeffer M, Meyer H. Zoonotic poxviruses. Vet Microbiol. 2010;140:229–36. https://doi.org/10.1016/j.vetmic.2009.08.026
3. Mauldin MR, McCollum AM, Nakazawa YJ, Mandra A, Whitehouse ER, Davidson W, et al. Exportation of monkeypox virus from the African continent. J Infect Dis. 2022;225:1367–76. https://doi.org/10.1093/infdis/jiaa559
4. Minhaj FS, Ogale YP, Whitehill F, Schultz J, Foote M, Davidson W, et al.; Monkeypox Response Team 2022. Monkeypox outbreak—nine states, May 2022. MMWR Morb Mortal Wkly Rep. 2022;71:764–9. https://doi.org/10.15585/mmwr.mm7123e1
5. Pan American Health Organization (PAHO). Mpox [cited 2023 Mar 10]. https://www.paho.org/en/monkeypox
6. World Health Organization (WHO). Global genomic surveillance strategy for pathogens with pandemic and epidemic potential, 2022–2032 [cited 2023 Mar 2]. https://www.who.int/publications/i/item/9789240046979
7. Isidro J, Borges V, Pinto M, Sobral D, Santos JD, Nunes A, et al. Phylogenomic characterization and signs of microevolution in the 2022 multi-country outbreak of monkeypox virus. Nat Med. 2022;28:1569–72. https://doi.org/10.1038/s41591-022-01907-y
8. Roychoudhury P, Sereewit J, Xie H, Nunley E, Bakhash SM, Lieberman NAP, et al. Genomic analysis of early monkeypox virus outbreak strains, Washington, USA. Emerg Infect Dis. 2023;29:644–6. https://doi.org/10.3201/eid2903.221446
9. Ministry of Health. Notifiable Diseases Information System—SINAN [in Portuguese] [cited 2023 Mar 10]. http://portalsinan.saude.gov.br
10. Menezes YR, Miranda AB. Severe disseminated clinical presentation of monkeypox virus infection in an immunosuppressed patient: first death report in Brazil. Rev Soc Bras Med Trop. 2022;55:e0392-2022. https://doi.org/10.1590/0037-8682-0392-2022

Address for correspondence: Felipe Campos de Melo Iani, Ezequiel Dias Foundation, Rua Conde Pereira Carneiro, 80—Gameleira, Belo Horizonte 30510-010, Brazil; email: felipe.iani@funed.mg.gov.br

Antimicrobial-Resistant Infections after Turkey/Syria Earthquakes, 2023

Anthony Rizk, Antoine Abou Fayad, Louis-Patrick Haraoui

Author affiliations: Geneva Graduate Institute, Geneva, Switzerland (A. Rizk); American University of Beirut, Beirut, Lebanon (A. Abou Fayad); Université de Sherbrooke, Sherbrooke, Québec, Canada (L.-P. Haraoui)

DOI: https://doi.org/10.3201/eid2906.230316

Increased rates of multidrug-resistant microbes have been reported after earthquakes. After the 2023 earthquakes in Turkey and Syria, the number of associated highly drug-resistant pathogens and nosocomial transmission will probably surge in hospitals treating injured patients. It is not too late to act to prevent antimicrobial-resistant infections from compounding these tragedies.

The 2023 earthquakes that affected Turkey and Syria, with Kahramanmaraş Province in Turkey at their epicenter, measured 7.8 and 7.5 on the Richter scale. The effects were devastating, making these the strongest earthquakes in Turkey since 1939. Combined with their multiple aftershocks, the earthquakes caused >50,000 deaths and severely damaged or collapsed >170,000 buildings (https://www.aljazeera.com/news/2023/2/25/death-toll-climbs-above-50000-after-turkey-syria-earthquakes). In their wake, the earthquakes left a growing humanitarian crisis. If previous experiences are any indication, we can also expect hospitals caring for the injured and wounded to struggle with highly antimicrobial-resistant infections, many of which will lead to excess illnesses and deaths.

Multidrug resistant microbes have often been reported after earthquakes and other natural disasters. Medical literature on earthquake-associated injuries, going as far back as the Marmara, Turkey, earthquake of 1999 (*1*), have consistently shown highly resistant microbial strains emerging in hospital settings and causing hospital-acquired infections in trauma patients. Antimicrobial-resistant *Acinetobacter baumannii* has been identified in disproportionately high rates from infections associated with large-scale earthquakes in Southeast Asia in 2004; northern Pakistan in 2005; Wenchuan, China, in 2008; central Italy in 2009; and Haiti in 2010 (Appendix, https://wwwnc.cdc.gov/EID/article/29/6/23-0316-App1.pdf).

Although earthquake-associated pathogens detected in hospital settings have been consistently multidrug resistant, their resistance profiles have varied. The etiology of antimicrobial resistance from earthquakes remains uncertain. After the Marmara earthquake of 1999, associated *A. baumannii* and *Pseudomonas aeruginosa* infections were mainly resistant to carbapenems, which had been preemptively administered in large numbers to patients before hospitalization (*1*). After the 2004 Southeast Asia earthquake, patients with multiple wounds admitted to the intensive care unit of the Cologne-Merheim Medical Center in Germany were reportedly contaminated with multidrug-resistant *A. baumannii*, extended-spectrum β-lactamase *Escherichia coli*, and methicillin-resistant *Staphylococcus aureus* (*2*). After the 2005 northern Pakistan earthquake, Kiani et al. reported emergence of multiply drug-resistant *Acinetobacter* spp., *Enterobacter* spp., and other gram-negative organisms, susceptible to amikacin only. Hospitals were overwhelmed with staff and antimicrobial drug shortages, and wounds were often treated empirically because of limited laboratory capacities (*3*). After the 2008 earthquake in Wenchuan, China, the predominant pathogen causing infections was *A. baumannii*; 1 hospital reported that >65% of *Acinetobacter* isolates were resistant to a wide range of antimicrobial drugs, except imipenem, and 24.6% of isolates were pan–drug resistant (*4*).

Since the 2023 Turkey/Syria earthquakes, multidrug resistance has not yet been reported. However, on the basis of the epidemiology of infections in earthquake-stricken regions, we expect hospitals in the region to struggle with containing nosocomial transmission of highly resistant pathogens that may increase deaths among hospitalized patients. Also of concern is the re-emergence of other infectious diseases, such as cholera, known to be precipitated by disaster settings (*5*). The Turkey/Syria earthquakes come on the heels of multiple crises in the region, many of which have been shown to influence the rising rates of multidrug resistance, as in the wake of the Iraq and Syrian conflicts (*6*). Rising rates of antimicrobial resistance are further compounded by the regionwide travel of wounded patients for treatment as healthcare infrastructure in Iraq and Syria collapsed (*7*). Medicine shortages, especially resulting from sanctions in Syria and Iraq and following the 2019 financial collapse in Lebanon, further compound selective pressures on microbes to develop specific resistance profiles.

Hospitals in and outside the region treating injuries from the Turkey/Syria earthquakes will probably observe a surge in highly resistant pathogens and nosocomial transmission. In addition to providing immediate care for the injured and displaced, relief efforts should therefore anticipate a probable increase in antimicrobial-resistant infections for which therapeutic options may be limited. Detecting and responding to this superimposed crisis urgently requires support and expansion of existing microbiology laboratory capacity. Recent initiatives, such as the deployment of telemicrobiology in northern Syria, are examples of how to rapidly assist local laboratory teams in settings of social disruption (*8*). Training healthcare workers on surgical techniques and wound care adapted to deal with traumatic injuries have also been shown to enhance wound healing and to limit complications such as chronic and recurrent skin and soft tissue infections, which are risk factors for antimicrobial resistance (*9*). Early-stage detection and aggressive infection-control practices (e.g., active surveillance, contact isolation, sampling of healthcare workers and hospital environments, and antimicrobial stewardship) during and after disasters play key roles in preventing resistant strains from becoming endemic to healthcare facilities (*10*). Healthcare facilities may need to consider patient decolonization through chlorhexidine bathing to forestall colonization by antimicrobial-resistant *Acinetobacter* strains (*10*). Communities affected by the recent earthquakes will probably experience their effects for months to come. It is not too late to act to prevent further complications from these natural disasters, such as antimicrobial-resistant infections, from compounding ongoing human tragedies.

This work was supported by the New Frontiers in Research Fund, Canada (NFRFE-2019-00444) (A.R. and L.-P.H.), the Fonds de Recherche du Quebec–Sante (282182) (L.-P.H.), and the Canadian Institute for Advanced Research (GS-0000000256) (L.-P.H.)

About the Author

Mr. Rizk is a PhD candidate in anthropology at the Geneva Graduate Institute, Switzerland. His research interests include scientific laboratory capacities and antimicrobial resistance.

References

1. Oncül O, Keskin O, Acar HV, Küçükardali Y, Evrenkaya R, Atasoyu EM, et al. Hospital-acquired infections following the 1999 Marmara earthquake. J Hosp Infect. 2002;51:47–51. https://doi.org/10.1053/jhin.2002.1205
2. Maegele M, Gregor S, Steinhausen E, Bouillon B, Heiss MM, Perbix W, et al. The long-distance tertiary air transfer and care of tsunami victims: injury pattern and microbiological and psychological aspects. Crit Care Med. 2005;33:1136–40. https://doi.org/10.1097/01.CCM.0000163269.42524.50
3. Kiani QH, Amir M, Ghazanfar MA, Iqbal M. Microbiology of wound infections among hospitalised patients following

the 2005 Pakistan earthquake. J Hosp Infect. 2009;73:71–8. https://doi.org/10.1016/j.jhin.2009.06.012
4. Tao C, Kang M, Chen Z, Xie Y, Fan H, Qin L, et al. Microbiologic study of the pathogens isolated from wound culture among Wenchuan earthquake survivors. Diagn Microbiol Infect Dis. 2009;63:268–70. https://doi.org/10.1016/j.diagmicrobio.2008.11.009
5. Kelly-Hope LA. Conflict and emerging infectious diseases. Emerg Infect Dis. 2008;14:1004–5, author reply 1005.
6. Haraoui LP, Valiquette L, Laupland KB. Antimicrobial resistance in conflicts. J Assoc Med Microbiol Infect Dis Can. 2018;3:119–22. https://doi.org/10.3138/jammi.2018.05.15
7. Dewachi O, Skelton M, Nguyen VK, Fouad FM, Sitta GA, Maasri Z, et al. Changing therapeutic geographies of the Iraqi and Syrian wars. Lancet. 2014;383:449–57. https://doi.org/10.1016/S0140-6736(13)62299-0
8. Karah N, Antypas K, Al-Toutanji A, Suveyd U, Rafei R, Haraoui LP, et al. Teleclinical microbiology: an innovative approach to providing web-enabled diagnostic laboratory services in Syria. Am J Clin Pathol. 2022;157:554–60. https://doi.org/10.1093/ajcp/aqab160
9. Abu-Sittah GS, Hoballah JJ, Bakhach J, editors. Reconstructing the war injured patient. Cham, Switzerland: Springer International Publishing; 2017.
10. Munoz-Price LS, Weinstein RA. *Acinetobacter* infection. N Engl J Med. 2008;358:1271–81. https://doi.org/10.1056/NEJMra070741

Address for correspondence: Louis-Patrick Haraoui, Hôpital Charles-Le Moyne, Casier 251, 3120 Blvd Taschereau, Greenfield Park, QC J4V 2H1, Canada; email: louis.patrick.haraoui@usherbrooke.ca

Detection of Severe Murine Typhus by Nanopore Targeted Sequencing, China

Panpan Qian, Xiaohua He, Mei Yang, Li Wei, Lihui Zhang, Xiqian Xing

Authors affiliation: The Affiliated Hospital of Yunnan University, Kunming, China

DOI: https://doi.org/10.3201/eid2906.221929

We report a case of murine typhus in China caused by *Rickettsia typhi* and diagnosed by nanopore targeted sequencing of a bronchoalveolar lavage fluid sample. This case highlights that nanopore targeted sequencing can effectively detect clinically unexplained infections and be especially useful for detecting infections in patients without typical signs and symptoms.

Murine typhus is caused by *Rickettsia typhi* bacteria transmitted by rat or cat flea vectors. Persons with murine typhus often have nonspecific or mild symptoms, such as fever, myalgia, and rash. In rare instances, murine typhus will cause atypical or multiple organ dysfunction syndrome (MODS) (*1*,*2*).

Murine typhus is an undifferentiated febrile illness, which makes it challenging to recognize and diagnose. We report a case of murine typhus and MODS in a patient without rash. We diagnosed murine typhus by using nanopore targeted sequencing (NTS) of a bronchoalveolar lavage fluid (BALF) sample, aiming to provide more reference for clinical practice.

A 60-year-old female farmer from Yunnan Province, China, had fatigue, anorexia, nausea, dizziness, and vomiting for 1 week. At admission, she was afebrile and hemodynamically stable and did not have headache, rash, or eschar. Chest computed tomography (CT) imaging showed pneumonia and a small plural effusion (Figure, panels A, B). By the next day, her condition had deteriorated. She experienced chills, fever (temperature 39°C), severe hypotension (70/53 mm Hg), dyspnea, and deterioration of the oxygenation index. Preliminary laboratory investigation demonstrated mild leukocytosis (13.86 × 10^9 cells/L), moderately elevated transaminase levels (alanine aminotransferase 197 U/L, aspartate aminotransferase 128 U/L), severe thrombocytopenia (12 × 10^9 platelets/L), coagulation disorder (D-dimer 49.8 μg/mL), elevated C-reactive protein (207.4 mg/L) and procalcitonin (4.65 ng/mL) levels, and respiratory failure (partial pressure of oxygen 58.9 mm Hg).

The patient was given intravenous meropenem and norepinephrine and was admitted on noninvasive ventilation. We then conducted tests for malaria, *Legionella*, influenza virus, SARS-CoV-2, HIV, herpes simplex virus, cytomegalovirus, Epstein-Barr virus IgM, *Roxiella burnettii* IgM (phase II antigen), *R. typhi* IgM, *Mycoplasma pneumoniae* IgM, *Chlamydia* IgM, respiratory syncytial virus IgM, and adenovirus IgM; results were all negative. In addition, testing of blood, urine, stool, and sputum cultures and bone marrow biopsy all produced negative results.

On admission day 5, she remained normotensive. Her body temperature dropped, but she still had a low-grade fever, body temperature fluctuating from 37.5°C to 38°C. However, the cause of her severe infection remained unclear. The next day, she underwent bronchoscopy. BALF was sent to undergo NTS analysis to Wuhan Dgensee Clinical Laboratory Co., Ltd (https://www.dgensee.com). Two days later, NTS results revealed *R. typhi* DNA.

NTS analysis yielded a total of 71,252 single-end reads. *R. typhi* had the highest relative abundance of 44.58% (n = 31,764 reads). Subsequently, we conducted quantitative PCR (qPCR) using a sequence from GenBank (accession no. WP_011190964) as the target gene to detect *R. typhi*. The qPCR results confirmed the NTS detection (Appendix, https://wwwnc.cdc.gov/EID/article/29/6/22-1929-App1.pdf).

After the murine typhus diagnosis, the patient was treated with doxycycline (100 mg every 12 h) beginning on admission day 9. Soon after, her body temperature, platelet count, and blood coagulation function returned to normal. Reexamination of

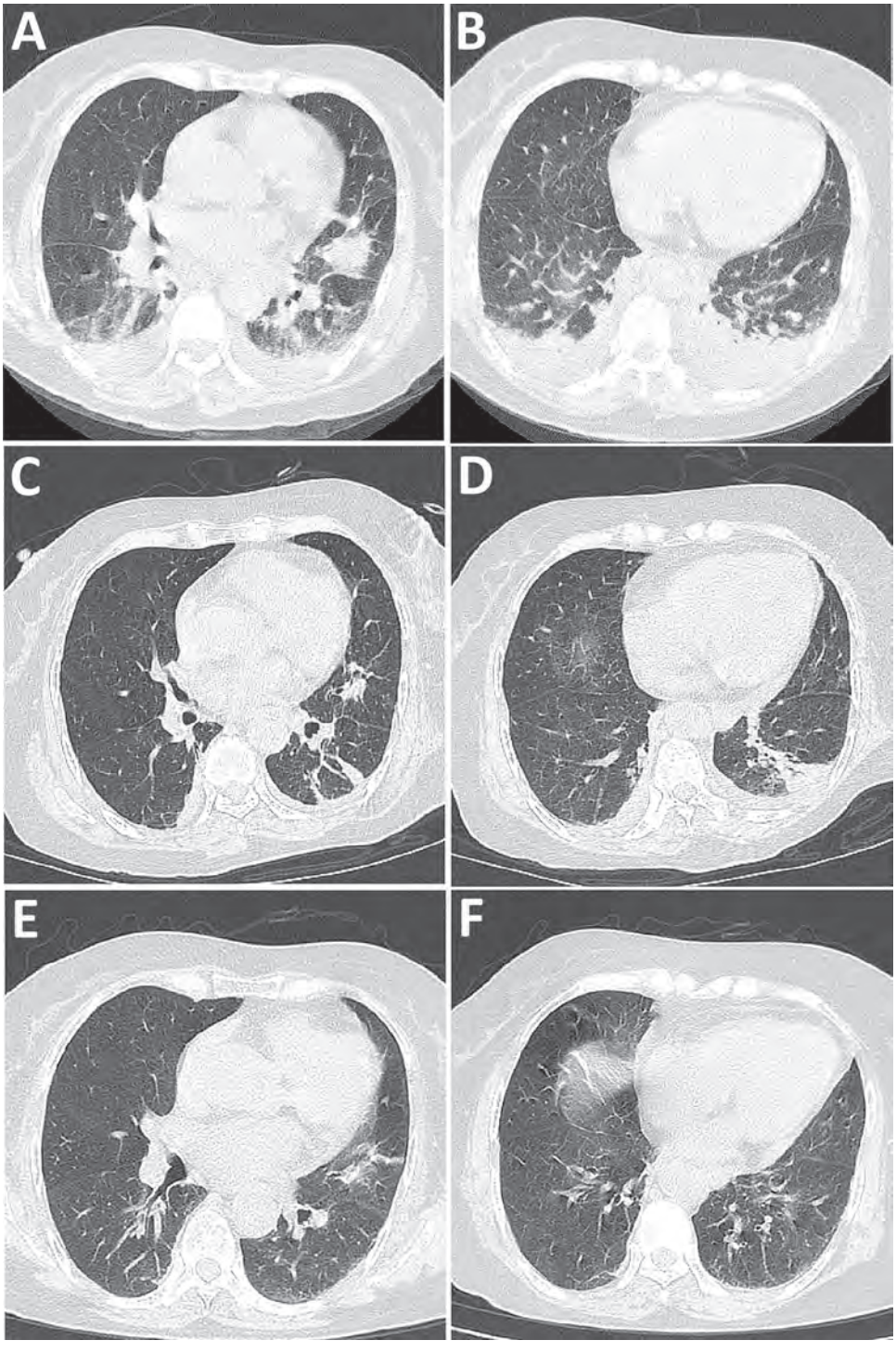

Figure. Chest computed tomography images from a patient with severe murine typhus detected by nanopore targeted sequencing, China. A, B) Images taken at hospital admission demonstrating pneumonic exudation of the left lung lingual segment and double lower lobes and small plural effusion. C, D) Improvement of pulmonary infiltrates after 14 days. E, F) Resolution of pulmonary infiltrates demonstrated 1 month after hospital discharge.

chest CT images showed improved pulmonary infiltrates (Figure, panels C, D), and she was discharged from the hospital. She continued doxycycline (100 mg 2×/d) for 14 days after discharge. At a 1-month follow-up, she had no symptoms of discomfort, and chest CT imaging showed resolving pulmonary infiltrates (Figure, panels E, F).

As an undifferentiated febrile illness, murine typhus can be challenging to diagnose in clinically mild or severe illness. Murine typhus can manifest with nonspecific symptoms and mimic other disease processes, making laboratory-confirmed diagnosis difficult without a high index of suspicion.

Diagnosis of murine typhus is usually performed by serologic testing and molecular analysis. Adaptation of modern serologic techniques for murine typhus diagnosis has substantially increased diagnostic accuracy, and serology was deemed the standard before the wide acceptance of molecular testing. Rickettsial infections require early diagnosis and treatment to prevent severe outcomes, but early diagnosis is rarely achieved by using serology (*3*). In addition to serology, the most common diagnostic method for murine typhus is qPCR (*4*). However, PCR has limitations, including being more sensitive during acute illness, such as the febrile phase, usually days 1–5 of illness, but possibly up to days 7–10 (*3*).

NTS is a groundbreaking technology that has the potential to overcome the shortcomings of both PCR and metagenomic next-generation sequencing, and next-generation sequencing is much less affected by antimicrobial drugs than is PCR (*5*–*7*). NTS has been used clinically and has shown high specificity and sensitivity (*6*). NTS combines long read length (>5,000 bp) and targeted amplification of 16S RNA gene for bacteria, *rpoB* for mycobacteria, and internal transcribed spacer (ITS) for fungi, all of which are free from interference of host background DNA (*8*,*9*). NTS can accurately detect causative pathogens in infectious samples and has a short 8–14-hour turnaround time.

In conclusion, we successfully detected *R. typhi* by using NTS in a febrile patient with MODS but without rash. NTS is a promising technology that can efficiently identify infectious pathogens early and has the potential to assist physicians in providing timely and precise treatment, especially for patients with nonspecific symptoms indicative of multiple disease processes.

Acknowledgments

We thank Dgensee, Wuhan, China for performing the targeted nanopore sequencing procedure and interpretation.

This work was supported by grants from the National Natural Science Foundation of China (grant no. 82160016), the Basic Research Program of Yunnan Province (grant no. 202201AY070001-265), and the Famous Doctors of High-Level Talent Training Support Program of Yunnan Province (grant no. YNWR-MY-2020-013).

About the author

Dr. Qian is a resident at the Affiliated Hospital of Yunnan University, Kunming, Yunnan, China. Her research interest is emerging infectious diseases.

References

1. Civen R, Ngo V. Murine typhus: an unrecognized suburban vectorborne disease. Clin Infect Dis. 2008;46:913–8. https://doi.org/10.1086/527443
2. Tsioutis C, Chaliotis G, Kokkini S, Doukakis S, Tselentis Y, Psaroulaki A, Gikas A. Murine typhus in elderly patients: a prospective study of 49 patients. Scand J Infect Dis. 2014;46:779–82. https://doi.org/10.3109/00365548.2014.943283
3. Paris DH, Dumler JS. State of the art of diagnosis of rickettsial diseases: the use of blood specimens for diagnosis of scrub typhus, spotted fever group rickettsiosis, and murine typhus. Curr Opin Infect Dis. 2016;29:433–9. https://doi.org/10.1097/QCO.0000000000000298
4. Abdad MY, Abou Abdallah R, Fournier PE, Stenos J, Vasoo S. A concise review of the epidemiology and diagnostics of rickettsioses: *Rickettsia* and *Orientia* spp. J Clin Microbiol. 2018;56:e01728-17. https://doi.org/10.1128/JCM.01728-17
5. Hasan MR, Rawat A, Tang P, Jithesh PV, Thomas E, Tan R, et al. Depletion of human DNA in spiked clinical specimens for improvement of sensitivity of pathogen detection by next-generation sequencing. J Clin Microbiol. 2016;54:919–27. https://doi.org/10.1128/JCM.03050-15
6. Fu Y, Chen Q, Xiong M, Zhao J, Shen S, Chen L, et al. Clinical performance of nanopore targeted sequencing for diagnosing infectious diseases. Microbiol Spectr. 2022;10:e0027022. https://doi.org/10.1128/spectrum.00270-22
7. Ciuffreda L, Rodríguez-Pérez H, Flores C. Nanopore sequencing and its application to the study of microbial communities. Comput Struct Biotechnol J. 2021;19:1497–511. https://doi.org/10.1016/j.csbj.2021.02.020
8. Petersen LM, Martin IW, Moschetti WE, Kershaw CM, Tsongalis GJ. Third-generation sequencing in the clinical laboratory: exploring the advantages and challenges of nanopore sequencing. J Clin Microbiol. 2019;58:e01315-9. https://doi.org/10.1128/JCM.01315-19
9. Huang Q, Fu A, Wang Y, Zhang J, Zhao W, Cheng Y. Microbiological diagnosis of endophthalmitis using nanopore targeted sequencing. Clin Exp Ophthalmol. 2021;49:1060–8. https://doi.org/10.1111/ceo.13992

Address for correspondence: Xiqian Xing, Department of Pulmonary and Critical Care Medicine, The Affiliated Hospital of Yunnan University, 176 Qingnian Rd, Kunming 650021, Yunnan, China; email: xingxiqian@ynu.edu.cn or xingxiqiankm@163.com

Mycobacterium marinum Infection after Iguana Bite in Costa Rica

Jordan Mah, Kyle Walding, Brooke Liang, Laurence Rinsky, Roshni Mathew, Indre Budvytiene, Niaz Banaei

Author affiliations: Stanford University School of Medicine, Stanford, California, USA (J. Mah, K. Walding, B. Liang, L. Rinsky, R. Mathew, N. Banaei); Stanford Health Care, Stanford (J. Mah, I. Budvytiene, N. Banaei)

DOI: https://doi.org/10.3201/eid2906.230062

Infections after reptile bites are uncommon, and microbial etiologies are not well defined. We describe a case of *Mycobacterium marinum* soft-tissue infection after an iguana bite in Costa Rica that was diagnosed through 16S rRNA sequencing and mycobacterial culture. This case informs providers of potential etiologies of infection after iguana bites.

Zoonotic infections associated with animal bite injuries are common and can result in severe illness (*1*,*2*). Approximately 5 million animal bites occur annually in North America, and 10 million injuries occur globally from dog bites alone (*2*,*3*). Pathogens causing infections after dog or cat bites are well described; pathogens from other animal bites are less well defined, although their oral microbiota are known (*1*). We report a case of cutaneous *Mycobacterium marinum* infection after an iguana bite to inform clinicians of potential infectious etiologies of lizard bites.

A previously healthy 3-year-old girl was on vacation with her family in Costa Rica. She was eating cake on the beach when an iguana approached her. While attempting to take the cake, the animal bit the dorsum of her left hand. She was immediately taken to a local clinic and found to have a single, superficial bite wound over the dorsum of her third metacarpal. The wound was immediately disinfected and irrigated; she was prescribed a 5-day course of oral amoxicillin. The family returned to the United States after the incident. Her wound completely resolved over the ensuing days without immediate complications.

Five months after the bite, her parents noted a small lump on the dorsum of her left hand that was not present previously. The child was otherwise well. The lump became progressively larger, erythematous, and mildly painful over the next 3 months (Figure, panel A). Because of persistent symptoms, her parents sought medical attention at Stanford Medicine Children's Health (Stanford, California, USA). Although ultrasound demonstrated findings suggestive of a ganglion cyst (Figure, panel B), the location

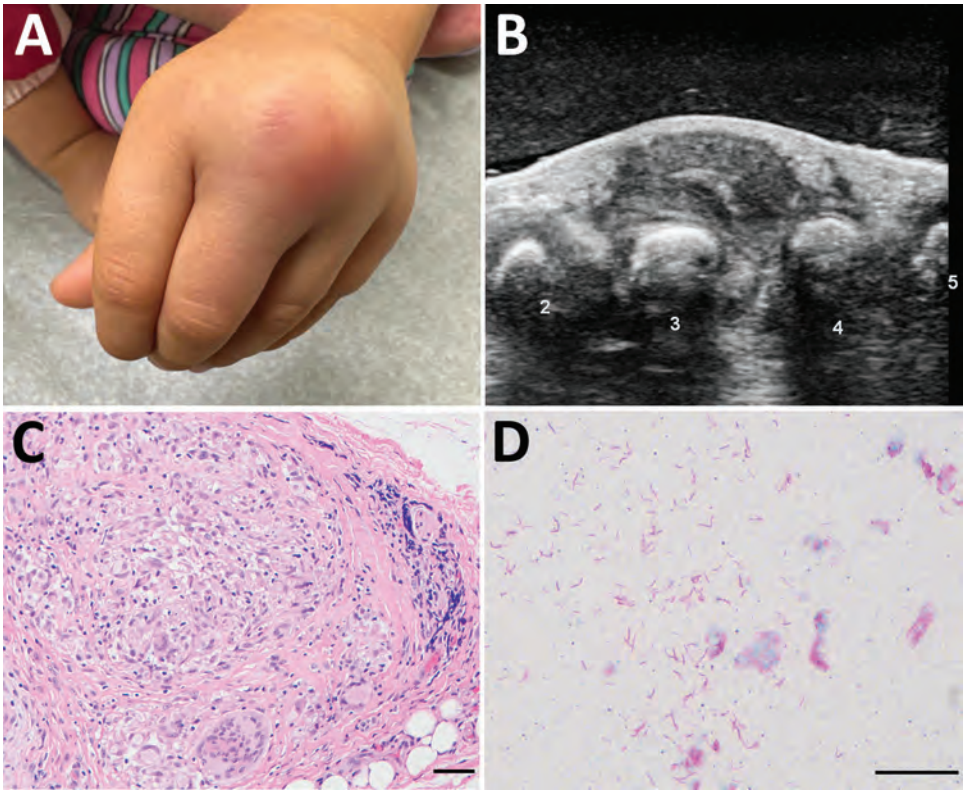

Figure. Gross and microscopic features of a mass involving the dorsum of the left hand in a 3-year-old girl with *Mycobacterium marinum* infection after iguana bite in Costa Rica. A) Erythematous lump over third and fourth digits. B) Ultrasound image, with numbers labeling the digits. C) Hematoxylin and eosin–stained soft tissue showing granulomatous inflammation. Scale bar indicates 10 μm. D) Fite stain highlighting numerous mycobacteria in an area of necrosis. Scale bar indicates 20 μm.

and symptoms were not consistent with this diagnosis. She saw an orthopedic surgeon who, given the progression and unusual clinical features, performed excision of the mass.

Surgical excision revealed a 2-cm, thick-walled mass adherent to the extensor tendons of the third and fourth digits, with extrusion of a thick, white, purulent material. Histopathology revealed extensive necrosis and necrotizing granulomatous inflammation with acid-fast bacilli seen by Fite staining (Figure, panels C, D). Bacterial 16S rRNA sequencing identified a sequence with 100% identity to *M. marinum* (GenBank accession no. OQ249694). Mycobacterial culture (Middlebrook 7H11 agar) incubated at 30°C grew photochromogenic colonies after 2 weeks that were consistent with *M. marinum*. The patient was started on rifampin and clarithromycin and gradually improved over the next 2 months.

Literature on the microbiologic etiologies of infected human wounds secondary to iguana bites is scarce; *Serratia marcescens* was reported in 3 cases and *Staphylococcus aureus* in 1 other (*1*). *Salmonella enterica* is a consideration for reptiles in general because 75%–90% of both wild and captive reptiles (including snakes, turtles, and iguanas) are colonized (*4*,*5*). Several studies have demonstrated that domestic reptiles can also harbor nontuberculous mycobacteria (NTM) because of their ubiquitous environmental presence (*4*). In a study of healthy pet reptiles, many were found to harbor NTM such as *M. fortuitum*, *M. peregrinum*, and *M. chelonae* (*6*). Reptiles can be asymptomatic carriers or can have NTM disease; cutaneous manifestations are the most common, with granulomatous lesions seen on histopathology (*4*,*6*). In this case, although the iguana is the most plausible source of *M. marinum*, we cannot rule out the possibility that the patient's wound was inoculated from an environmental source.

M. marinum, a slow-growing photochromogenic NTM, is an established environmental pathogenic mycobacterium found in fresh water and salt water (*7*). *M. marinum* causes necrotizing granulomatous disease in humans, where its immunopathogenesis mimics that of *M. tuberculosis,* with which it shares considerable genetic homology (*7*). In humans, *M. marinum* is associated with occupational or recreational exposures after a skin injury where a contaminated water source enables direct inoculation (*7*). *M. marinum* is taken up by local macrophages and, like *M. tuberculosis*, uses the type VII secretion system ESX-1 (ESAT-6 secretion system 1), escaping the phagosome into cytoplasm and triggering an inflammatory response to spread to other macrophages (*8*).

M. marinum causes disease in immunocompetent and immunosuppressed hosts; however, the incidence of cutaneous infections among children is low (*9*). The incubation period ranges from 3 weeks to 9 months, and symptoms are usually minimal and localized; systemic symptoms are generally absent (*7*). Common manifestations of *M. marinum* infections include subacute to chronic papulonodular skin lesions on the hand with a sporotrichoid spread, as the infection spreads along lymphatic vessels to regional lymph nodes (*7*). NTM, including *M. marinum,* are resistant to β-lactams because of β-lactamases, decreased cell permeability, and low affinity to penicillin-binding proteins, explaining why this patient did not respond to amoxicillin (*7*).

Isolation of *M. marinum* in culture is challenging because it is slow growing, requiring 28°C–32°C for optimal growth in vitro and incubation over several weeks (*7*,*10*). For this reason, bacterial sequencing is increasingly used for diagnosis because of its rapidity, sensitivity, and specificity. The cold-blooded nature of iguanas might enable them to serve as reservoirs for temperature-sensitive *M. marinum* (*4*). The genotypic and phenotypic evidence of *M. marinum* infection after an iguana bite in this report could inform clinicians of less commonly known bacterial etiologies after unusual zoonotic exposures.

J.M. and N.B. conceived the project. J.M., K.W., and B.L. drafted the manuscript. J.M. and B.L. prepared the figures. All authors provided critical appraisal of manuscript drafts. All authors critically revised the manuscript for important intellectual content and gave final approval of the version to be published and agreed to be accountable for all aspects of the work.

About the Author

Dr. Mah is a board-certified infectious diseases physician who is a trainee in medical microbiology at Stanford University. His research interests include tropical medicine, invasive fungal infections, mycobacterial infections, and infections in immunocompromised hosts.

References

1. Abrahamian FM, Goldstein EJC. Microbiology of animal bite wound infections. Clin Microbiol Rev. 2011;24:231–46.
2. Ellis R, Ellis C. Dog and cat bites. Am Fam Physician. 2014;90:239–43.
3. World Health Organization. Animal bites. 2018 [cited 2023 Jan 11]. https://www.who.int/news-room/fact-sheets/detail/animal-bites
4. Ebani VV. Domestic reptiles as source of zoonotic bacteria: a mini review. Asian Pac J Trop Med. 2017;10:723–8. https://doi.org/10.1016/j.apjtm.2017.07.020

5. Nakadai A, Kuroki T, Kato Y, Suzuki R, Yamai S, Yaginuma C, et al. Prevalence of *Salmonella* spp. in pet reptiles in Japan. J Vet Med Sci. 2005;67:97–101. https://doi.org/10.1292/jvms.67.97
6. Ebani VV, Fratini F, Bertelloni F, Cerri D, Tortoli E. Isolation and identification of mycobacteria from captive reptiles. Res Vet Sci. 2012;93:1136–8. https://doi.org/10.1016/j.rvsc.2012.05.006 PMID: 22657144
7. Aubry A, Mougari F, Reibel F, Cambau E. Mycobacterium marinum. Microbiol Spectr. 2017;5. https://doi.org/10.1128/microbiolspec.TNMI7-0038-2016
8. Osman MM, Shanahan JK, Chu F, Takaki KK, Pinckert ML, Pagán AJ, et al. The C terminus of the mycobacterium ESX-1 secretion system substrate ESAT-6 is required for phagosomal membrane damage and virulence. Proc Natl Acad Sci U S A. 2022;119:e2122161119. https://doi.org/10.1073/pnas.2122161119
9. Meoli A, Deolmi M, Iannarella R, Esposito S. Non-tuberculous mycobacterial diseases in children. Pathogens. 2020;9:553.
10. van Ingen J. Diagnosis of nontuberculous mycobacterial infections. Semin Respir Crit Care Med. 2013;34:103–9. https://doi.org/10.1055/s-0033-1333569

Address for correspondence: Niaz Banaei, Department of Pathology, Stanford University, 3375 Hillview Ave, Palo Alto, CA 94304, USA; email: nbanaei@stanford.edu

Microscopic Evidence of Malaria Infection in Visceral Tissue from Medici Family, Italy

Frank Maixner, Dennis Drescher, Giulia Boccalini, Dario Piombino-Mascali, Marek Janko, Nicole Berens-Riha, Bum Jin Kim, Michelle Gamble, Jolanthe Schatterny, Rory E. Morty, Melanie Ludwig, Ben Krause-Kyora, Robert Stark, Hyun Joo An, Jens Neumann, Giovanna Cipollini, Rudolf Grimm, Nicole Kilian, Albert Zink

Author affiliations: Eurac Research, Bolzano, Italy (F. Maixner, G. Boccalini, G. Cipollini, A. Zink); University Hospital Heidelberg, Heidelberg, Germany (D. Drescher, J. Schatterny, R.E. Morty, M. Ludwig, N. Kilian); Vilnius University, Vilnius, Lithuania (D. Piombino-Mascali); Technical University of Darmstadt, Darmstadt, Germany (M. Janko, R. Stark); Institute of Tropical Medicine, Antwerp, Belgium (N. Berens-Riha); University of Munich, Munich, Germany (N. Berens-Riha); Oregon State University, Corvallis, Oregon, USA (B.J. Kim); Chungnam National University, Daejeon, Korea (B.J. Kim, H.J. An); Heritage and Archaeological Research Practice, Edinburgh, Scotland, UK (M. Gamble); Kiel University, Kiel, Germany (B. Krause-Kyora); Ludwig Maximilian University, Munich (J. Neumann); Agilent Technologies, Santa Clara, California, USA (R. Grimm)

DOI: https://doi.org/10.3201/eid2906.230134

Microscopy of mummified visceral tissue from a Medici family member in Italy identified a potential blood vessel containing erythrocytes. Giemsa staining, atomic force microscopy, and immunohistochemistry confirmed *Plasmodium falciparum* inside those erythrocytes. Our results indicate an ancient Mediterranean presence of *P. falciparum*, which remains responsible for most malaria deaths in Africa.

The Medici family was a powerful family from Florence, Italy, that gained prominence under Cosimo de' Medici in the early 15th century (*1*). Dynastic power granted Medici family members a burial at the San Lorenzo Basilica in central Florence (Appendix Figure 1, panel A, https://wwwnc.cdc.gov/EID/article/29/6/23-0134-App1.pdf). Burial was preceded by an embalming procedure in which inner organs (viscera) were removed and placed in large terracotta jars (Appendix Figure 1, panel B).

In 2011, selected jars of organs from Medici family members were opened centuries after burial to examine their contents, revealing that multiple tissue pieces were still present (Appendix). The Institute for Mummy Studies at Eurac Research (Bolzano, Italy) received samples from the organs; we performed microscopic and molecular analysis (Appendix) of a 2.5 cm × 1.5 cm tissue piece (ID 1297) from 1 jar (Appendix Figure 1, panel C). Using microscopy, we identified a potential blood vessel containing erythrocytes (Figure, panel A). Diameters (7.24, SD ±0.14 μm; n = 37) and discocyte shapes of cells within the blood vessel were characteristic of erythrocytes (*2*). We conducted further microscopic evaluation of single cells and found the potential presence of a parasite that might have resided within the erythrocytes during the lifetime of the deceased family member. Giemsa staining of tissue sections confirmed our first impression (Figure, panel B) and suggested the parasite was *Plasmodium* spp.; members of this genus are the causative agent of different types of human malaria (*3*). We used atomic force microscopy to identify the ring stage, an immature developmental stage of *P. falciparum* that is dominant in peripheral blood of infected patients and a diagnostic

hallmark (Figure, panel C). We verified the presence of *P. falciparum* by using immunohistochemistry with polyclonal mouse antiserum against *Plasmodium* spp.–specific aldolase (Appendix Figure 1, panels D, E) and a monoclonal antibody against *P. falciparum*–specific histidine-rich protein HRPII (Appendix Figure 1, panels F, G). We confirmed results by using immunofluorescence analysis with antibody against *P. falciparum* endoplasmic reticulum resident protein Pf39 (Appendix Figure 1, panels H, I). All isotype controls were negative (Appendix Figure 1, panels E, G, I). Not all observed parasitized erythrocytes were labeled by the antiserum, likely because of tissue degradation over the centuries. We verified a progressed state of biomolecule degradation by additional DNA-based analysis.

We determined that parasitemia was 38% in the Medici tissue, which appeared high (Appendix

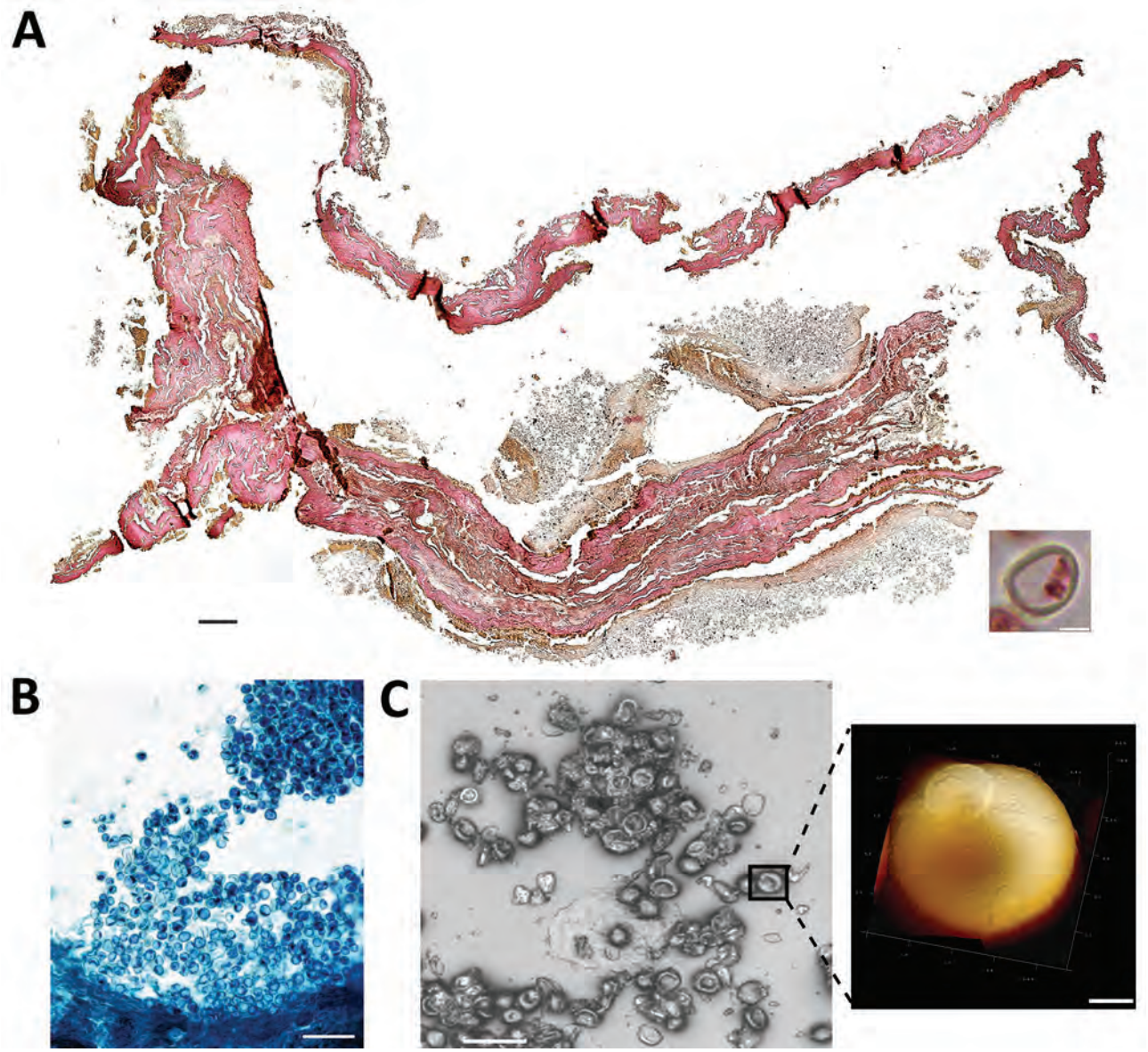

Figure. Microscopic analysis of malaria infection in visceral tissue from Medici family, Italy. We evaluated a 2.5 cm × 1.5 cm tissue piece (ID 1297) from 1 jar containing viscera of a Medici family member and identified a potential blood vessel containing erythrocytes. A) Histological cross section of the tissue stained with hematoxylin and eosin; scale bar indicates 200 µm. Inset shows a possible erythrocyte; scale bar indicates 3 µm. B) Giemsa staining of a paraffin section of viscera suggesting the presence of parasites within the erythrocytes. Scale bar indicates 50 µm. C) Atomic force microscopy (AFM) of the tissue section. An optical microscope was used to define appropriate sample areas for AFM imaging (left image); scale bar indicates 20 µm. Enlarged area at right shows a ring stage of *Plasmodium falciparum* in an erythrocyte; scale bar indicates 2 µm.

Figure 1, panel J). However, instead of peripheral blood, we investigated tissues that might have had higher than expected parasitemia from sequestration of erythrocytes parasitized by mature asexual developmental stages (trophozoite and schizonts) of *P. falciparum* (*4*). Erythrocytes were visible in the tissue and were not washed away after embedding, further suggesting the presence of malaria parasites because they can trigger blood coagulation that might have kept the cells in place (*5*). High parasitemia within tissues is likely dependent on *P. falciparum* developmental stages (*4*). Erythrocytes infected with juvenile ring stages can be found in the peripheral blood of patients, whereas mature developmental stages are absent (*6*). Erythrocytes that contain more mature developmental stages can adhere to endothelial cells that line blood vessels within inner organs (*6*).

The most striking parasite-derived erythrocyte modification is the establishment of secretory organelles, known as Maurer's clefts, that reside within the cytoplasm of terminally differentiated host erythrocytes infected with *P. falciparum* (*7*). Similar organelles also exist in the cytoplasm of erythrocytes infected by other pathogenic *Plasmodium* spp. (*7*). During *P. falciparum* infections, Maurer's clefts are crucial for initiating host-parasite interactions; they are responsible for severe disease and patient death by enabling protein trafficking that causes cytoadherence within organs (*4*). By using Giemsa staining, we observed delicate stipplings within the cytoplasm of infected erythrocytes in the Medici tissue, indicative of Maurer's clefts (Appendix Figure 1, panel J). We quantified the stipplings; numbers were comparable to what can be observed within infected erythrocytes of malaria patients and in vitro–infected erythrocyte cultures.

We performed glycan analysis by using mass spectrometry and molecular analyses (Appendix). We identified a unique glycan found in erythrocyte B antigen (Appendix Figure 2, panels A–D), further indicating the presence of erythrocytes in the tissue. However, parasite DNA was undetectable by PCR. Metagenomic sequencing showed only 0.06% of all reads were host DNA; 2 reads could be unambiguously assigned to *P. falciparum* (Appendix Figure 2, panel E).

Medici family members were known to hunt in marshlands around Florence and in Tuscany that served as breeding grounds for mosquito vectors capable of transmitting *Plasmodium* spp. parasites (*8*). In 2010, immunoassays were used to analyze bones of 4 Medici family members who might have died from malaria; *P. falciparum* was detected (*9*). Our observations agree with previous studies of ancient human remains, suggesting a Mediterranean presence of malaria from the era of ancient Egypt to modern times (*10*). Malaria remains a major health threat for persons in Africa, mostly affecting pregnant women and children. Malaria is a curable disease; however, persons in malaria-endemic areas still lack access to proper healthcare. Developing *Plasmodium* resistance to standard treatments further hampers positive therapeutic outcomes.

Acknowledgments

We thank Donatella Lippi and Elsa Pacciani for their support during the initial phase of the study.

Funding was provided by the European Regional Development Fund 2014–2020_CALL-FESR 2017 Research and Innovation_Autonomous Province of Bolzano-South Tyrol_Project: FESR1078-MummyLabs.

About the Author

Dr. Maixner is coordinator at the EURAC Institute for Mummy Studies and head of the ancient DNA laboratory. His research interests focus on genomic and relationship analysis of ancient human remains and identification of ancient pathogens that caused disease.

References

1. The Medici: citizens and masters. In: Black R, Law JE, editors. Villa I Tatti Series 32, the Harvard University Center for Italian Renaissance Studies. Cambridge (MA): Harvard University Press; 2015.
2. Kilian N, Dittmer M, Cyrklaff M, Ouermi D, Bisseye C, Simpore J, et al. Haemoglobin S and C affect the motion of Maurer's clefts in *Plasmodium falciparum*–infected erythrocytes. Cell Microbiol. 2013;15:1111–26. https://doi.org/10.1111/cmi.12102
3. World Health Organization. World malaria report 2021 [cited 2023 Jan 1]. https://www.who.int/teams/global-malaria-programme/reports/world-malaria-report-2021
4. Cyrklaff M, Sanchez CP, Kilian N, Bisseye C, Simpore J, Frischknecht F, et al. Hemoglobins S and C interfere with actin remodeling in *Plasmodium falciparum*–infected erythrocytes. Science. 2011;334:1283–6. https://doi.org/10.1126/science.1213775
5. Francischetti IMB, Seydel KB, Monteiro RQ. Blood coagulation, inflammation, and malaria. Microcirculation. 2008;15:81–107. https://doi.org/10.1080/10739680701451516
6. Lee WC, Russell B, Rénia L. Sticking for a cause: the falciparum malaria parasites cytoadherence paradigm. Front Immunol. 2019;10:1444. https://doi.org/10.3389/fimmu.2019.01444
7. Mundwiler-Pachlatko E, Beck HP. Maurer's clefts, the enigma of *Plasmodium falciparum*. Proc Natl Acad Sci USA. 2013;110:19987–94. https://doi.org/10.1073/pnas.1309247110

8. Menning CB. The noble hunt: the "Libro della caccia" of Angelo del Bufalo. Yale Univ Libr Gaz. 2001;76:27–35.
9. Fornaciari G, Giuffra V, Ferroglio E, Gino S, Bianucci R. *Plasmodium falciparum* immunodetection in bone remains of members of the Renaissance Medici family (Florence, Italy, sixteenth century). Trans R Soc Trop Med Hyg. 2010;104:583–7. https://doi.org/10.1016/j.trstmh.2010.06.007
10. Boualam MA, Pradines B, Drancourt M, Barbieri R. Malaria in Europe: a historical perspective. Front Med. 2021;8:691095. https://doi.org/10.3389/fmed.2021.691095

Address for correspondence: Albert Zink, Institute for Mummy Studies, Eurac Research, Viale Druso 1, 39100 Bolzano, Italy; email: albert.zink@eurac.edu

Enhanced Adenovirus Vaccine Safety Surveillance in Military Setting, United States

John Iskander, Scott Blanchet, Caitlin Springer, Patrick Rockwell, Dana Thomas, Satish Pillai

Author affiliations: United States Coast Guard, Washington, DC, USA (J. Iskander, D. Thomas, S. Pillai); United States Coast Guard Academy, New London, Connecticut, USA (S. Blanchet, C. Springer, P. Rockwell)

DOI: https://doi.org/10.3201/eid2906.230331

The US Coast Guard Academy began adenovirus vaccination of incoming cadets in 2022. Of 294 vaccine recipients, 15%–20% had mild respiratory or systemic symptoms within 10 days postvaccination but no serious adverse events after 90 days. Our findings support the continued use of adenovirus vaccines in congregate military settings.

Adenovirus infection results in considerable illness among congregate military populations (*1*). US Food and Drug Administration–approved use of a live, oral, bivalent adenovirus vaccine for military populations began in 2011 and was associated with substantial decreases in adenovirus infection incidence at US military basic training centers (*2*,*3*). The US Naval Academy introduced adenovirus vaccination in 2018 after a large adenovirus outbreak (*4*). An adenovirus outbreak involving ≈300 cadets occurred at the US Coast Guard Academy (CGA) in 2019 (*5*). Adenovirus vaccines were introduced for incoming first-year CGA cadets on June 28, 2022. To supplement postlicensure data on adenovirus vaccine safety (*6*), we monitored postvaccination signs and symptoms in those cadets.

We developed a monitoring system to account for military training features, such as restricted cellphone access and a time-sensitive, regimented curriculum. For sick call visits occurring ≤10 days after vaccination, the CGA clinic used a monitoring tool (Appendix, https://wwwnc.cdc.gov/EID/article/29/6/23-0331-App1.pdf) consisting of 17 postvaccination signs or symptoms obtained from clinical trial results (*7*,*8*). We measured vaccine uptake and inability to swallow pills and monitored cadets for 90 days after vaccination for US Food and Drug Administration–defined serious adverse events (*9*).

Cadets received an in-person briefing from CGA clinic staff on June 27, 2022. The CGA training cadre, with whom the cadets had daily contact, were briefed by clinic leadership on the paper-based reporting tool, reporting requirements, and referring ill cadets to the CGA clinic. Before vaccination, cadets were given the Centers for Disease Control and Prevention adenovirus vaccine information statement and opportunity to ask questions. Subsequently, if cadets sought care for illness at the CGA clinic, staff used the reporting tool to record whether any of the 17 signs and symptoms were present.

During the initial vaccination period (June 28–30, 2022), 293 (97.3%) of 301 first-year cadets received the adenovirus vaccine; 4 (1.3%) cadets were unable to swallow the vaccine. Of 4 cadets isolated for COVID-19 during the initial vaccination period, only 1 subsequently received the vaccine. Of 294 vaccinated cadets, a total of 159 (54.1%) received 1 other vaccine and 53 (18.0%) received ≥2 additional vaccines.

The average age of the 294 vaccine recipients was 18.25 years; 57% were male, and 43% female. During June 30–July 8, 2022, ≈100 first-year cadets sought care at the CGA clinic for illness, and 65 (22.1%) cadets reported ≥1 vaccine surveillance sign or symptom. Commonly reported signs and symptoms were cough (20.1%), sore throat (17.0%), headache (16.0%), fatigue (16.0%), nasal congestion (15.3%), and shortness of breath (11.6%) (Table). Frequencies of gastrointestinal symptoms among cadets seeking care at the clinic during the 10-day period after vaccination were 2.3% for abdominal pain, 3.7% for diarrhea, 4.0% for vomiting, and 8.3% for nausea (Table). During the 90 days after vaccination, no serious adverse events were reported, including hospitalization, Guillain-Barre syndrome, or death.

Table. Percentages of first-year US Coast Guard cadets reporting signs or symptoms within 10 days after adenovirus vaccination in study of enhanced adenovirus vaccine safety surveillance in military setting, United States*

Signs or symptoms	% Total†
Cough	20.1
Sore throat	17.0
Headache	16.0
Fatigue	16.0
Nasal congestion or rhinorrhea	15.3
Shortness of breath	11.6
Arthralgias or myalgias	10.5
Nausea	8.5
Fever, subjective or measured at >38.0°C	7.8
Increasing weakness in arms or legs	5.8
Numbness or tingling in hands or feet	4.8
Vomiting	4.1
Diarrhea	3.7
Abdominal pain	2.4
New rash	0.7
Dysuria	0.0
Hematuria	0.0

*Total number of vaccinated cadets was 294.
†Percentages sum to >100% because vaccine recipients reported multiple signs or symptoms.

During the enhanced postimmunization monitoring period, a concomitant COVID-19 outbreak affected ≈20% of first-year cadets. Of the 65 students who sought care at the CGA clinic and had ≥1 enhanced surveillance sign or symptom, 8 (12.3%) also tested positive for COVID-19.

The live adenovirus vaccine was well-tolerated; only 4 vaccination failures occurred, the cadets who could not swallow the medication. Of 294 vaccinated CGA cadets, <25% reported signs or symptoms during the monitoring period. Phase 1 adenovirus vaccine trial data (*7*) showed symptom occurrence reached 33% within 8 weeks postvaccination. The most common signs and symptoms reported among CGA first-year cadets corresponded with those noted in a large phase 3 adenovirus trial (*8*), including headache, sore throat, nasal congestion, and cough. In this cohort, rates for gastrointestinal symptoms (2.3%–8.3%) were lower than those reported in the phase 3 trial (*8*).

Shortness of breath in 11.6% of cadets did not clearly correspond to signs and symptoms identified in phase 1 or phase 3 trial safety data. Given that >25% of nonhospitalized adults with COVID-19 report shortness of breath (*10*), the concurrent COVID-19 outbreak might have contributed to reports of this specific symptom.

In conclusion, enhanced passive monitoring established after introducing adenovirus vaccination for incoming first-year CGA cadets did not identify any serious adverse events. Even with the receipt of multiple vaccines and an intercurrent COVID-19 outbreak, the signs and symptoms profile among cadets who had sick calls during the 10-day postvaccination period appears consistent with profiles reported in previous adenovirus vaccine trials. A positive COVID-19 test was observed for 12.3% of cadets who completed the surveillance questionnaire during their sick call, which might explain the 11.6% of cadets who reported shortness of breath. Our favorable real-world findings support continuing adenovirus vaccination of incoming CGA cadet classes and wider use of the vaccine in congregate military settings.

Acknowledgments

We thank Christopher Janik, Martin Newton, Garrett Heitmann, Benjamin Keller, Matthew Cuevas, Fahad Alsayyid, and Shane Steiner for providing logistic and technical support.

About the Author

Dr. Iskander is Chief of Preventive Medicine and Population Health for the United States Coast Guard in Washington, DC. His primary interests focus on immunization-related topics.

References

1. McNeill KM, Ridgely Benton F, Monteith SC, Tuchscherer MA, Gaydos JC. Epidemic spread of adenovirus type 4-associated acute respiratory disease between U.S. Army installations. Emerg Infect Dis. 2000;6:415–9. https://doi.org/10.3201/eid0604.000419
2. Radin JM, Hawksworth AW, Blair PJ, Faix DJ, Raman R, Russell KL, et al. Dramatic decline of respiratory illness among US military recruits after the renewed use of adenovirus vaccines. Clin Infect Dis. 2014;59:962–8. https://doi.org/10.1093/cid/ciu507
3. O'Donnell FL, Taubman SB. Follow-up analysis of the incidence of acute respiratory infections among enlisted service members during their first year of military service before and after the 2011 resumption of adenovirus vaccination of basic trainees. MSMR. 2015;22:2–7.
4. Rogers AE, Lu X, Killerby M, Campbell E, Gallus L, Kamau E, et al. Outbreak of acute respiratory illness associated with adenovirus type 4 at the U.S. Naval Academy, 2016. MSMR. 2019;26:21–7.
5. Chu VT, Simon E, Lu X, Rockwell P, Abedi GR, Gardner C, et al. Outbreak of acute respiratory illness associated with human adenovirus type 4 at the United States Coast Guard Academy, 2019. J Infect Dis. 2022;225:55–64. https://doi.org/10.1093/infdis/jiab322
6. McNeil MM, Paradowska-Stankiewicz I, Miller ER, Marquez PL, Seshadri S, Collins LC Jr, et al. Adverse events following adenovirus type 4 and type 7 vaccine, live, oral in the Vaccine Adverse Event Reporting System (VAERS), United States, October 2011–July 2018. Vaccine. 2019;37:6760–7. https://doi.org/10.1016/j.vaccine.2019.08.087
7. Lyons A, Longfield J, Kuschner R, Straight T, Binn L, Seriwatana J, et al. A double-blind, placebo-controlled study of the safety and immunogenicity of live, oral type 4 and type 7 adenovirus vaccines in adults. Vaccine. 2008;26:2890–8. https://doi.org/10.1016/j.vaccine.2008.03.037

8. Kuschner RA, Russell KL, Abuja M, Bauer KM, Faix DJ, Hait H, et al.; Adenovirus Vaccine Efficacy Trial Consortium. A phase 3, randomized, double-blind, placebo-controlled study of the safety and efficacy of the live, oral adenovirus type 4 and type 7 vaccine, in U.S. military recruits. Vaccine. 2013;31:2963–71. https://doi.org/10.1016/j.vaccine.2013.04.035
9. US Food and Drug Administration. CFR—Code of Federal Regulations Title 21, 21CFR312.32. Investigational new drug application [cited 2023 Apr 3]. https://www.accessdata.fda.gov/scripts/cdrh/cfdocs/cfCFR/CFRSearch.cfm?fr=312.32
10. Burke RM, Killerby ME, Newton S, Ashworth CE, Berns AL, Brennan S, et al.; Case Investigation Form Working Group. Symptom profiles of a convenience sample of patients with COVID-19—United States, January–April 2020. MMWR Morb Mortal Wkly Rep. 2020;69:904–8. https://doi.org/10.15585/mmwr.mm6928a2

Address for correspondence: John Iskander, United States Coast Guard Headquarters, 2703 Martin Luther King Jr Ave SE, Washington, DC 20593-7907, USA; email: John.K.Iskander@uscg.mil

Isolated Ocular Mpox without Skin Lesions, United States

Minh T. Nguyen, Akshay Mentreddy, Julie Schallhorn, Matilda Chan, Su Aung, Sarah B. Doernberg, Jennifer Babik, Kevin Miles, Katherine Yang, Emily Lydon, Daniel J. Minter, John Gonzales, Jessica Shantha, Thuy Doan, Gerami D. Seitzman

Author affiliations: University of California, San Francisco, California, USA (M.T. Nguyen, A. Mentreddy, J. Schallhorn, M. Chan, S. Aung, S.B. Doernberg, J. Babik, K. Miles, K. Yang, E. Lydon, D.J. Minter, J. Gonzales, J. Shantha, T. Doan, G.D. Seitzman); Francis I. Proctor Foundation, San Francisco (M.T. Nguyen, A. Mentreddy, M. Chan, J. Gonzales, J. Shantha, T. Doan, G.D. Seitzman)

DOI: https://doi.org/10.3201/eid2906.230032

We report a case of a 53-year-old HIV-negative patient in San Francisco, California, USA, with no classic mpox prodromal symptoms or skin lesions who experienced fulminant, vision-threatening scleritis, keratitis, and uveitis. Deep sequence analysis identified monkeypox virus RNA in the aqueous humor. We confirmed the virus on the cornea and sclera by PCR.

We report a case of ocular-only mpox infection in a 53-year-old man in San Francisco, California, USA. His medical history included chronic lymphocytic leukemia (CLL), inactive 2 years after treatment with obinutuzumab and venetoclax but with persistent lymphopenia. He reported male sexual partners but was HIV negative. Symptoms in his right eye began August 2022 as itching and nasal scleral redness (Figure, panel A). There was no fever, rash, or lymphadenopathy. Eye redness worsened; the patient sought care at an urgent care facility and was given erythromycin ointment. Continued vision loss led to an emergency department visit, resulting in a diagnosis of preseptal cellulitis, treated with trimethoprim/sulfamethoxazole plus amoxicillin/clavulanic acid.

In early September 2022, the patient sought care at a county eye clinic for purulent conjunctivitis and corneal epithelial defects. Clinicians suspected gonococcal conjunctivitis and administered intramuscular ceftriaxone and topical moxifloxacin 0.5%. Bacterial and fungal ocular cultures and herpetic viral PCR returned negative results. Topical prednisolone acetate 1% and oral valacyclovir failed to control the eye inflammation. Three weeks after initial symptoms appeared, the patient's ocular inflammation increased; keratic precipitates and a moderate corneal opacity developed. Uveitis and scleritis workups did not yield a specific diagnosis (Table).

In late September 2022, at a second opinion examination at a University of California clinic, the patient's right eye acuity was 20/640. Examination showed a nasal patch of avascular scleral necrosis (Figure, panel B), and corneal epithelial sloughing (Figure, panel C) with microcystic edema. Repeat ocular surface cultures and PCR were negative. Given the negative results of extensive infectious etiology testing, we prescribed oral prednisone (40 mg/d) for presumed undifferentiated necrotizing anterior scleritis and keratitis.

One week later, corneal inflammation worsened (Figure, panel D). Clinical deterioration on systemic steroids continued to raise suspicion for ocular infection; we stopped steroid treatments. Again, cultures and PCR remained negative. Without prednisone, the patient's limbal infiltrates worsened, with progressive corneal haze. White corneal endothelial plaques appeared. We performed anterior chamber paracentesis for cultures, viral PCR, and an RNA deep-sequencing (RNA-seq) protocol previously described (*1*). The patient's scleritis, keratitis, and anterior uveitis worsened (Figure, panels E, F). Right eye vision decreased to hand motion only. We performed a diagnostic scleral and corneal biopsy and initiated

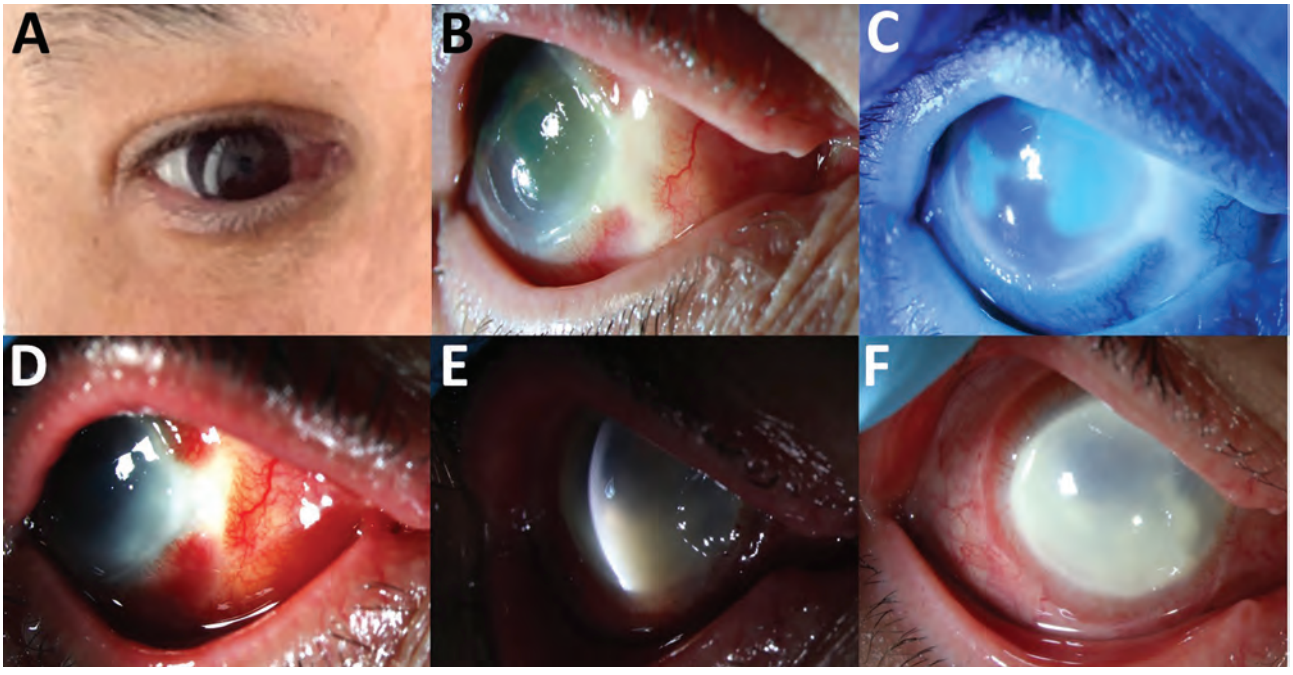

Figure. Clinical progression of ocular mpox in patient in California, USA. A) Initial manifestation of nasal scleral inflammation. B) Nasal scleral necrosis with surrounding scleritis. C) Corneal epithelial sloughing. D) Worsening scleritis and nasal keratitis. E) Corneal endothelial inflammatory plaque. Nasal area of corneal irregularity represents the area of biopsy. F) Progression of diffuse keratitis and corneal limbitis.

voriconazole for presumed fungal infection. The biopsy results returned negative for infection, and voriconazole was stopped.

Given the progressive clinical disease and negative infectious workup, we processed residual aqueous fluid for RNA-seq, which revealed a high number of reads aligning to monkeypox virus (MPXV) (Appendix Figure 1, https://wwwnc.cdc.gov/EID/article/29/6/23-0032-App1.pdf). Orthogonal testing from corneal and scleral swab specimens also returned positive results for MPXV by PCR. A nasal swab specimen obtained on the same day tested negative for MPXV by PCR.

When presented with those findings, the patient offered additional information regarding high-risk sexual activities, previously withheld because his definition of sexual activity included only penetrative intercourse. He described an encounter with a male partner with semen deposition into his right eye 2 weeks before the onset of his symptoms. He received the first dose of mpox vaccine for higher risk groups the week after this encounter. Several months later, during casual text messaging, the partner from this activity revealed a subsequent penile mpox diagnosis. (Appendix Figure 2).

Following treatment guidance from the Centers for Disease Control and Prevention, we initiated oral tecovirimat (600 mg 2×/d), topical trifluridine (6×/d), and weekly topical ophthalmic betadine washes (2). Four months into this course, worsening vision to light perception and repeat positive conjunctival mpox PCR led to inpatient admission for intravenous tecovirimat and cidofovir. Used in a compassionate-use capacity, tecovirimat and cidofovir have shown good activity against other orthopoxviruses, and in vitro and animal models have shown the antivirals to be effective against mpox (3). Unfortunately, after 3 weeks of inpatient treatment, the ocular disease did not improve. The patient's eye remained PCR positive for MPXV with an opacified and vascularized cornea.

Ocular manifestations of mpox during the 2010–2013 outbreak were associated with a more severe systemic presentation (4). However, during the recent 2022 outbreak, ocular findings do not appear to have correlated with systemic disease severity (5–7). Isolated ocular mpox in the absence of systemic or skin findings is exceedingly rare.

In conclusion, we describe a case of isolated ocular mpox with no skin lesions or systemic prodromal symptoms in a relatively immunocompromised patient. Because pertinent history and clinical suspicion were lacking, metagenomic RNA sequencing was highly valuable in helping identify the pathogen.

Table. Summary of laboratory and microbiology testing of patient with ocular mpox, California, USA

Test	Result
Laboratory and microbiology testing from serum or ocular surface scraping or swab specimen	
Human leukocyte antigen B27	Negative
Angiotensin-converting enzyme	Within reference range
Complement	Within reference range
Antineutrophilic cytoplasmic antibody	Within reference range
Antinuclear antibodies	Within reference range
Rheumatoid factor	Within reference range
Anti-cyclic citrullinated peptide	Within reference range
HIV antibody/antigen	Negative ×2
QuantiFERON-TB Gold*	Negative
Fluorescent treponemal antibody absorption	Negative ×2
Herpes simplex virus 1 DNA from ocular surface swab specimen	Negative ×2
Cytomegalovirus DNA from ocular surface swab specimen	Negative ×2
Varicella zoster virus DNA from ocular surface swab specimen	Negative ×2
Bacterial culture on blood, chocolate, Middlebrook agar	Negative ×2
Fungal culture on potato flake agar	Negative ×2
Monkeypox virus RNA from aqueous sample	Positive for MPXV
Monkeypox virus DNA from conjunctival swab specimen	Positive ×5
Testing from scleral and corneal biopsy	
Periodic acid Schiff for fungus	Negative for fungal organisms
Grocott's methamine silver	Negative for fungal organisms
Steiner	Negative for spirochetes
Acid-fast bacteria (Fite)†	Negative for acid-fast organisms
Trepona pallidum antibody	Negative
Herpes simplex virus 1 & 2	Negative
Varicella zoster virus	Negative
Complete blood count with differential obtained at the time of hospitalization	
Red blood cell count (reference 4.4–5.9 $\times 10^{12}$ cells/L)	4.45 $\times$ 10^{12} cells/L
Hemoglobin (reference 13.6–17.5 g/dL)‡	13.7 g/dL
Platelets (reference140–450 $\times 10^9$/L)‡	174 $\times$ 10^9/L
Leukocyte count (reference 3.4–10 $\times 10^9$ cells/L)	4.3 $\times$ 10^9 cells/L
Absolute neutrophils (reference 1.8 $\times$ 6.8 $\times$ 10^9 cells/L)	3.93 $\times$ 10^9 cells/L
Absolute monocytes (reference 0.2–0.8 $\times 10^9$ cells/L)‡§	0.06 $\times$ 10^9 cells/L
Absolute eosinophils (reference 0–0.4 $\times 10^9$ cells/L)	0
Absolute basophils (reference 0–0.1 $\times$ 10^9 cells/L)	0.01 $\times$ 10^9 cells/L
Absolute lymphocytes (reference 1–3.4 $\times$ 10^9 cells/L)‡§	0.33 $\times$ 10^9 cells/L

*QIAGEN, https://www.qiagen.com.
†Newcomer Supply, https://www.newcomersupply.com/product/afb-fite-stain-kit.
‡Hemoglobin (>10 g/dL) and platelet count (>100 $\times$ 10^9/L) do not meet criteria for active chronic lymphocytic leukemia and treatment.
§Indicates chronic lymphocytopenia.

Semen was the likely vehicle for direct transmission (*8*), although hand-to-eye contact with unobserved lesions or exposure through nondisclosed encounters cannot be excluded. Intraocular mpox involving the sclera, cornea, and anterior chamber, along with persistently PCR-positive ocular surface mpox, has a poor visual prognosis. There is no established treatment for ocular mpox (*9*). Continued mpox disease progression over several months is unusual and could raise suspicion of immunosuppression or treatment resistance.

Research reported in this manuscript was supported by the National Eye Institute of the National Institutes of Health under award no. R01EY03861 (TD), a Research to Prevent Blindness unrestricted grant, and the Pacific Huang Foundation. The content is solely the responsibility of the authors and does not necessarily represent the official views of the National Institutes of Health.

About the Author

Dr. Nguyen is a fellow in cornea and external disease at the University of California San Francisco and F.I. Proctor Foundation in San Francisco, California. His research interests include regenerative ophthalmology and ocular infectious diseases.

References

1. Doan T, Hinterwirth A, Worden L, Arzika AM, Maliki R, Abdou A, et al. Gut microbiome alteration in MORDOR I: a community-randomized trial of mass azithromycin distribution. Nat Med. 2019;25:1370–6. https://doi.org/10.1038/s41591-019-0533-0
2. Centers for Disease Control and Prevention. Interim clinical considerations for management of ocular mpox virus infection. 2022 [cited 2023 Feb 20]. https://www.cdc.gov/poxvirus/monkeypox/clinicians/ocular-infection.html
3. Frenois-Veyrat G, Gallardo F, Gorgé O, Marcheteau E, Ferraris O, Baidaliuk A, et al. Tecovirimat is effective against human monkeypox virus in vitro at nanomolar

concentrations. Nat Microbiol. 2022;7:1951–5. https://doi.org/10.1038/s41564-022-01269-8
4. Hughes C, McCollum A, Pukuta E, Karhemere S, Nguete B, Lushima RS, et al. Ocular complications associated with acute monkeypox virus infection, DRC. Int J Infect Dis. 2014;21:276–7. https://doi.org/10.1016/j.ijid.2014.03.994
5. Iñigo Martínez J, Gil Montalbán E, Jiménez Bueno S, Martín Martínez F, Nieto Juliá A, Sánchez Díaz J, et al. Monkeypox outbreak predominantly affecting men who have sex with men, Madrid, Spain, 26 April to 16 June 2022. Euro Surveill. 2022;27:2200471. https://doi.org/10.2807/1560-7917.ES.2022.27.27.2200471
6. Vusirikala A, Charles H, Balasegaram S, Macdonald N, Kumar D, Barker-Burnside C, et al. Epidemiology of early monkeypox virus transmission in sexual networks of gay and bisexual men, England, 2022. Emerg Infect Dis. 2022;28:2082–6. https://doi.org/10.3201/eid2810.220960
7. Thornhill JP, Barkati S, Walmsley S, Rockstroh J, Antinori A, Harrison LB, et al.; SHARE-net Clinical Group. Monkeypox virus infection in humans across 16 countries—April–June 2022. N Engl J Med. 2022;387:679–91. https://doi.org/10.1056/NEJMoa2207323
8. Lapa D, Carletti F, Mazzotta V, Matusali G, Pinnetti C, Meschi S, et al.; INMI Monkeypox Study Group. Monkeypox virus isolation from a semen sample collected in the early phase of infection in a patient with prolonged seminal viral shedding. Lancet Infect Dis. 2022;22:1267–9. https://doi.org/10.1016/S1473-3099(22)00513-8
9. Centers for Disease Control and Prevention. Ocular monkeypox—United States, July–September 2022. 2022 [cited 2022 Dec 15]. https://www.cdc.gov/mmwr/volumes/71/wr/mm7142e1.htm

Address for correspondence: Gerami D. Seitzman, University of California San Francisco—Ophthalmology, 490 Illinois St, San Francisco, CA 94158, USA; email: gerami.seitzman@ucsf.edu

National Surveillance of Pediatric Acute Hepatitis of Unknown Etiology, Japan, October 2021–December 2022

Shogo Otake, Chiaki Ikenoue, Natsu Sudani, Miho Kobayashi, Kensuke Takahashi, Tomoe Shimada, Itsuro Yoshimi, Tomoya Saito, Tomimasa Sunagawa

Author affiliations: Kobe University Graduate School of Medicine, Kobe, Japan (S. Otake); National Institute of Infectious Diseases, Tokyo, Japan (S. Otake, C. Ikenoue, N. Sudani, M. Kobayashi, K. Takahashi, T. Shimada, I. Yoshimi, T. Saito, T. Sunagawa)

DOI: https://doi.org/10.3201/eid2906.221579

Pediatric acute hepatitis of unknown etiology has been reported globally since April 2022. In Japan, 139 possible cases with onset dates after October 2021 were reported as of December 2022. Three patients required liver transplants, but none died. Rates of adenovirus positivity (11/125, 9%) were lower than those for other countries.

Severe acute hepatitis of unknown etiology (AHUE) in children has been reported globally since April 2022. By July 8, 2022, a total of 1,010 cases had been reported to the World Health Organization from 35 countries on the basis of the working case definitions (*1*). A definition for a confirmed case is not available, but probable cases are defined as acute hepatitis (non-A–E hepatitis) in persons ≤16 years of age with serum transaminase >500 IU/L (aspartate transaminase or aspartate aminotransferase) since October 1, 2021; epidemiologically linked cases are acute hepatitis (non-A–E hepatitis) in persons of any age who were close contacts with a probable case-patient since October 1, 2021. Of the 1,010 cases identified, 46 (5%) children required liver transplants, and 22 (2%) children died (*1*). We report pediatric AHUE cases in Japan and compare them with cases in other countries. Because the data for this study were taken from an epidemiologic investigation conducted by the government, the National Institute of Infectious Diseases did not require informed consent and ethical review (receipt no. 1442).

The Ministry of Health, Labor and Welfare (MHLW) of Japan issued the working case definitions of AHUE on April 27, 2022 (*2*), adopting the case definition published by the World Health Organization but limiting cases to hospitalized patients (Appendix Table 1, https://wwwnc.cdc.gov/EID/article/29/6/22-1579-App1.pdf). Physicians were instructed to exclude viral hepatitis A, B, C, and E through laboratory tests and report cases to public health centers. Laboratories at hospitals and local public health institutions performed microbiological testing recommended by MHLW (Appendix Table 2). Acute liver failure was considered a coagulopathy characterized by a prothrombin time and international normalized ratio of ≥2 or ≥1.5 with clinical encephalopathy (*3*).

As of December 31, 2022, a total of 139 probable AHUE cases with onset dates after October 1, 2021, had been reported throughout Japan without geographic clustering (Table). Six cases with unknown onset dates were excluded, and none were epidemiologically linked. Among the 139 patients, 3 (2%) underwent liver transplantation. Eleven (13%) of 85 patients met the definition of acute liver failure, 17 (18%) of 95 received intensive care, and none died (Table 1).

Of note, of 125 cases tested for adenovirus by PCR, 11 (9%) were positive (Appendix Table 3); however, adenoviruses were the most frequently detected pathogen in AHUE cases from Europe (52%) and the United Kingdom (66%) (*4*,*5*). Among the 11 adenovirus-positive cases, type 41 was identified in only 2 cases (18%) in Japan, unlike its frequent detection in England (*5*) (Appendix Table 1). Studies from the United Kingdom reported simultaneous increases in numbers of hospitalized hepatitis case-patients and detected adenoviruses cases (*5*). In Japan, the national surveillance system for viral hepatitis (Appendix Table 4), adenovirus, and adenovirus-associated syndromes (e.g., pharyngoconjunctival fever) did not identify unusual numbers or trends compared with previous years (*2*). The varying characteristics of reported AHUE cases among countries might be attributed to these differences.

Some reports have stated that SARS-CoV-2 spike protein acts as a superantigen, broadly stimulating T cells to induce hyperinflammation and

Table 1. Characteristics and laboratory findings of 139 cases that fulfilled the working case definition of pediatric acute hepatitis of unknown etiology, Japan, October 2021–December 2022*

Characteristic	Value
Median age, y (IQR)	4.4 (1.3–9.5)
<6 y of age	81/139 (58)
Sex	
M	74/139 (53)
F	65/139 (47)
Any comorbidities†	37/139 (26)
No comorbidities	98/139 (71)
Presence of comorbidities unknown	4/139 (3)
History of COVID-19 before onset of disease	15/132 (11)
Median duration from COVID-19 onset to hepatitis onset, d (range)	85 (14–300)
Persons ≥5 y who received ≥1 dose of COVID-19 vaccine	22/66 (33)
Any international travel in 2 mo before illness	0/130 (0)
Any contact with sick persons in 2 wk before illness	39/129 (30)
Treatment	
Steroid therapy	15/139 (11)
Immunoglobulin	6/139 (4)
Plasmapheresis	6/139 (4)
Hemodialysis	4/139 (3)
Liver transplantation	3/139 (2)
Outcome	
Acute liver failure	11/85 (13)‡
Hospitalized to ICU or HCU	17/95 (18)
Death	0/139 (0)
Median duration from symptom onset to hospital admission, d (IQR)	4 (2–7.5)
Median length of hospital stay, d (IQR)	10 (7–16)
Clinical symptoms§	
Fever 37.5°C or higher	89/138 (64)
Gastrointestinal symptoms: abdominal pain, diarrhea, or nausea/vomiting	75/138 (54)
Cough	29/138 (21)
Jaundice	29/138 (21)
White stools	10/138 (7)
Impaired consciousness	6/138 (4)
Median AST, IU/L (IQR)¶	764 (503–1,312)
Median ALT, IU/L (IQR)¶	838 (576–1,390)
Median total bilirubin, mg/dL (IQR)¶	1.00 (0.60–4.74)
Median PT-INR (IQR)¶	1.11 (1.02–1.32)
No. SARS-CoV-2 positive/no. tested (%)	10/134 (7)
Nucleic acid amplification test: PCR 101, LAMP 1, and NEAR 1	8/103 (8)
Antigen test	2/13 (15)
Type of test unknown	0/18 (0)

*Values are no. (%) except as indicated. Denominators consist of cases for which data are available. ALT, alanine aminotransferase; AST, aspartate aminotransferase; HCU, high-care unit; ICU, intensive care unit; IQR, interquartile range; LAMP, loop-mediated Isothermal amplification; NEAR, nicking enzyme amplification reaction; PT-INR, prothrombin time and international normalized ratio.
†Specific underlying conditions reported were psychomotor retardation (11, 8%), syndromes involving changes in chromosomes or genes (5, 4%), congenital heart disease (4, 3%), congenital metabolic disorder (3, 2%), low birthweight (3, 2%), endocrine disorder (3, 2%), autoimmune and collagen diseases (3, 2%), primary immunodeficiency syndrome (2, 1%), and other disorders (8, 6%) (atopic dermatitis, cloacal exstrophy, hydronephrosis, unilateral kidney agenesis and haemangioma).
‡Including 3 patients with encephalopathy.
§Some patients reported ≥1 sign/symptom.
¶Maximum values up to the time of reporting. Based on information from 136 (AST and ALT), 99 (total bilirubin), and 85 (PT-INR) cases.

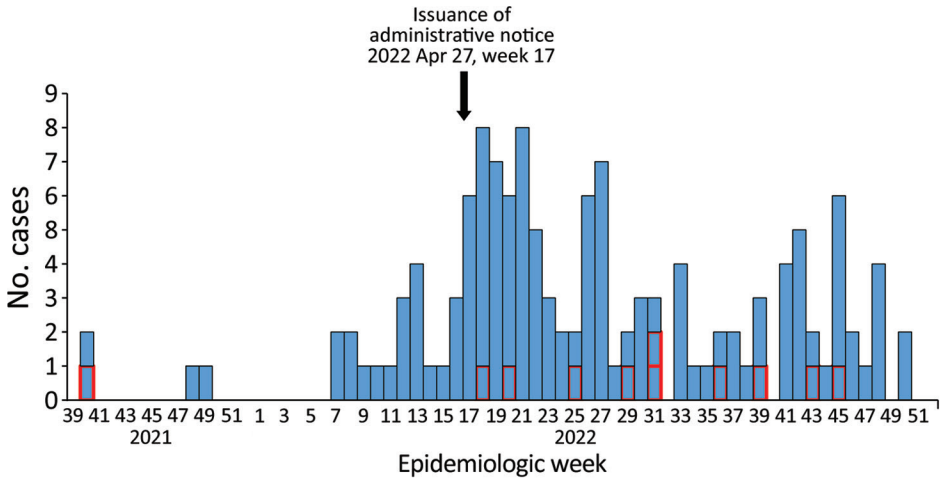

Figure. Cases of acute hepatitis of unknown etiology by week of onset in Japan, October 2021–December 31, 2022. The Ministry of Health, Labour, and Welfare Japan issued the working case definitions and administrative notice on April 27, 2022. In total, 139 probable cases with onset dates after October 1, 2021 (week 39, 2021), were reported as of December 31, 2022 (week 52, 2022). We excluded 6 cases for which onset dates were unavailable. Red outlines indicate cases fulfilling the diagnostic criteria for acute liver failure (n = 11).

potentially contributing to hepatitis (*6*). AHUE cases in Europe and United Kingdom revealed high rates of SARS-CoV-2 seropositivity (*4*,*5*) (Appendix Table 1). However, our study indicated low SARS-CoV-2 positivity (10/134, 7%) at the time of hospitalization for AHUE in Japan. Results of serologic tests for SARS-CoV-2 were unavailable because they were not required. The low proportion of patients with a history of COVID-19 before onset of AHUE (15/132, 11%) might explain the lower rates of seropositivity in Japan than for Europe and the United Kingdom.

Laboratory tests did not reveal a high frequency of any specific microorganism in Japan, and the distribution, other than for adenovirus, was similar to that reported in Europe (*4*). The cause of AHUE in Japan remains unknown. Cases reported in Japan were less severe than those reported in other countries (*1*,*2*,*4*,*5*,*7*) (Appendix Table 1), which might be because of differences in genetic predisposition that could affect inflammatory responses and clinical severity, as has been suggested with certain acute inflammatory diseases (*8*). The prevalence of the HLA-DRB1*04:01 allele, expressed by 89% of AHUE liver transplant cases in Scotland (*5*), is higher in the general population in Scotland than in Japan (8.9% vs. 1.0%) (*9*).

The first limitation of our study is that ascertainment bias might have affected microbiological testing results. The pathogens listed by MHLW (Appendix Table 2) might not have been examined uniformly and systematically, and the frequency of pathogens indicated in this report might not accurately reflect actual distribution. Second, the increase in reports after MHLW issued an administrative notice could be caused by reporting bias (Figure). Last, recall bias could have resulted in underestimates of the number of AHUE cases early in the study period.

In conclusion, we identified 139 pediatric AHUE cases in Japan during October 2021–December 2022 that differed in severity and adenovirus PCR positivity from cases in other countries. However, no unusual trends were found in this investigation. Japan might observe similar AHUE trends as in past years, as in the United States (*10*).

Acknowledgments

We thank the attending physicians, authorized staff at local public health centers, and members of the Ministry of Health, Labour and Welfare (Taito Kitano, Shouhei Nagae, Shuugo Sasaki, Jun Sugihara, and Mayumi Ueda) involved in data collections and case investigations. We thank the staff of Unit 4, Center for Surveillance, Immunization, and Epidemiologic Research, for contributing complementary surveillance information from the National Epidemiological Surveillance of Infectious Diseases system. We also acknowledge the work of the Prefectural and Municipal Public Health Institutes in Japan involved in microbiological testing. In addition, we thank Editage (http://www.editage.com) for editing and reviewing our manuscript for English publication.

This study was performed as a part of a grant funded by the Ministry of Health, Labour and Welfare (Research project on global disease intelligence and readiness for emerging diseases, 22HA2002).

About the Author

Dr. Otake is a researcher in field epidemiology and a pediatric infectious disease specialist at the National Institute of Infectious Diseases, Tokyo, Japan. His research interests are field epidemiology and pediatric infectious diseases.

References

1. World Health Organization. Severe acute hepatitis of unknown etiology in children—multi-country. 2022 Jul 12 [cited 2022 Oct 15]. https://www.who.int/emergencies/disease-outbreak-news/item/2022-DON400
2. National Institute of Infectious Diseases. Acute hepatitis of unknown etiology in children in Japan, October 2021–June 2022, as at Jun 23, 2022 (First report). 2022 Jul 27 [cited 2022 Oct 15]. https://www.niid.go.jp/niid/en/all-surveillance/2603-fetp/jissekijpn/11344-acute-hepatitis-of-unknown-etiology-in-children-in-japan-october-2021-june-2022-as-at-23-june-2022-first-report.html
3. Squires RH Jr, Shneider BL, Bucuvalas J, Alonso E, Sokol RJ, Narkewicz MR, et al. Acute liver failure in children: the first 348 patients in the pediatric acute liver failure study group. J Pediatr. 2006;148:652–8. https://doi.org/10.1016/j.jpeds.2005.12.051
4. European Centre for Disease Prevention and Control. Joint ECDC-WHO regional office for Europe hepatitis of unknown origin in children surveillance bulletin. 2022 Nov 25 [cited 2022 Dec 31]. https://www.ecdc.europa.eu/en/hepatitis/joint-hepatitis-unknown-origin-children-surveillance-bulletin
5. UK Health Security Agency. Investigation into acute hepatitis of unknown etiology in children in England. Technical briefing 4. 2022 Jul 26 [cited 2022 Oct 15]. https://assets.publishing.service.gov.uk/government/uploads/system/uploads/attachment_data/file/1094573/acute-hepatitis-technical-briefing-4.pdf
6. Brodin P, Arditi M. Severe acute hepatitis in children: investigate SARS-CoV-2 superantigens. Lancet Gastroenterol Hepatol. 2022;7:594–5. https://doi.org/10.1016/S2468-1253(22)00166-2
7. Cates J, Baker JM, Almendares O, Kambhampati AK, Burke RM, Balachandran N, et al.; Hepatitis of Unknown Etiology Group. Interim analysis of acute hepatitis of unknown etiology in children aged <10 years—United States, October 2021–June 2022. MMWR Morb Mortal Wkly Rep. 2022;71:852–8. https://doi.org/10.15585/mmwr.mm7126e1
8. Randolph HE, Fiege JK, Thielen BK, Mickelson CK, Shiratori M, Barroso-Batista J, et al. Genetic ancestry effects on the response to viral infection are pervasive but cell type specific. Science. 2021;374:1127–33. https://doi.org/10.1126/science.abg0928
9. Ikeda N, Kojima H, Nishikawa M, Hayashi K, Futagami T, Tsujino T, et al. Determination of HLA-A, -C, -B, -DRB1 allele and haplotype frequency in Japanese population based on family study. Tissue Antigens. 2015;85:252–9. https://doi.org/10.1111/tan.12536
10. Kambhampati AK, Burke RM, Dietz S, Sheppard M, Almendares O, Baker JM, et al. Trends in acute hepatitis of unspecified etiology and adenovirus stool testing results in children–United States, 2017–2022. MMWR Morb Mortal Wkly Rep. 2022;71:797–802. https://doi.org/10.15585/mmwr.mm7124e1

Address for correspondence: Tomoe Shimada, Center for Field Epidemic Intelligence, Research and Professional Development, National Institute of Infectious Diseases, J1601 Iidabashi Plano Stage Bldg, 2-7-2 Fujimi, Chiyoda-ku, Tokyo 102-0071, Japan; email: tomoes@niid.go.jp

etymologia revisited

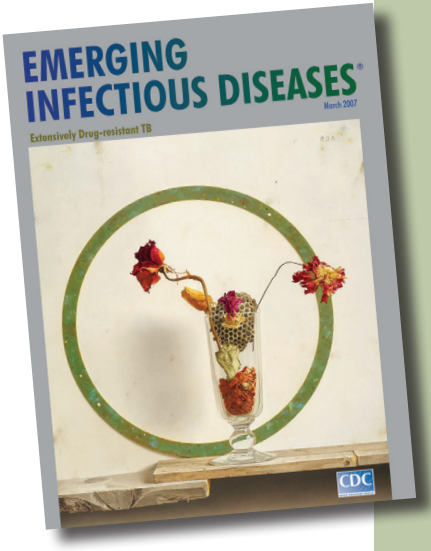

Originally published in March 2007

Norovirus

[nor′-o-vi′rəs]

Genus of viruses that cause viral gastroenteritis. Noroviruses are named after the original strain, "Norwalk virus," which caused an outbreak of acute gastroenteritis among children at an elementary school in Norwalk, Ohio, in 1968. Numerous outbreaks of disease with similar symptoms have been reported since, and the etiologic agents were called "Norwalk-like viruses" or "small round-structured viruses." Noroviruses are transmitted primarily through the fecal-oral route and are highly contagious; as few as 10 viral particles may infect a person.

Reference:

1. Mahy BWJ. A dictionary of virology. London: Academic Press; 2001; www.cdc.gov/ncidod/dvrd/revb/gastro/norovirus-qa.htm; www.medicinenet.com/norovirus_infection/article.htm

https://wwwnc.cdc.gov/eid/article/13/3/e1-1303_article

John Williamson (c.1730–c.1803), *Recovering Smallpox Patient*, c.1770 (detail)**.** Bust, pine, boiled linseed oil. 12.6 in x 5.7 in x 9.45 in/32 cm x 14.5 cm x 24 cm. Shetland Museum and Archives. Shetland Islands, Scotland, UK.

"Unassisted by Education, and Unfettered by the Rules of Art"

Byron Breedlove

The wig-stretching block appearing on this month's cover is thought to be the only surviving work from John Williamson, who lived on the Shetland Islands of Scotland. Williamson, perhaps better known by his nickname "Johnnie Notions" (sometimes spelled Johnie), proved to be skilled at many trades. *The Statistical Accounts of Scotland 1791–1845* describes him as "a singular instance of an uncommon variety of talents, being a tailor, a joiner, a clock and watch-mender, a blacksmith, and a physician." He was also, at various times in his life, a farmer, fisherman, and weaver. A self-taught physician, Williamson developed and administered smallpox inoculations for an estimated 3,000 patients during the late 18th century, primarily during the decade before Edward Jenner developed his smallpox vaccine in 1796. The procedure Williamson used, known as variolation, had been used for thousands of years, and it involves taking live virus from a smallpox patient and "inoculating" that virus onto the skin of a recipient who did not have the disease.

Ian D. Conacher, a physician and researcher, and Brian Smith, an archivist and author with the Shetland Archives, have each authored detailed accounts of Williamson's life and his work as an inoculator. Both authors provide historical context for how smallpox was introduced from the mainland of Scotland to Shetland and the devastating consequences resulting

Author affiliation: Centers for Disease Control and Prevention, Atlanta, Georgia, USA

DOI: https://doi.org/10.3201/eid2906.AC2906

from a series of smallpox outbreaks, curiously occurring in 20-year intervals (1700, 1720, 1740, and 1760). Both also draw from *The Statistical Accounts of Scotland 1791−1845,* which provides this account of Williamson's work:

> "Williamson was a local pioneer in the use of vaccines against smallpox. Unassisted by education, and unfettered by the rules of art. He is careful in providing the best matter and keeps it a long time before he puts it to use - sometimes 7 or 8 years. And, in order to lessen its virulence, he first dries it in peat smoke, and then puts it under the ground covered in camphor....by a small knife, made by his own hand, he gently raises a very little of the outer skin of the arm ....then puts in a very small quantity of the matter....The only plaister he uses, for healing the wound, is a bit of cabbage leaf."

Conacher noted that there is no evidence that Williamson caused any cases of smallpox or deaths among the people he inoculated. However, it is difficult to determine whether his techniques to reduce virulence of the virus were always successful. Variolation was inherently risky, in that, for some, the process could result in a full-blown case of smallpox. Regardless of the resulting severity, the individual recipient could then transmit the virulent smallpox virus to others.

According to the Shetland Museum and Archives, Williamson created the wig block for the Cheyne family, lairds at Tangwick Haa, Northmavine, Shetland, and "The face is modelled on an old man suffering from smallpox, the wood chosen because it was naturally marked with similar scarring." The archivist Smith wrote that "There is a strong tradition in Shetland that 'Johnie Notions' used as his model for this stretcher an old man from Hillswick whose face was marked with smallpox." A careful observer might conclude that, given the few pockmarks on the face, the man had experienced a relatively mild case of smallpox.

During that time in Europe, wigs were often favored by the wealthy and aristocratic classes but not simply to signal wealth and social status. Syphilis, which was widespread across Europe, caused hair loss and skin sores, so wigs helped disguise those symptoms. Blocks such as the one Williamson created from a piece of pine were essential for preening, shaping, and maintaining wigs.

During the last years of Williamson's life, Jenner developed the first vaccine against smallpox and envisioned the elimination of smallpox. In his 1801 treatise *On the Origin of the Vaccine Inoculation*, Jenner wrote, "the annihilation of the smallpox, the most dreadful scourge of the human species, must be the final result of this practice."

A good measure of control was achieved in many developed countries, largely via mass vaccination campaigns. However, because of poor health infrastructures in most developing countries, mass campaigns were not very successful, and smallpox circulation continued into the 20th century. In the 1960s, the deployment of an approach known as surveillance and containment—in which cases of smallpox were identified and traced and all those exposed and nearby were vaccinated—proved successful. Consequently, in 1980, the World Health Organization declared smallpox to be eradicated.

Although the smallpox virus (variola virus), the best known of the poxviruses affecting humans, no longer exists naturally, other poxviruses, including monkeypox virus, orf virus, molluscum contagiosum, yatapoxviruses, and parapoxviruses, can infect humans or other animals. The recent epidemic of mpox highlights the importance of continued vigilance, response, prevention, and innovation in public health efforts to control and treat diseases caused by poxviruses.

Bibliography

1. Centers for Disease Control and Prevention. Poxvirus [cited 2023 Apr 20]. https://www.cdc.gov/poxvirus
2. Centers for Disease Control and Prevention. Smallpox [cited 2023 Apr 20]. https://www.cdc.gov/smallpox
3. Conacher ID. The enigma of Johnnie "Notions" Williamson. J Med Biogr. 2001;9:208–12. https://doi.org/10.1177/096777200100900403
4. Sinclair, Sir John. *The Statistical Account of Scotland*, Yellmid and South, Shetland, Vol. 2, Edinburgh: William Creech, 1792, p. 569. University of Edinburgh, University of Glasgow. (1999) The Statistical Accounts of Scotland online service [cited 2023 May 1]. https://stataccscot.edina.ac.uk:443/link/osa-vol2-p569-parish-shetland-yellmid_and_south
5. Jenner E. On the origin of the vaccine inoculation. Med Phys J. 1801;5:505–8.
6. Nulman LA. Wigs: who wore them and why? [cited 2023 Apr 25]. http://www.kings-chapel.org/historyblog/wigs-who-wore-them-and-why
7. Shetland Museum and Archives. Artworks. Recovering smallpox patient [cited 2023 Apr 14]. https://artuk.org/discover/artworks/recovering-smallpox-patient-259654
8. Smith B. Camphor, cabbage leaves and vaccination: the career of Johnie "Notions" Williamson, of Hamnavoe, Eshaness, Shetland. Proc R Coll Physicians Edinb. 1998;28:395–406.

Address for correspondence: Byron Breedlove, EID Journal, Centers for Disease Control and Prevention, 1600 Clifton Rd NE, Mailstop H16-2, Atlanta, GA 30329-4027, USA; email: wbb1@cdc.gov

EMERGING INFECTIOUS DISEASES®

Upcoming Issue • Fungal Infections

- Nationwide Outbreak of *Candida auris* Infections Driven by COVID-19 Hospitalizations, Israel, 2021–2022
- Clinical and Mycologic Characteristics of Emerging Mucormycosis Agent *Rhizopus homothallicus*
- Rising Incidence of *Sporothrix brasiliensis* Infections, 2011–2022, Curitiba, Brazil
- Trajectory and Demographic Correlates of Antibodies to SARS-CoV-2 Nucleocapsid in Recently Infected Blood Donors, United States
- Triplex ELISA for Assessing Durability of *Taenia solium* Seropositivity after Neurocysticercosis Cure
- Sensitivity to Neutralizing Antibodies and Resistance to Type I Interferons in SARS-CoV-2 R.1 Lineage Variants, Canada
- Effect of Norovirus Inoculum Dose on Virus Kinetics, Shedding, and Symptoms
- Long-term Epidemiology and Evolution of Swine Influenza Viruses, Vietnam
- Estimating Waterborne Infectious Disease Burden by Exposure Route, United States, 2014
- Pulmonary Nontuberculous Mycobacteria, Ontario, Canada, 2020
- Increased Hospitalizations Involving Fungal Infections during COVID-19 Pandemic, United States, January 2020–December 2021
- Sexually Transmitted *Trichophyton mentagrophytes* Genotype VII Infection among Men Who Have Sex with Men
- Lumpy Skin Disease Virus Infection in Free-Ranging Indian gazelles (*Gazella bennettii*), Rajasthan, India
- Tuberculosis among Non–US-Born Persons and Persons >60 Years of Age, United States, 2019–2020
- Long-Term SARS-CoV-2 Antibody Seroprevalence in Blood Donors, Italy
- Novel High Pathogenicity Avian Influenza A(H5N1) Clade 2.3.4.4b Virus in Wild Birds, South Korea
- *Mycobacterium angelicum* Infection in Urinary Tract, French Polynesia
- Challenges in Forecasting Antimicrobial Resistance
- Epidemiology of Pathogens Listed as Potential Bioterrorism Agents, the Netherlands, 2009–2019

Complete list of articles in the July issue at https://wwwnc.cdc.gov/eid/#issue-300

Earning CME Credit

To obtain credit, you should first read the journal article. After reading the article, you should be able to answer the following, related, multiple-choice questions. To complete the questions (with a minimum 75% passing score) and earn continuing medical education (CME) credit, please go to http://www.medscape.org/journal/eid. Credit cannot be obtained for tests completed on paper, although you may use the worksheet below to keep a record of your answers.

You must be a registered user on http://www.medscape.org. If you are not registered on http://www.medscape.org, please click on the "Register" link on the right hand side of the website.

Only one answer is correct for each question. Once you successfully answer all post-test questions, you will be able to view and/or print your certificate. For questions regarding this activity, contact the accredited provider, CME@medscape.net. For technical assistance, contact CME@medscape.net. American Medical Association's Physician's Recognition Award (AMA PRA) credits are accepted in the US as evidence of participation in CME activities. For further information on this award, please go to https://www.ama-assn.org. The AMA has determined that physicians not licensed in the US who participate in this CME activity are eligible for AMA PRA Category 1 Credits™. Through agreements that the AMA has made with agencies in some countries, AMA PRA credit may be acceptable as evidence of participation in CME activities. If you are not licensed in the US, please complete the questions online, print the AMA PRA CME credit certificate, and present it to your national medical association for review.

Article Title

Case Studies and Literature Review of *Francisella tularensis*–Related Prosthetic Joint Infection

CME Questions

1. Your patient is a 52-year-old man with suspected *Francisella tularensis* prosthetic joint infection (PJI). On the basis of the case series of 3 cases of *F. tularensis* subsp. *holarctica*–related PJI in France between 2016 and 2019 and a review of 5 other cases reported in the literature by Ponderand and colleagues, which one of the following statements about clinical presentation and course of *F. tularensis* PJI is correct?

A. Clinical symptoms always began within 1 month of prosthetic joint placement
B. Symptoms were specific for tularemia
C. In 6 of 8 patients, clinical symptoms appeared away from the joint placement
D. All patients had severe infectious symptoms

2. According to the case series of 3 cases of *F. tularensis* subsp. *holarctica*–related PJI in France between 2016 and 2019 and review of 5 other cases reported in the literature by Ponderand and colleagues, which one of the following statements about diagnosis and laboratory findings of *F. tularensis* PJI is correct?

A. Joint aspiration or perioperative tissue cultures were positive in only 2 of 8 patients
B. *F. tularensis* was initially identified in 2 patients by matrix-assisted laser desorption/ionization time-of-flight mass spectrometry
C. *F. tularensis* was identified by molecular methods in 3 patients
D. When reported, inflammatory blood markers were usually in normal range

3. On the basis of the case series of 3 cases of *F. tularensis* subsp. *holarctica*–related PJI in France between 2016 and 2019 and review of 5 other cases reported in the literature by Ponderand and colleagues, which one of the following statements about treatment of *F. tularensis* PJI is correct?

A. Surgical treatment plus long-term (4–6 weeks) antimicrobial treatment led to favorable outcomes, with no relapse after 6 months of follow-up
B. All patients with tularemia PJI should have prosthesis removal
C. Clindamycin is recommended for first-line treatment of tularemia
D. Severe tularemia PJI should be treated with oral ciprofloxacin 800–1,000 mg daily for 10 days

Earning CME Credit

To obtain credit, you should first read the journal article. After reading the article, you should be able to answer the following, related, multiple-choice questions. To complete the questions (with a minimum 75% passing score) and earn continuing medical education (CME) credit, please go to http://www.medscape.org/journal/eid. Credit cannot be obtained for tests completed on paper, although you may use the worksheet below to keep a record of your answers.

You must be a registered user on http://www.medscape.org. If you are not registered on http://www.medscape.org, please click on the "Register" link on the right hand side of the website.

Only one answer is correct for each question. Once you successfully answer all post-test questions, you will be able to view and/or print your certificate. For questions regarding this activity, contact the accredited provider, CME@medscape.net. For technical assistance, contact CME@medscape.net. American Medical Association's Physician's Recognition Award (AMA PRA) credits are accepted in the US as evidence of participation in CME activities. For further information on this award, please go to https://www.ama-assn.org. The AMA has determined that physicians not licensed in the US who participate in this CME activity are eligible for AMA PRA Category 1 Credits™. Through agreements that the AMA has made with agencies in some countries, AMA PRA credit may be acceptable as evidence of participation in CME activities. If you are not licensed in the US, please complete the questions online, print the AMA PRA CME credit certificate, and present it to your national medical association for review.

Article Title

Neurologic Complications of Babesiosis, United States, 2011–2021

CME Questions

1. Your patient is a 43-year-old man admitted for babesiosis, who is now complaining of headache. On the basis of the record review of all 163 adult patients admitted to Yale-New Haven Hospital from January 2011 to October 2021 for laboratory-confirmed babesiosis by Locke and colleagues, which one of the following statements about the type and frequency of neurologic complications of babesiosis is correct?

A. One third of patients experienced 1 or more neurologic symptom during their hospital admission
B. The most frequent symptoms were headache, confusion/delirium, and impaired consciousness
C. Using the Glasgow Coma Scale (GCS), 6.1% of patients were classified as comatose
D. On lumbar puncture (LP), cerebrospinal fluid (CSF) showed marked pleocytosis

2. According to the record review by Locke and colleagues, which one of the following statements about risk factors predisposing patients to neurologic complications of babesiosis and outcomes is correct?

A. On multivariate analysis, patients with diabetes mellitus had 60% increased adjusted odds (aOR) of confusion/delirium and impaired consciousness
B. On multivariate analysis, stroke/transient ischemic attack (TIA) was significantly associated with confusion/delirium
C. Neurological symptoms were associated with high-grade parasitemia, renal failure, and preexisting history of diabetes mellitus
D. Overall, 11% of patients died during hospitalization

3. On the basis of the record review by Locke and colleagues, which one of the following statements about clinical implications of the type and frequency of neurologic complications of babesiosis and risk factors predisposing patients to neurologic complications is correct?

A. More research is needed into the pathological mechanisms underlying neurologic manifestations and long-term outcomes of babesiosis
B. Lyme disease is extremely difficult to differentiate from babesiosis
C. The study proves that the babesiosis agent itself causes neurologic complications
D. The study proves that vascular obstruction causes CNS complications in babesiosis